Synthesis and characterisation of the bacteriostatic effects of aminocarboxylate and aminophenolate ligands

RAMINDER SINGH MULLA

Synthesis and characterisation of the bacteriostatic effects of aminocarboxylate and aminophenolate ligands

Raminder Singh Mulla

A thesis submitted in partial fulfilment of the requirements for the degree of Doctor of Philosophy.

Department of Chemistry
Durham University
2016

Abstract

This thesis describes efforts towards the synthesis and evaluation of ligands that may be used in place of **EDTA**, a ligand that is slow to biodegrade after use, in antibacterial formulations. A number of synthetic strategies have been employed in the search for candidate ligands, such as substituting the carboxylate groups of **EDTA** with amide groups to form systems bearing 1 to 4 amide groups, using ligands which are able to form extremely stable complexes with Fe^{3+} on account of their phenolic donor groups, and the design and synthesis of ligands incorporating motifs known to be biodegradable.

To gauge the bacteriostatic efficacy of the studied ligands, optical-density based methods of monitoring the growth of *E. coli* were used, allowing ranking of the ligands according to their inhibitory power. Of the synthesised ligands, symmetrical **EDTA** bis-amides bearing strongly coordinating pendent groups (e.g. carboxylates and pyridines) gave the greatest extent of inhibition against *E. coli*. So as to understand the chemical reasons dictating the extent of inhibition of the studied ligands, thermodynamic characterisation (via pH- potentiometry and spectroscopic measurements) was undertaken. Comparison of the metal ion binding constants obtained for a selection of synthesised **EDTA** amides with those of other aminocarboxylate ligands, indicated that the amides almost always had smaller binding affinities for Ca^{2+}, Mg^{2+}, Fe^{3+}, Mn^{2+}, and Zn^{2+} , indicating that the strength of ligand binding to these ions is not the sole determinant of the efficacy for the **EDTA** amides.

Studies into the importance of association constants of a selection of known, commercially available aminocarboxylate ligands to Ca^{2+}, Mg^{2+}, Fe^{3+}, Mn^{2+}, and Zn^{2+} indicate that a certain level of Mg^{2+} binding (at the experimental pH) is relevant to inhibition, but this is not the case for phenolic ligands *if* the Fe^{3+} binding is sufficiently high. Assessment of a number of variables on the growth inhibition of *E. coli* showed that growth inhibition was most closely correlated with parameters pertaining to Fe^{3+} binding. ICP-MS studies show that aminocarboxylate ligands can extensively deplete manganese and iron from cells, which may not have been apparent from inspection of their Mn^{2+} binding constants. In constrast, the phenolic **EHPG** depleted iron almost exclusively. Based on the above, rational ligand design was attempted and some suggestions for future work have been given.

Contents

1. Introduction and aims **20**

1.1. EDTA: A brief history and problem statement . . . 20

1.2. Structure of bacterial cell walls . . . 22

1.2.1. General description . . . 22

1.2.2. The outer membrane: implications for permeability and infection . . . 23

1.2.3. Chelation-induced disruption of the Gram-negative outer membrane . . . 24

1.3. Bacterial metal homeostasis . . . 27

1.4. Some aspects of coordination chemistry . . . 29

1.4.1. The chelate and macrocyclic effects . . . 30

1.4.2. Selection of donor groups . . . 32

1.5. Biodegradability . . . 34

1.5.1. Experimental assessment of biodegradability . . . 34

1.5.2. Features of biodegradable compounds . . . 35

1.5.3. Biodegradation of EDTA, EDDS and GLDA . . . 36

1.6. Perspective and aims of the work . . . 39

2. An introduction to specialised techniques used in this work **42**

2.1. Choices of strain, buffer and media . . . 42

2.2. Quantitative ^{1}H NMR (qHNMR) studies . . . 42

2.2.1. Choice of experimental conditions . . . 43

2.2.2. Relation to molecular weights obtained by combustion analysis . . . 46

2.3. Optical density-mediated monitoring of bacterial cell growth . . . 47

2.4. Analysis of cellular metal content via ICP-MS . . . 50

2.5. Fluorescence competition using Fura-2 . . . 51

2.5.1. General background . . . 51

2.6. Measurement of partition coefficients . . . 56

3. Synthesis and growth inhibition studies of a series of EDTA amide ligands **59**

3.1. Motivations for the work . . . 59

3.2. Synthetic work . . . 61

3.2.1. Preparation of EDTA di-amides via EDTA di-anhydride . . . 61

3.2.2. Alternative synthetic routes: Approach and preliminary experiments . . . 62

3.2.3. Evaluation of a convergent route: use of α-haloamides . . . 65

3.2.4. Synthesis of EDTA mono-amides . . . 68

3.2.5. Synthesis of EDTA tetra-amides . . . 71

3.3. Assessment of antibacterial properties . . . 73
3.3.1. General remarks . . . 73
3.3.2. Effect of the number of carboxylates . . . 73
3.3.3. EDTA di-amides: effect of substituent . . . 76
3.4. Effect of $AmGly_2$ and EDTA on cellular metal content . . . 78
3.5. Metal complexation studies . . . 81
3.5.1. Potentiometric titrations on $AmGly_1$ and $AmGly_2$ (In collaboration with the University of Valencia) . . . 81
3.5.2. Ca^{2+} partitioning studies with Fura-2 . . . 86
3.5.3. Zn^{2+} partitioning studies with Fura-2 . . . 87
3.6. Structures of EDTA-amide metal complexes in the solid state (In collaboration with the University of Valencia) . . . 89
3.7. The relationship between metal affinity and biological activity . . . 95
3.8. Lipophilicity measurements . . . 96
3.8.1. Estimation of partition coefficients (*P*) . . . 96
3.9. Conclusions for this chapter . . . 98

4. Synthetic and biological studies on ligands bearing phenol groups 101
4.1. Introduction and motivations . . . 101
4.2. Synthetic approaches to HBED and EHPG ligands . . . 106
4.2.1. Strategy . . . 106
4.2.2. HBED derivatives . . . 108
4.2.3. Attempted synthesis of 4-NO_2-HBED . . . 113
4.2.4. Simple EHPG derivatives . . . 116
4.3. Assessment of biological properties . . . 117
4.3.1. Choice of buffer . . . 117
4.3.2. Importance of the phenolate groups . . . 117
4.3.3. Effect of the *para*- substituent on bacterial growth inhibition . . . 119
4.3.4. Comparisons between 4-R-HBED and 4-R-EHPG derivatives . . . 124
4.4. Relationship between metal ion affinities and bacterial growth inhibition . . . 126
4.5. Effect of EHPG on cellular metal content . . . 129
4.6. Lipophilicity measurements . . . 131
4.6.1. Estimation of partition coefficients . . . 131
4.7. Conclusions for this chapter . . . 132

5. Synthesis, and growth inhibition studies of commonly used aminocarboxylate ligands and some variants **134**

5.1. Introduction and motivation . . . 134
5.2. Ligand synthesis . . . 134
5.2.1. TETA . . . 134
5.2.2. AAZTA . . . 135
5.2.3. DO3A . . . 136
5.3. Growth inhibition studies . . . 136
5.3.1. General remarks . . . 136
5.3.2. Macrocycle ring size: effects on growth inhibition . . . 136
5.3.3. Acyclic octadentate ligands: effects on growth inhibition . . . 139
5.3.4. Heptadentate ligands: effects on growth inhibition . . . 140
5.4. Effect of AAZTA on cellular metal content . . . 142
5.5. Towards rational ligand design: Synthesis and properties of NOON . . . 144
5.5.1. Motivation and synthesis . . . 144
5.5.2. Metal binding studies on NOON (in collaboration with the University of Valencia) and its effect on *E. coli* growth . . . 146
5.6. Lipophilicity measurements . . . 151
5.7. What is the most important factor in predicting ligand efficacy? . . . 151
5.7.1. Introduction and strategy . . . 151
5.7.2. Assembly of a data set . . . 152
5.7.3. A simple model of metal speciation in TSB . . . 153
5.7.4. Analysis of the data . . . 155
5.8. Conclusions for this chapter . . . 156

6. Towards new ligand structures **158**

6.1. Introduction . . . 158
6.1.1. Motivations for the preparation of GLDA analogues . . . 160
6.1.2. DTPA as the basis for a biodegradable ligand . . . 162
6.2. Synthetic and biological studies of GLDA analogues . . . 163
6.2.1. Strategy . . . 163
6.2.2. Synthesis of intermediates via reductive amination of aldehydes directly onto l-Glutamic acid and derivatives . . . 164
6.2.3. Routes towards $HBGl_3$ employing reductive amination onto glycine derivatives 166
6.2.4. Synthesis of $HBGl_3$ via t-butyl ester protected intermediates . . . 169
6.2.5. Growth inhibition properties of $HBGl_3$ . . . 170

6.2.6. Towards the synthesis of $PyGl_3$ . . . 172
6.3. Towards the synthesis of RDTPMal-type ligands . . . 175
6.3.1. Strategy . . . 175
6.3.2. Linear synthesis based on reductive amination with triamines . . . 176
6.3.3. Linear synthesis based on triamine alkylation . . . 176
6.3.4. Linear synthesis based on aminomalonate derivatives as nucleophiles . . . 178
6.3.5. Synthesis of key intermediates for a convergent route . . . 180
6.4. Conclusions for this chapter . . . 182

7. Summary, conclusions and future work **183**
7.1. General conclusions . . . 183
7.1.1. Key findings . . . 183
7.2. Scope and limitations . . . 184
7.3. Suggestions for future work . . . 185

8. Experimental Procedures **188**
8.1. Synthesis: general remarks . . . 188
8.2. Synthesis and growth inhibition studies of a series of EDTA amide ligands . . . 189
8.2.1. 2,2‘-(3,10-Dioxo-1,12-diphenyl-2,5,8,11-tetraazadodecane-5,8-diyl)diacetic acid, hydrochloride dihydrate, $AmBn_2$ . . . 189
8.2.2. 5,8-Bis(carboxymethyl)-3,10-dioxo-2,5,8,11-tetraaza-dodecane-1,12-dicarboxylic acid, $AmGly_2$ . . . 190
8.2.3. [(Carbamoylmethyl){2-[(carbamoylmethyl)(carboxymethyl)amino]ethyl}amino]acetic acid, $AmNH_2$ . . . 190
8.2.4. [(2-{(Carboxymethyl)[2-(diethylamino)-2-oxoethyl]amino}ethyl) [2-(diethylamino)-2-oxoethyl]amino]acetic acid, $AmdiEt_2$ . . . 191
8.2.5. 2-{2-[(Carboxymethyl)(2-{(carboxymethyl)[2-(1-carboxyethylamino) -2-oxoethyl]amino}ethyl)amino]acetylamino}propionic acid, $AmAla_2$ . . . 192
8.2.6. [(2-{(Carboxymethyl)[2-(butylamino)-2-oxoethyl]amino}ethyl) [2-(butylamino)-2-oxoethyl]amino]acetic acid, $AmnBu_2$ . . . 192
8.2.7. Synthesis of α-haloamide intermediates . . . 193
8.2.8. Ethyl 2-amino-3-phenylpropionate hydrochloride, diethyl-phenylalaninate hydrochloride . . . 194
8.2.9. (2S)-2-(2-Chloroacetylamino)-3-methylbutyric acid, 6a . . . 194
8.2.10. tert-Butyl (2-chloroacetylamino)acetate, 6b . . . 195
8.2.11. 2-Chloro-1-{[(2-pyridyl)methyl]amino}-1-ethanone, 6c . . . 195
8.2.12. Ethyl 2-(2-chloroacetylamino)-3-phenylpropionate, 6d . . . 196

8.2.13. 1-(Butylamino)-2-chloro-1-ethanone, 6e 196
8.2.14. Ethyl [(benzyl){2-[(benzyl)(ethoxycarbonylmethyl)amino]ethyl}amino]acetate, 8 197
8.2.15. Ethyl (2-oxo-1-piperazinyl)acetate, 10 198
8.2.16. Tert-Butyl[(benzyl){2-[(benzyl)(tert-butoxycarbonylmethyl) amino]ethyl}amino]acetate, 11 198
8.2.17. Tert-Butyl {2-[(tert-butoxycarbonylmethyl)amino]ethylamino}acetate, 12 199
8.2.18. tert-Butyl-({2-[(tert-butoxycarbonylmethyl)(2-oxo-2-{[(2-pyridyl)methyl]amino}ethyl) amino]ethyl} (2-oxo-2-{[(2-pyridyl)methyl]amino}ethyl)amino)acetate, 13 200
8.2.19. ({2-[(Carboxymethyl)(2-oxo-2-{[(2-pyridyl)methyl]amino}ethyl)amino]ethyl}(2-oxo-2-{[(2-pyridyl)methyl]amino}ethyl)amino)acetic acid, $AmPy_2$ 201
8.2.20. Tert-Butyl [(tert-butoxycarbonylmethyl){2-[(benzyl)(tert-butoxycarbonylmethyl) amino]ethyl}amino]acetate, 14 202
8.2.21. Tert-Butyl{2-[(tert-butoxycarbonylmethyl)-N-tert-butoxycarbonylamino]ethylamino} acetate, [xv] 202
8.2.22. Tert-Butyl[(tert-butoxycarbonylmethyl){2-[(ethoxycarbonylmethyl)(tert-butoxycarbonyl methyl)amino]ethyl}amino]acetate, 16 203
8.2.23. tert-Butyl [(tert-butoxycarbonylmethyl){2-[(tert-butoxycarbonylmethyl){2-oxo-2-[(tert-butoxycarbonylmethyl)amino]ethyl}amino]ethyl}amino]acetate, 17 204
8.2.24. [(Carboxymethyl){2-[(carboxymethyl){2-[(carboxymethyl)amino]-2-oxoethyl}amino] ethyl}amino]acetic acid, $AmGly_1$ 204
8.2.25. tert-Butyl [(tert-butoxycarbonylmethyl){2-[(tert-butoxycarbonylmethyl)(2-oxo-2-{[(2-pyridyl)methyl]amino}ethyl)amino]ethyl}amino]acetate, 1:1 formate adduct, $AmPy_1$-tBu 205
8.2.26. [(Carboxymethyl){2-[(carboxymethyl)(2-oxo-2-{[(2-pyridyl)methyl]amino}ethyl)amino] ethyl}amino]acetic acid, $AmPy_1$ 206
8.2.27. Ethyl (2-{[2-(bis{2-[(ethoxycarbonylmethyl)amino]-2-oxoethyl}amino)ethyl]{2-[(ethoxy carbonylmethyl)amino]-2-oxoethyl}amino}acetylamino)acetate, 18 207
8.2.28. tert-Butyl (2-{[2-(bis{2-oxo-2-[(tert-butoxycarbonylmethyl)amino]ethyl}amino)ethyl]{2-oxo-2-[(tert-butoxycarbonylmethyl)amino]ethyl}amino}acetylamino)acetate, 19 . 208
8.2.29. Ethyl2-{2-[(2-{bis[2-(1-ethoxycarbonyl-2-phenylethylamino)-2-oxoethyl]amino}ethyl) [2-(1-ethoxycarbonyl-2-phenylethylamino)-2-oxoethyl]amino]acetylamino}-3-phenyl propionate, 20 209
8.2.30. (2-{[2-(Bis{2-[(carboxymethyl)amino]-2-oxoethyl}amino)ethyl]{2-[(carboxymethyl) amino]-2-oxoethyl}amino}acetylamino)acetic acid,hydrochloride salt, $AmGly_4$. 210
8.3. Synthetic and biological studies on ligands bearing phenol groups 211
8.3.1. o-[(2-{[(o-Hydroxyphenyl)methyl]amino}ethylamino)methyl]phenol, 4-H-21 . . . 211

8.3.2. 4-Fluoro-2-[(2-{[(5-fluoro-2-hydroxyphenyl)methyl]amino}ethylamino)methyl]phenol, 4-F-21 211
8.3.3. 4-Chloro-2-[(2-{[(5-chloro-2-hydroxyphenyl)methyl]amino}ethylamino)methyl]phenol, 4-Cl-21 212
8.3.4. 4-Bromo-2-[(2-{[(5-bromo-2-hydroxyphenyl)methyl]amino}ethylamino)methyl]phenol, 4-Br-21 213
8.3.5. 2-[(2-{[(2-Hydroxy-5-methoxyphenyl)methyl]amino}ethylamino)methyl]-4-methoxy phenol, 4-MeO-21 213
8.3.6. 2-Hydroxy-5-octylbenzaldehyde 214
8.3.7. 2-[(2-{[(2-Hydroxy-5-octylphenyl)methyl]amino}ethylamino)methyl]-4-octylphenol, 4-Oct-21 215
8.3.8. 2-[(2-{[(2-Hydroxy-5-nitrophenyl)methyl]amino}ethylamino)methyl]-4-nitrophenol, 4-NO_2-21 216
8.3.9. 1,2-Bis{[(o-methoxyphenyl)methyl]amino}ethane, 4-H-21-OMe 216
8.3.10. Ethyl {[(o-methoxyphenyl)methyl](2-{(ethoxycarbonylmethyl)[(o-methoxyphenyl) methyl]amino}ethyl)amino}acetate, 4-H-21-OMe-Et 217
8.3.11. Tert-Butyl{[(o-hydroxyphenyl)methyl](2-{[(o-hydroxyphenyl)methyl](tert-butoxy carbonyl methyl)amino}ethyl)amino}acetate, HBED-tBu 218
8.3.12. tert-Butyl {[(5-fluoro-2-hydroxyphenyl)methyl](2-{[(5-fluoro-2-hydroxyphenyl)methyl] (tert-butoxycarbonylmethyl)amino}ethyl)amino}acetate, 4-F-21-tBu 218
8.3.13. tert-Butyl{[(5-bromo-2-chlorophenyl)methyl](2-{[(5-chloro-2-hydroxyphenyl)methyl] (tert-butoxycarbonylmethyl)amino}ethyl)amino}acetate, 4-Cl-21-tBu 219
8.3.14. tert-Butyl {[(5-bromo-2- hydroxyphenyl)methyl] (2-{[(5-bromo-2- hydroxyphenyl) methyl] (tert-butoxy carbonylmethyl) amino}ethyl)amino} acetate, 4-Br-21-tBu . 220
8.3.15. tert-Butyl{[(2-hydroxy-5-methoxyphenyl) methyl](2-{[(2-hydroxy-5-methoxyphenyl)methyl](tert-butoxycarbonylmethyl)amino} ethyl)amino}acetate, 4-MeO-21-tBu 221
8.3.16. tert-Butyl{[(2-hydroxy-5-octylphenyl)methyl](2-{[(2-hydroxy-5-octylphenyl)methyl] (tert-butoxycarbonylmethyl)amino}ethyl)amino}acetate, 4-Oct-21-tBu 222
8.3.17. [(Benzyl){2-[(benzyl)(carboxymethyl)amino]ethyl}amino]acetic acid, BED 222
8.3.18. {[(5-Chloro-2-fluorophenyl)methyl](2-{(carboxymethyl)[(5-fluoro-2-hydroxyphenyl) methyl]amino}ethyl)amino}acetic acid, 4-F-HBED 223
8.3.19. {[(5-Chloro-2-hydroxyphenyl)methyl](2-{(carboxymethyl)[(5-chloro-2-hydroxyphenyl) methyl]amino}ethyl)amino}acetic acid, 4-Cl-HBED 224
8.3.20. {[(5-Bromo-2- hydroxyphenyl) methyl] (2-{[(5-bromo-2- hydroxyphenyl) methyl] (carboxymethyl) amino} ethyl)amino} acetic acid, 4-Br-HBED 224

8.3.21. {[(2-Hydroxy-5-methoxyphenyl)methyl](2-{(carboxymethyl)[(2-hydroxy-5-methoxy phenyl)methyl]amino}ethyl)amino}acetic acid, 4-MeO-HBED 225
8.3.22. {[(2-Hydroxy-5-octylphenyl)methyl](2-{(carboxymethyl)[(2-hydroxy-5-octylphenyl) methyl]amino}ethyl)amino}acetic acid, 4-Oct-HBED 226
8.3.23. Ethylene hydroxyphenyl acetic acid derivatives 226
8.4. Synthesis, and growth inhibition studies of commonly used aminocarboxylate ligands and some variants 228
8.4.1. 1,4-Dibenzyl-6-methyl-6-nitro-1,4-diazepane, 22 228
8.4.2. 6-Methyl-1,4-diazepin-6-ylamine, AAZ 228
8.4.3. Tert-Butyl {(tert-butoxycarbonylmethyl)[6-methyl-1,4-bis(tert-butoxycarbonylmethyl) -1,4-diazepin-6-yl]amino}acetate, AAZTA-tBu 229
8.4.4. {(Carboxymethyl)[1,4-bis(carboxymethyl)-6-methyl-1,4-diazepin-6-yl]amino}acetic acid, AAZTA, trifluoroacetate salt 230
8.4.5. tert-Butyl [4,10-bis(tert-butoxycarbonylmethyl)-1,4,7,10-tetraza-1-cyclododecyl] acetate hydrobromide, DO3A-tBu hydrobromide salt 230
8.4.6. [4,10-Bis(carboxymethyl)-1,4,7,10-tetraza-1-cyclododecyl]acetic acid, DO3A . 231
8.4.7. o-({2-[2-(2-{[(o-Hydroxyphenyl)methyl]-amino}ethoxy)-ethoxy]ethylamino}-methyl)phenol, 23 231
8.4.8. tert-Butyl-{[(o-hydroxyphenyl)-methyl]-{2-[2-(2-{[-(o-hydroxyphenyl)methyl]-(tert-butoxy-carbonylmethyl)-amino}ethoxy)-ethoxy]ethyl}-amino}acetate, NOON-tBu 232
8.4.9. {[(o-Oxyphenyl)methyl]{2-[2-(2-{(oxycarbonylmethyl)[(o-oxyphenyl)methyl]amino}ethoxy) ethoxy]ethyl}amino}acetate, NOON 233
8.5. Towards new ligand structures 235
8.5.1. 2-{[(o-Hydroxyphenyl)methyl]amino}glutaric acid, 24 235
8.5.2. Diisopropyl glutamate, hydrochloride salt 235
8.5.3. Isopropyl 1-[(o-hydroxyphenyl)methyl]-5-oxo-2-pyrrolidinecarboxylate, 25 . . . 236
8.5.4. Ethyl (2S)-1-[(o-hydroxyphenyl)methyl]-5-oxo-2-pyrrolidinecarboxylate, 26 . . . 237
8.5.5. Dimethyl 2-bromoglutarate, 27 237
8.5.6. Dimethyl 2-[bis(benzyl)amino]glutarate, 28 238
8.5.7. Methyl {[(o-hydroxyphenyl)methyl]amino}acetate, HB-28 239
8.5.8. o-(Benzyloxy)benzaldehyde, 29 239
8.5.9. Dimethyl 2-iodoglutarate, 27a 240
8.5.10. Methyl ({[o-(benzyloxy)phenyl]methyl}amino)acetate, HB-28-Bn 240
8.5.11. Dimethyl 2-({[o-(benzyloxy)phenyl]methyl}(methoxycarbonylmethyl)amino)glutarate, 30 241
8.5.12. Di-tert-butyl (2S)-2-{[(o-hydroxyphenyl)methyl]amino}glutarate, HB-31 242

8.5.13. Di-tert-butyl (2S)-2-{[(2-pyridyl)methyl]amino}glutarate Py-31 243
8.5.14. Di-tert-butyl (2S)-2-{(1R)-[(o-hydroxyphenyl)methyl](tert-butoxycarbonylmethyl) amino}glutarate, $HBGl_3$-tBu 244
8.5.15. (S)-2-{(Carboxymethyl)[(o-hydroxyphenyl)methyl]amino}glutaric acid, $HBGl_3$ . . 245
8.5.16. Di-tert-butyl (2S)-2-benzylaminoglutarate, hydrochloride salt, Bn-Glu-tBu . . . 245
8.5.17. Di-tert-Butyl(2S)-2-[(1R)-(benzyl)(tert-butoxycarbonylmethyl)amino]glutarate, $BnGl_3$ 246
8.5.18. Di-tert-butyl (2S)-2-[(tert-butoxycarbonylmethyl)amino]glutarate, 32 247
8.5.19. Di-tert-butyl (S)-2-{[(2-pyridyl)methyl](tert-butoxycarbonylmethyl)amino}glutarate, $PyGl_3$-tBu 248
8.5.20. Di-tert-butyl (2S)-2-{(1R)-(tert-butoxycarbonylmethyl)[(2-pyridyl)carbonyl]amino} glutarate, PyCO-Gl_3-tBu 249
8.5.21. 2-{2-[2-(3-Oxo-2H-isoindol-2-oyl)ethylamino]ethyl}-2H-isoindole-1,3-dione, 33 250
8.5.22. tert-Butyl {bis[2-(3-oxo-2H-isoindol-2-oyl)ethyl]amino}acetate, 33-tBu 250
8.5.23. 2-Amino-1-[(benzyl)(2-aminoethyl)amino]ethane, 35 251
8.5.24. Di-tert-butyl bromomalonate, 36 252
8.5.25. Di-tert-butyl bromomethylmalonate, Me-36 252
8.5.26. 2,2,2-Trifluoro-1-{2-[2-(2,2,2-trifluoroacetylamino)ethylamino]ethylamino}-1-ethanone, trifluoroacetate salt, [xxxvii] 253
8.5.27. {Bis[2-(2,2,2-trifluoroacetylamino)ethyl]amino}acetonitrile, 37-CN 253
8.5.28. tert-Butyl [bis(2-hydroxyethyl)amino]acetate, 39 254
8.5.29. Benzyl 2,5-dihydro-1H-pyrrole-1-carboxylate, 41 254
8.5.30. tert-Butyl [bis(2-chloroethyl)amino]acetate, 43 255
8.5.31. tert-Butyl [bis(2-iodoethyl)amino]acetate, 44 255
8.5.32. Diethyl {[(2,4-dimethoxyphenyl)methyl]amino}malonate, 45 256
8.5.33. Diethyl benzylaminomethylmalonate, 46 256
8.5.34. Di-tert-butyl benzylaminomalonate, 47 257
8.5.35. Di-tert-butyl (2-tert-butyldimethylsiloxyethylamino)malonate, 48 258
8.6. Determination of ligand stock solution concentrations via quantitative ^{1}H NMR 259
8.6.1. Preparation of t-butanol standard solution 259
8.6.2. Determination of ligand solution concentration 259
8.7. Analysis of biological properties 259
8.7.1. Preparation of overnight cultures of *E. coli* JM101 from freezer stocks 259
8.7.2. Assessment of relationship between colony forming units and optical density at 600nm (OD_{600}) 260

8.7.3. Growth inhibition studies on *E. Coli* JM101 . . . 260
8.7.4. Assessment of inhibitory concentrations against *E. Coli* JM101 for ICP-MS studies . . . 261
8.7.5. Preparation of ligand-treated cultures of *E. coli* JM101 for ICP-MS analysis . . 261
8.7.6. ICP-MS analysis of cell digests . . . 262
8.7.7. Assessment of *E. Coli* JM101 growth inhibition via a disc-diffusion based method . . . 262
8.8. Estimation of partition coefficients . . . 262
8.8.1. General procedure for the preparation of Fe^{3+} complexes of free ligands . . . 262
8.8.2. General procedure for estimating the partition coefficients of Fe^{3+} complexes . 264
8.8.3. Procedure for free ligand partition coefficients . . . 264
8.9. Fura-2 partitioning experiments . . . 265

A. Fura-2 partitioning protocol 266
A.1. Preparation . . . 266
A.1.1. Ligand stocks: . . . 266
A.1.2. Metal ion stocks: . . . 266
A.2. Selection of metal ion stock (Metal ion fluorescence titration) . . . 267
A.2.1. Fura-2 concentration adjustment . . . 267
A.3. Titration in plate . . . 267
A.4. Check for ligand autofluorescence . . . 267
A.5. Metal ion partitioning experiments . . . 268
A.5.1. Fura-2 First . . . 268
A.5.2. Ligand First . . . 268
A.6. Analysis of the data . . . 269

B. Some precursors to AAZTA ligands 270
B.1. Tert-butyl [6-methyl-6-nitro-4-(tert-butoxycarbonylmethyl)-1,4-diazepin-1-yl]acetate, NO_2-AAZ-tBu . . . 270
B.2. o-({4-[(o-Hydroxyphenyl)methyl]-6-methyl-6-nitro-1,4-diazepin-1-yl}methyl)phenol, NO_2-AAZ-HB . . . 272

C. A listing of single crystal X-ray structures 274
C.1. Structures of $AmGly_2$ . . . 275
C.1.1. Dipotassium salt . . . 275
C.1.2. Zwitterionic form . . . 276
C.1.3. Mg^{2+} complex . . . 277

C.2. Structure of $AmNH_2$ . . . 278
C.3. Structure of 6a . . . 279
C.4. Structure of methyl (2-bromoacetylamino)acetate . . . 280
C.5. Structures of $AmGly_1$ . . . 281
C.5.1. Free ligand . . . 281
C.5.2. Ca^{2+} complex . . . 282
C.6. Structure of 11 . . . 283
C.7. Structure of 4-H-21-OMe . . . 284
C.8. Structure of 4-R-21-tBu compounds . . . 285
C.8.1. Structure of 4-F-21-tBu . . . 285
C.8.2. Structure of 4-Cl-21-tBu . . . 286
C.8.3. Structure of 4-Br-21-tBu . . . 287
C.8.4. Structure of 4-MeO-21-tBu . . . 288
C.8.5. Structure of NOON-tBu . . . 289
C.9. Structures of NOON . . . 290
C.9.1. Free ligand . . . 290
C.9.2. Ca^{2+} complex . . . 291
C.10.Structure of 26 . . . 292
C.11.Structure of HB-28 . . . 293
C.12.Structure of NO_2-AAZ-HB . . . 294

D. Calculation of molecular weights from CHN data via JASPER 295

List of Figures

1. The structure of **EDTA** . . . 20
2. Commercially available biodegradable chelating ligands . . . 21
3. Simplified representations of Gram-positive, and Gram-negative cell walls . . . 22
4. The structure of *E. coli* **Lipid A** . . . 23
5. Antibacterials potentiated in the presence of **EDTA** . . . 25
6. The relationship between *P. aeruginosa* cell lysis and aminocarboxylate metal ion affinity 25
7. AFM-imaged membrane profiles of *E. coli* treated with **EDTA** . . . 26
8. The hexa-imidazole binding site of human calprotectin . . . 28
9. A graphical representation of the abundance of various metals in metalloproteins . . . 28
10. Some chelate ring sizes and their associated stability . . . 31
11. Equilibrium constants for open-chain and macrocyclic ligands . . . 32
12. The relationship between the Lewis acidity of a metal ion and the affinity to ligands containing anionic oxygen donors . . . 33
13. Biodegradability of some aromatic compounds . . . 36
14. Functional groups and their effect on biodegradability . . . 36
15. Compounds considered for use as ^{1}H NMR internal standards . . . 43
16. Representative *E. coli* JM101 growth curve experiments for **EDTA** and **NOTA** . . . 48
17. Typical dose response curves calculated from growth curves . . . 49
18. Example of the Increasing emission intensity of **Fura-2** in response to added Ca^{2+} . . . 51
19. Calibration of the corrected **Fura-2** emission intensity as a function of Ca^{2+} loading . . . 55
20. The effect of various aminocarboxylate ligands on the fluorescence of the **Ca-Fura-2** complex . . . 56
21. Charge states of **EDTA** . . . 57
22. Categories and examples of **EDTA** amide pendant groups . . . 61
23. Dose response curves for *E. coli* JM101 upon dosing with **EDTA**, **AmGly$_1$**, **AmGly$_2$** and **AmGly$_4$** 74
24. Dose response curve for *E. coli* JM101 upon dosing with **AmPhe$_4$** . . . 75
25. Dose response curves for *E. coli* JM101 upon dosing with **AmNH$_2$**, **AmBn$_2$**, **AmOMe$_2$**, **AmOH$_2$ and AmPy$_2$** . . . 78
26. Changes in the number of metal atoms per *E. coli* JM101 cell treated with **EDTA** at stationary phase measured by ICP-MS . . . 79
27. Changes in the number of metal atoms per *E. coli* JM101 cell with **AmGly$_2$** at stationary phase measured by ICP-MS . . . 80
28. Protonation states for **AmGly$_1$** and **AmGly$_2$** most relevant for metal complexation . . . 82
29. The effect of various **AmR$_2$** ligands on the fluorescence of the **Ca-Fura-2** complex . . . 86

30. The effect of various **AmR_2** ligands on the fluorescence of the **Zn-Fura-2** complex . . 87
31. Zn-Fura-2 demetalation as a function of incoming $AmGly_2$ and $AmOMe_2$ equivalents . 88
32. Single crystal structure of the Mg^{2+} complex of $AmGly_2$ 90
33. Crystal structure of **$AmTyr_2$** 92
34. Single crystal structure of the Ca^{2+} complex of $AmGly_1$ 93
35. Crystal structure of **Ca-12edtaenH_2** 94
36. A ranking of the *E. coli* JM101 growth inhibition at [**L**]=2.5 mM for the synthesised **AmR_x** ligands 99
37. Chelating ligands secreted by bacteria to solubilise and transport Fe^{3+} 102
38. Candidate ligands for the treatment of Fe^{3+} overload 103
39. A graphical representation of the selectivity of **HBED**, **EHPG** and **EDTA** at pH 7.4 . . . 106
40. Two disconnections toward **HBED** derivatives 107
41. Substituent effects on phenol pK_a 113
42. Comparison between *E. coli* growth inhibition characteristics for the bis-benzylated ligand **BED** and the bis-hydroxybenzylated ligand, **HBED** 118
43. Dose response curves for *E. coli* JM101 upon dosing with **4-F-HBED**, **4-Cl-HBED**, **4-Br-HBED** and **4-MeO-HBED** 120
44. Relationship between **4-R-HBED** and literature pK_a of their associated phenol groups 121
45. LB agar plates used for the disc diffusion experiment 123
46. Disc diffusion assay control plates 124
47. Dose response curves for *E. coli* JM101 upon dosing with **EHPG**, **4-Br-EHPG** and **4-Me-EHPG** 125
48. pK_a estimation for **4-Br-HBED** and **4-MeO-HBED** 127
49. The effect of the **BED**, **HBED**, **4-Br-HBED** and **4-Cl-HBED** ligands on the fluorescence of the **Ca-Fura-2** complex 128
50. The effect of the **BED**, **HBED**, **4-Br-HBED** and **EDTA** ligands on the fluorescence of the **Zn-Fura-2** complex 129
51. Effect of **EHPG** on the metal content of *E. coli* JM101 cells at stationary phase 130
52. Dose response curves for *E. coli* JM101 upon dosing with **EDTA**, **DOTA**, **NOTA** and **TETA** 137
53. Dose response curves for *E. coli* JM101 upon dosing with **DTPA** and **EGTA** 139
54. Dose response curves for *E. coli* JM101 upon dosing with **AAZTA**, **DO3A**, and **PN2C4** 141
55. Effect of **AAZTA** on the metal content of *E. coli* JM101 cells at stationary phase 143
56. Single crystal structure of the Ca^{2+} complex of **NOON** 145
57. Protonation states of **NOON** most relevant to metal ion binding 147
58. Dose response curves for *E. coli* JM101 upon dosing with **NOON** 150

59. Ligands considered in efforts towards a predictive model of *E. coli* JM101 growth inhibition in TSB . . . 152
60. Calculated $p(M^{n+})$ values in a model bacterial growth medium . . . 154
61. Correlations between *E. coli* growth relative to control and parameters related to Fe^{3+} binding . . . 156
62. Ligands with superior *E. coli* JM101 growth inhibition compared to **EDTA** . . . 158
63. Analogues of **GLDA** targeted for wide pH range performance . . . 160
64. Geometry-optimised models of the **Fe-GLDA** chelate . . . 161
65. A comparison between the pK_a values of glycine and 2-picolylamine . . . 161
66. log $K_a(Fe^{3+})$ and log $K_{a_{cond}}(Fe^{3+})$ values for **GLDA** and **HBIDA** . . . 162
67. Structure of **EDDM** . . . 162
68. **RDTPMal**, a candidate structure for a biodegradable analogue of **DTPA** . . . 163
69. Possible disconnections towards **$PyGl_3$** and **$HBGl_3$** . . . 163
70. Single crystal X-ray structure of **HB-28** . . . 167
71. Dose response curves for *E. coli* JM101 upon dosing with **EDTA**, **$HBGl_3$** and **GLDA** . 171
72. Disconnections evaluated for the synthesis of **RDTPMal-type** ligands . . . 175
73. Commercially available diethyl malonate derivatives . . . 175
74. Suggestions for further functionalisation of **48** . . . 181
75. Symmetrical **EDTA** bis-amides which display greater *E. coli* JM101 growth inhibition than **EDTA** . . . 183
76. α-haloamide intermediates prepared by Sherry . . . 186

List of Schemes

1. Routes to **EDTA** . . . 20
2. Examples of positive and negative entropy changes in ligand substitution reactions . . 29
3. Changes in steric interactions upon ligand coordination . . . 31
4. Biodegradation pathway for **EDTA** proposed for bacterial strains DSM9103 and BNC1. 37
5. The equilibrium between S,S'-**EDDS** and the weakly complexing biodegradation products formed by DSM9103 . . . 38
6. proposed biodegradation pathway for l-**GLDA** . . . 38
7. A popular route to **EDTA** diamide (**AmR_2**) ligands without recourse to protecting groups. . . . 61
8. Attempted synthesis of **$AmBn_1$** from anhydride **1** . . . 62
9. Disconnections and possible forward syntheses leading to **AmR_2** ligands. . . . 63
10. Attempted preparation of amide **2a** via carbodiimide coupling. HOBt: Hydroxybenzotriazole. . . . 64
11. Attempted preparation of **$AmGly_1$** via amide coupling. . . . 64
12. Ligands reported by the groups of Williams and Parker . . . 65
13. Preparation of **6f** using amide coupling chemistry . . . 66
14. Preparation of **8** via alkylation . . . 67
15. Preparation of key nucleophile **12** . . . 68
16. Synthesis of **$AmPy_2$** via a convergent route. . . . 68
17. Preparation of **15** using two different approaches . . . 69
18. Preparation of **$AmGly_1$** via a convergent route . . . 70
19. Preparation of **$AmPy_1$**. . . . 71
20. Key precursors to **AmR_4** type ligands . . . 71
21. The final **AmR_4** type ligands prepared. . . . 72
22. A possible forward synthesis of **4-R-HBED** type ligands. . . . 107
23. Wilson and Yunta routes for **4-R-EHPG** type ligands . . . 108
24. Preparation of **4-H-21** via one- and "two-pot" procedures. . . . 108
25. Scavenger-free deprotection of **11** . . . 112
26. *O*-protection strategies to enable selective amine alkylation in the presence of nitrophenols. . . . 115
27. Attempted syntheses of **4-NO_2-HBED-tBu** via aminoester **12** . . . 115
28. Preparation of **TETA**. . . . 135
29. Preparation of **AAZTA**. . . . 135
30. Preparation of **DO3A** . . . 136

31. Synthesis of the **NOON** ligand. 145
32. Synthesis of non-protected intermediate **24** via reductive amination 164
33. Reductive amination-cyclisation of diisopropyl glutamate to form lactam **25** 165
34. Thionyl chloride mediated esterification of **26** 166
35. Henig route to **27** 166
36. A test reaction between dibenzylamine and **27** confirming the absence of lactam formation. 167
37. Reductive amination of salicylaldehyde and pyridine-2-carboxaldehyde with methyl glycinate. 167
38. Test alkylation of **HB-28** using the more reactive electrophile **27a**. 168
39. Synthesis of **HB-28-Bn**, a protected analogue of **HB-28**, via reductive amination. . . 168
40. Synthesis of *O*- benzylated precursor **30** and attempted partial deprotection. 169
41. Reductive amination using a t-butyl protected derivative of glutamic acid to prevent lactam formation. 169
42. Successful synthesis of **HBGl$_3$**. 170
43. Synthesis of key intermediate **32** 172
44. Attempted enamine synthesis from **32** and 2-acetylpyridine. 174
45. Attempted reduction of **PyCO-Gl$_3$-tBu** 174
46. Synthetic pathway to linear triamine **34** and its undesired cyclisation to **34a**. Phth=Phthaloyl.176
47. Hydrazine-mediated synthesis of the stable linear triamine 35 177
48. Preparation of halogenated t-butyl malonates. 177
49. Selective terminal amine protection of diethylene triamine using ethyl trifluoroacetate. 177
50. Synthesis and hydrolysis of nitrile 37-CN 178
51. General approach to a protected **RDTPMal** precursor via “mustard-type” intermediates. 178
52. Alkylation of diethanolamine to prepare common intermediate **40**. 179
53. Cleavage of **41** to give carbonyl electrophile **42** as a substitute for **40**. 179
54. Conversion of diol **39** to dihalide electrophiles **43** and **44**. 179
55. Alkylation of TBDMS-protected ethanolamine with **36** 181
56. Proposed synthesis of **4-CF$_3$-HBED** 187
57. Waldron route to orthogonally functionalisable **AAZTA** precursors. 270
58. A three-step route to **NO$_2$-AAZTA-tBu**. 271
59. Synthesis of **NO$_2$-AAZ-HB**. 272

Declaration: The research described herein was undertaken at the Department of Chemistry at Durham University between October 2012 and December 2015. All of the work is my own, except where specifically stated otherwise. No part of it has previously been submitted for a degree at this or any other university.

Acknowledgements

This is in some ways the most difficult part to write. Perhaps bullet points may be better...

- **Prof. Gareth Williams,** for supervision, support and suggestions over these past few years, as well as offering me the opportunity to do this PhD.
- **Prof. David Parker** for helpful suggestions and wise words.
- **Prof. Nigel Robinson and his group** for guidance on the biological aspects of this work, undertaking ICP-MS analyses and generous access to microbiology facilities. **Dr. Gary Sharples** and **Marikka Beecroft** are also acknowledged for advice.
- **Tanya de Sa, Proctor and Gamble** for providing the support and funding this work.
- **Dr. Juan Aguilar** for his invaluable help in setting up the quantitative NMR experiments crucial to a great deal of work in this thesis.
- **The other members of the solution state NMR service** (Dr. Alan Kenwright, Catherine Heffernan, Dr. Raquel Belda Vidal) for running many a sample, and their advice.
- **Dr. Javier Pitarch-Jarque and Prof. Enrique Garcia-España** for potentiometric measurements on metal-ligand equilibria, and single crystal X-ray analyses of some metal complexes that crystallised out during their excellent work.
- **Dr. Dmitry Yufit** for a multitude of other crystal structure analyses.
- **The other analytical service personnel** (mass spec, elemental analysis, HPLC) for their professionalism and rapid turnaround of important data.
- **Aaron Brown and Malcolm Richardson** for glassblowing services (and more importantly, good conversation).
- **All of the members of CG1 past and present** for both moral and scientific support, and the good times, in the order I think I met them: Mickaële, Gemma, Victoria, Haz, Chris, Scott, David, Andrew, Maria, Emma, Mel, Ed, David O'Farrell, Bex and Jay (after all, you did offer me a chip and an onion ring to get on this list, and everyone has their price).
- **My Family**, Mum and Dad for raising me, Prithee for keeping me sane and the clan on either side, this one's for you.
- **The people I've met along the way** for their friendship. At the risk of sounding trite, you know who you are. I hope I've enriched your lives in the same way you have mine.

1. Introduction and aims

1.1. EDTA: A brief history and problem statement

Ethylenediaminetetraacetic acid, **EDTA** (***Figure 1***) is a hexadentate ligand that is used in a variety of domestic, industrial and health applications, e.g. food preservation, plant nutrition, surface cleaning and disinfection.[1, 2] These applications all rely on the ability of **EDTA** to strongly chelate a wide range of metal ions across a wide pH range and its low toxicity.[3] Some indications of the relevance to **EDTA** to modern life are that about 80,000 tonnes of **EDTA** are produced annually, and the ligand is included on the World Health Organisation's list of essential medicines.[4]

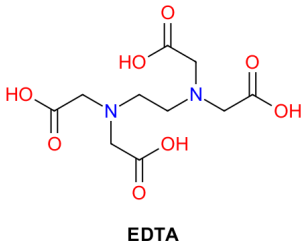

EDTA

Figure 1: The structure of **EDTA**. Donor groups are highlighted in colour.

EDTA was first synthesised by Munz in 1935 from ethylene diamine and chloroacetic acid,[5] but the current industrial synthesis utilises a condensation between ethylene diamine, formaldehyde and a cyanide source to prepare a nitrile intermediate which can then by hydrolysed (***Scheme 1***).

The first studies of **EDTA** after the filing of the Munz patent, were centred around thermodynamic studies of the metal complexes that the ligand formed, by Schwarzenbach[6] and others.[7]

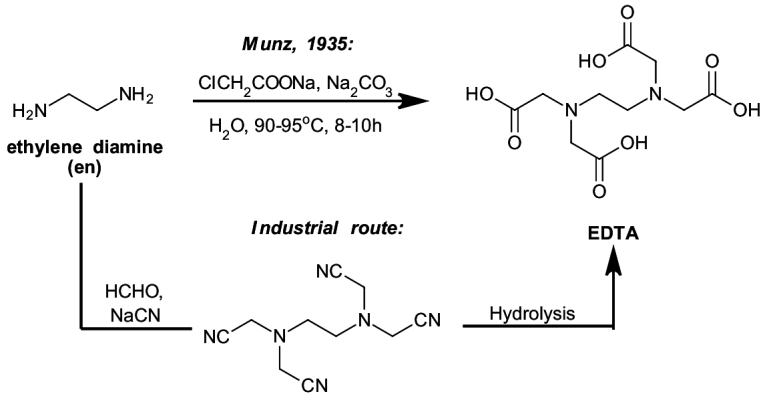

Scheme 1: The original 1935, and current industrial route to **EDTA**.

Soon after, studies on the use of **EDTA** to manipulate biological systems, especially on the applicability of **EDTA** as an anticoagulant,[8, 9] as a treatment for metal overload[10] and as a plant growth supplement,[11] were commenced, although the oldest work addressing the bacterial growth-inhibiting properties of **EDTA** may be from Johnson,[12] who demonstrated that the rate of *S. dysenteriae* was profoundly slowed by addition of the ligand above a threshold concentration. This combination of

fundamental studies elucidating the thermodynamic properties of metal-**EDTA** complexes, and the work on exploiting this newfound understanding in the “real world” from a very early stage, may be why the ligand is so widely used today.

A problematic aspect of this widespread use of **EDTA**, is that after use it accumulates in wastewater, and its disposal is complicated by its low biodegradability in nature. Indeed, it has been found that **EDTA** is present at higher concentrations than any other anthropogenic compound in European surface water.[13] Because of its long residence time in bodies of water, a concern is that unchecked **EDTA** use may lead to the leaching and mobilisation of toxic, heavy metal ions into water supplies intended for human consumption, and disruptions of the nitrogen balance of water bodies where **EDTA** is especially abundant.[14] Furthermore, the ability of **EDTA** to inhibit bacterial growth may lead to long-term, detrimental changes in aquatic ecosystems.[13]

It is because of these factors, that the use of **EDTA** has come under legislative scrutiny, and measures to limit its environmental impact have been put into place, including restrictions on its use in some US states and the limiting of its release into wastewater streams in Germany.[15] Based on such restrictions, alternatives to **EDTA** which are intended to be more biodegradable have been bought to market, like **MGDA**, **HIDS**, **EDDG**, **GLDA** and **EDDS** (***Figure 2***).[16] Of these, **EDDS** was evaluated by Procter and Gamble as an **EDTA** replacement that was more amenable to biodegradation,[17] but did not exhibit sufficient metal sequestration across the required pH range of 4-7 for it to function as a truly viable alternative, the same being true of **GLDA**.

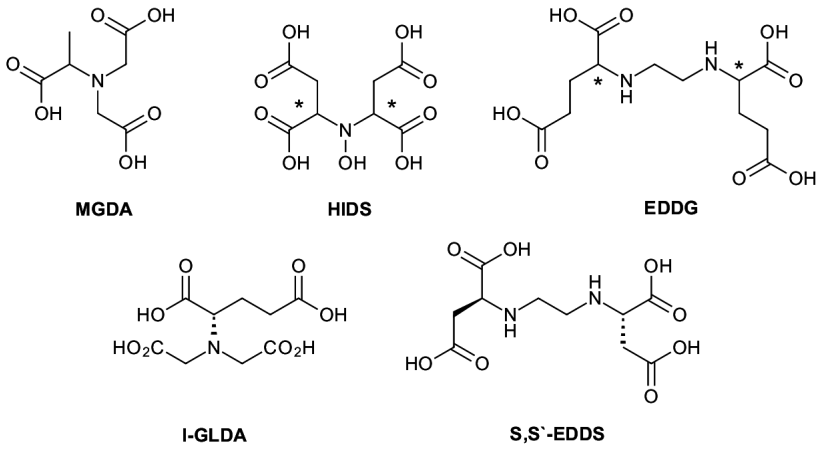

Figure 2: Commercially available biodegradable chelating ligands. Ligands that are known to exhibit enantioselective biodegradation have their most biodegradable isomer shown. Chiral compounds sold as racemates have their stereogenic centres marked with an asterisk.

Because of the shortcomings of the currently available biodegradable ligands, this thesis focuses on the synthesis of and evaluation of a wide range of alternative ligands, to be assessed on the basis of their bacterial growth inhibiting ability. Accordingly, a review of the factors underpinning ligand-mediated Gram-negative bacterial growth inhibition, chelate stability and the molecular features of a biodegradable compound follow.

1.2. Structure of bacterial cell walls

1.2.1. General description

Bacteria can be grouped into two general categories, Gram-positive and Gram-negative. Although both types of bacteria share common features such as a cytoplasmic membrane with embedded proteins, the cardinal difference between them is the structure of the cell walls (***Figure 3***). Gram-positive bacteria have a thick layer of peptidoglycan, a polymer comprised of sugar and amino acid fragments, and some species and strains also contain phosphate residues in their peptidoglycan layers which serve to bind Ca^{2+} and Mg^{2+} as an uptake mechanism for these ions. Gram-negative bacteria have a much thinner layer of peptidoglycan, but also have a secondary, outer membrane. This outer membrane is an asymmetric bilayer in which the layer in direct contact with the periplalsmic space is composed of phospholipids, which itself interfaces with a layer formed from molecules known as lipopolysaccharides (LPS), that are sugar-phospholipid conjugates.

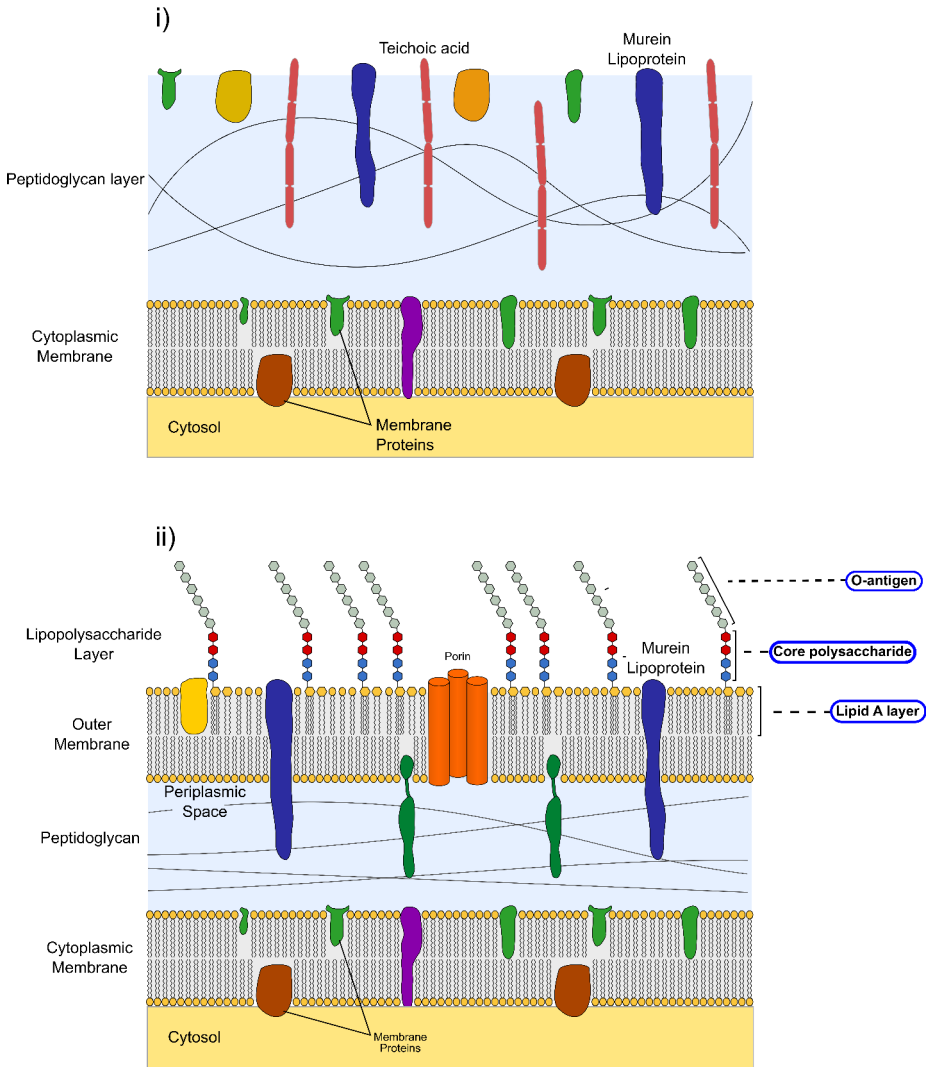

Figure 3: Simplified representations of **i)** the Gram-positive, and **ii)** Gram-negative cell walls. Adapted from the work of Jeff Dahl[18] under the terms of the GNU Free Documentation Licence.

The structure of lipopolysaccharide warrants further discussion, because of its central role in limiting the permeability of Gram-negative bacterial cells to a variety of foreign agents. The hydrophobic component of LPS, **Lipid A** (***Figure 4***), is conserved across many species of Gram-negative bacteria and anchors into the inner phospholipid layer of the outer membrane.[19] Phosphate groups are attached to the sugars that **Lipid A** contains, leading to a high negative charge density for each **Lipid A** unit. These phosphate groups are coordinated by Ca^{2+} and Mg^{2+} ions, and these interactions have profound implications for transport across the outer membrane, which will be discussed in ***Section 1.2.3***. Joining onto the sugar component of **Lipid A** is the core oligosaccharide, which is a species- and strain-dependent sequence of sugars that exhibits different degrees of phosphorylation depending on the organism in question.

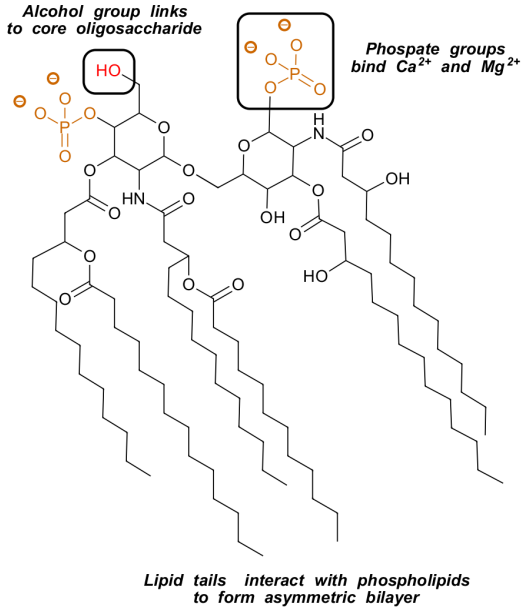

Figure 4: The structure of *E. coli* **Lipid A** , with key intermolecular interactions highlighted.

The outermost component of LPS projects into the outer environment and is called the *O*-antigen, present in most Gram-negative bacteria. This is a hydrophilic structure that contributes to the aqueous solubility of LPS, enables adhesion to host tissues and contributes to the pathenogenicity of some Gram-negative bacteria, but may not be present in all Gram-negative species and strains.

1.2.2. The outer membrane: implications for permeability and infection

The ability of LPS to bind[20] Ca^{2+} and Mg^{2+} confers mechanical stability[21] to the outer membrane with divalent cation binding increasing the ordering of isolated LPS, more so than the binding of other cations, like ammonium salts and Na^{+}.[22] In this way, interactions between LPS fragments and divalent cations can be considered similar to those in a coordination polymer. Such interactions also lead to a significant barrier to the diffusion of molecules above a certain size and polarity into a Gram-negative bacterial cell, and it is accepted that diffusion across the Gram-negative outer membrane

is restricted to a few types of molecules, e.g. small, hydrophilic molecules (up to ~600 g mol^{-1}) which can diffuse through proteins embedded within the outer membrane called porins.[23] This barrier renders Gram-negative bacteria invulnerable to many preservatives[24] and antibiotics that affect Gram-negative organisms after their transport into the cell.[25]

Unlike many Gram-positive pathogens like *Staphylococcus aureus* or *Clostridium difficile* then, whose growth and infections are treatable with a range of antibiotics, infections and growths of Gram-negative bacterial species like *Pseudomonas aeruginosa*, *Escherichia coli* and *Salmonella enterica* cannot be treated with as wide a range of compounds. Those antibiotics which are used, are often "drugs of last resort," with unpleasant side-effects.

Therefore, increasing the range of antibacterial compounds applicable to Gram-negative bacteria, alongside the development of tools to directly inhibit the growth of Gram-negative bacteria, is desirable. Given the sheer variety of locations in which Gram-negative bacterial species like *Pseudomonas aeruginosa* and *Escherichia coli* are able to thrive (the former even being able to grow in emulsions of toluene[26]), further utility would also be derived from the development of antibacterials that may also be applied to potential outbreak sites, e.g. soap dispensers and consumer formulations.[27] **EDTA** fulfils these roles rather well, but could also be exchanged for other powerful, broad-spectrum ligands, on account of the coordination interactions relevant to the stability of the LPS barrier.

1.2.3. Chelation-induced disruption of the Gram-negative outer membrane

A rich literature exists on the deliberate destabilisation of the Gram-negative outer membrane,[28] with a good deal of work focusing on *E. coli* and *P. aeruginosa* as model organisms. The phenomenon of **EDTA**-mediated LPS disruption was first reported by Leive,[29] who demonstrated that *E. coli* cells treated with **EDTA** became susceptible to actinomycin D, an antibiotic which is usually only effective against Gram-positive bacteria, within minutes of exposure to **EDTA**. Building on this, it was later found that in the presence of **EDTA**, the bactericidal effect of some amines like dodecylamine, **TRIS** or benzalkonium chloride against *E. coli* was drastically increased. This was assumed to be because **EDTA** treatment enabled penetration of these amines deep into the cell, resulting in lethal damage (***Figure 5***).[30]

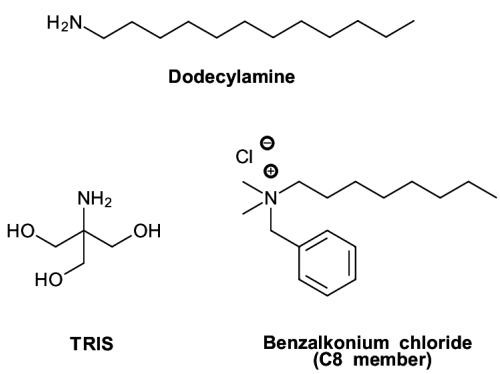

Figure 5: Antibacterials potentiated in the presence of **EDTA**.

The phenomenon of **EDTA**-induced potentiation of antibacterial agents was also observed in *P. aeruginosa* by Haque and Russell a few years later, who studied the effect of antibiotics typically unable to cross the Gram-negative cell wall, in conjunction with **NTA**, **IDA**, *trans*-**CDTA**, **HEDTA** and **EDTA**. The fact that these chelating ligands were all able to render *P. aeruginosa* susceptible to such antibiotics showed that chelation *in general* (provided sufficient metal ion content was complexed), was key to rendering Gram-negatives vulnerable antibiotics that were typically cell-impermeable.[31] Perhaps due to the more extensive phosphorylation of LPS belonging to *P. aeruginosa* compared to *E. coli*, it was also found that *trans*-**CDTA** and **EDTA** could effect *P. aeruginosa* cell lysis without an additive (***Figure 6***).[32, 33] To the author's knowledge, these works, alongside that of Spicer and Spooner,[34] are some of the only publications discussing the relation between metal ion binding properties of aminocarboxylate ligands and their capacity for disrupting Gram-negative bacterial growth.

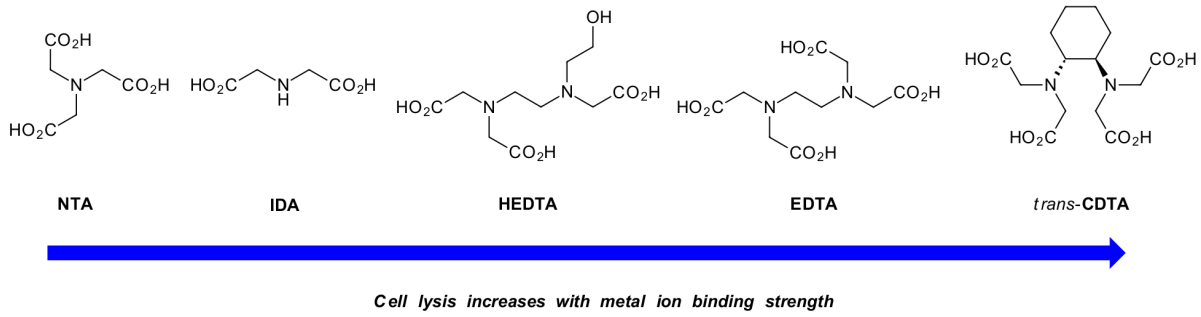

Figure 6: The relationship between *P. aeruginosa* cell lysis and aminocarboxylate metal ion affinity highlighted by Haque and Russell.[32]

Perhaps the most direct evidence for the role of Ca^{2+} and Mg^{2+} in LPS stabilisation came from experiments demonstrating that the addition of excess magnesium chloride completely restored the antibiotic resistance of a selection of *E. coli* strains.[29, 35] This effect was also observed in *P. aeruginosa*.[36] In fact, the addition of Mg^{2+} to Gram-negative bacterial cultures has become something of a way to "re-enforce" the structure of the LPS layer in a number of outer membrane studies.[37, 38] More recently, the use of atomic force microscopy gave a visual indication of the cellular damage **EDTA** can inflict on *E. coli* cells, allowing for the detection of pits formed in the outer membrane due to LPS stripping when the cells were treated with 100 mM **EDTA** (***Figure 7***).[39]

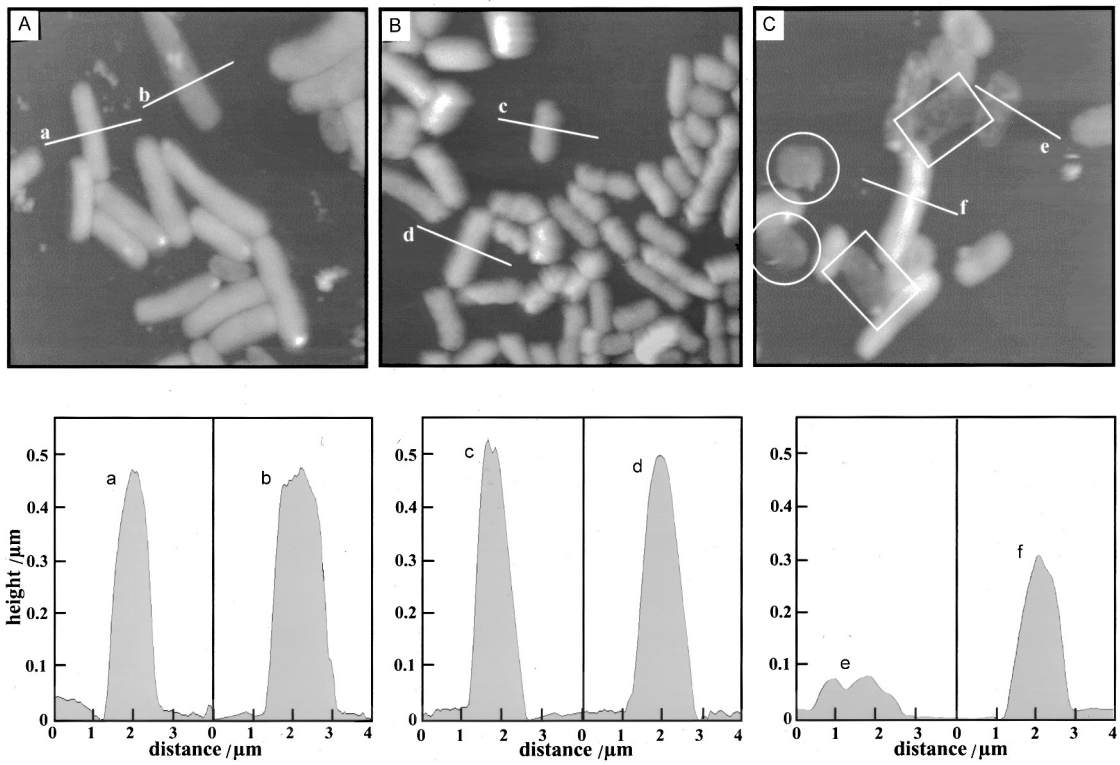

Figure 7: AFM-imaged membrane profiles of *E. coli* treated with **A**) 0 mM **EDTA**, **B**) 50 mM **EDTA** and **C**) 100 mM **EDTA**. Lowercase letters on the graphs represent the sampling location on the images of the cells. Adapted with permission from *Langmuir*, 2000, **16**, pp 2789–2796. Copyright 2000 American Chemical Society.

Polycations are also known to permeabilise the outer membrane through disorganisation, and the presence of multiple positive charges is a common feature in many compounds and natural extracts that are found to hinder Gram-negative bacterial growth. Because their mode of action is not dependent on chelation, they are not reviewed here, but the interested reader is directed to work by Vaara for further information.[40, 41]

From this work, it would therefore be reasonable to assume that a chelating ligand that exhibited sufficiently high Ca^{2+} and Mg^{2+} affinities would be an efficient outer membrane permeabilising agent, which could induce cell death on its own if the dose was high enough, or render treated cells susceptible to added antibacterials.

1.3. Bacterial metal homeostasis

It is believed that approximately one third of proteins contain a metal in some form,[42] where they perform a plethora of functions, from catalysis to conformational restriction (***Figure 1***).[43, 44] Bacteria, like all living organisms, require metals for their survival and growth and it is because of that, a shortage of relevant metal ions in an environment will limit their growth;[45] in fact, deliberate metal starvation is used as a way of controlling bacterial infection by infected host organisms, in a process known as nutritional immunity.[46]

Metal ions necessary for proper function are taken up into the cell either by the secretion of small molecules like siderophores for Fe^{3+} (covered further in ***Section 4.1***), active transport[47] or other, poorly-defined transport systems.[48] Systems to regulate cellular metal levels, like efflux pumps[49] or the repression of genes relevant to the transport of a certain metal, are also present,[50] because an excess of many metal ions (e.g. Fe^{3+}, Mn^{2+} or Cu^{+}) is also detrimental to cell health.

Table 1: Some examples of the use of metal ions in bacteria. Adapted from Wilkins.[43]

Biomolecule	Metal ion(s) present	Function of biomolecule	Function of metal ion(s)
Lipopolysaccharide (LPS) (Gram-negative bacteria)	Ca^{2+}, Mg^{2+}	Outer membrane permeability barrier	Links discrete LPS fragments together
Some ATPases (*E. coli*)	Ca^{2+}, Mg^{2+}	Hydrolysis of ATP for energy release	Enzyme cofactors
DNA (universal)	Mg^{2+}	Contains the genetic material of an organism	Structure stabilisation
Cytochrome P450 (*Pseudomonas sp.*)	Fe^{2+}, Fe^{3+}	Oxidative degradation of a variety of organic molecules	Electron source / sink and O_2 binding
Superoxide dismutase (*E. coli*)	Fe^{2+}, Fe^{3+} or Mn^{2+}, Mn^{3+}	Conversion of superoxide radical into H_2O_2 and O_2	Electron source / sink
Alkaline phosphatase (*E. coli*)	Zn^{2+}	Catalyses removal of phosphate groups	Lewis acid
Carbonic anhydrase	Zn^{2+}	Conversion of CO_2 to HCO_3^- and H^+	Lewis acid

These findings demonstrate that **EDTA**-induced growth inhibition will involve a component that cannot be attributed to LPS damage, i.e. the reduction of the metal content available to bacterial cells through chelation in general,[51] once again affirming that **EDTA** can be exchanged for other chelating ligands if an antibacterial effect is desired.

The disruption of metal homeostasis as an antibacterial strategy is an active field of study. For instance, the disruption of iron homeostasis has been shown to be an effective way to control bacterial growth by the work of Hider.[52–55] The antibacterial properties of human Calprotectin have also been investigated, and the activity of the protein has been assigned to its ability to bind Fe^{2+} and Mn^{2+} in a hexa-imidazole binding site (***Figure 8***).[56, 57]

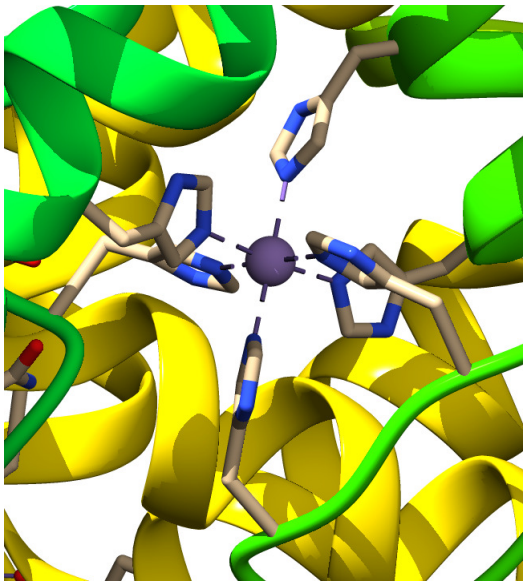

Figure 8: The hexa-imidazole binding site of human calprotectin coordinating Mn^{2+} (the purple sphere) in an octahedral geometry. This figure was rendered from the structure reported in Gagnon *et al*.[58]PDB code: 4XJK.

On the other hand, limited data about exactly which metal ion is the most important to Gram-negative bacterial growth and survival are available, and so it is prudent to design systems which can form stable complexes with as many of the metal ions (Ca^{2+}, Mg^{2+}, Zn^{2+} and the first row transition metals) that are commonly found in proteins, as possible (***Figure 9***). Thus, a review of the factors that influence ligand-metal complex equilibria, as a starting point for molecular design, is appropriate.

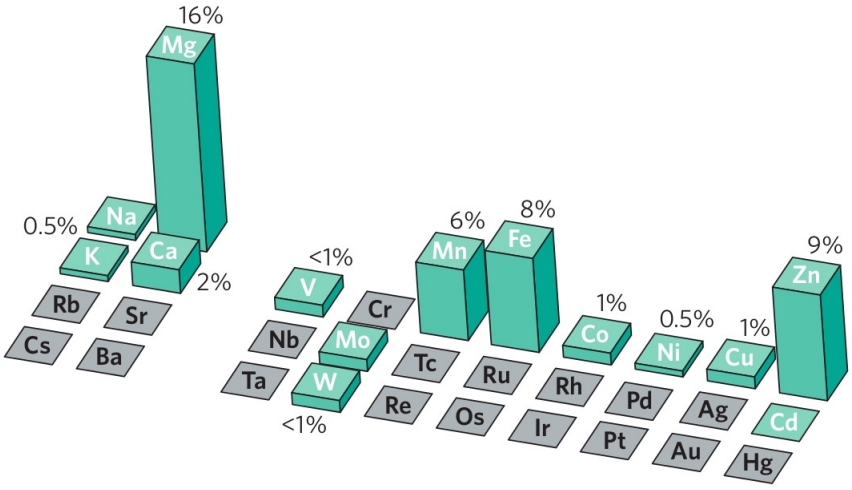

Figure 9: A graphical representation of the abundance of various metals in metalloproteins. Adapted by permission from Macmillan Publishers Ltd: Nature, 2009, **460** p. 823, copyright 2009.

1.4. Some aspects of coordination chemistry

Like all chemical reactions, metal complexation by a ligand can be treated as an equilibrium with enthalpic (*H*) and entropic (*S*) components, and with an extent of reaction that can be described by an equilibrium constant K_{eq} in the usual way (***Equations 1*** and ***2***).

$$\Delta G = \Delta H - T\Delta S \tag{1}$$

$$\Delta G = -RTlnK_{eq} \tag{2}$$

The enthalpic component ΔH, relates to factors such as charge neutralisation, the bond-making and bond-breaking events involved in the complexation reaction and strain factors in the metal-ligand complex. The entropic component ΔS, relates to changes in the freedom of motion available in the metal ion and the complex, as well as the degree of preorganisation of the complexing ligand and is best demonstrated with an example (***Scheme 2***).

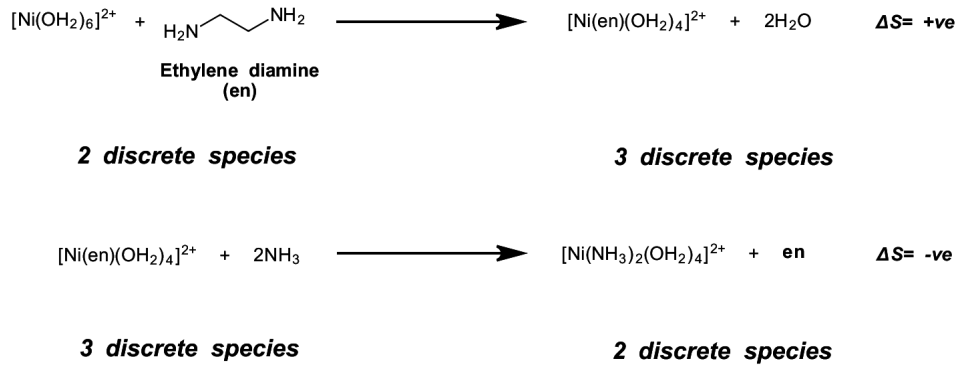

Scheme 2: Examples of positive and negative entropy changes in ligand substitution reactions. The change in entropy is positive if there are more species produced upon substitution, and vice-versa.

Naturally, the more negative ΔH is, and the more positive ΔS is, the more favourable the reaction is, which is expressed as a higher K_{eq}. Therefore to favour metal ion complexation, a ligand must be designed in such a way that many strong bonds are formed to the metal ions in question.

With regards to denticity, the transition metal ions (understood as being those with a partially filled *d*-subshell) will usually adopt a six-coordinate structure with a preference for an octahedral geometry, which minimises the steric interaction between ligand donor atoms, and allows for the optimal interaction of the ligand donor atom lone pairs with the *d*-orbitals of the metal ion. The coordination geometry of Zn^{2+} is somewhat more varied due to its completely filled *d*- orbitals meaning that any stabilisation component arises purely from the competition between steric crowding around the metal ion and maximising the number of interactions formed. In real terms, this means that octahedral geometries are common, but tetrahedral, trigonal planar and pentagonal bipyramidal geometries are also known.

The increased ionic radius of Ca^{2+}compared to Zn^{2+} (99 pm cf. 74 pm) means that higher coordination numbers are observed for Ca^{2+}, which commonly exhibits eight-coordination[59] because of the increased number of contacts that can arise without steric crowding. Because of its smaller size, Mg^{2+} typically exhibits octahedral geometry[60] since the incorporation of a higher number of ligands around the ion will be sterically unfavourable.

1.4.1. The chelate and macrocyclic effects

In considering a substitution reaction between an aquated metal ion and a monodentate ligand like ammonia, and the same reaction with the bidentate analogue ethylene diamine (***Scheme 2***), it is apparent that the latter is thermodynamically more favourable than would be expected if ΔG depended solely on the donor groups involved (***Table 2***).

Table 2: Examples of the chelate effect showing the increases in complex stability brought about when a chelating ligand is coordinated to a metal ion. Data from Huheey[61]

Ammonia complexes	ΔG / kJ mol^{-1}	ΔH / kJ mol^{-1}	ΔS / J mol^{-1} K^{-1}	**Ethylene diamine complexes**	ΔG / kJ mol^{-1}	ΔH / kJ mol^{-1}	ΔS / J mol^{-1} K^{-1}
$[Cu(NH_3)_2(H_2O)_4]^{2+}$	-44.7	-46	-4	$[Cu(en)(H_2O)_4]^{2+}$	-60.1	-55	+25
$[Cu(NH_3)_4(H_2O)_2]^{2+}$	-74.2	-92	-59	$[Cu(en)_2(H_2O)_2]^{2+}$	-111.8	-107	+29

This contribution to favourability is termed the *chelate effect*, and has both enthalpic and entropic components. In a chelating ligand like ethylene diamine, some of the steric strain arising from the necessarily close proximity of the amine groups in a metal complex is also present in the free ligand, meaning that the introduction of increased strain carries less of an energy penalty, than if two molecules of ammonia were coordinated adjacent to one another at the same metal core, since the ammonia molecule is not strained in the free state (***Scheme 3***). Desolvation effects also contribute; the reduced solvation of ethylene diamine compared to ammonia in the free state in aqueous media means that ethylene diamine has a reduced desolvation penalty compared to ammonia on complexation.[44]

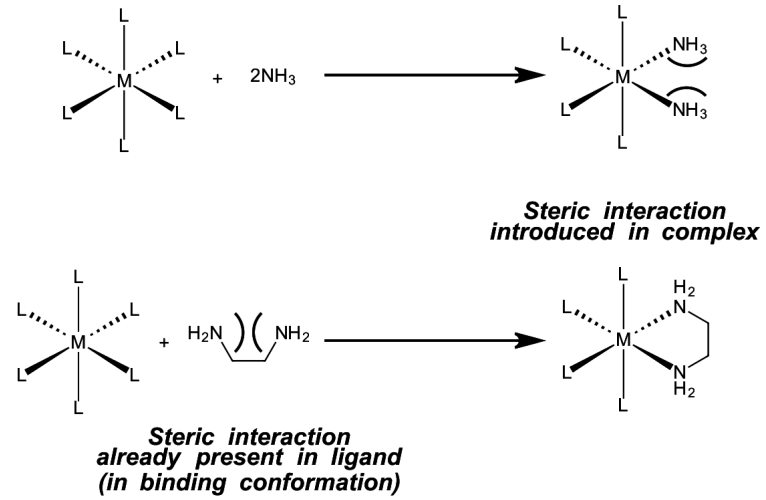

Scheme 3: Changes in steric interactions upon the coordination of two monodentate ligands, or a chelating ligand to a metal ion.

When a chelating ligand coordinates to a metal ion, a *chelate ring* is formed. Five and six-membered chelate rings are the most common ring sizes seen. Three and four-membered chelate rings are also known but are less stable owing to the strains present, much like in cyclic organic molecules (***Figure 10***). The properties of chelate rings have been systematically studied, and a number of excellent reviews published.[62, 63] As a general rule, ligands that can form five-membered chelate rings tend to be more selective for larger metal ions, and six-membered chelate rings are more selective for smaller metal ions, a feature which has been used in the design of chelating ligands selective for Be^{2+}.[64]

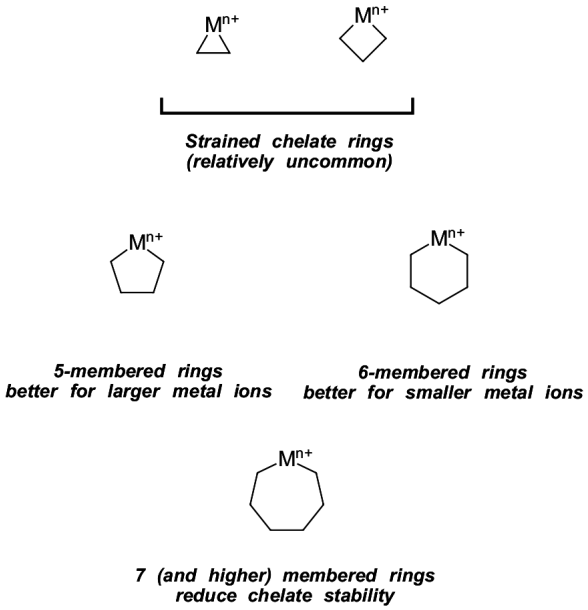

Figure 10: Some chelate ring sizes and their associated stability.

Even though the chelate effect relies upon the smaller changes in the strain of a ligand on coordination, and the increase in entropy when a ligand of high denticity displaces two or more ligands of lower denticity, as in ***Scheme 2***, there is still an entropic cost associated with the conformational restriction of a ligand upon binding to a metal ion. Preorganisation of a ligand, where the conformation of a chelating ligand is restricted, can be used used to mitigate this entropic cost, and is the reason why **CDTA** (***Figure 6***) forms more stable chelates than **EDTA**, for example. Similarly, the macrocyclic effect, where an appropriately "cyclised" chelating ligand displays much greater complex stability than an acyclic analogue is a form of preogranisation that can afford large increases in complex stability (***Figure 11***).

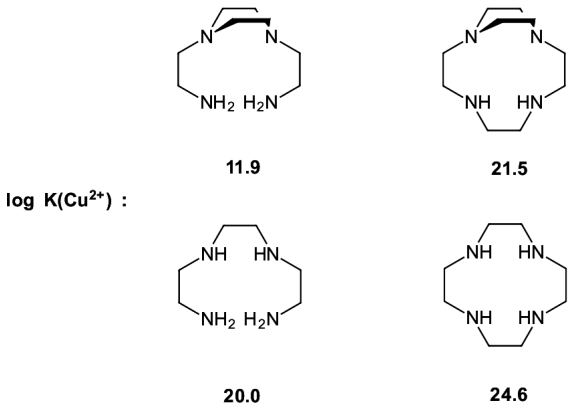

Figure 11: Equilibrium constants (for the $\frac{[ML]}{[M][L]}$ equilibrium) for open-chain and macrocyclic ligands, demonstrating the increase in complex stability due to preorganisation.

1.4.2. Selection of donor groups

The geometric and entropic contributions to chelate stability are complemented by an appropriate choice of donor atoms, matched to the metal ion(s) to be complexed. To optimise interactions between the donor atoms of a ligand and a metal ion then, orbital overlap should be maximised, an observation that was first described in the form of Hard-Soft Acid-Base theory (HSAB).

The theory states that "hard" metal ions (Lewis acids), which are small and highly charged will form more stable complexes with ligands that are also small and highly charged, or "hard" ligands (Lewis bases). Conversely, "soft" metal ions which are large, polarisable and have a low charge density, will form more stable complexes with similar ligands (***Table 3***).

Table 3: A selection of hard and soft ligands and metal ions. Data from Housecroft.[44]

Species	Hard	Soft
Ligands	F^-, Cl^-, H_2O, NH_3, RNH_2	I^-, RSH, R_2S, $[CN]^-$ (*C*-bound), RNC
Metal ions	Li^+, Mg^{2+}, Ca^{2+}, Mn^{2+}, Zn^{2+}, Fe^{3+}	Tl^+, Cu^+, Hg^{2+}, Cd^{2+}, Pd^{2+}, Pt^{2+}

The smaller orbitals found on hard metal ions and ligands, along with large HOMO-LUMO gaps on these species, lead to a reduced degree of covalency in the bonding interaction, whereas soft species have smaller HOMO-LUMO gaps. This does not necessarily lead to an increased degree of covalency in bonding, but does increase the likelihood of metal-ligand π-interactions between soft metal ions and ligands.[61]

Because many of the more abundant metal ions in biological systems are hard, a ligand designed for their successful complexation should contain hard donor groups also. An *excellent* review by Hancock and Martell[65] indicates that this would mean the incorporation of a number of oxygen and nitrogen donors. Carbonyl oxygen donors are more favourable than neutral, sp^3-hybridised oxygen donors for this purpose, because sp^3-hybridised oxygen donors impose more steric strain on the chelate rings that they are involved in, compared to carbonyl donors. This means that their use is more appropriate in ligands intended for larger metal ions, e.g. Pb^{2+}.

Charged oxygen donors are more useful still, and it has been shown that a linear relationship exists between the Lewis acidity of a metal ion (based on its affinity for hydroxide anion, OH^-) and the stability of a the chelate it forms with a ligand with anionic oxygen donors (***Figure 12***). The highly stable complex formed between catechol and Fe^{3+} is a prime example, where the hard, basic catechol ligand interacts strongly with the Lewis acidic metal ion, partially neutralising its charge.

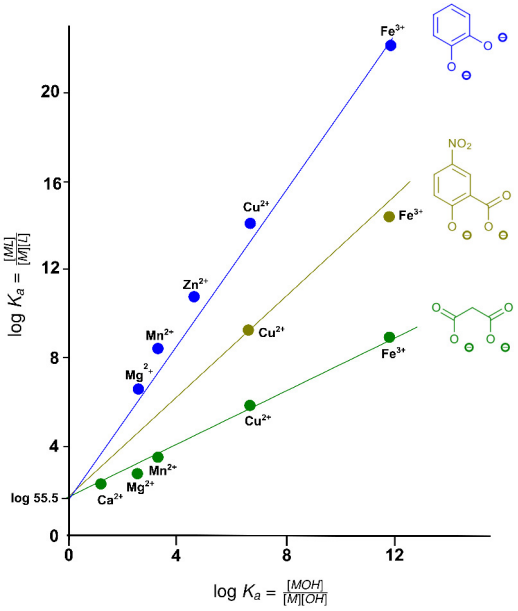

Figure 12: The relationship between the Lewis acidity of a metal ion and the affinity to ligands containing anionic oxygen donors. Data from Hancock and Martell.[65]

It is worth noting that in spite of these high metal ion affinities, the basicity of these ligands should also be taken into account. The higher the basicity, the greater the competition is at lower pH values between protons and metal ions for binding sites. For example, the effective binding strength of catechol to Fe^{3+} at pH 7 will be attenuated because of the large fraction of oxygen donors that exist

as neutral oxygen donors, as opposed to oxyanions.

A solution to this problem is the use of the carboxylate group, a charged oxygen donor that has a low basicity, meaning that it is more likely to interact with metal ions in solution over protons above a certain pH, depending on the pK_a of the conjugate acid. Furthermore, the low steric demand of the carboxylate donor group means that it is an ideal choice for interacting with a wide range of hard metal ions across a wide pH range, even though the interaction will be slightly weaker than with a more basic, charged ligand.

Although not as "hard" as anionic oxygen donors, amine donors are widely used in coordination chemistry due to their reactive lone pairs and easy functionalisation using a variety of techniques. This basicity results in a strong interaction between the orbitals of a metal ion and the ligand, giving large crystal field splitting in the case of transition metal ions, another source of stability. Of course, other donor atoms, such as phosphorus, sulphur, selenium and arsenic can be used, but due to their softness, are detrimental to the stability of complexes between a ligand and the metal ions in ***Table 1***. These atoms are better suited to complex formation with heavier, softer metal ions such as Cu^{+}, Ni^{2+}, Ag^{+} and Hg^{2+}, these all being less abundant in biological systems.

1.5. Biodegradability

The IUPAC definition[66] of biodegradability is "breakdown of a substance catalysed by enzymes *in vitro* or *in vivo*," and can be assessed in relation to the susceptibility of bulk materials like paper, cardboard and plastic, as well as their constituent compounds e.g. polymers and small molecules. The *de facto* standards for assessing biodegradability are those from the Organisation for Economic Co-operation and Development (OECD), but the United States Environmental Protection Agency (EPA) also recognises data generated from its own semi-empirical models.[67]

1.5.1. Experimental assessment of biodegradability

The procedures used to assess biodegradability vary according to the environment in which biodegradability information is sought. There are some shortfalls to these methods, even though they have been used to compile significant databases of the environmental properties of a variety of compounds. In addition, the geographical variance in microorganisms found in the sludge samples means that there will almost certainly be laboratory-to-laboratory variation in biodegradation tests undertaken, and even inoculum to inoculum. In general, the test for ready biodegradability is used, and when a substance is considered to be biodegradable, it is usually because it degrades within the 28 days for which the experiment runs.

In a typical ready biodegradability test, an inoculum from activated sludge (i.e. sewage effluent with large solids removed) is added to a defined growth medium along with the test substance,

and a parameter reflecting the metabolism of the bacteria measured, e.g. dissolved organic carbon content, carbon dioxide evolution, or the concentration of dissolved oxygen. Under these conditions, a substance is readily biodegradable if the parameter being monitored reaches a plateau within 28 days .[68] Biodegradability in seawater is measured using a very similar procedure.[69]

Even though a compound may not be readily biodegradable, it may still be susceptible to biodegradation over time. This can be tested through the use of the inherent biodegradability test, but it is not recommended that this test be applied to substances that can inhibit bacterial growth, limiting its scope somewhat. In this test, pre-conditioned activated sludge is added to a solution of test compound on a daily basis, for the duration of the test. At sampling intervals, the dissolved organic carbon content changes are measured until degradation is observed. Although the test can be run indefinitely, the authors suggest that no changes in dissolved organic carbon content within 12 weeks is taken as a lack of biodegradability.[70]

Biodegradability testing in soils is also possible, but is usually performed with a ^{14}C radiolabelled compound, with the evolution of carbon dioxide from the respiration of bacteria being measured via scintillation counter. The test is terminated after 64 days, or after 50% of the theoretical amount of labelled carbon dioxide has been evolved, whichever comes first.[71]

1.5.2. Features of biodegradable compounds

Through assembly of a large data set on the biodegradability of various compounds, Boethling and others identified molecular motifs that could be used to improve the biodegradability of small organic molecules.[72]These generalisations were deemed to be most appropriate for surfactants, plasticisers and ionic liquids because the speciation profile of these compounds tends to be relatively simple, not forming strong complexes to metal ions and exhibiting relatively few protonation states. Aminocarboxylate ligands are therefore less well covered by these generalisations, but an inspection of the structures of many biodegradable ligands illustrates incorporation of many of the motifs identified by Boethling, and it is for this reason that they are reviewed.

To prevent adsorption to solid material in wastewater, water solubility is advantageous in the design of a biodegradable compound, as is an incorporation of reactivity such that enzymatic transformations like oxidation, reduction, decarboxylation or hydrolysis of the molecule leads to products that can easily be metabolised, e.g. in **GLDA** (***Section 1.5.3***).

With regards to aromatic rings, although the role of substituent patterns are not clear, halogens and other electron-withdrawing groups are detrimental to biodegradation because they render the associated aromatic rings more resistant to oxygenase enzymes. Furthermore, nitrogen heterocycles like pyridine and pyrazine are not amenable to biodegradation for this reason. Even though the reasons are unclear, compounds containing quaternary carbons or branched alkyl chains are usually less biodegradable than those with linear alkyl chains (***Figure 13***).

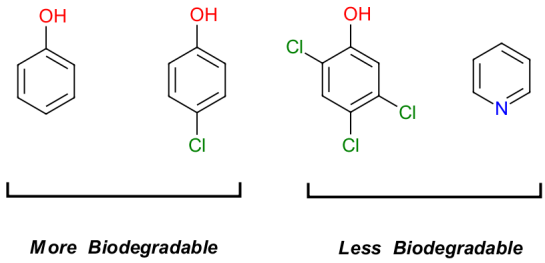

Figure 13: Biodegradability of some aromatic compounds.

The incorporation of hydrolysable groups also warrants mention, the use of esters and amides being conducive to aerobic biodegradation. Other oxygen-containing functional groups, with the exception of ether linkages, are also known to improve biodegradability. The use of esters is especially noteworthy, since esterase enzymes tend to have a wide substrate scope, and is a strategy commonly used in polymer chemistry to increase biodegradability. Tertiary amine groups, like ethers, are also known to impede biodegradation (***Figure 14***).

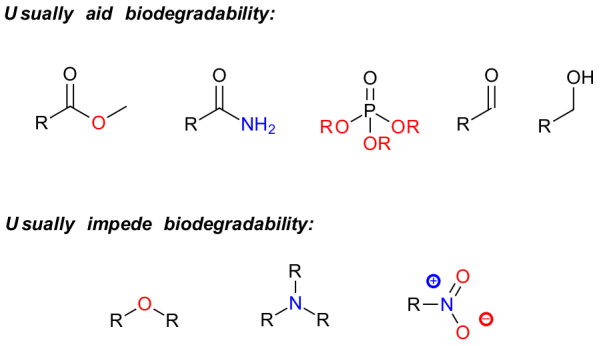

Figure 14: Functional groups and their effect on biodegradability.

1.5.3. Biodegradation of EDTA, EDDS and GLDA

In tests of the biodegradation of aminocarboxylate ligands, their speciation, in addition to their chemical structure is of crucial importance. As an example, in soil biodegradation studies on **EDTA**, it was found that the Cu^{2+}, Cd^{2+}, Fe^{3+}, Mn^{2+} and Zn^{2+} complexes of **EDTA** were more rapidly degraded than the Ni^{2+} complex.[73]

Even though **EDTA** is not readily biodegradable under typical environmental conditions, some bacterial strains and species that can metabolise **EDTA** have been isolated from activated sewage sludge. The growth of bacteria using **EDTA** as the sole carbon and nitrogen source has also been used to engineer bacteria that can degrade **EDTA**. In both cases, the enzymes responsible for **EDTA** degradation have been studied so as to understand the degradation pathway. Mixed cultures from wastewater plants that can degrade metal-**EDTA** complexes have also been identified, but the biochemistry and requirements for degradation in these cases are unclear.[74]

In work on two enzymes isolated from DSM9103,[75] it was proposed that an oxidation of **EDTA**

by monooxygenase enzymes, followed by successive decarboxylations was the primary pathway to degradation (***Scheme 4***).

Different metal **EDTA** complexes were also studied as enzyme substrates, with Mg^{2+}-**EDTA** being the most rapidly degraded by the enzyme system. The more stable the metal-**EDTA** complex was, the less rapidly it was degraded. In whole-cell investgations of the biodegradabtion of **EDTA** by DSM9103, transport experiments showed that the more stable (Zn^{2+}, Cu^{2+}, Co^{2+}, Ni^{2+} and Fe^{3+}) complexes of **EDTA** were not taken up by the bacteria, but were either demetallated or transmetallated to complexes that could be taken up into the cells, indicating the relevance of speciation for this particular organism.[76]

Two strains isolated from sewage, the *Pseudomonas sp.* LPM-410 and LPM-4, were found to be able to degrade **EDTA** and some of its metal complexes with log K_a values below ~16 (i.e. the Mg^{2+}, Ca^{2+}, Ba^{2+} and Mn^{2+} complexes of **EDTA**) in suspension, but was not able to degrade **NTA**, and the metabolic pathways and degradation products were not elucidated for these organisms.[77] Another strain, BNC1, was able to metabolise **EDTA** complexes that had a log K_a lower than ~12. The Zn^{2+} complex of **EDTA**, was an exception to this, and could be degraded in spite of its high K_a (log K_a= 16.44),[78] and was shown by Liu to degrade **EDTA** to ethylene diamine via successive decarboxylations in the same way as was observed for DSM9103 in ***Scheme 4***.[79] This pattern of bond formation and breaking has also been modelled via computational methods.[80]

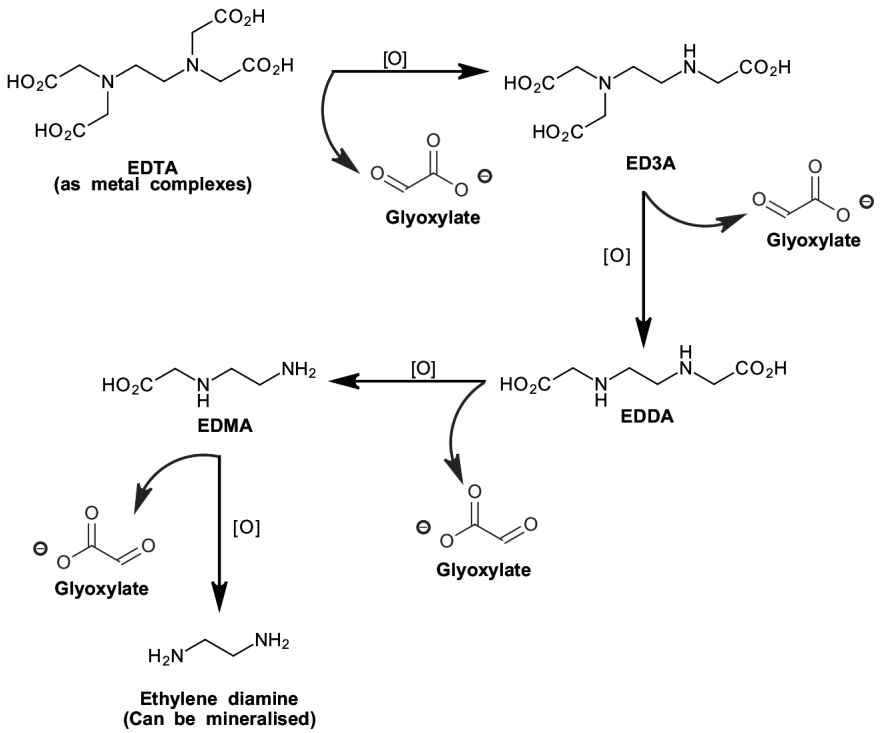

Scheme 4: Biodegradation pathway for **EDTA** proposed for bacterial strains DSM9103 and BNC1.

The stable Fe^{3+}-**EDTA** complex has been found to be degradable by other organisms such as an *E. coli* grown using the Fe^{3+}-**EDTA** complex as the sole nitrogen source. In this case, the formation of glyoxylate indicated that the degradation pathway may have been similar to that proposed for DSM9103 and BNC1.[81]An *Agrobacterium* strain that metabolised Fe^{3+}-**EDTA** but was unable to metabolise any of the deacylated products observed in the aerobic degradation processes in ***Scheme 4***, suggested that there may be alternate pathways for the degradation of Fe^{3+}-**EDTA**.[82]

Studies on the isomers of **EDDS**, showed that the S,S‘- isomer was degraded much more rapidly than the R,R‘- and R,S‘- isomers. Although this work by Schowanek used sewage sludge, precluding the identification of a single organism as being responsible for the biodegradation of **EDDS**, intermediates were proposed, showing that biodegradability was assisted when breakdown intermediates themselves could be metabolised by bacteria.[17] Another enzyme, a lyase isolated from the **EDTA** degrading strain DSM9103, allowed for elucidation of another degradation pathway for S,S‘-**EDDS**, involving an equilibrium between the ligand and fumarate (***Scheme 5***), demonstrating that deacylation may be a common reaction in the degradation of aminocarboxylate chelating agents. [83]

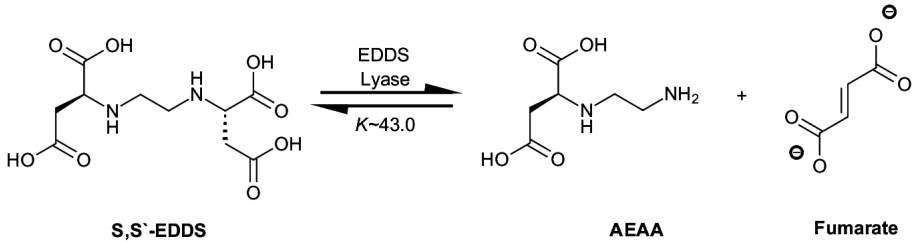

Scheme 5: The equilibrium between S,S‘-**EDDS** and the weakly complexing biodegradation products formed by DSM9103.[83]

GLDA, another aminocarboxylate, containing an asymmetric carbon, also exhibited different degradation rates for the *D*- and *L*- isomers when treated with activated sludge. Similar to the biodegradation pathways proposed for **EDTA** and **EDDS**, successive decarboxylation was proposed to be the pathway operating in the biodegradation of **GLDA** (***Scheme 6***).[84]

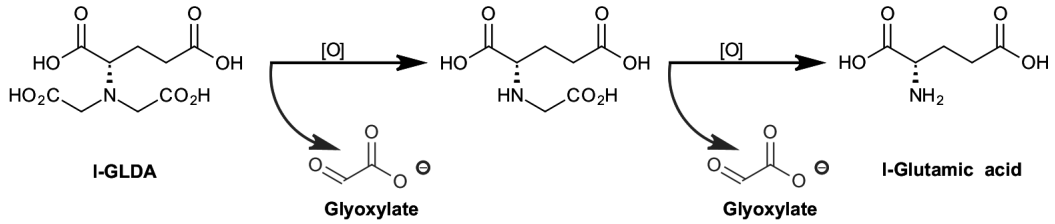

Scheme 6: The proposed biodegradation pathway for l-**GLDA**.[84]

When comparing **EDTA** and **EDDS** structurally, the differences in chelate strength arising from the differences in chelate ring sizes formed, as well as the substitution pattern at the ethylene diamine nitrogen atoms, were likely to be a major factor in their biodegradability. The work of Pitter and Sýkora elucidated how the structure and symmetry of ethylene diamine based units may affect the

biodegradability of the ligands they are incorporated into (***Table 4***).[85, 86]

Table 4: The effect of ethylene diamine functionalisation on biodegradation in activated sludge after 5 days.[85]

Structure	Extent of biodegradation / %
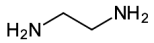	98
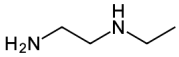	95
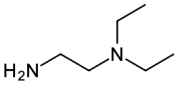	90
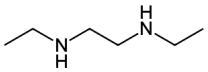	10
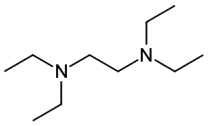	5

From the above data, it is apparent that the degree of amine substitution, as work discussed earlier suggests, affects biodegradability alongside the symmetry of the ethylene diamine fragment.

Overall, it would seem that the design of a chelating ligand that could form strong metal-ligand complexes but was also biodegradable could not necessarily be achieved by the incorporation of biodegradable features (***Section 1.5.2***) alone, but the incorporation of such features was *more likely* to render any synthesised ligand more biodegradable.

1.6. Perspective and aims of the work

From this survey of the literature presented, it is apparent that:

1. Despite being inexpensive to synthesise and its widespread usage, the low biodegradability of **EDTA** in typical wastewater streams may be an environmental problem, due to the changes in metal ion speciation it can induce. In addition, it may perturb the nitrogen and microbial economies of the bodies of water in which it is present.

2. Current readily biodegradable chelating ligands are not well-suited to replace **EDTA** for use within the pH range of 4-7.

3. A common use of **EDTA** in preservation systems is to enhance the activity of an active antimicrobial agent through disruption of the Gram-negative bacterial membrane. This damage is achieved through the sequestration of Ca^{2+} and Mg^{2+} ions from the LPS layer. For some species of Gram-negative bacteria, this damage can be lethal without an additional agent.

4. Although not thoroughly investigated, it is almost certain that **EDTA** and other chelating ligands exert antibacterial action through starving bacteria of essential metal ions, which are vital to proper cellular function. The most abundant metal ions in living organisms are Ca^{2+}, Mg^{2+} ,Zn^{2+} and the first row transition metals. Therefore, if a ligand is to be designed to disrupt normal bacterial cell function, it should form highly stable complexes with these ions.

5. The chelate and macrocyclic effects may be used to enhance ligand binding to these metal ions, alongside the use of hard donor groups, like amines, and anionic oxygen donors, taking into account their steric demand.

6. Generalisations for the structures of biodegradable organic molecules are known, but many of these do not apply to chelating ligands, for which the speciation of the ligand in test environments must also be considered.

7. For ligands known to be readily biodegradable such as **GLDA**, or **EDDS**, some features that are conducive to the biodegradability of small organic molecules are present, implying that the incorporation of molecular fragments known to enhance the biodegradability of non-chelating organic materials, into chelating ligands, is not without advantage.

With these points in mind, the primary aim of this work was to prepare a variety of ligands of different types, and evaluate their activity against Gram-negative bacteria in liquid media as a preliminary indicator of their performance. In spite of other metrics of ligand efficacy being available, this was chosen because it was likely to be both a factor of metal chelation and an industrially relevant parameter- **EDTA** being very frequently used in consumer care formulations to potentiate added preservative systems, as well as acting as a growth inhibitor in its own right. In doing so, it could be possible that strategies towards antibacterial ligand design may be uncovered, especially through a critical assessment of the thermodynamic characteristics of the ligands studied.

Accordingly, the following results and discussion describes different approaches to this problem. ***Chapter 2*** introduces the reader to some of the specialised techniques and the associated optimisation work needed to study the ligands in this thesis, as well as giving an overview of how the data used to construct this thesis has been interpreted. ***Chapter 3*** describes the synthesis of amides of **EDTA**, which incorporate hydrolysable amide linkages as a way to increase the rate of ligand metabolism in activated sludge, as well as using the amide groups to attach a variety of pendant groups that may affect *E. coli* growth inhbition. ***Chapter 4*** describes the synthesis of ligands bearing electron-rich aromatics in the form of phenol groups, and the effect of their extremely high Fe^{3+} affinities on the growth of *E. coli*.

Work described in ***Chapter 5*** aims to elucidate the properties of potent bacterial growth-inhibiting ligands in the hope of establishing design principles for use in future work. This is accomplished through a screening of a variety of aminocarboxylate ligands, and correlating their metal ion binding

constants to the inhibition characteristics observed, to see if any structural features can be tuned to optimise bacterial growth inhibition. Finally, ***Chapter 6*** describes synthetic efforts towards novel ligand systems incorporating biodegradable motifs, using observations in the preceding chapters to inform ligand design.

2. An introduction to specialised techniques used in this work

2.1. Choices of strain, buffer and media

Strain. An *E. coli* K-12 strain (JM101) was used as the model Gram-negative organism throughout this study. The K-12 strain is non-pathogenic and so can be handled without special precautions such as a microbiological safety cabinet, is readily available, and has a rapid doubling time enabling screening to be quickly and efficiently performed, meaning it is very widely used in microbiological research.[87] Despite its lack of *O*-antigen in typical culture conditions,[88] it retains the elements of lipopolysaccharide that act as a barrier to molecular entry and may be expected to display similar membrane character to other *E. coli* strains.

Media and buffers. Tryptone Soya Broth (TSB) was used for all growth inhibition studies because of its approval for sterility testing according to British Pharmacopoeia and Food and Drug Administration (FDA) standards. In contrast to Luria-Bertani (LB) medium, which is often used to study the effect of compounds against *E. coli*,[40, 89–92] TSB is buffered.[93] Consequently, if LB were used as the study medium, pH fluctuations could be expected to affect bacterial growth (***Section 2.3***) in addition to the test ligands.

In spite of the innate buffering capacity of TSB, introduction of an auxiliary buffer was necessary to stop the precipitation of many of the ligands. Dipotassium hydrogen phosphate (K_2HPO_4, M=174.18 g mol^{-1}) was chosen for this purpose. Because the presence of a test ligand would reduce solution pH, addition of a separate acidic component to the buffer was unnecessary. Depending on the type of ligand, different concentrations of dipotassium hydrogen phosphate were used in the buffers. For amides of **EDTA** and other aminocarboxylates (***Chapter 5***), 0.2 M K_2HPO_4 was used, since it gave a K_2HPO_4 concentration close to that of neat TSB upon dilution into the media prior to assay. Phenolate ligands required a concentration of 0.4M K_2HPO_4; their reduced solubility meant that higher pH values were necessary for dissolution.

2.2. Quantitative ^{1}H NMR (qHNMR) studies

The purification and storage of many of the ligand systems considered was complicated by their high hygroscopicity.[94–97] This hygroscopicity and, in some cases, alkali metal or acid salt formation would preclude the accurate preparation of stock solutions for many of the synthesised ligands for biological testing if a sample of solid ligand material were to be weighed into a vessel prior to dissolution. Even though corrections for the extent of hydration or salt formation could be attempted through the use of conventional combustion (CHN) analyses, reformulating the elemental composition would introduce a level of arbitrariness into interpreting the data.

For these reasons, an alternative method of determining stock solution concentration was sought. An optimal method would be one that is appropriate for all the compounds under study (not just those with a certain "label," e.g. ^{19}F environments or aromatic rings), capable of detecting organic impurities e.g. residual starting material and directly usable on the solution of a compound to be evaluated, in that solution concentration was *determined* and not estimated. Quantitative ^{1}H NMR satisfied all of these conditions and so was chosen for adaptation to the experimental set-up described in ***Section 8.7***.

2.2.1. Choice of experimental conditions

Although the work of Cullen[98] suggested that use of either internal or external referencing* methods would give similar accuracy and precision, an internally referenced method of determining concentration was chosen due to the relative ease of optimisation and insensitivity to probe tuning.[99] Briefly, this method requires addition of a known amount of material (an internal standard) to the NMR sample. The additional signal(s) from the standard may then be integrated against signals of the analyte to determine the analyte concentration.

An ideal internal standard should be non-hygroscopic, have a simple ^{1}H NMR spectrum that does not overlap with analyte signals, but is near the region of interest.[100] Furthermore, it is imperative that the nuclei of both analyte and standard are as close to being fully relaxed as possible. This is ensured by using a relaxation delay that is $\geqslant 5T_1$ (the spin-lattice relaxation time) of the signals of interest. Disodium succinate and t-butanol (***Figure 15***), were selected as candidate internal standards due to their low hygroscopicity[101] and use in previous quantitative ^{1}H NMR studies respectively.[102]

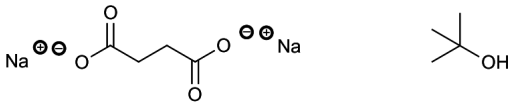

Disodium succinate **t-Butanol**

Figure 15: Compounds considered for use as ^{1}H NMR internal standards.

Measurement of the T_1values of these candidates in the presence or absence of dipotassium hydrogen phosphate was then undertaken as an assessment of how salt concentrations affected T_1 (***Table 5***), as well as providing a preliminary value for a sufficient relaxation delay time (***Table 5***).

*An internal reference is dissolved into the sample solution, whereas an external reference method relies on comparison of an analyte spectrum to calibration spectra.

Table 5: T_1 values obtained for disodium succinate and t-butanol via inversion recovery experiments under different conditions.

Entry	Internal standard[i]	Buffer	T_1 / s[ii]
1	^{t}BuOH	None (D_2O only)	2.29(3)[iii]
2	^{t}BuOH	100 mM K_2HPO_4 in D_2O	1.25(2)
3	Disodium succinate	None	2.50(2)
4	Disodium succinate	100 mM K_2HPO_4 in D_2O	2.50(4)

i) Concentration =50 mM in tube. **ii**) Ambient temperature. No attempt was made to deoxygenate the samples. Measurements taken on a Varian M400 NMR spectrometer operating at a proton resonance frequency of 400MHz. **iii**) Number in brackets corresponds to the plus-minus error of the last decimal place for the calculated value.

From these data, it is apparent that the presence of dipotassium hydrogen phosphate had no effect on T_1 for disodium succinate, and a decreased T_1 for t-butanol was observed when measured in the presence of the salt. Therefore, for quantitiative relaxation of either standard, a relaxation delay of at least 12.5 s was necessary.

Owing to structural similarities between **EDTA** and many of the other ligand systems used in this work, the T_1 values for the ethylenediamine or acyl protons of EDTA (H_a and H_b respectively, ***Table 6***), in the presence of both t-butanol and disodium succinate were then measured. The resulting data were used to determine whether elongation of this preliminary value of 12.5 s was necessary, i.e. if there were any proton environments that exhibited a T_1 > 2.5 s (***Table 6***).

Table 6: T_1 values obtained for the marked protons of EDTA in deuterated and partially non-deuterated solvent.

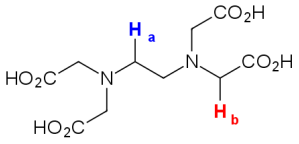

Entry	Internal standard[i]	[EDTA] / mM	Buffer[ii]	T_1[iii] (Standard) / s	T_1 (H_a) / s	T_1 (H_b) / s
1	^{t}BuOH	6.25	**A**	2.42(3)[iv]	0.438(4)	0.592(3)
2	^{t}BuOH	6.25	**B**	2.30(3)	0.336(3)	0.491(5)
3	Disodium succinate	6.25	**A**	2.55(4)	0.439(2)	0.588(1)
4	Disodium succinate	6.25	**B**	2.55(1)	0.342(2)	0.485(3)

i) Concentration= 50 mM in tube. **ii**) Buffer system **A**= 100 mM K_2HPO_4 in 50:50 (v/v) H_2O/D_2O; **B**= 100 mM K_2HPO_4 in D_2O. Samples containing H_2O were measured on a Varian VNMRS-600 NMR spectrometer operating at a proton resonance frequency of 600 MHz. The ROBUST5 pulse sequence was used to suppress the large water signal in these samples. **iii**) Ambient temperature. No attempt was made to deoxygenate the samples. **iv**) Number in brackets corresponds to the plus-minus error of the last decimal place for the calculated value.

The low T_1 values measured for both $\mathbf{H_a}$ and $\mathbf{H_b}$ under the experimental conditions clearly indicated that, in every case, the longest relaxation time was that of the standard. So, using a relaxation delay time suitable for the standard would also allow sufficient time for the quantitative relaxation of the relevant proton environments. The fact that these corresponded to ethylene and acyl fragments was especially useful, since these motifs were present in almost all of the ligands studied in this work. Because of this, their relaxation behaviour under these conditions could be expected to be similar to that of **EDTA** and exhibit similarly quantitative relaxation.

Based on the above data, t-butanol was selected as the internal standard, based on its slightly lower T_1 compared to disodium succinate, and its availability in a pure, anhydrous form, packaged under inert gas.* Elemental analysis results obtained for dehydrated disodium succinate also showed inconsistency across samples. Hence, any material used for standard solutions of disodium succinate would require repeated determination via elemental analysis, an impractical and time-consuming process.

The overall relaxation delay for the ^{1}H NMR experiment was set to 14 s, since this allowed for quantitative ($\geq 5T_1$) relaxation of the t-butanol standard and for any anomalously long relaxation times for either analyte or standard nuclei across a range of samples. Since the stock solutions to be quantified were in aqueous (non-deuterated) buffer, water supression was necessary†, the ROBUST5[103] pulse sequence being selected for this purpose. Once qHNMR spectra for the ligands of interest were acquired, the ligand peaks could be integrated against the t-butanol peak (set to 9H) and the ligand concentration (c_l) determined from ***Equation 5***, which is derived below:
The concentration ratio of t-butanol and the ligand is defined as:

$$\frac{c_l}{c_t} = \frac{(\frac{A_l}{n_l})}{(\frac{A_t}{n_t})} = (\frac{A_l}{n_l})(\frac{A_t}{n_t})^{-1} = \frac{A_l n_t}{n_l A_t} \tag{3}$$

c_l and c_t are the molar concentration of the analyte ligand and t-butanol, A_l and A_t are the integral values for the analyte peak of interest and t-butanol, n_l and n_t represent the number of protons in the environments from which A_l and A_t are measured in the ligand and t-butanol respectively.
When the t-butanol peak is set to 9H, then $A_t = n_t$ and ***Equation 3*** simplifies to:

$$\frac{c_l}{c_t} = \frac{A_l}{n_l} \tag{4}$$

Since c_t is known from the preparation of the standard solution of t-butanol in D_2O, rearranging for c_l leads to ***Equation 5***.

$$c_l = c_t(\frac{A_l}{n_l}) \tag{5}$$

*Sigma-Aldrich product number: 471712-100ML .

†The author thanks Dr. J. A. Aguilar for his assistance in acquiring T_1 values with application of the W5 pulse sequence and for the implementation of this quantitative method to an automated NMR spectrometer.

2.2.2. Relation to molecular weights obtained by combustion analysis

To test the devised qHNMR protocol more thoroughly, a direct comparison of the calculated molecular weights of some ligand samples obtained from CHN analyses and qHNMR was undertaken (***Table 7***). It was hoped that the reported molecular weight from either method would indicate the same or similar extent of hydrate and/or salt formation. With respect to combustion (CHN) analysis, a corrected molecular weight could be calculated by adjusting the expected molecular formula to fit the found empirical formula using a tool such as JASPER[104](the procedure for this is given in ***Appendix D***). A molecular weight for a given ligand could be obtained from qHNMR experiments by accurately weighing a given sample, and using the measured concentration c_l in a known sample volume v. Since c_l is known and $n = \frac{m}{M_r}$ (where n is the number of moles of the ligand, m is the sample mass (in g) and M_r is the molecular weight), ***Equation 6*** can be used.

$$M_r = \frac{m}{c_l v} = \frac{n_l m}{c_t A_l v} \tag{6}$$

The agreement between CHN and qHNMR molecular weights is generally very good (***Table 7***), demonstrating that the method was an acceptable substitute for the correction of molecular weights as well as for the quantification of stock solutions. It is on this basis that qHNMR was used as the primary method for ligand solution quantification throughout this work. Large discrepancies between the molecular weights predicted from the structures of the test ligands and those calculated from either CHN or qHNMR also served to emphasise the previously described shortcomings of relying on sample masses exclusively for solution concentration values.

Table 7: A comparison of the corrected molecular weights obtained from CHN and qHNMR methods.

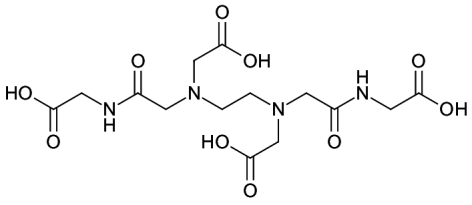

AmGly$_2$

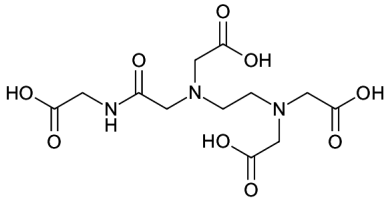

AmGly$_1$

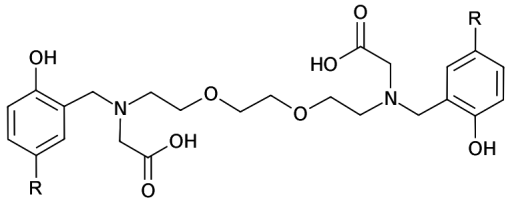

R=H, NOON
R=Br, Br-NOON

Compound	M_r / **g mol^{-1} (from structure)**	M_r / **g mol^{-1} (CHN)[i]**	M_r / **g mol^{-1} (qHNMR)[i]**	M_r **Ratio / No Units (CHN:qHNMR)**
AmGly$_1$	349	449	457	0.98
AmGly$_2$	406	424	422	1.0
H-NOON	477	580	581	1.0
Br-NOON	634	735	845	0.87

i) All samples were allowed to hydrate by keeping their open vials on the bench overnight prior to submission for analysis.

2.3. Optical density-mediated monitoring of bacterial cell growth

Once the concentration of a stock ligand solution had been determined, studies of the effects of the compounds described in this work on model bacterial species could be undertaken, using the culture conditions described earlier (***Section 2.1***). Optical density (OD) based methods were ideal because growth may be monitored continuously under highly automated conditions using a microplate reader, with which many experiments (variation of ligand concentration, species etc.) can be conducted in parallel. The basis of the method is that as a bacterial culture progresses through the various stages of growth, the number of cells in the culture will increase. If cellular aggregation is prevented via periodic shaking, a linear relationship exists between the number of live cells in suspension and the optical density at a certain wavelength, and so monitoring OD allows the for estimation of cell number after a suitable calibration procedure. Death phase cannot be followed using optical density measurements because reductions in the number of live cells are not usually accompanied by an OD reduction.

Plotting the OD of a culture as a function of time generates its *growth curve*, from which numerous parameters may be extrapolated such as: the doubling time, duration of the lag and log phases, and most importantly for the purposes of this work, the optical density once stationary phase is reached (***Figure 16***).

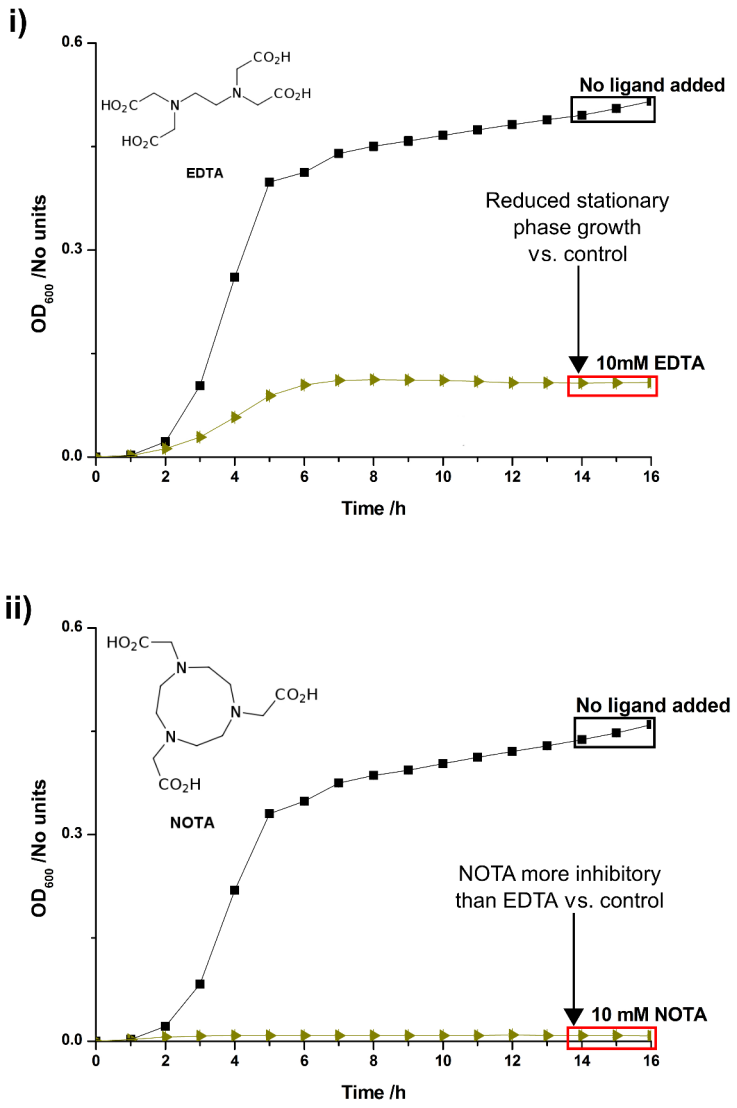

Figure 16: Representative *E. coli* JM101 growth curve experiments for **i) EDTA** and **ii) NOTA**, showing how differences in stationary phase bacterial populations can be observed via OD measurements at 600nm (OD_{600}). Values are the mean of three technical repeats. Error bars have been plotted (1σ), but their magnitude in these particular experiments renders them invisible.

Because of the linear response described previously, differences in stationary phase optical densities reflect the effect on growth that different ligands have. Comparison of the stationary phase OD thus allowed for a comparison of the bacterial inhibition effects of one ligand against another (***Figure 16, i*** and ***ii***).

Data obtained from a growth curve could be used to construct dose response curves, where stationary phase growth is expressed as a function of concentration. To enable comparison between experiments, stationary phase growth was expressed as a percentage (of the culture OD reached for untreated bacteria) and calculated in the following way: the final three data points from the positive control for a particular growth experiment (***Figure 16*** , curves **i)** and **ii)**, black rectangles) were averaged, as were those for a particular concentration (***Figure 16*** , curves **i)** and **ii)**, red rectangles). The average OD value for bacteria grown in the presence of a ligand was then divided by the average OD for the positive control to give the percentage extent of stationary phase growth, i.e. a value of 100% was equivalent to bacterial growth in buffer exclusively. Advantages of this approach were that the error in the growth relative to control could be estimated through error propagation expressions,[105] and fluctuations in the end-stage optical density could be averaged out. All growth curve experiments included **EDTA** as an "internal standard" against which experiment-to-experiment variation could be evaluated. An example plot and comparison is shown in ***Figure 17***.

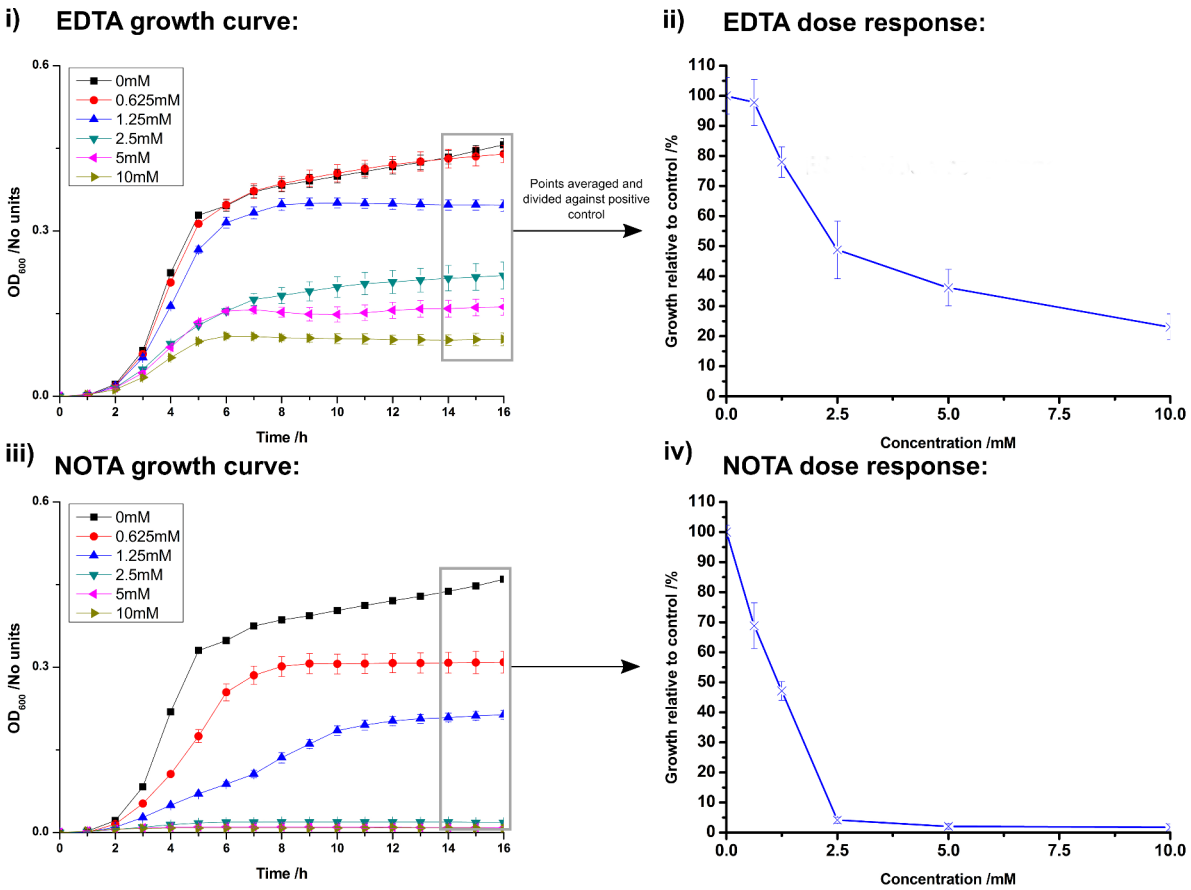

Figure 17: Typical dose response curves calculated from growth curves such as **i)** and **iii)**. Comparison of curves **ii)** and **iv)** demonstrate that **NOTA** inhibits bacterial growth to a a greater extent than **EDTA**, even at concentrations as low as 0.625 mM of ligand. Error bars for **ii)** and **iv)** represent two standard deviations of the mean, propagated from the standard deviation values of the relevant concentrations.

A standard design for the growth curve experiment in 96-well plates was chosen, using in-well concentrations of 10, 5, 2, 1.25, 0.625 and 0 mM (the positive control for unimpeded bacterial growth) in technical triplicate. The upper limit of 10 mM was selected due to the fact that commercial skincare formulations rarely exceed a ligand concentration of 5 mM, adjusting for molecular mass.

2.4. Analysis of cellular metal content via ICP-MS

Inductively coupled mass spectrometry (ICP-MS) is a versatile analytical technique used for the quantification of a variety of elements at low (parts per billion) concentrations. First commercialised in the 1980's, it has recently been adopted for studies on the metal content of biological systems. Coupled with other techniques, like laser ablation, the metal content of solid samples, e.g. bacteria in abscesses within organs, may also be interrogated.[106] Measurements of residual metal concentrations in media after treatment with a given agent are also possible.[56, 57]

To measure bacterial metal content, a large scale culture is grown, and the cells harvested at a certain point via centrifugation. After a washing procedure to remove residual media, the cells are digested in nitric acid to prepare a homogeneous solution and then diluted into a suitable matrix for analysis. Metal concentrations can then be determined in relation to a standard curve, which is prepared from accurate metal stock solutions for the metals of interest, using the same matrix as for the cells, and so is the approach adopted in this work.

There appear to be some differences in approaches to bacterial harvesting in the literature. One view is that cells should be harvested at mid-log phase, where the cells are most actively growing, and that their growth is synchronised, which has been used in interrogations of metal regulation systems in bacteria. This is because all of the cells in the culture will exhibit the same response to a perturbation in metal content.[107] Sampling a culture as a function of time has also been utilised to study the relationship between metal uptake and growth stages,[108] and to monitor increases in cellular Ag^{+} content in work on use of the ion as an antimicrobial.[109] Stationary phase sampling has also been used to monitor the effect of severe Zn^{2+} depletion in media on *E. coli* growth.[110] In this work, stationary phase sampling was employed to give an accurate reflection of the metal content of the *E. coli* culture and the associated dose response for a given ligand concentration.

Attempts were made to keep the ligand concentration to effect around 90% growth relative to control, because more inhibitory concentrations were likely to lead to changes in cellular metal content arising from mechanical factors arising from membrane damage.[39] As a consequence, fairly low ligand concentrations were necessary, leading to variability (up to 20%) in the growth relative to control. Therefore, it is advisable to consider these data as illustrative of the effect of a given ligand concentration on cellular metal content irrespective of dose, and not the effect of a set inhibitory dose of a ligand on cellular metal content.

2.5. Fluorescence competition using Fura-2

2.5.1. General background

As a rapid way to assess the affinities of the synthesised ligand systems for Ca^{2+} and Zn^{2+}, when classical potentiometric techniques were not available, competition experiments[111, 112] using the fluorescent probe **Fura-2** were performed (***Figure 18***).

First prepared by Tsien, this probe is designed to selectively bind Ca^{2+} over Mg^{2+}, a feature arising from its hard, octadentate donor set. On complexation of Ca^{2+} to **Fura-2**, there is a small hypsochromic shift of the emission maximum from 518 nm to 510 nm along with an increase in emission intensity. It was this increase in the emission intensity that was used to monitor the concentration of Ca^{2+} after calibration.

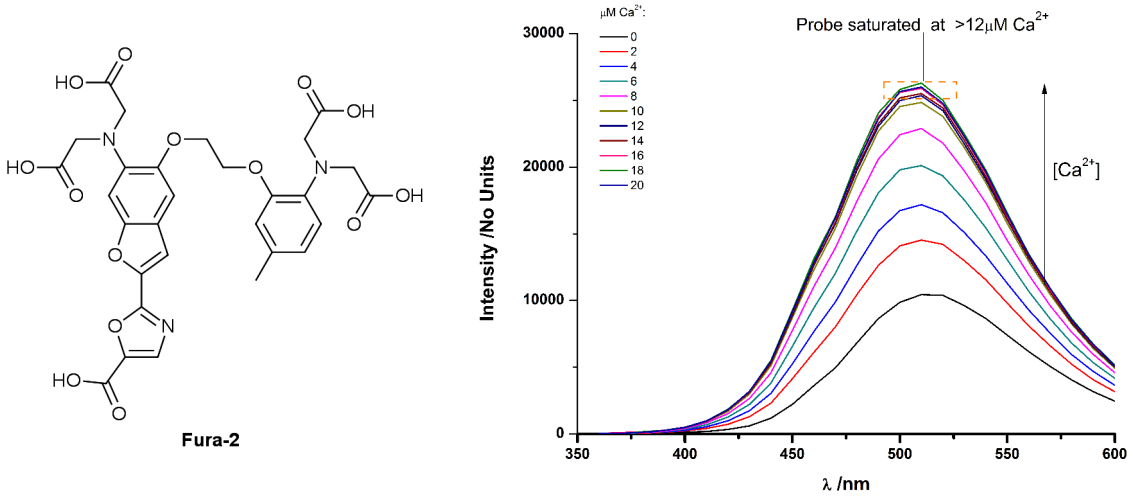

Figure 18: Example of the Increasing emission intensity of **Fura-2** in response to added Ca^{2+} as a result of complex formation. Measurements were performed in 96-well plates using 10mM HEPES (pH 7), 100mM KCl as the medium. The in-well concentration of **Fura-2** was 12.25μM, λ_{ex}=340 nm and T=26$\pm$0.5°C. Spectra are the average of three independently prepared wells using the same stock solutions.

The probe was selected on account of its Ca^{2+} affinity (log K_a $\approx$7 at 22°C) and Zn^{2+}affinity (log K_a $\approx$8.5 at 22°C),[113] meaning that it possessed Ca^{2+} and Zn^{2+} binding strengths that were close enough (usually to within four log units) to a number of other known aminocarboxylate ligands. The absence of fluorophores in the ligands prepared and studied in this work meant that the choice of reporter ligand was unconstrained.

The basis of this particular competition experiment is that pre-formed metal complexes of a given ligand of interest L^1 can be demetallated via the addition of a known concentration of another, different ligand L^2, resulting in a perturbation of the initial equilibrium between a metal ion M, and L^1. The resulting reaction can be expressed as per ***Equation 7***.

$$ML^1 + L^2 \overset{K_1}{\rightleftharpoons} ML^2 + L^1 \tag{7}$$

and so the equilibrium constant K_1, for this reaction is defined as:

$$K_1 = \frac{[ML^2][L^1]}{[ML^1][L^2]} \tag{8}$$

Even though the comparison of K_1 values from ligand to ligand in this experimental regime will give information on the influence of structure on metal affinity, a more useful constant would be that describing the complexation of L^1 to "free" metal (***Equations 9*** and ***10***), which can then be used to calculate speciation in more complex systems at a certain pH once the other relevant equilibria are known.

$$L^1 + M \overset{K_{a_{cond}}}{\rightleftharpoons} ML^1 \tag{9}$$

$$K_{a_{cond}} = \frac{[ML^1]}{[L^1][M]} \tag{10}$$

Provided the value of the equilibrium constant for the equilibrium between M and L^2 is known, i.e:

$$M + L^2 \overset{K_2}{\rightleftharpoons} ML^2$$

and so:

$$K_2 = \frac{[ML^2]}{[M][L^2]} \tag{11}$$

then ***Equation 11*** can be substituted into ***Equation 8*** to yield the conditional value for K_a, $K_{a_{cond}}$:

$$K_1 = \frac{[ML^2][L^1]}{[ML^1][L^2]}$$

$$\frac{1}{K_2} = \frac{[M][L^2]}{[ML^2]}$$

$$\frac{K_1}{K_2} = \frac{[L^1][M]}{[ML^1]} = \frac{1}{K_{a_{cond}}} \therefore$$

$$K_{a_{cond}} = \frac{[ML^1]}{[L^1][M]}$$

Because $K_{a_{cond}}$ values correspond to metal affinity at a certain pH, ligand pK_a values are needed to calculate absolute K_a values (***Equations 12 and 13***).[114]

$$K_{a_{cond}} = K_a\alpha = \frac{\alpha[ML^1]}{[L^1][M]} \tag{12}$$

$$\alpha = (1 + \beta_{H,1}[H] + \beta_{H,2}[H]^2 + \beta_{H,3}[H]^3 \ldots \beta_{H,n}[H]^n)^{-1} \tag{13}$$

A worked example follows:

If the $K_{a_{cond}}$ at pH 7.4 for the equilibrium between **EDTA** and its Zn^{2+} complex is desired, then the Schwarzenbach α-coefficient must first be calculated.

The pK_a values for **EDTA** are:

pKa_1= 10.17, so $K_{a_1}^{-1} = 10^{10.17} = \beta_{H,1}$

pKa_2= 6.11 so $K_{a_1}^{-1} = 10^{6.11} = \beta_{H,2}$

pKa_3= 2.68 so $K_{a_1}^{-1} = 10^{2.68} = \beta_{H,3}$

pKa_4= 2.00 so $K_{a_1}^{-1} = 10^{2.00} = \beta_{H,4}$

pKa_5= 1.50 so $K_{a_1}^{-1} = 10^{1.50} = \beta_{H,5}$

Since $pH = -log[H^+]$ then $[H^+] = 10^{-7.4}$, and so by substition into ***Equation 13***

$$\alpha = (1 + 10^{10.17}(10^{-7.4}) + 10^{6.11}(10^{-7.4})^2 + 10^{2.68}(10^{-7.4})^3 + 10^{2.00}(10^{-7.4})^4 + 10^{1.50}(10^{-7.4})^5)^{-1}$$

$$\alpha = (1 + 10^{2.77} + 10^{-8.69} + 10^{-19.52} + 10^{-27.6} + 10^{-35.5})^{-1}$$

$$\alpha = 0.0016$$

The log K_a value for the $\frac{[ML]}{[M][L]}$ equilibrium (M =Zn^{2+} and L = **EDTA**) is 16.44 so,

$$K_a = 10^{16.44}$$

From ***Equation 12,***

$$K_{a_{cond}} = \frac{\alpha[ML]}{[M][L]} = 0.0016 \times 10^{16.44} = 4.41 \times 10^{13}$$

Hence:

$$\log K_{a_{cond}} = 13.65$$

There is an extensive literature on association constants expressed as K_a as opposed to $K_{a_{cond}}$, allowing for much broader comparison of experimental and literature values, a deeper understanding of how structure affects sequestration ability.

Although equilibrium constants (K_2 in the above derivation) for M=Ca^{2+}, Zn^{2+} and L^2=**Fura-2** have been published for a variety of conditions (temperatures, ionic strengths etc.), no values have been determined for the conditions utilised in this work. Fortunately, the self-indicating nature of any ligand with a suitable reporter means that calibration of the response is a relatively simple process. Kits to correlate the amount of free Ca^{2+} in solution to emission intensity, from which an appropriate value of K_2 can be calculated, are commercially available and their constituents have been published.[113] Solutions to correlate free Zn^{2+} concentrations in solution to emission intensity can be made in an analogous way.

Even though $K_{a_{cond}}$ and K_a values could thus be obtained by titration of a known concentration of ligand against **Fura-2** to find equivalence points, a quicker way of estimating metal affinity was through the use of a single concentration of ligand, L^1. If a ligand that strongly bound Ca^{2+} or Zn^{2+} was used, the fluorescence of the relevant metal complex of **Fura-2** (also referred to as **Ca-Fura-2** or **Zn-Fura-2**) generated in situ would be quenched to a greater degree than when competed with a ligand that weakly bound Ca^{2+} or Zn^{2+} , all other things being equal. Since calibration essentially quantifies the amount of **Ca-Fura-2** or **Zn-Fura-2** , K_1 values can be calculated (***Equation 8***), provided an appropriate loading of Ca^{2+} or Zn^{2+} is used to keep emission in the linear range (***Figure 19***).

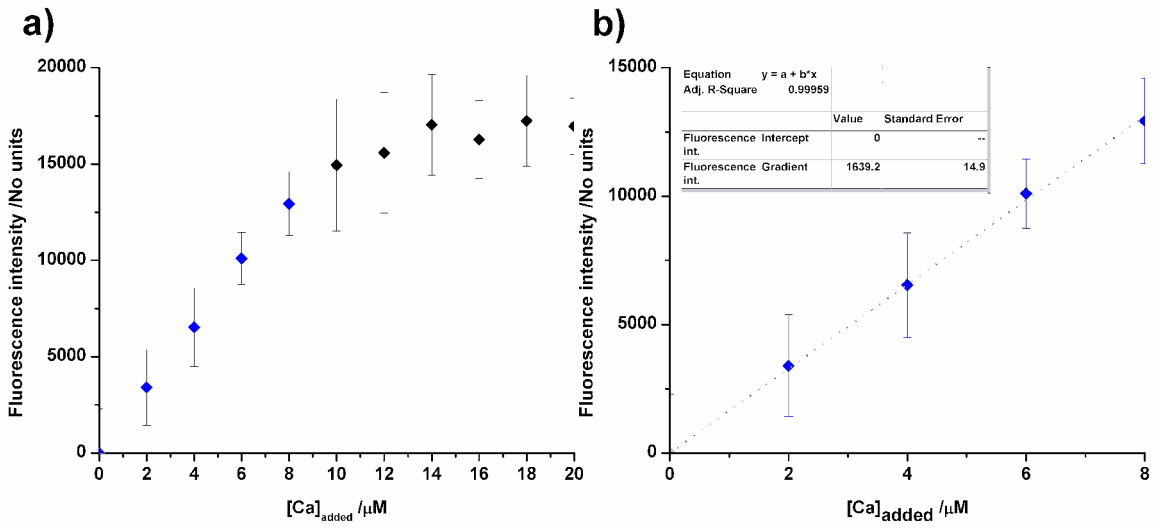

Figure 19: Calibration of the corrected **Fura-2** emission intensity as a function of Ca^{2+} loading. At substoichiometric loadings of Ca^{2+} (blue points on graph **a**) , a linear relationship between the in-well concentration of Ca^{2+} and emission intensity exists after subtraction of the emission spectrum of free **Fura-2**. Saturation occurrs when all of the free **Fura-2** is bound at higher Ca^{2+} loadings (black points). Applying a linear fit to the linear part of the curve (graph **b**), gives the relation from which the effect of incoming ligands on the concentration of **Ca-Fura-2** can be quantified. Error bars represent two standard deviations from the mean of three replicates. λ_{ex} =340 nm, λ_{em}=510 nm. [**Fura-2**]=12.25μM. Buffer: 10mM HEPES/100mM KCl at pH 7, T=26$\pm$1°C.

In this example, once the optimal Ca^{2+} loading was selected (for ***Figure 19***, [Ca^{2+}] added=8 μM), solutions of this concentration of **Ca-Fura-2** were prepared in a multiwell plate and a 10μM solution of a competing ligand added into the wells. The fluorescence at 510 nm could then be measured and used to calculate the amount of **Ca-Fura-2** remaining in the presence of a competing ligand. Once calculated, graphs reflecting the relative affinity of ligands in a given experiment could be plotted (***Figure 20***). From the observed quenching, orderings of ligand affinity for Ca^{2+} are determined. In this case, the order is **DOTA**>**EGTA**>**DTPA**>**NOTA**. For studies on Zn^{2+}, the process is essentially the same, except the monitored emission wavelength is not always 510 nm, and is reported in each case.

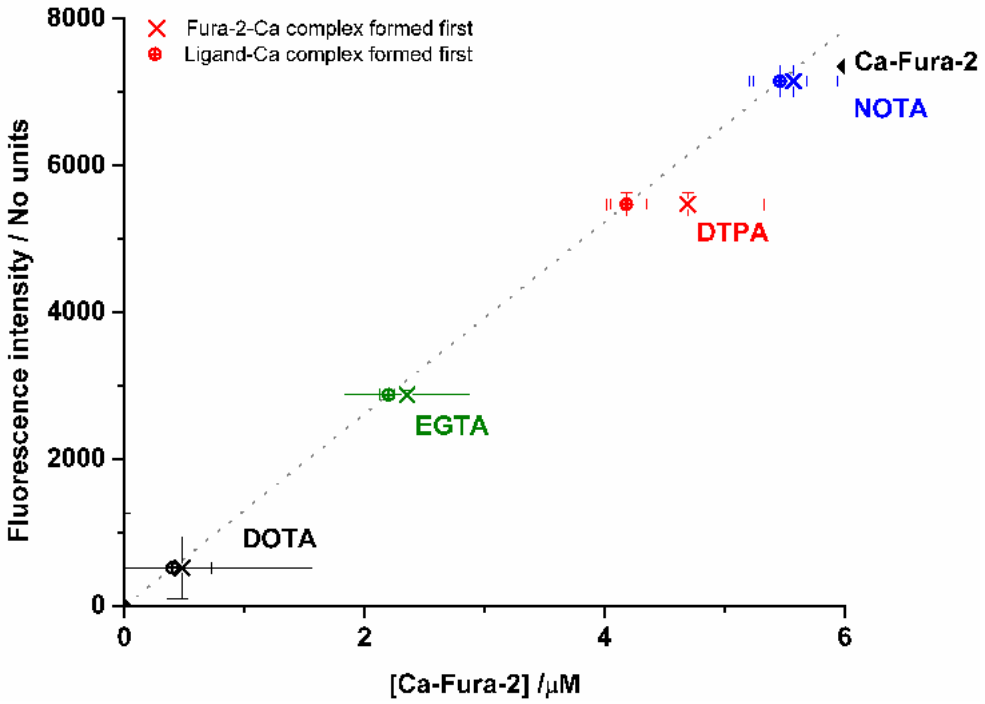

Figure 20: The effect of various aminocarboxylate ligands on the fluorescence of the **Ca-Fura-2** complex. Calibration function shown in grey. Error bars represent two standard deviations from the mean of three replicates and were propagated from the error in the fitted gradient to give the *x* axis error bars. λ_{ex} =340 nm, λ_{em}=510 nm. [**Fura-2**]=7.6μM, [**ligand**]=10μM. Buffer: 10mM HEPES/100mM KCl at pH 7, T=26$\pm$1°C.

To ensure that all measurements were taken at equilibrium, both orders of addition were tested, i.e. demetalation of a **Fura-2** complex, or the removal of metal from a metal-ligand complex by **Fura-2**. If the differences **Fura-2** emission intensities for each direction were statistically insignificant, as is the case in ***Figure 20***, then equilibration was assumed. In most cases, equilibrium was reached before readings were taken, with the exception of the reaction between **EDTA** and **Zn-Fura-2**.

2.6. Measurement of partition coefficients*

The partition coefficient, P describes the relative lipophilicity of a given compound A , and is defined as the ratio of the concentrations of A in an organic and an aqueous phase in contact with one another at equilibrium (***Equation 14***).

$$P = \frac{[A]_{org}}{[A]_{aq}} \tag{14}$$

The ligands and complexes studied throughout this work have pH-dependent solubilities and charge states (***Figure 21***), meaning pH control was necessary for these measurements. This was accomplished using a modified PBS buffer, allowing for interrogations of compound lipophilicity at physiological and growth experiment pH (usually 7.4) to be made, even though most (if not all) of the analytes would be ionised.

*Although the measurement of partition and distribution coefficients is far from a specialised technique, some modifications have been made to the traditional conditions[115] that warrant discussion.

Partition coefficients are useful for the characterisation of a variety of other properties of a compound. For example, the measurement of equilibrium quantities like pK_a, likelihood of emulsion formation, protein-ligand binding strength, permeability though biological membranes and the likelihood a compound will be pharmacologically active[116, 117]. It is perhaps because of the information that partition coefficients can yield that a number of semi-empirical models for the calculation of these quantities have been proposed for small organic molecules.[118] Since many of these models are most effective for relatively non-polar molecules with few charge states, their application to the highly polar, multiply ionisable ligands and their associated metal complexes covered in this work is inappropriate, and so experimental determinations of lipophilicity are preferable.

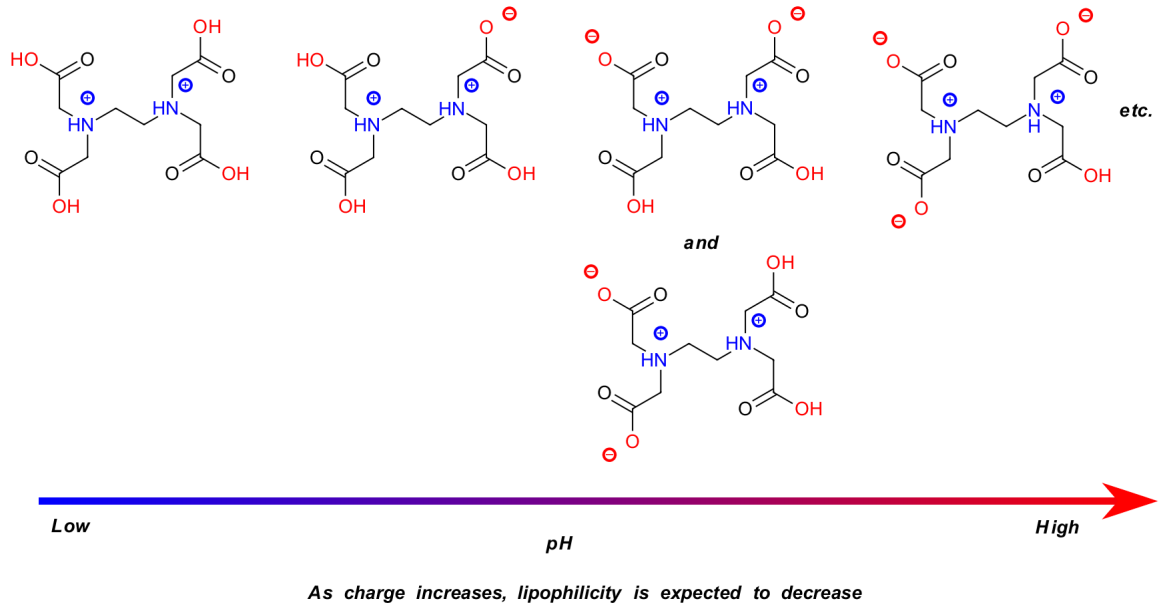

Figure 21: Charge states of **EDTA** (adapted from Szakács[119]) as a function of pH, demonstrating the need for pH control in partition coefficient measurements.

There is evidence that compounds with higher relative lipophilicity are generally better inhibitors of *E. coli* growth,[120–123] even though the membrane structure of Gram-negative bacteria limits cellular permeability (***Section 1.2***). Thus, the measurement of partition coefficients of selected ligands and their complexes may have enabled rationalisation of their dose responses, at least in part.

Typically, the aqueous and organic phase (typically octan-1-ol) are mixed together in a vessel such as a separating funnel, and a method of detection appropriate for the analyte is used to measure concentration ratios, once the phases are separated naturally, or by centrifugation. In this work, dichloroethane and chloroform were used as the organic phases due to their simple ^{1}H NMR spectra, meaning that measurements via ^{1}H NMR were not complicated by the splittings that octan-1-ol or butan-1-ol would exhibit. A variety of test compounds have been studied in the dichloroethane and chloroform organic phases and so a basis for comparison against literature values does exist.[116]

A linear relationship has also been demonstrated between dichloroethane-water and octanol-water

partition coefficients (P_{DCE} and P_{oct}, respectively). That is, compounds with a high P_{DCE} will likely have a high P_{oct} . There is also a correlation between P_{DCE} and chloroform-water partition coefficients (P_{CHCl_3}, ***Equation 15***).[124] As a consequence, experimentally determined P_{DCE} and P_{CDCl_3}values can be compared to P_{oct} values if desired.

$$logP_{CHCl_3} = 1.11(\pm 0.06) logP_{DCE} - 0.06(\pm 0.11) \quad (15)$$

With these factors in mind, a variation on the shake-flask method was used for all of the ligands and complexes under study, using ^{1}H NMR for the measurement of P_{CHCl_3} of the free ligands owing to the absence of other spectroscopic handles (in most cases), and UV-Vis spectroscopy for the measurement of P_{DCE} for transition metal complexes. Samples of each phase for UV-Vis measurements were diluted into DMSO prior to measurement to mitigate the influence of the solvent on the extinction coefficients of the complexes. In this way, if a linear relation held across a range of dilutions and absorbance in DMSO, the ratio of absorbances for the phases would give P_{DCE} , based on the Beer-Lambert law.[125]

LCMS could also be used to assess these quantities but it was avoided due to the necessity of time-consuming calibration procedures, and evidence of acid-mediated complex decomposition from the gradient solvent, resulting in inaccurate concentration ratios. The formation of noncovalent adducts in mass spectrometry is also well-known,[126] and could also lead to “false” readings. This would not be the case with the UV-Vis based method, where a comparison of the spectra of the aquated metal ions and metal-ligand complexes would give a reliable indicator of complexation, especially in the case of aminophenolate ligands.

3. Synthesis and growth inhibition studies of a series of EDTA amide ligands

3.1. Motivations for the work

EDTA amide ligands are ligands where one or more of the acid groups of **EDTA** have been exchanged for amides. This class of molecules have been known for at least the last four decades, and have been considered for many applications. These include radical traps, reagents for the processing of photographic film and as supporting ligands in MRI contrast agents. Yet, there is a distinct lack of both academic and patent literature on the use of this class of ligands as a means to control bacterial growth, despite the vast array of derivatives (> 900) reported.*

Guided by observations collected by Boethling[72] that incorporation of hydrolysable groups such as esters and amides into organic materials enhances aerobic biodegradability, these systems seemed lucrative targets, although there is a cost in replacing carboxylate donor groups with amides: complex stability is likely to be reduced leading to less extensive metal sequestration in liquid media (***Table 8***).

*This number was obtained by performing a substructure search in the Chemical Abstracts Service (SciFinder) database using the SMILES string O=C(N)CN(CC(=O)O)CCN(CC(N)=O)CC(O)=O in October 2015.

Table 8: Literature Zn^{2+} affinities for EDTA and some EDTA di-amide ligands. From these data and application of the Irving-Williams series, a crude estimate of the chelating behaviour of these ligands can be made for other metal ions.

Entry	Ligand	log $K_a(\frac{[ML]}{[M][L]})$ M=Zn^{2+}
a	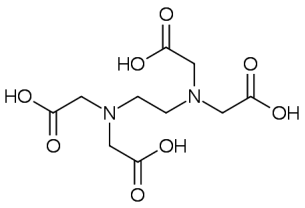 **EDTA**	16.44[i]
b	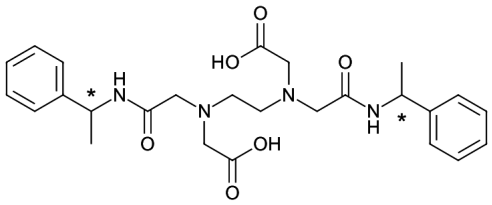 **EDTAMBA**	8.75[ii]
c	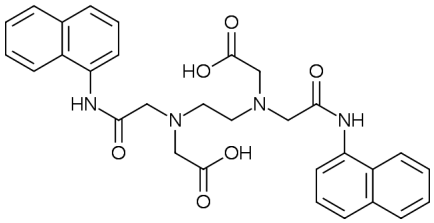 **EDTA1nap**	10.7[iii]

i) Averaged value from Danil de Namor. **ii)** *Via* potentiometric titration, I=0.1 M $KClO_4$. Values **i** and **ii** are from Danil de Namor *et al.*[127] **iii)** Via fluorescence titration I=0.01 M NaCl, T=25°C.[128]

Because of the limited understanding of the antibacterial effect of EDTA-amide ligands, a wide range of EDTA amides were targeted so that more information about the kind of amide substituents and the effect that they had on *E. coli* growth could be collected. Three general categories of pendent groups were selected for study to this end.

Symmetrical EDTA di-amides of type **AmR_2** (***Figure 22***) were the first ligands synthesised and tested, because many reports of gram-scale, protecting group-free and chromatography-free syntheses of a variety of these materials are in the literature. Synthesis typically proceeds via nucleophilic ring opening of anhydride **1**,[129–134] and the final **AmR_2** ligand is obtained via purification or crystallisation, making eventual scale-up a possibility (***Scheme 7***).

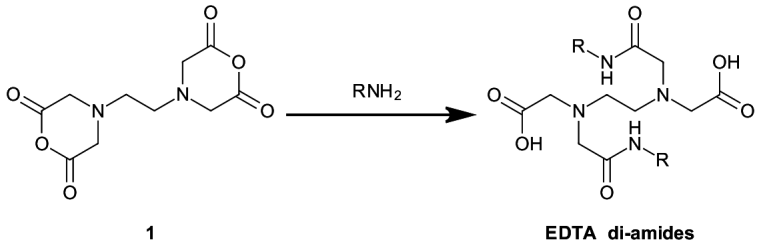

Scheme 7: A popular route to **EDTA** diamide (**AmR$_2$**) ligands without recourse to protecting groups.

Once a selection of **AmR$_2$** ligands was prepared, ligands of type **AmR$_1$** and **AmR$_4$** could then targeted for comparison after development of a suitable route (***Figure 22***).

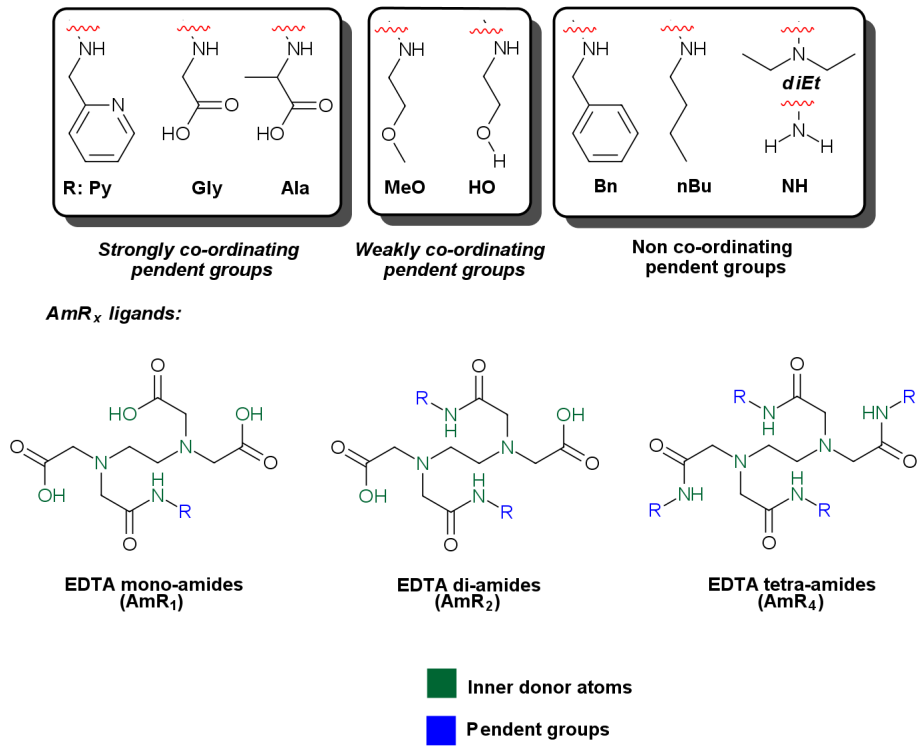

Figure 22: Categories and examples of pendant groups, archetypal ligand structures and the naming convention used in this chapter.

3.2. Synthetic work

3.2.1. Preparation of EDTA di-amides via EDTA di-anhydride

Following the array of reports in the literature described above, the first route to **AmR$_2$** ligands used involved reaction of anhydride **1** with a variety of amines in a polar aprotic solvent such as dimethylformamide or tetrahydrofuran at room temperature. Even though the presence of the desired molecules in crude material was confirmed via ES-LCMS, purification proved extremely difficult, if not impossible, due to the hygroscopicity of the compounds and their high polarity. This precluded the use of conventional purification methods like column chromatography or solvent extraction.

Attempts at purification via ion-exchange, based on methods for purifying amino acids[135–138] using concentration gradients of hydrochloric acid on a DOWEX 50WX8 resin, led to poor mass recovery and partial hydrolysis. Reverse-phase chromatography was somewhat successful and small amounts of **AmAla$_2$**, **AmdiEt$_2$** and **AmnBu$_2$** were isolable but samples contained trace impurities.

Finally, crystallisation and recrystallisation techniques were therefore used on crude products at a variety of pH values and solvent compositions (usually mixtures of water and acetone or the lower alcohols), but many derivatives failed to crystallise after cooling possibly due to high solubilities in water across a wide pH range. After some refinement the **AmR$_2$** ligands **AmGly$_2$**, **AmBn$_2$** and **AmNH$_2$** could be crystallised in a pure form, albeit in low to moderate yields, following dissolution of the crude material into $\geqslant$1 M hydrochloric acid (heating if necessary). Multi-gram batches of **AmGly$_2$** and **AmBn$_2$** could then be prepared, and in the cases, of **AmGly$_2$** and **AmNH$_2$**, crystals suitable for analysis via X-ray crystallography could be obtained.

Alternative synthetic pathways to **AmR$_2$** type ligands were investigated in order to facilitate access to other derivatives, because of the limited success of preparing such ligands via the anhydride route (***Section 3.2.2***).

3.2.2. Alternative synthetic routes: Approach and preliminary experiments

In the pursuit of a greater variety of **AmR$_x$** ligands (**x** = 2,3,4) (more R- groups, differing degrees of substitution), it was necessary to evaluate chemistry beyond the ring-opening of **1**, due to reasons covered earlier. It may be noted at this point that the attempted synthesis of **AmR$_1$** ligands based on the work of Jaeger[129] using **1**, one equivalent of amine and one equivalent of water were unsuccessful and gave **AmR$_2$** type ligands and **EDTA** instead (***Scheme 8***). This observation has been made independently by Scozzafava.[132]

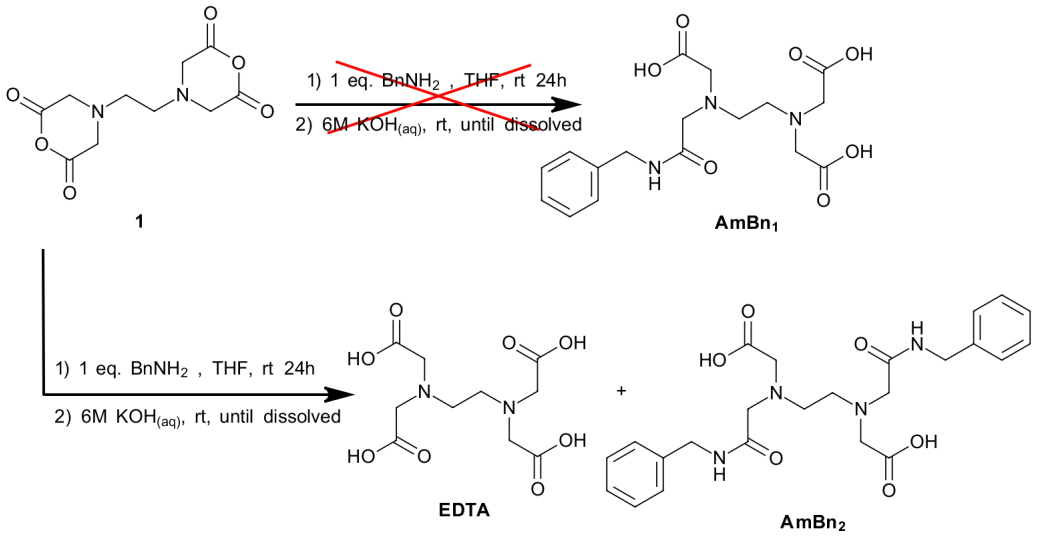

Scheme 8: Attempted synthesis of **AmBn$_1$** from anhydride **1**

Inspection of the **AmR$_2$** framework revealed a range of possible disconnections (***Scheme 9***) and following the accepted practice of disconnecting adjacent to a heteroatom,[139] two key disconnection points were identified (labelled **A** and **B** in ***Scheme 9***) from which forward syntheses could be devised.

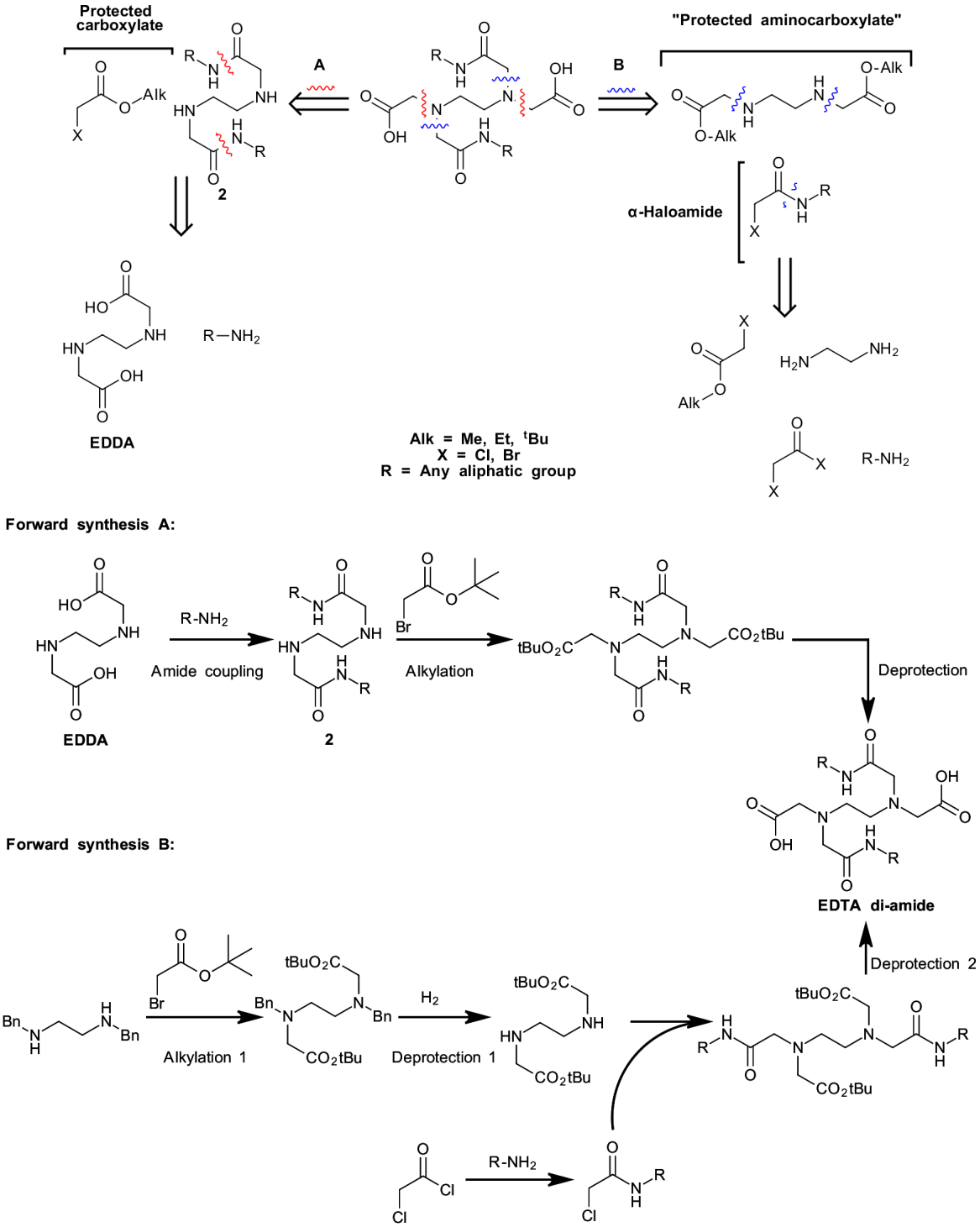

Scheme 9: Disconnections and possible forward syntheses leading to **AmR$_2$** ligands.

In this alkylation-based approach, carboxylic acid groups were to be introduced as their esters so that the solubility of the intermediates in organic solvents was improved and purification via normal phase chromatography was feasible. Methyl and ethyl esters were preferred in the earlier stages of this work, because of the ready availability of amino acid esters protected with these groups at very low cost. Esterification of the parent acids when ester derivatives were not commercially available was also facile. The linear route **A**, starting from the commercially available N,N'-ethylenediaminediacetic acid (**EDDA**) appeared more logical and had fewer steps compared to **B** and was evaluated in the first instance.

Carbodiimide coupling methods, used widely in peptide synthesis,[140] were used to attempt the preparation of amides of type **2** so that the carboxy groups of **EDDA** could be functionalised in one step. As a proof of concept for **A**, **EDDA** was coupled with diethylamine in water using EDC (1-Ethyl-3-(3-dimethylaminopropyl)carbodiimide) as the coupling agent to provide **2a**, the key intermediate to **AmdiEt$_2$** (***Scheme 10***).

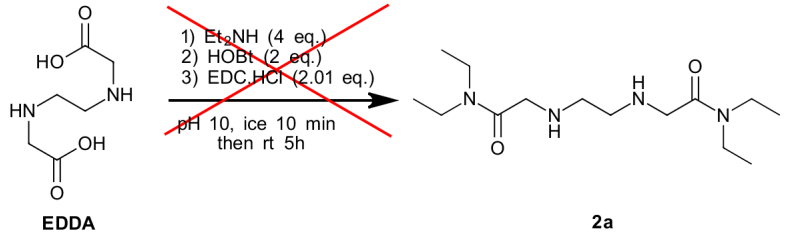

Scheme 10: Attempted preparation of amide **2a** via carbodiimide coupling. HOBt: Hydroxybenzotriazole.

While a polar aprotic solvent was desirable for this reaction, the insolubility of **EDDA** in anything other than aqueous base necessitated the use of aqueous conditions. Although the use of water in amide couplings is highly unconventional, examples of amide couplings in water have been published.[141, 142] Unfortunately, the reaction was unsuccessful and only **EDDA** was recovered. A variation as a route into **AmR$_1$** ligands was then attempted on **EDTA** directly to see if the solvent, or the interference of the secondary amines present was the cause of failure (***Scheme 11***).

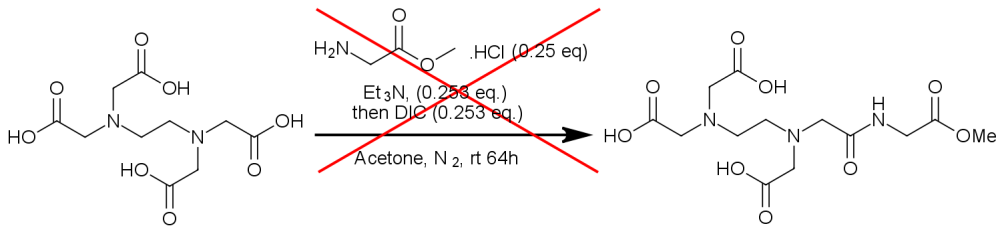

Scheme 11: Attempted preparation of **AmGly$_1$** via amide coupling.

The reaction did not proceed, though it is suspected that some conversion may be achieved, and the completed route may be an extremely quick way to afford diverse compounds. For reasons discussed in the next section, no such optimisation was attempted .

3.2.3. Evaluation of a convergent route: use of α-haloamides

Prompted by the abundance and structural diversity of ligands for various Ln^{3+} ions containing amide, carboxyl and amino groups in the literature and the presence of the same functional groups in the targeted EDTA amides, translation of this chemistry was thought to be useful. The similarity of many intermediates identified in disconnection **B** (***Scheme 9***) to those previously published, could suggest synthetic success. In this convergent approach, the aminocarboxylate fragment is prepared independently from the amide arm(s) and the two fragments are joined via alkylation (***Scheme 12***).

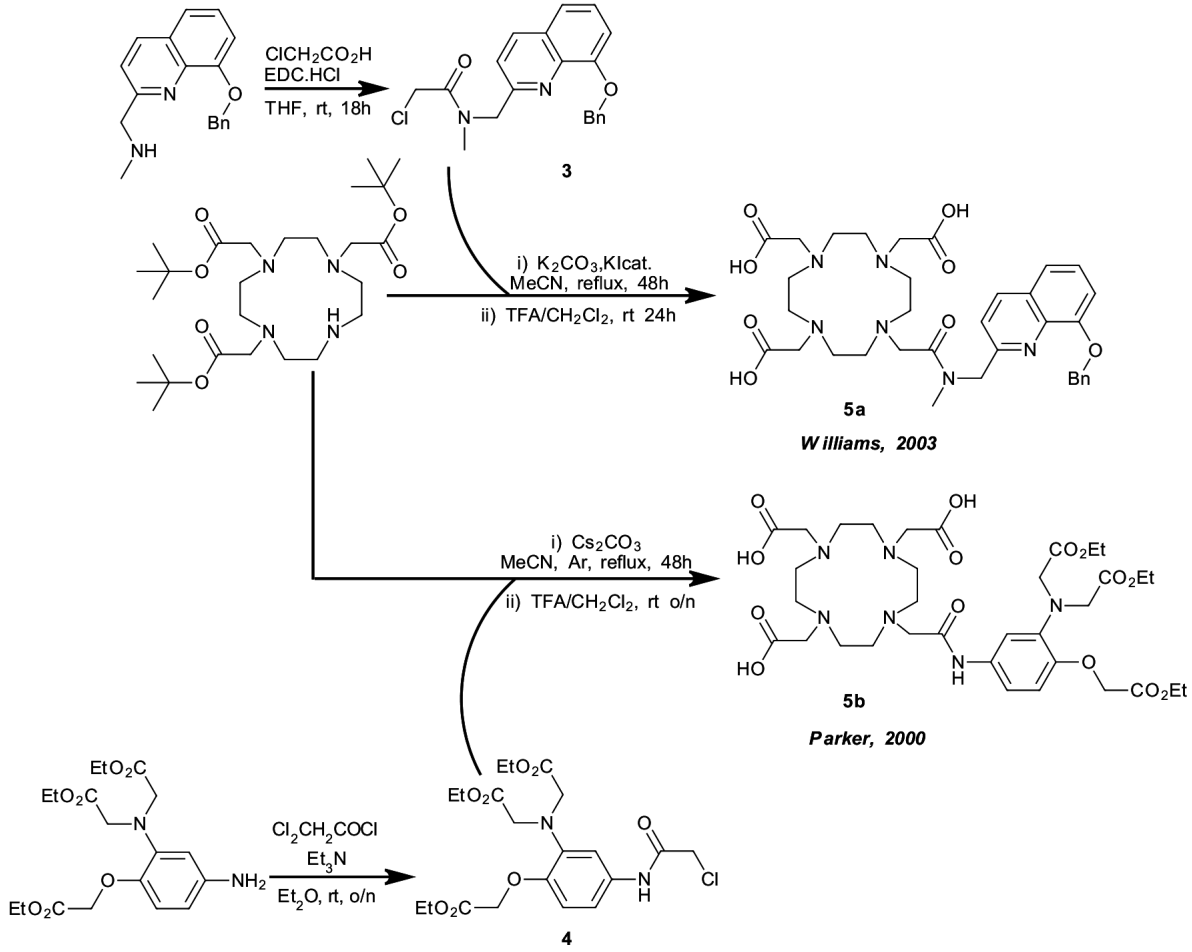

Scheme 12: Ligands reported by the groups of Williams[143] and Parker[144] using a strategy based on the incorporation of amide fragments at a later stage.

A drawback of route **B** (***Scheme 9***) is that in preparing the aminocarboxylate fragment, both amine, and carboxylate protection is usually necessary to prevent over-reaction, adding steps to the synthesis, but a distinct advantage over route **A** is that aminocarboxylate fragments can be exchanged and reacted with the same amide electrophile to access the $\mathbf{AmR_1}$, $\mathbf{AmR_2}$ and $\mathbf{AmR_4}$ substitution patterns bearing the same pendent group (***Section 3.2.4***).

With this in mind, work on the amide coupling method of choice to generate compounds of type **6** was commenced. The use of haloacetyl halides is commonplace for the preparation of these amides and was successfully employed to afford the compounds listed in ***Table 9*** in low to moderate yields.

Table 9: α-Haloamides prepared by reaction between chloroacetyl chloride and amines.

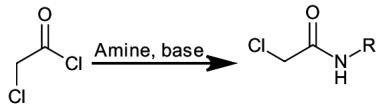

6a-e

Entry	Amine	Amide	Base	Solvent	Yield / %
a	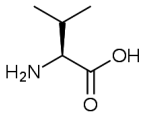	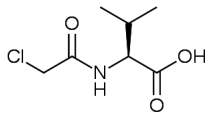	None[ii]	MeCN	28[iii]
b	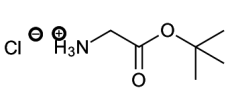	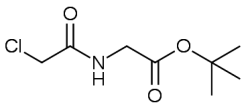	Et_3N	DCM	67
c	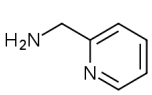	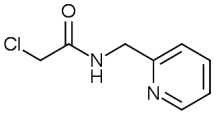	None	DCM	75[iv]
d	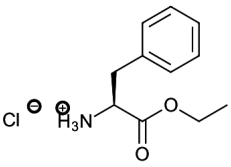	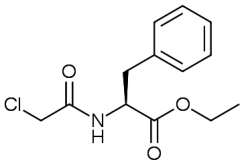	Et_3N	THF	25[iv]
e	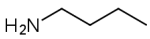	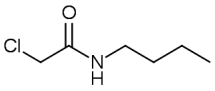	None[ii]	DCM	48

i) No protecting group was necessary for this transformation. **ii)** 2 equivalents amine used. **iii)** After recrystallisation. Stereochemical integrity of the product was verified by X-ray crystallography. **iv)** after column chromatography on silica.

In light of these low yields compared to the literature, a carbodiimide coupling procedure was applied to the synthesis of **6f** to see whether the approach could deliver superior yields (***Scheme 13***). This was not the case and so the haloacetyl halide route was adopted as the default method for the preparation of the desired amide electrophiles, given the low cost of the necessary reagents.

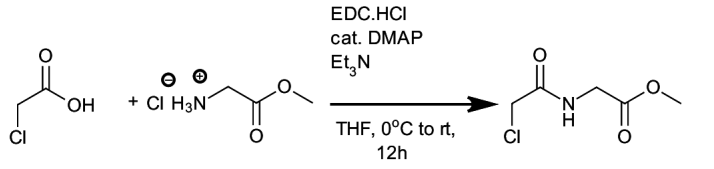

6f

Scheme 13: Preparation of **6f** using amide coupling chemistry.

With α-haloamides **6a-e** in hand, the next step was the construction of the aminocarboxylate fragments. As outlined in ***Section 3.2.3***, ethyl and methyl esters of the amino acid precursors to compounds of type **6** were used. To enable global deprotection via aqueous base[145] the use of the same

protecting groups for the carboxylates of the aminocarboxylate fragment was necessary and so intermediate **7** was reacted with ethyl bromoacetate to form intermediate **8** (***Scheme 14***). In theory **8** could then be debenzylated to provide the protected nucleophile **9** (***Table 10***) for further reactions.

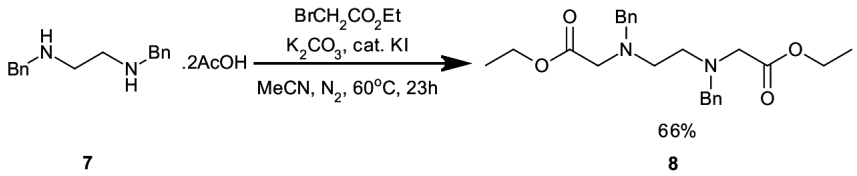

Scheme 14: Preparation of **8** via alkylation.

Hydrogenation with a palladium catalyst is typical for benzylamine deprotection and so was the first approach tested. Hydrogen gas or ammonium formate (transfer hydrogenation conditions[146, 147]),were trialled as reductants but a kinetically favoured 6-exo-tet cyclisation resulted under these conditions to form ketopiperazine **10** exclusively (***Table 10***).

Table 10: A survey of conditions used to debenzylate precursor **8**.

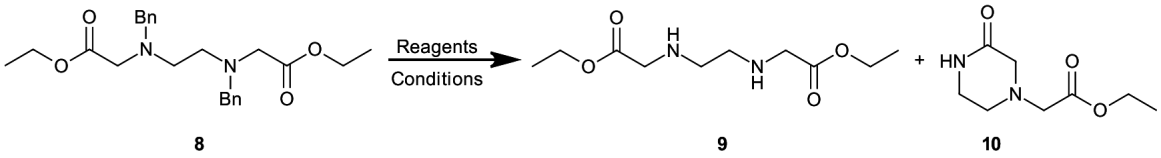

Entry	Reagents	Conditions	9:10 / %[i]
a	NH_4HCO_2, 5 mol% Pd (as 5 wt. % Pd/C)	EtOH, reflux 2h	0:100
b	H_2, 5 mol% Pd (as 5 wt. % Pd/C)[ii]	EtOH, rt 4h	0:100

i) Determined by ^{1}H NMR spectroscopy of the filtered reaction mixture. Data confirming the structure of **10** are reported in ***Section 8.2.15***. **ii)** Catalyst loadings for routine tranformations necessary across this work (debenzylation, imine and nitro reduction-see ***Section 5.2.2***) had already been determined and from these experiments $\geq$ 5 mol % palladium metal was necessary.

Parallel experiments on other substrates were performed to assess if an oxidative approach to debenzylation could prevent cyclisation,[148] but starting material was recovered exclusively. Other workers observed similar cyclisations and were unable to practically inhibit them without changing the carboxyl protecting group on the aminocarboxylate fragment.[149–151] Carboxyl protection via t-butyl groups was employed as a result. These groups are stable to bases and nucleophiles but precursors to $\mathbf{AmR_x}$ ligands bearing them could no longer be globally deprotected using base when carboxyl groups protected as methyl and ethyl esters were present in the same molecule.[152] In a manner analogous to **8**, aminoester **11** could be prepared using t-butyl bromoacetate as the alkylating agent, and hydrogenated smoothly to afford key nucleophile **12** (***Scheme 15***).

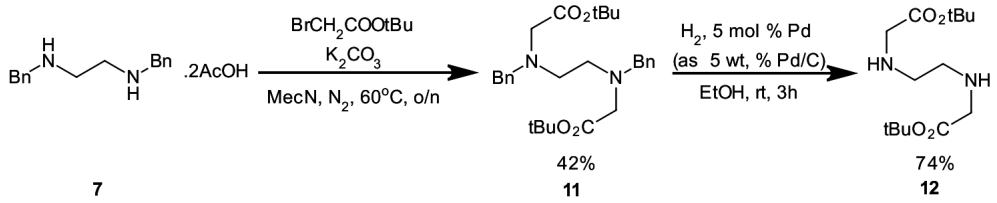

Scheme 15: Preparation of key nucleophile **12**

Now that procedures to afford the key nucelophile and electrophile in route **B** were in place, they were tested in the synthesis of **AmPy$_2$**, a ligand that could not be isolated in a pure form via the approach described in ***Section 3.2.1***. Synthesis and purification were smooth, and led to the synthesis of **AmPy$_2$** in 15% cumulative yield; a figure comparable to other multi-step syntheses of chelating ligands.[153–157]

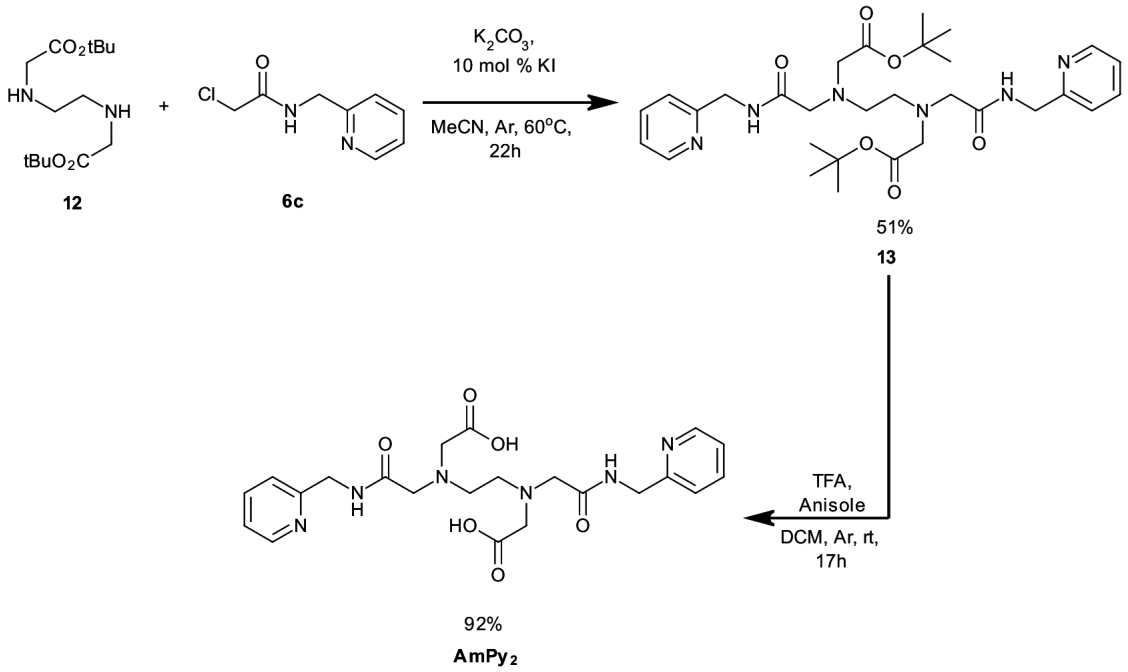

Scheme 16: Synthesis of **AmPy$_2$** via a convergent route.

3.2.4. Synthesis of EDTA mono-amides

It was mentioned in ***Section 3.2.3*** that use of the convergent route **B** (***Scheme*** 9) could be adapted to the different degrees of substitution of the **AmR$_x$** ligands desired by changing the aminocarboxylate fragment, for example, by preparing **14**, and adjusting the equivalents of α-haloamide and base used in the reaction. Following literature precedent,[158] a benzyl protecting group was used in the first alkylation step (***Scheme 17i***). The fact that there is only one possible isomer of this tris- homo-substituted ethylenediamine, and that the over-reaction product **EDTA tBu** is much less polar than **15**, enables the direct reaction of t-butyl bromoacetate with ethylene diamine to form **15**,[159] isolable after simple chromatography (***Scheme 17ii***).

Because the starting materials for either route are inexpensive, the direct route to **15** was used, on account of the time that could be saved, even if the yield was lower than if benzyl protection was employed.

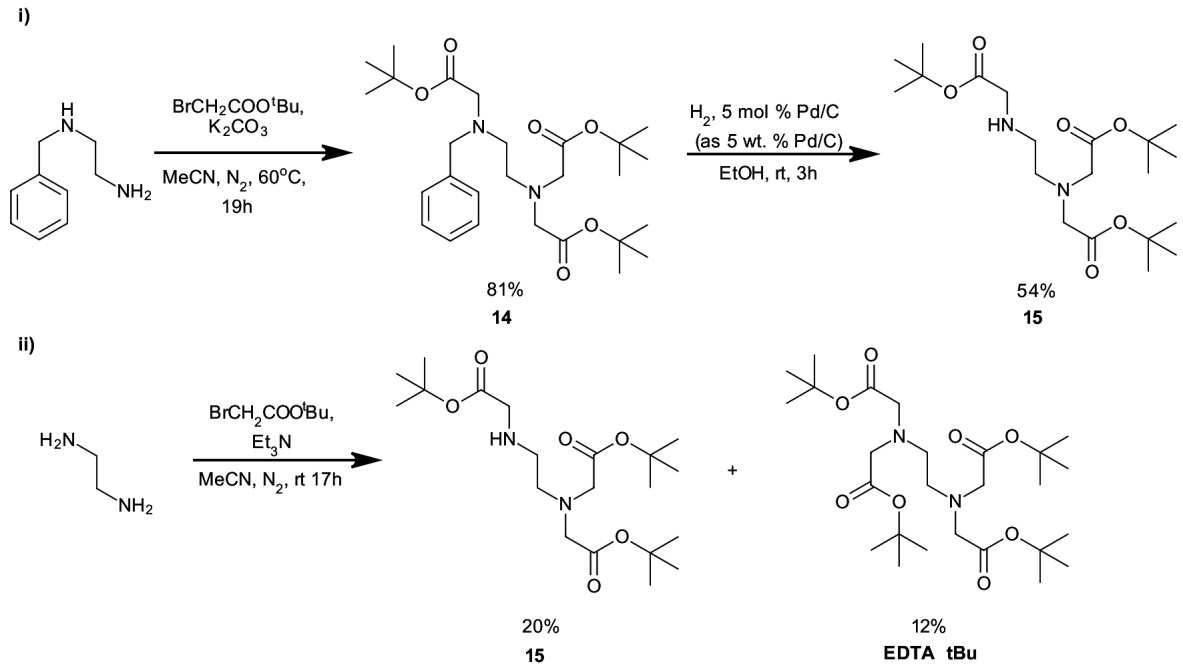

Scheme 17: Preparation of **15** in a **i)** two-step approach involving amine protection and **ii)** a direct route.

Once **15** was in hand, test alkylations were performed to optimise the base for future syntheses, since a variety of bases are reported for alkylations of this type in the literature. Using ethyl bromoacetate as a model alkylating agent, orthogonally protected aminoester **16** was prepared using the conditions in ***Table 11***. Successful preparation of **16** indicated both that **15** should be able to react with intermediates of type **6a-f** and that the use of caesium carbonate, due to its higher solubility in organic solvents, was detrimental to yield, since more thorough purification of the crude product was necessary.

As an aside, **16** is a complement to the orthogonally protected species prepared by Micklitsch,[158] and could be deprotected via aqueous base or trifluoroacetic acid in dichloromethane to afford one or three functionalisable carboxyl sites respectively.

Table 11: Influence of the base on alkylation yields.

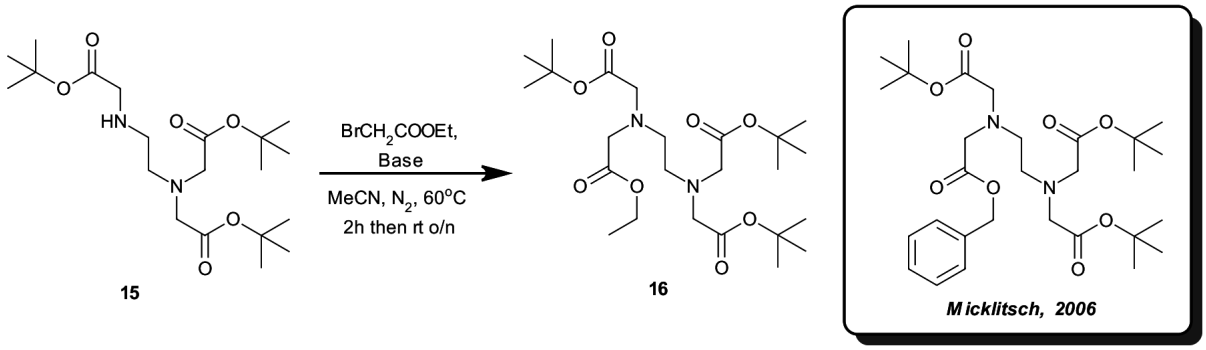

Entry	Base	Yield / %
a	K_2CO_3	90
b	Cs_2CO_3	59

Synthesis of the novel mono-amide **AmGly$_1$**was attempted using the optimised alkylation conditions. Initially, the low-cost, commercially available α-haloamide ethyl (2-chloroacetylamino)acetate and its methyl ester analogue **6f**, were used as alkylating agents. Despite evidence of conversion from ^{1}H NMR and TLC analyses, the crude material was not amenable to column chromatography, either not eluting at all (even using 100% MeOH), or co-eluting with impurities. α-Haloamide **6b** was then used as the alkylating agent to solve these problems, even though it is prepared from the far more costly t-butyl glycinate, and has the added advantage of subsequent trivial global deprotection. Using this combination of reagents gave an effective synthesis (***Scheme 18***).

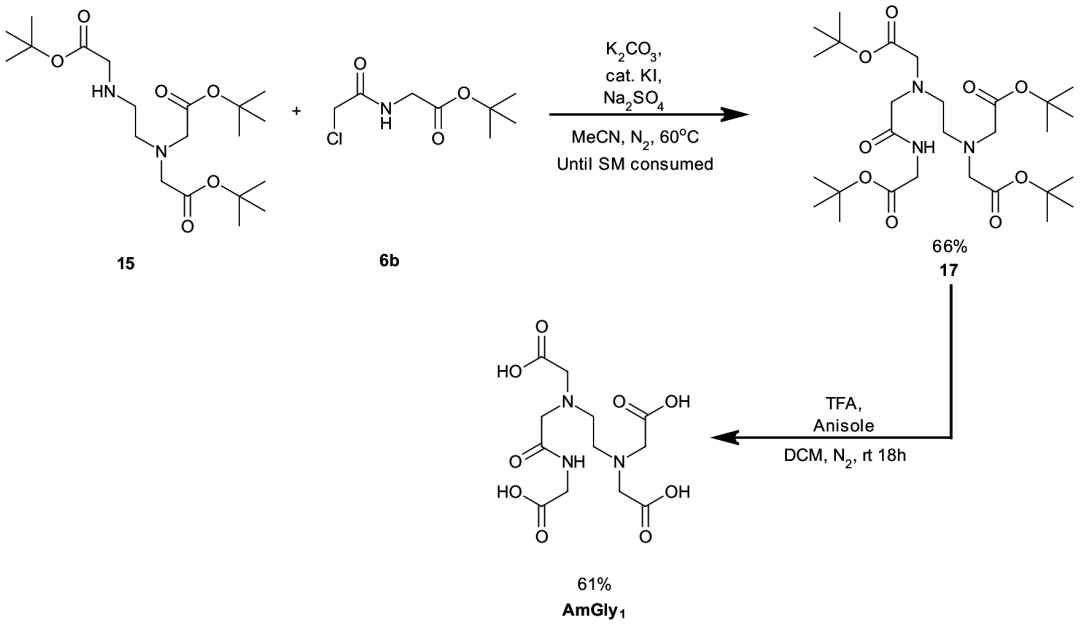

Scheme 18: Preparation of **AmGly$_1$** via a convergent route.

AmPy$_1$ could also be prepared in an analogous way (***Scheme 19***).

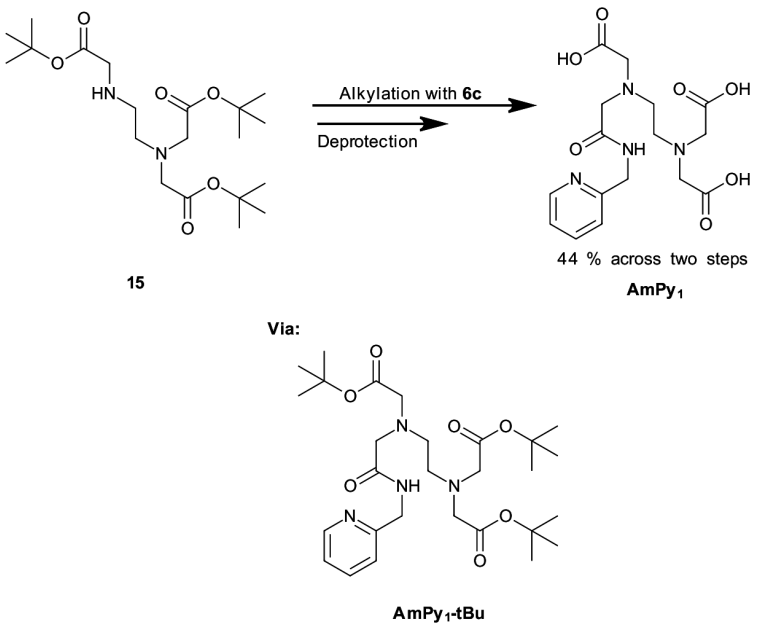

Scheme 19: Preparation of **AmPy$_1$**.

Analytical HPLC was performed for **AmGly$_1$** and **AmPy$_1$**, to assess the homogeneity of the final ligands, both of which showed one peak in their respective chromatograms. With a variety of **AmR$_1$** and **AmR$_2$** systems prepared, synthetic focus was turned to preparing ligands of type **AmR$_4$**.

3.2.5. Synthesis of EDTA tetra-amides

The synthesis of **AmR$_4$** type ligands was undertaken from ethylene diamine and haloamides **6b**, **6d** and **6g** using the appropriate deprotection chemistry so that the effect of substituting all of the carboxylate groups in the central donor set of the EDTA amides could be interrogated. In addition to the fundamental knowledge that could be gained regarding the alteration of the central donor set and its effect on *E. coli* growth, these molecules may exhibit enhanced biodegradability, much like dendrimers based on polyamide structures (***Scheme 20***).[160, 161]

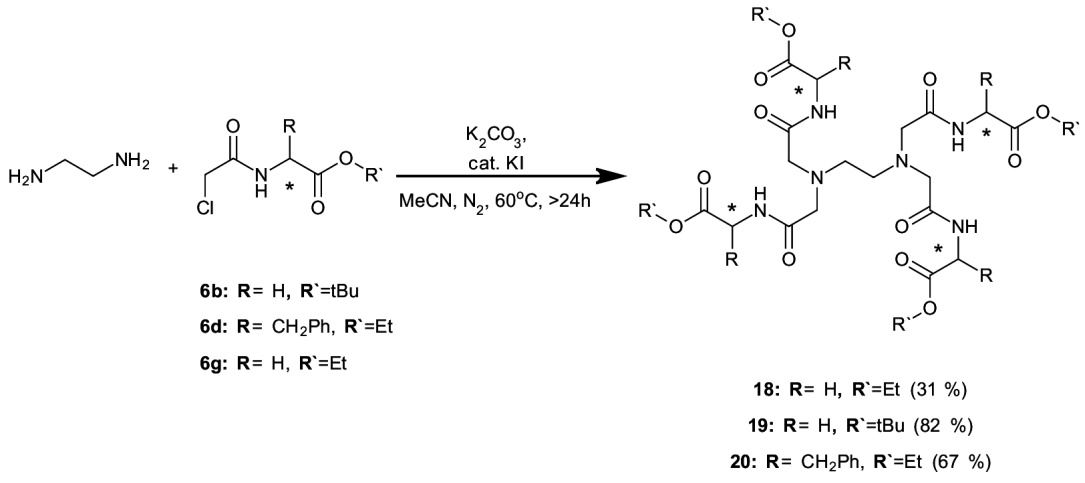

Scheme 20: Key precursors to **AmR$_4$** type ligands.

Compound **18**, was prepared from commercial reagents exclusively and so the synthesis was remarkably convenient. But following final deprotection using potassium hydroxide in a mixed water:methanol system and purification via ion-exchange chromatography, the cumulative yield was lower than when **AmGly$_4$** was synthesised via **19**. Although **AmGly$_4$** has previously been prepared via amide-coupling chemistry,[162] the alkylation route employed for the synthesis of **AmR$_1$** and **AmR$_2$** ligands was selected in light of the unsuccessful attempts at such couplings in this work (***Section 3.2.2***). The phenylalanine derived amide **AmPhe$_4$** was also prepared from the relevant ethyl ester precursor **20** (***Scheme 21***).

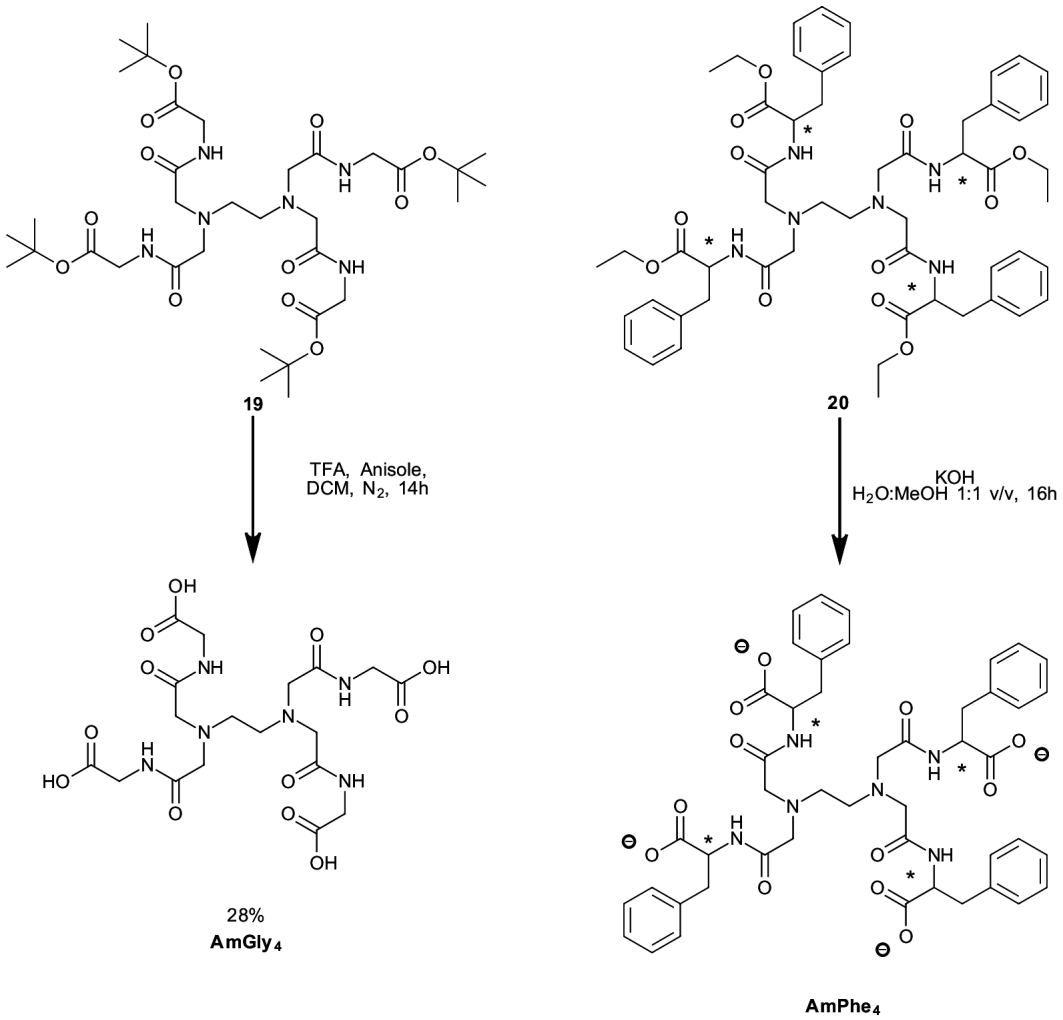

Scheme 21: The final **AmR$_4$** type ligands prepared.

With the final roster of ligands prepared and characterised, a study of their biological properties could now take place.

3.3. Assessment of antibacterial properties

3.3.1. General remarks

The experimental procedure for the growth curve assays is covered in ***Section 8.7***, and the background in ***Section 2.3*** . Because these experiments were performed in 96-well plates, and comparisons across experiments are drawn, an indicator of experiment to experiment variability is useful when dose responses are being discussed. For this reason, when dose responses for a ligand are presented, the EDTA dose response for the corresponding experimental run has been overlaid as a light grey curve. Since a goal of this work is the discovery of ligands that inhibit *E. coli* more severely than EDTA at the same or lower concentrations, it is hoped that the reader will find the overlays helpful in the comparison of data points and their statistical significance. For the data presented, the variation between **EDTA** runs is within the error of the experiment, meaning that data from different experimental runs may be compared.

3.3.2. Effect of the number of carboxylates

Analysing the growth inhibition characteristics for the ligands prepared above commenced with the analysis of **EDTA**, **AmGly$_1$**, **AmGly$_2$** and **AmGly$_4$** . These growth characteristics are described in ***Figure 23***.

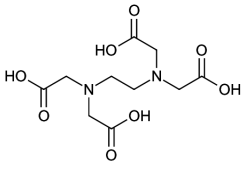

EDTA

[EDTA] / mM	Growth cf. control /%
0 (7.4)	100 ± 10
0.625 (7.4)	93 ± 8
1.25	75 ± 10
2.5	47 ± 12
5.0	33 ± 5
10.0 (7.3)	21 ± 3

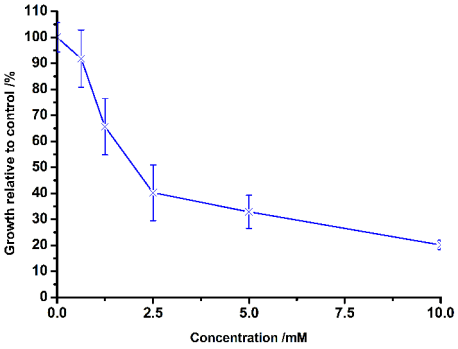

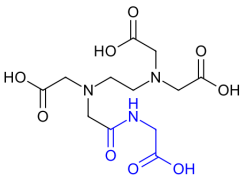

$AmGly_1$

[$AmGly_1$] / mM	Growth cf. control /%
0 (7.4)	100 ± 8
0.625 (7.5)	95 ± 6
1.25	71 ± 11
2.5	11 ± 1
5.0	31 ± 2
10.0 (7.3)	25 ± 4

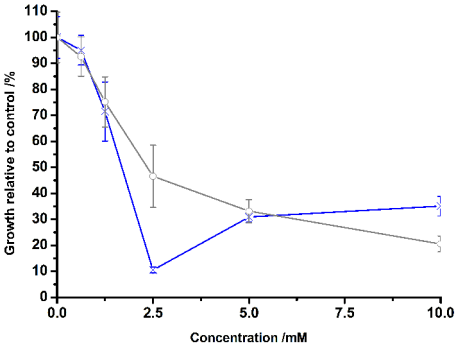

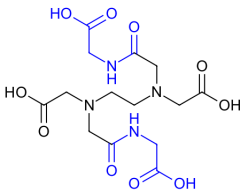

$AmGly_2$

[$AmGly_2$] / mM	Growth cf. control /%
0 (7.4)	100 ± 2
0.625 (7.5)	103 ± 8
1.25	74 ± 10
2.5	6 ± 1
5.0	4 ± 1
10.0 (7.3)	5 ± 1

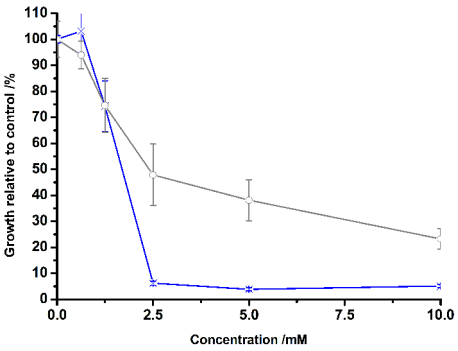

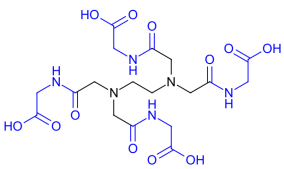

$AmGly_4$

[$AmGly_4$] / mM	Growth cf. control /%
0 (7.4)	100 ± 10
0.625 (7.3)	104 ± 9
1.25	97 ± 40
2.5	110 ± 14
5.0	101 ± 9
10.0 (7.6)	94 ± 8

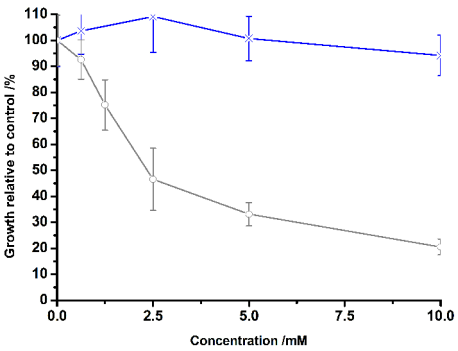

Figure 23: Dose response curves for *E. coli* JM101 upon dosing with **EDTA**, **$AmGly_1$**, **$AmGly_2$** and **$AmGly_4$** . Bacteria were incubated for 16 h at 37°C in a medium composed of of 90:10 v/v TSB: 10x ligand stock in 200mM K_2HPO_4 (in-well [K_2HPO_4] of 20mM). Values are the mean of three technical repeats. Both error bars and margins represent two standard deviations from the mean. Bracketed values are the pH of test solutions based in the same media used for the experiment. Blue lines represent the dose response of the ligand, and grey lines represent the dose response of EDTA.

It is immediately apparent that upon exchanging all of the carboxylate groups in **EDTA** with amides as is the case for **AmGly$_4$**, an **AmR$_x$** ligand loses all efficacy and no statistically significant growth inhibition is observed. Increasing the lipophilicity of an **AmR$_4$** ligand, as in the case of **AmPhe$_4$**, does not alter the inhibition profile (***Figure 24***).

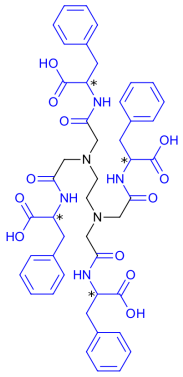

AmPhe$_4$

[AmPhe$_4$] / mM	Growth cf. control /%
0 (7.4)	100 ± 17
0.625 (7.5)	100 ± 13
1.25	98 ± 14
2.5	97 ± 14
5.0	99 ± 16
10.0 (7.4)	90 ± 21

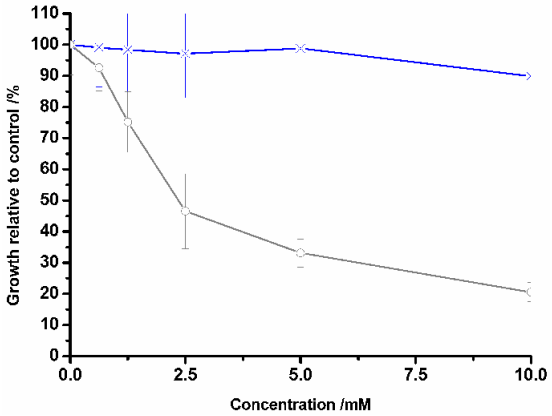

Figure 24: Dose response curve for *E. coli* JM101 upon dosing with **AmPhe$_4$**. Experimental conditions were identical to those described in ***Figure 23***. Values are the mean of three technical repeats. Both error bars and margins represent two standard deviations from the mean. Bracketed values adjacent to tabulated concentrations are the pH of test solutions based on the same media used for the growth curves. Blue lines represent the dose response of the ligand, and grey lines represent the dose response of EDTA.

These observations are unsurprising when considered in light of the detrimental effect that increased amide substitution has on metal affinity (***Table 12***), and the current understanding on the mechanism of chelation-induced bacterial growth inhibition (***Sections 1.2*** and ***1.3***). Work by Clapp[163] on the related ligand **EDTAM** serves to illustrate how profound this reduction in metal affinity can be when no carboxylate donor groups are present in the inner donor set (***Table 12***).

Table 12: The reduction in Ca^{2+} and Mg^{2+} affinities on substituting all of the carboxylate groups of **EDTA** with amide groups.

Entry	Ligand	log $K_a(\frac{[ML]}{[M][L]})$ M=Ca^{2+}	log $K_a(\frac{[ML]}{[M][L]})$ M=Mg^{2+}
a[i]	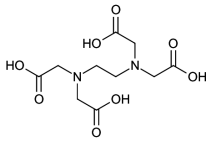 **EDTA**	10.61	8.83
b[ii]	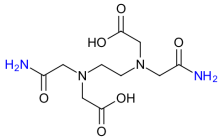 **EDTAM**	3.29	1.6

i) Data sourced from Martell and Smith. T=25°C, I=0.1M.[164] **ii)** Data from Clapp *et al.*[163] T=25°C, I=0.1M.

Because the metal affinity of **$AmGly_4$** and **$AmPhe_4$** is likely to be lower, by analogy to those measured for **EDTAM** giving correspondingly low inhibition power, no further work on **AmR_4** ligands was undertaken. Both **$AmGly_1$** and **$AmGly_2$** were more effective growth inhibiting agents than **EDTA**, even though their metal ion affinities should be lower than **EDTA** based on an inspection of their donor groups and the data in ***Tables 8*** and ***12***.

The apparent *increase* in growth when the cells are treated with higher concentrations of **$AmGly_1$** also warrants comment. To the author's knowledge such non-monotonic behaviour has been observed in the interaction between endocrine disruptors and their receptors,[165–167] but never before for the action of a chelating agent in bacterial growth inhibition. Such a response may be a signal of processes competing with metal starvation at high ligand concentration, like ligand hydrolysis or precipitation due to pH changes in the medium due to bacterial respiration. Precipitation is thought unlikely; pH measurement of a sample of 90:10 v/v TSB:0.2M K_2HPO_4 bacterial growth medium after overnight incubation of *E. coli* JM101 (once cellular material was removed via centrifugation) indicated a pH *increase*, which would lead to higher ligand solubility.

3.3.3. EDTA di-amides: effect of substituent

Dose responses were acquired for the other **AmR_2** materials to compare them to that of **$AmGly_2$**. This assessment allowed an initial evaluation of whether the presence of two amide groups in the inner donor set, or the choice of pendent groups gave a bacterial growth inhibition (***Figure 25***).

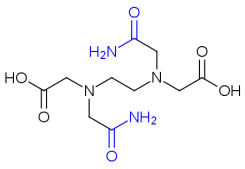

$AmNH_2$

[$AmNH_2$] / mM	**Growth cf. control /%**
0	100 ± 8
0.625 (7.6)	95 ± 7
1.25	90 ± 6
2.5	80 ± 5
5.0	48 ± 3
10.0 (7.4)	35 ± 3

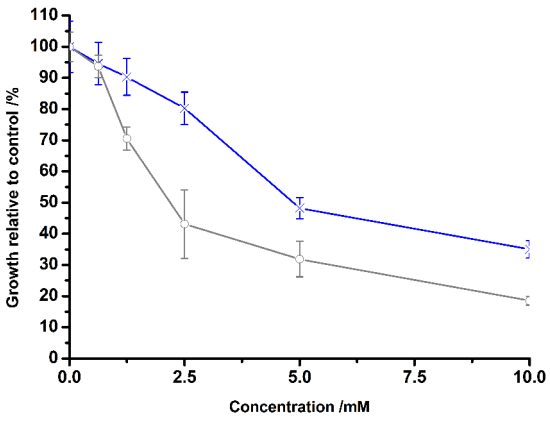

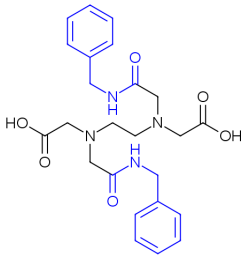

AmBn$_2$

[AmBn$_2$] / mM	Growth cf. control /%
0	100 ± 1
0.625 (7.6)	99 ± 2
1.25	94 ± 2
2.5	86 ± 2
5.0	66 ± 4
10.0 (7.2)	44 ± 2

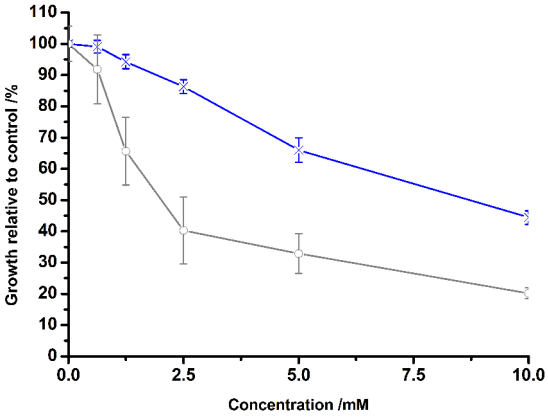

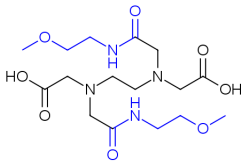

AmOMe$_2$

[AmOMe$_2$] / mM	Growth cf. control /%
0	100 ± 9
0.625 (7.5)	103 ± 11
1.25	101 ± 15
2.5	92 ± 6
5.0	47 ± 5
10.0 (7.1)	39 ± 6

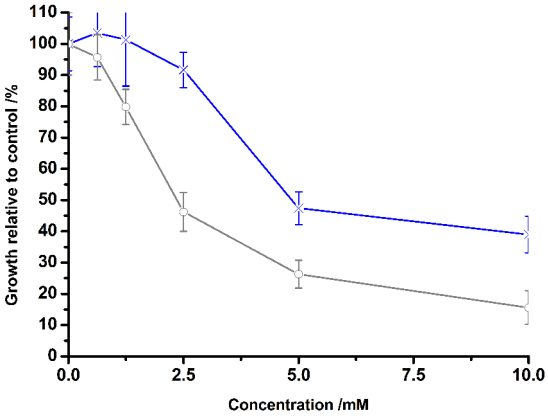

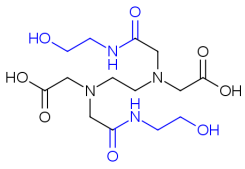

AmOH$_2$

[AmOH$_2$] / mM	Growth cf. control /%
0	100 ± 8
0.625 (7.9)	104 ± 8
1.25	104 ± 8
2.5	99 ± 7
5.0	84 ± 8
10.0 (7.1)	59 ± 6

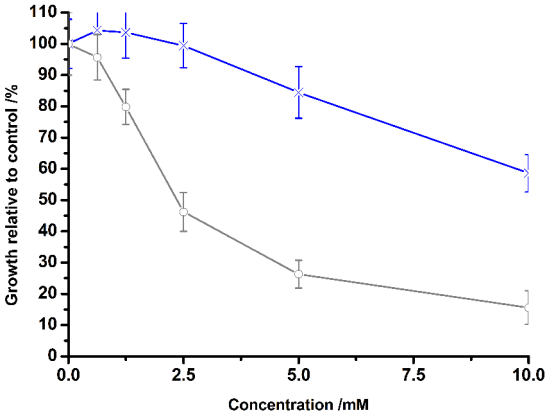

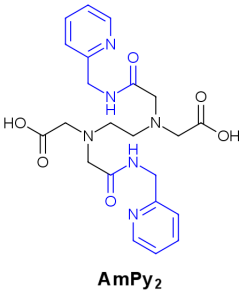

[$AmPy_2$] / mM	Growth cf. control /%
0	100 ± 2
0.625 (7.5)	97 ± 3
1.25	89 ± 4
2.5	45 ± 15
5.0	7 ± 2
10.0 (7.1)	2 ± 1

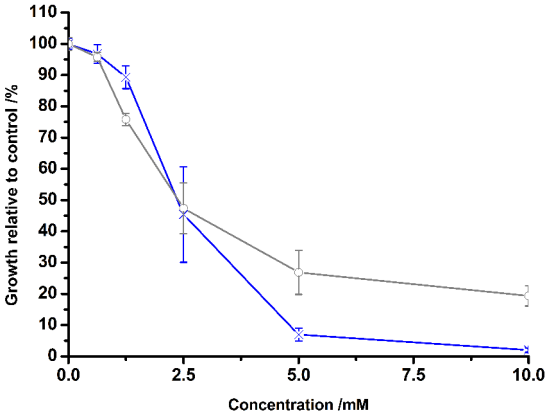

Figure 25: Dose response curves for *E. coli* JM101 upon dosing with **$AmNH_2$**, **$AmBn_2$**, **$AmOMe_2$**, **$AmOH_2$ and $AmPy_2$** . Experimental conditions were identical to those described in ***Figure 23***. Both error bars and margins represent two standard deviations from the mean. Bracketed values adjacent to tabulated concentrations are the pH of test solutions based on the same media used for the growth curves. Blue lines represent the dose response of the ligand, and grey lines represent the dose response of EDTA.

From these data, it is apparent that not all di-amide substitutions gave equal growth inhibition against *E. coli* and of the types of pendent group (***Figure 22***), those which were "strongly co-ordinating" gave greater growth inhibition as in the case of **$AmPy_2$** and **$AmGly_2$** (***Figure* 23**). This observation gives rise to what may be a general design principle for EDTA di-amides. When the dose responses of **$AmNH_2$**, **$AmBn_2$**, **$AmOMe_2$** and **$AmOH_2$** are considered in light of the possible lower metal ion affinities they may have (by analogy with similar **AmR_2** type ligands bearing non-coordinating pendant groups, as shown in ***Table 8***), the lower inhibition of *E. coli* growth, as for the **AmR_4** (***Figures 23 and 24***) ligands, is not unexpected.

These results seem to imply that strongly co-ordinating pendant groups on **AmR_2** ligands bolster metal binding in some way.

3.4. Effect of $AmGly_2$ and EDTA on cellular metal content

To directly assess the effect on *in cellulo* metal concentrations that incubating *E. coli* JM101 with **$AmGly_2$** and **EDTA** had, the metal concentrations of cells incubated in different concentrations of either ligand were interrogated through the use of ICP-MS (a background to the reasoning behind these experiments being given in ***Section 2.4***). Stationary phase cells were used in this part of the study, using concentrations of **$AmGly_2$** that measurably inhibited the growth of *E. coli* JM101 at stationary phase (10%) relative to control, as measured by use of a cell counter. Cells were incubated

in the presence of **EDTA** and **$AmGly_2$** in a mixture of 99:1 v/v TSB:0.2 M K_2HPO_4 containing 100x the concentration of the ligand under study. In each case, a blank containing no ligand (buffer exclusively) was run, against which the effects of metal depletion could be evaluated, and the data presented in ***Figure 26*** for **EDTA** and ***Figure*** for **$AmGly_2$**. These data represent some of the first insight into the effect of chelating ligands on the metal content of bacteria.[168, 169]

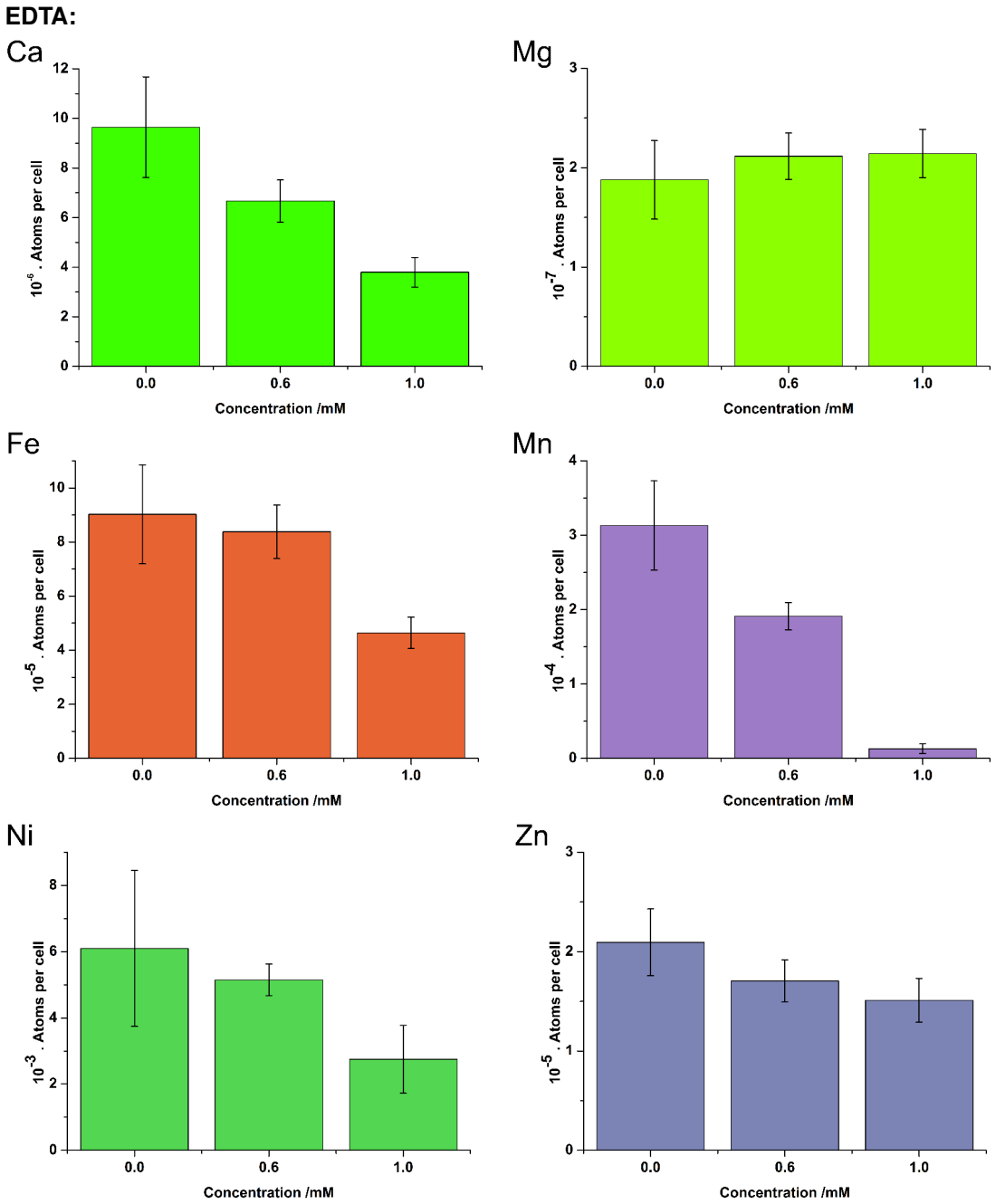

Figure 26: Changes in the number of metal atoms per *E. coli* JM101 cell at stationary phase measured by ICP-MS, following incubation with different concentrations of **EDTA**. Values are the average of three biological repeats. Error bars represent two standard deviations of the mean. Cells were incubated aerobically at 37°C for 16 h in a medium consisting of 99:1 v/v TSB:0.2 M K_2HPO_4 containing 100x [**EDTA**] prior to harvest.

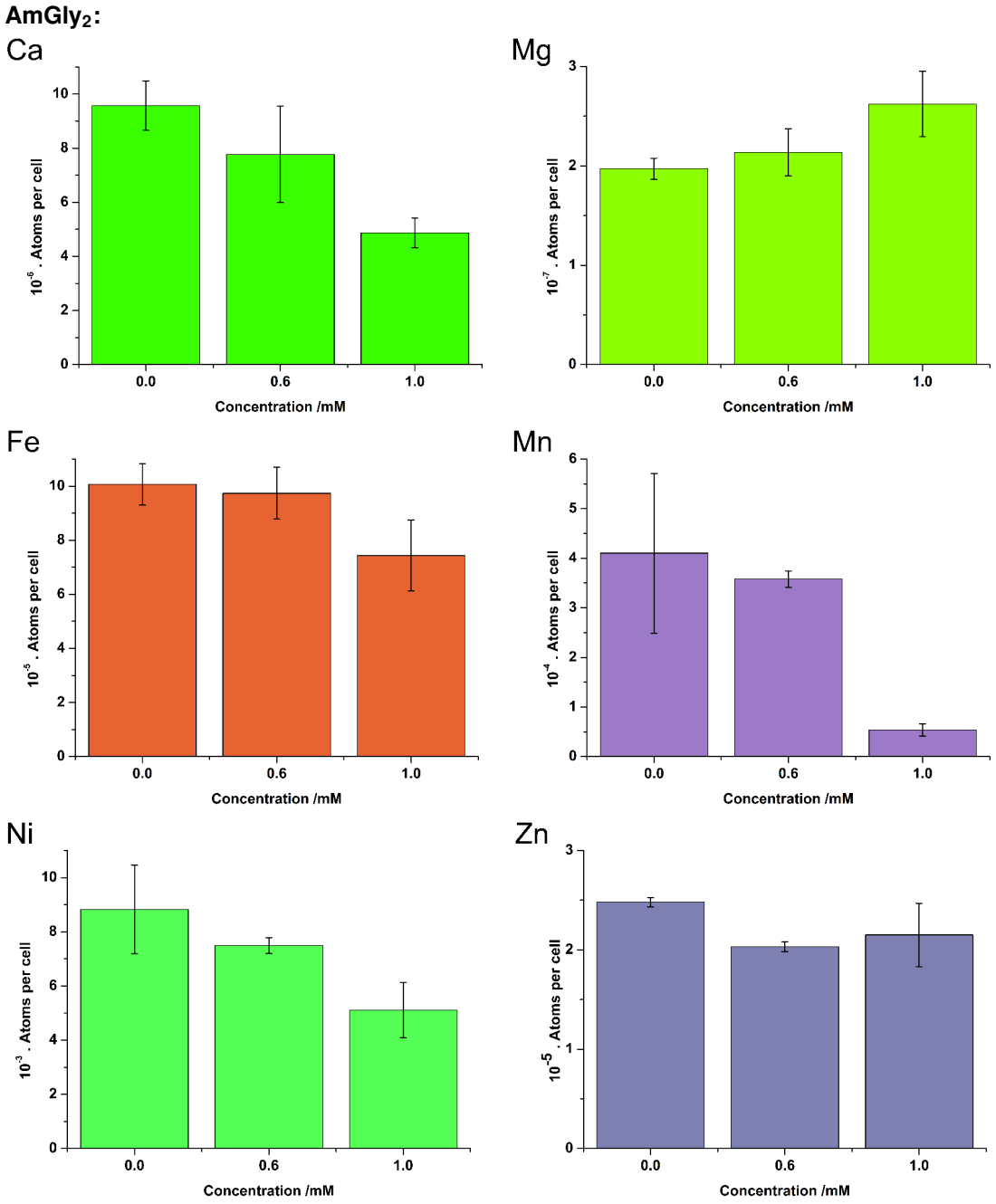

Figure 27: Changes in the number of metal atoms per *E. coli* JM101 cell at stationary phase measured by ICP-MS, following incubation with different concentrations of **AmGly$_2$**. Values are the average of three biological repeats. Error bars represent two standard deviations of the mean. Cells were incubated aerobically at 37°C for 16 h in a medium consisting of 99:1 v/v TSB:0.2 M K_2HPO_4 containing 100x [**AmGly$_2$**] prior to harvest.

For both **EDTA** and **AmGly$_2$**, the calcium concentration is reduced *in cellulo* , but **AmGly$_2$** affords less extensive depletion of the metal compared to **EDTA**. Depletion of calcium is not unexpected and may well be a signal of outer membrane disruption and lipopolysaccharide dispersion effects that the chelation of cellular group II metals brings about. More recently, the role of Ca^{2+} has been highlighted in the cell reproductive cycle,[170] and so the reduced stationary phase growth covered in ***Section 3.3*** may be a function of this effect also.

The concentrations of transition metals are also reduced; for instance that of iron, which is used in bacteria for protection against oxidative stress, for respiration and for reproduction. Given the high relative affinity for Fe^{3+} that **EDTA** has compared to **AmGly$_2$** (***Section 3.5***), the more extensive depleting effect it has compared to equal concentrations of **AmGly$_2$** is to be expected. *E. coli* also secretes *extremely* powerful Fe^{3+} chelators such as enterobactins to allow for uptake of Iron from the media into the cell, and so the tested ligands are likely in competition with such agents for Fe^{3+}.

The most striking depletion is that of manganese; based on the metal affinities of **EDTA** and **AmGly$_2$** and selectivities in solution, this observation is unexpected and represents a contradiction to the current understanding of chelator-induced cell damage as being a primarily by process mediated by Ca^{2+} and Mg^{2+} depletion. A good deal of attention has been directed towards the role of manganese in the survival and virulence of many bacterial species and strains. For instance, in *Salmonella sp.* , Mn^{2+} is used to protect against oxidative stress and is taken up from media most quickly in the log phase of growth. In *E. coli*, systems relevant to Mn^{2+} uptake are activated upon exposure to peroxide stress. It has also been proposed that Mn^{2+} sequestration by a host from a pathogen such as some *E. coli* or *Salmonella* strains is a defence mechanism against these pathogens.[108, 171–174] It is important to bear in mind that although the above findings demonstrate the importance of Mn^{2+} to bacterial growth, they do not show why such a pronounced depletion of Mn^{2+} is observed upon exposure to **EDTA** and **AmGly$_2$**, for which further work is necessary.

On the basis of data covered in the following section it is clear (and unsurprising) that **EDTA** and **AmGly$_2$** deplete transition and non-transition metals from *E. coli*. Yet the observation that **AmGly$_2$** gave more profound growth inhibition effects than **EDTA** at concentrations $\geq$2.5mM, despite the less extensive metal depletion it displayed at 1mM warrants further investigation.

3.5. Metal complexation studies

3.5.1. Potentiometric titrations on AmGly$_1$ and AmGly$_2$ (In collaboration with the University of Valencia)

At this point, the collection of some metal affinities via potentiometric titration was considered to assist in understanding the non-monotonic dose response of **AmGly$_1$** , the efficacy of **AmGly$_2$** and to elucidate the relationship, if any, between metal affinity and *in cellulo* metal depletion. It would *seem* that incorporating carboxylate pendent groups gave an increase in the first-row transition metal affinities of **AmGly$_1$** and **AmGly$_2$** compared to other **AmR$_x$** ligands and even **EDTA**, and could have led to more severe cellular metal depletion at lower concentrations. Since a pH range of 2-12 is conventionally used in a potentiometric titration, it was feasible that any pH-induced precipitation or hydroylsis events that may explain the observed dose response for **AmGly$_1$** would be observed during such experiments in the form of anomalous titration curves.

As an incentive, it is not uncommon to obtain X-ray quality crystals from samples of completed titrations at the extremes of pH. Where obtained, their analysis via X-ray crystallography provided structural information that could be used to further understand chelate stability (***Section 3.6***). Work in collaboration with the group of Prof. Enrique Garcia-España was thus commenced to characterise the binding of **AmGly$_1$** and **AmGly$_2$** to Ca^{2+} , Fe^{3+}, Mg^{2+}, Mn^{2+}, Zn^{2+} and H^+ ions. Binding data for **AmGly$_1$** and **AmGly$_2$** as a result of this study are listed and discussed below.

Protonation states. The most relevant protonation states for **AmGly$_1$** and **AmGly$_2$** with respect to complexation have been derived from chemical intuition because it is not trivial to determine the specific sites for deprotonation from pH-potentiometric experiments alone (***Figure 28***).[175]

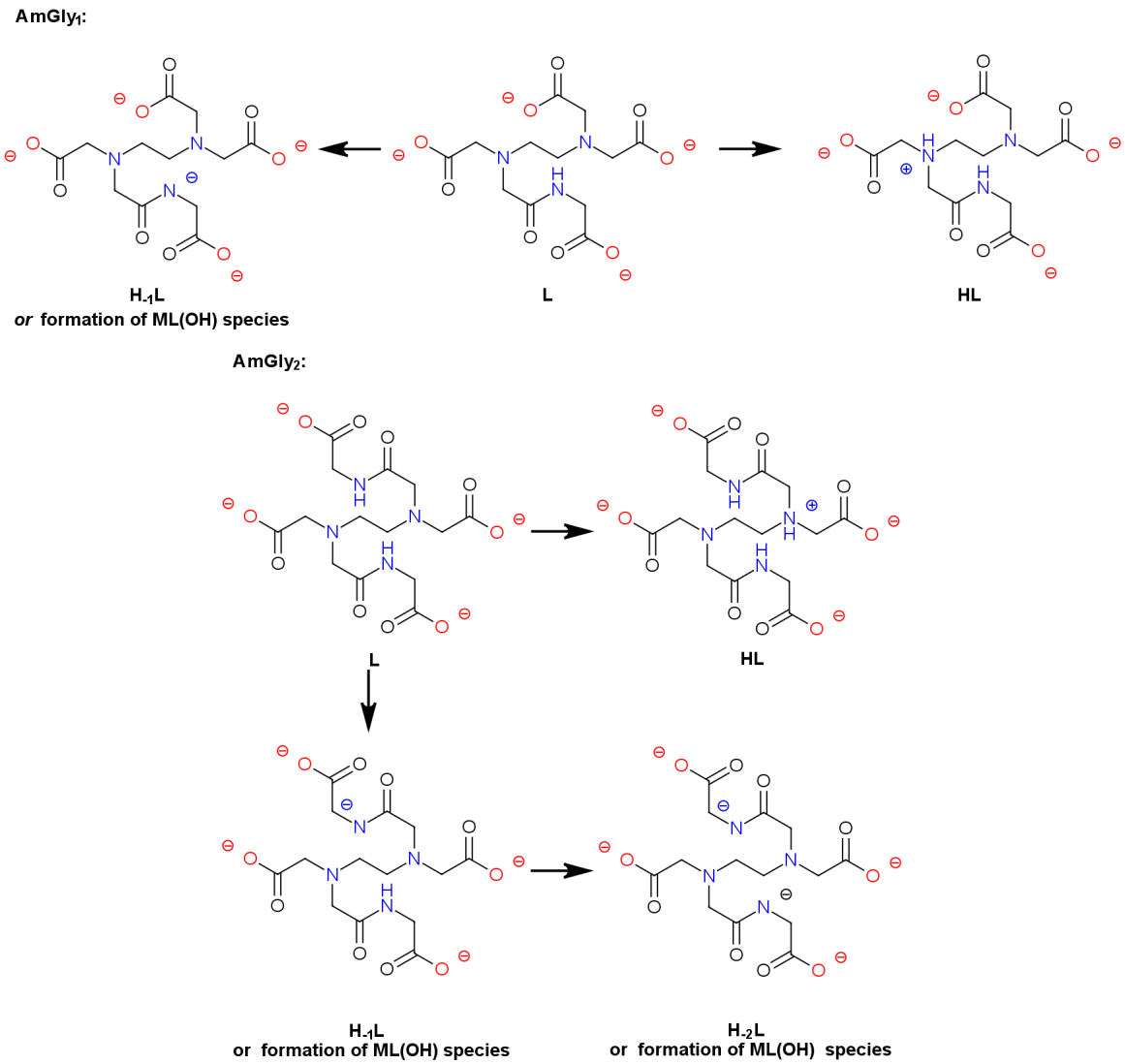

Figure 28: Protonation states for **AmGly$_1$** and **AmGly$_2$** most relevant for metal complexation.

Protonation constants. The agreement seen between the protonation constants published[176] for **AmGly$_2$** and from this work were pleasing, and discrepancies were attributed to the slight differences in experimental conditions. In the case of **AmGly$_2$**, similar pK_a values were also observed for other

AmR$_2$ type ligands,[127, 177]. From a comparison of entries ***a-d*** and ***e-h*** in ***Table 14***, the presence of two amide groups in **AmGly$_2$** lowers the pH at which a tertiary amine site of **AmGly$_2$** protonates to the cognate "**HL**" form (***Figure 28***) relative to **AmGly$_1$** or **EDTA**. This could be due to the electron withdrawing effect of the non-ionised amide groups.[127] Incidentally, the methylene bridges between the tertiary amine and amide groups of **AmGly$_2$** exhibit a higher chemical shift in the ^{1}H NMR spectrum at high pH, compared to the methylene bridges between the tertiary amine and the carboxylate groups suggesting the operation of such an inductive effect.

Table 14: Protonation constants for **AmGly$_1$ and AmGly$_2$** determined using pH-potentiometry, compared to reference values for **EDTA** (T=25°C, I=0.1 M unless otherwise indicated)[164] and previously published values for **AmGly$_2$**.[176] Values in brackets represent one standard deviation of the last significant figure. log K values without accompanying brackets are K_a values calculated from experimentally determined equilibria. Data for **AmGly$_1$** and **AmGly$_2$** are the average of two independent experiments, both performed at T=25°C and I=0.15 M KCl.

Entry	Equilibrium	Log K_a	Entry	Equilibrium	Log K_a	Entry	Equilibrium	Log K_a
	AmGly$_1$			**AmGly$_2$**			**EDTA**	
a	$\frac{[HL]}{[H][L]}$	9.76(1)	**e**	$\frac{[HL]}{[H][L]}$	7.26(1) *lit.* 7.37	**i**	$\frac{[HL]}{[H][L]}$	10.17
b	$\frac{[H_2L]}{[H][HL]}$	4.69(1)	**f**	$\frac{[H_2L]}{[H][HL]}$	4.18(2) *lit.* 4.38	**j**	$\frac{[H_2L]}{[H][HL]}$	6.11
c	$\frac{[H_3L]}{[H][H_2L]}$	4.19	**g**	$\frac{[H_3L]}{[H][H_2L]}$	3.53(2) *lit.* 3.51	**k**	$\frac{[H_3L]}{[H][H_2L]}$	2.68
d	$\frac{[H_4L]}{[H][H_3L]}$	2.27(2)	**h**	$\frac{[H_4L]}{[H][H_3L]}$	3.39(2) *lit.* 2.87	**l**	$\frac{[H_4L]}{[H][H_3L]}$	2.0
						m	$\frac{[H_5L]}{[H][H_4L]}$	1.5

i) Data taken at T=20°C, I=0.1 M.

Protonations at lower pH occur in similar ranges across **AmGly$_1$** and **AmGly$_2$**, but in all cases the protonation constants of **AmGly$_2$** are slightly lower, possibly due to the stronger inductive effect of the two amide groups. These protonations presumably occur on the acid groups in both **AmGly$_1$** and **AmGly$_2$**. Due to their distance from the amide groups the effect on protonation constant may not be as strong as for the amine protonations. Evidencing the role of amide groups in lowering protonation constants, it is seen that for EDTA all of the protonation constants are raised (***Table 14*** entries ***i-m***), relative to the amides.

Complexes of Calcium, Magnesium and Zinc. The most helpful equilibria are those expressed in the form $\frac{[ML]}{[M][L]}$, since they are independent of pH and so provide insight into how the ligand alone affects chelate stability. These data alongside the protonation constants for the complexes are presented in ***Table 15***.

Table 15: Metal-ligand association constants for **$AmGly_1$ and $AmGly_2$** determined using pH-potentiometry, compared to reference values for **EDTA** (T=25°C, I=0.1 M unless otherwise indicated)[164]. Values in brackets represent one standard deviation of the last significant figure. log K values without accompanying brackets are K_a values calculated from experimentally determined equilibria. Data for **$AmGly_1$** and **$AmGly_2$** are the average of two independent experiments, both performed at T=25°C and I=0.15 M KCl.

Entry	Equilibrium	Log K_a	Entry	Equilibrium	Log K_a	Entry	Equilibrium	Log K_a
	$AmGly_1$			**$AmGly_2$**			**EDTA**	
a	$\frac{[CaLH_{-1}][H]}{[CaL]}$	-11.56	**i**	$\frac{[CaLH_{-1}][H]}{[CaL]}$	-10.84			
b	$\frac{[CaL]}{[Ca][L]}$	9.31(2)	**j**	$\frac{[CaL]}{[Ca][L]}$	7.00(1)	**s**	$\frac{[CaL]}{[Ca][L]}$	10.61
c	$\frac{[CaHL]}{[H][CaL]}$	4.19	**k**	$\frac{[CaHL]}{[H][CaL]}$	3.39	**t**	$\frac{[CaHL]}{[H][CaL]}$	3.93[i]
			l	$\frac{[MgLH_{-1}][H]}{[MgL]}$	-10.69			
d	$\frac{[MgL]}{[Mg][L]}$	6.63(4)	**m**	$\frac{[MgL]}{[Mg][L]}$	5.10(2)	**u**	$\frac{[MgL]}{[Mg][L]}$	8.83
e	$\frac{[MgHL]}{[H][MgL]}$	5.6	**n**	$\frac{[MgHL]}{[H][MgL]}$	4.84	**v**	$\frac{[MgHL]}{[H][MgL]}$	3.85[i]
			o	$\frac{[ZnLH_{-2}][H]}{[ZnLH_{-1}]}$	-10.88			
f	$\frac{[ZnLH_{-1}][H]}{[ZnL]}$	-10.17	**p**	$\frac{[ZnLH_{-1}][H]}{[ZnL]}$	-9.07			
g	$\frac{[ZnL]}{[Zn][L]}$	14.11(3)	**q**	$\frac{[ZnL]}{[Zn][L]}$	10.41(2)	**w**	$\frac{[ZnL]}{[Zn][L]}$	16.44
h	$\frac{[ZnHL]}{[H][ZnL]}$	3.49	**r**	$\frac{[ZnHL]}{[H][ZnL]}$	3.59	**x**	$\frac{[ZnHL]}{[H][ZnL]}$	3.0

i) Data taken at T=20°C, I=0.1 M.

More extensive amide substitution, unsurprisingly, leads to reduced metal binding in all cases, this being due to the reduced donor strength an amide will possesses relative to a charged, carboxylate donor. The unstable [MLH_{-1}] and [MLH_{-2}] type species formed at high pH which are observed in the titrations of **AmGly$_1$** and **AmGly$_2$** (***Table 15, entries a,f,i,l,o***) could be due to the deprotonation of the amide groups of **AmGly$_1$** and **AmGly$_2$** but without further study of these complexes, e.g. via infrared spectroscopy, this assignment is not definite.

The electron-withdrawing character of the amide groups discussed in the previous section on protonation constants, is reflected in the reduced basicity of the Ca^{2+} and Mg^{2+} complexes of **AmGly$_2$** compared to **AmGly$_1$**, assuming that protonation takes place at a tertiary nitrogen site in both cases. In contrast, the Zn^{2+} complex of **AmGly$_2$** is slightly more basic than that of **AmGly$_1$**. Work from Santacruz[128] on the **EDTA1nap** ligand which has no peripheral coordinating groups, show very close agreement for the $\frac{[ZnL]}{[Zn][L]}$ equilibrium ($K_{\mathbf{EDTA1nap}}$= 10.1, $K_{\mathbf{AmGly_2}}$= 10.41, ***Table 8, entry c and Table 15, entry q***) showing that the protonation is not affected by the pendent carboxylates of **AmGly$_2$**.

Complexes of Iron and Manganese. Data for the transition metal complexes of **AmGly$_1$** and **AmGly$_2$** are presented in ***Table 16***.

Table 16: Transition metal-ligand association constants for **AmGly$_1$ and AmGly$_2$** determined using pH-potentiometry, compared to reference values for **EDTA** (T=25°C, I=0.1 M unless otherwise indicated)[164]. Values in brackets represent one standard deviation of the last significant figure. log K values without accompanying brackets are K_a values calculated from experimentally determined equilibria. Data for **AmGly$_1$** and **AmGly$_2$** are the average of two independent experiments, both performed at T=25°C and I=0.15 M KCl.

Entry	Equilibrium	Log K	Entry	Equilibrium	Log K	Entry	Equilibrium	Log K
	AmGly$_1$			**AmGly$_2$**			**EDTA**	
			g	$\frac{[FeLH_{-3}][H]}{[FeLH_{-2}]}$	-10.31			
			h	$\frac{[FeLH_{-2}][H]}{[FeLH_{-1}]}$	-10.11	**o**	$\frac{[Fe(OH_2)L][H]}{[Fe(OH)L]}$	-9.41[i]
a	$\frac{[FeLH_{-1}][H]}{[FeL]}$	-3.91	**i**	$\frac{[FeLH_{-1}][H]}{[FeL]}$	-3.61	**p**	$\frac{[Fe(OH)L][H]}{[FeL]}$	-7.49[i]
b	$\frac{[FeL]}{[Fe][L]}$	15.27(5)	**j**	$\frac{[FeL]}{[Fe][L]}$	11.81(2)	**q**	$\frac{[FeL]}{[Fe][L]}$	25.0
c	$\frac{[FeHL]}{[H][FeL]}$	3.06	**k**	$\frac{[FeHL]}{[H][FeL]}$	-	**r**	$\frac{[FeHL]}{[H][FeL]}$	1.3(1)[i]
d	$\frac{[MnLH_{-1}][H]}{[MnL]}$	-11.44	**l**	$\frac{[MnLH_{-1}][H]}{[MnL]}$	-10.33			
e	$\frac{[MnL]}{[Mn][L]}$	11.97(1)	**m**	$\frac{[MnL]}{[Mn][L]}$	9.28(2)	**s**	$\frac{[MnL]}{[Mn][L]}$	13.81
f	$\frac{[MnHL]}{[H][MnL]}$	3.62	**n**	$\frac{[MnHL]}{[H][MnL]}$	3.53	**t**	$\frac{[MnHL]}{[H][MnL]}$	3.1

i) Data taken at T=20°C, I=0.1 M.

Once again, the complexes that **AmGly$_1$** forms are more stable than those of **AmGly$_2$**. In fact, the stability of the Mn^{2+} complex of **AmGly$_1$** is similar to that of **EDTA**. Nevertheless, it is seen that amide

substitution once again decreases complex stability, especially so in the case of Fe^{3+}, likely due to the hard character of the ion and the charge stabilisation that results when Fe^{3+} is chelated by the tetranegative donor set of **EDTA**.

Work by Martell[176] using infra-red spectroscopy to investigate the coordination of Fe^{3+} to **$AmGly_2$** indicates that at higher pH the amide protons could be lost, enabling the assignment of the equilibria in ***Table 16 , entries h and i*** to the formation of complexes involving amide anions as donors. *

3.5.2. Ca^{2+} partitioning studies with Fura-2

For compounds where assessment via pH-potentiometry was not available, the relative Ca^{2+} affinity of a selection of EDTA-diamides was obtained via competition with **Fura-2** in the manner described in ***Section 2.5*** following a suitable calibration procedure. It is apparent that the **$AmGly_2$**-induced Ca^{2+} depletion from the **Ca-Fura-2** complex was more extensive than for the other **AmR_2** ligands which were statistically indistinguishable from one another in terms of Ca^{2+} scavenging ability (***Figure 29***).

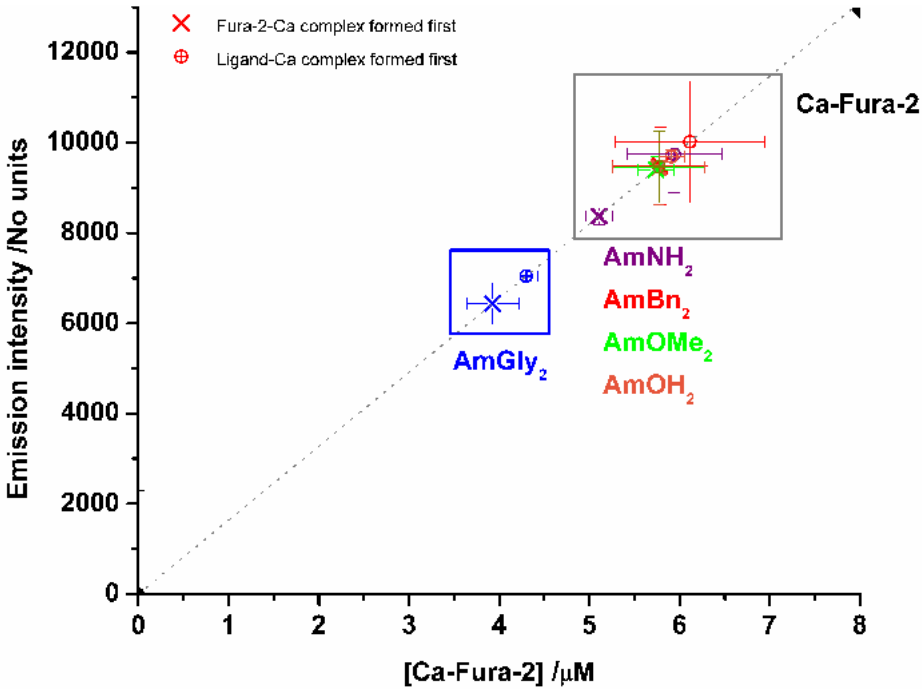

Figure 29: The effect of various **AmR_2** ligands on the fluorescence of the **Ca-Fura-2** complex, with calibration function shown in grey. Error bars represent two standard deviations from the mean of three replicates and were propagated from the error in the fitted gradient to give the *x* axis error bars. λ_{ex} =340 nm, λ_{em}=510 nm. [**Fura-2**]=12.25μM, [**AmR_2**]=10μM. Buffer: 10mM HEPES/100mM KCl at pH 7, T=26$\pm$1°C.

*The large discrepancy between these values and those of Martell does warrant closer examination and may be due to the differing approaches in calculating the stability constants; this work assumes that the complex between **$AmGly_2$** and Fe^{3+} forms over the course of the titration, whereas that of Martell assumes complete complex formation even at low pH.

Given the relation between $K_{a_{cond}}$ and K_a (also discussed in ***Section 2.5***), i.e. the fact that they are proportional to one another, the constant being the Schwarzenbach α-coefficient, then assuming the pK_a values between these **AmR$_2$** ligands are similar, the Ca^{2+} affinities will also be similar for these ligands.

3.5.3. Zn^{2+} partitioning studies with Fura-2

From the Irving-Williams series,[178] the binding of Zn^{2+} to **AmR$_2$** type ligands is expected to be stronger than that of Ca^{2+}. Based on this assumption and the equilibria presented in ***Table*** 8, Zn^{2+} partitioning studies were performed, in the hope that differences in binding strength between the ligands surveyed could be observed due to stronger interactions. Unfortunately, no significant differences between the **AmR$_2$** ligands were observed (***Figure 30***).

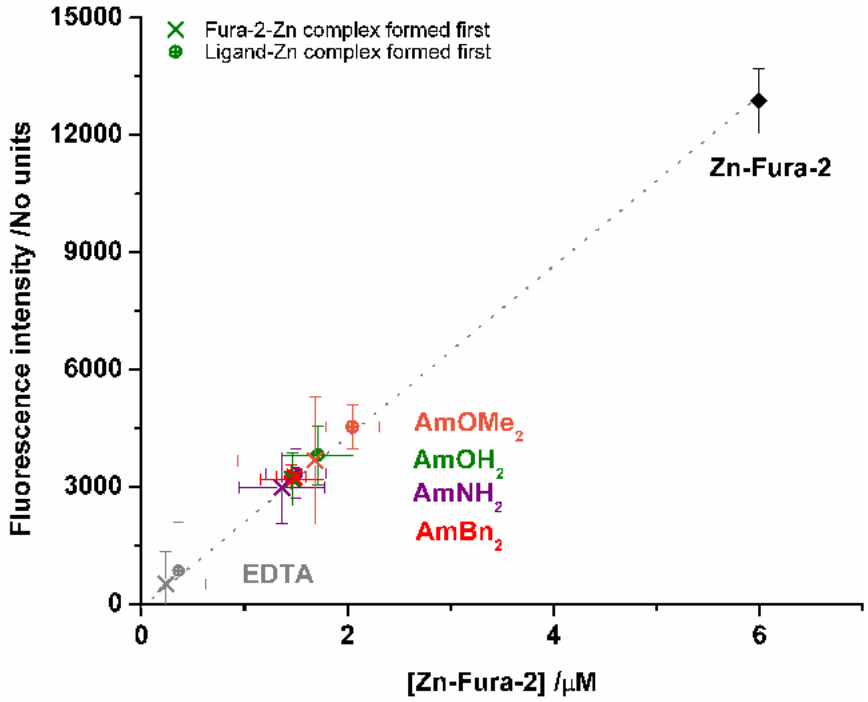

Figure 30: The effect of various **AmR$_2$** ligands on the fluorescence of the **Zn-Fura-2** complex, with calibration function shown in grey. Error bars represent two standard deviations from the mean of three replicates and were propagated from the error in the fitted gradient to give the *x* axis error bars. λ_{ex} =340 nm, λ_{em}=510 nm. [**Fura-2**]=9.8μM, [**AmR$_2$**]=10μM. Buffer: 10mM HEPES/100mM KCl at pH 7, T=26$\pm$1°C.

None of the **AmR$_2$** ligands studied exhibit stronger Zn^{2+} binding than **EDTA**, which is unsurprising given previous equilibrium information (***Table 8 and Table 15***). As an aside, when this experiment was performed it was noted that **EDTA** required a longer incubation time for equilibrium to be reached (ca. 30 minutes) than the **AmR$_2$** ligands. These kinetic effects may have profound effects on the inhibitory behaviour for the compounds and should not be overlooked, although they were beyond the scope of this work.

Given this partitioning data, it seems the **AmR_2** pendent groups are irrelevant to Zn^{2+} binding. If changing the pendent groups had no impact on Zn^{2+} binding, then a ligand with strongly coordinating pendent groups like **$AmGly_2$**would not be expected to bind more Zn^{2+} than any of the other **AmR_2** ligands, which would be in agreement with the potentiometric data, and something which called for experimental verification.

To investigate the effect of the pendent group on Zn^{2+} binding then, a variation on the Zn^{2+} partitioning experiment where the concentrations of **$AmOMe_2$**, **$AmGly_2$** were varied and competed against a constant concentration of **Zn-Fura-2** was performed. If the auxiliary groups of **$AmGly_2$** were binding Zn^{2+} to any appreciable degree, then **$AmGly_2$** ought to give greater **Zn-Fura-2** depletion than **$AmOMe_2$** at lower concentrations (***Figure* 31**), which would be observable in a reduced fluorescence intensity.

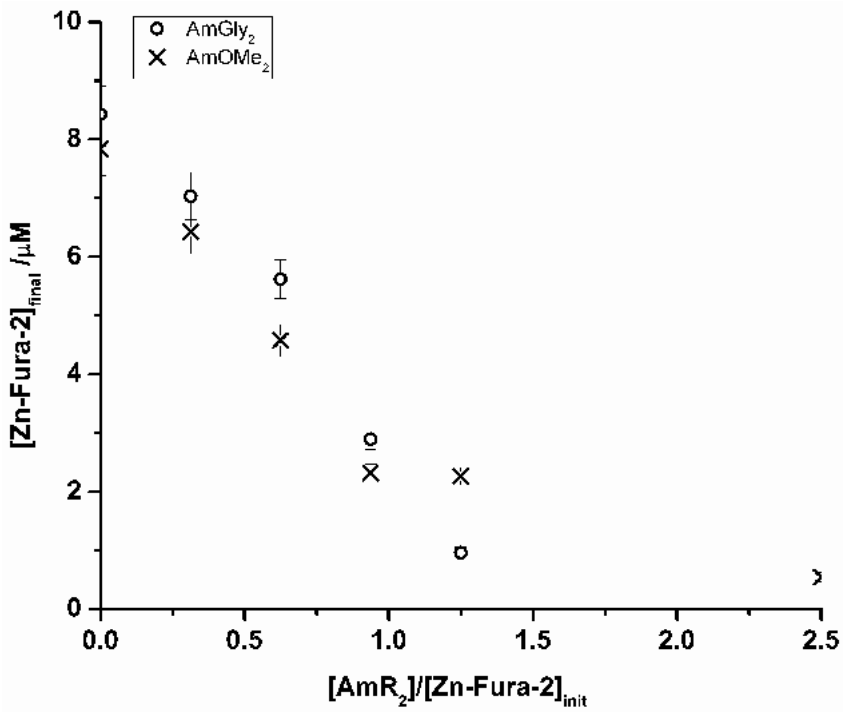

Figure 31: Zn-Fura-2 demetalation as a function of incoming **$AmGly_2$** and **$AmOMe_2$** equivalents. The error bars were estimated from the calibration function since only one run was performed. λ_{ex} =340 nm, λ_{em}=500 nm. [**Fura-2**]=10.0μM, [**AmR_2**]=10μM. Buffer: 10mM HEPES/100mM KCl at pH 7, T=26$\pm$1^{o}C.

There appears to be more extensive **Zn-Fura-2** demetalation for **$AmMeO_2$** at lower **AmR_2**:**Zn-Fura-2**, but the situation is reversed when the competing ligands are in excess. From this, it is implied that the pendent groups of **$AmGly_2$** *may* be involved in Zn^{2+} binding only when higher concentrations of **$AmGly_2$** are competed against **Zn-Fura-2**, possibly because of mass action or steric effects. Although the amide groups of **$AmGly_2$** can be treated as glycylglycine arms attached to a central ethylene diamine bridge, raising the possibility of complexes with higher nuclearity forming through the involvement of the pendent carboxylates, it appears that complexation of additional Zn^{2+}

ions is unfavourable based on ***Figure 31*** *and* preliminary titration data using two equivalents of Zn^{2+} (K_a = -1.51(3) for the $\frac{[Zn_2LH_{-2}][H]^2}{[Zn]^2[L]}$ equilibrium). This may be due to the first metal coordination event forcing **$AmGly_2$** into a geometry where the pendent carboxylates cannot interact with one another to form a chelating donor set (***Figure 34***).

In summary, based on the **Fura-2** studies, it can be seen that:

1. **$AmGly_2$** has a higher Ca^{2+} affinity than the **$AmNH_2$**, **$AmBn_2$**, **$AmOMe_2$** and **$AmOH_2$** ligands studied in this work, whose Ca^{2+} affinities are statistically indistinguishable from one another,

2. **$AmNH_2$**, **$AmBn_2$**, **$AmOMe_2$** and **$AmOH_2$**all have statistically indistinguishable Zn^{2+} affinities. All of these binding strengths are lower than those of **EDTA**.

3. The pendent carboxyl groups of **AmGly2** do not appear to assist in Zn^{2+} binding compared to another, **AmR_2** ligand, **$AmOMe_2$**.

3.6. Structures of EDTA-amide metal complexes in the solid state (In collaboration with the University of Valencia)

Structure of the Mg^{2+} complex of $AmGly_2$. This compound crystallised out of an aqueous solution at pH 11 following the addition of 1 equivalent of magnesium nitrate and slow evaporation, which is the first reported Mg^{2+} chelate of any **EDTA** di-amide* and demonstrates the lack of involvement of the peripheral carboxylate groups in chelation (***Figure 32***), substantiating the conclusions drawn from data in ***Table 8*** and ***Figures 3.5.3*** and ***31***. Although these groups do participate in an extended coordination network of **Mg-$AmGly_2$** molecules linked by hydrated Na^+ ions, possibly due to the crystallisation conditions. This behaviour is similar to other published structures of **EDTA**-amides with pendent coordinating groups such as carboxylic acids, phenols,[179] thioethers[180] and uracil derivatives[181], where the pendent groups either participate in hydrogen-bonding, co-ordination with alkali metals or have no discernible effect on the long-range structure.

*Based on a CCDC substructure search using the SMILES string O=C(N)CN(CC(O)=O)CCN(CC(=O)O)CC(=O)N as input on the WebCSD interface.

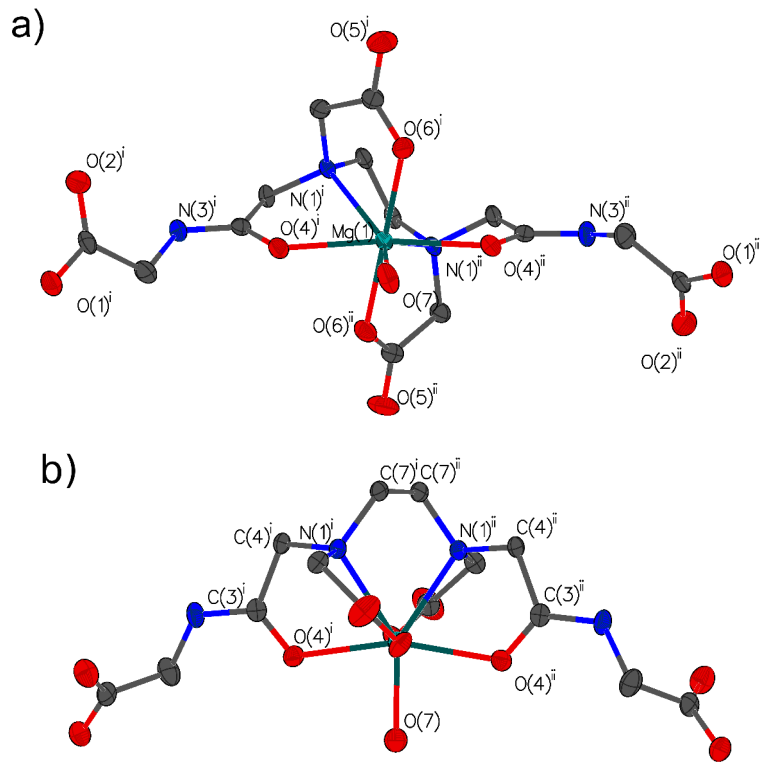

Figure 32: a) Single crystal structure of the Mg^{2+} complex of **$AmGly_2$** (**Mg-$AmGly_2$**, **$AmGly_2$** is in the "L" form, ***Figure 28***) viewed down the *b*- axis. **b)**: The same structure viewed perpendicular to the *b*-axis illustrating the equatorial coordination around the central Mg^{2+} ion. Counter-ions, hydrogen atoms and outer-sphere water molecules omitted for clarity. Ellipsoids represent 50% probability.

The Mg^{2+} ion displays an unusual seven-coordinate geometry in a distorted pentagonal bipyramidal arrangement with O(4)-Mg-N(1), $N(1)^{i}$-Mg-$N(1)^{ii}$ and O(4)-Mg-O(7) bite angles of 69.9°, 73.9°and 81.3° respectively. One **$AmGly_2$** ligand supplies six of the donor groups ($N(1)^{i}$, $N(1)^{ii}$, $O(4)^{i}$, $O(4)^{ii}$, $O(6)^{i}$ and $O(6)^{ii}$), and the seventh O(7), comes from water. In a plane defined by $O(4)^{i}$, O(7) and $O(4)^{ii}$ with Mg(1) as the central atom, $N(1)^{i}$ and $N(1)^{ii}$ are both out of plane by 18°. Bite angles close to 90° exist between $O(6)^{i}$, $O(6)^{ii}$ and O(7), indicating that the distortion observed in the coordination sphere arises due to the geometry that **$AmGly_2$** is forced into upon coordinating with Mg^{2+} and not "external" ligands exerting a steric influence. Other key measurements are enumerated in (***Table 17***). The interested reader is directed to ***Appendix C.1*** for a full listing refinement parameters.

Table 17: Selected angles and bond distances for **Mg-AmGly$_2$**. Bracketed values are the standard deviation of the last figure.

Bond lengths		Bond angles		Torsion angles	
Bond	**Length / Å**	**Atoms**	**Angle /°**	**Atoms**	**Angle /°**
Mg(1)—O(4)	2.2341(19)	O(4)^{i}—Mg(1)—O(4)^{ii}	162.53(13)	Mg(1)—O(4)—C(3)—N(3)	178.4(2)
Mg(1)—O(6)	2.088(2)	O(4)^{i}—Mg(1)—N(1)^{ii}	125.87(9)	Mg(1)—N(1)—C(4)—C(3)	39.5(2)
Mg(1)—N(1)	2.422(3)	O(4)^{i}—Mg(1)—N(1)^{i}	69.92(8)	Mg(1)—N(1)—C(7)^{i}—C(7)^{ii}	41.0(3)
Mg(1)—O(7)	2.051(3)	O(6)^{i}—Mg(1)—O(4)^{ii}	79.46(8)	O(4)—C(3)—C(4)—N(1)	-28.9(3)
O(4)—C(3)	1.244(4)	O(6)^{ii}—Mg(1)—O(4)^{ii}	100.66(8)	N(3)—C(3)—C(4)—N(1)	152.3(2)
N(1)—C(7)	1.480(4)	N(1)^{i}—Mg(1)—N(1)^{ii}	73.93(11)	C(4)—N(1)—C(7)^{i}—C(7)^{ii}	-78.7(3)
N(1)—C(4)	1.463(4)	O(6)^{ii}—Mg(1)—N(1)^{ii}	105.98(9)	C(7)—N(1)—C(4)—C(3)	160.4(2)

In an attempt to see how the selectivity of **AmGly$_2$** relates to structural factors, analogies can be drawn with published structures in the CCDC. * For example, the structure of the Zn^{2+} complex of the ligand **AmTyr$_2$** (CCDC entry code:TITJOW)[179] shows that the amide oxygen atoms interact more strongly with the metal ion than those of **AmGly$_2$** with Mg^{2+} from a comparison of bond lengths (d(Mg—O)=2.23 Å in **AmGly$_2$** cf. d(Zn—O)=2.13 Å in **Zn-AmTyr$_2$** , ***Figure*** 33).

*Unfortunately, most **AmR$_2$** complex structures deposited in the CCDC are for metals whose binding behaviour was not characterised in this work.

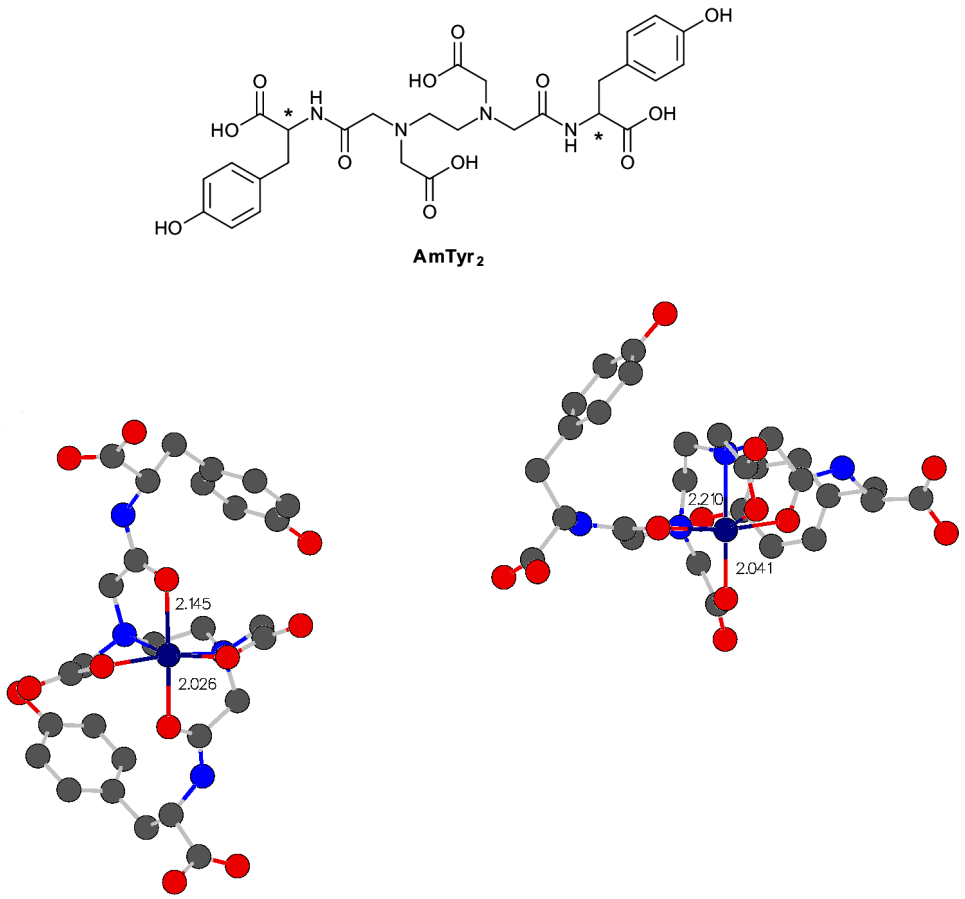

Figure 33: Crystal structure of **AmTyr$_2$** adapted from Fisher[179] with key bond lengths displayed.

In addition, the tertiary metal-amine interactions are stronger in **Zn-AmTyr$_2$** compared to **Mg-AmGly$_2$**(d(N-Mg) **Zn-AmTyr$_2$**= 2.13 Å cf. d(N-Mg) **Mg-AmGly$_2$** = 2.42 Å), yet the carboxylic acid-metal distances are almost the same. **Zn-AmTyr$_2$**, like other complexes of **AmR$_2$** ligands, exhibits a distorted coordination geometry possibly due to sub-optimal matching between the chelate ring size and metal ionic radius.

Ca complex of AmGly$_1$. In this binuclear complex, which crystallised from alkaline solution in the presence of stoichiometric $CaCl_2$, one of the carboxylate donors from a single **AmGly$_1$** ligand acts as a bridging ligand to another crystallographically identical Ca^{2+} core (***Figure 34***). Like **Mg-AmGly$_1$**, the Ca^{2+} ions in **Ca-AmGly$_1$** have water molecules (also coordinating with Na^+) coordinated to give the final eight-coordinate dicapped octahedral geometry around the metal ions. Once again the pendent carboxylate does not participate in chelation of the central (or other) Ca^{2+} ions, instead participating in networks through interactions with hydrated sodium cations giving a final polymeric structure (not shown).

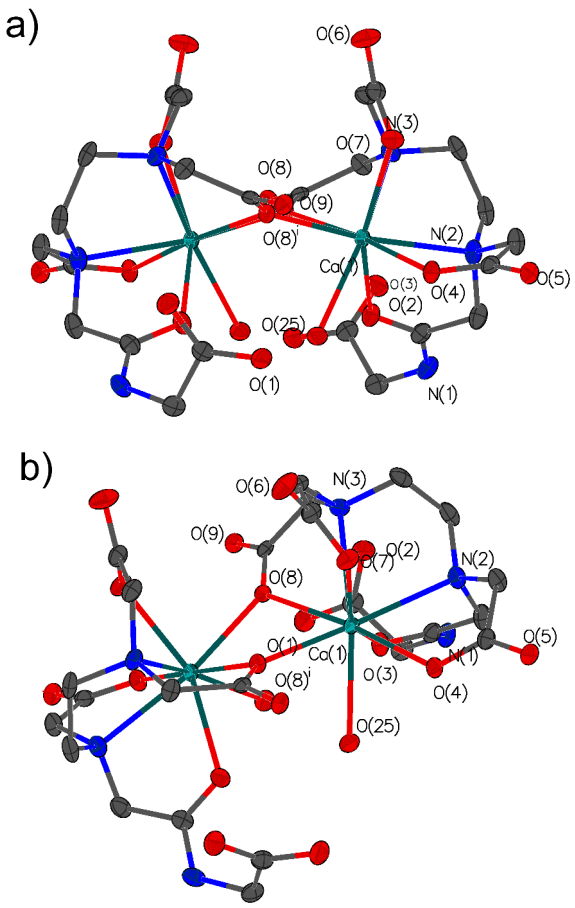

Figure 34: a) Single crystal structure of the Ca^{2+} complex of **AmGly$_1$** (**Ca-AmGly$_1$**, **AmGly$_1$** is in the "L" form, ***Figure 28***) viewed down the *c*- axis. **b)**: The same structure rotated to show the bridging carboxylate interaction. Counter-ions, hydrogen atoms and outer-sphere water molecules are omitted for clarity. Ellipsoids represent 50% probability.

Unlike **Mg-AmGly$_2$**, and **Zn-AmTyr$_2$**, all of the carbonyl-Ca^{2+} bond lengths are similar, indicating that the amide carbonyl oxygen O(3) has a bond strength to the central Ca^{2+} ion as the carboxylate oxygens. Comparison of the Ca^{2+}- tertiary amine bond lengths (d(Ca(1)—N(2)) and d(Ca(1)—N(3)) = 2.58 and 2.60 Å respectively) to those measured for the Ca^{2+} complex of **12edtaenH$_2$** (**Ca-12edtaenH$_2$**, CCDC entry: TEZSAS, ***Figure 35***),[182] shows that the tertiary amines in **Ca-AmGly$_1$** interact more strongly than those in **Ca-12edtaenH$_2$** (***Table 18***).

Table 18: Selected angles and bond lengths for **Ca-AmGly$_1$**. Bracketed values are the standard deviation of the last figure.

Bond lengths		Bond angles	
Bond	**Length / Å**	**Atoms**	**Angle /°**
Ca(1)—O(25)	2.536(3)	O(25)—Ca(1)—N(3)	163.92(10)
Ca(1)—O(4)	2.351(3)	O(25)—Ca(1)—N(2)	113.41(10)
Ca(1)—O(3)	2.421(3)	O(4)—Ca(1)—O(25)	71.15(9)
Ca(1)—O(7)	2.420(3)	O(4)—Ca(1)—N(2)	67.66(10)
Ca(1)—O(8)	2.449(3)	O(4)—Ca(1)—O(7)	78.26(10)
Ca(1)—O(8)^{i}	2.342(3)	O(4)—Ca(1)—O(8)	174.03(9)
Ca(1)—N(3)	2.597(3)	O(4)—Ca(1)—N(3)	122.76(10)
Ca(1)—N(2)	2.577(3)	N(2)—Ca(1)—N(3)	69.59(11)

The stronger interaction with the metal may arise from the presence of five C=O-calcium interactions in **Ca-AmGly$_1$** drawing the Ca^{2+} ion closer into the chelating cavity than in **Ca-12edtaenH$_2$**, which only has four C=O-calcium interactions. This is because of the structure of **12edtaenH$_2$** which appears to force one of the amide groups into a position where it is unable to coordinate to the central Ca^{2+} core. On comparison of their $\frac{[ML]}{[M][L]}$ association constants also, the large difference in Ca^{2+} between **AmGly$_1$** and **12edtaenH$_2$** (log K_a(**AmGly$_1$**)= 9.31 *cf.* log K_a(**12edtaenH$_2$**)= 3.5) may be due to the contributions of these bonds to chelate stability.

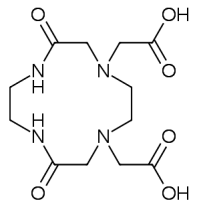

12edtaenH $_2$

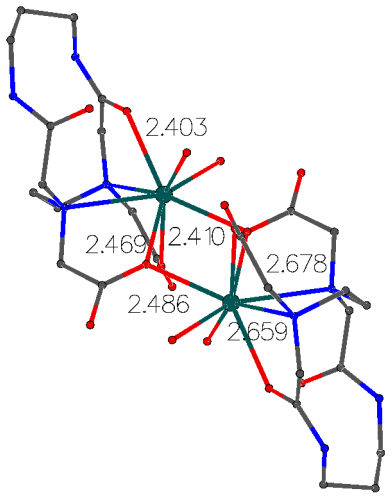

Figure 35: Crystal structure of **Ca-12edtaenH$_2$** adapted from Inoue[182] with key bond lengths displayed.

3.7. The relationship between metal affinity and biological activity

From the data discussed in ***Sections 3.3 and 3.5***, there seems to be little correlation between metal affinity for the ions studied and *E. coli* growth inhibition. In fact, based on the metal affinities obtained via potentiometry and the metal partitioning profiles obtained from **Fura-2** competition experments, it would be expected that **$AmGly_2$** would be inferior to **EDTA** for *E. coli* growth inhibition, in line with the metal uptake data presented in ***Figures 26 and 27***. Thus, the observation that **$AmGly_2$** is more effective than **EDTA** contradicts the understandings that chelating ligands are more effective as bacterial growth inhibitors when their metal affinity is higher,[31, 34, 183] and that Ca^{2+} and Mg^{2+} depletion are the main cause of growth inhibition in Gram-negative organisms exposed to chelating ligands,[1, 23, 184, 185]. This contradiction persists even when protonation constants are accounted for to calculate $K_{a_{cond}}$ values at a pH of 7.4 from $\frac{[ML]}{[M][L]}$ equilibria (***Figure 19***) using the Schwarzenbach α-coefficient described in (***Section 2.5***).

Table 19: $K_{a_{cond}}$ values calculated for pH=7.4 to closer reflect the metal affinity of **$AmGly_1$**, **$AmGly_2$** and **EDTA** in liquid media.

Row	Equilibrium quantity	$AmGly_1$	$AmGly_2$	EDTA
a	α-coefficient	4.34×10^{-3}	5.80×10^{-1}	1.61×10^{-3}
b	K_a (Ca^{2+})	9.31	7.00	10.61
c	$K_{a_{cond}}$ (Ca^{2+})	6.95	6.76	7.82
d	K_a (Mg^{2+})	6.63	5.10	8.83
e	$K_{a_{cond}}$ (Mg^{2+})	4.27	4.86	6.04
f	K_a (Fe^{3+})	15.27	11.81	25.0
g	$K_{a_{cond}}$ (Fe^{3+})	12.9	11.6	22.2
h	K_a (Mn^{2+})	11.97	9.28	13.81
i	$K_{a_{cond}}$ (Mn^{2+})	9.61	9.04	11.0
j	K_a (Zn^{2+})	14.11	10.41	16.44
k	$K_{a_{cond}}$ (Zn^{2+})	11.7	10.2	13.65

A further implication is that the greater inhibition of *E. coli* growth exhibited by **$AmGly_2$** and **$AmPy_2$** compared to **EDTA**, is not likely to arise from the strongly coordinating pendent groups increasing metal affinity. It also seems unlikely that multinuclear complex formation takes place based on the data in ***Figures 32-35***, and the **Fura-2** work described in ***Section 3.5.3***.

The measurement of partition coefficients was thus undertaken on **$AmGly_1$** and some **AmR_2** ligands to evaluate the influence of lipophilicity on bacterial growth inhibition and to determine if the ligands could operate *in cellulo*.

3.8. Lipophilicity measurements

3.8.1. Estimation of partition coefficients (*P*)

To gauge the lipophilicity of a representative selection of EDTA-Amides, the partition coefficients of the free ligands and their respective Fe^{3+} complexes were measured. The preparation of Fe^{3+} complexes was straightforward and adapted from literature procedures. Following stirring in aqueous solution, subtle pH changes could be used to precipitate uncomplexed Fe^{3+} as polymeric *hydroxo*-species.. The presence of the Fe^{3+} complex could then be confirmed by the presence of an LCMS peak at the expected m/z ratio, high-resolution mass spectrometry and comparison of calculated and observed isotope ratios.

Although it was desirable to keep the organic phase consistent to ease comparisons of free ligands and their Fe^{3+} complexes, the use of deuterated dichloroethane for the number of ^1H NMR measurements necessary was inconvenient when volumes conducive to accurate handling were used. Consequently, free ligand partition coefficients correspond to the quantity P_{CDCl_3} (***Section 2.6***), and were performed in the PBS*:$CDCl_3$ system. This is in contrast to the PBS:1,2-dichloroethane system used for the Fe^{3+} complexes, for which P_{DCE} is measured.

On account of their varied inhibition profiles, **EDTA**, **$AmGly_1$**, **$AmGly_2$** and **$AmBn_2$** and the heterocycle acridine (for which a P_{DCE} is known)[124] were selected for study. In the cases of **$AmGly_1$** and **$AmGly_2$**, the speciation in both the free and complexed states was known due to the potentiometric work described in ***Section 3.5***. Following an appropriate calibration procedure, absorbance monitoring in DMSO could then be used to measure the P_{DCE} values (**Table 20**).

*The PBS composition was different to the traditional recipe[186] and was prepared from: K_2HPO_4 0.075 mol dm^{-3}, KH_2PO_4 0.025 mol dm^{-3}, KCl 0.15 mol dm^{-3} and adjusted to pH 7.4 .

Table 20: PBS:1,2-Dichloroethane partition coefficients (P_{DCE}) for the Fe^{3+} complexes of **$AmGly_1$**, **$AmGly_2$**, **$AmBn_2$** and acridine at a buffer pH of ≈7.4 . Data are the average of two independent experiments. Error margins represent two standard deviations from the mean. Unless otherwise indicated, speciation curves generated from the data discussed in ***Section 3.5.1*** were used to determine ligand charges at the experimental pH.

Row	Species	Charge at pH	P_{DCE} / **No units**
a	**Fe-$AmGly_1$**	-2	0 ± 0[i] (extremely hydrophilic)
b	**Fe-$AmGly_2$**	-2	0 ± 0[i] (extremely hydrophilic)
c	**Fe-$AmBn_2$**	0[ii]	0.002 ± 0.006[i] (extremely hydrophilic)
d	**Fe-EDTA**	-0	0 ± 0[i] (extremely hydrophilic)
e	**Acridine**	0	Undefined[iii] (*lit.* 3.57)[124] (extremely hydrophobic)

i) No detectable absorption in dichloroethane layer. **ii)** Estimate based on the work of Santacruz[128] and Martell[176]. **iii)** No detectable absorption in buffer layer

Under the conditions of the experiment (without specialised techniques, extreme *P* values cannot be measured accurately)[124] it appears that neither the incorporation of lipophilic groups, as in the case of **Fe-$AmBn_2$**, or the number of amide groups (as shown by the lack of partitioning for **Fe-$AmGly_1$**) result in any increase in lipophilicity relative to **Fe-EDTA**. Based on the extremely low P_{DCE} values obtained for all of the complexes, it would not appear that, under the conditions of the growth curve experiments (***Section 3.3***), that any of these Fe^{3+} complexes will be able to traverse a lipid membrane.

The same can be said of the free ligands, the P_{CDCl_3} values of which were measured at a pD of approximately 7.4. From these data, it is surmised that these ligands are unlikely to be able to penetrate a lipid membrane, even when the apparent charge on a ligand is low (***Table 21***).

Table 21: PBS:chloroform partition coefficients (P_{CDCL_3}) for the ligands **$AmGly_1$**, **$AmGly_2$**and **$AmBn_2$**. Bracketed values are the measured pD of the buffer system. Unless otherwise indicated, speciation curves calculated from the data discussed in ***Section 3.5.1*** were used to determine ligand charges at the experimental pH.

Entry	Species	Charge at pH	P_{CDCl_3}/ **No units**
a	**$AmGly_1$**	-3 (7.4)	0[i]
b	**$AmGly_2$**	-3 or -4[ii] (7.4)	0[i]
c	**$AmBn_2$**	-1 or -2[ii, iii] (7.5)	0
d	**EDTA**	-2 or -3 (7.4)[ii,iv]	0[i]

i) No detectable signal in chloroform layer. **ii)** The experimental pH is close to the pK_a values of these ligands meaning appreciable amounts of either charge state are likely to be present. **iii)** Estimate based on the work of Danil de Namor.[127] **iv)** Estimate based on the work of Delgado.[187]

Based on the partition coefficient data shown above, it is suggested that the ligands may interact with the surface of the *E. coli* outer membrane (***Section 1.2***), but are unlikely to traverse the hydrophobic inner membrane to sequester intracellular metal in the event of outer membrane permeabilisation. If this is the case, then it is reasonable to assume that any metal that the cells are being starved of, resides in the aqueous growth medium, and has not been taken up into the cell, or resides on the cell surface, e.g. in certain metalloproteins.*

3.9. Conclusions for this chapter

A selection of $\mathbf{AmR_x}$ (**x**=1, 2, 4) ligands has been synthesised and characterised using two main approaches. The first of these was the nucleophilic ring-opening of the bis-anhydride of **EDTA** (***Scheme 7***) in a one-step synthesis in which protecting groups were unnecessary, and the second involved the use of successive alkylations on protected amine intermediates (***Scheme 9***). Although route **B** appeared more laborious at first glance, the difficulty in purifying the crude products furnished in attempts to prepare a number of $\mathbf{AmR_2}$ ligands from the bis-anhydride of **EDTA**, alongside the general applicability of route **B** to different degrees of amide substitution, *and* the facile chromatographic purification of the relevant intermediates, meant that it was selected as the primary method for the synthesis of the $\mathbf{AmR_x}$ ligands discussed in this part of the work.

The ability of the synthesised ligands to inhibit the growth of *E. coli* JM101 was then assessed, to give a ranking of the synthesised ligands (***Figure 36***). From these experiments, it was apparent that $\mathbf{AmR_2}$ ligands with pendent groups that are able to strongly coordinate to metal ions are the most inhibitory activity at a ligand concentration of 2.5 mM.

*While partition coefficient measurements of divalent metal cations such as Zn^{2+} or Mn^{2+} seemed lucrative to assess the effect of overall complex charge on lipophilicity, these measurements were not performed. This was after a consideration of the charges of the free ligands and their Fe^{3+} complexes, showing that the most and least charged forms of these ligands had been studied, and both forms were extremely hydrophilic. Since metal-specific effects on *P* are unlikely,[188] it is predicted that complexes of divalent metals with $\mathbf{AmGly_1}$, $\mathbf{AmGly_2}$ and $\mathbf{AmBn_2}$ will also reside in the buffer layer exclusively due to their respective charges.

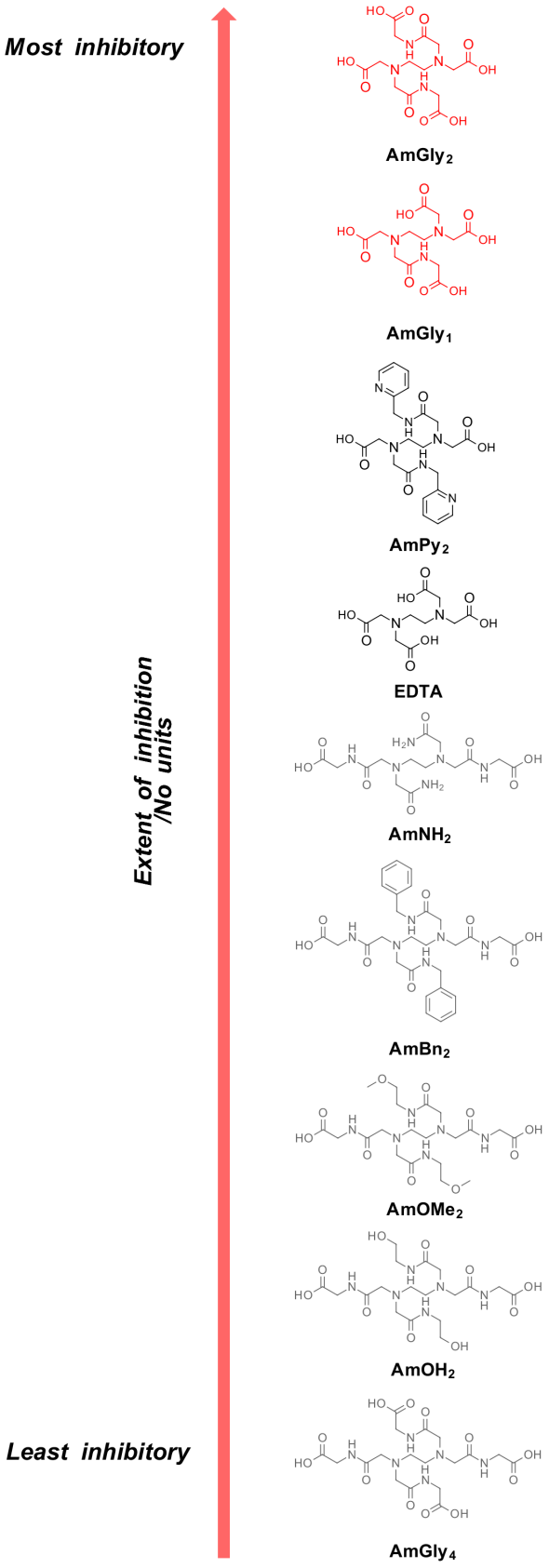

Figure 36: A ranking of the *E. coli* JM101 growth inhibition at [**L**]=2.5 mM for the synthesised **AmR$_x$** ligands (**AmPhe$_4$** excluded). Strongly inhibiting ligands are shown in red, moderately inhibiting ligands in black, and weakly inhibiting ligands in grey.

Metal ion binding data for the binding of **$AmGly_1$** and **$AmGly_2$** to Ca^{2+}, Mg^{2+}, Fe^{3+}, Mn^{2+} and Zn^{2+}, were collected by potentiometric titration, in collaboration with the University of Valencia, alongside estimations of the binding strength of **$AmBn_2$, $AmNH_2$, $AmOH_2$** and **$AmOMe_2$** to Ca^{2+} and Zn^{2+} using **Fura-2** competition experiments. These competition experiments showed that the binding strength of these ligands to Ca^{2+} and Zn^{2+}, is statistically indistinguishable under the experimental regime used.

It has also been found that the cellular manganese concentration of *E. coli* JM101 is reduced drastically when cultures are treated with **EDTA** or **$AmGly_2$**, which suggests that these ligands may exert an inhibitory effect beyond the disruption of the *E. coli* LPS outer layer. Consideration of the metal depletion data alongside the metal ion binding and inhibition data for *E. coli* collected for these ligands, indicates that there is little correlation between metal ion affinity (even when adjusted for solution pH) and the extent of inhibition, but there may be a link to the extent of manganese depletion and Mn^{2+} affinity.

To see whether membrane effects could be assigned to the unexpected, superior inhibition of **$AmGly_2$** compared to **EDTA** , partition coefficients were measured for selected free ligands and their Fe^{3+} complexes. No significant partitioning into the organic layers used were observed, indicating membrane activity is unlikely to contribute to inhibition effects. It is suggested that the kinetics of metal binding for ligands that are more effective than **EDTA** in the inhibition of *E. coli* (i.e. **$AmGly_2$** and **$AmPy_2$**) are considered as an additional line of enquiry into their success, on account of the short lag phase observed in their growth curves and the importance of lag phase to metal uptake and cell health.[108, 189]

4. Synthetic and biological studies on ligands bearing phenol groups

4.1. Introduction and motivations

Iron (in both +2 and +3 oxidation states) is important to bacterial life. As an example, the ability of the metal to cycle between oxidation states (+2 and +3) may be why iron cores are found in many bacterial superoxide dismutase enzymes,[190] which transform the reactive oxygen species O_2^- into oxygen or hydrogen peroxide. Cytochromes, which are important for respiratory processes, can also contain iron cores (e.g. Cytochrome d in *E. coli*)[191]. Such cores are implicated in the reduction of molecular oxygen into water as part of the electron transfer chain.

Fe^{3+} is the dominant oxidation state in aerobic environments and is speciated primarily as polynuclear, insoluble complexes at neutral to alkaline pH, meaning that the free, soluble Fe^{3+} concentration is very low.[192] It is no surprise then, that bacteria and plants have evolved elegant transport systems which enable solubilisation and movement of environmental Fe^{3+} into their respective cell membranes. Such systems contribute to the virulence of pathogenic bacteria in vertebrate hosts by enabling iron acquisition from host organisms (where most of the iron is either intracellular or complexed),[193] facilitating pathogen growth.

These iron transport systems generally work by secreting *extremely* powerful Fe^{3+} chelating ligands such as those in ***Figure 37***. The Fe^{3+} complexes of these molecules are then recognised by cell membrane receptors and can then be moved into the cytoplasm where further reactions take place to liberate the ion for use *in cellulo*.[43, 194]

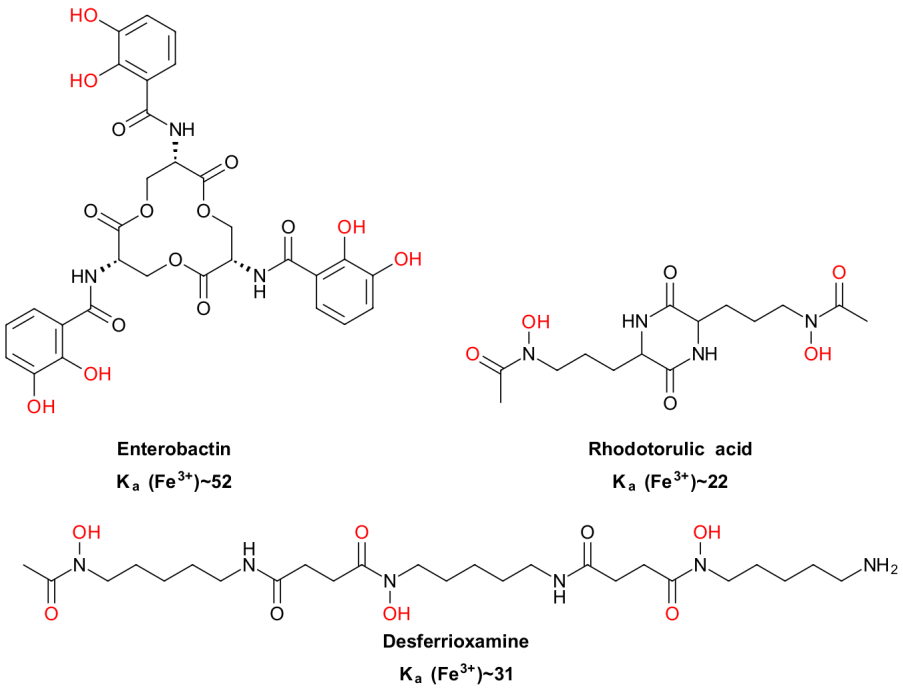

Figure 37: Chelating ligands secreted by bacteria to solubilise and transport Fe^{3+}. Donor atoms for the Fe^{3+} chelates of these ligands are shown in red. K_a values correspond to the $log(\frac{[ML]}{[M][L]})$ equilibrium (the deprotonated ligand + metal) for Enterobactin[195] and Desferrioxamine[196] and $log(\frac{[ML_2]}{[M][L]^2})$ for Rhodotorulic acid.[197]

The receptors for the iron complexes of these molecules are rather specific. For example, when the unnatural enantiomer (prepared from D-Serine) of enterobactin is incubated with an *E. coli* mutant unable to synthesise enterobactin, growth inhibition is observed. Inhibition is not observed if the mutant is incubated in the presence of the laboratory-synthesised, but naturally occurring enantiomer prepared from L-Serine (***Figure 37***).[198] This suggests that reducing the concentration of available Fe^{3+} in solution via complexation with ligands which bacteria are unable to recognise and transport, could be a strategy to control their growth.

An excess of iron is also problematic for many organisms, leading to extensive cell damage and organ death. Accordingly, attention has been directed to the design and synthesis of Fe^{3+} chelators (including desferrioxamine) that can be administered as therapeutics to those suffering from diseases such as Haemochromatosis, or who have undergone blood transfusions.[52] Because the efficacy of these therapeutic candidates usually relies primarily on their ability to sequester Fe^{3+} from a host organism or patient, many of the metal affinities for these molecules are known. Often, they are quoted in terms of their p(Fe^{3+}), where $p(Fe^{3+}) = -log[Fe^{3+}_{free}]$. This is a more biologically relevant measure of metal affinity independent of ligand speciation (***Figure 38***).

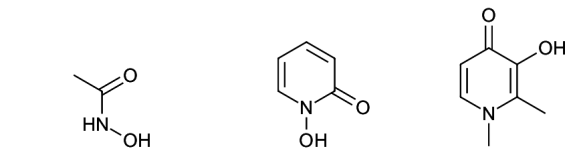

Acethydroxamic acid **1,2-HOPO** **Deferiprone**

p(Fe^{3+})=13 **p(Fe^{3+})=16** **p(Fe^{3+})=21**

Figure 38: Candidate ligands for the treatment of Fe^{3+} overload, with p(Fe^{3+}) at pH 7.4 shown. In this case $[Fe^{3+}_{total}] = 10^{-6}M$ and $[L] = 10^{-5}M$. Data from Zhou.[52]

A consistent feature of many of these high-affinity Fe^{3+} ligands is the presence of hard, ionisable oxygen donor atoms, typically in the form of phenolates and hydroxamates, which match well to the hard Fe^{3+} ion. Some element of preorganisation,[65] e.g. the macrocycle of Enterobactin, the rigidity of bidentate donor ligands reported by Hider[53, 183, 199, 200] and the diketopiperazine of Rhodotorulic acid, is also common. Consequently, these features were deemed desirable in any ligands to be studied.

In choosing whether to focus on hydroxamates or phenolate donors, the iron affinity of ligands bearing these groups was compared (***Table 22***), and it was apparent that the complexes involving phenolate donors were more stable than those involving hydroxamates (the pK_a values for both are similar). Ligands incorporating phenolates could also be more lipophilic, opening up the possibility of ligand-membrane interactions that could affect dose response.

Table 22: Literature Fe^{3+} affinities for the hydroxamate ligand **$^{i}Pr_2$-EDTA-DX**,[201] the phenolic ligand **HBED**[202] and **EDTA**.[164]

Entry	Ligand	log $K_a(\frac{[ML]}{[M][L]})$ M=Fe^{3+}
a	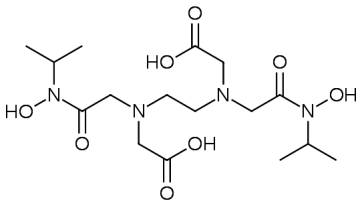 **$^{i}Pr_2$-EDTA-Dx**	30.2[i]
b	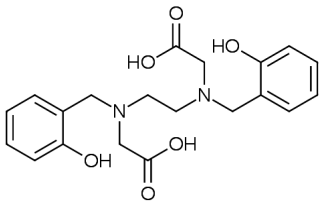 **HBED**	39.0[ii]
c	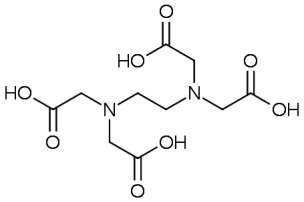 **EDTA**	25.0

i) Obtained by spectrophotometry, T=25°C, I=0.1 M. **ii)** Obtained via competitive potentiometric titration, T=25°C, I=0.1 M.

Another advantage of phenolate ligands was that the relationship between phenol oxygen lone pair availability and antibacterial activity could be studied by changing the *ortho*- and *para*- substituents on the phenolic donor. This meant the generation of quantitative structure-activity data was a possibility. Furthermore, a relationship between lone pair availability and potential activity for **EHPG** (also known as **EDDHA**) derivatives has been alluded to by Yunta *et al.*[203, 204]That is, the more electron-withdrawing a substituent *para*- to the oxygen donor in a phenol group, the higher the $p(Fe^{3+})$ of the ligand will be, and the more Fe^{3+} the ligand will be able to sequester (***Table 23***).

Table 23: Electronic effects on $p(Fe^{3+})$ for **EHPG** and its derivatives, from the work of Yunta.[203] As the *para*- substituent becomes more electron withdrawing, $p(Fe^{3+})$ increases. For this data pH=7.5 , $[Fe^{3+}_{total}] = 10^{-6}M$ and $[L] = 1.1x10^{-6}M$. Both *meso*- and *rac*- diastereomers were present in the analysed sample.

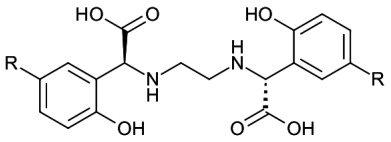

***meso*-4-R-EHPG**

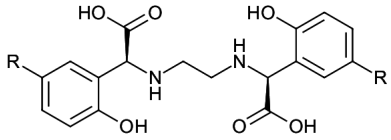

***rac*-4-R-EHPG**
(exists as two enantiomers)

Entry	R=	$p(Fe^{3+})$
a	-H (**EHPG**)	25.2
b	-Me (**4-Me-EHPG**)	25.7
c	$-SO_3H$	27.2

Based on the range of information available for **HBED** and **EHPG** ligands, it was decided to focus primarily on these ligand frameworks. While the work laid out in this chapter is therefore centred around the effect of Fe^{3+} chelation on bacterial growth, an ability to sequester other biologically relevant first-row transition metals was desirable, and is predicted at physiological pH (***Figure 39***).

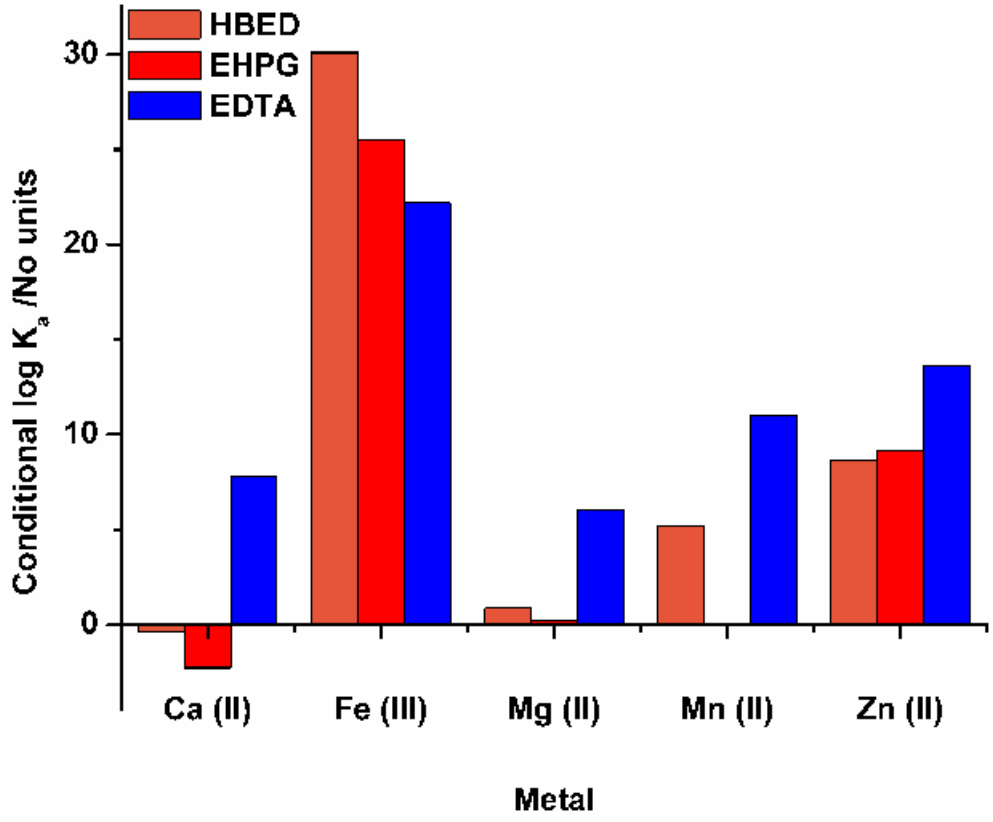

Figure 39: A graphical representation of the selectivity of **HBED**, **EHPG** and **EDTA** at pH 7.4 . **HBED** pK_a and K_a values from Eplattenier[205] , **EHPG** pK_a values from Bannochie.[206] K_a values were from Frost. Mn^{2+} values for **EHPG** could not be calculated due to the instability of the **Mn^{2+}-EHPG** complex to oxidation.[207]

4.2. Synthetic approaches to HBED and EHPG ligands

4.2.1. Strategy

Though both **HBED** and **EHPG** (***Tables 22*** and ***23*** respectively) have been known for a long time, and a number of approaches reported for their preparation,[208] it was thought productive to survey disconnections and forward syntheses of these molecules, and adopt those that appeared most fruitful either in terms of yield or convenience, as was done for the **AmR_x** ligands (***Section 3.2.2***).

Disconnections for **4-R-HBED** systems were evaluated first. Because disconnection **B** would require the preparation of aminoester **12** (***Scheme 22***), it was not considered in the first instance, due to the more inconvenient synthesis associated with it (***Figure 40***).

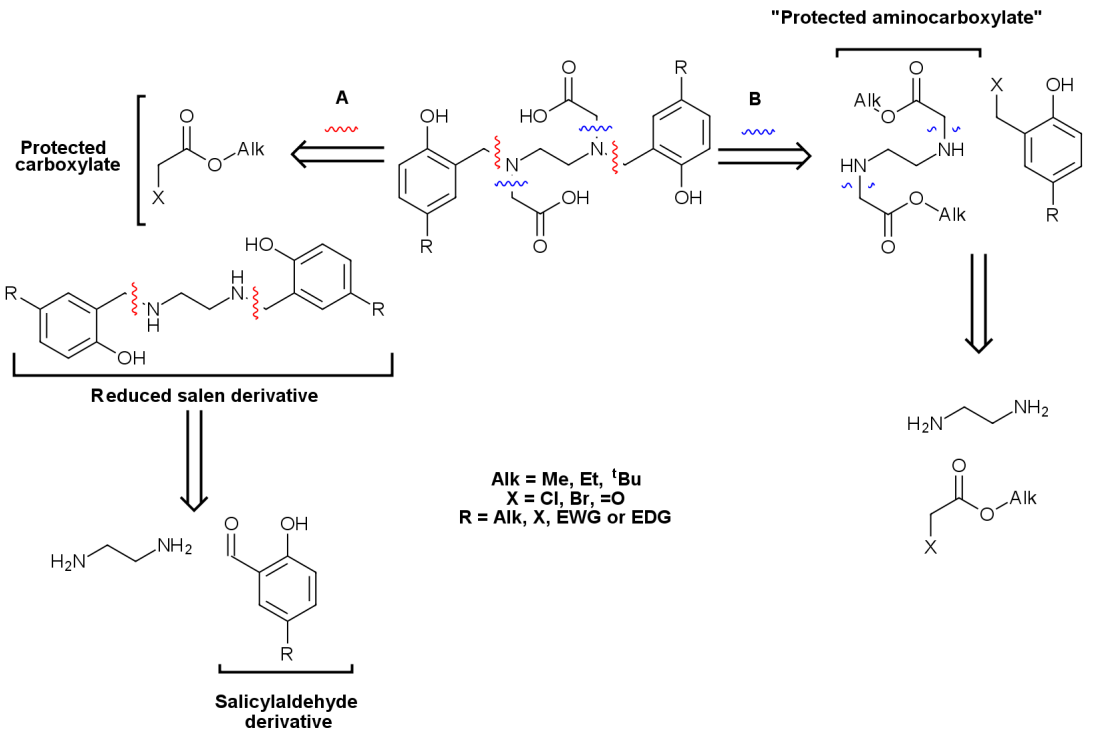

Figure 40: Two disconnections toward **HBED** derivatives.

Disconnection **A** was much more attractive, because of the commercial availability of the necessary salicylaldehyde derivatives, and use of selective reductive amination chemistry to prepare the corresponding reduced salen derivatives (conditions for the preparation of which are known). Protecting groups would be unnecessary at this stage of the synthesis, and the synthesis simpler (***Scheme 22***). If necessary, certain salicylaldehyde derivatives could be prepared via formylation of the corresponding phenol via the Riemer-Tiemann,[209] Duff,[210] or Skattebøl[211] reactions.

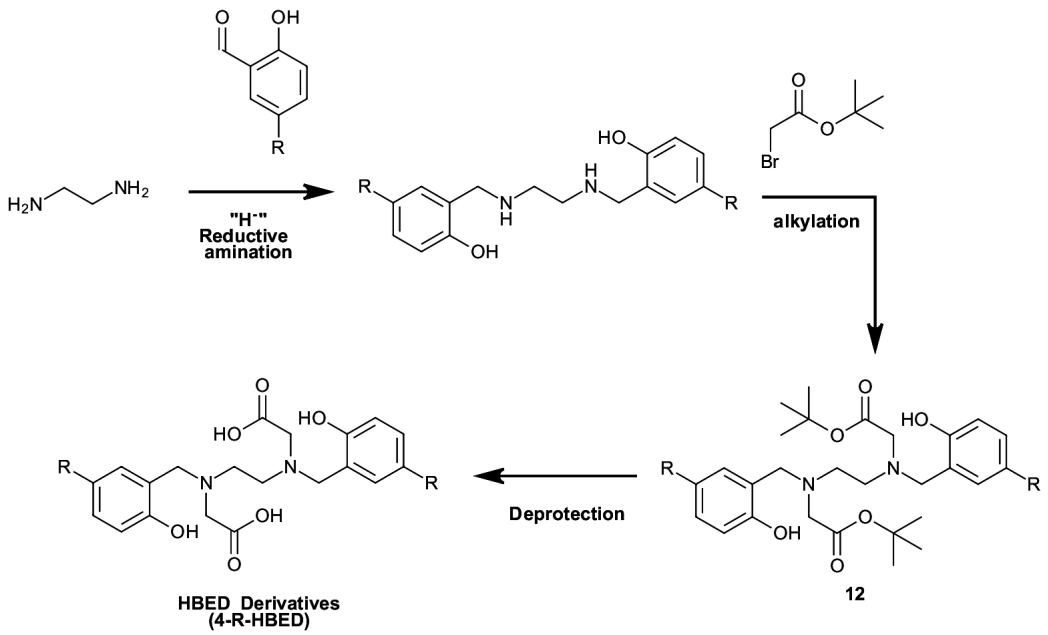

Scheme 22: A possible forward synthesis of **4-R-HBED** type ligands.

No survey of disconnections was necessary for the preparation of **4-R-EHPG** ligands because the routes proposed by Yunta[203] and Wilson[212] are complementary and could be used to access a wider range of derivatives more quickly than would be possible if a single route was utilised (***Figure 23***).

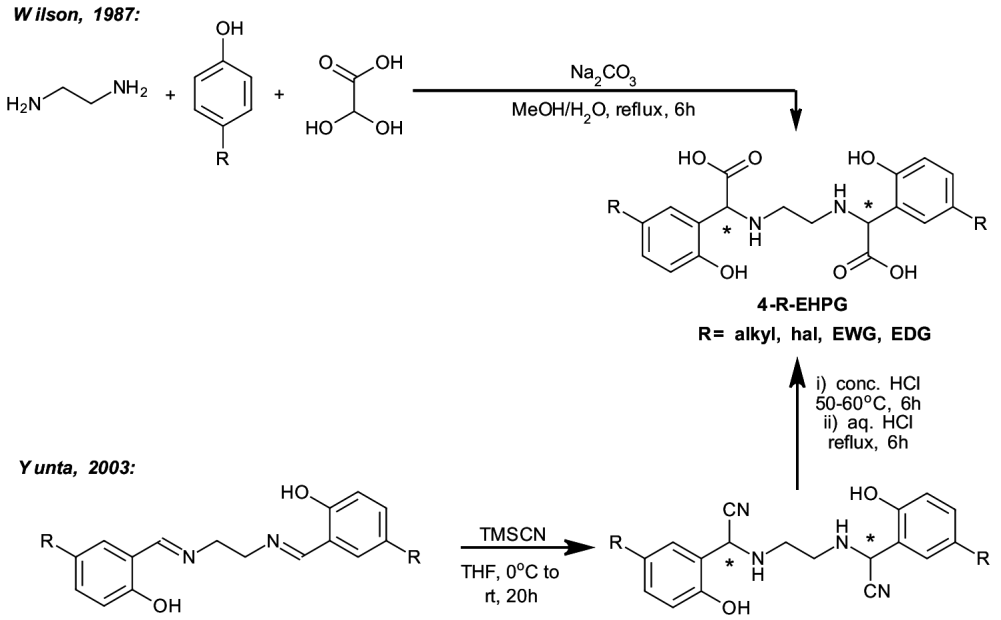

Scheme 23: Wilson[212] and Yunta[203] routes for **4-R-EHPG** type ligands.

4.2.2. HBED derivatives

A number of conditions have been reported (mostly in the patent literature)[213] for the reductive amination necessary for the synthesis of the representative reduced salen derivative **4-H-21**. Since these conditions were better suited to large-scale preparations, some adaptations were necessary to run the reactions on a laboratory scale. As a test of reductive amination conditions, **4-H-21** was prepared in two ways, either in one pot, or via reduction of the isolated imine in a "two-pot" procedure (***Scheme 24***).

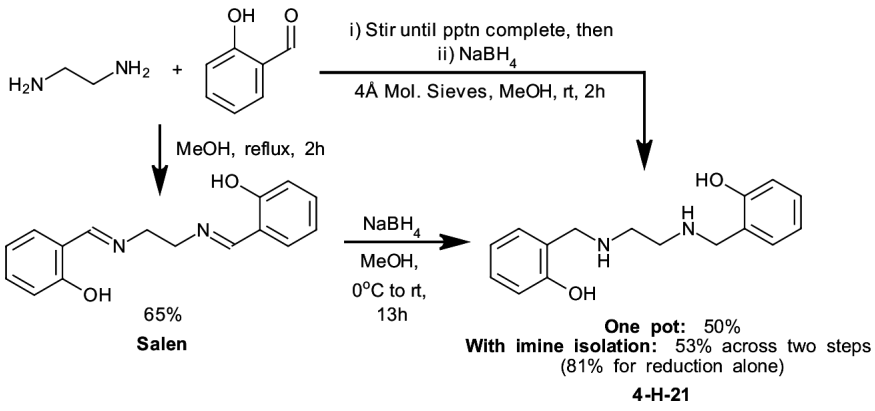

Scheme 24: Preparation of **4-H-21** via one- and "two-pot" procedures.

While the overall yield for **4-H-21** is almost the same, it was found that a two-pot reductive amination protocol where the intermediate imine was isolated[214] was far more reproducible than the reported one-pot procedure.[215]. Consequently, when the salicylaldehyde *para*- substituent was varied to prepare **4-NO_2-21**, **4-Cl-21**, **4-Br-21** and **4-MeO-21**, the two pot procedure was used. Typically, sodium borohydride in an alcoholic solvent was used as the reducing agent, with the relevant reduced salen being isolated by extraction or precipitation out of aqueous solution. A modified Skattebøl reaction[216] was used to prepare 4-n-octyl-salicylaldehyde from 4-n-octylphenol, which was reductively aminated to form **4-Oct-21** in much the same way.[217] Solubility and purification issues precluded the use of alcoholic sodium borohydride to prepare **4-F-21**, which was prepared instead from its imine via catalytic hydrogenation (***Table 24***)[208].

Table 24: Reduction conditions used to prepare the **4-R-21** aminophenols.

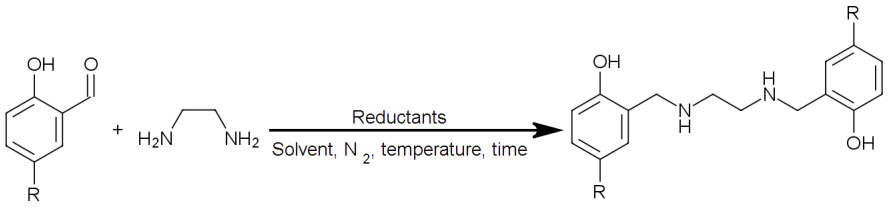

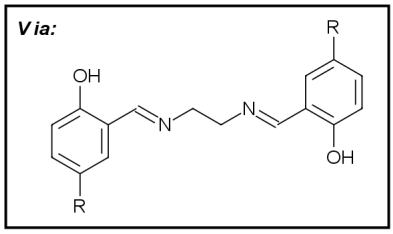

Entry	R=	Reductant(s)	Solvent[i]	Temp. / °C[i]	Time / h[i]	Yield / %[ii]
a	**F**	H_2, 5 mol. % Pd/C	THF:MeOH[iii]	50-60°C	24	61
b	**Cl**	$NaBH_4$	THF:MeOH[iii]	rt	21	67
c	**Br**	$NaBH_4$	THF:MeOH[iii]	rt	2	86
d	**OMe**	$NaBH_4$	MeOH	rt	17	71
e	**C_8H_{17} (Oct)**	$NaBH_4$	THF:MeOH[iv]	rt	2	60
f	**NO_2**	$NaBH_4$	THF:MeOH[iii]	rt	21	87

i) For reduction step only. **ii)** Across two steps (imine formation and reduction). All are unoptimised. **iii)** 1:1 v/v Mixture. **iv)** 8:2 v/v Mixture.

Once these derivatives were in hand, alkylation was attempted on **4-H-21**, using t-butyl bromoacetate and potassium carbonate (a base selected as a result of work covered in ***Table 11***) or with chloroacetic acid and aqueous sodium hydroxide. Unfortunately in the first case, phenol *O*- alkyla-

tion was observed in addition to amine alkylation, whereas the second did not proceed at all. Two alternatives to circumvent overreaction were trialled in parallel; the use of a weaker base, potassium hydrogen carbonate (potassium bicarbonate) or protection of the phenol groups as their methyl ethers, from precursor **4-H-21-OMe** (***Table 25***).

Table 25: Approaches for the chemoselective alkylation of amine groups in **4-R-21** type precursors.

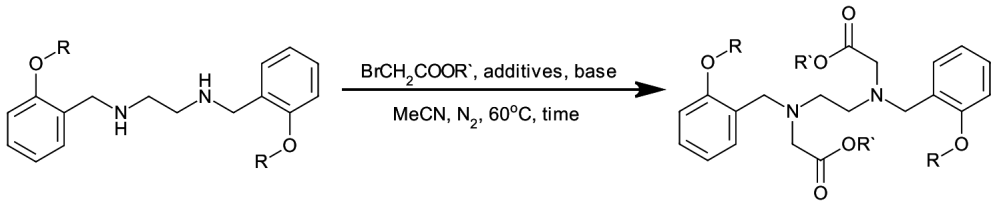

R=H: 4-H-21
R=Me: 4-H-21-OMe

R=H, R`=^{t}Bu: 4-H-21-tBu
R=Me, R`=Et: 4-H-21-OMe-Et

Entry	Additives	Base	Time / h[i]	Yield / %
a	KI, Na_2SO_4	$KHCO_3$	16	86
b	-	Et_3N	2	41

i) Refers to discontinuation of heating.

Both strategies were successful, meaning that *O*- protection was superfluous. Potassium bicarbonate was therefore the base of choice for chemoselectively alkylating the amine groups of **4-F-21**, **4-Cl-21**, **4-Br-21** and **4-MeO-21**, which were alkylated using t-butyl bromoacetate to form ester precursors to the substituted **HBED** ligands. Use of an alcoholic solvent was necessary for the preparation of **4-F-21-tBu** and **4-Cl-21-tBu**, because significant amounts of *O*- alkylation were observed in acetonitrile. It is possible that the use of isopropanol meant that the phenolic oxygens were more solvated and less likely to act as nucelophiles compared to the neighbouring amines, resulting in the desired selectivity, or changes in the relative pK_a values of the bases. A mixed solvent system comprised of acetonitrile and ethyl acetate was used to prepare **4-Oct-21-tBu** from **4-Oct-21** on account of its low solubility in acetonitrile alone (***Table 26***).

Table 26: Alkylation conditions used to prepare **4-R-21-tBu**.

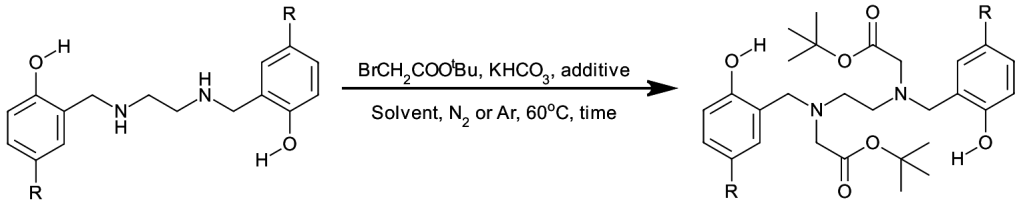

R= F: 4-F-21
R= Cl: 4-Cl-21
R= Br: 4-Br-21
R= OMe: 4-MeO-21
R= $^{n}C_8H_{17}$: 4-Oct-21

R= F: 4-F-21-tBu
R= Cl: 4-Cl-21-tBu
R= Br: 4-Br-21-tBu
R= OMe: 4-MeO-21-tBu
R= $^{n}C_8H_{17}$: 4-Oct-21-tBu

Entry	R=	Additive	Solvent	Time / h[i]	Yield / %[ii]
a	**F**	-	^{i}PrOH	24	45
b	**Cl**	-	^{i}PrOH	21	46
c	**Br**	KI	MeCN	22	44
d	**OMe**	-	MeCN	17	67
e	**C_8H_{17} (Oct)**	-	EtOAc:MeCN[iii]	24	73

i) Times are unoptimised and refer to discontinuation of heating. **ii)** After precipitation or column chromatography. **iii)** 1:1 v/v Mixture.

Remarkably (with the exceptions of **4-Oct-21-tBu** and **4-H-21-tBu**), most of the t-butyl esters could be isolated without chromatographic purification, using a simple precipitation from hexane or diethyl ether assisted by ultrasonic agitation. This allowed for their preparation in modest, but acceptable yields. If desired, further purification/decolourisation could be undertaken via recrystallisation. Further to this, single crystals suitable for analysis via X-ray crystallography could easily be grown, all of which show intramolecular N···H—O hydrogen bonding, and changes in space group depending on the *para*-substituent (***Appendix C.8***).

To assess the contribution of the phenol groups to the *E. coli* inhibitory activity of these **HBED** derivatives, aminoester **11** (***Scheme 15***) was deprotected prior to the **HBED** precursors to give the benzylated **BED** ligand, which lacks the -OH groups of **HBED**. Inspection of the ^{1}H NMR and ES-MS data for a deprotected sample of **11** indicated that ring alkylation by liberated t-butyl cation had taken place to give the side product (***Scheme 25***) and that the addition of a t-butyl cation scavenger was necessary.

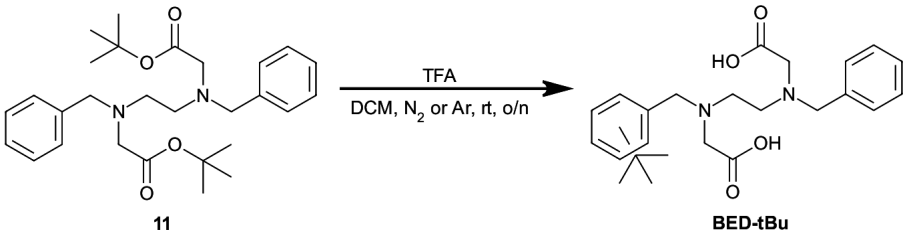

Scheme 25: Scavenger-free deprotection of **11** leading to nonspecific ring-alkylation.

Triethylsilane was used as the t-butyl cation scavenger and seemed to stop the formation of significant amounts of **BED-tBu**,[218] but this scavenging ability did not translate to the deprotection of the more electron-rich phenolic ligands, for which anisole was selected.[219] 1,4-dimethoxybenzene was used as the scavenger for the deprotection of **4-MeO-21-tBu** (***Table 27***).

Table 27: Deprotection conditions used for the aromatic ligands in this chapter.

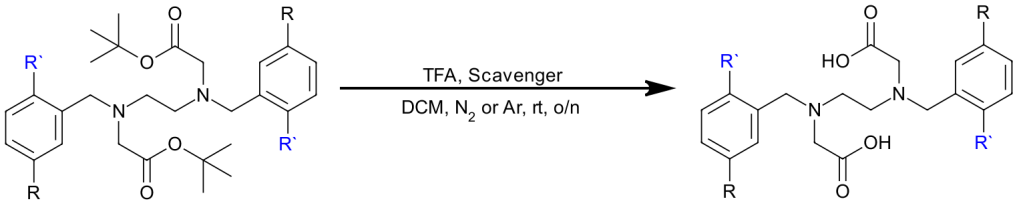

R= H, **R`**=H: **11**
R= F, **R`**=OH: **4-F-21-tBu**
R= Cl, **R`**=OH: **4-Cl-21-tBu**
R= Br, **R`**=OH: **4-Br-21-tBu**
R= OMe, **R`**=OH: **4-MeO-21-tBu**
R= $^{n}C_8H_{17}$, **R`**=OH: **4-Oct-21-tBu**

R= H, **R`**=H: **BED**
R= F, **R`**=OH: **4-F-HBED**
R= Cl, **R`**=OH: **4-Cl-HBED**
R= Br, **R`**=OH: **4-Br-HBED**
R= OMe, **R`**=OH: **4-MeO-HBED**
R= $^{n}C_8H_{17}$, **R`**=OH: **4-Oct-HBED**

Entry	R=	R‘=	Scavenger	Yield / %[i]
a	**H**	**H**	Et_3SiH	29
c	**F**	**OH**	Anisole	45
d	**Cl**	**OH**	Anisole	74
e	**Br**	**OH**	Anisole	76
f	**OMe**	**OH**	1,4-DMB	67
g	**C_8H_{17} (Oct)**	**OH**	Anisole	73

i) Based on recovered mass (assumed to be speciated as shown in the scheme) after ion exchange treatment.

4.2.3. Attempted synthesis of 4-NO_2-HBED

As the data in ***Table 23*** show, the extent of Fe^{3+} sequestration is greater when a phenol donor bears an electron withdrawing group. Hence, the synthesis of a ligand bearing strongly electron-withdrawing groups conjugated to the phenolic oxygens was desirable. A prime candidate was the nitro group, which was chosen on account of the low-cost of 5-nitrosalicylaldehyde and the drastic effect nitro substitution has on phenol pK_a (***Figure 41***).

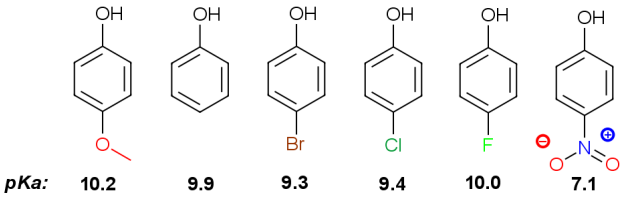

Figure 41: Substituent effects on phenol pKa.[220]

Non-selective nitration on **HBED** to afford a mixture of isomers of **4-NO_2-HBED** has been reported[221]. This approach was not pursued, a route employing non-chromatographic exclusively was desired, and so alkylation of the amino groups of **4-NO_2-21** was the basis of the first synthetic strategies pursued due to the relative ease that other protected, **4-R-21** intermediates were furnished. Unfortunately, in all cases, overalkylation at the phenolic oxygen sites was observed by ES-LCMS in all cases and ^{1}H NMR did not indicate the formation of sufficient amounts of product to warrant any attempt at isolation (***Table 28***).

Table 28: A survey of alkylation conditions towards the synthesis of **4-NO_2-HBED-R'**.

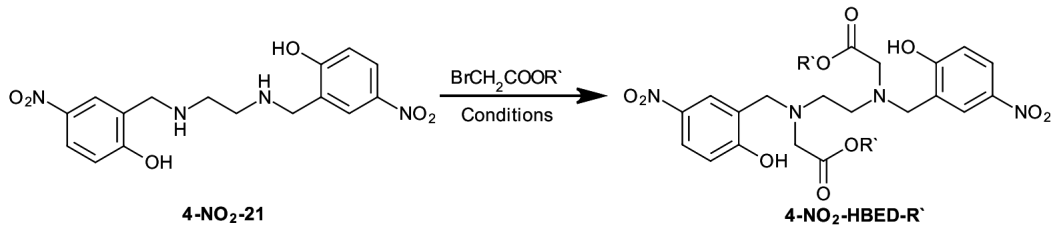

4-NO_2-21 **4-NO_2-HBED-R`**

Entry	R'=	Solvent	Base	Temp. /°C	Time / h	Outcome
a	Et	MeCN	$KHCO_3$	60	25	overalkylation, lactam formation, **pdt. observed**[i]
b	tBu	MeCN	Et_3N	60	21	overalkylation, **pdt. observed**[i]
c	Et	MeCN	Et_3N	rt	24	overalkylation, lactam formation[i]
d	Et	DMF	$^iPr_2NEt$	-30	4.5	overalkylation, **pdt. observed**[i]
e	tBu	^{i}PrOH	$KHCO_3$	60	24	overalkylation (exclusively)[ii]

i) By ES-LCMS. **"Pdt."** refers to the **4-NO_2-21-R'** product in the scheme. **ii)** By ^{1}H NMR.

Protection of the phenol group seemed to be a solution to the observed overreaction and a variety of protection strategies were considered both on 5-nitrosalicylaldehyde and **4-NO_2-21**. Inspired by the work of Gale *et al.* on the synthesis of a precursor to a manganese-based redox probe, where t-butyldiphenylsilyl (TBDPS) protection was employed (***Scheme 26***).[222] Application of the same protection protocol to **4-NO_2-21** was attempted, but failed at the phenol protection step (no conversion was observed after twenty-four hours, monitoring by ES-LCMS), possibly because of the unfavourable steric interactions that two TBDPS groups in close proximity would have. Greater attention was directed to the protecting the 5-nitrosalicylaldehyde precursor prior to reductive amination as a result.

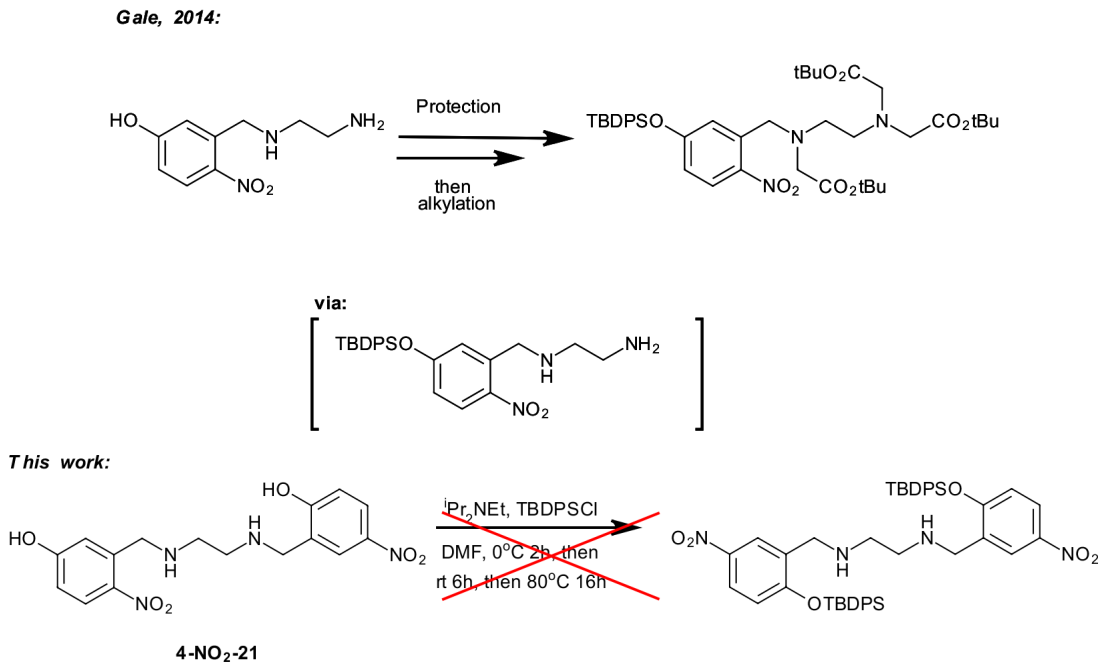

Scheme 26: *O*-protection strategies to enable selective amine alkylation in the presence of nitrophenols.

Preparation of *O*- protected derivatives like TBDMS, Boc[219] and benzoyl adducts was unsuccessful and starting material was recovered in all cases. Minimal conversion of 5-nitrosalicylaldehyde to its allyl ether was observed when reacted with allyl bromide in dimethylformamide using caesium carbonate as base, but a practical yield could not be obtained. These observations are somewhat unexpected, given the overreaction of **4-NO$_2$-21** covered above.

The final strategies trialled towards **4-NO$_2$-HBED** involved decoupling the amino groups from the phenol and using **12** as the nucleophile in reductive amination, or alkylation sequences using 5-nitrosalicylaldehyde or a Koshland-1 type reagent. Reaction monitoring via ES-LCMS led to the observation of **4-NO$_2$-HBED-tBu** and **24** but neither were observed by ^{1}H NMR after workup in either case (***Scheme 27***).

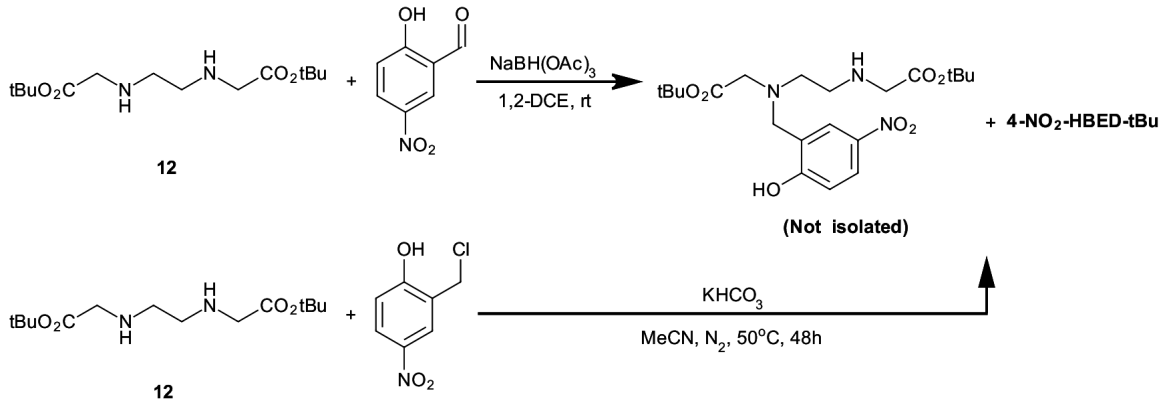

Scheme 27: Attempted syntheses of **4-NO$_2$-HBED-tBu** via aminoester **12**.

Based on these outcomes, a re-examination of the synthetic strategy is necessary to selectively access **4-NO_2-HBED**. This was not attempted due to the range of simple **HBED** derivatives that had already been accessed, although none of them were endowed with particularly electron-withdrawing groups.

4.2.4. Simple EHPG derivatives

As mentioned previously (***Section 4.1***), there is a wide range of equilibrium data published for **EHPG** and some of its derivatives. From a biodegradability perspective, the presence of asymmetric carbon atoms and secondary amines [72] in the **EHPG** parent structure meant the ligand and its complexes *may* be able to degrade in soils more readily than those of **HBED** and its derivatives. The complexes that **EHPG** forms are slightly less stable than those of **HBED** because of the increased strain of chelate ring formation in the former,[205] and less stable chelates are sometimes more biodegradable.[223] As seen in ***Section 3.7***, decreases in metal affinity may not affect the extent of bacterial growth inhibition in a linear way. Consequently, if the **HBED** derivatives were found to be problematic in downstream studies then **EHPG** analogues could be used as replacements.

Using the route of Wilson,[212] **4-Br-EHPG** and **4-Me-EHPG** were prepared in low, but workable yields (***Scheme 23***). Because there are two chiral centres in the EHPG structure, two diastereomers are produced from the reaction, in a 1:1 ratio (determined by ^{1}H NMR integration ratios). These can be separated if desired, but no attempt was made due to the small differences in metal affinity observed between isomers.[206] The synthesis of an electron-poor derivative, **4-NO_2-EHPG** was also attempted, but resulted in the formation of a resinous product exclusively.

Table 29: EHPG derivatives prepared using the route of Wilson (***Scheme 23***).

Entry	R =	Yield / %[i]
a	-Me	18
b	-Br	8
c	-NO_2	0

i) Combined yield for both diasteromers.

The Strecker-type reactions outlined by Yunta[203, 204] and Frost[207] were anticipated to give better yields for electron poor imines than the Wilson route (becuase the phenol is not a nucleophile), so the synthesis of **4-NO_2-EHPG** was attempted, but starting material was recovered exclusively. The small pK_a differences between cyanide anion and 4-nitrophenol (***Figure 41***) meant alcoholysis of the trimethylsilyl cyanide reagent was likely, meaning some form of *O*- protection will be necessary in future work on this chemistry.

Though this was a modest selection of **EHPG** derivatives, some biological comparison to the prepared **4-R-HBED** ligands was now possible.

4.3. Assessment of biological properties

4.3.1. Choice of buffer

The poor aqueous solubility of the **4-R-HBED** and **4-R-EHPG** series rendered the use of 0.2 M K_2HPO_4 impractical. Although keeping the buffer system consistent across the work presented in this thesis would be desirable, it was found that by increasing the concentration of K_2HPO_4 in the buffer to 0.4 M, dissolution of the ligands was eased. The buffer change also affected the outcome of the *E. coli* inhibition experiments, in that much more severe growth inhibition was observed at higher concentrations of **EDTA** compared to tests run under 0.2 M K_2HPO_4. In some experimental runs, concentrations of the ligands under study gave very large error margins, possibly due to precipitation over the course of these growth experiments. It is due to this, that the author recommends avoiding direct comparison of the data presented below and those in ***Sections 3.3***, above a ligand concentration of 2.5 mM, where the differences in the **EDTA**-induced growth inhibition at different buffer concentrations become most profound.

4.3.2. Importance of the phenolate groups

The growth inhibition properties of **BED** and **HBED** are presented in (***Figure 42***).

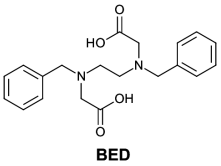

BED

[BED] / mM	Growth cf. control /%
0 (7.4)	100 ± 8
0.625 (7.8)	105 ± 7
1.25	111 ± 8
2.5	108 ± 7
5.0	110 ± 7
10.0 (7.6)	110 ± 6

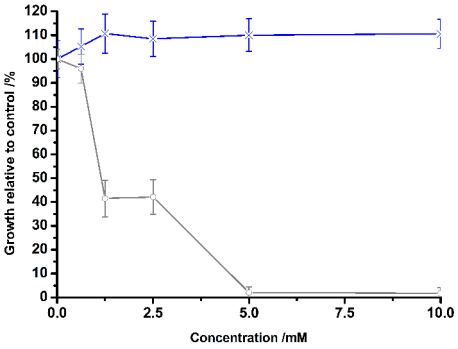

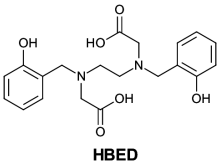

HBED

[HBED] / mM	Growth cf. control /%
0 (7.4)	100 ± 12
0.625 (7.9)	38 ± 5
1.25	44 ± 7
2.5	42 ± 4
5.0	31 ± 6
10.0 (7.9)	18 ± 2

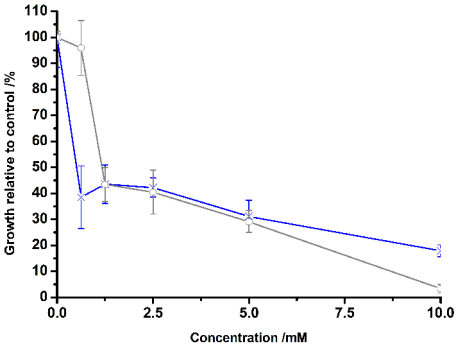

Figure 42: Comparison between *E. coli* growth inhibition characteristics for the bis-benzylated ligand **BED** and the bis-hydroxybenzylated ligand, **HBED**. Bacteria were incubated for 16 h at 37°C in a medium composed of of 90:10 v/v TSB: 10x ligand stock in 400mM K_2HPO_4 (in-well [K_2HPO_4] of 40mM). Values are the mean of three technical repeats. Both error bars and margins represent two standard deviations from the mean. Bracketed values are the pH of test solutions based in the same media used for the experiment. Blue lines represent the dose response of the ligand, and grey lines represent the dose response of EDTA.

Although this appears to be a redundant experiment (it is certain that **HBED** has a higher metal affinity than **BED** for the metal ions under consideration in this work) a desire to examine the scope of the non-linear relationship between metal affinity and growth inhibition covered in ***Chapter 3*** was the motivation for this study. It have been, for example, that the solution conformation, or relative hydrophobicity of **BED** afforded it unexpected potency compared to **HBED**. That the data show this is not the case and such parameters are likely inconsequential, was reassuring.

The dose response of **HBED** exhibits a greater growth inhbition than **EDTA** at a concentration of 0.625 mM. Increasing the **HBED** concentration does not increase growth inhibition, unlike the behaviour seen for **EDTA**. This implies that the pathways operating for these phenolate ligands may be different to those of the aminocarboxylates, possibly because of their Fe^{3+} complexing ability and selectivity. ICP-MS experiments discussed in ***Section 4.5*** appear to substantiate this.

4.3.3. Effect of the *para-* substituent on bacterial growth inhibition

With the importance of the phenol hydroxyl group established, an understanding of the importance of lone pair availability could be gained by obtaining the dose responses of **4-F-HBED**, **4-Cl-HBED**, **4-Br-HBED** and **4-MeO-HBED** (***Figure 43***).

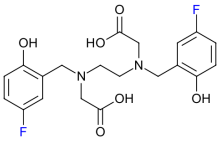

4-F-HBED

[4-F-HBED] / mM	Growth cf. control /%
0	100 ± 10
0.625 (7.7)	35 ± 3
1.25	39 ± 4
2.5	35 ± 4
5.0	37 ± 4
10.0	33 ± 7

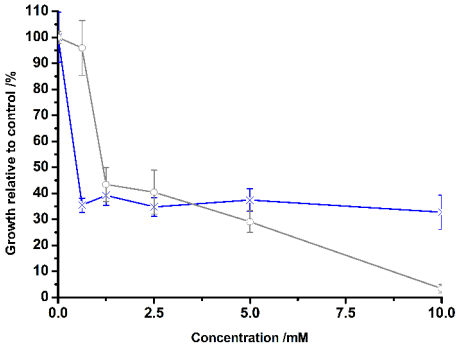

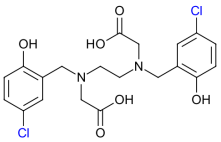

4-Cl-HBED

[4-Cl-HBED] / mM	Growth cf. control /%
0	100 ± 8
0.625 (8.1)	95 ± 6
1.25	71 ± 11
2.5	11 ± 1
5.0	31 ± 2
10.0 (8.0)	25 ± 4

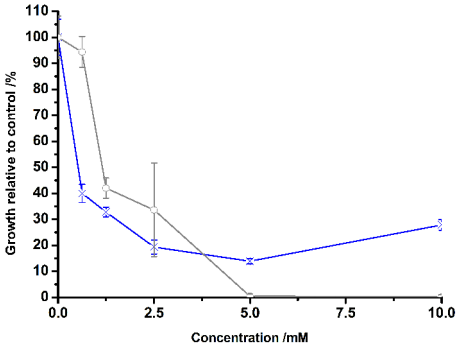

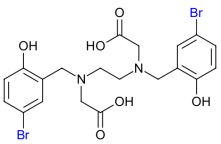

4-Br-HBED

[4-Br-HBED] / mM	Growth cf. control /%
0	100 ± 5
0.625 (7.9)	39 ± 5
1.25	10 ± 4
2.5	5 ± 1
5.0	12 ± 3
10.0 (7.6)	14 ± 6

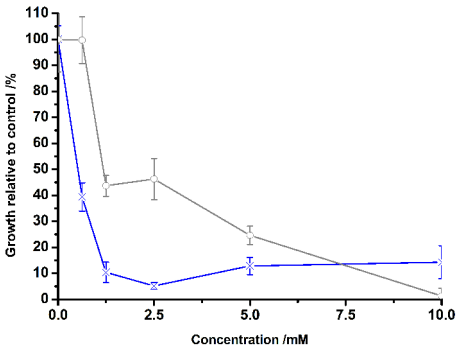

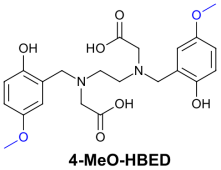

4-MeO-HBED

[4-MeO-HBED] / mM	Growth cf. control /%
0	100 ± 4
0.625 (8.0)	52 ± 4
1.25	51 ± 8
2.5	51 ± 3
5.0	51 ± 5
10.0 (9.6)	66 ± 12

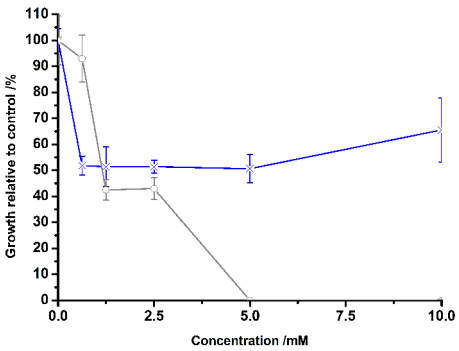

Figure 43: Dose response curves for *E. coli* JM101 upon dosing with **4-F-HBED**, **4-Cl-HBED**, **4-Br-HBED** and **4-MeO-HBED**. Bacteria were incubated for 16 h at 37°C in a medium composed of of 90:10 v/v TSB: 10x ligand stock in 400mM K_2HPO_4 (in-well [K_2HPO_4] of 40mM). Values are the mean of three technical repeats. Both error bars and margins represent two standard deviations from the mean. Bracketed values adjacent to tabulated concentrations are the pH of test solutions based on the same media used for the growth curves. Blue lines represent the dose response of the ligand, and grey lines represent the dose response of EDTA.

It is apparent that **HBED** derivatives bearing more "electron-withdrawing" substituents display greater growth inhibition compared to a derivative like **4-MeO-HBED**. This is unsurprising, especially in light of the $p(Fe^{3+})$ data shown for the **4-R-EHPG** systems (***Table 23***) and literature pK_a values (***Figure 41***) for substituted phenols. This is attributable to the "electron rich" phenol being more basic and associating with protons in solution more readily than metal ions, limiting the efficacy of the ligand at pH values below the pK_a of the methoxyphenol group[203].

In fact, it is possible to show something of a correlation between the pKa for a parent phenol of a **4-R-HBED** ligand and the observed *E. coli* growth inhibition at 2.5 mM, a concentration chosen because the corresponding growth inhibition of *E. coli* for the **EDTA** control experiment has the same value across independent experiments (***Figure 44***), indicating that the data for the **4-R-HBED** systems at this concentration are reproducible.

R=	pK_a	Growth cf. control /%
H	9.9	42 ± 4
F	10.0	52 ± 4
Cl	9.4	51 ± 8
Br	9.3	51 ± 3
OMe	10.2	51 ± 5

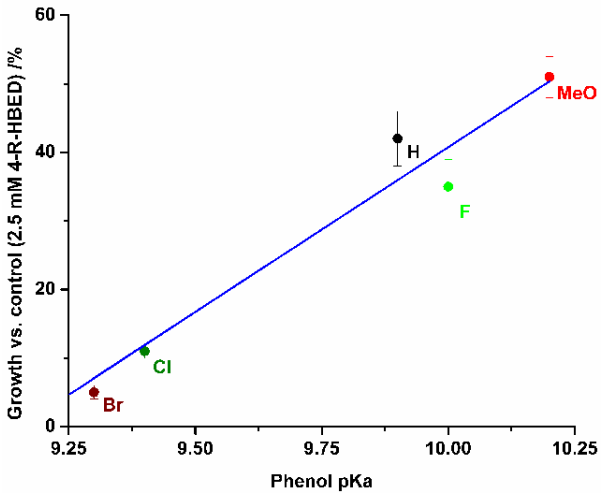

Figure 44: Relationship between **4-R-HBED** at [**4-R-HBED**]=2.5 mM and the literature pK_a (***Figure 41***) of their associated phenol groups. Bacteria were incubated for 16 h at 37°C in a medium composed of of 90:10 v/v TSB: 10x ligand stock in 400mM K_2HPO_4 (in-well [K_2HPO_4] of 40mM). Values are the mean of three technical repeats.

A design guideline to optimise the growth inhibition for these phenolic donors emerged as a result of this study; this being that optimal growth inhibition for these bacteria is observed for **4-R-HBED** ligands bearing groups that reduce the pK_a of the parent phenol. Nonetheless, it is necessary to substantiate this finding by performing dose response/growth curve experiments with **4-R-HBED** systems bearing much more strongly electron-withdrawing groups. It is also apparent that increasing the concentration of these substituted ligands past a certain point has little effect on the observed growth inhibition, much like **HBED**. Therefore smaller concentrations may be used to generate the same effect under the experimental conditions, however the origin of this effect is unknown.

Interactions between bacterial membanes and a given ligand could be enhanced by increasing the lipophilicity of a given ligand structure. For this reason **4-Oct-HBED** was prepared as an example of a highly lipophilic **4-R-HBED** type system to show whether lipophilicity was an important factor in the

activity of these compounds. Owing to the insolubility of the ligand in aqueous media, a disc-diffusion based method was used,[224–227]where sterile discs made from filter paper containing solutions of **4-Oct-HBED** (in a 3:1 v/v DMSO:H_2O solvent system) at different concentrations were loaded onto agar plates seeded with bacteria (***Figure 45***). As a control, the solvent system was tested for inhibitory properties in an analogous way, because DMSO is known to be toxic to certain cell lines.[228] In these tests, no discernible zone of inhibition was found and the negative control (which contained no bacteria) did not display evidence of contamination (***Figure 46***).

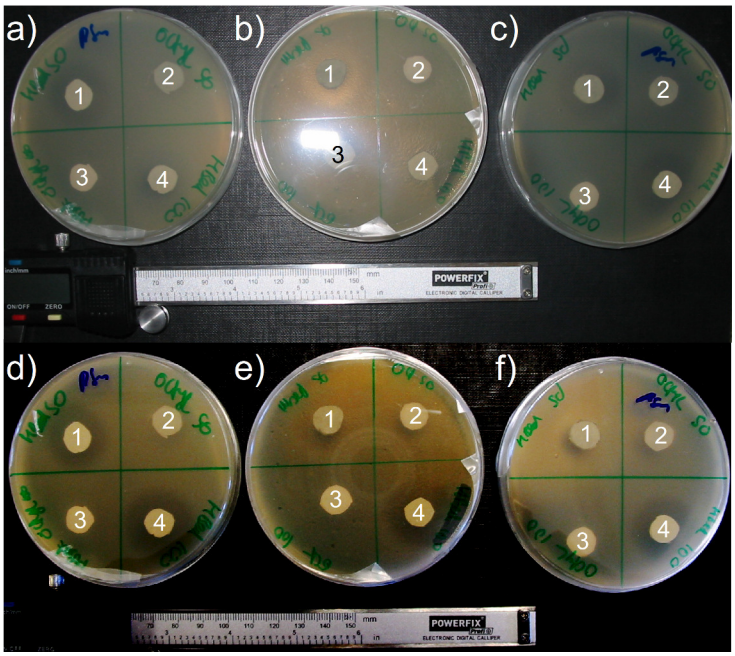

(a) LB agar plates for the disc-diffusion experiment on *E. coli* JM101 divided into four sections containing discs impregnated with **1)** 50 mM **HBED**, **2)** 50 mM **4-Oct-HBED**, **3)** 100 mM **4-Oct-HBED** and **4)** 100 mM **HBED**. Plates were incubated overnight at 37°C before being photographed at different angles to emphasise the zones of inhibition on each plate. Plates **a)**-**c)** are replicates of one another resulting in three biological replicates. Plates in images **d)**-**f)** are actually plates **a)**-**c)** but have subject to image processing to enhance contrast.

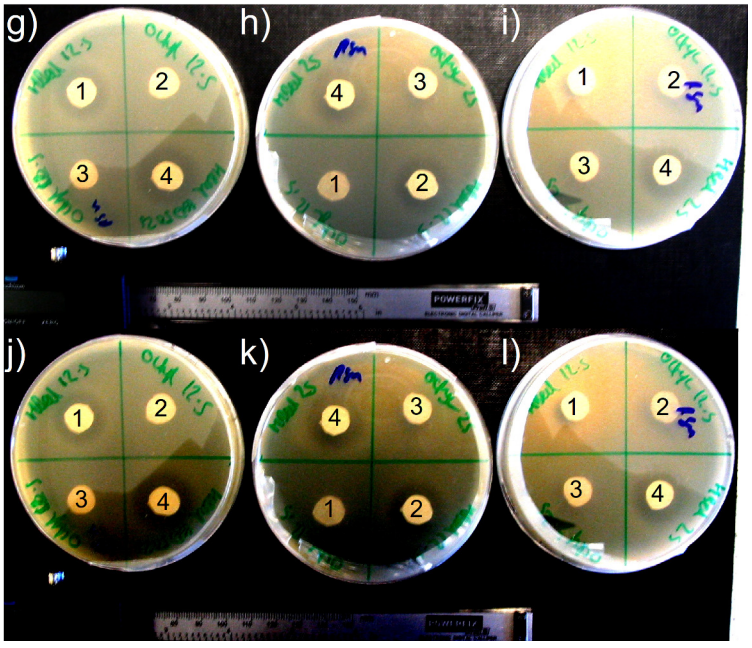

(b) LB agar plates for the disc-diffusion experiment on *E. coli* JM101 divided into four sections containing discs impregnated with **1)** 12.5 mM **HBED**, **2)** 12.5 mM **4-Oct-HBED**, **3)** 25 mM **4-Oct-HBED** and **4)** 25 mM **HBED**. Plates were incubated overnight at 37°C before being photographed . Plates in images **j)**-**l)** are actually plates **g)**-**f)** photographed at a different angle to emphasise the zones of inhibition. Three biological replicates have therefore been performed. In this case both photographs have been processed to enhance contrast.

Figure 45: LB agar plates used for the disc diffusion experiment.

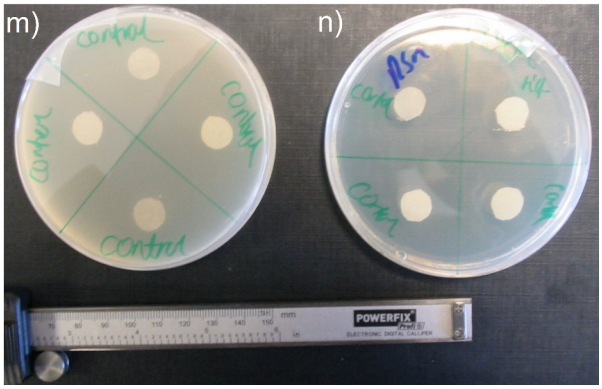

Figure 46: LB agar plate divided into four sections containing discs impregnated with 3:1 v/v DMSO:H_2O as a vehicle control. No inhibition zone was observed for the positive control **m)**, no growth was observed on the negative control **n)**.

The disc-diffusion experiment relies on the compound diffusing from the disc, into the agar which affects the growth of the bacteria seeded on it. The greater the diameter of the *zone of inhibition* is, the more inhibitory a compound is. From ***Figures 45a*** and ***45b***, **HBED** exhibits an inhibitory effect but **4-Oct-HBED** does not, across the concentration range. This may be due to the higher molecular mass[229] of **4-Oct-HBED** compared to **HBED** and/or the hydrophobicity of **4-Oct-HBED** which could hinder diffusion.[226] Since the coordination environments of **HBED** and **4-Oct-HBED** are almost identical (**4-Oct-HBED** will probably have slightly more basic phenolic oxygen donors), it is suspected that these matrix effects are the reason why no inhibition is observed in the case of this ligand.

4.3.4. Comparisons between 4-R-HBED and 4-R-EHPG derivatives

4-Br-HBED was a superior inhibitor of *E. coli* growth compared to the other **4-R-HBED** systems based on data presented in ***Section 4.3.3***. In order to examine if the 4-Br substitution also led to better inhibition for **4-R-EHPG**-type systems, the dose responses for **4-Br-EHPG** and **EHPG** (both containing a 1:1 mixture of either diastereoisomer) were obtained. Given the small differences between the $p(Fe^{3+})$ values of **4-Me-EHPG** and **EHPG**, evaluation of the impact of such small differences could also be assessed (***Figure 47***) by comparison of this pair of ligands.

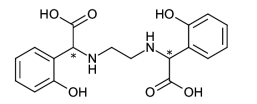

EHPG

[EHPG] / mM	Growth cf. control /%
0	100 ± 17
0.625 (7.8)	69 ± 9
1.25	66 ± 12
2.5	unrel.[i]
5.0	6 ± 2
10.0	5 ± 4

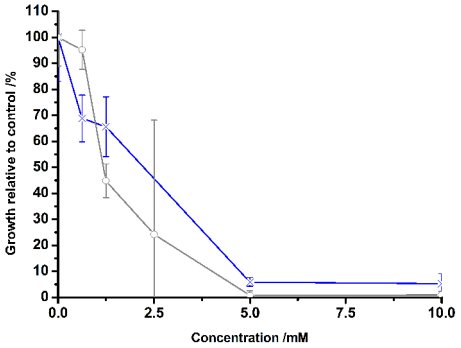

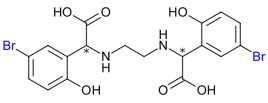

4-Br-EHPG

[4-Br-EHPG] / mM	Growth cf. control /%
0	100 ± 10
0.625 (8.1)	44 ± 9
1.25	39 ± 3
2.5	28 ± 4
5.0	3 ± 1
10.0 (8.0)	2 ± 1

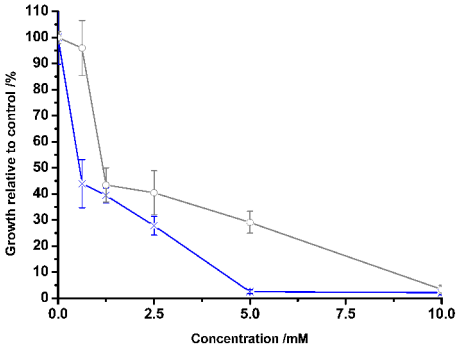

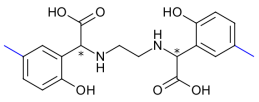

4-Me-EHPG

[4-Me-EHPG] / mM	Growth cf. control /%
0	100 ± 12
0.625 (7.9)	62 ± 6
1.25	58 ± 6
2.5	unrel.[i]
5.0	5 ± 1
10.0 (7.6)	3 ± 0

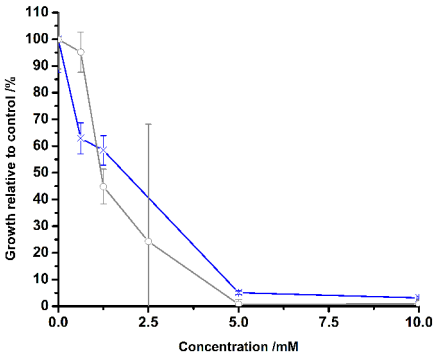

i) Excluded due to high error margins.

Figure 47: Dose response curves for *E. coli* JM101 upon dosing with **EHPG**, **4-Br-EHPG** and **4-Me-EHPG**. Bacteria were incubated for 16 h at 37°C in a medium composed of of 90:10 v/v TSB: 10x ligand stock in 400mM K_2HPO_4 (in-well [K_2HPO_4] of 40mM). Values are the mean of three technical repeats. Both error bars and margins represent two standard deviations from the mean. Bracketed values adjacent to tabulated concentrations are the pH of test solutions based on the same media used for the growth curves. Blue lines represent the dose response of the ligand, and grey lines represent the dose response of EDTA.

Once again, the **EDTA** dose response is inconsistent across experiments, but shows that the data can be compared for responses at 1.25mM, where **4-Br EHPG** is superior. No statistically significant improvement to bacterial growth inhibition is observed between **EHPG** and **4-Me-EHPG**, meaning that the small difference in p(Fe^{3+}) reported[203] does not lead to enhanced growth inhibition. **4-Br-EHPG** shows a greater inhibition of bacterial growth than **EHPG** analogous to that which **4-Br-HBED** exhibits, compared to **HBED**. At higher concentrations (10 mM), there is no significant difference in inhibitory effects between these **EHPG** derivatives. An interesting difference between the **4-R-EHPG**

and **4-R-HBED** dose responses, is that the **4-R-EHPG** dose responses do not plateau at a certain concentration, the reason for which is unclear.

4.4. Relationship between metal ion affinities and bacterial growth inhibition

When the K_a data is considered alongside the pK_a values for the **HBED** and **EHPG** structures using the treatment described in ***Section 2.5***, the conditional stability constants, $K_{a_{cond}}$ are obtained. The significance of the phenolate groups warrant comment. If these groups are protonated, many metal affinities are affected profoundly (***Table 30***), and a clear selectivity for Fe^{3+} in solution becomes apparent (***Figure 39***).

Table 30: $K_{a_{cond}}$ values calculated for pH=7.4 to closer reflect the metal affinity of **HBED**, **EHPG** and **EDTA** in liquid media. **HBED** pK_a and K_a values from Eplattenier[205] , **EHPG** pK_a values from Bannochie.[206] K_a values were from Frost. Mn^{2+} values for **EHPG** could not be calculated due to the instability of the **Mn^{2+}-EHPG** complex to oxidation.[207]

Row	Equilibrium quantity	HBED	EHPG	EDTA
a	α-coefficient	2.34×10^{-10}	2.74×10^{-10}	1.61×10^{-3}
b	K_a (Ca^{2+})	9.29	7.29	10.61
c	$K_{a_{cond}}$ (Ca^{2+})	-0.34	-2.27	7.82
d	K_a (Fe^{3+})	39.7	35.1	25.0
e	$K_{a_{cond}}$ (Fe^{3+})	30.1	25.5	22.2
f	K_a (Mg^{2+})	10.5	9.76	8.83
g	$K_{a_{cond}}$ (Mg^{2+})	0.87	0.20	6.04
h	K_a (Mn^{2+})	14.8	-	13.81
i	$K_{a_{cond}}$ (Mn^{2+})	5.17	-	11.0
j	K_a (Zn^{2+})	18.3	18.7	16.44
k	$K_{a_{cond}}$ (Zn^{2+})	8.67	9.14	13.65

Conditional affinities could be used to explain the differing dose responses of **EHPG** and **HBED**. For instance, the lower affinities **EHPG** has towards Ca^{2+} and Mg^{2+} compared to **HBED** may mean that higher concentrations of **EHPG** than **HBED** are necessary to permeabalise the outer membrane of *E. coli* prior to *intracellular* iron chelation. Given the apparent sensitivity of growth inhibition to the phenolic donor pK_a for the **4-R-HBED** and **4-R-EHPG** ligands and the dramatic decreases in $K_{a_{cond}}$ if the phenol groups are considered to be protonated, it was postulated that a *para-* substituent induced lowering of phenol basicity may give large increases in conditional metal affinities for the systems studied.

Since potentiometry was not available to determine the pK_a values of these ligands (and may not have been practical for ligands like **4-MeO-HBED** which was suspected to bear extremely basic phenol groups on the basis of data in ***Figure 41***), this notion was first tested by monitoring changes in the UV-Vis spectra of **4-Br-HBED** and **4-MeO-HBED** as a function of pH, to allow estimation of

the apparent pK_a* of the phenol groups for each ligand (***Figure 48***). These systems were chosen because they were the most and least inhibitory **HBED** derivatives tested at **[4-R-HBED]**=2.5mM respectively. Because the pK_a values for **HBED** were known, their re-determination was not crucial.

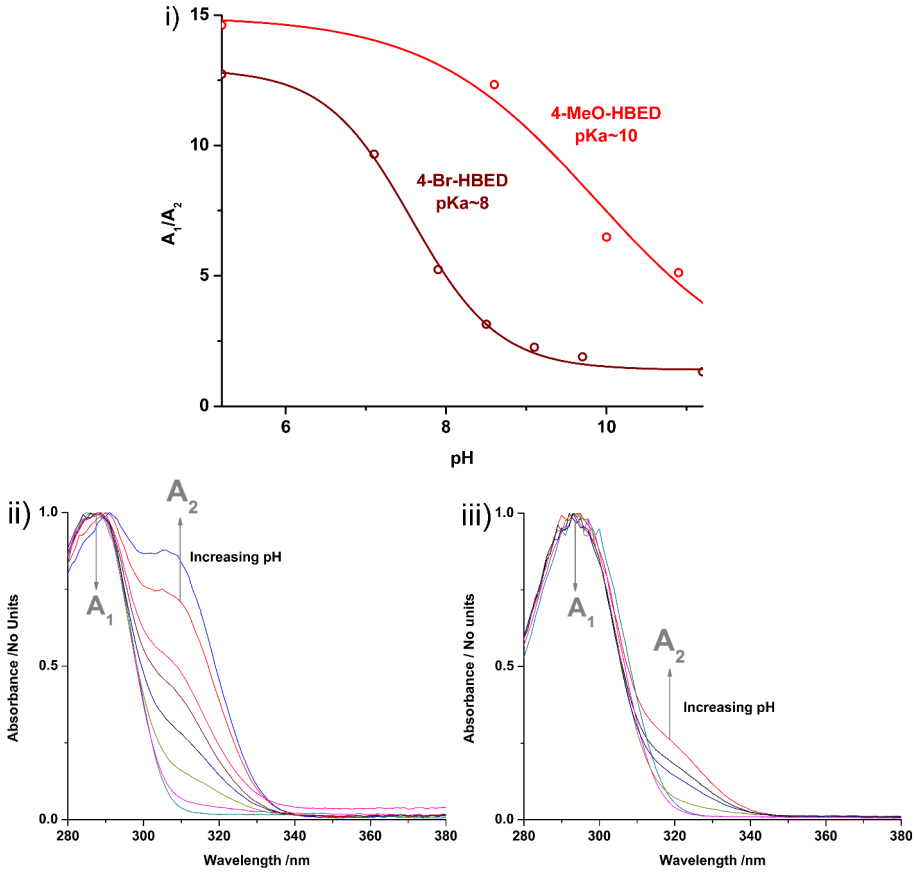

Figure 48: i) pK_a estimation for **4-Br-HBED** and **4-MeO-HBED**. Measurements were performed at room temperature in 15mM KCl. A sigmoidal fit was applied to the pH-absorbance profiles, the reported pK_a being the midpoint of the sigmoid function in either case. For **4-Br-HBED**, A_1=287 nm, A_2=307 nm. For **4-MeO-HBED**, A_1=294 nm, A_2=319 nm. The stacked spectra for **ii) 4-Br-HBED** and **iii) 4-MeO-HBED**, are also shown.

A lower pK_a is observed for **4-Br-HBED** compared to **4-MeO-HBED**, meaning that the value for the α-coefficient (see ***Section 2.5***) for **4-Br-HBED** will be higher, and so the $K_{a_{cond}}$ values calculated for **4-Br-HBED** will be closer to the actual K_a values for a given pH, compared to **4-MeO-HBED**. If the metal ion binding strengths for **4-Br-HBED** and **4-MeO-HBED** are similar, the result of this lower pK_a, and correspondingly lower α-coefficient will be that **4-Br-HBED** will form more stable complexes with metal ions under conditions of lower pH. This can be attributed to a greater fraction of the phenol donors in solution existing as the metal-binding phenoxide form for **4-Br-HBED** compared to **4-MeO-HBED**.

Monitoring of the depletion of Ca^{2+} from **Ca-Fura-2** in the usual competitive manner for **BED**, **HBED**, **4-Br-HBED** and **4-Cl-HBED** was then performed to see if these pK_a-based effects could induce or enhance Ca^{2+} binding. From the collected data (***Figure 49***), it appears that none of the

*Under these experimental conditions, the ionisations of individual phenol groups could not be monitored

tested ligands (with the exception of the **EDTA** control) can sequester Ca^{2+} from **Ca-Fura-2** under these conditions.

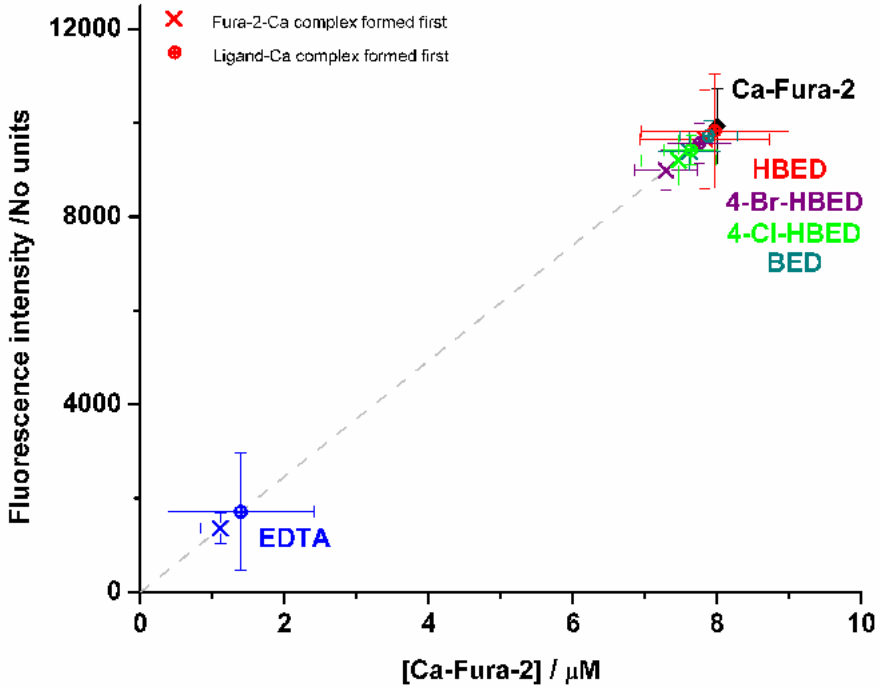

Figure 49: The effect of the **BED**, **HBED**, **4-Br-HBED** and **4-Cl-HBED** ligands on the fluorescence of the **Ca-Fura-2** complex, with calibration function shown in grey. Error bars represent two standard deviations from the mean of three replicates and were propagated from the error in the fitted gradient to give the *x* axis error bars. λ_{ex} =340 nm, λ_{em}=510 nm. [**Fura-2**]=10.5μM, [**L**]=10μM. Buffer: 10mM HEPES/100mM KCl at pH 7, T=26$\pm$1°C.

Using a slightly different ligand set (**BED**, **HBED** , **4-Br-HBED** and **EDTA**) due to material constraints, an analogous experiment was performed using Zn^{2+}. Based on the projected higher binding strength of Zn^{2+} to these systems, it was hoped that substituent induced changes in metal binding strength would be detectable (***Figure 50***).

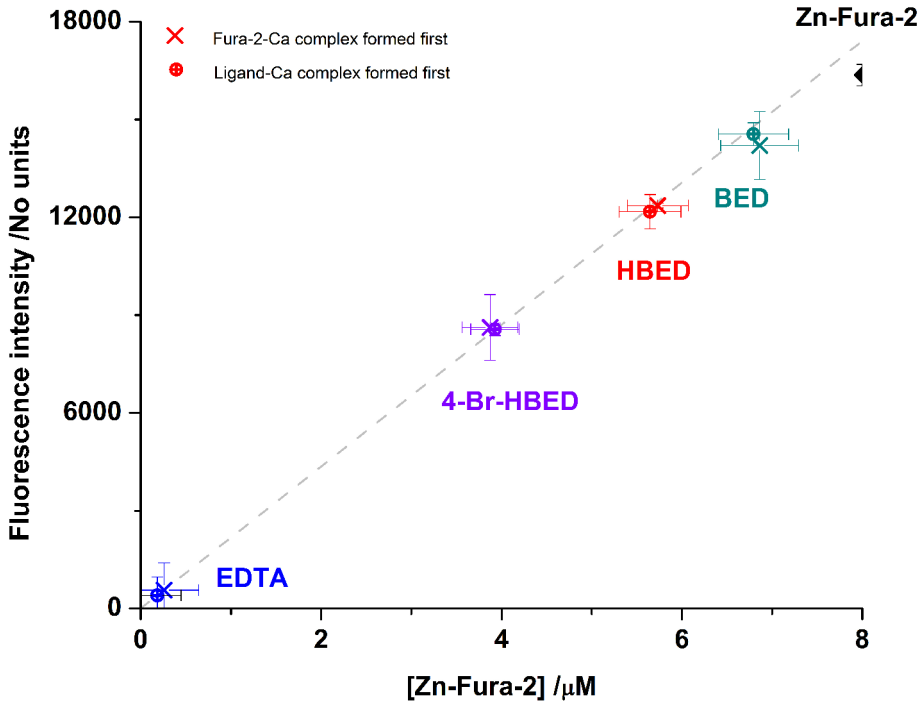

Figure 50: The effect of the **BED**, **HBED**, **4-Br-HBED** and **EDTA** ligands on the fluorescence of the **Zn-Fura-2** complex, with calibration function shown in grey. Error bars represent two standard deviations from the mean of three replicates and were propagated from the error in the fitted gradient to give the *x* axis error bars. λ_{ex} =340 nm, λ_{em}=500 nm. [**Fura-2**]=10.0μM, [**L**]=10μM. Buffer: 10mM HEPES/100mM KCl at pH 7, T=26$\pm$1°C.

Gratifyingly, the data show that **4-Br-HBED** exhibits a higher binding strength than **BED** and **HBED** under the experimental conditions. Based on the pK_a estimates, this order arises because of the higher concentration of phenoxide donors **4-Br-HBED** can provide. As an aside, the participation of the phenol hydroxyl groups in Zn^{2+} binding for **HBED** and **4-Br-HBED** is demonstrated by the inferior zinc binding of the non-hydroxylated **BED** ligand, and the contribution of readily ionised donor groups by the superior zinc binding of **EDTA**. Though it is unwise to assume that *all* of the metal affinities for **4-Br-HBED** are raised due to the pKa-altering effects of the bromo- substituents, the author proposes this to be the reason why **4-Br-HBED** is a more effective inhibitor of *E. coli* growth than **HBED** itself. Such an explanation also ties in to trends discussed previously (***Table 23***).

4.5. Effect of EHPG on cellular metal content

The selectivity for Fe^{3+} these phenolate donors possess in the experimental pH range (***Figure 39***) compared to **EDTA**, **AmGly$_1$** and **AmGly$_2$** (***Table 19***), made interrogation of their effect on cellular metal content lucrative. So, analysis of cell digests treated with **EHPG** via ICP-MS was performed in the manner described in (***Section 8.7***). Quantitative data for calcium, magnesium, copper, iron manganese and zinc were obtained from the experiment in this case (***Figure 51***).

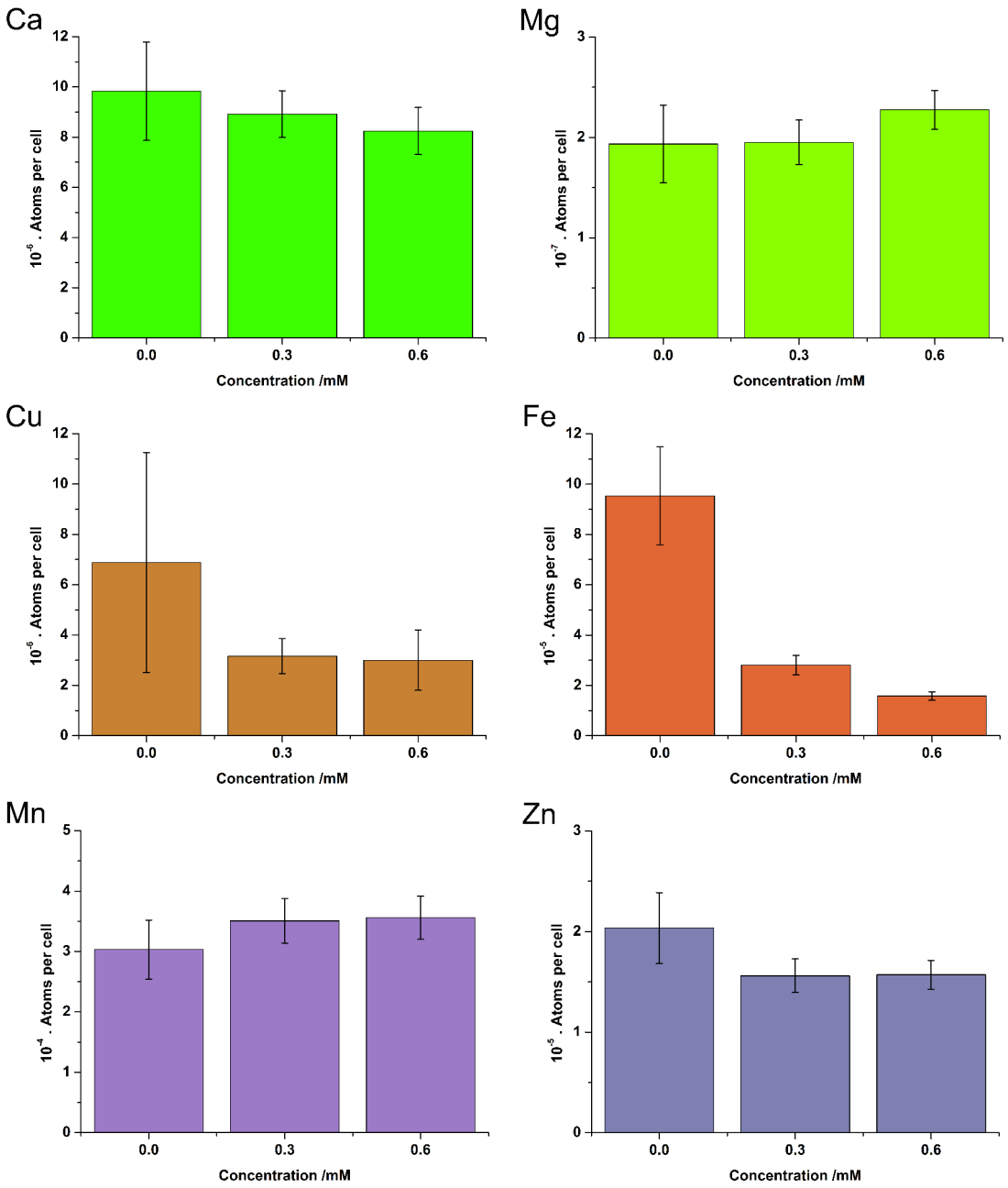

Figure 51: Effect of **EHPG** on the metal content of *E. coli* JM101 cells at stationary phase. Values are the average of three biological repeats. Error bars represent two standard deviations of the mean. Cells were incubated aerobically at 37°C for 16 h in a medium consisting of 99:1 v/v TSB:0.4 M K_2HPO_4 containing 100x [**EHPG**] prior to harvest.

Compared to the perturbations of cellular metal seen for **EDTA** and **AmGly$_2$** (***Figures 26*** and ***27***) where manganese is most severely affected, the concentration of iron *in cellulo* is reduced to a greater extent than the other metals measured. In light of the selectivity of **EHPG** at experimental pH (***Figure 39***), such a reduction is to be expected. Zinc concentrations would also be expected to significantly fall, but this is not the case, and may be due to a transmetalation of the **Zn-EHPG** complex by Iron as the system approached equilibrium.

A greater depletion of iron compared to manganese raises the possibility that phenolic ligands like **EHPG** perturb different cellular functions compared to **EDTA** and **AmGly$_2$**. However, there is some

overlap between the functions of iron and manganese in bacteria,[171] meaning that further work must be done to confirm or deny this. Owing to the weak binding of **EHPG** to calcium and magnesium at physiological pH, outer membrane permeabialisation effects are unlikely to be operating at the concentrations studied.[29, 35] Therefore, any chelated metal has most likely been removed from the growth medium by **EHPG** outcompeting some of the Fe^{3+} transport molecules secreted by *E. coli* for Fe^{3+} (***Figure 37***). Evidence for the absence of membrane activity could be gathered by studying the lipophilicity of free and Fe^{3+}-complexed **EHPG**, and is the subject of ***Section 4.6***.

4.6. Lipophilicity measurements

4.6.1. Estimation of partition coefficients

Lipophilicity measurements on a selection of free phenolic ligands and their Fe^{3+} complexes could yield information about the possibility of Fe^{3+} transport across the *E. coli* membrane and the location of metal (from the cell or from the media) sequestration. As was previously discussed, a relationship between *E. coli* growth inhibition and higher lipophilicity also exists (***Section 2.6***) and so bioactivity may be predicted from such measurements.

Measurements of the P_{DCE} for the Fe^{3+} complexes (***Table 31***) and P_{CDCl_3} for the free ligands, were performed using UV-Vis and ^{1}H NMR based methods respectively. Although UV-Vis could also be used to monitor the partitioning of the free ligands described in this chapter (once suitable wavelengths were identified), ^{1}H NMR was selected to allow fairer comparison with the data collected for the $\mathbf{AmR_2}$ systems (***Table 21***). Reasons for the use of different solvents for the free ligands and complexes are described in ***Sections 2.6*** and ***3.8.1***. The synthesis of the Fe^{3+} complexes is discussed in ***Section 8.8.1***.

Table 31: PBS:1,2-Dichloroethane partition coefficients (P_{DCE}) for the Fe^{3+} complexes of **HBED**, **4-BrHBED**, **EHPG** and **4-Me-EHPG** at a buffer pH of $\approx$7.4 . Data are the average of two independent experiments. Error margins represent two standard deviations from the mean.

Entry	Species	Charge at pH	P_{DCE} / No units
a	**Fe-HBED**	-1	0 ± 0[i] (extremely hydrophilic)
b	**Fe-4-Br-HBED**	-1[ii]	0.3 ± 0.03 (slightly hydrophilic)
c	**Fe-EHPG**	-1	0.0 ± 0[i] (extremely hydrophilic)
d	**Fe-4-Me-EHPG**	-1[ii]	0 ± 0[i] (extremely hydrophilic)

i) No detectable absorption in dichloroethane layer. **ii)** Estimated by analogy with **HBED** and **EHPG** speciation data.[205, 206]

Clearly, the most lipophilic complex is that of **4-Br-HBED** (***Table 31***, entry **b**), which is the only system that demonstrates measurable partitioning into the organic phase, raising the possibility that

Fe-4-Br-HBED could traverse the cell membrane and act as a growth inhibitor in its own right, although additional work to assess whether this was mode of action would be necessary. In spite of this interesting result, it is suspected that the putatively higher metal binding affinity of **4-Br-HBED** relative to **HBED** is the primary cause of growth inhibition (***Section 4.4***).

Compared to the **AmR_2** ligands, the **4-R-HBED** and **4-R-EHPG** systems exhibited lower charges in their free states versus their complexes because of the high pK_a of the phenol groups, and were expected to have different partitioning behaviour on account of this, especially in the case of **4-Br-HBED** (***Table 32***).

Table 32: PBS:chloroform partition coefficients (P_{CDCL_3}) for the ligands **HBED**, **4-Br-HBED** and **EHPG**. Bracketed values are the measured pD of the buffer system. Speciation curves from the literature[205, 206] were used to determine ligand charges at the experimental pH.

Entry	Species	Charge at pH	P_{CDCl_3} / No units
a	**HBED**	0 (8.9)[i,ii]	0[iii]
b	**4-Br-HBED**	0 or -1 (7.7)[iv]	0[iii]
c	**EHPG**	0 (7.7)	0[iii]

i) Attempts to use a lower, more reasonable buffer pH led to sample precipitation. **ii) 98%** of the **HBED** in solution calculated to be in the zwitterionic form. **iii)** No detectable signal in chloroform layer. **iv)** Estimated from the **HBED** speciation data and the apparent pKa calculated from ***Figure 48***. An emulsion was formed, but was easily broken by centrifugation.

For these measurements, it is assumed that the zwitterionic form is responsible for the observed partitioning behaviour. Despite the low-to-neutral charge of the ligands at experimental pH values, it is a characteristic of many amino acids in their isoelectric range[230] for solubility in both organic and aqueous media to decrease.[231]

Since these compounds were used at a lower pH in media for all biological studies, the zwitterionic forms, whose partitioning behaviour has now been estimated, would predominate, and so at lower pH the studied **4-R-HBED** and **4-R-EHPG** ligands would be unlikely to interact with cell membranes. Therefore, these phenolic ligands much like the **AmR_2** ligands, will probably exert their metal depletion effects by reducing the concentration of metal ions available to the cells in the growth media.

4.7. Conclusions for this chapter

Derivatives of ligands based on the **HBED** and **EHPG** parent structures bearing electron donating, or mildly electron-withdrawing substituents in the position *para*- to the phenol donor oxygen, have been synthesised. In most cases, syntheses can be performed without column chromatography, which enables scale-up. Characterisation of *E. coli* growth inhibition at various concentrations reveals that the lone pair availability of these phenolate donors influences the performance of these systems. The form of the dose response for these phenolic ligands differs from that seen for the aminocarboxylate ligands in ***Chapter 3***, in that the effects at low and high concentration are much the same for the **4-**

R-HBED systems. For the **4-R-EHPG** systems tested, the situation is slightly different, in that higher concentrations of ligands of this type give greater growth inhibition, but the cause of this is unknown. In both cases, the **4-Br-** derivative gives the greatest growth inhibition for a given concentration.

Consideration of the metal affinities of **HBED** and **EHPG** demonstrate the importance of factoring in the pK_a values of the phenol groups, and show that at pH$\approx$7.4, Fe^{3+} and Zn^{2+} are the metals most likely to be sequestered, and that Ca^{2+} and Mg^{2+} complexes of these ligands are not so stable in comparison to those of **EDTA**. This was substantiated by the absence of significant Ca^{2+} complexation in competition experiments using **Fura-2** and ICP-MS experiments on **EHPG**, which showed iron to be the metal most depleted *in cellulo*.

Zn^{2+} binding was also assessed for selected ligands. The data showed that **4-Br-HBED** competed more successfully for Zn^{2+} against **Zn-Fura-2** than did **HBED**, tallying with previously published work, which showed that less basic phenolate ligands are more effective sequestrants of metal ions at lower pH, probably due to more extensive ionisation of the phenol groups of **4-Br-HBED**. Due to the high pK_a values of the phenol groups in these ligands, none of them sequester Zn^{2+} as effectively as **EDTA**. The relevance of lipophilicty for these ligands was also considered, but aside from the slight partitioning observed for **Fe-4-Br-HBED**, none of the species evaluated were detected in the organic layers used, suggesting that their site of action is extracellular.

5. Synthesis, and growth inhibition studies of commonly used aminocarboxylate ligands and some variants

5.1. Introduction and motivation

From work in ***Chapters 3*** and ***4***, it was shown that the the extent of *E. coli* growth inhibition for symmetrical bis-amides of **EDTA** was not linked to the magnitude of K_a and $K_{a_{cond}}$ values, or to the metals that were most extensively depleted from cells incubated with **EDTA** or **AmGly$_2$**. In contrast, the iron depletion from cells incubated with the phenolic ligand **EHPG** was consistent with its high $K_{a_{cond}}(Fe^{3+})$, and based on estimations of pK_a values for **4-R-HBED** derivatives, a relationship between $K_{a_{cond}}(Fe^{3+})$ and *E. coli* growth inhibition could also be inferred.

These outcomes indicated that the relationship between metal ion affinities and adverse effects on cellular growth is more complex than once thought,[31, 32] and further investigation towards a more detailed model of chelation-induced growth inhibition was warranted. This could be conducted by characterising the growth inhibition properties of ligands whose metal ion affinities (especially for Ca^{2+}, Fe^{3+}, Mg^{2+}, Mn^{2+}, and Zn^{2+}, see ***Section 1.3***), were well characterised.

Aminocarboxylate systems were ideal for this purpose, since the metal binding behaviour of these ligands is often rigorously examined on account of their use in medicine e.g. as supporting ligands in Gd^{3+} [232–234]and Mn^{2+} based[235, 236] contrast agents like Dotarem and Magnevist. Many of these ligands were commercially available; those which were not could be synthesised trivially. Furthermore, databases (curated by IUPAC and NIST) containing a wealth of stability constant data for aminocarboxylate ligands are also available,[237] and allow rapid retrieval of thermodynamic data, making the search for trends in ligand behaviours much easier.

Perusal of IUPAC SCDBase entries for candidate ligands also showed that many aminocarboxylate ligands have different selectivities between certain metal ions, e.g. Ca^{2+} and Mg^{2+}, arising from their structure[63] or donor atoms.[65] This meant that interrogation of the effect of metal ions to different extents on growth inhibition may be experimentally realised. This could lead to a way to modify existing ligand structures to optimise metal ion affinity, and in turn growth inhibition.

5.2. Ligand synthesis

These ligand syntheses have been reported previously, or are trivial deprotections. Some small modifications to the reported procedures were made in the interests of convenience and reproducibility.

5.2.1. TETA

TETA, a ligand commonly used as a ligand for ^{64}Cu in positron emission tomography imaging,[238] was prepared via basic hydrolysis from its tetra-ethyl ester **TETAEt**. Initially, lithium hydroxide was

used, but complete reaction was extremely slow because of its lower relative solubility. Therefore, potassium hydroxide in a mixed MeOH:H_2O (1:1 v/v) solvent system (***Scheme 28***) was employed in an optimised preparation. Residual potassium hydroxide was removed by subjecting the crude product to ion exchange prior to biological study.

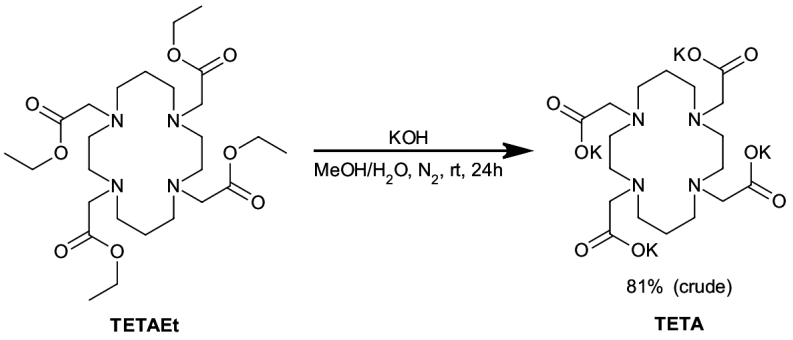

Scheme 28: Preparation of **TETA**.

5.2.2. AAZTA

A heptadentate donor, **AAZTA** was pursued because of the low cost of the starting materials. This ligand was intended for use in next-generation Gd^{3+}-based MRI contrast agents, and was synthesised using an adaptation of the method of Aime.[239] Some optimisation of the catalyst loading was necessary for the combined nitro- reduction/ debenzylation step, which was performed without specialised equipment* using transfer hydrogenation methodology[146, 147] (***Scheme 29***). Because the ligand was isolated as its trifluoroacetate salt after ester deprotection, ion-exchange treatment was used to convert a sample of the material to the hydrochloride salt for biological work.

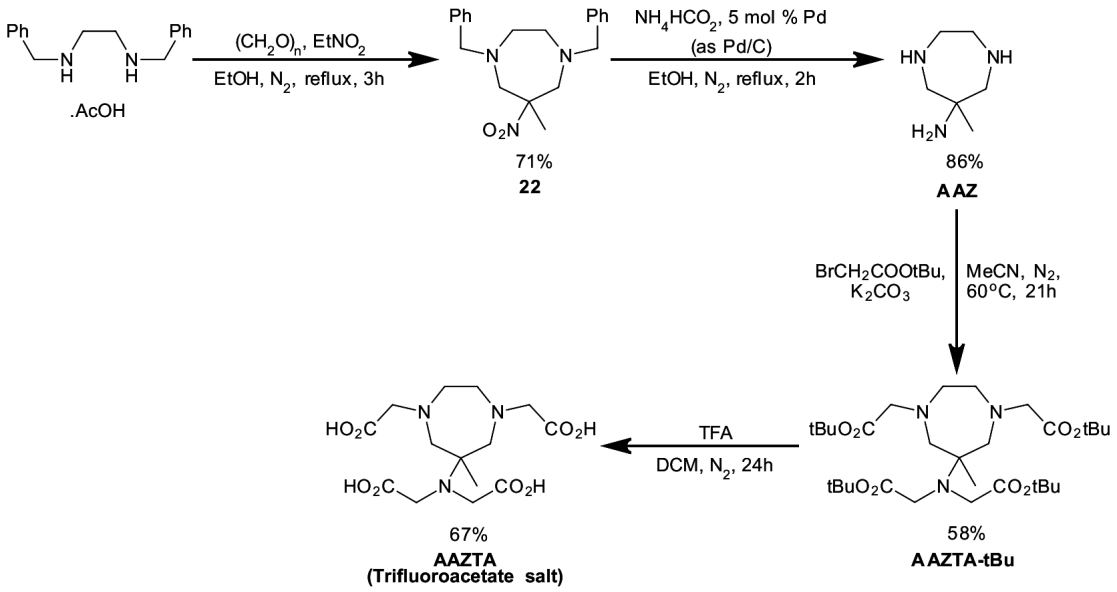

Scheme 29: Preparation of **AAZTA**.

*The reported procedure calls for a supply of hydrogen at 28 MPa, an extremely high hydrogen pressure.

5.2.3. DO3A

The t-butyl ester of this ligand, **DO3A-tBu** is used extensively as a precursor in the synthesis of functionalised **DOTA** ligands such as those in ***Chapter 3***. **DO3A** itself, however, has received less attention as a chelator in its own right; this is probably due to the lanthanide complexes of **DO3A** being less kinetically and thermodynamically stable than complexes based on a **DOTA**-type ligand. Aside from the novelty of studying **DO3A** in an antibacterial context, a comparison of the biological activities of **DO3A** and **AAZTA** would serve to demonstrate the effect of changing a carboxylate donor to an amine, even if the orientation of the donor groups were different. **DO3A-tBu** was therefore synthesised according to methods developed in this group,[240] followed by t-butyl ester deprotection in the usual way (***Scheme 30***).

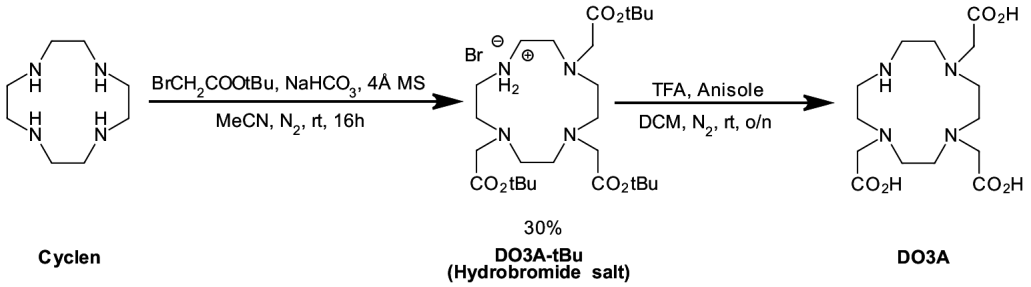

Scheme 30: Preparation of **DO3A**. A final yield is not reported because of the hygroscopicity of the ligand.

5.3. Growth inhibition studies

5.3.1. General remarks

Because of the high aqueous solubility of the ligands tested in the following sections 0.2M K_2HPO_4 was used as the buffer, meaning that cross comparison between the data to follow and those presented in ***Chapter 3,*** and data up to a ligand concentration of 2.5 mM for systems studied in ***Chapter 4,*** is possible. As for work in the previous chapters, the **EDTA** dose response is shown in grey for each experiment as an indicator of experimental reliability.

5.3.2. Macrocycle ring size: effects on growth inhibition

Three well-known ligand systems, **DOTA**, **NOTA** and **TETA**, were tested for their dose response (***Figure 52***), on account of the metal affinities and selectivities that were reported for each.

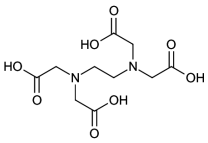

EDTA

[EDTA] / mM	Growth cf. control /%
0	100 ± 6
0.625 (7.5)	98 ± 8
1.25	78 ± 5
2.5	49 ± 10
5.0	36 ± 6
10.0 (7.2)	23 ± 4

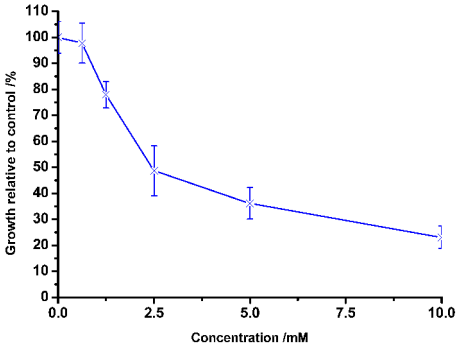

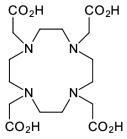

DOTA

[DOTA] / mM	Growth cf. control /%
0	100 ± 5
0.625 (7.2)	99 ± 5
1.25	43 ± 8
2.5	13 ± 12
5.0	12 ± 1
10.0 (7.0)	11 ± 1

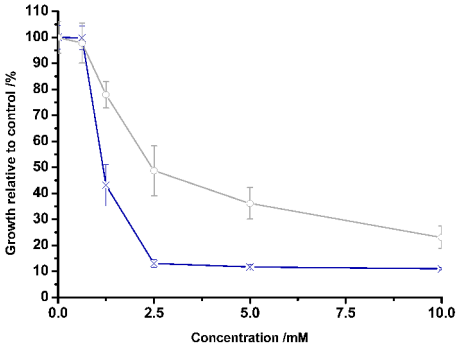

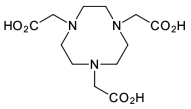

NOTA

[NOTA] / mM	Growth cf. control /%
0	100 ± 2
0.625 (7.1)	69 ± 8
1.25	47 ± 3
2.5	4 ± 1
5.0	2 ± 1
10.0 (7.0)	2 ± 1

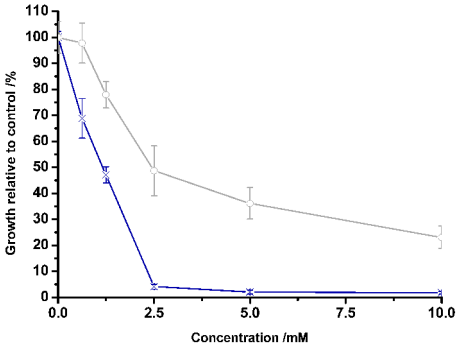

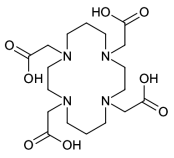

TETA

[TETA] / mM	Growth cf. control /%
0	100 ± 17
0.625 (7.4)	99 ± 13
1.25	103 ± 13
2.5	103 ± 16
5.0	103 ± 18
10.0 (7.2)	91 ± 12

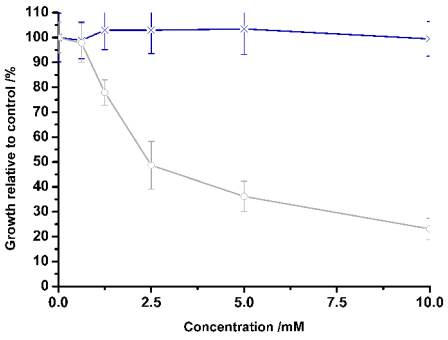

Figure 52: Dose response curves for *E. coli* JM101 upon dosing with **EDTA**, **DOTA**, **NOTA** and **TETA**. Bacteria were incubated for 16 h at 37°C in a medium composed of of 90:10 v/v TSB: 10x ligand stock in 200mM K_2HPO_4 (in-well [K_2HPO_4] of 20mM). Values are the mean of three technical repeats. Both error bars and margins represent two standard deviations from the mean. Bracketed values adjacent to tabulated concentrations are the pH of test solutions based on the same media used for the dose response experiment. Blue lines represent the dose response of the ligand, and grey lines represent the dose response of EDTA.

The data show that **TETA** does not significantly inhibit *E. coli* JM101 growth, and that at concentrations $\geq$1.25 mM, **NOTA** is more inhibitory than **DOTA**. The shapes of the dose responses are similar with the extent of inhibition reaching a plateau at 2.5 mM for both of these ligands, in contrast to the more gradual dose response observed for **EDTA**.

Based on structure alone, it seems that smaller macrocycles are better growth inhibitors of *E. coli* JM101, most likely due to the selectivity these ligands would have for the first row transition metals. More information could be gleaned, however, through a comparison of the metal association constants of these ligands (***Table 33***).

Table 33: log $K_{a_{cond}}$ values calculated for pH = 7.4 to closer reflect the metal ion affinity of **DOTA**, **NOTA**, **TETA** and **EDTA** in liquid media.

Entry	Equilibrium quantity	DOTA[i]	NOTA[ii]	TETA[iii]	EDTA[iv]
a	α-coefficient	1.50 x 10^{-7}	9.56 x 10^{-5}	7.57 x 10^{-7}	1.61 x 10^{-3}
b	log K_a (Ca^{2+})	16.37	8.92	8.53	10.61
c	log $K_{a_{cond}}$ (Ca^{2+})	9.55	4.90	2.41	7.82
d	log K_a (Mg^{2+})	11.2	9.69	3.01	8.83
e	log $K_{a_{cond}}$ (Mg^{2+})	4.33	5.67	-3.11	6.04
f	log K_a (Fe^{3+})	29.4	28.3	26.5	25.0
g	log $K_{a_{cond}}$ (Fe^{3+})	22.6	24.3	20.4	22.2
h	log K_a (Mn^{2+})	19.9	14.9	11.3	13.81
i	log $K_{a_{cond}}$ (Mn^{2+})	13.1	10.9	5.18	11.0
j	log K_a (Zn^{2+})	20.8	18.3	16.4	16.44
k	log $K_{a_{cond}}$ (Zn^{2+})	14.0	14.2	10.3	13.65

i) pK_a and Zn^{2+} values from Anderegg.[241] Ca^{2+} $Mg^{2+}$and Fe^{3+} values from Clarke.[242, 243] Mn^{2+} value from Bianchi.[244] **ii)** pK_a values from Van der Merwe.[245] Ca^{2+} and Mg^{2+} values from Bevilacqua. [246] Fe^{3+} value from Clarke.[242] Mn^{2+} value from Cortes.[247] Zn^{2+} value from Hama.[248] **iii)** pK_a , Ca^{2+} , Mg^{2+} and Fe^{3+} values from Clarke.[242] Mn^{2+} value from Chaves.[249] Zn^{2+} value from Delgado.[250] **iv)** All **EDTA** values from Martell.[164]

From these data, the poor inhibition of **TETA** was assigned to its lower metal ion affinities compared to **DOTA** and **NOTA**. Although the metal ion affinities for **DOTA** and **NOTA** are similar, **NOTA** has higher affinities for Fe^{3+} and Mg^{2+} (entries ***e*** and ***g***), and it may be possible that the increased Fe^{3+} affinity (at the experimental pH) of **NOTA** compared to **DOTA** is the cause of the degree of inhibition it exhibits, similar to the observation in ***Chapter 4*** that **HBED** derivatives projected to have a higher $K_{a_{cond}}(Fe^{3+})$ will display greater growth inhibition.

It is also interesting to note that the only major difference between the metal ion binding characteristics of **DOTA** and **EDTA** is the higher $K_{a_{cond}}$ of **DOTA** for Ca^{2+}, which could imply that the increased outer membrane permeabilisation of **DOTA** may be capable of, compared to **EDTA** might be the cause of the greater inhibition it exhibits. **DOTA** also has slow complexation kinetics,[251] which may be of importance.

5.3.3. Acyclic octadentate ligands: effects on growth inhibition

The powerful inhibition that the octadentate ligands **AmGly$_2$**, **AmPy$_2$**, and **DOTA** (***Figures 23***, ***25*** and ***52***, respectively) displayed, prompted a study of other octadentate ligands, to gauge the importance of ligand denticity to growth inhibition. To this end, the acyclic ligands **EGTA** and **DTPA** were selected for study (***Figure 53***).

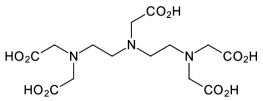

DTPA

[DTPA] / mM	Growth cf. control /%
0	100 ± 7
0.625 (7.5)	38 ± 4
1.25	7 ± 1
2.5	6 ± 1
5.0	6 ± 1
10.0 (7.3)	5 ± 1

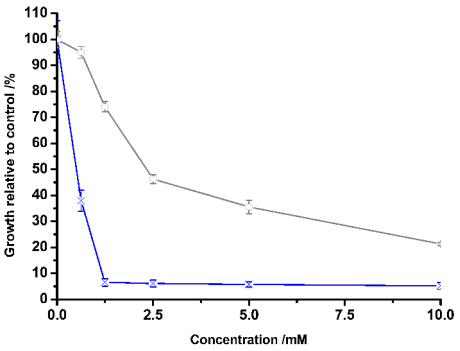

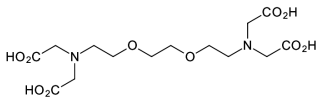

EGTA

[EGTA] / mM	Growth cf. control /%
0	100 ± 5
0.625 (7.4)	96 ± 4
1.25	92 ± 4
2.5	92 ± 3
5.0	92 ± 3
10.0 (7.0)	90 ± 4

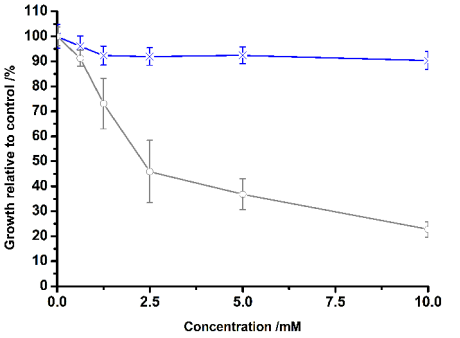

Figure 53: Dose response curves for *E. coli* JM101 upon dosing with **DTPA** and **EGTA**. Bacteria were incubated for sixteen hours at 37°C in a medium composed of of 90:10 v/v TSB: 10x ligand stock in 200mM K_2HPO_4 (in-well [K_2HPO_4] of 20mM). Values are the mean of three technical repeats. Both error bars and margins represent two standard deviations from the mean. Bracketed values adjacent to tabulated concentrations are the pH of test solutions based on the same media used for the dose response experiment. Blue lines represent the dose response of the ligand, and grey lines represent the dose response of EDTA.

From the above, and for **TETA**, it could be seen that higher denticity was not a key determinant for *E. coli* growth inhibition, and once again, consultation of metal ion affinity data was used to see if other trends were apparent (***Table 34***). The data for **AmGly$_2$** have also been shown for comparison.

Table 34: $K_{a_{cond}}$ values calculated for pH= 7.4 to closer reflect the metal ion affinity of **DTPA**, **EGTA,** **$AmGly_2$** and **EDTA** in liquid media.

Entry	Equilibrium quantity	DTPA	EGTA[ii]	$AmGly_2$	EDTA
a	α-coefficient	4.3 x 10^{-5}	2.98 x 10^{-4}	5.80 x 10^{-1}	1.61 x 10^{-3}
b	K_a (Ca^{2+})	10.7	11.0	7.00	10.61
c	$K_{a_{cond}}$ (Ca^{2+})	6.33	7.48	6.76	7.82
d	K_a (Mg^{2+})	9.30	5.30	5.10	8.83
e	$K_{a_{cond}}$ (Mg^{2+})	4.93	1.78	4.86	6.04
f	K_a (Fe^{3+})	28.0	20.5	11.81	25.0
g	$K_{a_{cond}}$ (Fe^{3+})	23.6	17.0	11.6	22.2
h	K_a (Mn^{2+})	15.6	12.3	9.28	13.81
i	$K_{a_{cond}}$ (Mn^{2+})	11.2	8.78	9.04	11.0
j	K_a (Zn^{2+})	18.3	14.4	10.41	16.44
k	$K_{a_{cond}}$ (Zn^{2+})	13.9	10.9	10.2	13.65

i) pK_a, $Ca^{2+}$and Mg^{2+} values from Anderegg (2005).[241] Fe^{3+} and Zn^{2+} values from Caravan.[252] Mn^{2+} value from Anderegg (1959).[253] **ii)** pK_a values from Anderegg.[254] Ca^{2+} value from Wright.[255] Mg^{2+} value from Smith.[256] Fe^{3+} value from Schroeder.[257] Mn^{2+} value from Holloway.[258] Zn^{2+} value from Doi.[259]

From these data and those for the macrocyclic ligands, it would appear that if a ligand had a low Mg^{2+}affinity, it would display inferior inhibition, this being highlighted by comparison of the metal ion affinity values for **EGTA** and **$AmGly_2$**, which are similar for Ca^{2+}, Mn^{2+} and Zn^{2+}(entries ***c, i*** and ***k***). What is especially noteworthy is that **EGTA** possesses a far higher $K_{a_{cond}}$ value for Fe^{3+} than **$AmGly_2$**, but a much lower value for Mg^{2+} (entries ***e*** and ***g***), yet **$AmGly_2$** displayed much greater *E. coli* growth inhibition than did **EGTA** (***Figures 23*** and ***53***). This behaviour is also observed for **TETA** (***Figure 52*** and ***Table 33***) .

The apparent importance of Mg^{2+} affinity for these ligands may suggest that a ligand-induced outer membrane disruption process is a mechanism of inhibition operating for aminocarboxylate ligands, but not for the phenolate ligands covered in ***Chapter 4.*** These systems (**4-R-HBED** and **4-R-EHPG** derivatives), had extremely low Ca^{2+} and Mg^{2+} affinities, yet still inhibited bacterial growth. It is on this basis that the study of the interactions of some "magnesium dependent" ligands like **$AmGly_2$** or **NOTA** with a suitable membrane mimic is suggested, to clarify the role of Mg^{2+} sequestration in cell damage.[21, 260]

5.3.4. Heptadentate ligands: effects on growth inhibition

Now that the inhibitory effect of a set of hexadentate and octadentate ligands had been determined, the inhibitory effects of the heptadentate ligands were investigated. This was motivated by the observed depletion of manganese from *E. coli* JM101 by aminocarboxylate ligands, meaning that extensive sequestration of the metal could give strong inhibitory effects. There is a higher percentage of seven-coordinate complexes for Mn^{2+} reported in the CSD than for Fe^{2+}, Fe^{3+} and Zn^{2+} as a fraction

of all of the complexes reported for these metal ions,[261] and the higher selectivity that **DO3A** has for Mn^{2+} over Ca^{2+} binding compared to **DOTA** has recently been shown, alluding to the possibility that heptadentate ligands are strong Mn^{2+} binding units in general.[262] Thus, **AAZTA**, **DO3A** and **PN2C4** were studied to see what effect (if any) reducing denticity from eight- to seven- had on the dose response (***Figure 54***).

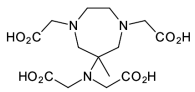

AAZTA

[AAZTA] / mM	Growth cf. control /%
0	100 ± 5
0.625 (7.4)	96 ± 5
1.25	6 ± 2
2.5	3 ± 0
5.0	2 ± 2
10.0 (7.2)	2 ± 2

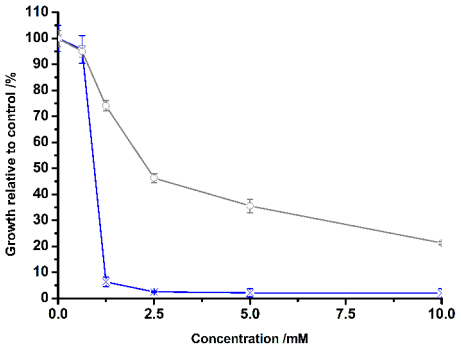

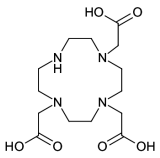

DO3A

[DO3A] / mM	Growth cf. control /%
0	100 ± 3
0.625 (7.4)	89 ± 4
1.25	79 ± 2
2.5	53 ± 1
5.0	31 ± 2
10.0 (7.2)	23 ± 1

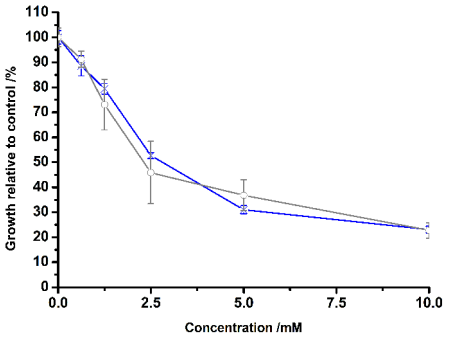

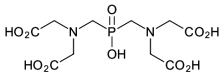

PN2C4

[PN2C4] / mM	Growth cf. control /%
0	100 ± 4
0.625 (7.7)	60 ± 12
1.25	47 ± 2
2.5	48 ± 5
5.0	41 ± 8
10.0 (7.4)	29 ± 4

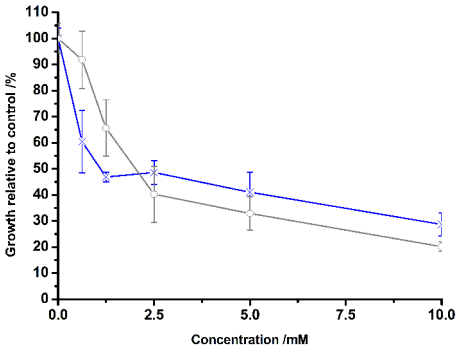

Figure 54: Dose response curves for *E. coli* JM101 upon dosing with **AAZTA**, **DO3A**, and **PN2C4**. Bacteria were incubated for 16 hours at 37°C in a medium composed of of 90:10 v/v TSB: 10x ligand stock in 200mM K_2HPO_4 (in-well [K_2HPO_4] of 20mM). Values are the mean of three technical repeats. Both error bars and margins represent two standard deviations from the mean. Bracketed values adjacent to tabulated concentrations are the pH of test solutions based on the same media used for the growth curves. Blue lines represent the dose response of the ligand, and grey lines represent the dose response of EDTA.

Remarkably, **AAZTA** is the most inhibitory of these ligands, presumably due to the lowered pK_a of the amine donors compared to those in **DO3A**, which exhibits a much weaker growth inhibition than **DOTA**. Unfortunately, the absence of sufficiently comprehensive metal ion binding data for **AAZTA**,

DO3A and **PN2C4** precluded a full inspection of the metal ion affinities of these ligands in light of their dose response. With this in mind, it can be seen from ***Table 35*** that **DO3A** has slightly higher metal ion affinities than **AAZTA**, with the exception of Ca^{2+} (entry ***c***), suggesting that outer membrane permeabilisation, or kinetic effects may be operating for **AAZTA**.

Table 35: $K_{a_{cond}}$ values calculated for pH=7.4 to closer reflect the metal ion affinity of **AAZTA**, **DO3A**, **PN2C4** and **EDTA** in liquid media. All data for **AAZTA** were at T=25°C and I=0.1M and taken from Baranyai *et al.*[263] pK_a, Ca^{2+} and Zn^{2+} values for **PN2C4** from Kálmán.[264] Mg^{2+} value from Tircsó[265]

Entry	Equilibrium quantity	AAZTA	DO3A	PN2C4	EDTA
a	α-coefficient	1.3 x 10^{-4}	1.98 x 10^{-7}	6.77 x 10^{-3}	1.61 x 10^{-3}
b	K_a (Ca^{2+})	12.76	12.6	7.66	10.61
c	$K_{a_{cond}}$ (Ca^{2+})	8.88	5.87	5.49	7.82
d	K_a (Mg^{2+})	8.31	11.6	7.65	8.83
e	$K_{a_{cond}}$ (Mg^{2+})	4.42	4.94	5.48	6.04
f	K_a (Mn^{2+})	15.4	19.4	-	13.81
g	$K_{a_{cond}}$ (Mn^{2+})	11.6	12.7	-	11.0
h	K_a (Zn^{2+})	18.0	21.6	15.9	16.44
i	$K_{a_{cond}}$ (Zn^{2+})	14.1	14.9	13.7	13.7

There is only a small difference in metal ion affinities between **EDTA** and **AAZTA**, but a marked difference exists in their dose response. On this basis, it is suggested that **AAZTA** may have a higher Fe^{3+} affinity compared to **EDTA** at pH 7.4, and experimental confirmation of this may be useful.

5.4. Effect of AAZTA on cellular metal content

As the ICP-MS data in ***Chapter 3*** showed, manganese is the metal most extensively depleted from *E. coli* JM101 cells by **EDTA** and **$AmGly_2$** , and this depletion could not be predicted from inspection of the metal ion affinities for either ligand alone. Along these lines, the similar metal ion affinities, but strikingly different dose responses of **EDTA** and **AAZTA** at pH 7.4, prompted an investigation of the effect of **AAZTA** on *E. coli* cellular metal content (***Figure 29***), to see if any further information could be obtained regarding the observed inhibition profile.

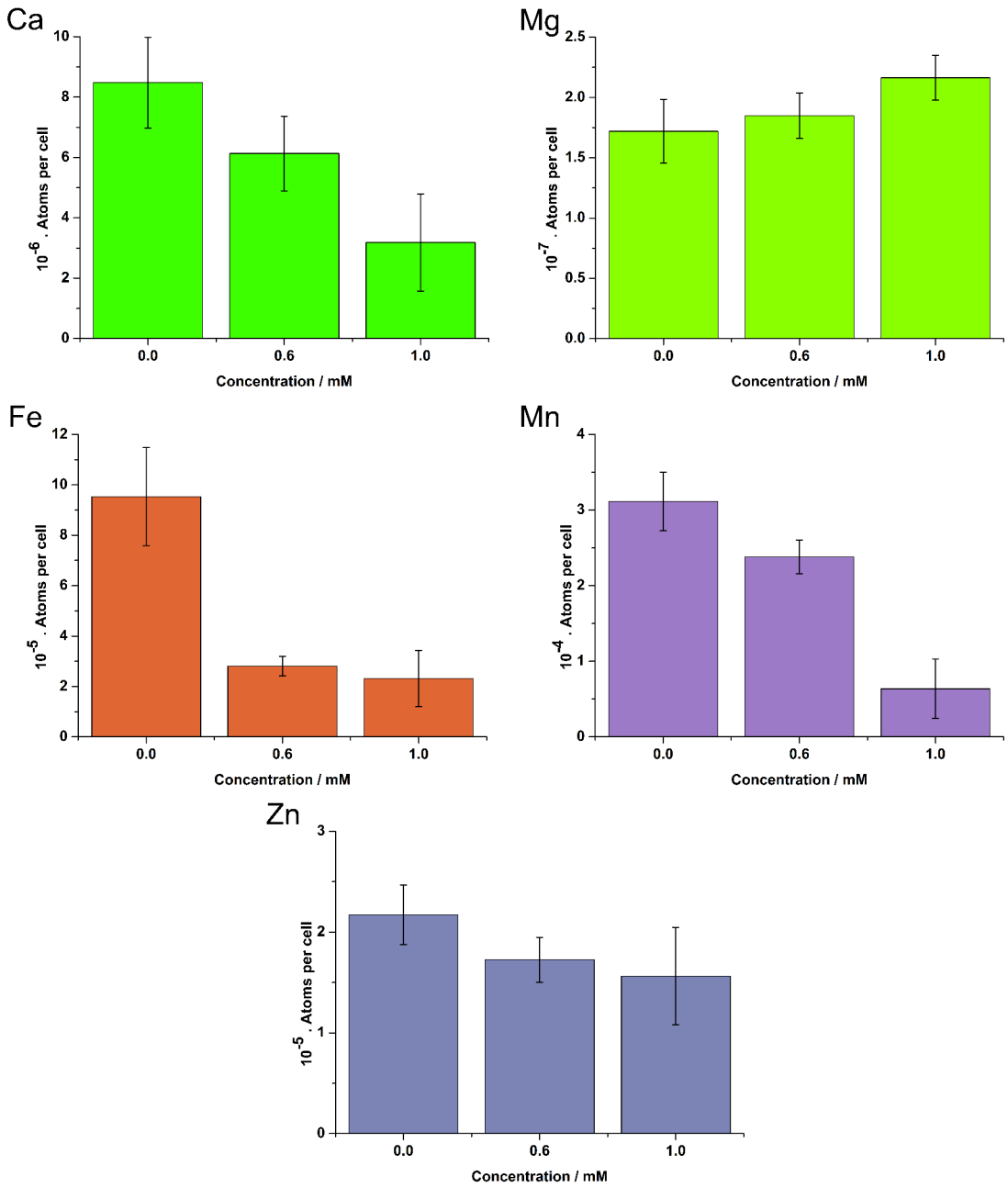

Figure 55: Effect of **AAZTA** on the metal content of *E. coli* JM101 cells at stationary phase. Values are the average of three biological repeats. Error bars represent two standard deviations of the mean. Cells were incubated aerobically at 37°C for 16 hours in a medium consisting of 99:1 v/v TSB:0.2 M K_2HPO_4 containing 100x [**AAZTA**] prior to harvest.

In this case, iron *is* depleted from the cells, in addition to manganese. Although **EDTA** depletes both of these metals at 1.0mM, the depletion is not as drastic as that observed for **AAZTA**. Without an assessment of the Fe^{3+} binding strength of **AAZTA** however, no certain conclusions can be made on the origin of this phenomenon and so such a study should be considered in future work.

Studies on abcessed organs in mice also show simultaneous iron and manganese deficiencies compared to neighbouring tissues,[106, 266] and reductions of iron and manganese concentrations in growth media treated with human Calprotectin leading to *E. coli* growth inhibition have been reported.[56, 57] Because there is some overlap between the roles of manganese and iron in bacteria,[174]

the simultaneous starvation of these metals may be one of the reasons behind the enhanced toxicity of **AAZTA** at lower concentrations compared to to **EDTA**, **AmGly$_2$** or **EHPG**. That the effects on manganese and iron observed for **AAZTA** are also seen in the natural world as part of an antimicrobial defence strategy[173, 193] was highly gratifying.

5.5. Towards rational ligand design: Synthesis and properties of NOON

5.5.1. Motivation and synthesis

The observations that **EHPG** depleted iron from *E. coli* JM101 selectively (***Figure 51***), and that phenolate donor ligands have very low Ca^{2+} and Mg^{2+} affinities at pH 7.4 (***Figure 39*** and ***Table 30***), but were still capable of inhibiting *E. coli* growth, and that **TETA** and **EGTA** exhibited limited *E. coli* growth inhibition (***Sections 5.3.2*** and ***5.3.3***) was intriguing, considering the low $K_{a_{cond}}$ values **HBED**, **EHPG**, **TETA** and **EGTA** all had for Ca^{2+} and Mg^{2+}.

At this point, it was thought that enough information had been gathered on a sufficiently wide variety of ligands and their effects on cellular metal content to attempt the design of an analogue of a known ligand that exhibited weak growth inhibition by bolstering its Fe^{3+} affinity through optimising the donor groups.

In this case, **EGTA** was selected as the base ligand, because of its low Fe^{3+} affinity and the possibility of enhancing the Fe^{3+} affinity by substituting some carboxylate donors with phenolates. If this was successful, the resulting ligand would have low affinities for Ca^{2+} and Mg^{2+} at pH 7.4, but a high Fe^{3+} affinity. This could result in a metal ion affinity and selectivity profile similar to that of **HBED** or **EHPG**, and possibly similar growth inhibition behaviour, if the supposition that very high ligand-Fe^{3+} affinity can compensate for low affinities for other metal ions, leading to significant inhibition, was true.

The test structure that was selected was {[(o-Hydroxyphenyl)methyl]{2-[2-(2-{(carboxymethyl)[(o-hydroxyphenyl)methyl]amino}ethoxy)ethoxy]ethyl}amino}acetic acid (**NOON**), which could easily be prepared by using the reductive amination-alkylation-deprotection sequence used to prepare the **4-R-HBED** systems in ***Chapter 4*** (***Figure 31***).

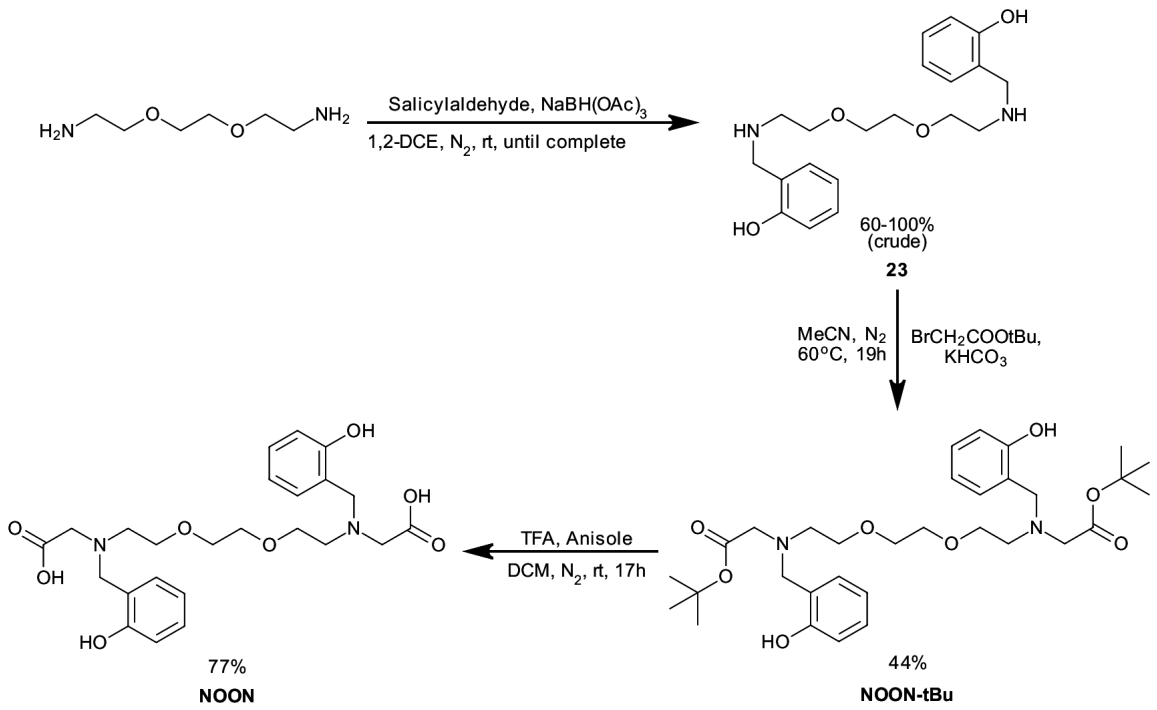

Scheme 31: Synthesis of the **NOON** ligand.

As with many of the other phenolate ligands, chromatography was unnecessary for any part of the synthesis, and single crystal X-ray crystal structures have been obtained for **NOON-tBu**, **NOON** and the **Ca-NOON*** complex, which is one of only two examples of an N_2O_6 ligand saturating the Ca^{2+} coordination sphere in 1:1 stoichiometry (***Figure 56*** and ***Appendix C***).[267]

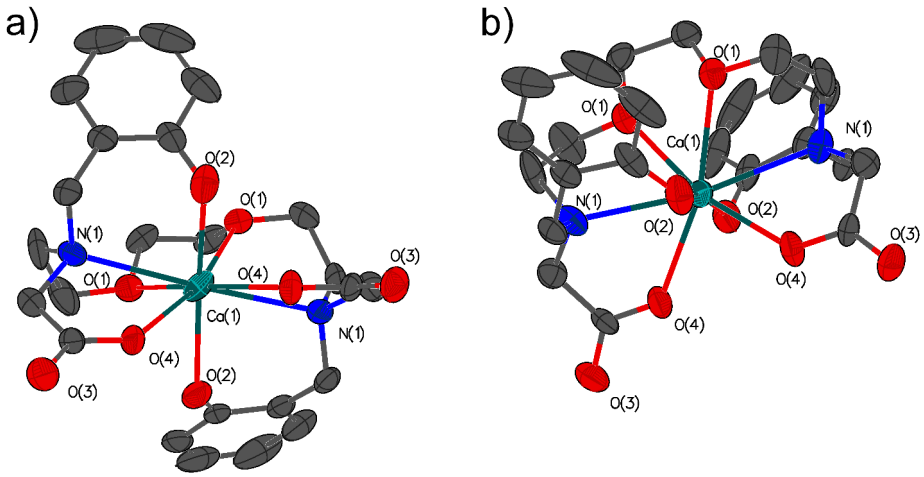

Figure 56: a) Single crystal structure of the Ca^{2+} complex of **NOON** (**Ca-NOON**, the **NOON** ligand is in the "L" form, ***Figure 57***) viewed down the *a*- axis. **b)**: The same structure viewed perpendicular to the *a*-axis illustrating the equatorial coordination around the central Ca^{2+} ion. Counter-ions, hydrogen atoms and outer-sphere water molecules omitted for clarity. Ellipsoids represent 50% probability.

*Species was crystallised and solved by Javier Pitarch-Jarque (University of Valencia)

Measurements of the chelate rings **NOON** forms show that pronounced angle strains are apparent, manifested in the form of large deviations of the bite angles from the ideal bond angles of pentagonal and hexagonal rings (108 and 109º respectively, ***Table 36***).

Table 36: Selected angles and bond distances for **Ca-NOON**. Bracketed values are the standard deviation of the last figure.

Bond lengths		**Bond angles**	
Bond	**Length / Å**	**Atoms**	**Angle /º**
O(1)—Ca(1)	2.591(3)	O(1)—Ca(1)—O(1)	64.26
O(2)—Ca(1)	2.330(3)	O(1)—Ca(1)—O(2)	79.41(11)
O(4)—Ca(1)	2.502(7)	N(1)—Ca(1)—O(1)	64.12(10)
N(1)—Ca(1)	2.746(4)	N(1)—Ca(1)—O(4)	76.5

On comparison to **Ca-AmGly$_1$** structure discussed in ***Section 3.6***, it is also apparent that the donor atom-Ca^{2+} bond lengths in the **Ca-NOON** complex are all substantially longer than those observed in **Ca-AmGly$_1$**. These strained angles suggest that the ligand may be better suited for larger metal ions than Ca^{2+}, Mg^{2+}, Fe^{3+}, Mn^{2+} or Zn^{2+}, something which was also suggested from the following metal ion affinity data. An entropic component may also be at play, in that the long, flexible linker that **NOON** contains will have its conformational freedom reduced more severely than a shorter chain, such as an ethylene diamine upon coordination to a metal ion (***Section 1.4.1***).

5.5.2. Metal binding studies on NOON (in collaboration with the University of Valencia) and its effect on *E. coli* growth

The proton and metal ion binding characteristics of **NOON** were then studied, so as to obtain an understanding of how the structure of the ligand affected the interactions it had, thereby allowing a greater understanding of its bacterial growth-inhibiting behaviour.

Protonation constants. The most relevant protonation states for metal ion binding are displayed in ***Figure 57***.

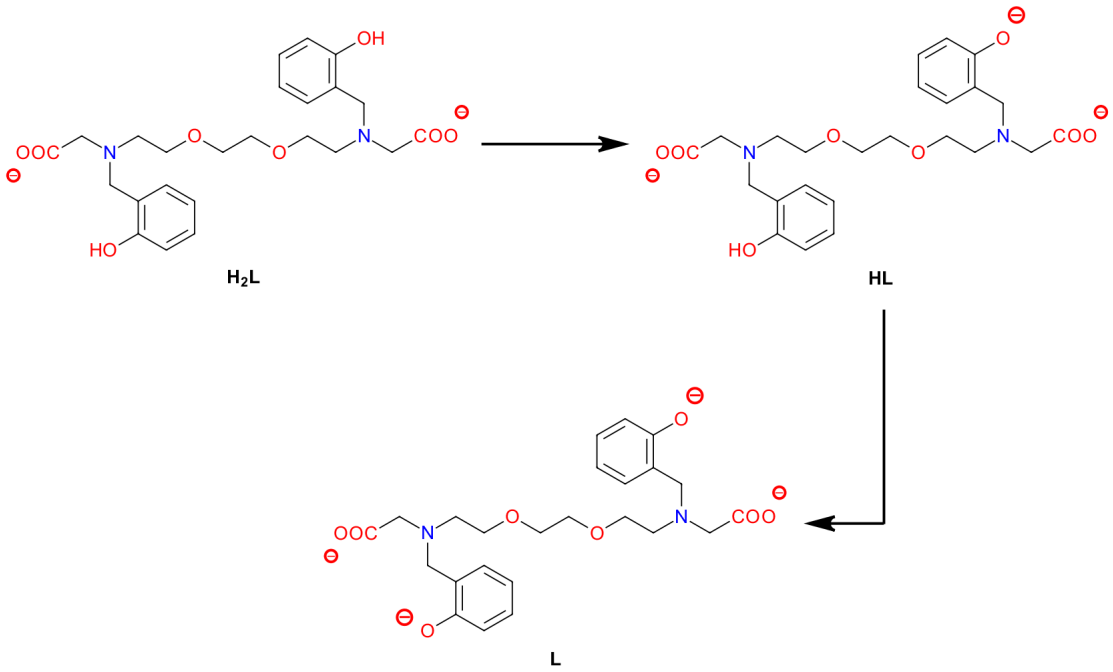

Figure 57: Protonation states of **NOON** most relevant to metal ion binding. Donor groups are highlighted using colour.

Protonation constants are shown in ***Table 37*** alongside those of **HBED** for comparison.

Table 37: Protonation constants for **NOON** determined using pH-potentiometry and UV-Vis titration, compared to reference values for **HBED** (T=25°C, I=0.1 M unless otherwise indicated). Values in brackets represent one standard deviation of the last significant figure. log K_a values without accompanying brackets are K_a values calculated from experimentally determined equilibria . Data for **NOON** are the average of two independent experiments, both performed at T=25°C and I=0.15 M KCl.

Entry	Equilibrium	log K_a	Entry	Equilibrium	log K_a
	NOON			**HBED**[i]	
a	$\frac{[HL]}{[H][L]}$	12.17(1)	**g**	$\frac{[HL]}{[H][L]}$	12.46
b	$\frac{[H_2L]}{[H][HL]}$	10.88(1)	**h**	$\frac{[H_2L]}{[H][HL]}$	11.00
c	$\frac{[H_3L]}{[H][H_2L]}$	8.34(1)	**i**	$\frac{[H_3L]}{[H][H_2L]}$	8.32
d	$\frac{[H_4L]}{[H][H_3L]}$	7.56(1)	**j**	$\frac{[H_4L]}{[H][H_3L]}$	4.64
e	$\frac{[H_5L]}{[H][H_4L]}$	2.65(3)	**k**	$\frac{[H_5L]}{[H][H_4L]}$	2.53
f	$\frac{[H_6L]}{[H][H_5L]}$	1.61(1)	**l**	$\frac{[H_5L]}{[H][H_4L]}$	1.70

i) Data for entries **g-j** from Eplattenier.[205] Entries **k-l** from Motekaitis.[268]

In general, the pK_a values for the phenol groups of **NOON** are very similar to those for **HBED**, indicating that going from the ethylene bridge in **HBED** to the bis-ether bridge in **NOON** has very little effect on the ionisation behaviour of the groups in each case. The origin of the large difference between the fourth protonation event for either ligand (***entries d*** and ***j***) is uncertain, because the site of protonation for **NOON** is unknown, but it is possible that short range interactions between heteroatoms and already protonated sites in **HBED** that cannot form in **NOON** are responsible.

Complexes of Calcium, Magnesium and Zinc. Data are presented in ***Table 38***.

Table 38: Metal-ligand association constants for **NOON** determined using pH-potentiometry, compared to reference values for **NOON** (T=25°C, I=0.1 M unless otherwise indicated). Values in brackets represent one standard deviation of the last significant figure. log K values without accompanying brackets are K_a values calculated from experimentally determined equilibria . Data for **NOON** are the average of two independent experiments, both performed at T=25°C and I=0.15 M KCl.

Entry	Equilibrium	log K_a	Entry	Equilibrium	log K_a
	NOON			**HBED**[i]	
a	$\frac{[CaL]}{[Ca][L]}$	7.34(5)	**j**	$\frac{[CaL]}{[Ca][L]}$	9.29
b	$\frac{[CaHL]}{[H][CaL]}$	9.96	**k**	$\frac{[CaHL]}{[H][CaL]}$	5.52
c	$\frac{[CaH_2L]}{[H][CaHL]}$	8.67	**l**	$\frac{[CaH_2L]}{[H][CaHL]}$	2.02
d	$\frac{[MgL]}{[Mg][L]}$	5.32(5)	**m**	$\frac{[MgL]}{[Mg][L]}$	10.51
e	$\frac{[MgHL]}{[H][MgL]}$	10.77	**n**	$\frac{[MgHL]}{[H][MgL]}$	6.20
f	$\frac{[MgH_2L]}{[H][MgHL]}$	9.41	**o**	$\frac{[MgH_2L]}{[H][MgHL]}$	2.21
g	$\frac{[ZnL]}{[Zn][L]}$	12.17(3)	**q**	$\frac{[ZnL]}{[Zn][L]}$	18.95
h	$\frac{[ZnHL]}{[H][ZnL]}$	10.34	**r**	$\frac{[ZnHL]}{[H][ZnL]}$	8.17
i	$\frac{[ZnH_2L]}{[H][ZnHL]}$	7.51	**s**	$\frac{[ZnH_2L]}{[H][ZnHL]}$	5.83

i) Data for entries **j-o** from Eplattenier.[205] Entries **q-s** from Motekaitis.[268]

From these data, it is obvious that **NOON** forms less stable complexes than **HBED** to Ca^{2+}, Mg^{2+} and Zn^{2+} at high pH, which *may* be due to the steric strain induced in the resulting complexes of **NOON** as suggested by the crystal structure above. It would seem that this effect outweighs the increased stability that octadentate coordination of **NOON** to Ca^{2+} may contribute relative to **HBED**. The complexes that **NOON** forms are much more basic compared to those of **HBED**; this may also lead to a route to “acid-mediated” decomplexation that increases the *rate* of dissociation of the complexes of **NOON** relative to those of **HBED**.

Table 39: Transition metal-ligand association constants for **NOON** determined using pH-potentiometry, compared to reference values for **HBED** (T=25°C, I=0.1 M unless otherwise indicated). Values in brackets represent one standard deviation of the last significant figure. log K_a values without accompanying brackets are K_a values calculated from experimentally determined equilibria. Data for **NOON** are the average of two independent experiments, both performed at T=25°C and I=0.15 M KCl.

Entry	Equilibrium	log K	Entry	Equilibrium	log K
	NOON			**HBED**[i]	
a	$\frac{[FeL]}{[Fe][L]}$	25.68	**g**	$\frac{[FeL]}{[Fe][L]}$	39.01
b	$\frac{[FeHL]}{[H][FeL]}$	7.54	**h**	$\frac{[FeHL]}{[H][FeL]}$	1.51
c	$\frac{[FeH_2L]}{[H][FeHL]}$	4.42			
e	$\frac{[MnL]}{[Mn][L]}$	11.16	**i**	$\frac{[MnL]}{[Mn][L]}$	14.78
f	$\frac{[MnHL]}{[H][MnL]}$	10.20	**j**	$\frac{[MnHL]}{[H][MnL]}$	9.98
			k	$\frac{[MnH_2L]}{[H][MnHL]}$	5.56

i) Data for entries **g-h** from Ma.[202] Entries **i-k** from Eplattenier.[205]

Complexes of Iron and Manganese. As was hoped, the incorporation of the phenol groups increased the Fe^{3+} affinity of the deprotonated **NOON** ligand relative to **EGTA**, but once again, the change in bridge from the ethylene bridge of **HBED** to the bis-ether bridge of **NOON** reduced the stability of the **Fe^{3+}-NOON** complex dramatically compared to the **Fe^{3+}-HBED** complex. Much like the reduced stability of the **Fe^{3+}-EHPG** complex relative to the **Fe^{3+}-HBED** complex (***Section 4.4***), these data also serve to show the importance of the spatial arrangement of donor groups in maximising complex stability even when the individual donor groups form extremely strong interactions with the metal ions in question (***Section 1.4.2***). A similar reduction in Mn^{2+} complex stability is also observed compared to the hexa-coordination of **HBED**, which was likewise assigned to the sub-optimal selection of donor atoms and bridge length.

With these metal ion binding data in hand, calculation of the Schwarzenbach α-coefficient and the metal ion binding constants at pH 7.4 was now possible (***Table 40***).

Table 40: $K_{a_{cond}}$ values calculated for pH=7.4 to closer reflect the metal affinity of **NOON** in liquid media, with the values for **HBED** included for comparison.

Row	Equilibrium quantity	NOON	HBED
a	α-coefficient	6.33×10^{-11}	2.34×10^{-10}
b	K_a (Ca^{2+})	7.34	9.29
c	$K_{a_{cond}}$ (Ca^{2+})	-2.86	-0.34
d	K_a (Fe^{3+})	25.7	39.7
e	$K_{a_{cond}}$ (Fe^{3+})	15.5	30.1
f	K_a (Mg^{2+})	5.32	10.5
g	$K_{a_{cond}}$ (Mg^{2+})	-4.89	0.87
h	K_a (Mn^{2+})	11.2	14.8
i	$K_{a_{cond}}$ (Mn^{2+})	0.96	5.17
j	K_a (Zn^{2+})	12.2	18.3
k	$K_{a_{cond}}$ (Zn^{2+})	2.27	8.67

As with the other phenolic ligands discussed in this work, the high pK_a values for **NOON** mean that Ca^{2+} and Mg^{2+} ions are unlikely to be sequestered under the conditions of the dose response experiment, and so outer membrane permeabilisation is very unlikely. It is also evident that the only metal ions that may interact with **NOON** will be Fe^{3+} and Zn^{2+}, but the stark difference in $K_{a_{cond}}(Zn^{2+})$ and $K_{a_{cond}}(Fe^{3+})$ mean that **NOON** is extremely selective for Fe^{3+}. In spite of this, it is probable that the value of $K_{a_{cond}}(Fe^{3+})$ for **NOON**, relative to **EGTA**, was the reason why the ligand did not exhibit any significant bacterial growth inhibitory activity against *E. coli* (***Figure 58***), in that the Fe^{3+} affinity was not sufficiently high to give the same effects on bacterial growth seen for **HBED** and **EHPG**.

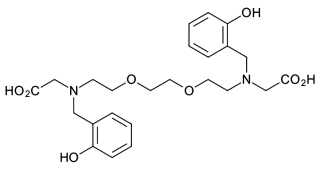

NOON

[NOON] / mM	Growth cf. control / %
0	100 ± 18
0.625 (7.9)	101 ± 17
1.25	104 ± 16
2.5	97 ± 20
5.0	93 ± 16
10.0 (8.3)	87 ± 16

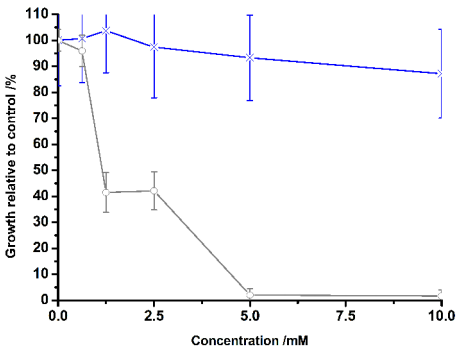

Figure 58: Dose response curves for *E. coli* JM101 upon dosing with **NOON**. Bacteria were incubated for 16 hours at 37°C in a medium composed of of 90:10 v/v TSB: 10x ligand stock in 400mM K_2HPO_4 (in-well [K_2HPO_4] of 40mM). Values are the mean of three technical repeats. Both error bars and margins represent two standard deviations from the mean. Bracketed values adjacent to tabulated concentrations are the pH of test solutions based on the same media used for the dose response experiment. Blue lines represent the dose response of the ligand, and grey lines represent the dose response of EDTA.

Due to these disappointing results, studies on **NOON** were discontinued. It is recommended that the design of another ligand, perhaps with lower pK_a values and designed to have less strained chelate rings is investigated to evaluate the relevance of extremely high Fe^{3+} affinities on bacterial growth inhibition. It is proposed however, that **NOON** may be usable as an Fe^{3+} buffer for biological assays in a role similar to **EGTA**, which is often used as a Ca^{2+} buffer due to its high selectivity for Fe^{3+} in solution.

5.6. Lipophilicity measurements

Though previous partition coefficient estimations in ***Chapters 3*** and ***4*** showed no evidence of partitioning for the ligands and complexes tested, the same study was performed here to afford data for the analysis discussed in ***Section 5.7***. Only the Fe^{3+} complexes of **DTPA**, **EGTA** and **NOTA** were considered (***Table 41***). These complexes were likely to be more lipophilic than the free ligands, which were almost certain not to partition into the organic phase.

Table 41: PBS:1,2-Dichloroethane partition coefficients (P_{DCE}) for the Fe^{3+} complexes of **DTPA**, **EGTA** and **NOTA** at a buffer pH of $\approx$7.4 . Data are the average of two independent experiments. Error margins represent two standard deviations from the mean.

Entry	Species	Charge at pH	P_{DCE} / No units
a	**Fe-DTPA**	-2[i]	0$\pm$0[ii] (extremely hydrophilic)
b	**Fe-EGTA**	-1[iii]	0.0$\pm$0.0[ii] (slightly hydrophilic)
c	**Fe-NOTA**	-0[iv]	0.0$\pm$0[ii] (extremely hydrophilic)

i) Calculated from Caravan *et al.*[252] **ii)** No detectable absorption in dichloroethane layer. **iii)** Calculated from Schroeder[257] **iv)** Calculated from Clarke and Martell.[242]

The absence of measurable partitioning is consistent with the behaviour of other iron complexes studied, and indicates that their membrane permeation is unlikely.

5.7. What is the most important factor in predicting ligand efficacy?

5.7.1. Introduction and strategy

No one molecular property considered throughout this work appeared to dictate the inhibitory power of a ligand in liquid media, meaning that rational ligand design with the aim of maximising growth inhibition at low concentrations would be difficult. Because the identification of the most relevant parameters for *E. coli* growth inhibition would greatly facilitate ligand design for other workers, efforts were turned to the development of a preliminary model of *E. coli* growth inhibition through using combinations of variables.

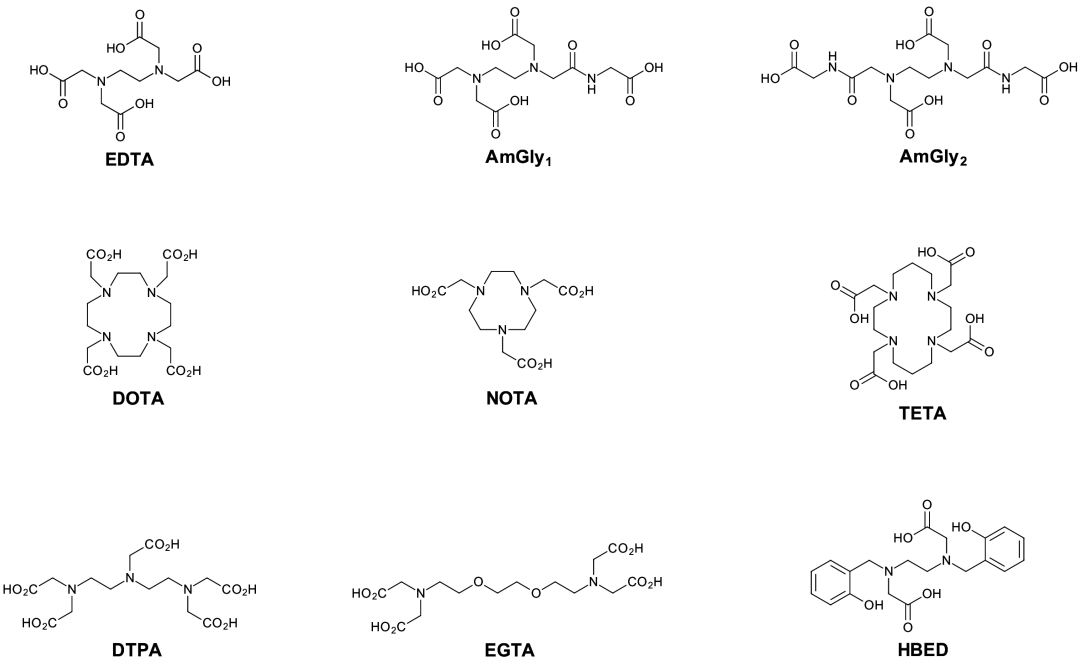

Figure 59: Ligands considered in efforts towards a predictive model of *E. coli* JM101 growth inhibition in TSB.

This study began by selecting ligands that had already been tested for inhibition, but which also had known protonation constants and metal ion affinities (Ca^{2+}, Mg^{2+}, Fe^{3+}, $Mn^{2+}$and Zn^{2+}) along with partition coefficients (***Figure 59***), to provide a pool of data.

Once the candidate ligands were selected, the data set to be used could now be constructed.

5.7.2. Assembly of a data set

Although high metal ion affinities were key to growth inhibition, the question of which metal(s) were of greatest importance remained unanswered. Because it was not certain which formulation of the metal ion affinity for a ligand gave the closest relationship to *E. coli* growth inhibition, both $K_{a_{cond}}$ and K_a values for a set of metal ions were entered into the data set. Structural features of the ligands, such as denticity and number of atoms in each chelate ring, were also incorporated as auxiliary parameters which did not affect growth inhibition at a given concentration, but did influence metal ion affinity.

Up until now, the concentrations of the metal ions in media has not been discussed, partly because of the limited relevance metal ion concentrations had in the previous discussions on structure with the extent of growth relative to control. Metal ion concentrations in media (both complex and defined) vary by orders of magnitude, and so if a metal ion is present in low concentration in a liquid medium, the metal ion affinity a ligand required for complete (or close to complete) sequestration will need to be higher.

Conversely, metal ion affinities for metal ions present at higher concentrations in the medium need

not be so high, provided enough of the ligand is available for complete sequestration. Therefore, the magnitude of some metal ion affinities will be more important than others, and this will be dictated by the composition of the media. This raised the possibility that tracking ligand effects on free metal ion concentrations *in situ* could give better correlations and the observed growth relative to control (referred to as *GRC* for brevity). [269]Because of the number of equilibria involved and their interrelation with one another, experimental measurement of free metal ion concentrations was not possible. To overcome this, a simple computational model was employed.

5.7.3. A simple model of metal speciation in TSB

The speciation modelling program HySS[270] and equilibrium data obtained from the SCDbase or potentiometric work covered earlier (***Sections 3.5.1***) were used to model the interaction between the ligands in ***Figure 59*** and the metal content of TSB, for which the values of Damo *et al*.[56] were used after applying a correction for the 90% v/v TSB used in the growth inhibition experiments.

Because TSB is a complex medium, some approximations were necessary. These were that:

- The pH of the simulated media is 7.4, at a temperature of 25°C.
- All iron present in the simulation is in the +3 oxidation state. Indeed, Fe^{2+} would also be present, but the absence of added reducing agents and non-anaerobic conditions meant that Fe^{3+} was likely to be the predominant oxidation state *in situ*. Similarly, all manganese was considered to be in the +2 oxidation state.
- Trace metal ions such as those of copper and cobalt were not considered, meaning that only Ca^{2+}, Mg^{2+}, Fe^{3+}, Mn^{2+} and Zn^{2+} were simulated.
- Because it is impossible to know what the ligating species in TSB are, no competing ligands, e.g. peptides, amino acids or simple inorganic ligands were incorporated into the model. This implied that all of the metal ion content in the simulation existed as hydrated species available for binding, or “free” metal, and that in reality, the free metal ion concentrations would be lower than would be calculated.
- No hydroxo- complexes of the formula $[ML(OH)_n]^{x-}$, where $n > 1$ were formed.

Working within these approximations, free metal ion concentrations could then be calculated for media in the presence or absence of a given ligand at a set concentration (***Figure 60***). Because of the large variation in the values of free metal ion concentrations, these concentrations have been expressed as $p(M^{n+})$ values, where $p(M^{n+}) = -log[M^{n+}]$. Because of the way $p(M^{n+})$ is formulated, a higher $p(M^{n+})$ is reflective of a *lower* free metal ion concentration.

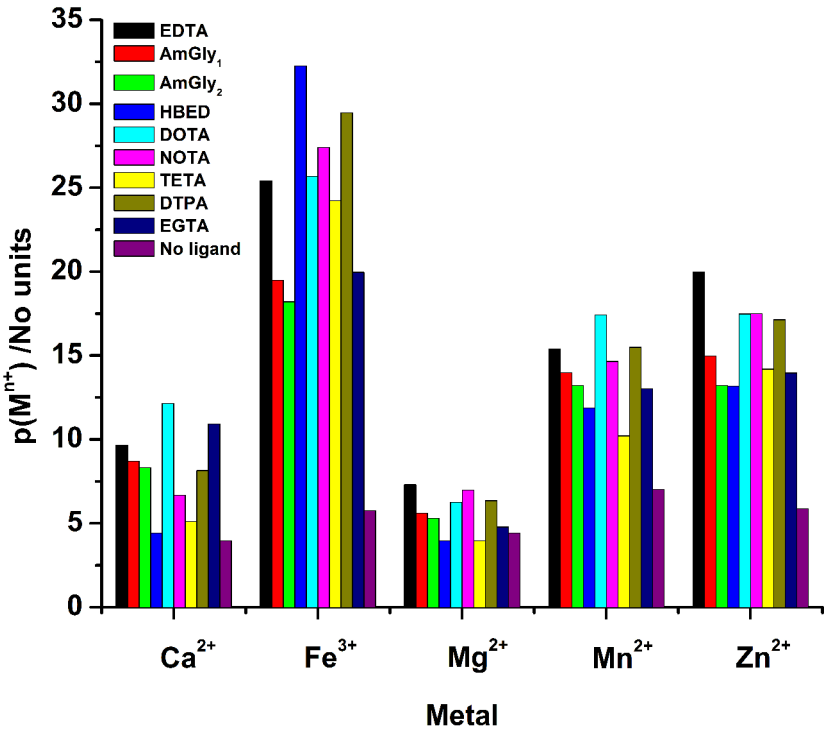

Figure 60: Calculated $p(M^{n+})$ values in a model bacterial growth medium for the test ligands at [**L**]=2.5 mM.

It is noteworthy that aminocarboxylate ligands such as **DOTA**, **NOTA**, and **DTPA** that exhibit higher $p(M^{n+})$ values in the model gave lower GRC at 2.5 mM of ligand. The $p(Fe^{3+})$ values for these ligands are slightly higher than for **EDTA**, and may have contributed to the increased inhibition observed for **DOTA**, **NOTA**, and **DTPA** at lower concentrations cf. **EDTA**.

Now that estimates of the effects on metal ion concentrations were available for each ligand, they could be incorporated into the final data set for correlation analysis (***Table 42***).

Table 42: Ligand properties and associated transformations checked for correlations with GRC at [**L**]=2.5 mM.

Row	Structural features	Equilibrium properties	Modelled medium data
a	Total number of atoms participating in all possible chelate rings	α-coefficient	$[Ca^{2+}]_{free}$
b	Number of donor atoms	log $K_{a_{cond}}(Ca^{2+})$	$[Mg^{2+}]_{free}$
c	Charge on free ligand (pH =7.4)	log $K_{a_{cond}}(Mg^{2+})$	$[Fe^{3+}]_{free}$
d	P_{DCE} (Fe^{3+} complex)	log $K_{a_{cond}}(Fe^{3+})$	$[Mn^{2+}]_{free}$
e	P_{CDCl_3} (free ligand)	log $K_{a_{cond}}(Mn^{2+})$	$[Zn^{2+}]_{free}$
f		log $K_{a_{cond}}(Zn^{2+})$	$100(\frac{[Ca^{2+}]_{free}}{[Ca^{2+}]_{total}})$
g		$\sum logK_{a_{cond}}(M^{n+})$	$100(\frac{[Mg^{2+}]_{free}}{[Mg^{2+}]_{total}})$
h		$\prod logK_{a_{cond}}(M^{n+})$	$100(\frac{[Fe^{3+}]_{free}}{[Fe^{3+}]_{total}})$
i		$K_{a_{cond}}(Ca^{2+})$	$100(\frac{[Mn^{2+}]_{free}}{[Mn^{2+}]_{total}})$
j		$K_{a_{cond}}(Mg^{2+})$	$100(\frac{[Zn^{2+}]_{free}}{[Zn^{2+}]_{total}})$
k		$K_{a_{cond}}(Fe^{3+})$	$p(Ca^{2+})_{free}$
l		$K_{a_{cond}}(Mn^{2+})$	$p(Mg^{2+})_{free}$
m		$K_{a_{cond}}(Zn^{2+})$	$p(Fe^{3+})_{free}$
n		$\sum K_{a_{cond}}(M^{n+})$	$p(Mn^{2+})_{free}$
o		$\prod K_{a_{cond}}(M^{n+})$	$p(Zn^{2+})_{free}$
p		$K_a(Ca^{2+})$	$\sum[M^{n+}]_{free}$
q		$K_a(Mg^{2+})$	$log(\sum[M^{n+}]_{free})$
r		$K_a(Fe^{3+})$	$100(\frac{\sum[M^{n+}]_{free}}{\sum[M^{n+}]_{total}})$
s		$K_a(Mn^{2+})$	
t		$K_a(Zn^{2+})$	

5.7.4. Analysis of the data

The small sample size used meant that the use of multiple regression and linear discriminant analysis methods to determine the most important contributor to growth inhibition in the data set was inappropriate.[271] Therefore, simpler methods of assessing correlations were used, the most useful being the nonparametric Spearman rank correlation coefficient, a measure similar to the Pearson correlation coefficient, but adapted for data that does not follow a normal distribution (the small sample size and absence of multiple ligands in the data set with identical metal affinities meant that this was the case). Using the Spearman correlation coefficient, no significant ($p < 0.05$) correlations between GRC at 2.5mM and the equilibrium parameters in ***Table 42*** were found.

If the candidate set of ligands was truncated to simple aminocarboxylates however (thus excluding **HBED**, **AmGly$_1$** and **AmGly$_2$**), it was apparent that quantities related to Fe^{3+} sequestration (***Figure 61***) showed the strongest correlation to the GRC at 2.5 mM.

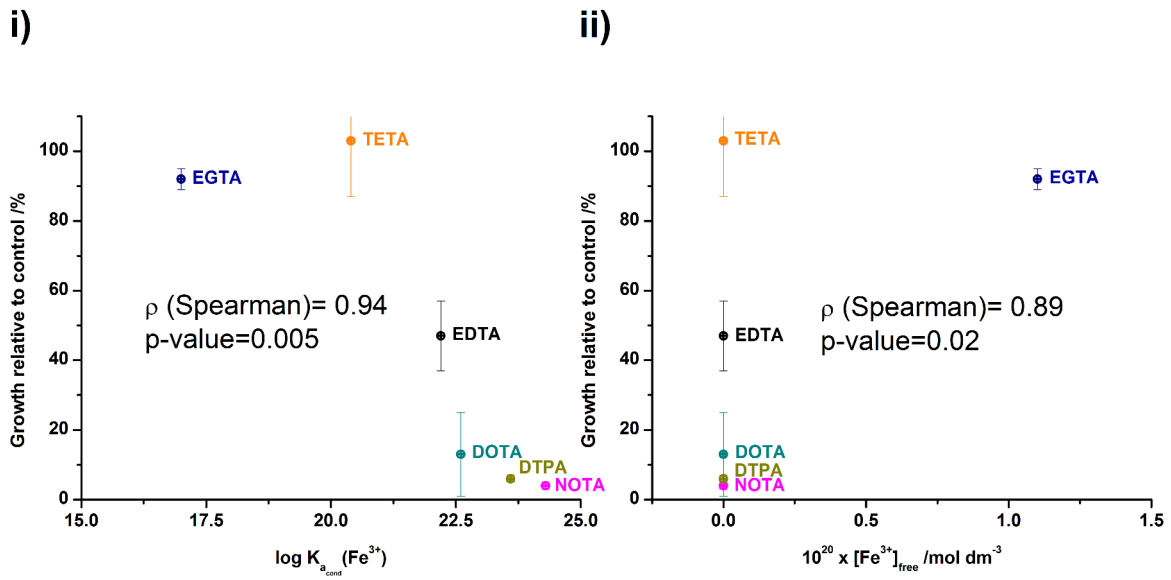

Figure 61: Correlations between *E. coli* growth relative to control at 2.5mM and **i)** log $K_{a_{cond}}(Fe^{3+})$, and **ii)** the molar concentration of free Fe^{3+} in the model media. Error bars represent two standard deviations from the mean of three technical repeats.

The monotonic, non-linear relationship between log $K_{a_{cond}}(Fe^{3+})$ underlines the importance of the ion for the various cellular processes of *E. coli*, which was covered earlier (***Section 4.1***). Owing to the small sample size used for the development and validation of this model, it is of limited use. Nevertheless, these correlations indicated that a greater ability to sequester Fe^{3+} in the model growth media may lead to reduced GRC values for aminocarboxylate ligands. Further work will be necessary to extend this model to more “aytpical” ligands bearing amide, phenol and other groups.

5.8. Conclusions for this chapter

A collection of commonly used ligands were tested for their growth inhibition properties against *E. coli* JM101, and the outcomes considered in light of their conditional metal ion affinities. For aminocarboxylates, ligand denticity did not appear to be a major factor for growth inhibition. Two different profiles of chelation induced bacterial growth inhibition are proposed, based on the apparent importance of the Mg^{2+} affinity of aminocarboxylate ligands to *E. coli* growth inhibition, and the observation that phenolic ligands like **EHPG** and **HBED** are capable of inhibiting bacterial growth even though they are unlikely to bind Mg^{2+} particularly well. To see whether increasing Fe^{3+} affinity could increase *E. coli* growth inhibition, an analogue of **EGTA**, the novel ligand **NOON**, was synthesised. Unfortunately, the high pK_a values of **NOON** meant that metal ion binding in media was attenuated to the point where it was ineffective as a growth inhibitor.

Studies on cellular metal content of *E. coli* cells treated with different concentrations of **AAZTA**, a powerful inhibitor of *E. coli* growth, were also undertaken, and showed simultaneous iron and manganese depletion; an effect that has recently been observed with human calprotectin, which has been shown to act as a bacterial growth inhibitor.

Based on a model of TSB and elementary statistical methods, a tentative link between Fe^{3+} affinity for aminocarboxylate ligands at pH 7.4 and *E. coli* growth inhibition has been identified. Because of the low sample size (six ligands) used however, the evaluation of a greater number of ligands to test the relevance of such a link is necessary. If such work is fruitful, then a principle for the design of aminocarboxylate ligands that are strong inhibitors of *E. coli* growth, i.e. the need for a high Fe^{3+} affinity at the pH of use, will have been established.

6. Towards new ligand structures

6.1. Introduction

The presence of tertiary amines in the ligands most inhibiting of *E. coli* growth (e.g. **$AmGly_2$**, **4-Br-HBED**, **NOTA** and **DTPA**) was likely to render such systems non-biodegradable (***Figure 62***).[72] Consequently, if one of these ligands were to be used as an **EDTA** alternative, the environmental impact would also be uncertain. A solution to this problem then, may be the synthesis of ligands with a similar inhibition profile to those in ***Figure 62,*** but which also incorporated certain "biodegradable" structural features, like chiral carbon atoms, secondary amines and electron-rich aromatic groups.

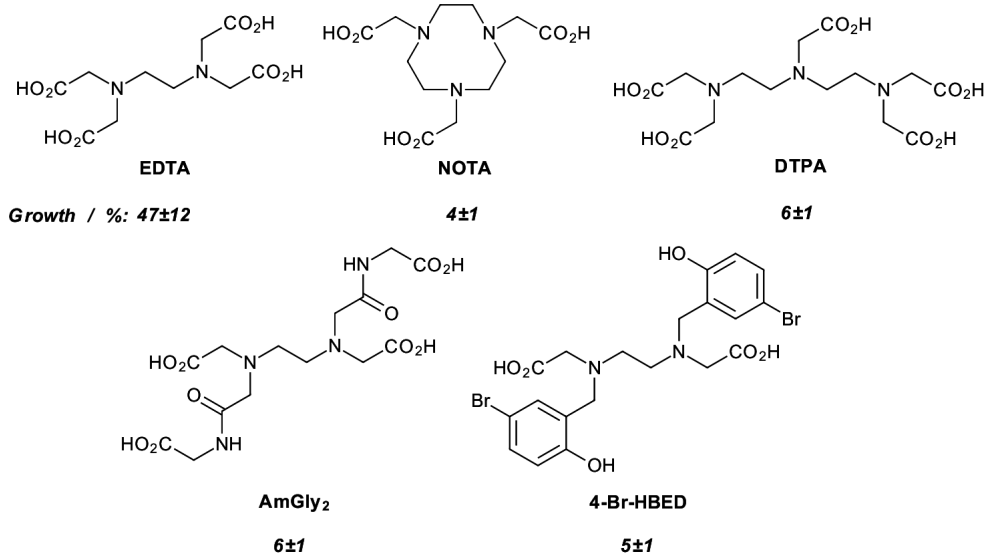

Figure 62: Ligands with superior *E. coli* JM101 growth inhibition compared to **EDTA**, as measured by percentage growth relative to control (at [**L**]=2.5 mM, italicised).

A complementary approach, where analogues of ligands known to be biodegradable are synthesised, could also be useful. Many biodegradable ligands currently in mass production, e.g. **EDDS**[17] or **NTA**, have significant shortcomings, such as low metal ion affinities and the need for a high operating pH (***Table 43***).

Table 43: log $K_{a_{cond}}$ values calculated for pH=7.4 to closer reflect the metal ion affinities of **EDDS**, **NTA** and **EDTA** in liquid media. All data presented were measured at T=25°C and *I*=0.1M.

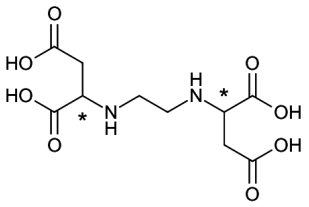

EDDS

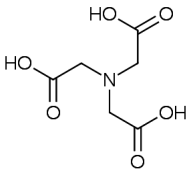

NTA

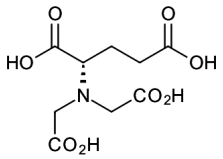

GLDA

Row	Equilibrium quantity	EDDS[i]	NTA[ii]	GLDA[v]	EDTA
a	α-coefficient	1.51 x 10^{-3}	2.51 x 10^{-3}	9.83 x 10^{-3}	1.61 x 10^{-3}
b	log K_a (Ca^{2+})	4.58	6.31	5.9	10.61
c	log $K_{a_{cond}}$ (Ca^{2+})	1.76	3.71	3.9	7.82
d	log K_a (Mg^{2+})	5.82	5.36	5.2	8.83
e	log $K_{a_{cond}}$ (Mg^{2+})	3.00	2.76	3.2	6.04
f	log K_a (Fe^{3+})	20.6	24.0[iii]	15.3	25.0
g	log $K_{a_{cond}}$ (Fe^{3+})	17.8	21.4[iii]	13.3	22.2
h	log K_a (Mn^{2+})	8.97	-[iv]	7.6	13.81
i	log $K_{a_{cond}}$ (Mn^{2+})	6.14	-[iv]	5.6	11.0
j	log K_a (Zn^{2+})	13.6	10.5	11.5	16.44
k	log $K_{a_{cond}}$ (Zn^{2+})	10.8	7.93	9.5	13.65

i) EDDS values for pK_a, Fe^{3+}, Mn^{2+} and Zn^{2+} from Orama.[272]All values correspond to the S,S- isomer. Ca^{2+} and Mg^{2+} values from Gorelov.[273]The measured isomer could not be ascertained. **ii) NTA** pK_a values from Majlesi[274], Ca^{2+} data from Craggs[275], Mg^{2+} data from Bohigian[276] and Fe^{3+} data from Motekaitis.[277] **iii)** Overall stability constant for the formation of an ML_2 complex. **iv)** Data not available. **v)** All data from the AkzoNobel GLDA product guide[278]

Synthetic approaches towards analogues of biodegradable ligands are uncommon in the literature, and so the development of a general route in itself could facilitate the study of analogues by other workers.

Based on the strategies proposed above for the synthesis of biodegradable ligands, structures based on analogues of **DTPA** and **GLDA** were considered. The reasons for these choices are discussed below.

6.1.1. Motivations for the preparation of GLDA analogues

GLDA (***Table 43***) is well known as a readily biodegradable ligand based on l-glutamic acid, sold by AkzoNobel under the trade name Dissolvine® GL. A number of patents (ca. 350)* have been granted describing its use in niches similar to **EDTA**, e.g. in cleaning, personal care, soil treatment and cosmetics. The metal ion affinities for **GLDA** are somewhat low, meaning that **GLDA** is unlikely to be as active as **EDTA** at similar concentrations *in situ* (***Table 43***).

As with all aminocarboxylate ligands, the metal ion affinities increase as a function of pH, and in the case of **GLDA**, the optimum pH range for metal sequestration is 8-10 for Ca^{2+}, Mg^{2+}, Mn^{2+} and Zn^{2+}.[278] For certain applications, where a low pH is necessary, e.g. in shampoo, this is problematic. Therefore, the preparation of an analogue of **GLDA** which retained good metal affinity across a wide pH range was a clear way to address this shortcoming. An alternative strategy to raise the effective pH range was based on exploiting the relationship observed between log $K_{a_{cond}}(Fe^{3+})$ and *E. coli* growth inhibition (***Section 5.7***), as well as the reduced influence of low $K_{a_{cond}}$values for Ca^{2+}, Mg^{2+}, Mn^{2+} and Zn^{2+} on *E. coli* inhibition when $K_{a_{cond}}(Fe^{3+})$ was especially high (***Section 4.3***). Based on these lines of reasoning, two **GLDA** analogues, **$PyGl_3$** and **$HBGl_3$** were targeted for synthesis (***Figure 63***).

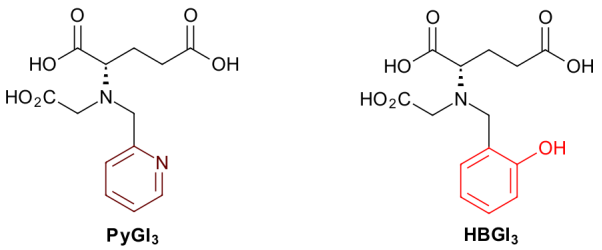

Figure 63: Analogues of **GLDA** targeted for wide pH range performance (**$PyGl_3$**), and stronger Fe^{3+} binding (**$HBGl_3$**) compared to the **GLDA** parent structure.

$PyGl_3$ was selected based on an inspection of the pK_a values for **GLDA**, with the first protonation event being assignable to the central amine. This protonation would contribute to a disruption in the chelate ring formation that is less likely to be present in di-, or poly-amine ligands, because of their ability to form chelate rings with a metal ion even if one of the amines is protonated (***Figure 64***).

*Based on searching patents related to CAS No: 58976-65-1 (**GLDA** as the free acid) in the SciFinder database (January 2016).

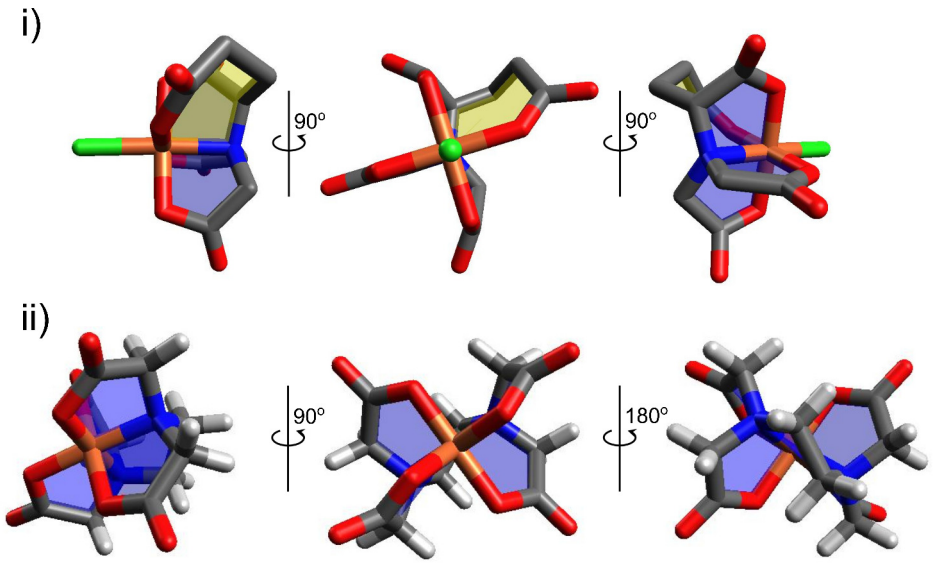

Figure 64: Geometry-optimised (UFF) models of **i)** the **Fe-GLDA** chelate, showing how all of the chelate rings involve the sole amine group, and **ii)** the **Fe-EDTA** chelate. In this case, if one of the amine groups is protonated, not all of the chelate rings will be affected. Because no single crystal X-ray structures of **GLDA** or its metal complexes have been reported, a guess of the coordination mode was necessary.

It would be useful then, to lower the pK_a of the central nitrogen atom by the attachment of a nearby electron-withdrawing group which was also capable of coordination. Based on these factors, and literature pK_a values, a picolyl group was chosen for the purpose (***Figure 65***).

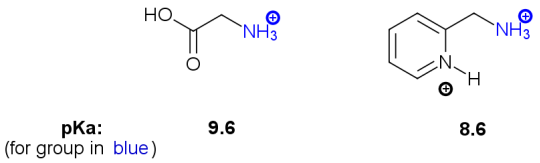

Figure 65: A comparison between the pK_a values[279] of glycine and 2-picolylamine.

$HBGl_3$ on the other hand, would likely have a higher pK_a value for the amine group than **GLDA**, but would be structurally similar to the **HBIDA** ligand, which possesses a high $K_a(Fe^{3+})$, and a correspondingly high $K_{a_{cond}}$ (Fe^{3+}) at pH 7.4 (***Figure 66***). By analogy to **HBIDA**, it could be anticipated that **$HBGl_3$** would exhibit a higher Fe^{3+} affinity across a wide pH range, and a stronger inhibitory effect against *E. coli* compared to **GLDA**.

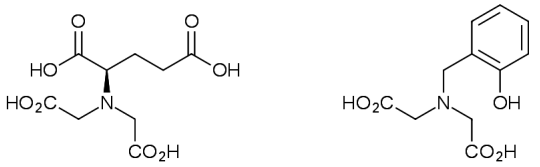

GLDA **HBIDA**

log K_a:	15.3	22.4
log K_{acond} (pH 7.4):	13.3	17.2

Figure 66: log $K_a(Fe^{3+})$ and log $K_{a_{cond}}(Fe^{3+})$ values for **GLDA** and **HBIDA**[280], indicating the contribution of the phenol group to Fe^{3+} complex stability at physiological pH.

6.1.2. DTPA as the basis for a biodegradable ligand

DTPA and **NOTA** were among the most inhibitory ligands tested in this work, but the experimentally demonstrated poor biodegradability of **DTPA**[223] and the low biodegradability predicted for **NOTA**[281] prompted a consideration of how their environmental properties could be improved through the synthesis of analogues. In this case, a **DTPA** based structure was chosen in preference to a **NOTA** based one because of the high cost of the **NOTA** ligand and the parent macrocyclic triamine, as well as the somewhat lengthy syntheses required to access **NOTA** derivatives.[236, 282]

Drawing from the biodegradability of **EDDS**,[17] and **EDDM** (***Figure 67***),[16] a system containing secondary amines was envisaged. As a way of enhancing metal ion affinities compared to **EDDS** which forms some six-membered chelate rings, five-membered chelate rings defined by amine and carboxylate donors were desired in targeted structures. The incorporation of a tertiary amine was also hoped to increase metal ion affinities relative to **EDDM**.[283]

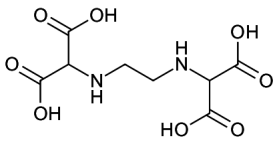

EDDM

Figure 67: Structure of **EDDM**, a biodegradable ligand incorporating malonate donor units.

The conceived structure, **RDTPMal** (***Figure 68***), was predicted to be readily biodegradable in the free state and would also be one of few ligands to incorporate malonate units as donors in a chelating ligand, if the synthesis was successful.

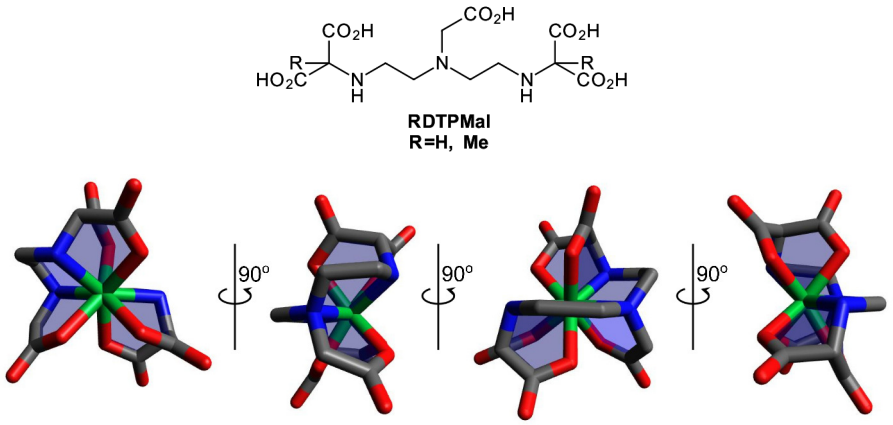

Figure 68: RDTPMal, a candidate structure for a biodegradable analogue of **DTPA**, and a simulated eight-coordinate complex for the R=H structure. Five-membered chelate rings formed are highlighted in blue.

6.2. Synthetic and biological studies of GLDA analogues

6.2.1. Strategy

The obvious starting material in this case was l-glutamic acid, which could be subject to stepwise functionalisation at the amine group. An ester derivative could be used for a possible pathway (***Figure 69***, route **B**). Alternatively, a pre-functionalised amine precursor could be coupled to an α-haloglutarate electrophile prepared[284] from l-glutamic acid (***Figure 69***, route **A**).

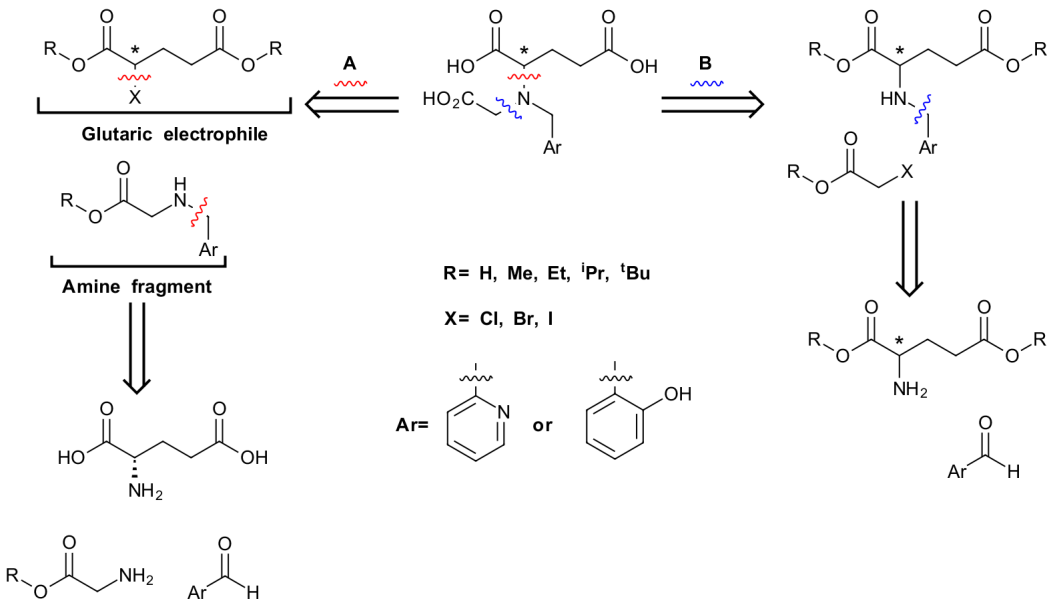

Figure 69: Possible disconnections towards **PyGl$_3$** and **HBGl$_3$**.

To minimise the number of protection/deprotection steps necessary, reductive amination was chosen to install the aromatic fragments in disconnections **A** and **B** in preference to alkylation. This decision was also influenced by the fact that pyridine-2-carboxaldehyde and salicylaldehyde are commod-

ity chemicals, and the preparation of pure oxoacetates is difficult because of their high reactivity.[285] This meant that the addition of the final carboxylate groups to prepare precursors to **PyGl$_3$** and **HBGl$_3$** was probably the more straightforward approach.

6.2.2. Synthesis of intermediates via reductive amination of aldehydes directly onto l-Glutamic acid and derivatives

Initially, a synthesis devoid of any form of protecting group chemistry was trialled. l-Glutamic acid was reacted with salicylaldehyde under the reductive amination conditions described by Sreenivasulu.[286] This convenient procedure could be conducted on a large scale and so was used to afford **24** for further alkylation studies (***Scheme 32***).

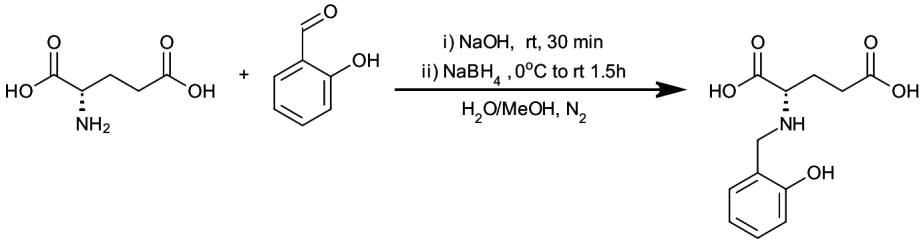

58%
24

Scheme 32: Synthesis of non-protected intermediate **24** via reductive amination.

Alkylations of **24** under a variety of conditions to prepare **HBGl$_3$** or a monoester precursor were unsuccessful (***Table 44***), presumably due to the interference of the carboxylate groups. Informed by results in ***Section 4.2***, it appeared that protection of all of the carboxylate groups as their esters in precursors to **PyGl$_3$** and **HBGl$_3$** was necessary.

Table 44: Unsuccessful alkylation conditions used towards the synthesis of **$HBGI_3$**.

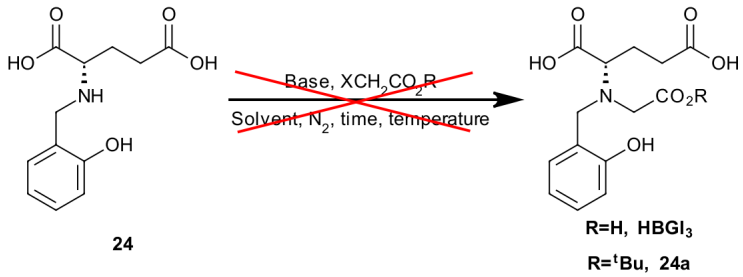

Row	X=	R=	Solvent	Base	Temp. /°C	Time / h	Outcome
a	Cl	H	H_2O	$KHCO_3$	rt	22	No reaction[i]
b	Cl	H	H_2O	Na_2CO_3	60	24	No reaction[i]
c	Br	tBu	H_2O[ii]	NaOH	60	48	Complex mixture[i]
d	Br	tBu	DMF	$KHCO_3$	60	48	No reaction[i]
e	Br	tBu	DMF	Et_3N	60	44	No reaction[i]
f	Br	tBu	MeCN	Et_3N	60	44	No reaction[i]

i) By ES-LCMS. **ii)** Tetra(n-butyl)ammonium bromide added as phase transfer catalyst.

Ethyl and isopropyl esters of glutamic acid were chosen as the amine sources, since they could be made on a large scale using low-cost materials and simple procedures. Methyl esters were not investigated because of their known propensity to cyclise to lactams under reductive amination conditions,[150, 151] a behaviour also seen when diisopropyl glutamate was reacted with salicylaldehyde (***Scheme 33***) to give highly functionalised lactam **25**. This showed that the increased steric hindrance of isopropyl compared to methyl groups was insufficient to inhibit cyclisation.

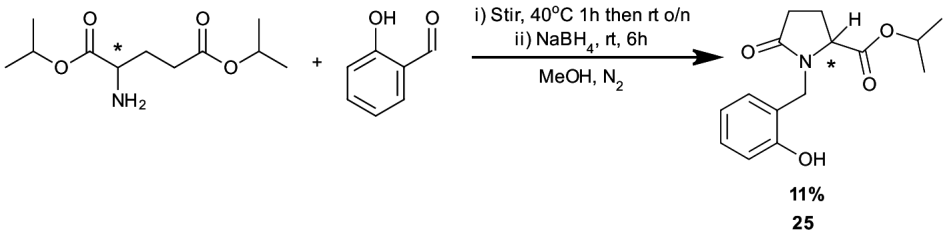

Scheme 33: Reductive amination-cyclisation of diisopropyl glutamate to form lactam **25**.

Because lactam formation requires a sufficiently nucleophilic amine, direct ester protection on **24** could be possible under acidic conditions, so that the amine functionality remained protonated. This was not the case, and in a thionyl chloride mediated esterification (***Scheme 34***), lactam **26** was the only isolable product. It is interesting that **26** retained the *S*- stereochemistry of glutamic acid, in spite of the possibility of acid-catalysed racemisation under these somewhat harsh conditions.

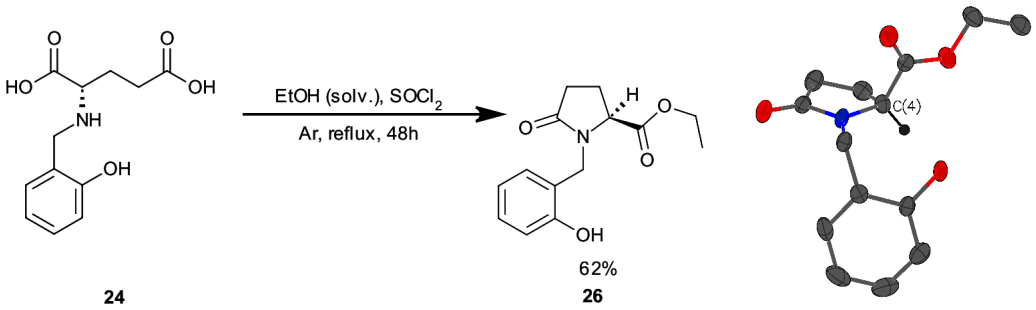

24 26

Scheme 34: Thionyl chloride mediated esterification of **24** leading to lactam formation. A single crystal X-ray structure of lactam **26** was obtained, showing the *S*- configuration at C(4). The hydrogen atom attached to C(4) has been coloured black for clarity. Ellipsoids represent 50% probability.

Two options were apparent in addressing this cyclisation problem: either the development of a route based on disconnection **A**, or the use of t-butyl ester protecting groups. Because t-butyl ester protection is nontrivial, and di-t-butyl glutamate is a costly starting material, the use of simple alkyl esters as protecting groups was investigated first. The resulting aminoesters could be used as alkylating agents (simple glutamic acid esters can be transformed to glutaric halides) to enable the key reaction for disconnection **A** . If this was not fruitful, then the use of t-butyl ester intermediates would be employed as a "method of last resort."

6.2.3. Routes towards $HBGl_3$ employing reductive amination onto glycine derivatives

Development of a route based on disconnection **A** (***Figure 69***), required the preparation of two fragments for coupling in a convergent synthesis. The first was the glutarate electrophile, which could easily be prepared from l-glutamic acid using a diazotisation reaction followed by Fischer esterification to afford α-bromoester **27** in low but workable yields (***Scheme 35***).

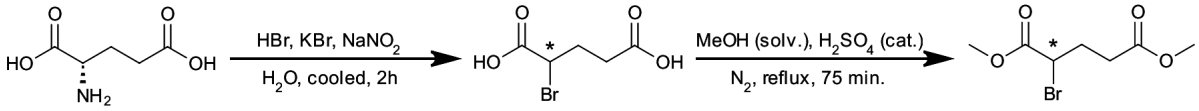

22% (across two steps)

27

Scheme 35: Henig[284] route to **27**, an electrophile for subsequent amine alkylation.

The suppression of cyclisation in this route relied on the fact that once the amine and glutarate fragments were coupled togther, a tertiary amine would result. Even though tertiary amines are nucleophilic, attack of an ester group by a tertiary amine would give an unstable tetrahedral intermediate that would collapse back to the starting materials, as opposed to forming a lactam. To confirm the feasibility of alkylation, and the absence of lactam formation before pursuing the route further, a test alkylation between **27** and dibenzylamine was performed. Because this amine is somewhat

hindered, the reaction times necessary for alkylations of amine fragments of the type described in ***Figure 69*** could be estimated (***Scheme 36***) from this experiment.

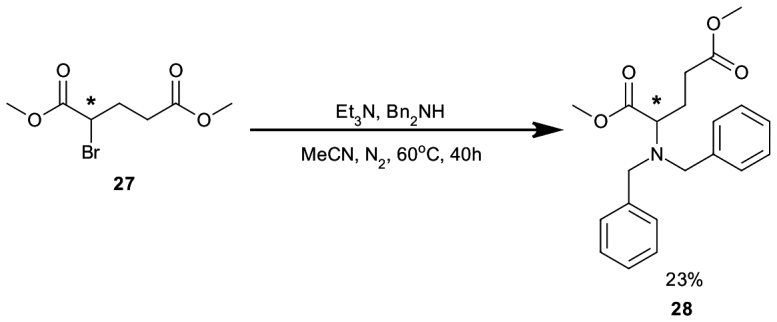

Scheme 36: A test reaction between dibenzylamine and **27** confirming the absence of lactam formation.

No lactam products were isolated, and purification proved straightforward. Therefore synthesis of the amine fragments **HB-28** and **Py-28** (for coupling to **27**) via reductive amination, was undertaken by reacting methyl glycinate with the appropriate aromatic aldehyde. Initially, sodium borohydride was used to prepare **HB-28**, but the recovery of large amounts of 2-hydroxybenzyl alcohol meant that sodium triacetoxyborohydride was used as the reducing agent (***Scheme 37***) in subsequent work.

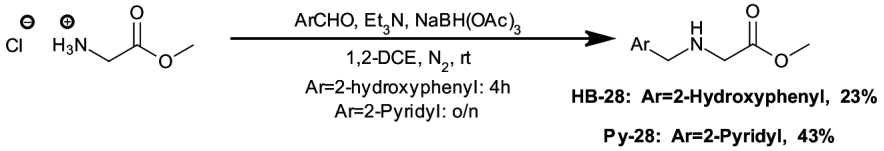

Scheme 37: Reductive amination of salicylaldehyde and pyridine-2-carboxaldehyde with methyl glycinate.

Based on ES-LCMS data, reaction of these substrates with **27** proceeded. In spite of this, no evidence of product formation was present in the ^{1}H NMR spectra of the crude or purified reaction products, meaning that the reaction conditions likely needed optimisation to give workable yields.

One possible explanation came from inspection of a single crystal X-ray structure of **HB-28**, which showed the presence of a hydrogen bonding interaction between the amine lone pair and phenol O-H group, which could lead to the deactivation of **HB-28** as a nitrogen nucleophile (***Figure 70***).

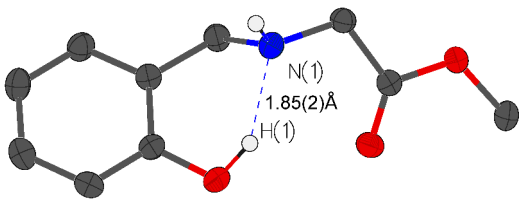

Figure 70: Single crystal X-ray structure of **HB-28** showing the hydrogen bond between the phenol O-H and amine groups. Ellipsoids represent 50% probability.

On the other hand, compounds of type **4-R-21** (***Table 26***), readily underwent alkylation with t-butyl bromoacetate. Moreover, it is unlikely that any sort of intramolecular hydrogen bond would exist in **Py-28**, which also has a less sterically hindered secondary amine group, meaning that some other factor was accountable for the low yields of these reactions. Increasing the reactivity of electrophile **27** to generate the *iodo*- derivative **27a** via the Finkelstein reaction followed by reaction with **HB-28** also did not lead to appreciable product formation (***Scheme 38***).

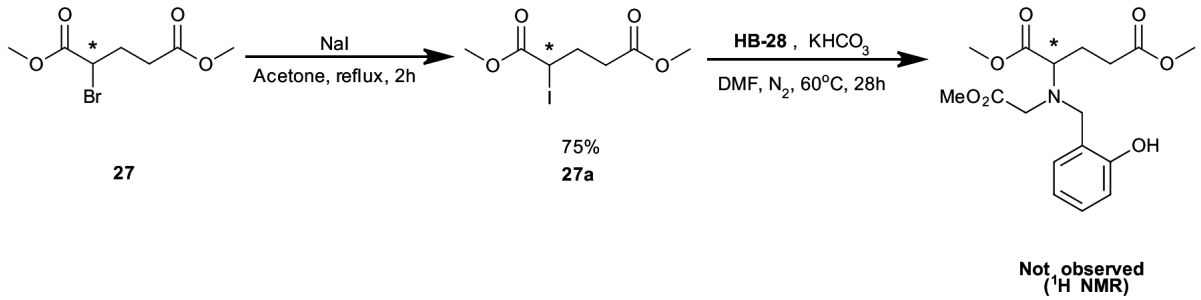

Scheme 38: Test alkylation of **HB-28** using the more reactive electrophile **27a**.

Inspired by the work of Prins *et al*,[287] showing that the synthesis and purification of bulky, tripodal hydroxybenzylamine ligands was facilitated by protection of the phenol groups as their benzyl ethers, the protected amine fragment **HB-28-Bn** was synthesised using the benzyl ether of salicylaldehyde, **29** as the reductive amination substrate (***Scheme 39***). This synthesis proceeded in a higher yield than that of **HB-28**, probably because of the presence of the benzyl ether in **HB-28-Bn** results in improved organic solubility and a more efficient isolation by solvent extraction as a result.

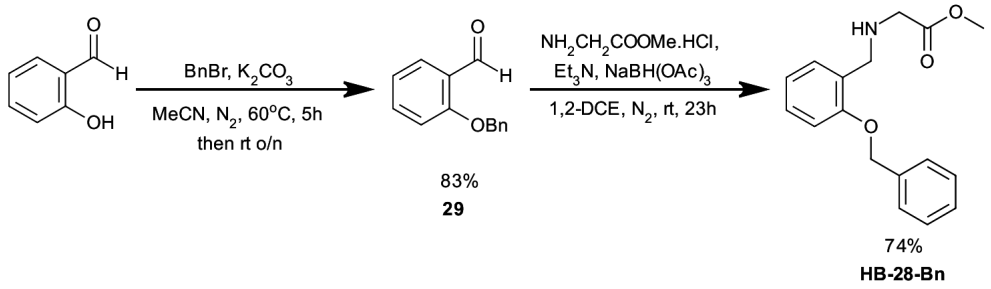

Scheme 39: Synthesis of **HB-28-Bn**, a protected analogue of **HB-28**, via reductive amination.

Remarkably, the reaction between **HB-28-Bn** and **27a** proceeded smoothly in contrast to the reaction of **27** with **HB-28**. Although slow, monitoring of the reaction via GC-MS indicated that conversion did increase over time to furnish precursor **30**, which was inert to benzyl group removal under reductive conditions (***Scheme 40***).

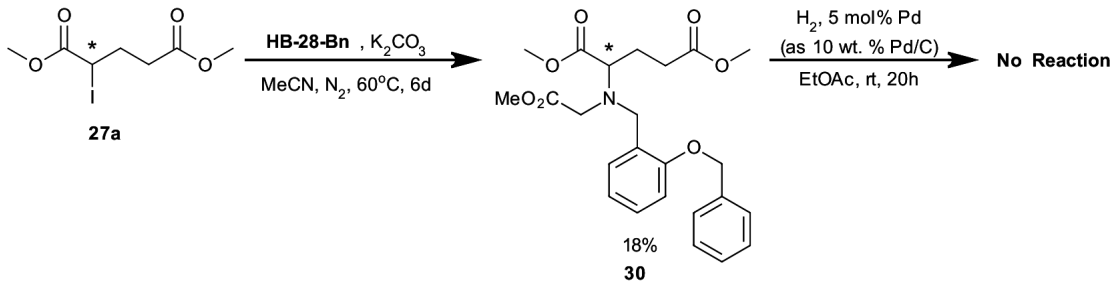

Scheme 40: Synthesis of *O*- benzylated precursor **30** and attempted partial deprotection.

At this point, t-butyl esters were used as carboxylate protecting groups, due to the failure of this partial deprotection, and the large number of steps (six in total) necessary to generate **30**.

6.2.4. Synthesis of $HBGl_3$ via t-butyl ester protected intermediates

Exploiting the inertness to nucleophilic attack that t-butyl ester protection imparts to carbonyl groups (***Section 3.2.3***), reductive amination procedures analogous to those in ***Schemes 37*** and ***33*** were performed on di-t-butyl glutamate to afford **HB-31** and **Py-31** (***Scheme 41***). Using this protocol, no lactam formation was observed, and as an added advantage, column chromatography was unnecessary for **HB-31**.

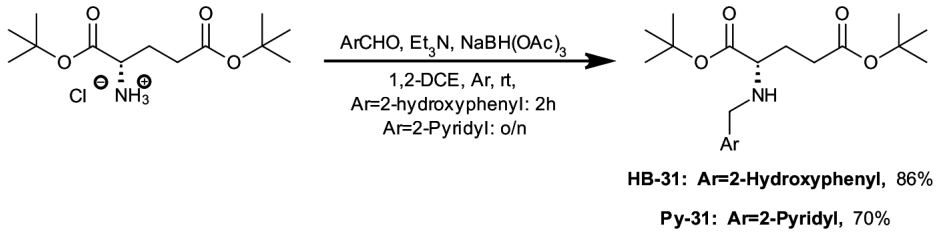

Scheme 41: Reductive amination using a t-butyl protected derivative of glutamic acid to prevent lactam formation.

The subsequent alkylation of **HB-31** using t-butyl bromoacetate, although extremely slow, was straightforward and **$HBGl_3$-tBu** was isolable in low but sufficient yield (***Scheme 42***). This low rate of reaction was expected based on a survey of other alkylations that would have a similar steric demand around the nitrogen atom,[288, 289] in addition to reaction time necessary to access **HB-28-Bn** (***Scheme 41***). The low yield of the final deprotection to afford **$HBGl_3$** was unexpected and has been attributed to the hygroscopicity of the **$HBGl_3$** (as the trifluoroacetate salt) leading to mechanical losses.

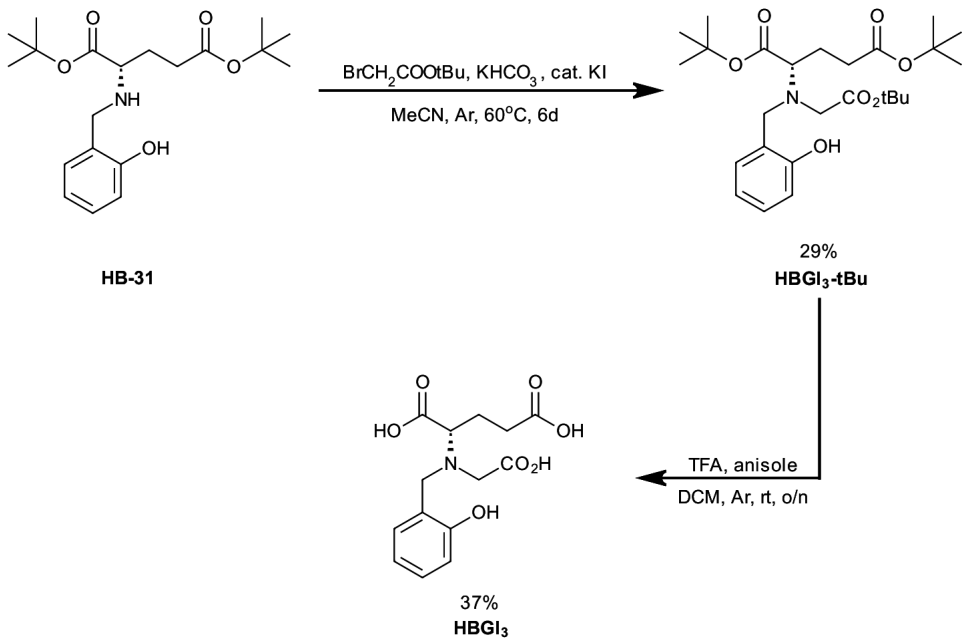

Scheme 42: Successful synthesis of **$HBGI_3$**.

Despite the presence of trace impurities in a representative sample of **$HBGI_3$** as detected by ^{1}H NMR*, sample homogeneity indicated by analytical HPLC analysis (UV detection) and the only impurity peak in an ES-LCMS spectrum being assignable to $[M\text{-}4H\text{+}NH_4]^-$, led to the decision that samples of **$HBGI_3$** were suitable for assay (***Section 6.2.5***). As an aside, the trifluoroacetate salt of **$HBGI_3$** exhibited a higher level of purity based on ^{1}H NMR and ES-LCMS measurements, implying that any side products formed were likely attributable to the workup conditions used.

It would be useful to reduce the reaction time necessary to furnish **$HBGI_3$-tBu**. To achieve this, a variety of conditions including microwave heating and alternative solvents were tested, but none were as high-yielding as those in ***Scheme 42***. Even though extensive conversion of **HB-31** to **$HBGI_3$-tBu** after two hours could be achieved by running the reaction in ***Scheme 42*** in dimethylformamide at 120°C, impurities that could not be removed by column chromatography from samples of **$HBGI_3$-tBu** made in this way meant that this modification was not especially useful.

6.2.5. Growth inhibition properties of $HBGI_3$

With **$HBGI_3$** in hand, the effect of the phenol donor group in a glutamic acid based chelator could now be interrogated. As with the studies in ***Chapters 3*** and ***5***, 0.2M K_2HPO_4 was used as the buffering agent (***Figure 71***).

*Ca. 94% purity based on the ratio of the sum integrals not assignable to **$HBGI_3$**: sum of integrals assignable to **$HBGI_3$**.

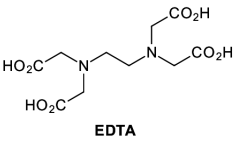

EDTA

[EDTA] / mM	Growth cf. control /%
0	100 ± 3
0.625	91 ± 3
1.25	65 ± 13
2.5	46 ± 12
5.0	33 ± 9
10.0	21 ± 5

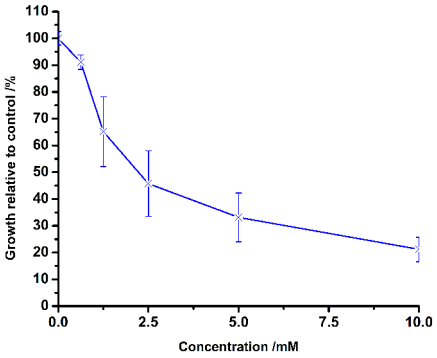

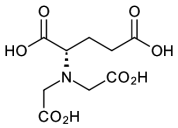

GLDA

[GLDA] / mM	Growth cf. control /%
0	100 ± 2
0.625	99 ± 2
1.25	98 ± 2
2.5	97 ± 3
5.0	95 ± 2
10.0	89 ± 2

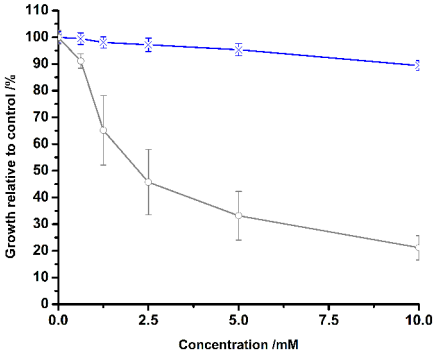

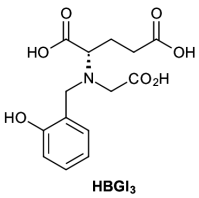

$HBGI_3$

[$HBGI_3$] / mM	Growth cf. control /%
0	100 ± 4
0.625	98 ± 10
1.25	100 ± 4
2.5	100 ± 3
5.0	97 ± 5
10.0	87 ± 4

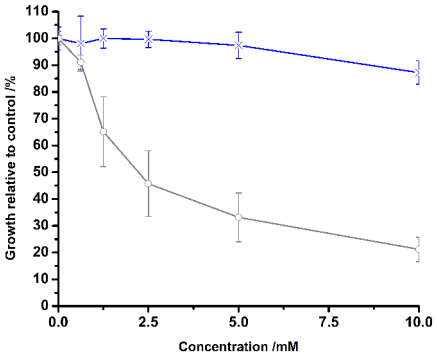

Figure 71: Dose response curves for *E. coli* JM101 upon dosing with **EDTA**, **$HBGI_3$** and **GLDA**. Bacteria were incubated for 16 h at 37°C in a medium composed of of 90:10 v/v TSB: 10x ligand stock in 200mM K_2HPO_4 (in-well [K_2HPO_4] of 20mM). Values are the mean of three technical repeats. Both error bars and margins represent two standard deviations from the mean. Blue lines represent the dose response of the ligand, and grey lines represent the dose response of EDTA.

It can be seen that neither of the glutamic acid based ligands match the inhibition of **EDTA**, which is understandable based on the metal ion affinity data in ***Table 43***; the metal ion affinities of **GLDA** are lower than those of **EDTA** at the experimental pH. At the range of concentrations studied, no significant difference between the dose responses of **GLDA** and **$HBGI_3$** could be observed. Based on this outcome, it can be surmised that the difference in conditional metal ion affinities between **GLDA** and **$HBGI_3$** is small, and changing one of the carboxylate groups attached to the amine for another donor may not be an appropriate way to prepare enhanced **GLDA** analogues. To confirm whether this is the case, structural and metal binding data are necessary.

6.2.6. Towards the synthesis of $PyGl_3$

Alkylation of **Py-31** with t-butyl bromoacetate proceeded in extremely low (< 5%) yield, presumably due to nonselective alkylation at the amine and pyridyl nitrogen atoms. As a result, n-butyl lithium was used to attempt deprotonation of the aliphatic amine group to increase selectivity, but this approach was unsuccessful with only starting material being recovered (***Table 45***).

Table 45: Conditions used for the attempted alkylation of **Py-31**.

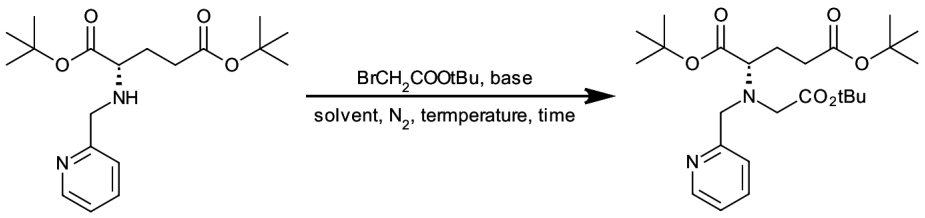

Row	Base	Solvent	Temperature /°C	Time / h	Yield / %
a	K_2CO_3	MeCN	60	24	<5
b	^{n}BuLi	THF	-78[i]→rt	23[ii]	0

i) For two hours in the absence of t-butyl bromoacetate. **ii)** At room temperature, after addition of the alkylating agent.

To circumvent problems of chemoselectivity, the order of reaction at the amine group of di-t-butyl glutamate was reversed; the protected carboxyl group was introduced first, followed by a second alkylation using picolyl chloride[290–292] as the reagent. Much like the preparation of the aminocarboxylate fragments in ***Chapter 3***, a benzyl protection strategy was used to prepare **32**. Alternatively, activated zinc dust[293] could be used to convert the starting hydrochloride salt of di-t-butyl glutamate to its free base, which could easily be monoalkylated, circumventing the need for benzyl protection (***Scheme 43***).

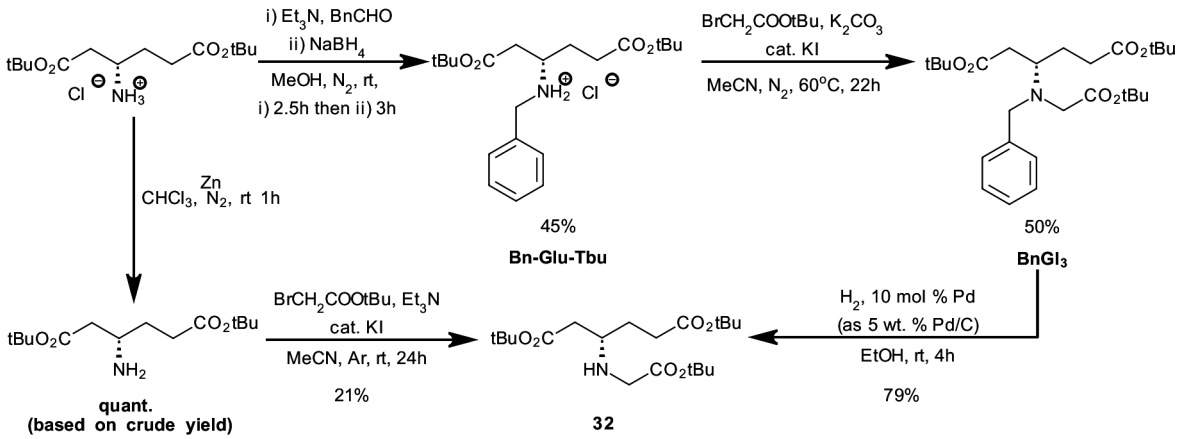

Scheme 43: Synthesis of key intermediate **32** via direct alkylation, or benzyl protected precursors.

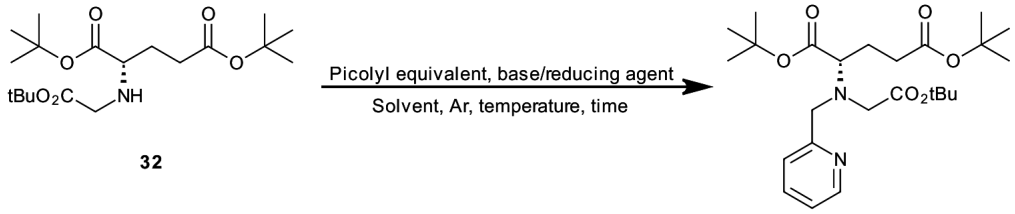

32 **PyGl$_3$-tBu**

Row	Picolyl equivalent	Base	Reducing agent	Solvent	Temp. /°C	Time	Outcome[i]
a	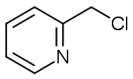	K_2CO_3 (cat. KI)	-	MeCN	60	38h	Partial conversion to **PyGl$_3$-tBu**, (not isolated)
b	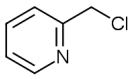	K_2CO_3 (cat. KI)	-	MeCN	70	5d	**32** consumed. Complex mixture
c	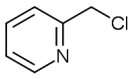	K_2CO_3 (cat. KI)	-	DMF	120	21h	No conversion
d	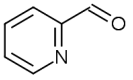	-	$NaBH_4$	-	rt	20h	No conversion
e[ii]	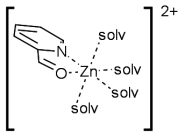	-	$NaBH_4$	MeOH	rt	19h	No conversion
f	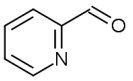	-	$NaBH(OAc)_3$	1,2-DCE	rt	29h	1% **PyGl$_3$-tBu** isolated
g	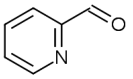	TMEDA	$SiCl_3H$	DCM	rt	2d	No conversion

i) Reaction monitoring was via ES-LCMS. **ii)** Complex structure predicted from ES-MS.

Table 46: Alkylation and reductive amination conditions evaluated for the preparation of **PyGl$_3$-tBu** from **32**.

The alkylation conditions used (***Table 46,*** rows ***a-c***) did not afford complete conversion of **32** to **PyGl$_3$-tBu** (monitoring by ES-LCMS), and **32** was recovered exclusively after chromatography. Changing the electrophile from picolyl chloride to pyridine-2-carboxaldehyde and performing the second amine functionalisation via reductive amination was then evaluated. Using secondary amines as reductive amination substrates can lead to rather variable yields, but examples of sterically hindered tertiary amines prepared in this way are known,[294] suggesting the method could be fruitful in this case. Since the typical sodium acetoxyborohydride mediated reductive amination conditions were low-yielding, an increase of the electrophilicity of the aldehyde was sought by complexing pyridine-

2-carboxaldehyde with Zn^{2+},[295] prior to reductive amination. Hypervalent silicon[296] was also evaluated for use in this reduction, however neither of these alternative reductions led to the isolation of practical amounts of **PyGl$_3$-tBu** (***Table 46,*** rows ***d-h***).

At this point, the stability of the iminium intermediate was thought to be the cause of the inefficient reaction; it could be possible that the crowding around the C=NR$^+$ function to be reduced meant that the intermediate decomposed before reduction. In the hope that an enamine analogue might be more stable, possibly to the point of being isolated prior to reduction, a Lewis-acid promoted[297] reaction between **32** and 2-acetylpyridine was carried out (***Scheme 44***). Under these conditions, no enamine formation was observed, despite the known utility of titanium tetrachloride in the preparation of highly hindered enamines. Instead, a partially deprotected[298] derivative of **32** was observed by ES-LCMS.

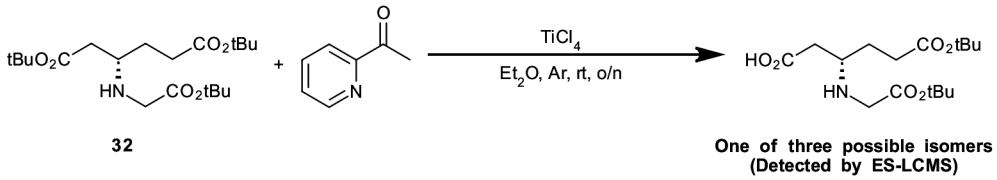

Scheme 44: Attempted enamine synthesis from **32** and 2-acetylpyridine.

A final pathway proceeding via tertiary amides was then studied, based on recent reports of the use of trialkoxysilanes in highly chemoselective reductions.[299] To form the precursor **PyCO-Gl$_3$-tBu**, picolinoyl chloride was reacted with **32** using catalytic DMAP. Difficulties were incurred in reproducing the procedure (***Section 8.5.20***). The **PyCO-Gl$_3$-tBu** that was generated was then contacted with trimethoxysilane and zinc (II) acetate (***Scheme 45***).

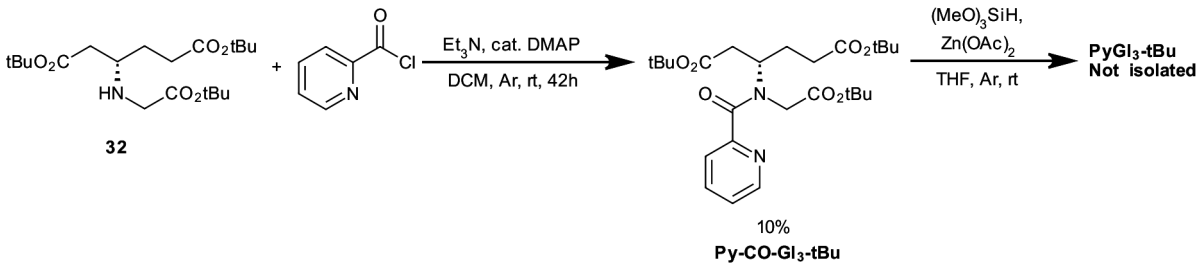

Scheme 45: Attempted reduction of **PyCO-Gl$_3$-tBu**.

Based on the failure to isolate any reduction product, i.e. **PyGl$_3$-tBu**, this particular avenue of work was discontinued. It is hoped that in future work, the novel intermediates described here can be utilised for the preparation of other glutamic acid based chelating agents.

6.3. Towards the synthesis of RDTPMal-type ligands

6.3.1. Strategy

Literature precedent was lacking for many of the fragments identified in this retrosynthesis, meaning that no one approach could be favoured over another from the outset (***Figure 72***). Like the other ligands considered throughout this thesis, multiple disconnections were feasible.

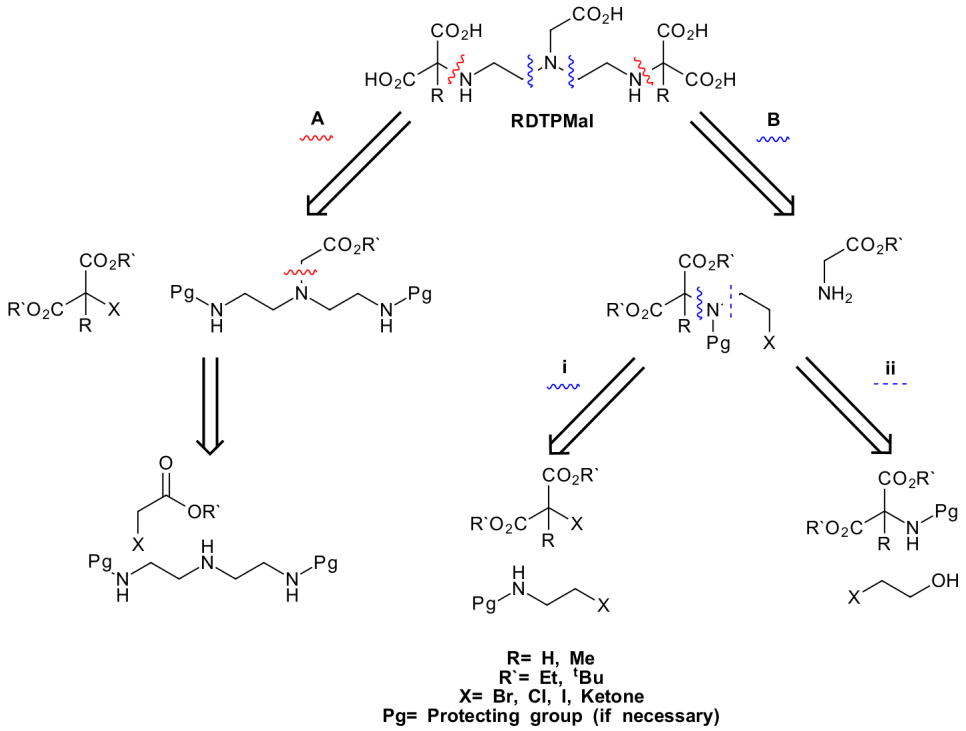

Figure 72: Disconnections evaluated for the synthesis of **RDTPMal-type** ligands.

In this retrosynthesis, disconnection **A** would give a linear route relying on a triamine motif that was functionalised in sequence, whereas disconnection **B** would lead to the generation of an electrophile that could be coupled with an alkyl ester of glycine. As with the aminocarboxylate equivalents in ***Chapter 3***, amine protection was likely to be necessary to control the extent of addition of the relevant electrophiles to the concerned amine nucleophiles.

So as to use readily available materials for the study of these syntheses, diethyl malonate derivatives were used in preliminary work (***Figure 73***).

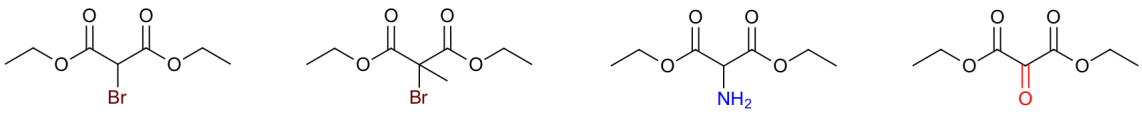

Figure 73: Commercially available diethyl malonate derivatives.

Additionally, the lactam formations encountered earlier in this chapter (***Schemes 33*** and ***34***) and in ***Chapter 3***, were unlikely to occur in the reactions involving malonates, because of the absence of primary or secondary amines and ester carbon atoms that were five or six bonds apart. Based on this characteristic, it was assumed that there would be little difference in reactivity between ethyl and t-butyl malonates and so they could be interchanged at a later stage to enable global deprotection.

6.3.2. Linear synthesis based on reductive amination with triamines

Working along disconnection **A**, with a view to minimising the use of protecting groups, the reductive amination of **34** with diethyl ketomalonate was evaluated as a fairly straightforward route to a **RDTPMal** precursor. The ability of diethyl ketomalonate to act as a partner in reductive amination reactions,[300] along with the literature precedent for the preparation of **34** via a Gabriel synthesis, meant these were ideal candidates for preliminary studies (***Scheme 46***). This approach was quickly abandoned, due to difficulty in inhibiting the cyclisation of **34** to the corresponding ketopiperazine;[149] a somewhat unexpected side reaction given the inertness of the t-butyl group.

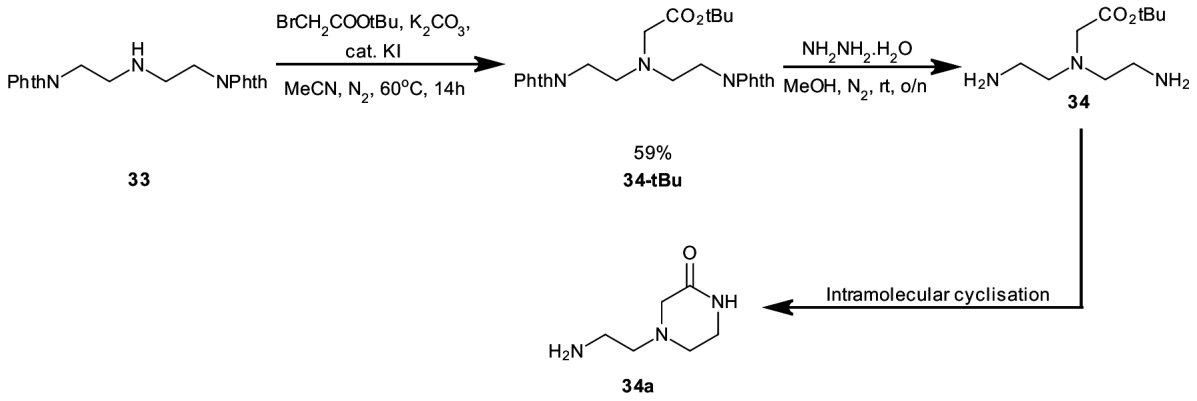

Scheme 46: Synthetic pathway to linear triamine **34** and its undesired cyclisation to **34a**. Phth=Phthaloyl.

Preliminary reactions along disconnection **B** using diethyl ketomalonate as a reductive amination substrate resulted in the recovery of diethyl hydroxymalonate exclusively. Because of this, alongside the inability to prevent cyclisation of **34**, the secondary amine protecting group on the triamine fragment and the central amine protection were varied, and alkyl halomalonates were used for functionalisation of the terminal amines.

6.3.3. Linear synthesis based on triamine alkylation

Benzyl protected intermediate **35** was prepared via a similar phthalimide protection-alkylation-deprotection sequence, proceeding smoothly to give the triamine fragment necessary for synthesis along disconnection **A** (***Scheme 47***).[301] Once alkylated by a halomalonate, the benzyl group of **35** could then be cleaved, and the central nitrogen alkylated with a more useful fragment.[302–305]

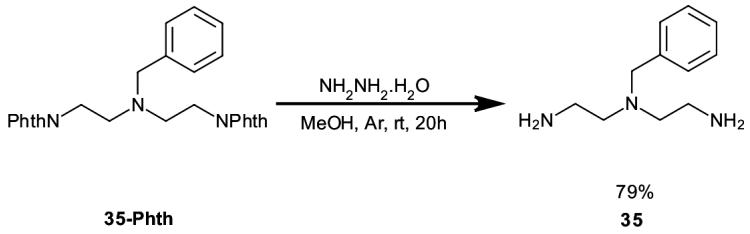

Scheme 47: Hydrazine-mediated synthesis of the stable linear triamine **35**.

Once **35** was in hand, alkylation of the terminal amines was attempted using **36** and the methylated, non-enolisable **Me-36**, both prepared using a variation on the methods of Trost (***Scheme 48***).[306, 307]

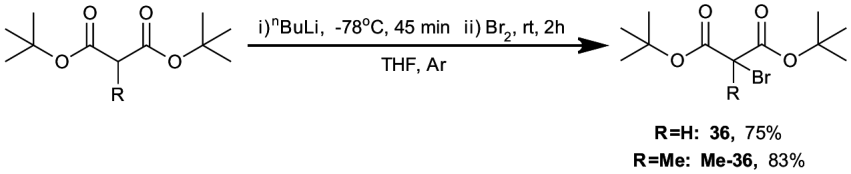

Scheme 48: Preparation of halogenated t-butyl malonates.

Terminal amine protecting groups were not applied to **35**, to see whether the steric bulk of **36** or **Me-36** were sufficient to effect a single substitution for each amine.[308] In both of these cases, minimal to no conversion was observed.

Some initial work was carried out based on the elegant protection protocol of O'Sullivan (***Scheme*** 49),[309] followed by the use of benzyl and t-butyl ester groups to block the central amine, but the requisite alkylation reactions on **37** were problematic, with poor conversion and suspected decomposition upon chromatographic purification.

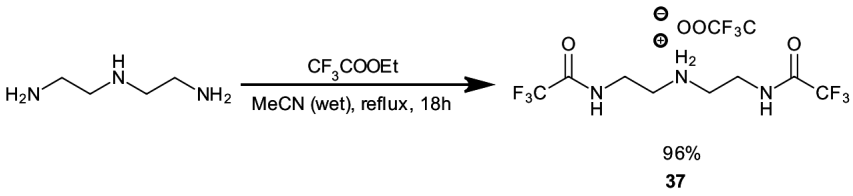

Scheme 49: Selective terminal amine protection of diethylene triamine using ethyl trifluoroacetate.

In contrast, alkylation of **36** with chloroacetonitrile to introduce a nitrile function which could act as a masked carboxylate equivalent, was successful. Although the trifluoroacetamide hydrolysis to produce free triamine **38** was facile (***Scheme 50***), the need for harsh conditions for nitrile hydrolysis at a later stage in the synthesis meant that concomitant decarboxylation of the malonate fragments was likely, and so the use of trifluoroacetamide-protected triamines was discontinued.

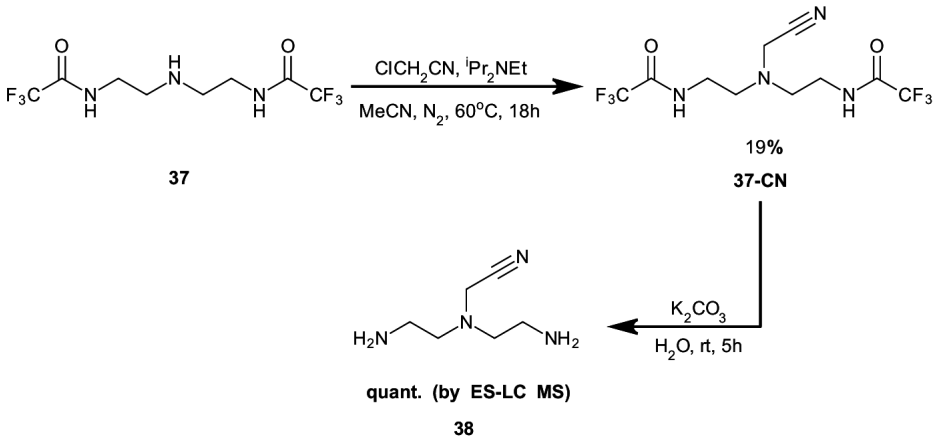

Scheme 50: Synthesis and hydrolysis of nitrile **37-CN**.

6.3.4. Linear synthesis based on aminomalonate derivatives as nucleophiles

The propensity of triamine **34** to cyclise and the lack of reaction of malonate electrophiles with **35** prompted a reversal of polarity for the fragments identified in disconnection **A**, in that the triamine used was exchanged for a protected monoamine bearing leaving groups in the β-position, not unlike a nitrogen mustard (***Scheme 51***).

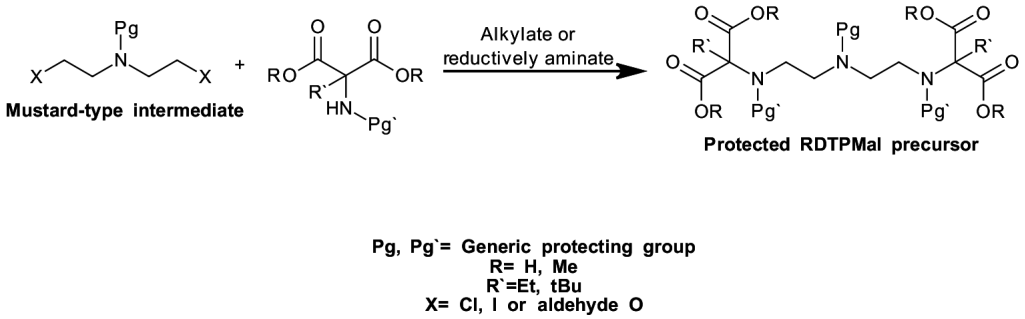

Scheme 51: General approach to a protected **RDTPMal** precursor via “mustard-type” intermediates.

Once again, to minimise the number of protection steps in the route, reductive amination was to be tested first as a way of furnishing the terminal secondary amines. A first approach to the required carbonyl fragment **40**, was the oxidation of diol **39** which was easily prepared from diethanolamine (***Scheme 52***). From a survey of oxidation conditions and substrates, it was clear that selective oxidation methods were necessary to prevent side reactions involving the ester and amine groups in **39**. To this end, the activated DMSO, or hypervalent iodine-mediated oxidations seemed like ideal candidates, but attempts at generating **40** from **39** under Swern, Pfitzner-Moffatt and Dess-Martin conditions[310] resulted only in the recovery of starting material, or the formation of complex mixtures from which no product was isolable.

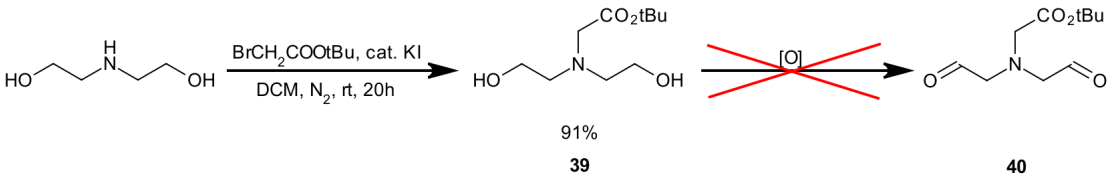

Scheme 52: Alkylation of diethanolamine to prepare common intermediate **40**.

A report by Fricke[311] indicated similar problems when the central amine of 3-pyrroline was not protected as an amide prior to oxidative cleavage, and also, that di-aldehydes of form **42** were very unstable and prone to hydration. The need for an alternative protection procedure would therefore give a different, yet suitable electrophile (***Scheme 53***). Using a similar procedure to generate **42** via the cleavage method of Nicolaou [312] gave a successful synthesis according to ^{1}H NMR, but attempts to trap **42** via reductive amination failed.

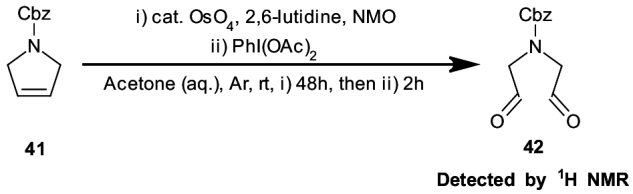

Scheme 53: Cleavage of **41** to give carbonyl electrophile **42** as a substitute for **40**.

Activation of diol **39** was then performed via reaction with thionyl chloride to generate alkylating agent **43** (***Scheme 54***), the reaction of which was studied with diethyl aminomalonate and protected aminomalonate (***Table 47***, rows ***a-c***). Even though **43** was observed to cyclise when these reactions were monitored via ES-LCMS, it was anticipated that this cyclisation would enhance reactivity[313] because of the charge on the aziridinium ion, a characteristic which is also exploited in chemotherapeutics.[314]

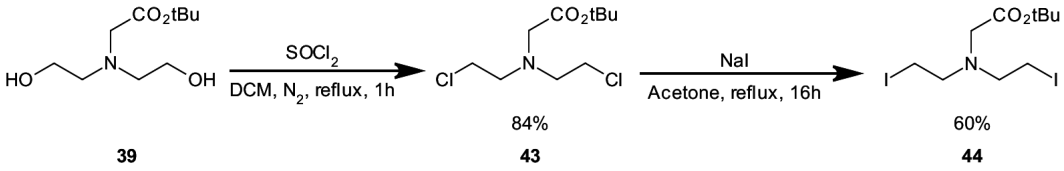

Scheme 54: Conversion of diol **39** to dihalide electrophiles **43** and **44**.

Reactions of **43** appeared to proceed, but ^{1}H NMR of the crude reaction mixture indicated that some side products had also been formed, and that conversion was limited (***Table 47***, row ***c***). Suspecting the low reactivity of **43** as the reason behind low conversion, the Finkelstein reaction was used to convert **43** into the corresponding diiodo derivative (***Scheme 54***), which was reacted with the aminomalonates in rows ***c-f*** in ***Table 47*** , prepared based on the method of Ugarizza.[315] In these cases also, minimal conversion was observed. This failure led to the study of routes based on disconnection **A** being discontinued (***Table 47***, rows ***d-f***).

Table 47: Conditions and outcomes of aminomalonate alkylations with **43** and **44**.

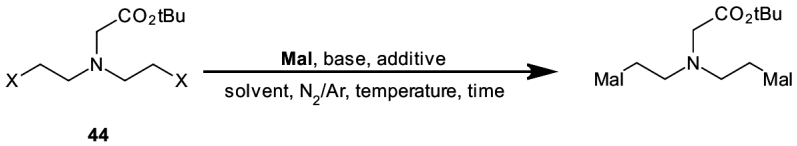

44

Row	X=	Mal=	Base	Additive	Solvent	Temp. /°C	Time / h	Outcome
a	Cl	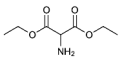	Et_3N	KI[i]	MeCN	rt	25	Poor conversion, no product observed[ii]
b	Cl	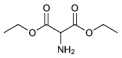	Et_3N	KI[i]	MeCN	60	19	Product mass not observed, malonate recovered[iii]
c	Cl	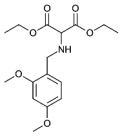 **45**	$KHCO_3$	KI[i]	MeCN	60	48	Target mass observed[ii], crude ^1H NMR ambiguous
d	I	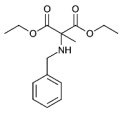 **46**	K_2CO_3	-	MeCN	60	84	Halide consumed[ii], malonate recovered[iii]
e	I	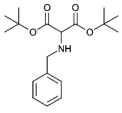 **47**	Et_3N	-	MeCN	60	25	No conversion, starting materials recovered[iii]
f	I	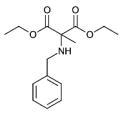 **46**	K_2CO_3	-	DMF	120	56	Target mass absent.[ii] Product absent in crude ^1H NMR

i) Potassium iodide added at 25 mol% with respect to a single chloride group. **ii)** By ES-LCMS. **iii)** By ^1H NMR.

6.3.5. Synthesis of key intermediates for a convergent route

It was possible that the steric crowding around the reacting centres in the linear triamines and aminomalonates described complicated the coupling of these fragments in either configuration. A search on the chemistry of aminomalonates also revealed that in many cases, intramolecular cyclisation was used to prepare malonates with a tertiary nitrogen functionality, unless the electrophile used was particularly active, e.g. an acyl halide.[107, 316–319]

Using this information, it was hoped that moving the key bond formation away from the malonate would give a more viable route than using the triamine or mustard intermediates. Informed by the ease of transforming diol **39** into dichloride **43**, ethanolamine was to be used as a precursor to prepare the aminomalonate electrophile used for disconnection **B** (***Figure 72***).

To start, ethanolamine was benzylated under reductive amination conditions[320] and then alkylation

was attempted either with or without *in situ* protection of the hydroxy group as a TMS ether. In these cases, products could be identified from ES-LCMS traces. Thus, alkylation of 2-benzylaminoethanol resulted in malonate addition at both the N and O terminals. When alcohol protection was employed, the TMS ether was partially cleaved, presumably during extractive workup. This was somewhat expected given the known lability of the TMS group.[145]

From these observations, a more robust TBDMS ether was used to *O*- protect ethanolamine. Because of the lack of conversion incurred previously when aminomalonate derivatives were reacted with **43** and **44**, (***Table 47***), the nitrogen protecting group was to be introduced later. Once the protected alcohol was in hand, alkylation with t-butyl bromomalonate proceeded smoothly in reasonable yield (***Scheme 55***).

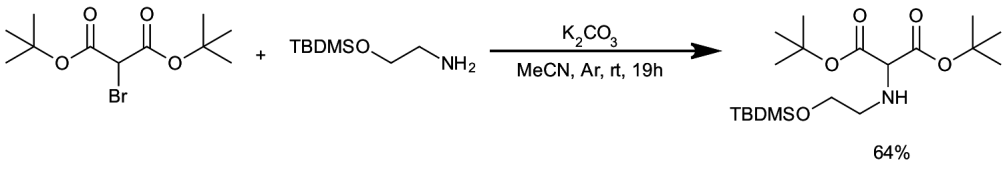

36 **48**

Scheme 55: Alkylation of TBDMS-protected ethanolamine with **36** to prepare a potential intermediate to **RDTPMal** type systems.

Because reactive electrophiles were reported to be particularly effective in functionalising aminomalonates, an attempt was made to prepare the N-Boc derivative of **48**, but these reactions were unsuccessful. Time constraints precluded development of the route, but the author suggests that it is on exploitation of this intermediate that further work be conducted (***Figure 74***).

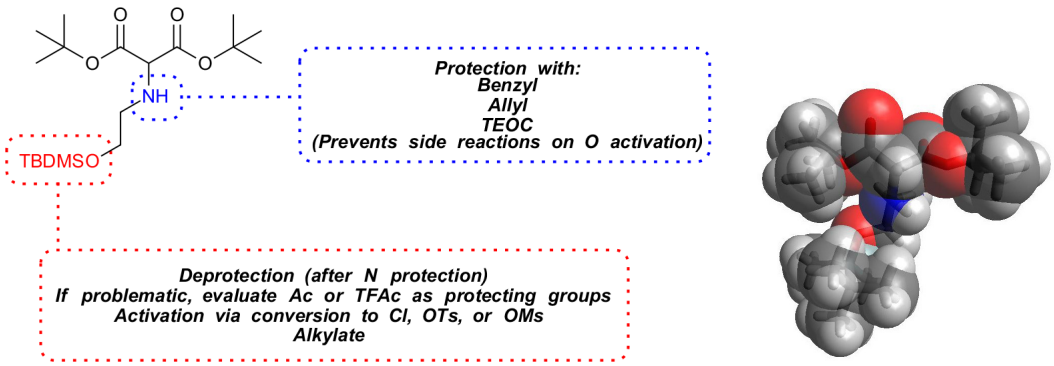

Figure 74: Suggestions for further functionalisation of **48** to prepare a key electrophile along disconnection **B**. An MMFF94 optimised model of **48** to illustrate the steric shielding of the nitrogen atom.

6.4. Conclusions for this chapter

Synthetic efforts towards two **GLDA** analogues **$PyGl_3$** and **$HBGl_3$**, each designed with different inhibition-enhancing features, have been described. Of these two systems the phenolate appended **$HBGl_3$** was successfully prepared, representing a new way to differentiate the amino group of glutamic acid. Unfortunately, **$HBGl_3$** did not display greater *E. coli* inhibition than **GLDA** itself, which may be a function of the low metal ion affinities of these types of ligand. **$PyGl_3$** on the other hand, was not synthesised because of the inaccessibility of the precursor **$PyGl_3$-tBu** in practical yields.

Linear and convergent routes towards an octadentate ligand structure, **RDTPMal**, inspired by **DTPA** and **EDDS**, were also evaluated, with reactions along linear routes to key precursors involving aminomalonates being complicated by insufficient conversion to product to warrant further development. In pursuing a convergent route, a precursor to a useful electrophile has been synthesised, and suggestions for its subsequent transformation into a useful electrophile are given.

7. Summary, conclusions and future work

7.1. General conclusions

In order to identify an alternative to **EDTA** that could be used at lower concentrations *in situ,* but may also have been more biodegradable, the following approaches were taken:

1. Synthesis of amide ligands based on the **EDTA** structure.
2. Synthesis of a set of phenolic ligands derived from the **HBED** and **EHPG** frameworks, with electron-donating or -withdrawing groups.
3. Screening the growth inhibition properties of several commonly used aminocarboxylate ligands, with a view to relating biological effects to metal ion affinities.
4. The preparation of novel ligands inspired by systems known to be readily biodegradable.
5. Using the structure of strongly inhibiting ligands as a basis for more biodegradable ligand designs.

E. coli JM101 was used as the model organism in all growth inhibition studies.

7.1.1. Key findings

1. Of all the **EDTA** amides studied, when the pendent groups were strongly coordinating, e.g. carboxyl or pyridyl, greater *E. coli* inhibition compared to **EDTA** was observed (***Figure 75***). No single reason for the greater extent of inhibition despite the lower metal affinities could be pinpointed from the structural and thermodynamic data collected.

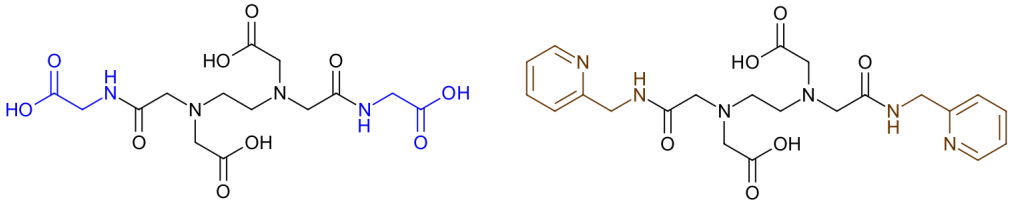

Figure 75: Symmetrical **EDTA** bis-amides which display greater *E. coli* JM101 growth inhibition than **EDTA**.

2. For “simple” aminocarboxylate ligands containing amine, carboxylate and ether groups exclusively, there is a positive correlation between $K_{a_{cond}}$ values, especially $K_{a_{cond}}(Fe^{3+})$, and the growth inhibition of *E. coli* JM101 cells. If a simple aminocarboxylate ligand had a low $K_{a_{cond}}(Mg^{2+})$, e.g. **EGTA** or **TETA**, then the ligand displayed poor growth inhibition characteristics.

3. Even though the phenolic ligands studied in this work are not expected to bind Mg^{2+} appreciably, they are still capable of inhibiting *E. coli* growth. Accordingly, it is proposed that their extremely high $K_{a_{cond}}(Fe^{3+})$ values compensate for the deficiencies in Mg^{2+} binding that they may have.

4. The lower the pK_a of a parent phenol a **HBED** derivative is based on, the more inhibitory the resulting ligand will be. This finding may enable the design of "tunable" phenolic ligands that can give a specific extent of inhibition.

5. ICP-MS studies show that different ligands will deplete different cellular metals, and the extent of this depletion may not be obvious from the inspection of metal ion affinities alone. For instance, **EDTA** and **AmGly$_2$** deplete manganese most extensively, **EHPG** depletes iron, and a particularly inhibitory aminocarboxylate ligand, **AAZTA**, depletes both manganese and iron. This simultaneous depletion has recently been observed in studies on the antibacterial properties of human calprotectin.[56, 57, 106] The differing depletion behaviours observed suggest that there may not be a general route for ligand-induced *E. coli* growth inhibition.

6. The phenolic donor **HBGl$_3$** was designed and synthesised, as a potentially improved **GLDA** analogue. Unfortunately **HBGl$_3$** did not exhibit significantly greater inhibition of *E. coli* growth compared to **GLDA**. The synthetic route towards **HBGl$_3$** is novel and may be used for the construction of other analogues.

7. Work towards a biodegradable analogue of **DTPA**, the **RDTPMal** skeleton, was also initiated. If bought to fruition, this system may represent an extremely inhibitory, yet environmentally friendly ligand.

8. From an applicability perspective, **AmGly$_2$** is perhaps the most promising system studied. This is attributed to its one-step synthesis from **EDTA** dianhydride and glycine, meaning large quantities can be made at low cost.

7.2. Scope and limitations

This study represents one of the first steps towards a detailed interrogation of the thermodynamic properties (metal ion-ligand binding constants, partition coefficients) of aminocarboxylate ligands, and the impact of such ligands on the growth inhibition of *E. coli* JM101 by the respective ligands. A link has been alluded to in the literature,[31] but had remained unexamined for close to fifty years. In older work, no mention was made of the importance of the *magnitude* of metal ion binding strength, or which metal ions were the most important to sequester, merely that greater chelating ability leads to greater growth inhibition.

Even though a correlation has been found between Fe^{3+} chelate stability and bacterial growth inhibition, correlation, of course, does not imply causation. Indeed, there is likely a perturbation of

the underlying metal ion transport systems that Fe^{3+} chelation affects, the extent of this perturbation being regulated by the binding constant. Moreover, the sample set that the correlation was identified for was extremely small. Therefore to solidify this relationship, the study of more aminocarboxylate ligands is necessary.

For phenolate and other more specialised ligands for Fe^{3+}, a relationship between Fe^{3+} depletion and biological activity, at least in the fields of chelation therapy and antibacterials[52], is known. Work in this thesis *alludes* to this relation also holding for *E. coli* growth inhibition for **4-R-HBED** ligands. For the identification of a more concrete link, the author believes that a full characterisation of binding constants for the **4-R-HBED** systems is necessary. Much as this would be desirable and indeed possible, during the time allotted for the completion of this work, circumstances beyond our control precluded these studies in collaboration with a third party.

Most importantly, these relations hold in aqueous media at a set temperature and within a defined pH range. In consumer products, there are no such well-defined conditions, and large quantities of surfactant, alcohols, and salts will drastically affect the metal ion complexation properties of any added ligand. To extend the models presented here then, further work in these non-aqueous media is necessary. Some aspects of biodegradability have been discussed, but experimental assessment of efforts to improve the biodegradation of the classes of ligands discussed is a clear omission in this work.

Finally, many novel intermediates have been prepared in this work for use in new routes to known ligand classes. The similarity of these intermediates to those used to prepare ligands used for lanthanide and other metal based imaging modalities is notable, and it is hoped that the preparations of these intermediates are of use in this wider context.

7.3. Suggestions for future work

Detailed suggestions for future work have been mentioned in the preceding chapters, and so the following is intended to address more general themes arising from the work in this thesis.

General remarks. As a priority, the assessment of ligand biodegradability according to OECD guidelines should be performed, with the resulting data informing future ligand design. If these tests demand more material than can practically be synthesised, the incorporation of an isotopic label into analyte ligands can be considered, to serve as a handle for metabolite analysis. Recent advances in techniques to monitor the interactions between membranes and disrupting agents also make studies into the action of the ligands synthesised in this work against model lipopolysaccharide systems a lucrative target, the expertise for which is present in this department (Prof. Colin Bain)[321], and further afield (Prof. Jeremy Lakey, Newcastle).[21, 260]

Work on symmetrical EDTA bis-amides. This unusual class of ligands warrants further study on a few fronts. The first is whether the enhanced inhibition effect seen for **AmGly$_2$** and **AmPy$_2$**, which was assigned to the presence of coordinating groups as amide substituents, was truly general. This could be confirmed or refuted very easily by the synthesis of other EDTA bisamides with coordinating groups such as phosphonates, phenolates and so on. Some useful α-haloamide intermediates that could be used to this end have been prepared by the group of Sherry.[322, 323]

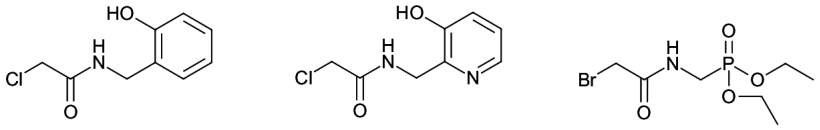

Figure 76: α-haloamide intermediates prepared by Sherry.

For this class of ligands, kinetics may be of importance. Preliminary studies of the time to equilibrium were made, but were complicated by metal ion hydrolysis at pH values close to 7. Many rigorous studies into kinetic stability circumvent this problem through the use of low pH values,[252, 262–264, 282, 324, 325] but such conditions are inappropriatefor this work, because low pH studies would not reflect or rationalise complexation behaviour at pH 7. It is on the basis of the observation that **EDTA** appeared to take longer to complex to Zn^{2+} than **AmGly$_2$**, that the suggestion to study kinetics has been made. Furthermore, the lag phase of some bacterial species is when cellular metal content is accumulated most rapidly. If a ligand cannot take up metal ions as quickly as a bacterial cell, lower inhibition may result.

Work on phenolate ligands. Clearly, the determination of protonation and metal ion binding constants would greatly help in elucidating the relationship between pK_a values and bacterial growth inhibition. In addition, if the relationship between lowered phenol pK_a and growth inhibition is confirmed through further studies, then the preparation of a phenolate ligand bearing strongly electron withdrawing groups may be a worthwhile synthetic excursion. Once prepared, then assessment of the bacterial growth inhibition of such a ligand would indicate whether or not the relationship between pK_a and bacterial growth inhibition holds across a wider range than was assessed in the work discussed earlier. Based on the difficulty of preparing **4-NO$_2$-HBED**, an alternative target, **4-CF$_3$-HBED** and an accompanying route are suggested, using Hartwig's trifluoromethylator^{TM} complex (***Scheme 56***).[326]

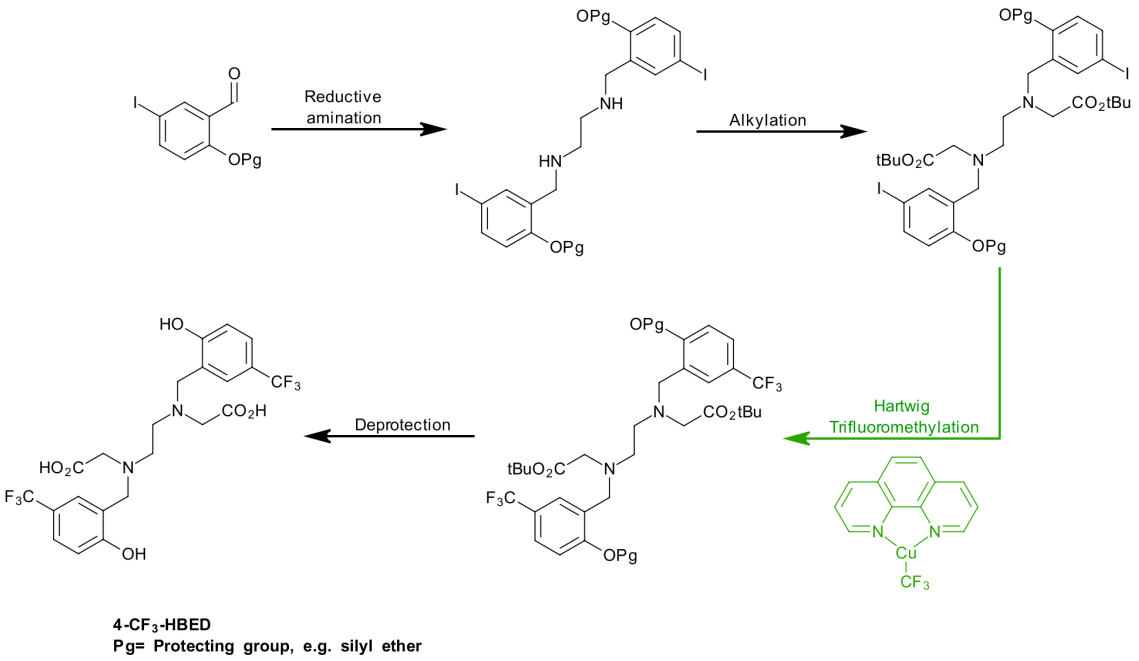

Scheme 56: Proposed synthesis of **4-CF_3-HBED**, an electron poor **HBED** derivative. The key trifluoromethylation step is highlighted in green.

8. Experimental Procedures

8.1. Synthesis: general remarks

Materials. Reagents were obtained from commercial sources and used without further purification unless otherwise stated. Solvent extractions were performed in a 100 cm^3 separating funnel with ca. 50 cm^3 for each phase, unless otherwise stated. For procedures involving dry solvent, glassware was oven-dried for at least eight hours prior to use. Dedicated oxygen-free nitrogen or argon cylinders (BOC, UK) were used to provide an inert atmosphere. Compounds **$AmOMe_2$** and **$AmOH_2$** were synthesised and characterised by Dr. C. Santos, and her donation of the materials is gratefully acknowledged.

Instrumentation. *NMR:* Routine ^1H (400MHz) and ^{13}C NMR (101MHz) spectra were acquired on Bruker Avance 400, or Varian Mercury 400 NMR spectrometers. Two-dimensional NMR (COSY, NOESY, HSQC and HMBC) and certain ^1H / ^{13}C NMR spectra were acquired by the solution state NMR service at Durham University on Varian VNMRS-600 (600 MHz) or VNMRS-700 (700 MHz) instruments. Where visible, signals corresponding to $CDCl_3$ were referenced to δ=7.26 ppm in ^1H NMR spectra and δ=77.2 ppm for ^{13}C spectra.

Mass spectrometry: ES-MS data (positive and negative ionisation modes) were obtained on a Waters TQD mass spectrometer interfaced with an Acquity UPLC system. ASAP experiments were performed on a Waters Xevo QToF mass spectrometer. GC-MS (EI ionisation) was performed on an Agilent instrument equipped with a 5973 model quadrupole mass spectrometer.

FT-IR: All infra-red spectra were recorded on a Perkin-Elmer Spectrum 90 spectrometer equipped with an ATR stage. Substances for analysis were used neat unless otherwise indicated.

Chromatography: TLC was performed on either alumina or silica using Merck foil-backed TLC plates. Column chromatography on silica was undertaken in one of two ways. Method i) involved the use of a standard glass column and silica sourced from Fluorochem Limited and elution was performed according to the method of Clark Still.[327] Method ii) involved the use of a Teledyne Combiflash instrument equipped with RediSep Rf silica cartridges to perform automated elution. Analytical and preparative HPLC was performed by the chromatography service at Durham University.

X-Ray Crystallography and Elemental Analysis: All structural data was collected at 120K and solved by Dr. D.S Yufit (Durham University). Elemental analyses were performed by either i) Mr. Stephen Boyer (London Metropolitan University elemental analysis service) or ii) Dr. Emily Unsworth using a Exeter CE-440 Elemental Analyser device.

Melting points: Melting points were taken on a Gallenkamp melting point apparatus.

8.2. Synthesis and growth inhibition studies of a series of EDTA amide ligands

8.2.1. 2,2'-(3,10-Dioxo-1,12-diphenyl-2,5,8,11-tetraazadodecane-5,8-diyl)diacetic acid, hydrochloride dihydrate, $AmBn_2$

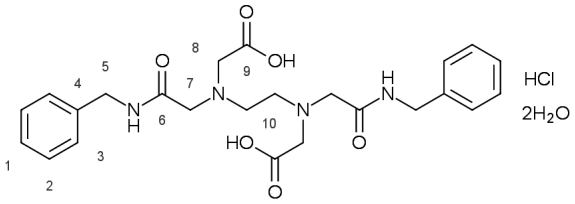

A solution of benzylamine (0.70 cm^3, 0.69 g, 6.41 mmol) in dry tetrahydrofuran (10 cm^3) was added dropwise to a suspension of EDTA bis-anhydride (0.76 g, 2.97 mmol), also in dry tetrahydrofuran (10 cm^3). The resulting off-white mixture was stirred at room temperature under nitrogen for 24 hours, during which time a large amount of white precipitate was observed. The solvent was then removed *in vacuo* to yield a white powder, which was dissolved in de-ionised water, and filtered to remove insoluble particulates. The water was subsequently removed *in vacuo*, to yield an off-white/yellow solid (1.26 g), that were dried under high-vacuum while being heated at 50°C for 4 hours. The resulting yellow material was dissolved in aqueous hydrochloric acid (3% w/w, ca. 60 cm^3) and the solution filtered to afford beautiful white crystals of **$AmBn_2$**, that were also dried under high vacuum to afford the title compound as the di-hydrated hydrochloride salt (white solid, 0.43 g, 0.79 mmol, 27%). *Elem. Anal. Found (Service i):* C, 52.8; H, 6.21; N, 10.8; Cl, 5.81 (Cl content found by gravimetric analysis against $AgNO_3$) ($C_{24}H_{35}ClN_4O_8$ requires C, 53.1; H, 6.50; N, 10.32; Cl, 6.53%); mp 70-72°C; ν_{max}/cm^{-1}(ATR) 3032 (carboxylic acid O-H st), 1732 (acid C=O st), 1666 (amide C=O st), 1236 (br, ethylene diamine C-N st); δ_H(700 MHz, D_2O, pD≈14) 7.44 – 7.12 (m, 10H, ***H1-3***), 4.33 (s, 4H, ***H5***), 3.18 (s, 4H, ***H7***), 3.08 (s, 4H, ***H8***), 2.59 (s, 4H, ***H10***);δ_C(176 MHz, D_2O pD≈14) 179 (***C9***) , 174 (***C6***) , 137 (***C4***) , 129 (***C1***) ,128 (***C2/3***) , 127 (***C2/3***) , 59 (***C7***) , 58 (***C8***) , 53 (***C10***) , 43 (***C5***); m/z (ES-MS^+) 471 (100%, $[M+H]^+$, M= $C_{24}H_{30}N_4O_6$).

8.2.2. 5,8-Bis(carboxymethyl)-3,10-dioxo-2,5,8,11-tetraaza-dodecane-1,12-dicarboxylic acid, $AmGly_2$

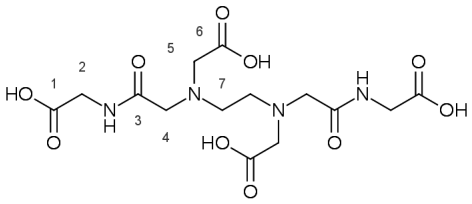

EDTA bis-anhydride (1.50 g, 5.85 mmol), and glycine (1.78 g, 23.7 mmol) were stirred under nitrogen in dry dimethylformamide for 6 hours, initially in an ice bath and then at room temperature. Following solvent removal *in vacuo*, an aqueous solution of hydrochloric acid (7.6% w/w, ca. 20 cm^3) was added to the crude solid. The resulting suspension was boiled, and left to cool overnight to afford a fine white precipitate that was filtered, and dried to constant mass (0.94 g, 2.32 mmol, 40%). Recrystallisation of 0.22g of this material from water afforded a white crystalline solid (0.13 g). Further recrystallisations from water afforded crystals suitable for structural analysis via X-ray crystallography. *Elem. Anal. Found (Service i):* C, 41.43; H, 5.38; N, 13.82;($C_{14}H_{22}N_4O_{10}$requires C, 41.38; H, 5.46; N, 13.79%); mp 221-225°C (dec.)*; ν_{max}/cm^{-1}(ATR) 3020 (COOH O-H st), 1730 (carboxylic acid C=O st), 1666 (amide C=O st), 1304 (acid C-O st), 1108 (br, ethylene diamine C-N st); δ_H(600 MHz, D_2O, pD≈14) 3.79 (s, 4H, ***H2***), 3.31 (s, 4H, ***H4***), 3.22 (s, 4H, ***H5***), 2.72 (s, 4H, ***H7***);δ_C(151 MHz, D_2O pD≈14) 179 (***C1***) , 177 (***C6***) , 174 (***C3***) , 59 (***C5***) , 58 (***C4***), 52 (***C7***) , 43 (***C2***); m/z (ES-MS^+) 407 (100%, $[M+H]^+$, M= $C_{14}H_{22}N_4O_{10}$); X-ray crystallography: $C_{14}H_{22}N_4O_{10}$, M_r= 406.36, orthorhombic ($P2_12_12$); *a* = 17.3349(11) Å, *b* = 9.3065(5) Å, *c* = 5.3951(4) Å; crystal size = 0.3599 × 0.1611 × 0.0820 mm^3; T= 120K.

8.2.3. [(Carbamoylmethyl){2-[(carbamoylmethyl)(carboxymethyl)amino]ethyl}amino]acetic acid[329], $AmNH_2$

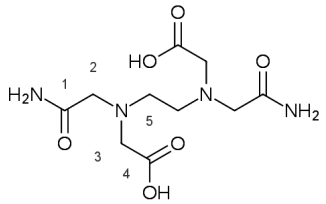

In a modification to the published procedure, EDTA bis-anhydride (0.26 g, 1.03 mmol), was suspended in a saturated solution of ammonia in ethanol (ca. 6 wt% ammonia, 20 cm^3) and stirred at room temperature under nitrogen for 20 hours, during which, a white precipitate was observed. Volatile material was then removed *in vacuo*, to yield a white powder that was subsequently dis-

*A wide melting point range which is accompanied by decomposition is typical of amino acids.[328]

solved in aqueous hydrochloric acid (1.2 M, 5 cm^3). After a few minutes, a white precipitate was observed and collected by filtration and dried under high vacuum to afford the product as a white powder (0.13 g, 0.434 mmol, 43%). Diffusion of acetone into an aqueous solution of this powder afforded crystals suitable for analysis by X-ray diffraction; mp 178-185°C (dec.) ; δ_H(600 MHz, D_2O, pD≈14) 3.18 (s, 4H, ***H3***), 3.10 (s, 4H, ***H2***), 2.57 (s, 4H, ***H5***); δ_C(151 MHz, D_2O pD≈14, Na_2CO_3 added δ=166ppm) 178 (***C4***) , 176 (***C1***) , 58 (***C3***) , 57 (***C2***) , 51 (***C5***); m/z (ES-MS^-) 289 (100%, $[M-H]^-$); HR-MS Found 289.1136, $C_{10}H_{17}N_4O_6$ $[M-H]^-$ requires 289.1148; X-ray crystallography: $C_{10}H_{18}N_4O_6$, M_r= 290.28, orthorhombic (Fdd2); *a* = 32.9984(14) Å, *b* = 14.0107(6) Å, *c* = 5.3942(2) Å; crystal size = 0.37 × 0.094 × 0.06 mm^3; T= 120K.

8.2.4. [(2-{(Carboxymethyl)[2-(diethylamino)-2-oxoethyl]amino}ethyl)[2-(diethylamino)-2-oxoethyl]amino]acetic acid, $AmdiEt_2$

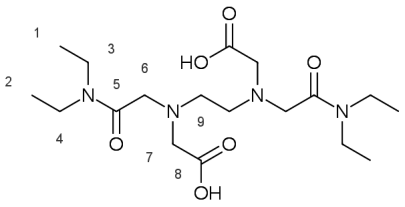

EDTA bis-anhydride (0.16 g, 0.633 mmol) was suspended in anhydrous N,N-dimethylformamide (2 cm^3) and diethylamine (0.13 cm^3, 12.7 mmol) was added at once via a Gilson pipette. The mixture was then stirred overnight under nitrogen, after which time the reaction solvent was removed *in vacuo* using toluene as a co-solvent for rotary evaporation. The resulting semi-solid was added to water followed by the addition of sodium carbonate to yield a homogeneous solution of final concentration 80 mg/ml. Preparative high-performance liquid chromatography (Sunfire C18 preparative HPLC column) on this solution allowed for the isolation of the title compound (0.06 g, 88% pure*) as a pale yellow oil. δ_H(400 MHz, D_2O) 4.28 (s, 4H, ***H7***), 3.86 (s, 4H, ***H6***), 3.57 (s, 4H, ***H9***), 3.39 (q, J = 7.2 Hz, 4H, ***H4***), 3.29 (q, J = 7.2 Hz, 4H, ***H4***), 1.16 (t, J =7.2 Hz, 6H, ***H1***), 1.11 (t, J = 7.1 Hz, 6H, ***H2***); δ_C(101 MHz, D_2O) 171 (***C8***) , 165 (***C5***) , 57 (***C7***) , 56 (***C6***) , 51 (***C9***) , 42 (***C3***), 41 (***C4***), 13 (***C1***) , 12 (***C2***); (ES-MS^+) 403 (100%, $[M+H]^+$); HR-MS Found 403.2564 , $C_{18}H_{35}N_4O_6$ $[M+H]^+$ requires 403.2557.

*In this instance, purity is defined as the total integral in the ^1H NMR spectrum divided by the integration of peaks attributatble to the title compound.

8.2.5. 2-{2-[(Carboxymethyl)(2-{(carboxymethyl)[2-(1-carboxyethylamino) -2-oxoethyl]amino}ethyl)amino]acetylamino}propionic acid, $AmAla_2$

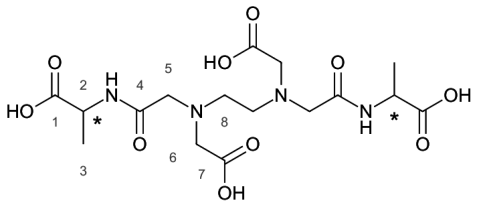

The preparation of this compound was analogous to that in section ***8.2.4,*** except the following amounts were used: EDTA bis-anhydride (0.21 g, 0.820 mmol), alanine (0.15g, 1.65 mmol). A colourless sticky oil was obtained after preparative HPLC (0.09 g, 96% pure). δ_H(400 MHz, D_2O) 3.36 (q, J = 7.3 Hz, 2H, ***H2***), 2.90 (s, 4H, ***H6***), 2.89 (s, 4H, ***H5***), 2.33 (s, 4H, ***H8***), 0.38 (d, J = 7.3 Hz, 6H, ***H3***); δ_C(101 MHz, D_2O pD ≈11) 180 (***C1***) , 179 (***C7***) , 174 (***C4***) , 59 (***C6***) , 58.5 (***C5***) , 53 , 51 (***C8 or C2***) , 18 (***C3***); (ES-MS$^+$) 435 (100%, $[M+H]^+$); HR-MS Found 435.1734 , $C_{16}H_{27}N_4O_{10}$ $[M+H]^+$ requires 435.1727.

8.2.6. [(2-{(Carboxymethyl)[2-(butylamino)-2-oxoethyl]amino}ethyl)[2-(butylamino)- 2-oxoethyl]amino]acetic acid, $AmnBu_2$

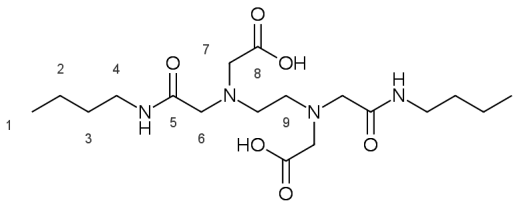

The preparation of this compound was analogous to that in section ***8.2.4,*** except the following quantities were used: EDTA bis-anhydride (0.13 g, 0.52 mmol), *n*-butylamine (0.10 cm^3, 1.06 mmol). A white solid was obtained after preparative HPLC (0.024g, 0.06 mmol). δ_H(400 MHz, D_2O) 3.78 (s, 4H, ***H7***), 3.68 (s, 4H, ***H6***), 3.28 (s, 4H, ***H9***), 3.21 (t, J = 8.2 Hz, 4H, ***H4***), 1.55 – 1.41 (m, 4H, ***H3***), 1.39 – 1.21 (m, 4H, ***H2***), 0.86 (t, J = 7.4 Hz, 6H, ***H1***); δ_C(101 MHz, D_2O, pD≈10) 179 (***C8***) , 174 (***C5***) , 59 (***C7***) , 58.6 (***C6***) , 53 (***C9***) , 39 (***C4***) , 31 (***C3***) , 20 (***C2***) , 13 (***C1***); (ES-MS$^-$) 401 (100%, $[M-H]^-$); HR-MS Found 401.2402 , $C_{18}H_{33}N_4O_6$ $[M-H]^-$ requires 401.2400.

8.2.7. Synthesis of α-haloamide intermediates

TMSCl-mediated preparation of amino acid methyl esters: General procedure[330] The amino acid of interest was charged into a round bottom flask and suspended in methanol (ca. 50 cm^3). TMSCl (ca. 2.2 equiv. per carboxylic acid group) was then added dropwise to the stirring suspension at room temperature under nitrogen. Once addition was complete, stirring was continued for 24 hours, and a decrease in the opacity of the reaction mixture was noted. The homogeneous solution was then concentrated *in vacuo*, initially to give a viscous oil which was re-dissolved in methanol (ca. 250 cm^3), agitated via ultrasound and re-concentrated (3x cycles). Diethyl ether was then added to the oil which was once again agitated via ultrasound (3x cycles) to afford the product, either as an white/off-white solid, or an oil. Since the products were to be used in further transformations, no attempt was made to determine their stereochemical integrity until their incorporation into either key intermediates or final products.

Methyl-2-aminopropionate hydrochloride. l-Alanine (1.88 g, 21.0 mmol), TMSCl (5.9 cm^3, 46.3 mmol) were used. Off-white powder (2.79 g, 20.0 mmol, 95%). δ_H(400 MHz, D_2O, pD$\approx$4) 4.20 (q, J = 7.3 Hz, 1H), 3.83 (s, 3H), 1.55 (d, J = 7.3 Hz, 3H); δ_C(101 MHz, D_2O pD$\approx$4) 171 , 54 , 49 , 15; (ES-MS^+) 104.3 (100 %, $[M+H-HCl]^+$, M= $C_4H_{10}ClNO_2$).

Methyl-2-pyrrolidinecarboxylate hydrochloride. l-Proline (1.84 g, 16.0 mmol), TMSCl (4.5 cm^3, 35.5 mmol) were used. Yellow-pink oil after exhaustive drying under high vacuum (2.23 g, 13.5 mmol, 84%). δ_H(400 MHz, $CDCl_3$) 10.62 (s, 1H), 9.22 (s, 1H), 4.46 (m, 1H), 3.80 (s, 3H), 3.57 (m, 1H), 3.47 (m, 1H), 2.39 (m, 1H), 2.05 (m, 3H); (ES-MS^+) 130.0 (100 %, $[M+H-HCl]^+$, M= $C_6H_{12}ClNO_2$).

Dimethyl-2-aminoglutarate hydrochloride. l-Glutamic acid (2.51 g, 17.1 mmol), TMSCl (8.7 cm^3, 68.5 mmol) were used. Off-white waxy solid (2.78 g, 13.1 mmol, 77%). δ_H(400 MHz, D_2O, pD$\approx$4) 4.21 (m, 1H), 3.82 (s, 3H), 3.72 (s, 3H), 2.65 (m, 2H), 2.27 (m, 2H); (ES-MS^+) 176.4 (100 %, $[M+H-HCl]^+$, M= $C_7H_{14}ClNO_4$).

8.2.8. Ethyl 2-amino-3-phenylpropionate hydrochloride, diethyl-phenylalaninate hydrochloride[331]

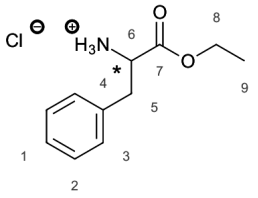

l-Phenylalanine (5.0 g, 30.3 mmol) was supended in ethanol (50 cm^3) and thionyl chloride (3.2 cm^3, 44.1 mmol) was added dropwise to the cooled reaction mixture. Once addition was complete, the reaction mixture was allowed to warm to room temperature under nitrogen. After 5 hours, dissolution of the suspended solid was observed, and the mixture was allowed to stir overnight prior to being refluxed for 2.5 hours. Concentration of the reaction mixture in *vacuo* until the appearance of a solid residue that was filtered off then followed. The solid was washed with diethyl ether, leading to the precipitation of further solid from the filtrate. The combined solids were filtered and dried under high vacuum to afford the title compound (3.8 g, 17.1 mmol, 57%) as a white solid. δ_H(400 MHz, D_2O) 7.49 – 7.20 (m, 5H, ***H1, H2, H3***), 4.40 (dd, J = 7.4, 6.1 Hz, 1H, ***H6***), 4.29 (q, J = 7.2 Hz, 2H, ***H8***), 3.34 (dd, J = 14.5, 6.1 Hz, 1H, ***H5***), 3.25 (dd, J = 14.5, 7.4 Hz, 1H, ***H5***), 1.26 (t, J = 7.2 Hz, 3H, ***H9***); δ_C(101 MHz, D_2O) 170 (***C7***), 134 (***C4***) , 129.5 , 129, 128 (***C1, C2, C3***) , 64 (***C8***) , 54 (***C6***) , 36 (***C5***) , 13 (***C9***) ; (ES-MS^+) 194.0 (100 %, $[M+H-HCl]^+$, M= $C_{11}H_{16}ClNO_2$).

8.2.9. (2S)-2-(2-Chloroacetylamino)-3-methylbutyric acid[332], 6a

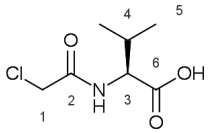

L-valine (2.32 g, 19.8 mmol) was suspended in acetonitrile (10 cm^3, dried over molecular sieves) and stirred under nitrogen while chloroacetyl chloride (0.8 cm^3, 10.1 mmol) was added dropwise. Once addition was complete, the reaction mixture was then heated to 60ºC for 2 hours, and left to cool to room temperature prior to filtration. Diethyl ether was added to the filtrate until a solid precipitated. The resulting suspension was then concentrated *in vacuo* and hexane added to enact further precipitation. All of the precipitate was then collected and recrystallised in ethyl acetate/hexane. The resulting needle-like crystals were collected at the pump, and dried under high vacuum to give the title compound (0.56 g, 2.89 mmol, 28%). Slow evaporation of a sample of these crystals from ethanol gave crystals suitable for single-crystal X-ray analysis. δ_H(400 MHz, D_2O) 4.29 (d, J = 5.9 Hz, 1H, ***H3***), 4.18 (s, 1H, ***H1***), 4.18 (s, 1H, ***H1***), 2.22 (dh, J = 7.0, 5.9 Hz, 1H, ***H4***), 0.96 (dd, J = 7.0, 5.9 Hz,

6H, ***H5***); δ_C(101 MHz, D_2O) 175 (***C6***) , 170 (***C2***) , 59 (***C3***) , 42 (***C1***) , 30 (***C4***) , 18 (***C5***) , 17 (***C5***) ; (ES-MS^-) 192.0 (100 %, $[M-H]^-$, M= $C_7H_{12}ClNO_3$); the stereochemical assignment of the title compound was confirmed by X-ray crystallography: $C_7H_{12}NO_3Cl$, M_r=193.63, orthorhombic ($P2_12_12$); *a* = 12.2940(4) Å, *b* = 14.2498(5) Å, *c* = 5.5498(2); crystal size =0.452 × 0.096 × 0.03 mm^3; T= 120K.

8.2.10. tert-Butyl (2-chloroacetylamino)acetate,[333] 6b

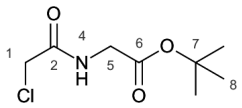

A solution of triethylamine (3 cm^3, 21.2 mmol) in anhydrous dichloromethane (30 cm^3) was used to suspend glycine t-butyl ester hydrochloride (1.00 g, 5.99 mmol). The resulting mixture was then cooled using a dry ice/acetone bath and allowed to stir under nitrogen for 10 minutes prior to the dropwise addition of a solution of chloroacetyl chloride (0.54 cm^3, 7.41 mmol) in dichloromethane (20 cm^3) over a period of 40 minutes, following which the reaction mixture was allowed to warm to room temperature overnight and filtered. The filtrate was washed with saturated aqueous sodium carbonate (2x) , aqueous hydrochloric acid (1 mol dm^{-3}, 2x) and then with brine. Drying of the organic layer over magnesium sulphate followed by solvent removal *in vacuo* gave the title compound (0.84 g, 4.03 mmol, 67%) as an oil that rapidly solidified to a solid. δ_H(400 MHz, $CDCl_3$) 7.06 (t, 1H, ***H4***), 4.08 (s, 2H, ***H1***), 3.98 (d, 2H, ***H5***), 1.49 (s, 9H, ***H8***); GC-MS (EI^+) 208 ($M^{\bullet+}$, M= $C_8H_{14}ClNO_3$).

8.2.11. 2-Chloro-1-{[(2-pyridyl)methyl]amino}-1-ethanone[323], 6c

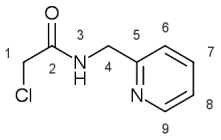

Anhydrous dichloromethane (50 cm^3), was used to dissolve chloroacetyl chloride (1.93cm^3, 24.2 mmol) and the solution cooled using a dry ice/acetone bath under nitrogen. 2-Aminomethylpyridine (2.5 cm^3, 24.5 mmol) was then added dropwise via syringe. As addition proceeded, the reaction mixture became purple and a solid precipiated. At this point, the reaction was bought to room temperature and more dichloromethane (as much as was necessary to enable free stirring) was added. The reaction mixture was then allowed to stir at room temperature for a further 20 hours and the mixture bought to basic pH via the addition of aqueous sodium carbonate (pH $\geq$10) before washing the crude mixture in the same. The organic layer was then dried over magnesium sulphate and the solvent removed *in vacuo*. The residue was purified via column chromatography (method i, silica, dichloromethane:tetrahydrofuran 70:30 v/v) to afford the title compound (3.31g, 17.9 mmol, 75%) as

a yellow oil that solidified to a brown solid upon refrigeration. δ_H (400 MHz, $CDCl_3$) 8.55 (ddd, 1H, ***H9***), 7.86 (s, 1H, ***H3***), 7.66 (ddd, 1H, ***H7***), 7.24 (dd, 1H, ***H6***), 7.20 (ddd, 1H, ***H8***), 4.58 (d, 2H, ***H4***), 4.10 (s, 2H, ***H1***); δ_C(101 MHz, $CDCl_3$) 166.1 (***C2***), 155.5 (***C9***), 149.2 (***C5***), 136.9 , 122.6 (***C7***), 122.2, 44.6, 42.6.

8.2.12. Ethyl 2-(2-chloroacetylamino)-3-phenylpropionate[334], 6d

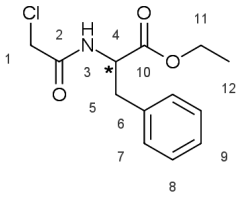

Triethylamine (2.5 cm^3, 18.0 mmol) was added to a solution of diethyl-phenylalaninate hydrochloride (3.29 g, 14.3 mmol) in dry tetrahydrofuran (20 cm^3), and the resulting mixture was cooled in an ice bath. Chloroacetyl chloride (1.7 g, 21.3 mmol) was then added dropwise within 1 hour, and the resulting brown mixture was allowed to stir overnight under nitrogen, after which time the solvent was removed *in vacuo* and the residue partitioned between dichloromethane and aqueous hydrochloric acid (3x). The organic layer was washed with water (3x), dried using magnesium sulphate and concentrated *in vacuo* prior to final purification via column chromatography (method ii, elution in 40:60 v/v ethyl acetate:hexanes) to give the title compound as a beige solid (1.45 g, 5.38 mmol, 25 %). δ_H(400 MHz, $CDCl_3$) 7.40 – 7.10 (m, 5H, ***H7, H8, H9***), 7.00 (d, 1H, ***H3***), 4.87 (m, 1H, ***H4***), 4.21 (q, J = 7.1 Hz, 2H, ***H11***), 4.05 (s, 2H, ***H7***), 3.18 (m, 2H, ***H5***), 1.27 (t, J = 7.1 Hz, 3H, ***H12***); δ_c(101 MHz, $CDCl_3$) 171 (***C10***) , 166 (***C2***) , 135 , 129 , 128.6 , 127 (***C6, C7, C8, C9***), 62 (***C11***) , 53 (***C4***) , 42 (***C1***) , 38 (***C5***) , 14 (***C12***).

8.2.13. 1-(Butylamino)-2-chloro-1-ethanone[289], 6e

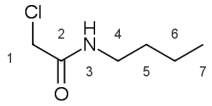

Chloroacetyl chloride (7.5 g, 66.4 mmol) was dissolved in dichloromethane (50 cm^3) and sodium carbonate (14.6 g, 0.14 mol) added. Butylamine (7.2 cm^3, 72.8 mmol) was added dropwise to the suspension at room temperature leading to the evolution of gas. Once addition was complete the reaction mixture was stirred for an hour under nitrogen and solids were then filtered off. Water and then aqueous hydrochloric acid (ca. 1 mol dm^{-3}) were used to wash the yellow filtrate in a separating funnel. The organic layer was then dried with magnesium sulphate prior to solvent removal *in vacuo* to afford the title compound as a yellow liquid (4.8 g, 32.1 mmol, 48%). δ_H(700 MHz, $CDCl_3$) 6.76 (d,

1H, ***H3***), 3.94 (s, 2H, ***H1***), 3.20 (td, 2H, ***H4***), 1.43 (tt, 2H, ***H5***), 1.27 (qt, 2H, ***H6***), 0.84 (t, 3H, ***H7***); δ_C(176 MHz, $CDCl_3$) 166 (***C2***), 43 (***C1***) , 40 (***C4***) , 31 (***C5***) , 20 (***C6***) , 13.75 (***C7***); (ES-MS^+) 151.8 (100 %, $[M+H]^+$, M= $C_6H_{12}ClNO$).

8.2.14. Ethyl [(benzyl){2-[(benzyl)(ethoxycarbonylmethyl)amino]ethyl}amino]acetate, 8

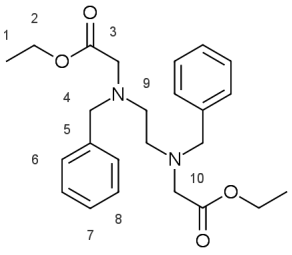

To a Schlenk tube equipped with a pressure-equalising dropping funnel was added a solution of N,N'-dibenzylethylene diamine diacetate (0.53 g, 1.47 mmol) in acetonitrile (ca. 4 cm^3, dried over molecular sieves). Potassium carbonate (1.02 g, 7.39 mmol) was added to the solution and the suspension stirred at room temperature under nitrogen while a solution of ethyl bromoacetate (0.35 cm^3, 3.16 mmol) in dry acetonitrile (2 cm^3) was added dropwise over 6 minutes. Once the reagent was added, heating at 60°C under nitrogen was commenced and the reaction monitored by TLC (ethyl acetate:hexanes). Completion was indicated within 10 hours, but heating was maintained for a further thirteen hours after completion. Solids were then removed by filtration through Celite® and the filtrate concentrated *in vacuo*. The resulting oil was purified by column chromatography (method ii, ethyl acetate:hexanes gradient, title compound eluted in ca. 30% v/v ethyl acetate). The concentrated fractions containing **8** also contained some residual ethyl bromoacetate; this was easily removed by heating combined fractions to 50°C under high vacuum to give the title compound (0.4 g, 0.97 mmol, 66%) as a colourless oil with a pleasant odour. ν_{max}/cm^{-1}(ATR) 2842 (sp^3C-H st), 1731 (C=O ester st), 1183 (C-O st); δ_H(700 MHz, $CDCl_3$) 7.61 – 7.2 (m, 10H, ***H6, H7, H8***), 4.13 (d, J = 7.1 Hz, 4H, ***H2***), 3.77 (s, 4H, ***H4***), 3.35 (s, 4H, ***H10***), 2.82 (s, 4H, ***H9***), 1.24 (d, J = 7.1 Hz, 6H, ***H1***); δ_C(176 MHz, $CDCl_3$) 171 (***C3***) , 139 (***C5***) , 127-9 (***C6-8***) , 60 (***C2***) , 58 (***C4***) , 54 (***C10***), 52 (***C9***) , 14 (***C1***); (ES-MS^+) 413.5 (100%, $[M+H]^+$); HR-MS Found 413.2434 , $C_{24}H_{33}N_2O_4$ $[M+H]^+$ requires 413.2440.

8.2.15. Ethyl (2-oxo-1-piperazinyl)acetate, 10

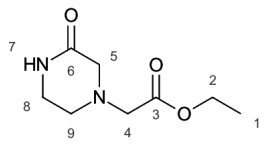

Ester **8** (0.14 g, 0.34 mmol) and ammonium formate (0.32 g, 5.07 mmol) were dissolved in ethanol (10 cm^3) and the solution was subject to three vacuum purge/nitrogen fill cycles prior to the addition of 5% palladium on charcoal (37 mg, 0.02 mmol wrt Pd). The vessel was then evacuated and filled with nitrogen for another three cycles and then refluxed for 2 hours (when quantitative conversion had been attained by ^{1}H NMR). The reaction mixture was subsequently cooled to room temperature and filtered through Celite®. Removal of the solvent *in vacuo* gave the title compound (0.03 g, 0.16 mmol, 47%) as a yellow oil. ν_{max}/cm^{-1}(ATR) 3312 (N-H st), 2936 (sp^3C-H), 1738 (C=O ester), 1636 (C=O amide), 1199 (C-O st); δ_H (600 MHz, $CDCl_3$) 4.15 (q, J = 7.5, 2H, ***H2***), 4.07 (s, 2H, ***H8***), 3.50 (s, 2H, ***H4***), 3.35 (t, J = 5.5 Hz, 2H, ***H6***), 3.07 (t, J = 5.5 Hz, 2H, ***H5***), 1.85 (s, 1H, ***H7***), 1.22 (t, J = 7.5 Hz, 3H, ***H1***); δ_C(176 MHz, $CDCl_3$) 170 (***C9***) , 169 (***C3***) , 61 (***C2***) , 50 (***C4***) , 49 (***C6***) , 48 (***C8***), 43 (***C5***) , 14 (***C1***); (ES-MS^+) 187.2 (100 %, $[M+H]^+$); HR-MS Found 187.1082 , $C_8H_{15}N_2O_3$ $[M+H]^+$requires 187.1083.

8.2.16. Tert-Butyl-[(benzyl){2-[(benzyl)(tert-butoxycarbonylmethyl)amino]ethyl}amino]acetate, 11[157]

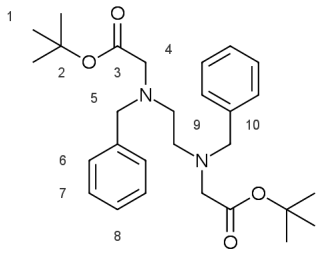

N,N'-dibenzylethylenediamine diacetate (1.25g, 3.47 mmol) was suspended in acetonitrile (20 cm^3, dried over molecular sieves) in a Schlenk tube equipped with a pressure-equalising funnel. Excess potassium carbonate (2.15g, 15.6 mmol) and sodium sulphate (ca. 0.5g) were then added to the suspension which was stirred at room temperature under nitrogen. t-Butyl bromoacetate (1.07 cm^3, 7.30 mmol) was subsequently added dropwise to the suspension and addition was complete within 10 minutes. The reaction mixture was then heated to 60°C and monitored via TLC (silica, ethyl acetate/hexanes 80:20 v/v). Typically, the reaction was complete within 4 hours but could be left overnight with no observable degradation at this temperature. Upon completion, the reaction mixture

was cooled to room temperature and filtered through Celite® to give a straw-coloured filtrate which was concentrated in vacuo to a viscous oil that was purified by column chromatography (method ii, 0:100→100:0 v/v ethyl acetate:hexanes, compound eluted in ca. 30:70 v/v ethyl acetate:hexanes). Fractions containing the pure compound were recombined and the solvent removed *in vacuo* to give a colourless oil that crystallised to a white solid upon standing (0.68 g, 1.45 mmol, 42%). Slow evaporation of a sample of this solid from a mixture of acetone and water gave crystals suitable for X-ray crystallography. Similarly, very large crystals may also be grown through recrystallisation of the purified residue in hexanes. mp 62-64°C; ν_{max}/cm^{-1}(ATR) 2978 (sp^{3}C-H st), 1719 (ester C=O st), 1149 (aliphatic ester asymm. C-O st), 1116 (aliphatic ester symm. C-O st); δ_H(700 MHz, $CDCl_3$) 7.66 – 6.72 (m, 10H, ***H6***, ***H7, H8***), 3.77 (s, 4H, ***H5***), 3.25 (s, 4H, ***H4***), 2.80 (s, 4H, ***H3***), 1.44 (s, 18H, ***H1***); δ_C(176 MHz, $CDCl_3$) 171 (***C3***) , 139 (***C10***) , 129 (***C7***) , 128 (***C6***) , 127 (***C8***) , 81 (***C2***) , 59 (***C5***) , 55 (***C4***) , 52 (***C9***) , 28 (***C1***); (ES-MS$^+$) 469 (100%, $[M+H]^+$, M= $C_{28}H_{40}N_2O_4$); X-ray crystallography: $C_{28}H_{40}N_2O_4$, M_r=468.62, tetragonal (P-4); *a* = 22.2406(6) Å, *b* = 22.2406(6) Å, *c* = 5.4929(2) Å; crystal size =0.48 × 0.24 × 0.2 mm^3; T= 120K.

8.2.17. Tert-Butyl {2-[(tert-butoxycarbonylmethyl)amino]ethylamino}acetate,[157] 12

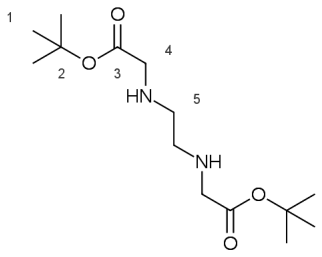

Catalytic transfer hydrogenation method: In a two-neck round bottom flask equipped with a condenser **11** (0.25 g, 0.53 mmol) was dissolved in ethanol (ca. 40 cm^3). Ammonium formate (0.71 g, 11.3 mmol) was then added to the stirring solution which was subsequently agitated in an ultrasonic bath to ensure complete dissolution. The colourless mixture was then subjected to three vacuum purge/ nitrogen fill cycles. Once complete, 5 wt. % palladium on charcoal (0.074 g, 0.035 mmol wrt Pd) was added to the reaction mixture under a fast flow of nitrogen, after which three further vacuum purge/fill cycles were performed prior to refluxing the reaction mixture under nitrogen. Reaction progress was monitored by ^{1}H NMR* and completion was typically reached in 3 hours, over the course of which solid white matter deposited on the walls of the condenser. Once complete, the reaction mixture was cooled to room temperature and allowed to stir for at least fifteen minutes prior to filtration through Celite® and concentration *in vacuo*. The resulting oil was purified by column chromatography on silica (method i, isocratic elution in 95:5 v/v methanol:dichloromethane) to afford

*Monitoring was performed by taking an aliquot of the reaction mixture, filtering the sample (typically through a syringe filter) and concentrating the filtrate *in vacuo*. The residue could then be analysed for the loss of benzyl groups by dissolution in $CDCl_3$ prior to the acquisition of an ^{1}H NMR spectrum.

the title compound as a colourless to yellow oil (0.1 g, 0.34 mmol, 65%).

Hydrogen gas method: **11** (0.63 g, 1.34 mmol) was dissolved in ethanol (ca. 50 cm^3) in a two-necked round bottom flask equipped with a two-way valve secured to the round bottom flask via a Keck clip. The resulting colourless solution was subject to three cycles of vacuum purging and nitrogen filling after which 5 wt. % palladium on charcoal (0.14 g, 0.066 mmol wrt Pd) was added under a flow of nitrogen. The nitrogen line was then replaced with a balloon containing hydrogen gas, and the reaction mixture was then evacuated and backfilled with hydrogen three times. Reaction progress was monitored by ^{1}H NMR and completion was typically observed within 3 hours. The workup and purification procedure could be carried out in the same way as the catalytic transfer hydrogenation method described above to give a colourless oil (0.29 g, 1.01 mmol, 74%). If filtration was carried out carefully, column chromatography could be bypassed leading to higher, sometimes quantitative yields. ν_{max}/cm^{-1}(ATR) 3334 (free N-H st), 3104 (H-bonded N-H st), 2977 (sp^3C-H st), 1730 (C=O ester), 1148 (C-O st); δ_H(700 MHz, $CDCl_3$) 3.23 (s, 4H, ***H4***), 2.64 (s, 4H, ***H5***), 1.89 (s, 2H, ***H6***), 1.39 (s, 18H, ***H1***); δ_C(176 MHz, $CDCl_3$) 172 (***C3***) , 81 (***C2***) , 51 (***C4***) , 49 (***C5***) , 28 (***C2***); (ES-MS^+) 289.1 (100%, $[M+H]^+$); HR-MS Found 289.2118 , $C_{14}H_{29}N_2O_4$ $[M+H]^+$ requires 289.2127.

8.2.18. tert-Butyl-({2-[(tert-butoxycarbonylmethyl)(2-oxo-2-{[(2-pyridyl)methyl]amino} ethyl)amino]ethyl}(2-oxo-2-{[(2-pyridyl)methyl]amino}ethyl)amino)acetate, 13

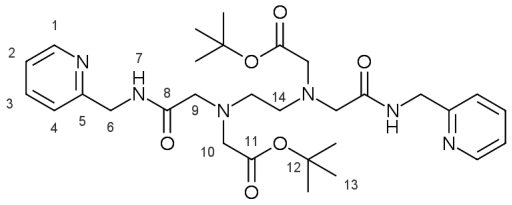

Aminoester **12** (0.47 g, 1.6 mmol) was dissolved in acetonitrile (4 cm^3, dried over molecular sieves) and α-haloamide **6c** (0.68 g, 3.7 mmol) added at once prior to the addition of potassium carbonate (0.7 g, 5 mmol) and a catalytic amount of potassium iodide (0.027g, 0.16 mmol). Heating was commenced under argon at 60^{o}C for 22 hours, at which point only spots visible by both short-wave UV and PMA staining were observed following TLC analysis (silica, dicholomethane:methanol 90:10). After cooling to room temperature, the reaction mixture was partitioned between water and dichloromethane and the dichloromethane layer extracted. The aqueous layer was extracted with dichloromethane a further two times and the combined organic extracts dried over magnesium sulphate and the solvent removed *in vacuo*. The residue was purified via preparative reverse-phase column chromatography (water:acetonitrile , 0.1% v/v formic acid as additive 0:100$\rightarrow$100:0 compound eluted in ca. 50:50 v/v water:acetonitrile) to afford the title compound (0.479 g, 0.82 mmol, 51%) as a brown oil. δ_H (600 MHz, $CDCl_3$) 8.49 (ddd, J = 5.0, 2.0, 1.0 Hz, 2H, ***H1***), 8.41 (t, J = 5.5

Hz, 2H, ***H7***), 7.62 (dd, J = 7.5, 2.0 Hz, 2H, ***H3***), 7.25 (d, J = 7.5 Hz, 2H, ***H4***), 7.16 (ddd, J = 7.5, 5.0, 1.0 Hz, 2H, ***H2***), 4.56 (d, J = 5.5 Hz, 4H, ***H6***), 3.36 (s, 4H, ***H9***), 3.30 (s, 4H, ***H10***), 2.82 (s, 4H, ***H14***), 1.41 (s, 18H, ***H13***); δ_C(151 MHz, $CDCl_3$) 171.6 (***C8***), 170.3 (***C11***), 157.2 (***C5***), 149.1 (***C1***), 137.0 (***C3***), 122.8 (***C2***), 122.1 (***C4***), 81.8 (***C12***), 59.1 (***C9***), 57.1 (***C10***), 53.6 (***C14***), 44.4 (***C6***), 28.3 (***C13***); (ES-MS^+) 585.2 (100 %, $[M+H]^+$); HR-MS Found 585.3403, $C_{30}H_{45}N_6O_6$ $[M+H]^+$requires 585.3401.

8.2.19. ({2-[(Carboxymethyl)(2-oxo-2-{[(2-pyridyl)methyl]amino}ethyl)amino]ethyl} (2-oxo-2-{[(2-pyridyl)methyl]amino}ethyl)amino)acetic acid, $AmPy_2$

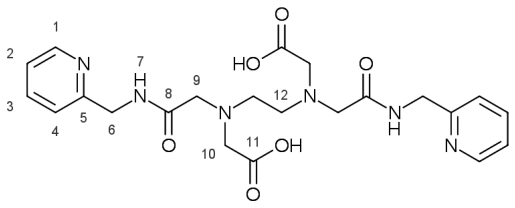

Aminoester **13** (0.458 g, 0.78 mmol) was dissolved in dichloromethane (4 cm^3) prior to the addition of anisole (0.16 cm^3, 1.5 mmol) and trifluoroacetic acid (3 cm^3) and the solution stirred under argon for 17 hours under argon. Volatiles were then removed in vacuo and the residue redissolved in dichloromethane which was removed *in vacuo*. Concentrated hydrochloric acid (ca. 5 cm^3) was then used to emulsify the residue, which was also removed *in vacuo* to afford the product as its trifluoroacetate salt which was a buff solid (0.38 g). The solid was dissolved in the minimum volume of 1 mol dm^{-3} hydrochloric acid and loaded onto DOWEX 1X8 (chloride form) that had been pre-washed with 1 mol dm^{-3} hydrochloric acid and then water. Once loaded onto the resin, elution of the compound was achieved with 1 mol dm^{-3} hydrochloric acid (ca. 100 cm^3). Removal of the solvent *in vacuo* followed by further drying under high vacuum gave the title compound (0.34 g, 0.72 mmol, 92 %) as light brown solid. t_R (H_2O:MeOH, UV detection); 1.33 min; δ_H (600 MHz, D_2O, pD≈6) 8.28 (d, 2H, ***H1***), 7.71 (dd, 2H, ***H2***), 7.38 – 7.06 (m, 4H, ***H3***, ***H4***), 4.31 (s, 4H, ***H6***), 3.71 (s, 4H, ***H9***), 3.39 (s, 4H, ***H10***), 3.11 (s, 4H, ***H12***); δ_C(151 MHz, D_2O, pD≈6) 174.3 (***C11***), 170.1 (***C8***), 155.6 (***C5***), 147.5 (***C1***) , 139.4 (***C2***), 123.4 and 122.1 (***C3***, ***C4***), 57.5 (***C10***), 56.6 (***C9***), 52.1 (***C12***), 43.7 (***C6***); (ES-MS^+) 473.2 (100 %, $[M+H]^+$); HR-MS Found 473.2139, $C_{22}H_{29}N_6O_6$ $[M+H]^+$requires 473.2149.

8.2.20. Tert-Butyl [(tert-butoxycarbonylmethyl){2-[(benzyl)(tert-butoxycarbonylmethyl) amino]ethyl}amino]acetate, 14[158]

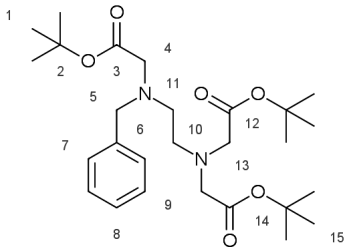

N-benzylethylenediamine (1.0 cm^3, 6.52 mmol) was dissolved in acetonitrile (25 cm^3 , dried over molecular sieves) and potassium carbonate (3.7 g, 26.8 mmol) added. While the mixture was at room temperature under nitrogen, t-butyl bromoacetate (3.22 cm^3, 22 mmol) was added dropwise within 10 minutes, and once addition was complete, the temperature was raised to 60°C. The reaction mixture was heated for 19 hours and then cooled and filtered and the concentrated filtrate was then purified by column chromatography (method ii, compound elution in ethyl acetate:hexanes started at 20:80 v/v) to give of the title compound as a colourless-to-yellow oil (2.67 g, 5.42 mmol, 81 %). δ_H(600 MHz, $CDCl_3$) 7.34 – 7.17 (m, 5H, ***H7, H8, H9***), 3.79 (s, 2H, ***H5***), 3.43 (s, 4H, ***H13***), 3.25 (s, 2H, ***H3***), 2.88 – 2.78 (m, 4H, ***H10, H11***), 1.44 (s, 9H, ***H1***), 1.42 (s, 18H, ***H15***); δ_C(151 MHz, $CDCl_3$) 171.1 (***C12***) , 171.0 (***C3***) , 139 (***C6***) , 127-9 (***C7, C8, C9***) , 81.0 (***C14***) , 80.9 (***C2***) , 59 (***C5***), 56 (***C13***) , 55 (***C4***) , 52.5 (***C10***) , 52 (***C11***) , 29 (***C1***) , 28 (***C15***); GC-MS (EI^+) 402.3 ($M^{+\bullet}$, M= $C_{27}H_{44}N_2O_6$).

8.2.21. Tert-Butyl{2-[(tert-butoxycarbonylmethyl)-N-tert-butoxycarbonylamino]ethylamino} acetate,[158] 15

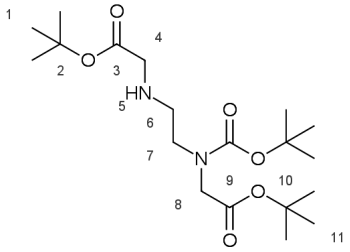

Via debenzylation of 14. The method used was identical to that described in section ***8.2.17***. Both catalytic transfer hydrogenation and hydrogen gas methods may be employed, but the substrate used was compound **14** (1.05 g, 2.13 mmol), ammonium formate (2.68 g, 42.5 mmol), 5 wt. % palladium on charcoal (0.27 g, 0.127 mmol wrt Pd). Purification was by column chromatography (method i, 10:90 v/v ethyl acetate:hexanes→60:40 ethyl acetate:hexanes). After drying the combined pure fractions under high vacuum, the title compound was obtained as a colourless to yellow oil (0.45 g, 1.16 mmol, 54 %).

Via alkylation of ethynene diamine. Ethylene diamine (0.5 cm^3, 7.5 mmol) and triethylamine (4.2 cm^3, 30 mmol) were dissolved in acetonitrile (37 cm^3, dried over molecular sieves), and a solution of t-butyl bromoacetate (3.32 cm^3, 22.6 mmol in 15 cm^3 in acetonitrile) was added dropwise to the mixture, which was then stirred at room temperature under argon for 17 hours under argon. After this, the reaction vessel was placed in the freezer (ca. 30 min) during which time a solid precipitated. This precipitate was filtered off, and the filtrate concentrated *in vacuo,* redissolved in dichloromethane, and then washed with water and then brine. The dichloromethane layer was then dried over magnesium sulphate, concentrated *in vacuo* and the residue purified by column chromatography (method i, silica, diethyl ether:hexanes 0:100→100:0 compound eluted in diethyl ether) to afford the title compound (0.60 g, 1.5 mmol, 20%).δ_H(400 MHz, $CDCl_3$) 3.43 (s, 4H, ***H8***), 3.29 (s, 2H, ***H4***), 2.85 (t, 2H, ***H6***), 2.65 (t, 2H, ***H7***), 2.12 (s, 1H, ***H5***), 1.44 (s, 9H, ***H1***), 1.43 (s, 18H, ***H11***); δ_C(101 MHz, $CDCl_3$) 171.4 (***C9***) , 171 (***C3***) , 81 (***C10***) , 80.6 (***C2***) , 56 (***C8***) , 54 (***C4***) , 52 (***C7***) , 47 (***C6***) , 28 (***C1, C11***).

8.2.22. Tert-Butyl[(tert-butoxycarbonylmethyl){2-[(ethoxycarbonylmethyl)(tert-butoxycarbonylmethyl)amino]ethyl}amino]acetate, 16

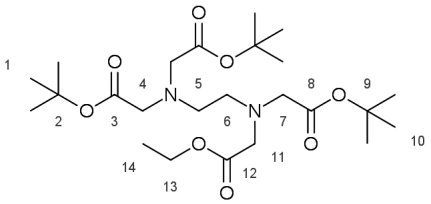

A stock solution of **15** (3 cm^3, 0.096 mol dm^3, 0.29 mmol) was placed into a Schlenk tube equipped with a septum. Potassium carbonate (0.077 g, 0.56 mmol) and potassium iodide (4.5 mg, 0.03 mmol) were then suspended in the solution. After a brief stirring period, ethyl bromoacetate (35 μL, 0.32 mmol) was added at once via a Gilson pipette. The reaction mixture was then heated to 60°C under airtight conditions and reaction progress was monitored at hourly intervals via GC-MS. Consumption of both **15** and ethyl bromoacetate was observed 2 hours after the reaction was initiated but the mixture was allowed to heat for a further 15 hours. Once cooled, the reaction mixture was filtered and concentrated *in vacuo* to yield the title compound as an orange oil (0.13 g, 0.26 mmol, 90%). The reaction was also performed with caesium carbonate (0.178 g, 0.55 mmol) instead of potassium carbonate as the base, all other reactant quantities being identical. Heating was maintained for thirteen hours after the consumption of starting materials as observed by GC-MS. The title compound was isolated after repeated filtration, and removal of the solvent from the filtrate *in vacuo* to give the title compound as a yellow oil (0.085 g, 0.17 mmol, 59%). ν_{max}/cm^{-1}(ATR) 2978 (sp^3C-H st), 1725 (ester C=O st), 1139 (C-O st); δ_H(600 MHz, $CDCl_3$) 4.12 (q, J = 7.1 Hz, 2H, ***H13***), 3.56 (s, 2H, ***H11***), 3.45 (s, 2H, ***H7***), 3.43 (s, 4H, ***H4***), 2.84 (s, 4H, ***H5, H6***), 1.42 (s, 27H, ***H1, H10***), 1.23 (t, J = 7.1 Hz, 3H, ***H14***); δ_C(151 MHz, $CDCl_3$) 172 (***C12***) , 171 (***C1***) , 170.8 (***C10***) , 81 (***C9***), 80.9 (***C2***), 60 (***C13***)

, 56 (*C**11***) , 55 (*C**4***) , 53, 52.5 (*C**5**, C**6***) , 28 (*C**1**, C**10***) , 14 (*C**13***); GC-MS (EI$^+$) 488.4 (11%, M$^{+\bullet}$), 387 (40%, M-^{t}BuOC=O); (ES-MS$^+$) 489.7 (100 %, [M+H]$^+$), 512.2 (70 %, [M+Na]$^+$) ; HR-MS Found 489.3176 , $C_{24}H_{45}N_2O_8$ [M+H]$^+$ requires 489.3159.

8.2.23. tert-Butyl [(tert-butoxycarbonylmethyl){2-[(tert-butoxycarbonylmethyl) {2-oxo-2-[(tert-butoxycarbonylmethyl)amino]ethyl}amino]ethyl}amino]acetate, 17

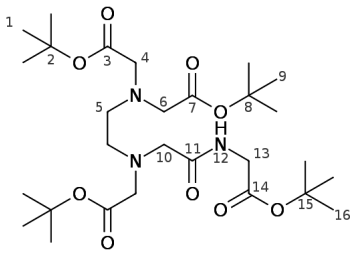

Aminoester **15** (0.20 g, 0.50 mmol) and haloamide **6b** (0.12 g, 0.58 mmol) were dissolved in acetonitrile (1.5 cm^3, dried over molecular sieves). Potassium carbonate (0.14 g, 1.01 mmol), potassium iodide and sodium sulphate (ca. 25 mg each) were then added and the mixture was heated at 60^{o}C under nitrogen. Reaction progress was monitored by TLC (alumina, ethyl acetate:hexanes 50:50) and ^{1}H NMR techniques. Once a steady state was observed with respect to the depletion of **[xv]** from the ^{1}H NMR spectrum, the reaction mixture was cooled to room temperature, filtered concentrated *in vacuo* and purified by column chromatography (method i, alumina, ethyl acetate:hexanes 50:50, isocratic) to afford the title compound (0.19 g, 0.33 mmol, 66%) as a yellow oil. ν_{max}/cm^{-1}(ATR) 2977 (sp^{3}C-H st), 1730 (ester C=O st), 1675 (amide C=O st), 1147 (C-O st);δ_H(700 MHz, $CDCl_3$) 8.52 (t, J = 6.0 Hz, 1H, *H**12***), 3.93 (d, J = 6.0 Hz, 2H, *H**13***), 3.42 (s, 4H, *H**4***), 3.35 (m, 4H, *H**6**, H**10***), 2.81 (s, 4H, *H**5***), 1.52 – 1.36 (m, 36H, *H**1**, H**9**, H**16***); δ_C(176 MHz, $CDCl_3$) 172.2 (*C**7***) , 170.5 (*C**3***) , 169.1 (*C**14*** or C***11***) , 81.4 - 81.0 (*C**2**, C**8**, C**15***) , 58.3 (*C**10***) , 56.5 (*C**10***) , 55.4 (*C**4***) , 52.8-52.2 (*C**5***, *C**6***) , 41.7 (*C**13***) , 28.1 - 28.0 (*C**1**, C**9**, C**16***); (ES-MS$^+$) 574.7 (100%, [M+H]$^+$); HR-MS Found 574.3705 , $C_{28}H_{52}N_3O_9$ [M+H]$^+$ requires 574.3704.

8.2.24. [(Carboxymethyl){2-[(carboxymethyl){2-[(carboxymethyl)amino]-2-oxoethyl}amino] ethyl}amino]acetic acid, AmGly$_1$

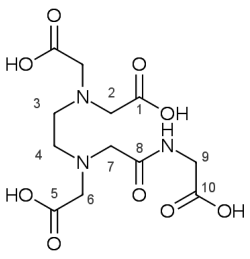

Amide **17** (0.54 g, 0.94 mmol) and anisole (0.44 cm^3 4.07 mmol), were dissolved in dichloromethane (2 cm^3), and trifluoroacetic acid (4 cm^3) was added to the yellow solution which was allowed to stir at room temperature under nitrogen for 18 hours. Volatiles were then removed *in vacuo* and the residue redissolved in dichloromethane which was once again removed *in vacuo*. Diethyl ether was then added to the residual oil and the mixture agitated ultrasonically to afford a white precipitate that was collected via centrifugation. This solid was dissolved in 1 mol dm^{-3} hydrochloric acid and passed through a short column of DOWEX 1X8 (chloride form) that had been pre-washed with 1 mol dm^{-3} hydrochloric acid and water. Once loaded onto the resin, elution of the compound was achieved with 1 mol dm^{-3} hydrochloric acid (ca. 100 cm^3). Removal of the solvent *in vacuo* followed by further drying under high vacuum gave the title compound (0.2 g, 0.57 mmol, 61%) as an off-white solid. t_R (H_2O:MeOH, MS detection); 1.63 min; δ_H (700 MHz, D_2O, pD≈8) 3.64 (s, 2H, ***H9***), 3.13 (s, 2H, ***H7***), 3.02 (s, 2H, ***H6***), 2.95 (s, 4H, ***H2***), 2.47 (t, J = 6.0 Hz, 2H, ***H4***), 2.43 (t, J = 6.0 Hz, 2H, ***H3***); δ_C(176 MHz, D_2O, pD≈8) 179.6 (***C1***), 179.3 (***C5***), 176.7 (***C10***), 173.8 (***C8***), 58.9 (***C6***), 58.7 (***C2***), 57.9 (***C7***), 52.2 (***C4***), 51.9 (***C3***), 43.1 (***C9***); (ES-MS^+) 551.7 (100 %, $[M+H]^+$); HR-MS Found 551.3449 , $C_{28}H_{47}N_4O_7$ $[M+H]^+$ requires 551.3445.

8.2.25. tert-Butyl [(tert-butoxycarbonylmethyl){2-[(tert-butoxycarbonylmethyl)(2-oxo-2-{[(2-pyridyl)methyl]amino}ethyl)amino]ethyl}amino]acetate, 1:1 formate adduct, $AmPy_1$-tBu

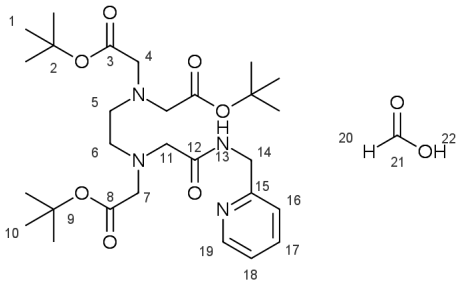

Aminoester **15** (0.53 g, 1.3 mmol) and haloamide **6c** (0.26, 1.4 mmol) were dissolved in acetonitrile (4.3 cm^3, dried over molecular sieves) and potassium carbonate (0.36 g, 2.6 mmol) and potassium iodide (0.04 g, 0.24 mmol) were suspended in the solution. The reaction mixture was then heated at 60°C under argon until ^1H NMR analysis indicated the consumption of starting aminoester **16** (within 24 hours). Acetonitrile was then removed *in vacuo* and the residue partitioned between dichloromethane and saturated sodium carbonate. The organic layer was extracted (3x) and dried over magnesium sulphate. The residue was purified via preparative reverse-phase column chromatography (water:acetonitrile, 0.5% v/v formic acid as additive 0:100→100:0 compound eluted in ca. 50:50 v/v water:acetonitrile) to afford the title compound (0.57 g, 0.96 mmol, 74%). ν_{max}/cm^{-1}(ATR) 3250 (acid O-H st), 2980 (sp^3 C-H st), 1730 (acid/ester C=O st), 1670 (amide C=O st), 1150

(acid/ester C-O st);δ_H (700 MHz, $CDCl_3$) 9.39 (t, J = 6.0 Hz, 1H, ***H13***), 9.06 (s, 1H, ***H22***), 8.94 (d, J = 5.5 Hz, 1H, ***H19***), 8.13 (dd, 1H, ***H17***), 8.11 (s, 1H, ***H20***) 7.75 (d, 1H, ***H16***), 7.61 (dd, 1H, ***H18***), 4.84 (d, J = 5.5 Hz, 2H, ***H14***), 3.87 (s, 2H, ***H11***), 3.76 (s, 4H, ***H4***), 3.71 (s, 2H, ***H7***), 3.24 (t, J = 5.0 Hz, 2H, ***H5***), 3.19 (t, J = 5.0 Hz, 2H, ***H6***), 1.47 (s, 1H, ***H10***), 1.44 (s, 1H, ***H1***); δ_C(176 MHz, $CDCl_3$)* 170.3 (***C12***), 168.4 (***C3***), 168.2 (***C8***), 162.9 (***C21***), 155.2 (***C15***), 143.7 (***C19***), 143.0 (***C17***), 124.7 (***C16***), 124.2 (***C18***), 117.1 (***C12***), 83.1 (***C2***), 83.0 (***C9***), 57.3 (***C11***), 55.1 (***C7***), 54.8 (***C4***), 51.8 (***C6***), 50.7 (***C5***), 41.5 (***C14***), 28.0 (***C10***), 27.9 (***C1***); (ES-MS^-) 595.6 (100 %, $[M-H]^-$, M= $C_{28}H_{46}N_4O_7$);

8.2.26. [(Carboxymethyl){2-[(carboxymethyl)(2-oxo-2-{[(2-pyridyl)methyl]amino}ethyl) amino]ethyl}amino]acetic acid, $AmPy_1$

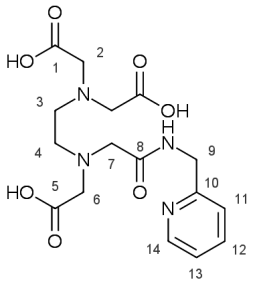

Amide **$AmPy_1$-tBu** (0.57g, 0.96 mmol) was dissolved in dichloromethane (2 cm^3) and anisole (0.35 cm^3, 3.2 mmol) dissolved. Trifluoroacetic acid (2 cm^3) was then added and the mixture was stirred under argon for 17 hours, after which time volatiles were removed *in vacuo*. A semi-solid material was then isolated after trituration in diethyl ether (50 cm^3) of the resulting residue using ultrasonic agitation, and the material collected via centrifugation. Aqueous hydrochloric acid (1 mol dm^3, ca. 50 cm^3) was the used to dissolve the solid, and then removed *in vacuo* to afford a buff solid. The solid was then redissolved in hydrochloric acid (1 mol dm^3, minimum volume) and the residue loaded onto DOWEX 1X8 (chloride form) that had been pre-washed with 1 mol dm^{-3} hydrochloric acid and water. Once loaded onto the resin, elution of the compound was achieved with water (ca. 100 cm^3) and then hydrochloric acid (1 mol dm^3, ca. 100 cm^3). Removal of the solvent *in vacuo* followed by further drying under high vacuum gave the title compound (0.22 g, 0.58 mmol, 60%) as an orange-brown solid. t_R (H_2O:MeOH, UV detection); 1.24 min; δ_H (600 MHz, D_2O, pD≈11) 8.32 (d, 1H, ***H14***), 7.72 (dd, 1H , ***H12***), 7.22 (m, 2H, ***H11, H13***), 4.40 (s, 2H, ***H9***), 3.23 (s, 2H, ***H7***), 3.11 (m, 6H, ***H3, H4, H6***), 2.65 (s, 4H, ***H2***); δ_C(151 MHz, D_2O, pD≈11) 179.3, 178.1 (***C1***, ***C5***) , 175.1 (***C8***), 156.6 (***C10***), 148.4 (***C14***), 138.4 (***C12***), 122.9 , 121.6 (***C12, C13***), 58.9 (***C4***), 58.4 (***C7***), 58.2 (***C3***), 52.4, 51.9 (***C1***, ***C6***), 44.0 (***C9***); (ES-MS^+) 383.2 (100 %, $[M+H]^+$); HR-MS Found 383.1570 , $C_{16}H_{23}N_4O_7$ $[M+H]^+$ requires 383.1567.

*Some impurity peaks, not reported, were present.

8.2.27. Ethyl (2-{[2-(bis{2-[(ethoxycarbonylmethyl)amino]-2-oxoethyl}amino)ethyl]{2-[(ethoxycarbonylmethyl)amino]-2-oxoethyl}amino}acetylamino)acetate, 18

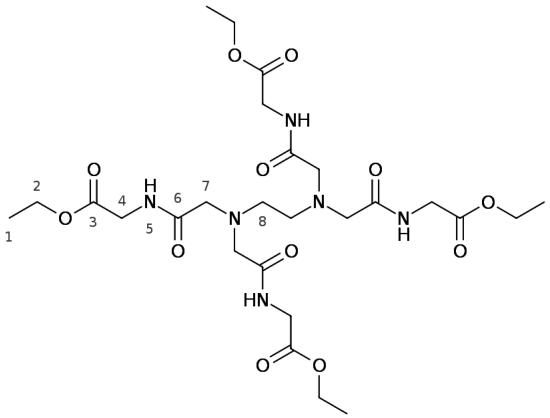

A solution of Ethyl (2-chloroacetylamino)acetate (1.08 g, 6.04 mmol) in acetonitrile (4 cm^3, dried over molecular sieves) was added dropwise to a solution of ethylene diamine (96 μL, 1.44 mmol) in acetonitrile (4 cm^3) in which potassium carbonate (0.99 g, 7.17 mmol) and sodium sulphate were suspended. Once the addition was complete (within 5 minutes), the mixture was heated to 60°C under nitrogen and the reaction was monitored using TLC (silica, dicholomethane:methanol 90:10) and ^{1}H NMR techniques. Since completion was not observed after 62 hours, a grain of potassium iodide was added as a catalyst and the reaction was allowed to stir for a further 28 hours at which point completion was indicated by ^{1}H NMR spectroscopy. After cooling the mixture to room tempature and filtering off solids, the filtrate was concentrated *in vacuo* and partitioned between dichloromethane and aqueous hydrochloric acid (pH 1-2). The extracted aqueous layer was then brought to pH 14 by adding solid sodium hydroxide and the resulting emulsion extracted with ethyl acetate (3x ca. 50 cm^3). The organic layer was subsequently washed with brine, dried over magnesium sulphate and concentrated *in vacuo* to afford the title compound (0.28 g, 0.44 mmol, 31%) as a yellow oil. ν_{max}/cm^{-1}(ATR) 3288 (amide N-H), 2982 (sp^3C-H), 1740 (ester C=O), 1656 (amide C=O), 1195 (ester C-O); δ_H(700 MHz, $CDCl_3$) 7.90 (d, J = 7.0 Hz, 4H, ***H5***), 4.20 (q, J = 7.5 Hz, 8H, ***H2***), 3.98 (d, J = 7.0 Hz, 8H, ***H4***), 3.33 (s, 8H, ***H7***), 2.86 (s, 4H, ***H8***), 1.26 (t, J = 7.5 Hz, 12H, ***H1***); δ_C(176 MHz, $CDCl_3$) 171.1 (***C3***) , 171.0 (***C6***) , 61.4 (***C2***) , 58.1 (***C7***) , 40.9 (***C8***), 14.03 (***C1***); (ES-MS^+) 633.7 (100%, $[M+H]^+$); HR-MS Found 633.3097 , $C_{26}H_{45}N_6O_{10}$ $[M+H]^+$ requires 633.3095.

8.2.28. tert-Butyl (2-{[2-(bis{2-oxo-2-[(tert-butoxycarbonylmethyl)amino]ethyl}amino)ethyl]{2-oxo-2-[(tert-butoxycarbonylmethyl)amino]ethyl}amino}acetylamino)acetate, 19

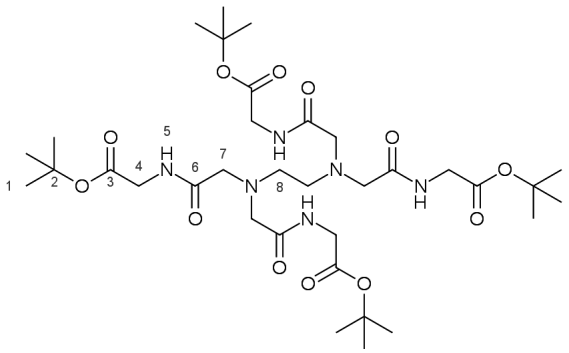

Ethylene diamine (45μL, 0.67 mmol) was dissolved in acetonitrile (7 cm^3, dried over molecular sieves) and haloamide **6b** (0.6 g, 3 mmol) added at once prior to the addition of potassium carbonate (2.33 g, 16.9 mmol) and potassium iodide (0.1 g, 0.6 mmol). The reaction mixture was then heated at 60°C for 26 hours under nitrogen. After cooling to room temperature, the reaction mixture was filtered, the solvent removed *in vacuo* and the residue purified by column chromatography (method i, alumina, dichloromethane:methanol 100:0→95:5 v/v) to afford the title compound (0.41 g, 0.55 mmol, 82%). δ_H (700 MHz, $CDCl_3$) 7.79 (t, J = 6.0 Hz, 4H, ***H5***), 3.87 (d, J = 6.0 Hz, 8H, ***H4***), 3.29 (s, 8H, ***H7***), 2.84 (s, 4H, ***H8***), 1.42 (s, 36H, ***H1***);δ_C(176 MHz, $CDCl_3$) 171.4 (***C3***), 170.1 (***C6***), 82.3 (***C2***), 58.6 (***C7***), 53.4 (***C8***), 41.9 (***C4***), 28.3 (***C1***); (ES-MS^+) 745.1 (100 %, $[M+H]^+$); HR-MS Found 745.4340, $C_{34}H_{61}N_6O_{12}$ $[M+H]^+$requires 745.4347.

8.2.29. Ethyl2-{2-[(2-{bis[2-(1-ethoxycarbonyl-2-phenylethylamino)-2-oxoethyl]amino} ethyl)[2-(1-ethoxycarbonyl-2-phenylethylamino)-2-oxoethyl]amino]acetylamino} -3-phenylpropionate, 20

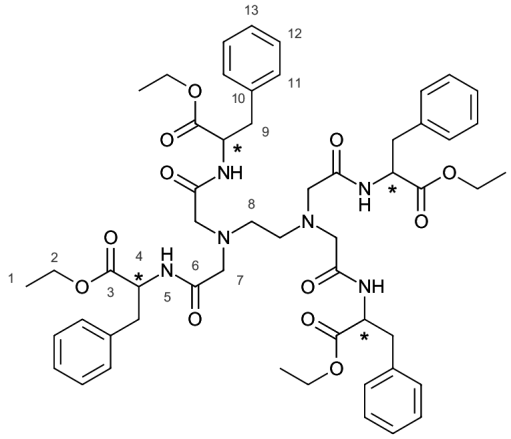

Ethylene diamine (36 μL, 0.54 mmol) was dissolved in acetonitrile (11 cm^3, dried over molecular sieves) along with haloamide **6d** (0.594 g, 2.20 mmol). Potassium carbonate (0.37 g, 2.7 mmol) and potassium iodide (0.01 g, 0.06 mmol) were then suspended in the solution which was heated under nitrogen at 60°C for 65 hours. After cooling to room temperature, solids were filtered off and the filtrate concentrated *in vacuo* prior to purification via column chromatography (method i, alumina, 0:100 dichloromethane:methanol→95:5 v/v) to afford the title compound (0.36 g, 0.36 mmol, 67%) as a yellow-brown oil. ν_{max}/cm^{-1}; 3300 (amide N-H st), 1670 (amide C=O st); δ_H (600 MHz, $CDCl_3$) 7.54 (s, 4H, ***H5***), 7.23 (dd, 8H, ***H11***), 7.19 (d, 4H, ***H13***), 7.14 (d, 8H, ***H12***), 4.79 (dd, 4H, ***H4***), 4.14 (q, J = 7.0, 8H, ***H5***), 3.38 – 2.76 (m, 16H, ***H7, H9***), 2.46 (s, 4H, ***H8***), 1.22 (t, J = 7.0 Hz, 12H, ***H1***); δ_C(151 MHz, $CDCl_3$) 172.3 (***C3, C6***), 136.4 (***C10***), 129.1 (***C12***), 128.5 (***C11***) , 126.9 (***C13***), 61.6 (***C2***), 58.1 (***C8***), 57.7 (***C7***), 53.30 (***C4***), 37.5 (***C9***), 14.1 (***C1***); (ES-MS^+) 993.4 (100 %, $[M+H]^+$); HR-MS Found 993.4970, $C_{54}H_{69}N_6O_{12}$ $[M+H]^+$requires 993.4973.

8.2.30. (2-{[2-(Bis{2-[(carboxymethyl)amino]-2-oxoethyl}amino)ethyl]{2-[(carboxymethyl) amino]-2-oxoethyl}amino}acetylamino)acetic acid,hydrochloride salt, $AmGly_4$

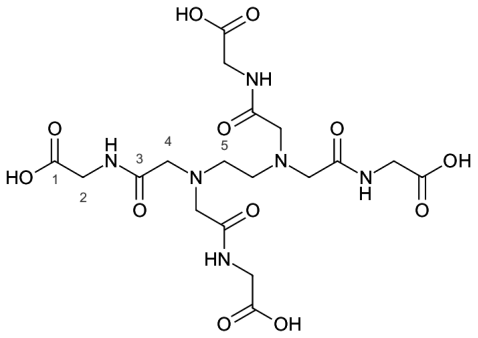

Via amide 18: Amide **18** (0.28 g, 0.44 mmol), was dissolved in methanol (5 cm^3) and an aqueous solution of potassium hydroxide (0.1 g, 1.78 mmol in 5 cm^3) was added to the methanolic solution which was then stirred under nitrogen. Reaction progress was monitored by ES-LCMS and upon consumption of the starting material volatiles were evaporated *in vacuo*. The crude residue was dissolved in concentrated ammonium hydroxide and loaded onto a DOWEX 1X8 anion exchange column (hydroxide form) that was first eluted with water until a reduction in pH was noted, and then aqueous hydrochloric acid (1 mol dm^{-3}) to elute the ligand. Concentration of fractions containing the product (determined via ES-LCMS) *in vacuo* afforded the title compound (77 mg, 34% based on M_r=520.5 g mol^{-1}) as an off-white solid.

Via amide 19: Amide **19** (0.41 g, 0.55 mmol) was dissolved in dichloromethane (4 cm^3) and anisole (0.26 cm^3, 2.4 mmol) added prior to the addition of trifluoroacetic acid (3 cm^3). The solution was then stirred under nitrogen for 14 hours. Volatiles were then removed *in vacuo* and the residue precipitated from diethyl ether using ultrasonic agitation. The precipitate was collected by centrifugation, dissolved in aqueous hydrochloric acid (1 mol dm^{-3}) and the solvent removed *in vacuo*. The residue was then re-dissolved in aqueous hydrochloric acid (1 mol dm^{-3}) and loaded onto a column DOWEX 1X8 (chloride form) that had been pre-washed with 1 mol dm^{-3} hydrochloric acid and water. Once loaded onto the resin, the compound was eluted using 1 mol dm^{-3} hydrochloric acid (ca. 100 cm^3) to give the title compound (0.08 g, 0.15 mmol 28% based on M_r=520.5 g mol^{-1}) as a yellow solid. δ_H(700 MHz, D_2O) 4.04 (s, 8H, ***H2***), 3.91 (s, 8H, ***H4***), 3.34 (s, 4H, ***H5***); δ_C(176 MHz, D_2O) 172.8 (***C1***) , 169.3 (***C3***) , 56.4 (***C4***) , 52.3 (***C5***) , 41.0 (***C2***); (ES-MS^-) 519.3 (100%, $[M-H]^-$); HR-MS Found 519.1687 , $C_{18}H_{27}N_6O_{12}$ $[M-H]^-$ requires 519.1687.

8.3. Synthetic and biological studies on ligands bearing phenol groups

8.3.1. o-[(2-{[(o-Hydroxyphenyl)methyl]amino}ethylamino)methyl]phenol, 4-H-21[214]

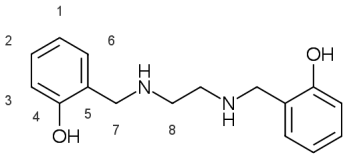

Salicylaldehyde (1.46 g, 12.0 mmol) was dissolved in methanol (60 cm^3) and ethylene diamine (0.4 cm^3, 5.98 mmol) was added at once to the solution which was stirring under nitrogen. Rapid precipitation was observed, and the suspension was refluxed for 2 hours. The yellow solid residue was isolated via filtration and dried under high vacuum to afford salen (1.04 g) which was suspended in methanol (60 cm^3) and allowed to stir under nitrogen prior to the portionwise addition of sodium borohydride (0.6 g, 15.9 mmol) at 0ºC . As addition progressed, discolouration of the reaction mixture from yellow to pinkish-white was observed. Once the addition was complete the mixture was stirred at room temperature for 13 hours. A white solid was then filtered off and the filtrate treated with aqueous sodium acetate (minimum volume to enact precipitation). Collection of the combined solids by filtration gave the title compound (0.86 g, 3.16 mmol, 53% based on ethylene diamine as limiting reagent) as a white crystalline solid. δ_H(700 MHz, $CDCl_3$) 7.16 (m, 1H, ***H2***), 6.97 (m, 1H, ***C6***), 6.83 (m, 1H, ***H3***), 6.75 (m, 1H, ***H1***), 3.99 (s, 4H, ***H7***), 2.83 (s, 4H, ***H8***); δ_c(176 MHz, $CDCl_3$) 157.9 (***C4***), 128.9 (***C2***), 128.4 (***C6***), 122.1 (***C5***), 119.2 (***C1***), 116.4 (***C3***), 52.6 (***C7***), 47.8 (***C8***); (ES-MS^-) 271.1 (100 %, $[M-H]^-$); HR-MS Found 273.1610 , $C_{16}H_{21}N_2O_2$ $[M+H]^+$ requires 273.1603.

8.3.2. 4-Fluoro-2-[(2-{[(5-fluoro-2-hydroxyphenyl)methyl]amino}ethylamino)methyl]phenol, 4-F-21[208]

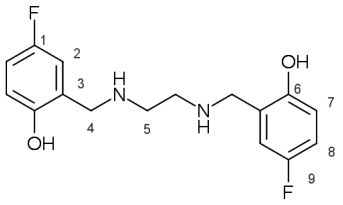

5-Fluorosalicylaldehyde (1.0 g, 7.1 mmol) was dissolved in methanol (17 cm^3) and ethylene diamine (0.23 cm^3, 3.4 mmol) was added and the mixture stirred under nitrogen at room temperature for 20 minutes to afford the precursor imine as a yellow precipitate (0.87 g, 2.9 mmol, 85 %). A sample of the imine (0.56g, 1.8 mmol) was then suspended in tetrahydrofuran:methanol (40 cm^3, 1:1 v/v) and the vessel flushed with nitrogen via three purge-backfill cycles. The suspension was then heated under nitrogen to dissolve the imine. 10% Palladium on charcoal (0.1 g, 5 mol% wrt. Pd) was then charged under a stream of nitrogen and a hydrogen balloon attached. The hydrogen was introduced by a

further three purge-backfill cycles and the reaction mixture heated at 50-60°C for 24 hours. After cooling to room temperature and refilling the flask with nitrogen, the reaction mixture was filtered through Celite® and the solvent removed *in vacuo* to give the title compound (0.41 g, 1.4 mmol, 72% wrt imine) as a pale yellow solid. δ_H (400 MHz, $CDCl_3$) 6.86 (m, 2H, ***H2***), 6.76 (dd, J = 9.0, 5.0 Hz, 2H, ***H8***), 6.70 (dd, J = 9.0, 3.0 Hz, 2H, ***H7***), 3.96 (s, 4H, ***H4***), 2.84 (s, 4H, ***H5***);δ_F (376 MHz, $CDCl_3$) -125.60 (td, J = 9.0, 5.0 Hz, ***F9***); (ES-MS^-) 307.2 (100 %, $[M-H]^-$, M= $C_{16}H_{18}F_2N_2O_2$).

8.3.3. 4-Chloro-2-[(2-{[(5-chloro-2-hydroxyphenyl)methyl]amino}ethylamino)methyl]phenol, 4-Cl-21[214]

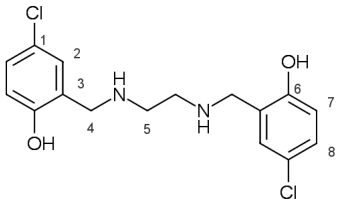

5-Chlorosalicylaldehyde (0.75 g, 4.8 mmol) was dissolved in chloroform (25 cm^3) and ethylene diamine (157μL, 2.3 mmol) added via Gilson pipette, following which, molecular sieves were charged into the reaction mixture. The mixture was then heated at 40°C under nitrogen for 17 hours, after which, the molecular sieves were removed via filtration and the solvent removed from the yellow filtrate *in vacuo* to afford the intermediate imine (0.72 g). After isolation, the imine was dissolved in a methanol:tetrahydrofuran solvent system (50 cm^3, 1:1 v/v) and sodium borohydride (0.5 g, 13.2 mmol) was added portionwise to the solution. Once addition was complete, the reaction mixture was stirred under nitrogen for 1 hour, another batch of sodium borohydride (0.5g, 13.2 mmol) was added, and the reaction mixture allowed to stir at room temperature for a further 20 hours. Volatiles were then removed *in vacuo*, and the residue partitioned between water and dichloromethane (2x). The combined organic layers were then washed with brine, dried over magnesium sulphate and the solvent removed *in vacuo* to afford the title compound (0.54 g, 1.6 mmol, 67%) as an off-white solid. δ_H (400 MHz, $CDCl_3$) 7.12 (dd, J = 8.5, 2.5 Hz, 2H, ***H8***), 6.96 (d, J = 2.5 Hz, 2H, ***H2***), 6.76 (d, J = 8.5 Hz, 2H, ***H7***), 3.96 (s, 4H, ***H4***), 2.83 (s, 4H, ***H5***); δ_C (101 MHz, $CDCl_3$) 156.7 (***C6***), 128.9 , 128.3, 124.0, 123.5, 117.9 (***C1, C2, C3, C7, C8***), 52.4 (***C4***), 47.9 (***C5***).

8.3.4. 4-Bromo-2-[(2-{[(5-bromo-2-hydroxyphenyl)methyl]amino}ethylamino)methyl]phenol, 4-Br-21[291]

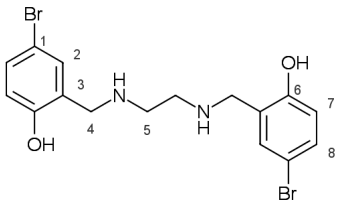

5-Bromosalicylaldehyde (1.85 g, 9.20 mmol) was dissolved in methanol (40 cm^3) and stirred under nitrogen for 5 minutes prior to the addition of ethylene diamine (0.3 cm^3, 4.44 mmol) leading to rapid precipitation of a yellow solid. The suspension was allowed to stir under nitrogen for 6 hours prior to collection of the solid imine (1.73 g, 4.06 mmol, 91%) by filtration. This solid was then dissolved in a 1:1 (v/v) mixture of tetrahydrofuran:methanol (30 cm^3), sodium borohydride (0.86 g, 22.7 mmol) was added portionwise over 3 minutes, and the mixture was stirred under nitrogen for 2 hours, over which time the solution decolourised. Aqueous hydrochloric acid (10 cm^3, 1 mol dm^{-3}) was then added dropwise to the reaction mixture and stirring was continued until precipitation of a white solid was observed. Filtration and washing of the precipitate with diethyl ether followed by drying of the solid under high vacuum led to isolation of the title compound (1.66 g, 3.86 mmol, 95%) as a white solid. δ_H (700 MHz, $CDCl_3$) 7.26 (m, 2H, ***H8***), 7.10 (d, 2H, ***H2***), 6.72 (d, 2H, ***H7***), 3.96 (s, 4H, ***H4***), 2.82 (s, 4H, ***H5***); δ_C(176 MHz, $CDCl_3$); 157.2 (***C6***) , 131.8 (***C8***) , 131.2 (***C2***) , 124.1 (***C3***) , 118.4 (***C7***) , 111.1 (***C1***) , 52.2 (***C4***) , 47.9 (***C5***); (ES-MS$^+$) 430.8 (100 %, $[M+H]^+$,M= $C_{16}H_{18}Br_2N_2O_2$).

8.3.5. 2-[(2-{[(2-Hydroxy-5-methoxyphenyl)methyl]amino}ethylamino)methyl]-4-methoxy phenol, 4-MeO-21[335]

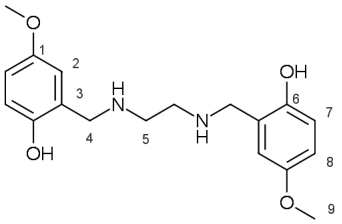

5-Methoxysalicylaldehyde (0.5 cm^3, 4.0 mmol) was dissolved in methanol (20 cm^3), ethylene diamine (0.13 cm^3, 2.1 mmol) was added and the mixture stirred at room temperature under nitrogen until a yellow solid (the target imine) precipitated. The solid (0.69 g)* was filtered off, and redissolved in methanol (15 cm^3). Sodium borohydride (1.08 g, 28 mmol) was added portionwise under ice and the mixture allowed to warm to room temperature. Stirring at room temperature under nitrogen was continued for a further 17 hours after which the reaction mixture was quenched with water (50

*The crude imine was most likely wet.

cm^3) and transferred to a separating funnel. This layer was washed with chloroform (100 cm^3) and extracted. The aqueous layer was washed a further three times with chloroform (50 cm^3) and the combined organic extracts washed with brine, dried over magnesium sulphate and dried *in vacuo*, to afford the title compound (0.49 g, 1.5 mmol, 71%), as a buff solid. δ_H (400 MHz, $CDCl_3$) 6.78 (m, 4H, ***H7, H8***), 6.58 (dd, 2H, ***H2***), 3.97 (s, 4H, ***H4***), 3.76 (s, 6H, ***H9***), 2.85 (s, 4H, ***H5***); δ_C (101 MHz, $CDCl_3$) 152.6, 151.9, 122.8, 116.8, 114.4, 113.7 (***C1,C2,C3,C6,C7,C8***), 55.8 (***C4***), 52.7 (***C9***), 47.9 (***C5***); (ES-MS^-) 331.3 (100 %, $[M-H]^-$, M= $C_{18}H_{24}N_2O_4$).

8.3.6. 2-Hydroxy-5-octylbenzaldehyde

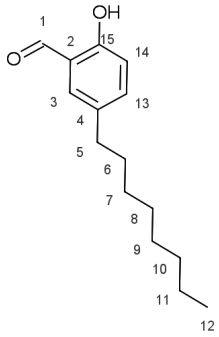

4-n-octylphenol (2.0 g, 9.69 mmol), paraformaldehdye (1.96 g, 65.3 mmol) and magnesium chloride (1.33 g, 14.5 mmol) were added to dry tetrahydrofuran (40 cm^3). To the suspension was added distilled, anhydrous triethylamine (5.0 cm^3, 35.8 mmol), leading to the formation of a cloudy white suspension. The apparatus was then flushed with nitrogen using three vacuum purge/nitrogen fill cycles and then refluxed under the same inert atmosphere for 60 hours during which the mixture adopted an increasingly yellow colour. Once cooled to room temperature, the mixture was acidified with aqueous hydrochloric acid (1 mol dm^{-3}) leading to a loss of colour. The resulting biphasic mixture was partitioned between ethyl acetate and water (3x), and the combined organic extracts were dried over magnesium sulphate and concentrated *in vacuo*. The resulting oil was purified by column chromatography (method i, silica, diethyl ether: hexanes, compound eluted in 10:90 diethyl ether hexanes v/v) to afford the title compound (1.68 g, 7.18 mmol, 74%) as a colourless oil. ν_{max}/cm^{-1} (ATR); 2923 (sp^3 C-H st), 1654 (aldehyde C=O st); δ_H (600 MHz, $CDCl_3$) ; 10.84 (s, 1H, ***H15***), 9.87 (s, 1H, ***H1***), 7.34 (m, 2H, ***H13, H14***), 6.91 (d, 1H, ***H3***), 2.59 (t, 2H, ***H5***), 1.58 (m, 2H, ***H6***), 1.29 (m, 10H, ***H7, H8, H9, H10, H11***), 0.88 (t, 3H, ***H12***); δ_C(151 MHz, $CDCl_3$) 197.0 (***C1***), 160.1 (***C15***), 134.7, 133.2, 120.7 ,117.7 (***C3***, ***C4, C13, C14***), 35.1 (***C5***) , 32.2 (***C6***) , 31.8 (***C7***) , 29.8 (***C8***), 29.6 (***C9***) , 29.5 (***C10***), 23.0 (***C11***) , 14.5 (***C12***); GC-MS (EI^+) 234 ($M^{+\bullet}$, M= $C_{15}H_{22}O_2$).

8.3.7. 2-[(2-{[(2-Hydroxy-5-octylphenyl)methyl]amino}ethylamino)methyl]-4-octylphenol, 4-Oct-21

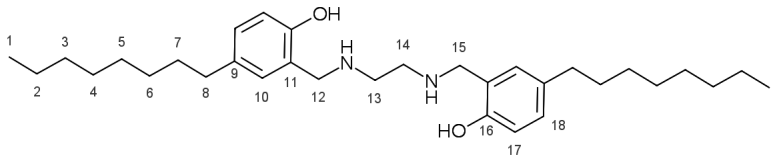

2-Hydroxy-5-octylbenzaldehyde (1.23 g, 5.25 mmol) was dissolved in chloroform (30 cm^3) and ethylene diamine (0.17 g, 2.54 mmol) added. The yellowing solution was then heated at 40°C under nitrogen and the reaction monitored by TLC (silica, ether:hexanes 50:50 v/v). The starting material appeared consumed within 2 hours and so the mixture was cooled to room temperature and allowed to stir for a further 2 hours at room temperature prior to removal of the solvent *in vacuo* to afford a yellow solid (the intermediate imine). The solid was then dissolved in a mixture of warmed tetrahydrofuran and methanol (50 cm^3, 80:20 v/v), sodium borohydride (0.45 g, 11.8 mmol) was added in portions and the reaction mixture was stirred at room temperature under nitrogen and monitored by TLC (silica, dichloromethane:methanol 90:10 v/v). Once the starting material was consumed (within 2 hours), the solvent was removed *in vacuo* and the residue repeatedly dissolved in dichloromethane and filtered through celite until no precipitation was observed from the filtrate. The solvent was again removed *in vacuo* and the resulting solid recrystallised from ethanol to afford the title compound (0.76 g, 1.5 mmol, 60%) as white flakes. ν_{max}/cm^{-1} (ATR); 3271 (amine N-H st) 2918 (sp^3 C-H st), 1116 (phenol C-O st); δ_H(600 MHz, $CDCl_3$) 6.97 (dd, J = 8.0, 2.0 Hz, 2H, ***H17***) , 6.78 (d, J = 2.0 Hz, 2H, ***H10***), 6.74 (d, J = 8.0 Hz, 2H, ***H18***), 3.96 (s, 4H, ***H12***), 2.84 (s, 4H, ***H13***), 2.48 (t, 4H, ***H8***), 1.55 (m , 4H, ***H7***), 1.37 – 1.13 (m, 20H, ***H6***, ***H5***, ***H4***, ***H3***, ***H2***), 0.88 (t, 6H, ***H1***); δ_C(151 MHz, $CDCl_3$); 156.0 (***C18***), 134.0 (***C15***), 129.0 (***C16***), 128.7 (***C10***), 122.2 (***C11***), 116.4 (***C17***), 53.1 (***C12***), 48.3 (***C13***), 35.5 (***C8***), 32.2 (***C7***), 32.1 (***C6***), 29.9 (***C5***), 29.7 (***C4***), 29.6 (***C3***), 23.0 (***C2***), 14.5 (***C1***); (ES-MS^-) 495.3 (100 %, $[M-H]^-$, M= $C_{32}H_{52}N_2O_2$).

8.3.8. 2-[(2-{[(2-Hydroxy-5-nitrophenyl)methyl]amino}ethylamino)methyl]-4-nitrophenol, 4-NO_2-21[291]

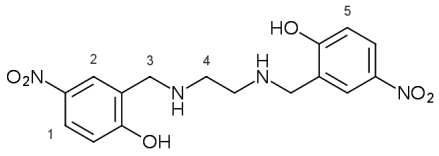

5-nitrosalicylaldehyde (1.02 g, 6.2 mmol) was dissolved in methanol and ethylene diamine (0.21 cm^3, 3.1 mmol) added to the solution, resulting in the immediate precipitation of a yellow powder that was collected by filtration (0.97 g) after the suspension was allowed to stir under nitrogen for 30 minutes. The yellow powder was then dissolved in tetrahydrofuran:methanol (10 cm^3, 1:1 v/v) and sodium borohydride (0.3 g, 8 mmol) added portionwise. The solution was stirred at room temperature under nitrogen for 21 hours prior to the dropwise addition of aqueous hydrochloric acid (10 cm^3, 1 mol dm^{-3}) to precipitate the title compound (0.96 g, 2.7 mmol, 87%), which was isolable by filtration. δ_H (400 MHz, D_2O) 6.46-7.99 (m, 6H, ***H1, H2, H5***), 3.70 (s, 4H, ***H3***), 2.80 (s, 4H, ***H4***);* (ES-MS^-) 360.9 (100 %, $[M-H]^-$, M= $C_{16}H_{18}N_4O_6$).

8.3.9. 1,2-Bis{[(o-methoxyphenyl)methyl]amino}ethane, 4-H-21-OMe

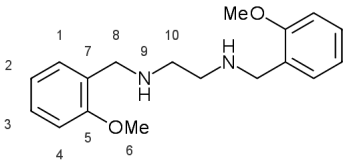

Ethylenediamine (0.58 cm^3, 8.68 mmol) was added to a methanolic (43 cm^3) solution of 2-methoxy benzaldehyde (2.38 g, 17.5 mmol) and stirred for 3 hours at room temperature under nitrogen prior to the portionwise addition of sodium borohydride (2.9 g, 76.6 mmol) over 3 hours. Once addition was complete, the solution was then stirred for 22 hours at room temperature and filtered through Celite® followed by solvent removal *in vacuo.* The resulting material was partitioned between dichloromethane and aqueous hydrochloric acid (3x, pH $\approx$1) and the combined aqueous extracts were treated with sodium hydroxide pellets until the formation of an emulsion was observed (pH>10). This emulsion was washed with ethyl acetate (3x), dried with magnesium sulphate and concentrated *in vacuo* to give the title compound as a colourless oil (2.0 g, 6.67 mmol, 77%), that crystallised to an off-white solid upon standing. Slow evaporation of a sample of this solid from diethyl ether gave crystals suitable for analysis via X-ray crystallography. ν_{max}/cm^{-1}(ATR) 3292 (free N-H st), 2830 (sp^3C-H st), 1025 (C-O st); δ_H (700 MHz, $CDCl_3$) 7.23 – 7.17 (m, 4H, ***H1, H3***), 6.89 (m, 2H, ***H2***), 6.84 (d, 2H, ***H4***), 3.79 (s , 6H, ***H6***), 3.76 (s, 4H, ***H8***), 2.72 (s, 4H, ***H10***), 1.97 (s, 2H, ***H9***);

*The poor solubility of this compound precluded acquisition of an acceptable ^{13}C NMR spectrum

δ_C(176 MHz, $CDCl_3$) 157.6 (***C5***) , 129.8 (***C3*** or ***C1***), 128.4 (***C7***) , 128.1 (***C3*** or ***C1***), 120.3 (***C2***) , 110.2 (***C4***) , 55.2 (***C6***), 49.0 (***C8***) , 48.5 (***C10***); (ES-MS^+) 301.0 (100 %, $[M+H]^+$); HR-MS Found 301.1907 , $C_{18}H_{25}N_2O_2$ $[M+H]^+$requires 301.1916 ; X-ray crystallography: $C_{18}H_{24}N_2O_2$, M_r=195.21, monoclinic ($P2_{1/n}$); *a* = 7.2450(3) Å, *b* = 5.5692(3) Å, *c* = 20.0255(9) ; crystal size = 0.49 × 0.25 × 0.14 mm^3; T= 120 K.

8.3.10. Ethyl {[(o-methoxyphenyl)methyl](2-{(ethoxycarbonylmethyl)[(o-methoxyphenyl) methyl]amino}ethyl)amino}acetate, 4-H-21-OMe-Et

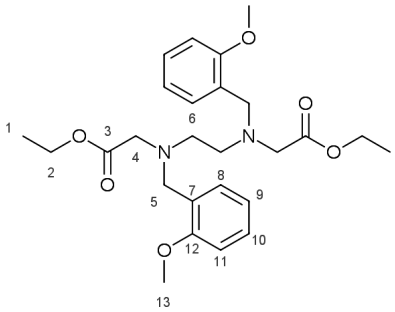

4-H-21-OMe (0.21 g, 0.7 mmol) was dissolved in acetonitrile (3.5 cm^3) and triethylamine (0.25 cm^3, 1.80 mmol) added to the stirred solution at room temperature. Ethyl bromoacetate (0.16 cm^3, 1.44 mmol) was then added at once to give a white suspension and the mixture heated to 60°C under nitrogen for 2 hours. Close monitoring by TLC (silica, dichloromethane:methanol 9:1) indicated completion within 90 minutes. The reaction mixture was then cooled to room temperature and partitioned between aqueous hydrochloric acid and dichloromethane, the organic layer being extracted and concentrated *in vacuo*. Diethyl ether (125 cm^3) was added to the residual oil and the mixture agitated by ultrasound after which the diethyl ether was decanted off to leave a colourless oil that was purified via column chromatography (method i, alumina, ethyl acetate:hexanes:triethylamine 0:98:2→50:48:2 v/v) to afford the title compound (0.14 g, 0.29 mmol, 41 %) as a colourless oil. ν_{max}/cm^{-1}(ATR) 2938 (sp^3 C-H st), 1736 (ester C=O st), 1601 (aromatic C-C st), 1027 (C-O st); δ_H (700 MHz, $CDCl_3$) 7.35 (d, 2H, ***H8***), 7.21 (m, 2H, ***H10***), 6.90 (m, 2H, ***H9***), 6.83 (d, 2H, ***H11***), 4.14 (q, J = 7.1 Hz, 4H, ***H2***), 3.84 (s, 4H, ***H5***), 3.77 (s, 6H, ***H13***), 3.40 (s, 4H, ***H4***), 2.90 (s, 4H, ***H6***), 1.25 (t, J = 7.1 Hz, 6H, ***H1***); δ_C(176 MHz, $CDCl_3$) 172.0 (***C3***) , 158.1 (***C7***) , 131.0 (***C8***) , 128.4 (***C10***) , 127.1 (***C7***) , 120.7 (***C9***) , 110.6 (***C11***), 60.4 (***C2***) , 55.5 (***C13***) , 54.9 (***C4***) , 52.8 (***C6***) , 52.3 (***C5***) , 14.6 (***C1***); (ES-MS^+) 473.0 (100 %, $[M+H]^+$); HR-MS Found 473.2647 , $C_{18}H_{37}N_2O_6$ $[M+H]^+$requires 473.2652.

8.3.11. Tert-Butyl{[(o-hydroxyphenyl)methyl](2-{[(o-hydroxyphenyl)methyl](tert-butoxy carbonylmethyl)amino}ethyl)amino}acetate, HBED-tBu

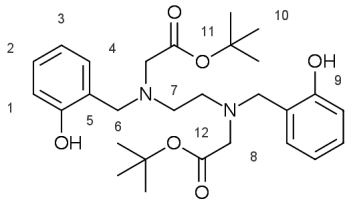

Acetonitrile (2 cm^3, dried over molecular sieves) was used to partially dissolve **4-H-21** (0.1 g, 0.37 mmol) in a Schlenk tube. Potassium bicarbonate (0.15 g, 0.75 mmol), potassium iodide (cat.) and sodium sulphate (ca. 0.2 g) were then added to the suspension followed by the dropwise addition of t-butyl bromoacetate (0.11 cm^3, 0.74 mmol). Once addition was complete, the reaction mixture was heated to 60°C for 16 hours under nitrogen, although consumption of **4-H-21** was observed by TLC (SiO_2, ethyl acetate:hexanes 50:50) after four hours. Once cooled to room temperature, the reaction mixture was filtered through Celite® concentrated *in vacuo* and purified by column chromatography (method i, SiO_2, ethyl acetate:hexanes 20:80→50:50) to afford the product as a colourless oil (0.16 g, 86%).* ν_{max}/cm^{-1}(ATR) 3327 (br, phenol O-H st), 2978 (sp^3C-H st), 1727 (ester C=O st), 1151 (C-O st); δ_H (400 MHz, $CDCl_3$) 9.69 (s, 2H, ***H9***), 7.17-6.76 (m, 8H, ***H1, H2, H3, H4)***, 3.71 (s, 4H, ***H8***), 3.16 (s, 4H, ***H6***), 2.68 (s, 4H, ***H7***), 1.46 (s, 18H, ***H10***); δ_C(101 MHz, $CDCl_3$) 170.1 (***C12***), 157.5 (***C9***) , 129.3 (***C12***) , 129.2 , 121.6 , 119.2 , 116.4 (***C1, C2, C3, C4***), 82.1 (***C11***) , 58.0 (***C8***) , 55.5 (***C6***) , 50.1 (***C7***) , 28.1 (***C10***); (ES-MS^-) 495.3 (100 %, $[M-H]^-$, M= $C_{28}H_{40}N_2O_6$).

8.3.12. tert-Butyl {[(5-fluoro-2-hydroxyphenyl)methyl](2-{[(5-fluoro-2-hydroxyphenyl)methyl] (tert-butoxycarbonylmethyl)amino}ethyl)amino}acetate, 4-F-21-tBu

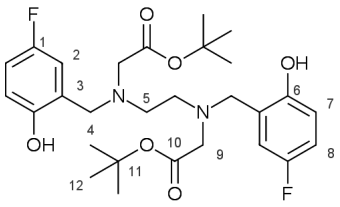

Aminophenol **4-F-21** (0.38 g, 1.2 mmol) was dissolved in anhydrous isopropanol (6.2 cm^3) and potassium bicarbonate (0.31 g, 3.1 mmol) was suspended in the solution to which t-butyl bromoacetate (0.37 cm^3, 2.5 mmol) was added at once. After the mixture was heated at 60°C under nitrogen for 27 hours, during which time the mixture clarified, hot filtration was performed. Once the solvent was removed from the filtrate *in vacuo*, the residue was dissolved in boiling hexanes leading to the formation of a yellow solution containing traces of an oily brown residue. The yellow solution was decanted

*after mass adjustment for the presence of adventitious high vacuum grease.

from the brown oil, and precipitation induced by ultrasonic agitation and cooling. This precipitate was then recrystallised from ethyl acetate to afford the title compound (0.29 g, 0.54 mmol, 45 %) as yellow crystals. Slow evaporation of this material from chloroform gave crystals suitable for X-ray crystallography. mp 132-134°C; δ_H (700 MHz, $CDCl_3$); 9.46 (s, 2H, ***H6***), 6.87 (dd, J = 8.5, 3.0 Hz, 2H, ***H8***), 6.77 (dd, J = 8.5, 5.0 Hz, 2H, ***H7***), 6.63 (dd, J = 8.5, 3.0 Hz, 2H, ***H2***), 3.69 (s, 4H, ***H4***), 3.16 (s, 4H, ***H9***), 2.68 (s, 4H, ***H5***), 1.46 (s, 18H, ***H12***); δ_C(176 MHz, $CDCl_3$); 170.1 (***C10***), 156.1 (d, J = 237.0 Hz) (***C1***) , 153.5 (***C6***), 122.6 (d, J = 7.0 Hz) (***C3***), 117.31 (d, J = 8.0 Hz) (***C7***), 115.7 (dd, J = 23.0, 12.0 Hz) (***C8***), 82.5 (***C11***), 57.7 (***C4***), 55.5 (***C9***), 50.3 (***C5***), 28.2 (***C12***); δ_F(376 MHz, $CDCl_3$); -126.15 (dd) (***F1***); (ES-MS$^-$) 535.2 (100 %, $[M-H]^-$); HR-MS Found 535.2618, $C_{28}H_{37}N_2O_6F_2$ $[M-H]^-$requires 535.2620; X-ray crystallography: $C_{28}H_{38}N_2O_6F_2$, M_r=536.60, monoclinic ($P2_1/c$); *a* = 13.1139(10) Å, *b* = 10.2607(7) Å, *c* = 10.8035(6); crystal size = 0.36 × 0.24 × 0.12 mm^3; T= 120K.

8.3.13. tert-Butyl{[(5-bromo-2-chlorophenyl)methyl](2-{[(5-chloro-2-hydroxyphenyl)methyl](tert-butoxycarbonylmethyl)amino}ethyl)amino}acetate, 4-Cl-21-tBu

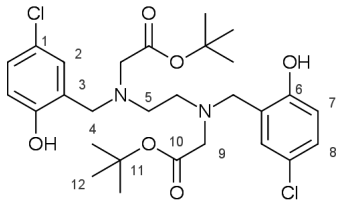

Aminophenol **4-Cl-21** (0.54 g, 1.6 mmol) was dissolved in anhydrous isopropanol (10 cm^3) and potassium bicarbonate (0.38g, 3.8 mmol) was suspended in the solution. t-Butyl bromoacetate (0.49 cm^3, 3.3 mmol) was added at once and the mixture heated to 60°C under nitrogen. After the starting material was consumed (ca. 15 hours) as monitored by TLC (ethyl acetate:hexanes 50:50 v/v), the reaction mixture was cooled to room temperature and filtered. The solid residue was then suspended in hot dichloromethane, filtered again and the solvent removed from the filtrate *in vacuo*. Ultrasonic agitation of the resulting oil in hexanes led to precipitation of the title compound (0.42 g, 0.74 mmol, 46%) as a white solid. Slow evaporation of this material from warm acetone gave crystals suitable for structural analysis via X-ray crystallography. mp 150-151°C δ_H (700 MHz, $CDCl_3$) ; 9.74 (s, 2H, ***H6***), 7.13 (dd, J = 8.5, 2.5 Hz, 2H, ***H8***), 6.89 (d, J = 2.5 Hz, 2H, ***H2***), 6.79 (m, 2H, ***H7***), 3.68 (s, 4H, ***H4***), 3.16 (s, 4H, ***H9***), 2.67 (s, 4H, *H*5), 1.46 (s, 18H, ***H12***); δ_C(176 MHz, $CDCl_3$); 170.1 (***C10***), 156.2 (***C6***), 129.3 (***C8***), 129.1 (***C2***), 123.8 (***C1***), 123.2 (***C3***), 118.0 (***C7***), 82.6 (***C11***), 57.8 (***C4***), 55.4 (***C9***), 50.2 (***C5***), 28.2 (***C12***); (ES-MS$^+$) 569.1 (100 %, $[M+H]^+$); HR-MS Found 569.2173, $C_{28}H_{39}N_2O_6Cl_2$ $[M+H]^+$requires 569.2185; X-ray crystallography: $C_{28}H_{38}N_2O_6Cl_2$, M_r=569.50, monoclinic ($P2_1/c$); *a* = 15.0443(5) Å, *b* = 8.8106(3) Å, *c* = 11.2961(4); crystal size = 0.38 × 0.23 × 0.08 mm^3; T= 120K.

8.3.14. tert-Butyl {[(5-bromo-2- hydroxyphenyl)methyl] (2-{[(5-bromo-2-hydroxyphenyl)methyl] (tert-butoxy carbonylmethyl) amino}ethyl)amino} acetate, 4-Br-21-tBu

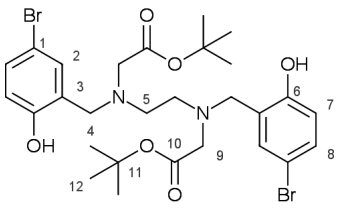

Aminophenol **4-Br-21** (0.75 g, 1.74 mmol) was dissolved in acetonitrile (10 cm^3, dried over molecular sieves) and potassium hydrogen carbonate (0.70 g, 6.98 mmol) and potassium iodide (8 mg, 0.05 mmol) were added. The mixture was then stirred for at room temperature prior to the addition of t-butyl bromoacetate (0.54 cm^3, 3.68 mmol). After addition, the reaction mixture was heated to 60°C under nitrogen for 22 hours and then allowed to cool to room temperature prior to dilution with diethyl ether and removal of solid material by filtration. The solid material was then suspended in boiling ethyl acetate, filtered while hot and the solvent of the filtrate removed *in vacuo* to isolate the title compound (0.50 g, 0.76 mmol, 44%) as a white solid. Slow evaporation of this material from warm acetone gave crystals suitable for structural analysis via X-ray crystallography. mp 184-186°C; ν_{max}/cm^{-1}; 3250 (phenol O-H st), 2980 (sp^3 C-H st), 1150 (ester C-O); δ_H (700 MHz, $CDCl_3$) ; 9.74 (s, 2H, ***H6***), 7.28 (dd, J =8.5, 2.5 Hz, 2H, ***H8***), 7.03 (d, J = 2.5 Hz, 2H, ***H2***), 6.73 (d, J = 8.5 Hz, 2H, ***H7***), 3.68 (s, 4H, ***H4***), 3.15 (s, 4H, ***H9***), 2.65 (s, 4H, ***H5***), 1.46 (s, 18H, ***H12***); δ_C(176 MHz, $CDCl_3$); 170.1 (***C10***) , 156.7 (***C6***) , 132.2 (***C2***) , 131.9 (***C8***) , 123.8 (***C3***) , 118.5 (***C7***) , 111.0 (***C1***) , 82.6 (***C11***) , 57.7 (***C4***) , 55.4 (***C9***) , 50.2 (***C5***) , 28.2 (***C12***); (ES-MS^-) 657.1 (100 %, $[M-H]^-$); HR-MS Found 657.1164, $C_{28}H_{39}N_2O_6Br_2$ $[M-H]^-$requires 657.1175; X-ray crystallography: $C_{28}H_{38}N_2O_6Br_2$, M_r=658.42, triclinic (P_1); *a* = 6.03170(10) Å, *b* = 9.8716(2) Å, *c* = 12.9407(2); crystal size = 0.28 × 0.14 × 0.08 mm^3; T= 120K.

8.3.15. tert-Butyl{[(2-hydroxy-5-methoxyphenyl)methyl](2-{[(2-hydroxy-5-methoxyphenyl)methyl](tert-butoxycarbonylmethyl)amino}ethyl)amino}acetate, 4-MeO-21-tBu

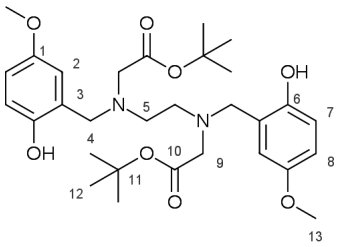

Aminophenol **4-MeO-21** (0.2g, 0.6 mmol), was dissolved in anhydrous acetonitrile (4 cm^3) and potassium bicarbonate (0.15g, 1.5 mmol) and t-butyl bromoacetate (0.19 cm^3, 1.3 mmol) were added at once. The mixture was then stirred at 60°C under nitrogen until most of the starting material was consumed (typically within 4 hours, monitored by TLC on silica, diethyl ether:hexane 1:1 v/v). The reaction mixture was then filtered and the filtrate concentrated to an oil *in vacuo* prior to purification by via column chromatography (method ii, diethyl ether:hexanes 0:100→50:50 compound eluted in ca. 30:70 v/v diethyl ether:hexanes). The title compound (0.12g, 0.21 mmol, 36%) crystallised out of the eluent medium as a white solid. Slow evaporation of a sample of this material from warm acetone gave samples suitable for x-ray crystallography. If desired, column chromatography could be bypassed via ultrasonic agitation of a suspension of the previously described concentrated oil in hexanes, followed by filtration of the resulting precipitate to afford the title compound (0.23 g, 67% starting from 0.25 g **4-MeO-21**). mp 134-136°C; δ_H (700 MHz, $CDCl_3$); 6.82 (d, J = 9.0 Hz, 2H, *H**7***), 6.74 (dd, J = 9.0, 3.0 Hz, 2H, *H**8***), 6.50 (d, J = 3.0 Hz, 2H, *H**2***), 3.76 (s, 4H, *H**4***), 3.72 (s, 6H, *H**13***), 3.26 (s, 4H, *H**9***), 2.82 (s, 4H, *H**5***), 1.45 (s, 18H, *H**12***); δ_C(176 MHz, $CDCl_3$); 169.7 (*C**10***), 152.7 (*C**1***), 151.1 (*C**6***), 121.8 (*C**3***), 117.3 (*C**7***), 115.4 (*C**2***), 114.7 (*C**8***), 82.6 (*C**11***), 57.5 (*C**4***), 55.9 (*C**13***), 55.3 (*C**9***), 50.4 (*C**5***), 28.2 (*C**12***); (ES+MS^+) 561.2 (100 %, $[M+H]^+$); HR-MS Found 561.3189, $C_{30}H_{45}N_2O_8$; $[M+H]^+$requires 561.3176; X-ray crystallography: $C_{30}H_{44}N_2O_8$, M_r=560.67, triclinic (P-1); *a* = 6.4286(2) Å, *b* = 10.1382(4) Å, *c* = 12.8531(4); crystal size = 0.49 × 0.24 × 0.14 mm^3; T= 120K.

8.3.16. tert-Butyl{[(2-hydroxy-5-octylphenyl)methyl](2-{[(2-hydroxy-5-octylphenyl)methyl](tert-butoxycarbonylmethyl)amino}ethyl)amino}acetate, 4-Oct-21-tBu

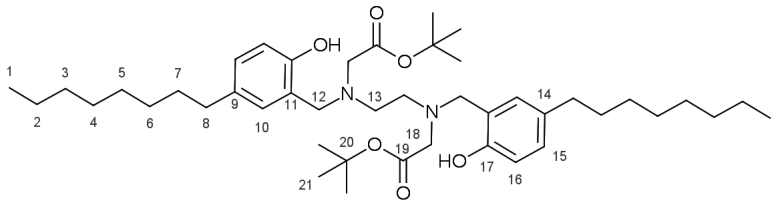

Aminophenol **4-Oct-21** (0.40 g, 0.81 mmol) was dissolved in an acetonitrile:ethyl acetate mixture (6 cm^3, 1:1 v/v) and potassium bicarbonate (0.32 g, 3.2 mmol) was then suspended in the reaction mixture that was then heated to 60°C. Once at temperature, t-butyl bromoacetate (0.25 cm^3, 1.7 mmol) was added dropwise and heating was continued until the starting material was observed to be consumed by TLC (silica, dichloromethane:methanol). After 24 hours the reaction mixture was cooled to room temperature, filtered and the filtrate concentrated *in vacuo*. The residue was then purified by column chromatography (method i, SiO_2, ethyl acetate:hexanes 0:100→10:90) to afford the title compound (0.43 g, 0.59 mmol, 73%) as a colourless oil. ν_{max}/cm^{-1}; 3290 (phenol O-H st), 2920 (sp^3 C-H st), 1730 (ester C=O st), 1150 (ester C-O); δ_H (700 MHz, $CDCl_3$) 9.46 (s, 2H, ***H17***), 6.97 (d, J=8.0 Hz, 2H, ***H15***), 6.75 (d, J = 8.0 Hz, 2H, ***H16***), 6.70 (s, 2H, ***H10***), 3.70 (s, 4H, ***H12***), 3.18 (s, 4H, ***H18***), 2.70 (s, 4H, ***H13***), 2.47 (t, J = 8.0 Hz, 4H, ***H8***), 1.53 (m, 4H, ***H7***), 1.45 (s, 18H, ***H21***), 1.28 (m, 20H, ***H6***, ***H5***, ***H4***, ***H3***, ***H2***), 0.88 (t, 6H, ***H1***); δ_C(176 MHz, $CDCl_3$) 170.0 (***C19***) , 155.2 (***C17***), 133.5 (***C9***), 129.0 (***C10***), 128.9 (***C15***) , 121.2 (***C11***), 116.1 (***C16***), 81.9 (***C20***), 58.0 (***C12***), 55.5 (***C18***), 50.4 (***C13***), 35.0 (***C8***), 31.9 (***C7***), 31.8 (***C6***), 29.5 (***C5***), 29.3 (***C4***), 29.2 (***C3***), 28.0 (***C21***), 22.6 (***C2***), 14.1 (***C1***); (ES-MS^+) 725.3 (100 %, $[M+H]^+$); HR-MS Found 725.5466, $C_{44}H_{73}N_2O_6$ $[M+H]^+$ requires 725.5469.

8.3.17. [(Benzyl){2-[(benzyl)(carboxymethyl)amino]ethyl}amino]acetic acid, BED[336]

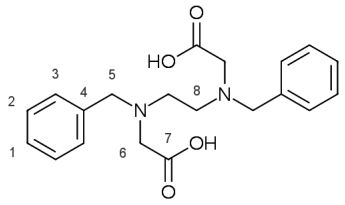

Aminoester **11** (0.69 g, 1.5 mmol) dissolved in dichloromethane (4 cm^3) and triethylsilane (1.2 cm^3, 7.5 mmol) added. Trifluoroacetic acid (3 cm^3) was then added at once to the solution, which was stirred at room temperature under nitrogen for 21 hours. Volatiles were then removed *in vacuo* and diethyl ether added to the oily residue to give a white precipitate (0.25 g) that was isolated via centrifugation. This white solid was suspended in aqueous hydrochloric acid (1 mol dm^{-3}) and

loaded onto a pad of DOWEX 50WX8 (H^+ form). The compound was then eluted using a sequence of aqueous hydrochloric acid (100 cm^3, 1 mol dm^{-3}), water (100 cm^3) and finally ammonia (100 cm^3, 10 mol dm^{-3}). The ammoniacal fractions were subject to solvent removal *in vacuo*, to afford the product (0.16 g, 0.46 mmol, 31%, based on the di-ammonium salt) as a white solid. δ_H (700 MHz, D_2O, pD≈14) 7.36 (m, 10H, ***H1, H2, H3***), 3.71 (s, 4H, ***H5***), 3.07 (s, 4H, ***H6***), 2.73 (s, 4H, ***H8***); δ_C (176 MHz, D_2O, pD≈14) 178.7 (***C7***), 137.3 (***C4***), 130.1 (***C3***), 128.4 (***C2***), 127.5 (***C1***), 57.6 (***C5***), 57.2 (***C6***), 50.2 (***C8***); (ES-MS^+) 357.2 (100 %, $[M+H]^+$); HR-MS Found 357.1817 , $C_{20}H_{25}N_2O_4$ $[M+H]^+$requires 357.1814.

8.3.18. {[(5-Chloro-2-fluorophenyl)methyl](2-{(carboxymethyl)[(5-fluoro-2-hydroxyphenyl) methyl]amino}ethyl)amino}acetic acid, 4-F-HBED

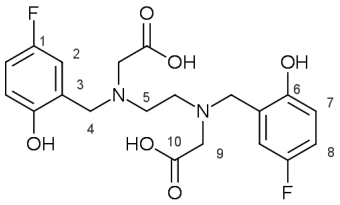

Aminoester **4-F-21-tBu** (0.2 g, 0.4 mmol) was dissolved in dichloromethane (2 cm^3) and anisole (0.10 cm^3, 0.93 mmol) added prior to the addition of trifloroacetic acid (2 cm^3) and the mixture stirred at room temperature under nitrogen for 13 hours. Volatiles were then removed *in vacuo*, and the residual oil was triturated in diethyl ether under ultrasonic agitation to afford a white precipitate that was collected under centrifugation. Aqueous hydrochloric acid (10 cm^3, 1 mol dm^{-3}) was used to dissolve the precipitate using heating if necessary, and the solvent removed *in vacuo* to afford the title compound (0.12 g, 0.37 mmol, 73%) as an off-white solid. t_R (H_2O:MeOH, UV detection); δ_H (600 MHz, D_2O, pD≈8); 6.81 (td, J = 9.0, 3.0 Hz, 2H, ***H7***), 6.64 (dd, J = 9.0, 3.0 Hz, 2H, ***H8***), 6.57 (dd, J = 9.0, 4.5 Hz, 2H, ***H2***), 3.50 (s, 4H, ***H4***), 3.01 (s, 4H, ***H9***), 2.52 (s, 4H, ***H5***); δ_C (151 MHz, D_2O, pD≈8); 178.2 (***C10***), 155.7 (d, J = 234.0 Hz) (***C1***), 152.6 (***C6***) , 123.9 (d, J = 7.0 Hz) (***C3***), 116.6 (d, J = 8.0 Hz) (***C2***), 115.9 (d, J = 23.0 Hz) (***C7***), 115.1 (d, J = 23.0 Hz) (***C8***), 57.6 (***C9***), 56.0 (***C4***), 49.3 (***C5***); δ_F (576 MHz, D_2O, pD≈8) -125.97 (td, J = 9.0, 4.5 Hz) (***F1***); (ES-MS^-) 423.2 (100 %, $[M-H]^-$, M= $C_{20}H_{22}F_2N_2O_6$).

8.3.19. {[(5-Chloro-2-hydroxyphenyl)methyl](2-{(carboxymethyl)[(5-chloro-2-hydroxyphenyl) methyl]amino}ethyl)amino}acetic acid, 4-Cl-HBED

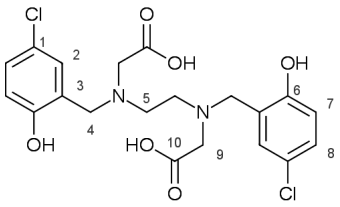

Aminoester **4-Cl-21-tBu** (0.283 g, 0.497 mmol) was dissolved in dichloromethane (2 cm^3) and anisole (0.12 cm^3, 1.1 mmol) added. Trifluoroacetic acid (2 cm^3) was then added and the solution was stirred at room temperature under nitrogen for 24 hours. Volatiles were removed *in vacuo*, the residue redissolved in dichloromethane, the solvent removed again to give an oil. Ultrasonic agitation of the oil in ether precipitated a white solid that was collected by centrifugation. Dissolution of the solid in aqueous hydrochloric acid (~ 1 mol dm^{-3}) followed by a final round of rotary evaporation to afford the title compound (0.17 g, 0.37 mmol, 74%) as a glassy solid. t_R (H_2O:MeOH, UV detection); 8.55 min; δ_H (700 MHz, D_2O, pD≈8); 7.03 (dd, J = 8.5, 2.5 Hz, 2H, ***H8***), 6.83 (d, J = 2.5 Hz, 2H, ***H2***), 6.56 (d, J = 8.5 Hz, 2H, ***H8***), 3.47 (s, 4H, ***H4***), 3.02 (s, 4H, ***H9***), 2.53(s, 4H, ***H5***); δ_C(176 MHz, D_2O, pD≈8); 177.5 (***C10***), 156.0 (***C6***) , 129.3 (***C2***), 129.0 (***C8***), 124.0 (***C3***), 122.7 (***C1***), 117.6 (***C7***) , 57.3 (***C4***) , 55.8 (***C9***) , 49.0 (***C5***); δ_F(376 MHz, D_2O, pD≈8) No detectable signals; (ES-MS^+) 457.1 (100 %, $[M+H]^+$, M= $C_{20}H_{22}Cl_2N_2O_6$).

8.3.20. {[(5-Bromo-2- hydroxyphenyl) methyl] (2-{[(5-bromo-2- hydroxyphenyl) methyl](carboxymethyl) amino} ethyl)amino} acetic acid, 4-Br-HBED

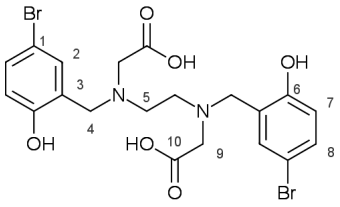

Protected amino acid **4-Br-21-tBu** (0.3 g, 0.46 mmol) was dissolved in a mixture of dichloromethane (3 cm^3) and anisole (0.11 cm^3). Trifluoroacetic acid (3 cm^3, 39.2 mmol) was then added at once and the mixture was stirred under nitrogen for 14 hours. Volatiles were then removed *in vacuo* and the solid residue was taken up in dichloromethane and agitated ultrasonically prior to removal of the solvent *in vacuo* (3x). This white residue was taken up in diethyl ether, agitated ultrasonically, centrifuged and the diethyl ether decanted off (3x). Aqueous hydrochloric acid (1 mol cm^{-3}, ca. 5 cm^3) was then used to partially dissolve the dried solid prior to its removal *in vacuo* followed by removal of residual water by drying the glassy white solid under high vacuum to afford the title

compound (0.19 g, 0.35 mmol, 76%). t_R (H_2O:MeOH, UV detection); 8.93 min; δ_H (700 MHz, D_2O, pD≈11) ; 7.20 (dd, J = 8.5, 2.5 Hz, 2H, ***H8***), 6.91 (d, J = 2.5 Hz, 2H, ***H2***), 6.58 (d, J = 8.5 Hz, 2H, ***H7***), 3.27 (s, 4H, ***H4***), 3.13 (s, 4H, ***H9***), 2.45 (s, 4H, ***H5***); δ_C(176 MHz, D_2O, pD≈11); 178.0 (***C10***) , 156.8 (***C6***) , 132.4 (***C8***) , 132.2 (***C2***) , 124.6 (***C3***) , 118.2 (***C7***) , 110.3 (***C1***) , 57.4 (***C4***) , 55.2 (***C9***) , 48.1 (***C5***); (ES-MS^-) 545.0 (100 %, $[M-H]^-$); HR-MS Found 544.9919, $C_{20}H_{23}N_2O_6Br_2$ $[M+H]^+$requires 544.9923.

8.3.21. {[(2-Hydroxy-5-methoxyphenyl)methyl](2-{(carboxymethyl)[(2-hydroxy-5-methoxyphenyl)methyl]amino}ethyl)amino}acetic acid, 4-MeO-HBED

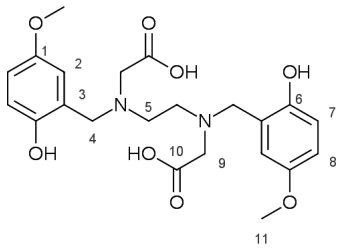

Aminoester **4-MeO-21-tBu** (0.09 g, 0.2 mmol) was dissolved in dichloromethane (2 cm^3) and 1,4-dimethoxybenzene (0.055 g, 0.40 mmol) added, followed by trifluoroacetic acid (2 cm^3) and the solution stirred at room temperature under nitrogen for 20 hours. Volatiles were then removed *in vacuo* and diethyl ether added to the residue that was then subject to ultrasonic agitation to precipitate a white solid that was isolated by centrifugation. The precipitate was redissolved in aqueous hydrochloric acid (ca. 10 cm^3, 1 mol dm^{-3}) using heating if necessary, and the solvent removed *in vacuo* to afford the title compound (0.07 g, 0.16 mmol, 80%) as an off-white to yellow solid. t_R (H_2O:MeCN, UV detection); 3.90 min; (700 MHz, D_2O, pD≈11) 6.66 (dd, J = 9.0, 3.0 Hz, 2H, ***H8***), 6.55 (d, J = 9.0 Hz, 2H, ***H7***), 6.44 (d, J = 3.0 Hz, 2H, ***H2***), 3.60 (s, 6H, ***H11***), 3.43 (s, 4H, ***H4***), 3.01 (s, 4H, ***H9***), 2.47 (s, 4H, ***H5***); (176 MHz, D_2O, pD≈11) 178.6 (***C10***), 151.6 (***C1***), 150.6 (***C6***), 123.8 (***C3***), 116.4 (***C7***), 115.1 (***C2***), 114.5 (***C8***), 57.9 (***C9***), 56.2 (***C4***), 55.9 (***C11***), 49.3 (***C5***); δ_F(376 MHz, D_2O, pD≈11) No detectable signals; (ES+MS^+) 449.1 (100 %, $[M+H]^+$); HR-MS Found 449.1922 , $C_{22}H_{29}N_2O_8$ $[M+H]^+$requires 449.1924.

8.3.22. {[(2-Hydroxy-5-octylphenyl)methyl](2-{(carboxymethyl)[(2-hydroxy-5-octylphenyl) methyl]amino}ethyl)amino}acetic acid, 4-Oct-HBED

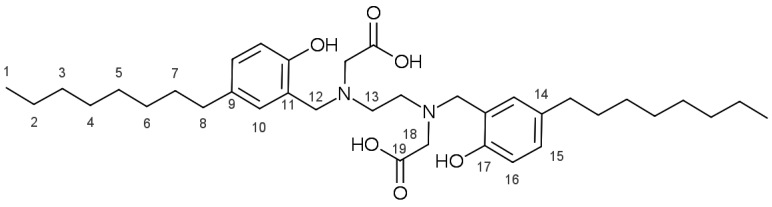

Aminoester **4-Oct-21-tBu** (0.25g, 0.3 mmol) was dissolved in dichloromethane (2 cm^3) and anisole (0.09 cm^3, 0.8 mmol) added. Trifluoroacetic acid (2 cm^3) was added to the reaction mixture, which was allowed to stir at room temperature under nitrogen for 15 hours. Volatiles were then removed *in vacuo* and the residue reprecipitated from diethyl ether and the precipitate collected via centrifugation. The resulting solid was then boiled in concentrated hydrochloric acid (ca. 5 cm^3), and the solvent removed *in vacuo* to give the title compound (0.15 g, 0.25 mmol, 71%) as a waxy, off-white solid. δ_H(700 MHz, DMSO-d^6) 7.01 (d, J = 2.0 Hz, 2H, ***H10***), 6.99 (dd, J = 8.0, 2.0 Hz, 2H, ***H15***), 6.79 (d, J = 8.0 Hz, 2H, ***H16***), 4.00 (s, 4H, ***H18***), 3.63 (s, 4H, ***H12***), 3.19 (s, 4H, ***H13***), 2.42 (t, J = 7.5 Hz, 4H, ***H8***), 1.48 (q, J = 7.5 Hz, 4H, ***H7***), 1.23 (m, 10H, ***H6***, ***H5***, ***H4***, ***H3***, ***H2***), 0.84 (t, 6H, ***H1***); δ_C(176 MHz, DMSO-d^6) 170.1 (***C19***), 154.1 (***C17***), 132.7 (***C9***), 131.5 (***C11***) , 129.6 (***C15***), 115.2 (***C16***), 52.6 (***C18***), 52.0 (***C12***), 49.38 (***C13***), 34.10 (***C8***), 31.2 (***C7***), 31.0 (***C6***), 28.7 (***C5***), 28.6 (***C4***), 28.5 (***C3***), 22.0 (***C2***), 13.8 (***C1***); The poor solubility of **4-Oct-HBED** in anything other than DMSO prevented solution phase mass spectrometric characterisation.

8.3.23. Ethylene hydroxyphenyl acetic acid derivatives:[212]

General method. A suspension of glyoxylic acid hydrate in water (4 mol dm^{-3}) raised to pH≈9 with sodium carbonate (ca. 0.5 equivalents) was contacted with a methanolic (3 mol dm^{-3}) solution of the para-substituted phenol (1 equivalent wrt glyoxylic acid). Following a short stirring period, a methanolic solution of ethylene diamine (5 mol dm^{-3}, 0.5 equivalents wrt glyoxylic acid) was added at once and the cloudy solution was refluxed for 6 hours during which time a loss of turbidity was observed. Once cooled to room temperature, the reaction mixture was diluted into water (ca. 5-6 x total reaction mixture volume) and the nonpolar organic material removed by washing the aqueous solution with diethyl ether (2x ca. 10 cm^3). Ethanol was added to the aqueous layer until an increase in turbidity was observed in the aqueous layer, and the solution heated until translucent. Concentrated hydrochloric acid was subsequently used to precipitate the product by lowering the pH to 3-4. The hot solution was then left to cool and stand for at least an hour. The title compounds were then collected by filtration and washed first with hot aqueous ethanol (50:50 ethanol:water v/v) and then hot ethanol prior to drying under high vacuum.

(5-Bromo-2-hydroxyphenyl)(2-{[(5-bromo-2-hydroxyphenyl)carboxymethyl]amino}ethylamino) acetic acid , (4-Br-EHPG). Glyoxylic acid hydrate (0.92 g, 9.99 mmol), sodium carbonate (0.53 g, 5.03 mmol), p-bromophenol (0.97 g, 10.1 mmol), ethylene diamine (335μL, 5.01 mmol). Yellow-brown solid (0.22 g, 0.41 mmol, 8 %). ν_{max}/cm^{-1}(ATR) 3092 (broad, carboxylic acid, phenol O-H st), 1644 (carboxylic acid C=O st), 1272 (phenol C-O st), 816 (aromatic C-Br st); δ_H (400 MHz, D_2O) 7.11 – 7.00 (m, 8H), 6.49 – 6.39 (m, 4H), 4.37 (s, 2H), 4.31 (s, 2H), 2.59 (m, 4H), 2.50 (m, 4H); δ_C(101 MHz, D_2O, carbonate δ=166*) 176.8 , 160.4 , 130.4 , 129.7 , 126.4 , 119.1 , 104.9 , 60.9 , 43.5; (ES-MS$^-$) 514.6 (100 %, based on 2x ^{79}Br [M-H]$^-$); HR-MS Found 516.9608 , $C_{18}H_{19}N_2O_6{}^{79}Br_2$ [M+H]$^+$requires 516.9610.

(2-{[Carboxy(2-hydroxytolyl)methyl]amino}ethylamino)(2-hydroxytolyl)acetic acid, (4-Me-EHPG). Glyoxylic acid hydrate (2.55 g, 27.7 mmol), p-cresol (2.99 g, 27.6 mmol), sodium carbonate (1.5 g, 14.2 mmol) ethylene diamine (0.92 cm^3, 13.6 mmol). Buff-coloured solid (0.93 g, 2.39 mmol, 18%); δ_H (400 MHz, D_2O, pD$\approx$14) 6.89 – 6.75 (m, 8H), 6.65 – 6.43 (m, 4H), 4.23 (s, 2H), 4.13 (s, 2H), 2.60 (m, 4H), 2.49 (m, 4H), 2.05 (s, 6H), 2.05 (s, 6H); δ_C(101 MHz, D_2O, carbonate δ=166) 176.6 , 153.9 , 128.2 , 128.0 , 126.4 , 122.6 , 115.5 , 62.4 , 43.4 , 18.0; (ES-MS$^-$) 387 (100 %, [M-H]$^-$, M= $C_{20}H_{24}N_2O_6$).

*The close proximity of signals corresponding to *meso-* and *rac-* isomers precludes unambiguous identification of each carbon signal, hence only peak per "pair" of peaks is reported.

8.4. Synthesis, and growth inhibition studies of commonly used aminocarboxylate ligands and some variants

8.4.1. 1,4-Dibenzyl-6-methyl-6-nitro-1,4-diazepane, 22[239]

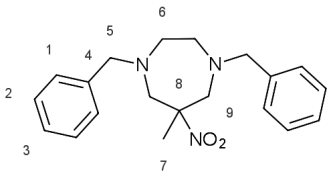

Paraformaldehyde (2.1 g, 83.5 mmol), nitroethane (1.79 ml, 25.1 mmol) and N,N'-dibenzylethylene diamine diacetate (9.11 g, 25.3 mmol) were added to ethanol (40 cm^3) and refluxed for 3 hours. The solvent was removed *in vacuo*, and the black viscous oil was partitioned between saturated potassium carbonate solution and dichloromethane. The organic layer was extracted, dried with magnesium sulphate, and concentrated *in vacuo* to afford a light brown oil, which was subjected to column chromatography (method i, silica, compound eluted in dichloromethane) to give a light yellow oil (6.0 g, 71%) that solidified to a waxy material after standing for a few weeks. δ_H (700 MHz, $CDCl_3$) 7.36 – 7.13 (m, 10H, ***H1, H2, H3***), 3.72 (d, J = 13.2 Hz, 2H, ***H5***), 3.59 (d, J = 13.2 Hz, 2H, ***H5***), 3.54 (d, J = 14.1 Hz, 2H, ***H9***), 2.90 (d, J = 14.1 Hz, 2H, ***H9***), 2.57 (ddd, J = 11.0, 8.2, 6.6 Hz, 2H, ***H6***), 2.51 (ddd, J = 12.0, 8.2, 6.6 Hz, 2H, ***H6***), 1.28 (s, 3H, ***H7***); δ_C(176 MHz, $CDCl_3$) 139 (***C4***) , 129 , 128 , 127 (***C1, C2, C3***) , 92 (***C8***) , 64 (***C9*** or ***C5***) , 63.6 (***C9*** or ***C5***) , 58 (***C6***) , 25 (***C7***) ; GC-MS (EI^+) 293 ($M\text{-}NO_2^{+\bullet}$, M= $C_{20}H_{25}N_3O_2$), 252 ($M\text{-}^iPr\text{-}NO_2^{+\bullet}$), 91 ($\text{-}PhCH^{+\bullet}$).

8.4.2. 6-Methyl-1,4-diazepin-6-ylamine*, AAZ

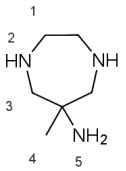

In a two-neck round bottom flask equipped with a condenser, **22** (1.25 g, 3.68 mmol) was dissolved in ethanol (ca. 100 cm^3) and ammonium formate (4.64 g, 77.7 mmol) was added to the solution which was left to stir under nitrogen until the majority of the solid dissolved. The vessel was then evacuated and back-filled with nitrogen (3x cycles) prior to the addition of 5% palladium on charcoal (0.6 g, 0.28 mmol wrt Pd). After this addition, the vessel was evacuated and back-filled with nitrogen a further three times and the mixture refluxed until the loss of benzyl groups was observable by ^1H NMR (2 hours). Following cooling to room temperature, the black mixture was filtered thorough Celite®, the

*Due to the reported reactivity of this compound,[337] thorough characterisation was not attempted. Instead, a full characterisation of the final aminocarboxylic acid is offered as evidence of structure.

solvent removed *in vacuo* to give a yellow residue which was redissolved in dichloromethane to give a white precipitate that was also filtered through Celite®. Removal of the solvent *in vacuo* gave the title compound as a yellow oil (0.41 g, 3.17 mmol, 86%). Alternatively, hydrogen gas in a baloon could be employed in the manner described in ***Section 8.2.17***. δ_H(400 MHz, $CDCl_3$) 2.91 (m, 2H, *H**1***), 2.81 (m, 2H, *H**1***), 2.68 (d, J = 13.5 Hz, 2H, *H**3***), 2.61 (d, J = 13.5 Hz, 2H *H**3***), 1.97 (s, 4H, *H**2**, H**5***), 1.00 (s, 3H, *H**4***); (ES-MS$^+$) 130.0 (100 %, $[M+H]^+$, M= $C_6H_{15}N_3$).

8.4.3. Tert-Butyl {(tert-butoxycarbonylmethyl)[6-methyl-1,4-bis(tert-butoxycarbonylmethyl) -1,4-diazepin-6-yl]amino}acetate, AAZTA-tBu

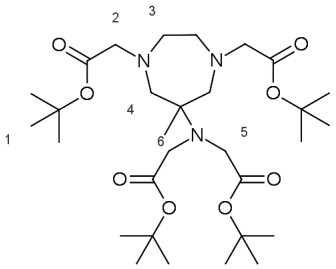

AAZ, (0.41 g, 3.17 mmol) was dissolved in acetonitrile (25 cm^3) and potassium carbonate (2.70 g, 20.0 mmol) was added. t-Butyl bromoacetate (2.08 cm^3, 16.1 mmol) in acetonitrile (30 cm^3) was then added dropwise into the mixture at room temperature. Once the addition was complete the mixture was heated at 60^{o}C under nitrogen for 21 hours, when TLC (hexanes:ethyl acetate:triethylamine 89:10:1 v/v) showed consumption of the starting material. Solids were removed by filtration and the filtrate was purified via column chromatography (method i, column diameter= 2.5 cm, length=25 cm, compound eluted in 20:79:1 v/v ethyl acetate:hexanes:triethylamine) to give the title compound as a yellow-tinged oil (1.07 g, 1.83 mmol, 58%). δ_H(400 MHz, $CDCl_3$) 3.60 (s, 4H, *H**5***), 3.19 (s, 4H, *H**2***), 2.95 (d, J = 14.1 Hz, 2H, *H**4***), 2.69 (m, 2H, *H**3***), 2.59 (m, 2H, *H**3***), 2.54 (d, J = 14.1 Hz, 2H, *H**4***), 1.36 (m, 18H, *H**1***), 1.01 (s, 3H, *H**6***); (ES-MS$^+$) 586.2 (100 %, $[M+H]^+$, M= $C_{30}H_{55}N_3O_8$).

8.4.4. {(Carboxymethyl)[1,4-bis(carboxymethyl)-6-methyl-1,4-diazepin-6-yl]amino}acetic acid, AAZTA, trifluoroacetate salt

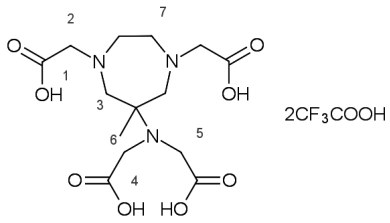

AAZTA-tBu (1.07 g, 1.83 mmol) was dissolved in trifluoroacetic acid (1.4 cm^3) and stirred under nitrogen for 24 hours. The acid was then removed *in vacuo* and the solid residue suspended in dichloromethane, agitated via ultrasound and the solvent removed *in vacuo* (3x). Diethyl ether was used to suspend the increasingly white solid which was agitated in the same way prior to final solvent removal *in vacuo* and drying under high vacuum to afford the title compound (0.72 g, 1.22 mmol, 67%) as a white solid. *Elem. Anal. Found (Service ii):* C, 36.8; H, 4.46; N, 7.28; ($C_{18}H_{25}F_6N_3O_{12}$ requires C, 36.9; H, 4.28; N, 7.13); δ_H (700 MHz, D_2O δ=4.79 ppm) 3.08 (m, 8H, ***H5, H2***), 2.73 (m, 4H, ***H7***), 2.54 (m, 4H, ***H3***), 0.83 (s, 3H, ***H6***); δ_C(176 MHz, D_2O $Na_2CO_3$$\delta$=166) 179 , 178 (***C1 or C4)*** , 63 , 62 (***C2 or C5***) , 60 , 56 , 54 (ring carbons) , 15 (***C6***); (ES-MS^+) 362.4 (100 %, $[M\text{-}CF_3COOH+H]^+$); HR-MS Found 362.1589 , $C_{14}H_{24}N_3O_8$ $[M\text{-}CF_3COOH+H]^+$requires 362.1563.

8.4.5. tert-Butyl [4,10-bis(tert-butoxycarbonylmethyl)-1,4,7,10-tetraza-1-cyclododecyl]acetate hydrobromide, DO3A-tBu hydrobromide salt[240]

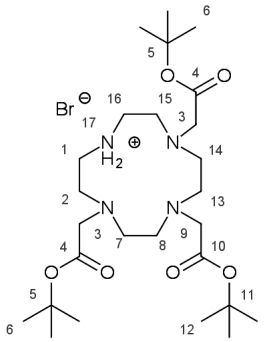

Cyclen (0.50 g, 2.9 mmol) was dissolved in acetonitrile (19 cm^3, dried over molecular sieves) and t-butyl bromoacetate (1.29 cm^3, 8.80 mmol) was added at once prior to the suspension of sodium bicarbonate (0.75 g, 8.9 mmol) and a catalytic amount of potassium iodide (ca. 25 mg) in the solution. A small amount of 4Å molecular sieves (ca. 0.5 g) were then added, and the reaction mixture stirred for 16 hours under nitrogen. Solids were then removed via filtration and washed with acetonitrile, and the filtrate concentrated *in vacuo.* The concentrated residue was then partitioned between water and dichloromethane and the organic layer extracted (3x 50 cm^3). The combined organic extracts

were dried over magnesium sulphate and the solvent removed *in vacuo* to give the crude residue which was recrystallised twice from toluene to give the title product (0.51 g, 0.86 mmol, 30%) as an off-white crystalline solid. δ_H (400 MHz, $CDCl_3$) 10.02 (s, 2H, ***H17***), 3.37 (s, 4H, ***H3***), 3.28 (s, 2H, ***H9***), 3.09 (t, 4H, ***H1, H16***), 2.90 (m, 8H, ***H7***, ***H8***, ***H13***, ***H14***), 1.45 (s, 18H, ***H6***), 1.45 (s, 9H, ***H12***); δ_C(101 MHz, $CDCl_3$) 170.5 , 169.6 (***C4***, ***C10***), 82.0, 81.8 (***C5, C11***), 58.2 , 51.4, 49.2, 48.4, 47.5 (***C1, C2, C3***, ***C7***, C**8**, ***C9, C13, C14, C15, C16***), 28.3, 28.2 (***C6***, ***C12***); (ES-MS$^+$) 515.2 (100 %, $[M+H-HBr]^+$, M= $C_{26}H_{50}N_4O_6Br$)

8.4.6. [4,10-Bis(carboxymethyl)-1,4,7,10-tetraza-1-cyclododecyl]acetic acid, DO3A*

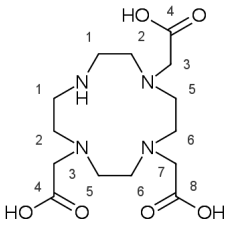

DO3A-tBu hydrobromide (0.2 g, 0.34 mmol) was dissolved in dichloromethane (2 cm^3) and anisole (0.12 cm^3, 1.1 mmol) added to the solution. To this solution, trifluoroacetic acid (2 cm^3) was added at once, and the reaction mixture allowed to stir at room temperature overnight. Volatiles were then removed *in vacuo*, redissolved in dichloromethane which was also removed *in vacuo*. A white solid was precipitated from the residue by the addition of diethyl ether, and this solid was collected via centrifugation. The solid was then dissolved in aqueous hydrochloric acid (1 mol dm^{-3}, ca. 10 cm^3), and then loaded onto a DOWEX 1X8 anion exchange resin (chloride form). The title compound was isolated after elution from the resin using a further equivalent of hydrochloric acid (1 mol dm^{-3}, ca. 100 cm^3) as an extremely hygroscopic off-white solid (0.15 g)after removal of the solvent *in vacuo.* δ_H (400 MHz, D_2O, pD≈12) 3.33 (m, 2H, ***H7***), 3.23 (m, 4H, ***H3***), 2.83-2.93 (m, 16H, ***H1***, ***H2***, ***H5***, ***H6***).

8.4.7. o-({2-[2-(2-{[(o-Hydroxyphenyl)methyl]-amino}ethoxy)-ethoxy]ethylamino}-methyl)phenol,

23

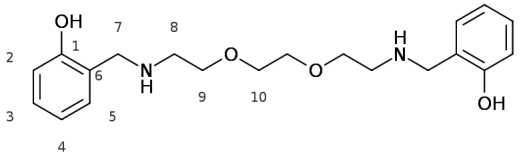

*A ^{13}C NMR was not collected due to insufficient material. Quantitative ^1H NMR showed that no organic impurities were present in the sample used for biological study.

Method 1: Indirect reductive amination using sodium borohydride. A solution of salicylaldehyde (0.73 cm^3, 6.85 mmol) in ethanol (17 cm^3, dried over molecular sieves) was stirred under nitrogen while 2-[2-(2-Aminoethoxy)ethoxy]ethanamine (0.5 cm^3, 3.41 mmol) was added dropwise. The resulting yellow mixture was allowed to stir for a further 3 hours prior to the portionwise addition of sodium borohydride (0.51 g, 13.5 mmol) over 20 minutes. Following the addition a loss of colour was noted, and stirring at room temperature was maintained overnight. Removal of the solvent *in vacuo* and subsequent partitioning between aqueous sodium acetate (2x, pH 9-10), followed by washing of the evaporated organic layer (dissolved in chloroform) with brine led to the isolation of a faint orange oil (0.25 g, 0.69 mmol, 20%) upon drying the organic layer with magnesium sulphate and removal of the solvent *in vacuo*. ν_{max}/cm^{-1}(ATR) 3304 (N-H st), 2862 (br phenol O-H st), 1255 (C-O st), 1103 (C-O st); δ_H (700 MHz, $CDCl_3$) 7.15 (dd, J = 8.0, 0.5 Hz, 2H, ***H3***), 6.96 (d, J = 7.5 Hz, 2H, ***H2***), 6.82 (d, J = 8.0 Hz, 2H, ***H5***), 6.77 (dd, J = 7.5, 1.0 Hz, 2H, ***H4***), 3.99 (s, 4H, ***H7***), 3.61 (m, J = 5.0 Hz, 8H, ***H9, H10***), 2.82 (t, J = 5.0 Hz, 4H, ***H8***); δ_C(176 MHz, $CDCl_3$) 158.6 (***C1***) , 129.0 (***C2***) , 128.7 (***C3***) , 122.7 (***C6***) , 119.3 (***C4***) , 116.7 (***C5***) , 70.7 (***C9***) , 70.0 (***C8***) , 52.6 (***C7***) , 48.1 (***C8***); (ES-MS^+) 361.3 (100 %, $[M+H]^+$); HR-MS Found 361.2122, $C_{20}H_{29}N_2O_4$ $[M+H]^+$requires 361.2127.

Method 2: Direct reductive amination using sodium acetoxyborohydride. Salicylaldehyde (0.8 cm^3, 7.50 mmol) was dissolved in 1,2-dichloroethane (16 cm^3) and 2-[2-(2-Aminoethoxy) ethoxy] ethanamine (0.5 cm^3, 3.41 mmol) was added to afford a yellow solution to which was added sodium triacetoxyborohydride (2.9 g, 13.7 mmol), leading to discolouration of the reaction mixture. Reaction progress was monitored by TLC (silica, ethyl acetate) and saturated aqueous potassium carbonate was used to quench the reaction mixture upon completion, followed by dilution of the biphasic mixture with dichloromethane. The organic layer was then extracted, dried with magnesium sulphate and the solvent removed *in vacuo* giving a yellow oil (1.23 g) that was used without further purification.*

8.4.8. tert-Butyl-{[(o-hydroxyphenyl)-methyl]-{2-[2-(2-{[-(o-hydroxyphenyl)methyl]-(tert-butoxy-carbonylmethyl)-amino}ethoxy)-ethoxy]ethyl}-amino}acetate, NOON-tBu

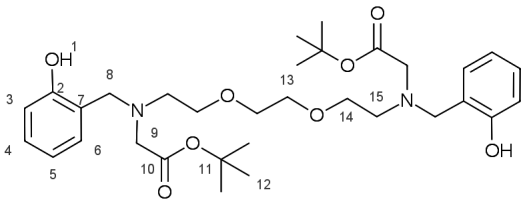

Aminophenol **23** (0.71 g, 2.0 mmol) was dissolved in dry acetonitrile (4 cm^3) and sodium sulphate (ca. 0.2 g), potassium biocarbonate (0.311 g, 3.11 mmol) were suspended in the solution. t-butyl

*While the NMR data of this product shows visible impurities, subsequent alkylation steps followed by column chromatography or trituration of the resulting product, lead to their facile removal.

bromoacetate (0.25 cm^3, 1.70 mmol) was then added dropwise to the stirred mixture that was heated to 60°C for 19 hours under nitrogen once addition was complete. After cooling to room temperature, the reaction mixture was filtered through Celite®and the solvent from the filtrate was removed *in vacuo* to afford the title compound (0.52 g, 0.88 mmol, 44%).

In an earlier variant of this procedure, **23** (0.28 g, 0.78 mmol) was reacted and worked up in an analogous manner, but **NOON-tBu** was isolated by column chromatography (method ii, ethyl acetate:hexanes 0:100→60:40, compound eluted in ca. 30:70 ethyl acetate:hexanes) to afford the product as a colourless oil that rapidly solidified to a white solid (0.16 g, 0.27 mmol, 35%). Slow evaporation of a sample of this material from warm acetone gave samples suitable for x-ray crystallography. mp 97-98°C; δ_H (700 MHz, $CDCl_3$) 9.99 (s, 2H, ***H1***), 7.16 (ddd, 2H, ***H4***), 6.96 (dd, 2H, ***H6***), 6.83 (dd, 2H, ***H3***), 6.76 (m, 2H, ***H5***), 3.90 (s, 4H, ***H8***), 3.59 (t, J = 5.5 Hz, 4H, ***H14***), 3.57 (s, 4H, ***H13***), 3.36 (s, 4H, ***H9***), 2.85 (t, J = 5.5 Hz, 4H, ***H15***), 1.46 (s, 18H, ***H12***); δ_C(176 MHz, $CDCl_3$) 170.0 (***C10***) , 157.7 (***C2***) , 129.0 (***C6***) , 128.9 (***C4***) , 121.9 (***C7***) , 119.0 (***C5***) , 116.3 (***C3***) , 81.6 (***C11***) , 70.3 (***C13***) , 68.9 (***C14***) , 57.4 (***C8***) , 55.5 (***C9***) , 52.4 (***C6***) , 28.1 (***C12***); (ES-MS^+) 589.4 (100 %, $[M+H]^+$); HR-MS Found 589.3495 , $C_{32}H_{49}N_2O_8$ $[M+H]^+$requires 589.3489; X-ray crystallography: $C_{32}H_{48}N_2O_8$, M_r=588.72, orthorhombic ($Pca2_1$); *a* = 10.5409(5) Å, *b* = 10.0117(5) Å, *c* = 29.6434(14) ; crystal size = 0.28 × 0.16 × 0.05 mm^3; T= 120K.

8.4.9. {[(o-Oxyphenyl)methyl]{2-[2-(2-{(oxycarbonylmethyl)[(o-oxyphenyl)methyl] amino}ethoxy)ethoxy]ethyl}amino}acetate, NOON

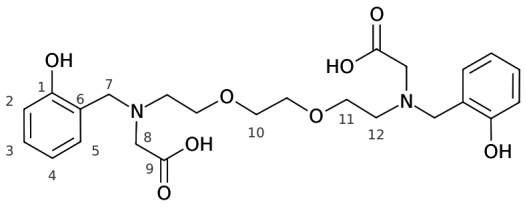

NOON-tBu (0.4 g, 0.68 mmol) was dissolved in dichloromethane (2.5 cm^3), and anisole (0.15 g, 1.38 mmol) was added prior to the addition of trifluoroacetic acid (2.5 cm^3). The resulting mixture was stirred under nitrogen for seventeen hours and volatiles were then removed *in vacuo*. The solid residue was then redissolved in dichloromethane and the solvent evaporated. Diethyl ether was then added to the residue to precipitate a solid which was collected via centrifugation, dissolved in aqueous hydrochloric acid (1 mol dm^{-3}, ca. 10 cm^3) and the solvent removed in vacuo to afford a buff, hygroscopic solid (0.25 g, 0.53 mmol, 77 %). Slow evaporation of a neutral solution of this material gave single crystals suitable for X-ray crystallography; t_R (H_2O:MeOH, UV detection); 5.24 min;δ_H (700 MHz, D_2O, pD≈14) 7.22 (ddd, 2H, ***H3***), 7.15 (dd, 2H, ***H2***), 6.83 (td, 2H, ***H4***), 6.80 (dd, 2H, ***H5***), 3.83 (s, 4H, ***H7***), 3.62 (t, J = 6.0 Hz, 4H, ***H11***), 3.53 (s, 4H, ***H10***), 3.26 (s, 4H, ***H8***), 2.79 (t, J = 5.7 Hz, 4H, ***H12***); δ_C(176 MHz, D_2O, pD≈14) 178.2 (***C9***) , 157.9 (***C1***) , 130.1 (***C2***) , 129.1

(***C3***) , 123.2 (***C1***) , 118.7 (***C4***) , 116.3 (***C5***) , 69.2 (***C10***) , 67.6 (***C11***) , 57.4 (***C8***) , 56.2 (***C7***) , 52.0 (***C12***); (ES-MS$^+$) 477.2 (100 %, $[M+5H]^+$); HR-MS Found 477.2231 , $C_{24}H_{33}N_2O_8$ $[M+5H]^+$requires 477.2237; X-ray crystallography: $C_{24}H_{32}N_2O_8$ x 5.33 H_2O, M_r=572.62, trigonal (P-3); *a* = 18.8263(5) Å, *b* = 18.8263(5) Å, *c* = 7.2192(2) ; crystal size = 0.28 × 0.03 × 0.03 mm^3; T= 120K.

8.5. Towards new ligand structures

8.5.1. 2-{[(o-Hydroxyphenyl)methyl]amino}glutaric acid[286], 24

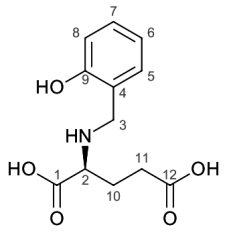

l-Glutamic acid (1.0 g, 6.83 mmol) was suspended in a mixture of water and methanol (50:50 v/v, 40 cm^3) and dissolved via the addition of sodium hydroxide (0.5 g, 12.5 mmol) to afford a homogeneous solution. Salicylaldehyde (0.72 cm^3, 6.79 mmol) was then added to the solution to give a yellow precipitate, which was left to stir for 30 minutes prior to immersion of the reaction vessel in an ice bath followed by the portionwise addition of sodium borohydride (0.5 g, 13.2 mmol) over a further 30 minutes. After 1 hour of stirring, a loss of colour was observed and the reaction mixture was acidified to pH 6 using acetic acid and concentrated *in vacuo*. Trituration using an ultrasonic bath of the residue in ethanol (125 cm^3), followed by collection of the resulting white solid via filtration and washing with diethyl ether (125 cm^3), led to the isolation of the title compound after the solid was dried under high vacuum (0.99 g, 3.91 mmol, 58 %). δ_H (400 MHz, D_2O) 7.40 – 6.70 (m, 4H, ***H5***, ***H6***, ***H7***, ***H8***), 4.06 (d, J = 13.5 Hz, 1H, ***H3***), 3.90 (d, J = 13.5 Hz, 1H, ***H3***), 3.34 (t, 1H, ***H2***), 2.24 , 1.96 (m, 4H, ***H10***, ***H11***); δ_C(101 MHz, D_2O) 181.8 , 177.5 (***C1***, ***C12***) , 159.8 (***C9***) , 130.3 , 130.0 , 121.5 , 117.7 , 117.2 (***C4***, ***C5***, ***C6***, ***C7***, ***C8***) , 61.9 (***C2***) , 48 , 34 , 28 (***C3***, ***C10***, ***C11***); (ES-MS^-) 252.0 (100 %, $[M\text{-}H]^-$, M= $C_{12}H_{15}NO_5$).

8.5.2. Diisopropyl glutamate, hydrochloride salt

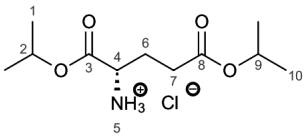

l-Glutamic acid (3.18 g, 21.6 mmol) was suspended in isopropanol (130 cm^3) and thionyl chloride (10 cm^3, 0.14 mol) was added to the stirring mixture dropwise. Once addition was complete, the mixture was stirred under nitrogen for 19 hours and then heated to 50°C for fifteen hours. After removal of solvent *in vacuo* and trituration with isopropanol (ca. 125 cm^3) and diethyl ether (3 x ca. 125 cm^3) a colourless oil was isolated which became a white, waxy solid (4.8 g, 17.9 mmol, 83%) upon standing in a freezer for a week. *Elem. Anal. Found (Service ii):* C, 49.34 ; H, 8.28 ; N, 5.23 ; ($C_{11}H_{22}ClNO_4$requires C, 49.26; H, 8.23; N, 5.19 %); δ_H(700 MHz, $CDCl_3$) 8.82 (s, 3H, ***H5***), 5.10

(m, 1H, ***H9***), 4.98 (m, 1H, ***H2***), 4.20 (m, 1H, ***H4***), 2.60 (m, 2H, ***H7***), 2.36 (m, 2H, ***H7***), 1.28 (m, 6H, ***H10***), 1.21 (d, 6H, ***H1***); δ_C(176 MHz, $CDCl_3$) 172 (***C8***) , 168 (***C3***) , 71 (***C9***) , 68 (***C2***) , 53 (***C4***) , 30 (***C7***) , 25 (***C6***) , 22 (***C1***), 21.64 (***C10***); (ES-MS$^+$) 232.0 (100 %, $[M+H]^+$); HR-MS Found 232.1556 , $C_{11}H_{22}NO_4$ $[M+H]^+$ requires 232.1549.

8.5.3. Isopropyl 1-[(o-hydroxyphenyl)methyl]-5-oxo-2-pyrrolidinecarboxylate, 25

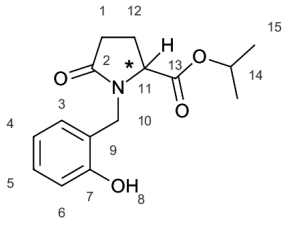

Diisopropyl glutamate hydrochloride (0.61 g, 2.28 mmol) and salicylaldehyde (0.28 g, 2.28 mmol) were dissolved in methanol (6 cm^3) and stirred under nitrogen at 40^{o}C for 1 hour, and then at room temperature overnight. Then, sodium borohydride (0.41 g, 10.9 mmol) was then added portionwise and the mixture stirred at room temperature for 6 hours. Solids were then filtered off and the filtrate concentrated *in vacuo* prior to re-dissolution in dichloromethane and the removal of precipitates via filtration. The filtrate was then washed with aqueous hydrochloric acid, extracted, dried using magnesium sulphate and the solvent removed *in vacuo* to provide an oil that was purified via column chromatography (method ii, ethyl acetate:hexanes compound eluted in 30:70 v/v ethyl acetate:hexanes) to afford the title compound (87 mg, 0.31 mmol, 11%) as a pink oil. ν_{max}/cm^{-1}(ATR) 3182 (br, phenol O-H st), 1735 (ester C=O st), 1660 (amide C=O st), 1103 (C-O st); (700 MHz, $CDCl_3$) 8.79 (s, 1H, ***H8***), 7.22 (m, 1H, ***H5***), 7.02 (m, 1H, ***H3***), 6.94 (m, 1H, ***H6***), 6.79 (m, 1H, ***H4***), 5.00 (m, J = 6.3 Hz, 1H, ***H14***), 4.68 (d, J = 15.2 Hz, 1H, ***H10***), 4.17 (dd, J = 9.3, 3.3 Hz, 1H, ***H11***), 4.10 (d, J = 15.1 Hz, 1H, ***H10***), 2.60 (m, 1H, ***H1***), 2.40 (m, 1H, ***H1***), 2.32 (m, 1H, ***H12***), 2.08 (m, 1H, ***H12***), 1.28 (d, J = 6.3 Hz, 3H, ***H15***), 1.16 (d, J = 6.3 Hz, 3H, ***H15***); δ_C(176 MHz, $CDCl_3$) 178 (***C2***) , 171 (***C13***) , 156 (***C7***) , 131 (***C3***) , 130.5 (***C5***) , 121 (***C9***) , 120 (***C4***) , 118 (***C6***) , 70 (***C14***) , 61 (***C11***) , 43 (***C10***) , 29 (***C1***) , 23 (***C12***) , 22 (***C15***) , 21.6 (***C15***); (ES-MS$^+$) 278.0 (100 %, $[M+H]^+$); HR-MS Found 278.1412, $C_{15}H_{20}NO_4$ $[M+H]^+$requires 278.1392.

8.5.4. Ethyl (2S)-1-[(o-hydroxyphenyl)methyl]-5-oxo-2-pyrrolidinecarboxylate, 26

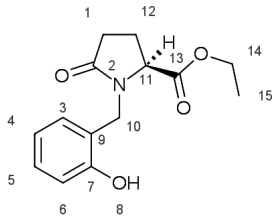

Amino acid **24** (0.42 g, 1.66 mmol) was suspended in ethanol (7 cm^3) and thionyl chloride (0.6 cm^3, 8.27 mmol) was added dropwise. The suspension was then refluxed for 48 hours under argon, cooled and then filtered. the filtrate was then concentrated *in vacuo* to give a white solid that was triturated with ethanol using ultrasound (3 x), and then diethyl ether (3 x), the solvent being removed *in vacuo* between cycles. Dichloromethane was used to suspend the resulting solid which was filtered through Celite® and the solvent removed from the pink filtrate to afford the title compound (0.27 g, 1.03 mmol, 62 %) as a pink crystalline solid. Single crystals suitable for structural and stereochemical determination via X-ray crystallography were grown from this solid via slow evaporation from acetone. mp 111-112°C; ν_{max}/cm^{-1}(ATR) 3069 (br, phenol O-H st), 2978 (sp^3C-H st), 1739 (ester C=O st), 1660 (amide C=O st), 1203 (C-O st); δ_H (600 MHz, $CDCl_3$) 8.76 (s, 1H, ***H8***), 7.22 (td, J = 7.7, 1.6 Hz, 1H, ***H5***), 7.02 (dd, J = 7.5, 1.6 Hz, 1H, ***H3***), 6.94 (d, J = 7.7 Hz, 1H, ***H6***), 6.79 (td, J = 7.5, 1.6 Hz, 1H, ***H4***), 4.64 (d, J = 15.1 Hz, 1H, ***H10***), 4.21 (m, 1H, ***H13***), 4.18 – 4.11 (m, 2H, ***H13, H14***), 4.06 (dq, J = 10.8, 7.1 Hz, 1H, ***H14***), 2.60 (m, 1H, ***H1***), 2.41 (m, 1H, ***H1***), 2.34 (m, 1H, ***H12***), 2.11 (m, 1H, ***H12***), 1.22 (t, J = 7.1 Hz, 3H, ***H15***); δ_C(151 MHz, $CDCl_3$) 178 (***C2***) , 171 (***C13***) , 156 (***C7***) , 131 (***C3***) , 130 (***C5***) , 121 (***C9***) , 118 (***C6***) , 62 (***C14***) , 60 (***C11***) , 43 (***C10***) , 29 (***C1***) , 23 (***C12***), 14 (***C15***); (ES-MS^+) 264.0 (100 %, $[M+H]^+$); HR-MS Found 264.1243 , $C_{14}H_{18}NO_4$ $[M+H]^+$requires 264.1236 ; X-ray crystallography: $C_{14}H_{17}NO_4$, M_r=263.29, triclinic (P1); *a* = 6.8353(3) Å, *b* = 7.5669(3) Å, *c* = 7.7552(3) ; crystal size = 0.28 × 0.21 × 0.14 mm^3; T= 120K.

8.5.5. Dimethyl 2-bromoglutarate[284], 27

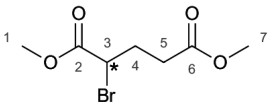

l-Glutamic acid (7.94 g, 54.0 mmol) was dissolved in aqueous hydrobromic acid (2 mol dm^{-3}, 48 cm^3) and potassium bromide (26.0 g, 218 mmol) was added. Sodium nitrite (8.10 g, 117 mmol) was then added portionwise to the ice-cooled solution over a period of 2 hours leading to the evolution of an orange gaseous product. Once addition was complete, the solution was acidified with concentrated sulphuric acid and the organic-soluble material was extracted with diethyl ether (3x), dried over magnesium sulphate and concentrated *in vacuo* to afford 4.15 g of a yellow oil (2-bromoglutaric

acid, 19.6 mmol 36% based on crude yield). Methanol (70 cm^3) was used to dissolve this oil and concentrated sulphuric acid (0.7 cm^3) was added to the solution that was refluxed under nitrogen for 75 minutes. After cooling to room temperature the solvent was removed *in vacuo* and the residue partitioned between saturated sodium carbonate and diethyl ether. The organic layer was extracted, dried over magnesium sulphate concentrated *in vacuo* and then purified via column chromagraphy (method i, silica, ethyl acetate:hexanes 0:100→20:80 compound eluted in ca. 10:90 v/v ethyl acetate:hexanes) to give the title compound (2.79g, 11.7 mmol, 60% based on 2-bromoglutaric acid) as a yellow oil. δ_H (600 MHz, $CDCl_3$) 4.37 (dd, 1H, ***H3***), 3.78 (s, 3H, ***H1***), 3.68 (s, 3H, ***H7***), 2.52 (m, 2H, ***H5***), 2.38 (m, 1H , ***H4***), 2.28 (m, 1H, ***H4***); δ_C(151 MHz, $CDCl_3$) 172.6 (***C6***) , 169.9 (***C2***) , 53.2 (***C1***) , 52.0 (***C7***) , 44.7 (***C3***) , 31.4 (***C5***) , 29.9 (***C4***); GC-MS (EI^+) 238.9 ($M^{\bullet+}$, M= $C_7H_{11}BrO_4$), 209.9 (M-2Me$^{\bullet+}$), 180.9 (M-2Me-$O_2^{\bullet+}$).

8.5.6. Dimethyl 2-[bis(benzyl)amino]glutarate, 28

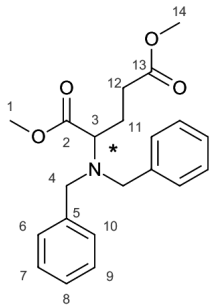

A solution of haloester **27** (0.4 g, 1.69 mmol) in acetonitrile (4 cm^3, dried over molecular sieves) was prepared and allowed to stir at room temperature under nitrogen in a Schlenk tube prior to the addition of triethylamine (0.5 cm^3, 3.61 mmol) at once followed by the dropwise addition of dibenzylamine over fifteen minutes (0.39 cm^3, 2.03 mmol). The brown solution was heated at 60^{o}C for 40 hours under nitrogen leading to the formation of a precipitate that was filtered off after cooling to room temperature. The filtrate was concentrated *in vacuo* and partitioned between diethyl ether and water; the organic layer was washed with brine, dried over magnesium sulphate and concentrated *in vacuo* prior to purification of the yellow residue via column chromatography (method ii, dichloromethane:methanol 100:0→90:10) to afford the product as a yellow oil (0.14 g, 0.39 mmol, 23%). δ_H (600 MHz, $CDCl_3$) 7.37 – 7.27 (m, 8H, ***H6, H7, H9, H10***), 7.24 (m, 2H, ***H8***), 3.89 (d, J = 14.0 Hz, 2H, ***H4***), 3.77 (s, 3H, ***H1***), 3.54 (s, 3H, ***H14***), 3.52 (d, J = 14.0 Hz, 2H, ***H4***), 3.35 (m, 1H, ***H3***), 2.45 (m, 1H, ***H11***), 2.31 (m, 1H, ***H11***), 2.02 (m, 2H, ***H12***); δ_C(151 MHz, $CDCl_3$) 173.5 (***C13***) , 172.9 (***C2***) , 139.4 (***C5***) , 129.1 , 128.4 , 127.2 (***C6***, ***C7, C8, C9***) , 59.8 (***C3***) , 54.6 (***C14***) , 51.6 (***C4***) , 51.3 (***C1***) , 30.5 (***C11***) , 24.5 (***C12***); ($ES\text{-}MS^+$) 356.2 (100 %, $[M+H]^+$); HR-MS Found 356.1854 , $C_{21}H_{26}NO_4$ $[M+H]^+$requires 356.1862.

8.5.7. Methyl {[(o-hydroxyphenyl)methyl]amino}acetate, HB-28

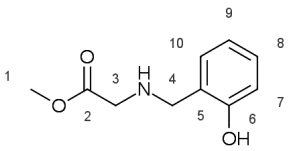

Glycine methyl ester hydrochloride (1.01 g, 8.01 mmol) was added to a solution of triethylamine (1.2 cm^3, 8.60 mmol) in 1,2-dichloroethane (30 cm^3) followed by the addition of salicylaldehyde (0.87 cm^3, 8.89 mmol). The reaction mixture was subsequently stirred under nitrogen for 10 minutes prior to the addition of sodium triacetoxyborohydride (2.10 g, 9.9 mmol) and monitored via TLC (90:10 dichloromethane:methanol) and ES-MS techniques until the absence of starting material and derivative imines were observed (within 4 hours). The mixture was then quenched with aqueous, saturated potassium bicarbonate (30 cm^3) and the biphasic mixture was stirred for a few minutes prior to extraction of the organic layer with dichloromethane (2x). The combined extracts were dried with magnesium sulphate and concentrated *in vacuo* to a yellow solid which was purified by column chromatography (method ii, dichloromethane:methanol, compound eluted in 90:10 v/v dichloromethane:methanol) to give the title compound as a crystalline sold (0.36 g, 1.84 mmol, 23%). Slow evaporation of a sample from acetonitrile gave crystals suitable for analysis by X-ray crystallography. δ_H (400 MHz, $CDCl_3$) 7.22 – 6.75 (m, 4H, ***H7, H8, H9, H10***), 4.00 (s, 2H, ***H4***), 3.76 (s, 3H, ***H1***), 3.45 (s, 2H, ***H3***); δ_C (101 MHz, $CDCl_3$) 172 (***C2***) , 158 (***C5***) , 130 , 129 , 122 , 120 , 117 (***C6***, ***C7***, ***C8***, ***C9***, ***C10***), 53 (***C4***), 52.5 (***C1***) , 49 (***C3***); (ES+MS^+) 196 (100 %, $[M+H]^+$, M= $C_{10}H_{13}NO_3$); X-ray crystallography: $C_{10}H_{13}NO_3$, M_r=195.21, orthorhombic (P_{bca}); *a* = 9.2513(8) Å, *b* = 9.0842(8) Å, *c* = 22.8517(19) ; crystal size = 0.42 × 0.18 × 0.16 mm^3; T= 120K.

8.5.8. o-(Benzyloxy)benzaldehyde, 29

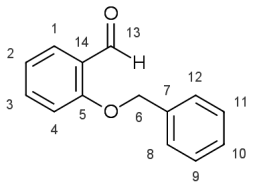

Potassium carbonate (5 g , 36.2 mmol) and potassium iodide (0.13 g, 0.78 mmol) was suspended in a solution of salicylaldehyde (2 cm^3, 18.8 mmol) in acetonitrile (60 cm^3, dried over molecular sieves) that was stirred at room temperature under nitrogen. A solution of benzyl bromide (2.4 cm^3, 20.2 mmol) in acetonitrile (60 cm^3) was then added dropwise to this suspension at room temperature over 30 minutes. Once addition was complete, the mixture was heated at 60°C for 5 hours and then stirred overnight at room temperature. Solids were then filtered off and the filtrate concentrated *in vacuo*.

The title compound was obtained after purification of the filtrate by column chromatography (method i, silica, diethyl ether:hexanes 0:100→20:80 v/v) as a yellow oil (3.31 g, 15.6 mmol, 83%). δ_H(400 MHz, $CDCl_3$) 10.57 (s, 1H, ***H13***), 7.86 (d, 1H, ***H1***), 7.54 (ddd, 1H, ***H2***), 7.41-7.05 (m, 7H, ***H3***, ***H4***, ***H8, H9, H10, H11, H12***), 5.20 (s, 2H, ***H6***); δ_C (101 MHz, $CDCl_3$) 190.0 (***C13***) , 161.3 (***C5***) , 136.4 , 136.17 , 129.02 , 128.75 , 128.57 , 127.57 , 125.49 , 121.30 , 113.31 (***C1, C2, C3, C4, C8, C9, C10, C11, C12***), 70.8 (***C6***); GC-MS (EI^+) 212 ($M^{\bullet+}$, M= $C_{14}H_{12}O_2$), 183 (M-$CHO^{\bullet+}$).

8.5.9. Dimethyl 2-iodoglutarate, 27a

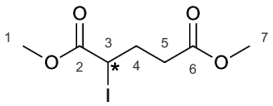

Sodium iodide (2.22 g, 13.4 mmol) was partially dissolved in acetone (12 cm^3) and ester **27** (0.66 g, 2.76 mmol) was added at once forming a yellow-orange solution that was refluxed for 2 hours. Volatiles were then removed *in vacuo* and the resulting brown solid was triturated in diethyl ether and then filtered. Concentration of the filtrate *in vacuo* afforded the product as a brown oil (0.59 g, 2.06 mmol, 75%). δ_H(400 MHz, $CDCl_3$) 4.46 (t, 1H, ***H3***), 3.75 (s, 3H, ***H1***), 3.68 (s, 3H, ***H7***), 2.45 (m, 2H, ***H5***), 2.28 (m, 2H, ***H4***); δ_C(101 MHz, $CDCl_3$) 172.1 (***C6***) , 171.3 (***C2***) , 52.8 (***C1***) , 51.7 (***C7***) , 33.2 (***C3***) , 30.8 (***C5***) , 18.9 (***C4***); GC-MS (EI^+) 286.0 ($M^{\bullet+}$, M= $C_7H_{11}IO_4$), 256.0 (M-$2Me^{\bullet+}$).

8.5.10. Methyl ({[o-(benzyloxy)phenyl]methyl}amino)acetate, HB-28-Bn

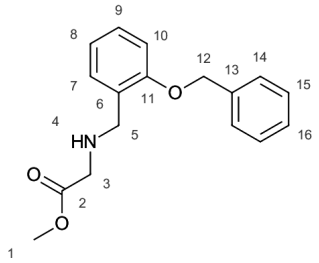

Ether **29** (0.51 g, 2.4 mmol) was dissolved in 1,2-dichloroethane (10 cm^3) and methyl glycinate hydrochloride (0.33g, 2.6 mmol) was suspended in the mixture prior to the addition of triethylamine (0.5 cm^3, 3.6 mmol) and sodium triacetoxyborohydride (1.01g, 4.77 mmol). The reaction mixture was then stirred at room temperature under nitrogen for 17 hours prior to the addition of a solution of saturated sodium carbonate. Dichloromethane was then added to the biphasic mixture and the organic layer extracted, dried over magnesium sulphate and the solvent removed *in vacuo* to afford the title compound (0.50 g, 1.8 mmol, 74%) as a colourless oil. δ_H (700 MHz, $CDCl_3$) 7.44 (m, 2H, ***H14***), 7.38 (m, 2H, ***H15***), 7.32 (m, 1H, ***H16***), 7.28 (dd, 1H, ***H7***), 7.22 (dd, 1H, ***H9***), 6.93 (m, 2H, ***H8, H10***), 5.08 (s, 2H, ***H12***), 3.89 (s, 2H, ***H5***), 3.63 (s, 3H, ***H1***), 3.40 (s, 2H, ***H3***), 2.64 (s, 1H, ***H4***);

δ_C(176 MHz, $CDCl_3$) 172.7 (***C2***), 156.8 (***C11***), 137.1 (***C13***), 130.0 (***C7***), 128.6 (***C15***), 128.5 (***C9***), 127.9 (***C16***), 127.9 (***C6***), 127.2 (***C14***), 120.8 (***C8***), 111.8 (***C10***), 69.9 (***C12***), 51.6 (***C1***), 50.0 (***C3***), 48.5 (***C5***).

8.5.11. Dimethyl 2-({[o-(benzyloxy)phenyl]methyl}(methoxycarbonylmethyl)amino)glutarate, 30

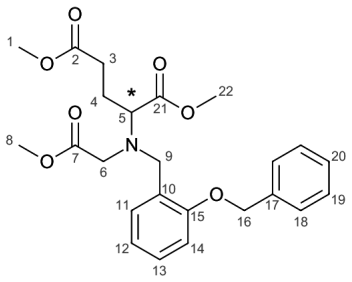

Alkyl iodide **27a** (0.18 g, 0.63 mmol) and amine **HB-28-Bn** (0.17 g, 0.60 mmol) were dissolved in acetonitrile (3 cm^3, dried over molecular sieves) and potassium carbonate (0.17 g, 1.23 mmol) added. The reaction mixture was then heated at 60°C under nitrogen for 6 days. Once cooled to room temperature, solids were filtered off and the solvent removed from the filtrate in vacuo. The residue was then purified by column chromatography (method ii, ethyl acetate:hexanes 0:100→100:0 compound eluted in ca. 30:70 v/v ethyl acetate:hexanes) to afford the title compound (0.07 g, 0.11 mmol, 18%) as a colourless oil. ν_{max}/cm^{-1}(ATR) 1730 (ester C=O st), 1200 (ester C-O st); δ_H (600 MHz, $CDCl_3$) 7.46 (d, 1H, ***H11***), 7.42 (dd, 2H, ***H19***), 7.38 (dd, 2H, ***H18***), 7.32 (m, 1H, ***H20***), 7.20 (m, 1H, ***H13***), 6.95 (dd, 1H, ***H12***), 6.89 (d, 1H, ***H14***), 5.07 (s, 2H, ***H16***), 4.04 (d, J = 14.0 Hz, 1H, ***H9***), 3.84 (d, J = 14.0 Hz, 1H, ***H9***), 3.62 (s, 3H), 3.61 (s, 3H, ***H8***, ***H22***), 3.59 (s, 3H, ***H1***), 3.56 (s, 1H, ***H6***), 3.48 (m, 2H, ***H5***, ***H6***), 2.44 (m, 2H, ***H3***), 1.97 (m, 2H, ***H4***); δ_C(151 MHz, $CDCl_3$) 173.9 (***C2***), 173.3, 172.3 (***C7***, ***C21***), 157.1 (***C15***), 137.7 (***C17***), 130.8 (***C11***), 128.6 (***C18***), 128.4 (***C13***), 127.9 (***C20***), 127.3 (***C19***), 127.2 (***C10***), 120.9 (***C12***), 111.9 (***C14***), 70.1 (***C16***), 62.1 (***C5***), 51.9 (***C6***), 51.5 (***C8***, ***C22***), 51.5 (***C1***), 51.3 (***C8***, ***C22***), 50.0 (***C9***), 30.3 (***C3***), 25.0 (***C4***); (ES-MS^+) 444.5 (100 %, $[M+H]^+$); HR-MS Found 444.2026, $C_{24}H_{30}NO_7$ $[M+H]^+$requires 444.2022.

8.5.12. Di-tert-butyl (2S)-2-{[(o-hydroxyphenyl)methyl]amino}glutarate, HB-31

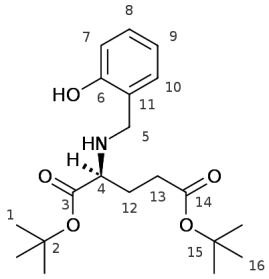

l-Glutamic acid di-*tert* butyl ester hydrochloride (0.5 g, 1.69 mmol) was suspended in 1,2-dichloro ethane (10 cm^3) and triethylamine (0.26 cm^3, 1.86 mmol) was added to the stirred mixture under nitrogen prior to the addition of salicylaldehyde (0.175 cm^3, 1.65 mmol) at once. The resulting pale yellow suspension was stirred under nitrogen for 20 minutes and sodium triacetoxyborohydride (0.78g, 3.68 mmol) was added. After 3 hours of stirring at room temperature a further equivalent of sodium triacetoxyborohydride (0.8g, 3.77 mmol) was added and the reaction mixture was allowed to stir for a further 36 hours under nitrogen at which point the reaction was judged to be complete by TLC. A saturated aqueous potassium bicarbonate (20 cm^3) solution was then used to quench the reaction mixture, which was diluted with, and extracted from dichloromethane (3x). The organic extracts were recombined and washed with brine prior to solvent removal *in vacuo*. Purification of the resulting oil via column chromatography (method i, silica, 0$\rightarrow$20% ethyl acetate:hexanes) led to the isolation of the title molecule (0.45g, 1.23 mmol, 75%) as a colourless oil. ν_{max}/cm^{-1}(ATR) 2976 (sp^3C-H), 1724 (ester C=O st), 1149 (ester C-O st); δ_H (700 MHz, $CDCl_3$) 7.18 (dd, J = 8.0, 1.5 Hz, 1H, ***H8***), 6.96 (d, J = 7.5, 1.5 Hz, 1H, ***H10***), 6.85 (dd, J = 8.0, 1.0 Hz, 1H, , ***H7***), 6.78 (dd, J = 7.5, 1.0 Hz, 1H, ***H9***), 4.04 (d, J = 13.5 Hz, 1H, ***H5***), 3.74 (d, J = 13.5 Hz, 1H, ***H5***), 3.24 (dd, ***H4***), 2.32 (m, 2H, ***H12***), 1.97 (m, 1H, ***H13***), 1.88 (m, 1H, ***H13***), 1.50 (s, 9H, ***H1***), 1.42 (s, 9H, ***H16***); δ_C(176 MHz, $CDCl_3$) 173.0 (***C3***) , 172.0 (***C14***) , 157.9 (***C6***) , 129.2 (***C8***) , 128.8 (***C10***) , 122.3 (***C11***) , 119.4 (***C8***) , 116.7 (***C7***) , 82.3 (***C2***) , 80.9 (***C15***) , 60.0 (***C4***) , 51.1 (***C5***) , 31.9 (***C13***), 28.5 (***C12***) , 28.3 (***C1***) , 28.2 (***C16***); (ES-MS^+) 366.2 (100 %, $[M-H]^-$); HR-MS Found 366.2288, $C_{20}H_{32}NO_5$ $[M+H]^+$requires 366.2280.

8.5.13. Di-tert-butyl (2S)-2-{[(2-pyridyl)methyl]amino}glutarate Py-31

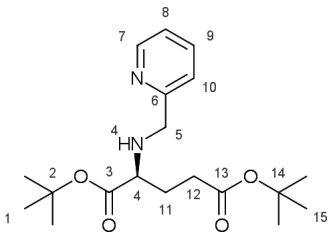

l-Glutamic acid di-*tert* butyl ester hydrochloride (0.5 g, 1.69 mmol) and triethylamine (0.28 cm^3, 2.00 mmol) were added to 1,2-dichloroethane (10 cm^3) followed by pyridine 2-carboxaldehyde (0.15 cm^3, 1.61 mmol). The yellow solution was then allowed to stir at room temperature under nitrogen for 10 minutes prior to the addition of sodium triacetoxyborohydride (1.1 g, 5.19 mmol) at once. The reaction was monitored by TLC (dichloromethane:methanol 90:10 v/v), and was complete within an overnight period. The reaction mixture was then quenched with a saturated aqueous solution of potassium carbonate, diluted with dichloromethane and transferred to a separating funnel for extraction of the organic layer which was then washed with brine and dried with magnesium sulphate. Removal of the solvent *in vacuo* followed by purification of the residual oil via column chromatography (method i, silica, compound eluted in dichloromethane:methanol ca. 95:5 v/v) led to isolation of the title compound (0.42 g, 1.20 mmol, 70%) as a yellow oil. ν_{max}/cm^{-1} (ATR) 2974 (sp^3 C-H st), 1722 (ester C=O st), 1143 (ester C-O st); δ_H (700 MHz, $CDCl_3$) 8.53 (d, 1H, ***H7***), 7.63 (dd, 1H, ***H9***), 7.37 (d, 1H, ***H10***), 7.14 (dd, 1H, ***H8***), 3.96 (d, J = 14.5 Hz, 1H, ***H5***), 3.77 (d, J = 14.5 Hz, 1H, ***H7***), 3.19 (dd, 1H, ***H4***), 2.38 (m, 2H, ***H12***), 2.12 (s, 1H, ***H4***) 1.95 (m, 1H, ***H11***), 1.86 (m, 1H, ***H11***), 1.46 (s, 9H, ***H1***), 1.42 (s, 9H, ***H15***); δ_C(176 MHz, $CDCl_3$) 174.0 (***C3***) , 172.5 (***C13***) , 159.7 (***C6***) , 149.1 (***C7***) , 136.4 (***C9***) , 121.9 (***C10***) , 121.8 (***C8***) , 81.3 (***C2***) , 80.2 (***C14***) , 61.0 (***C4***) , 53.4 (***C5***) , 32.0 (***C12***) , 28.6 (***C11***) , 28.1 (***C1***, ***C15***); (ES-MS^+) 351.2 (100 %, $[M+H]^+$); HR-MS Found 351.2275, $C_{19}H_{31}N_2O_4$ $[M+H]^+$requires 351.2284.

8.5.14. Di-tert-butyl (2S)-2-{(1R)-[(o-hydroxyphenyl)methyl](tert-butoxycarbonylmethyl) amino}glutarate, $HBGl_3$-tBu

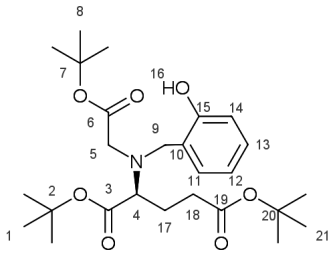

HB-31, (0.40 g, 1.10 mmol) was dissolved in acetonitrile (5 cm^3, dried over molecular sieves) and potassium hydrogen carbonate (0.22, 2.20 mmol) was suspended in the stirred solution. t-Butyl bromoacetate (0.17 cm^3, 1.16 mmol) was then added at once and the mixture heated to 60°C under nitrogen. Reaction progress was monitored by TLC (ethyl acetate:hexanes 20:80 v/v), and after 23 hours a catalytic amount of potassium iodide was added after which heating was maintained for a further 6 days, at which point the consumption of starting material was observed by TLC. Upon cooling to room temperature, the reaction mixture was filtered, concentrated *in vacuo* and the target compound isolated by column chromatography (method ii, ethyl acetate:hexanes 0:100→30:70 compound eluted in ca. 15:85 v/v ethyl acetate:hexanes) as a colourless oil (0.14 g, 0.29 mmol, 28%). ν_{max}/cm^{-1} (ATR) 3340 (O-H st), 2977 (sp^3 C-H st), 1722 (ester C=O st); 1137 (C-O st); δ_H (700 MHz, $CDCl_3$) 9.12 (s, 1H, ***H16***), 7.17 (dd, 1H, ***H13***), 6.96 (ddd, ***H11***), 6.86 (dd, ***H14***), 6.75 (ddd, 1H, ***H12***), 3.91 (d, J = 13.5 Hz, 1H, ***H9***), 3.73 (d, J = 13.5 Hz, 1H, ***H9***), 3.59 (d, J = 18.0 Hz, 1H , ***H5***), 3.26 (d, J = 18.0 Hz, 1H, ***H5***), 3.22 (dd, 1H, ***H4***), 2.24 (m, 1H, ***H18***), 2.12 (m, 1H, ***H18***), 1.89 (m, 1H, ***H17***), 1.78 (m, 1H, ***H17***), 1.48 (s, 9H, ***H21***), 1.47 (s, 9H, ***H8***), 1.35 (s, 9H, ***H1***); δ_C(176 MHz, $CDCl_3$) 172.3 (***C19***) , 172.0 (***C6***) , 171.2 (***C3***) , 157.3 (***C15***) , 130.2 (***C11***) , 129.5 (***C13***) , 121.6 (***C10***) , 119.3 (***C12***) , 116.6 (***C14***) , 82.4 (***C20***) , 81.8 (***C7***) , 80.4 (***C2***) , 60.5 (***C4***) , 55.9 (***C9***) , 51.5 (***C5***) , 31.8 (***C18***) , 28.3 (***C21***) , 28.1 (***C8***) , 28.0 (***C1***) , 24.7 (***C18***); (ES-MS^+) 480.5 (100 %, $[M+H]^+$); HR-MS Found 480.2948, $C_{26}H_{42}NO_7$ $[M+H]^+$requires 480.2961.

8.5.15. (S)-2-{(Carboxymethyl)[(o-hydroxyphenyl)methyl]amino}glutaric acid, $HBGl_3$

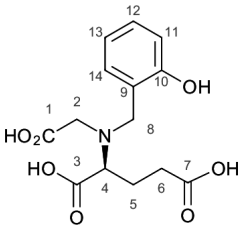

$HBGl_3$ (0.5 g, 1.0 mmol) was dissolved in dichloromethane (1 cm^3) and anisole (0.1 cm^3, 0.93 mmol) added, prior to the addition to trifluoroacetic acid (1 cm^3). The solution was stirred at room temperature under argon for 17 hours, followed by removal of volatiles *in vacuo*. The residue was then redissolved in dichloromethane, which was also removed *in vacuo.* Diethyl ether was then added to this residue and a yellow-while solid was precipitated after this suspension was agitated using an ultrasonic bath. The solid was collected via centrifugation, dissolved in aqueous hydrochloric acid (1 mol dm^{-3}), and eluted through a column of DOWEX 1X8 (chloride form) that had been pre-washed with 1 mol dm^{-3} aqueous hydrochloric acid and water. Once loaded onto the resin, elution of the compound was achieved with 1 mol dm^{-3} aqueous hydrochloric acid (ca. 100 cm^3). Removal of the solvent *in vacuo* followed by further drying under high vacuum gave the title compound (0.12 g, 0.39 mmol, 37 % based on mass).* t_R (H_2O:MeOH, UV detection); 4.14 min; ν_{max}/cm^{-1} (ATR) 2960 (O-H st), 1730 (acid C=O st), 1220 (acid C-O st); δ_H (700 MHz, D_2O) 7.23 (ddd, 1H, ***H13***), 7.19 (dd, 1H, ***H12***), 6.83 (ddd, 1H, ***H13***), 6.80 (dd, 1H, ***H11***), 4.45 (d, J = 13.0 Hz, 1H, ***H8***), 4.34 (d, J = 13.0 Hz, 1H, ***H8***), 4.02 (dd, 1H, ***H4***), 3.99 (d, 2H, ***H2***), 2.57 (dt, J = 17.5, 6.5 Hz, 1H, ***H6***), 2.48 (dt, J = 17.5, 7.5 Hz, 1H, ***H6***), 2.13 (dd, 2H, ***H5***); δ_C (176 MHz, D_2O) 176.0 (***C7***), 170.3 (***C3***), 169.0 (***C1***), 155.4 (***C10***), 132.5 (***C14***), 132.3 (***C12***), 120.7 (***C13***), 115.6 (***C11***), 115.2 (***C9***), 64.1 (***C4***), 54.7 (***C8***), 52.2 (***C2***), 30.1 (***C6***), 21.1 (***C5***); (ES-MS^+) 312.1 (100 %, $[M+H]^+$); HR-MS Found 312.1079, $C_{14}H_{18}NO_7$ $[M+H]^+$requires 312.1083.

8.5.16. Di-tert-butyl (2S)-2-benzylaminoglutarate, hydrochloride salt, Bn-Glu-tBu

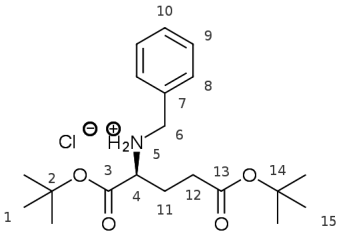

*Although the ^1H NMR spectrum of this compound exhibits impurity peaks (~6% of total integration value) that could not be assigned, the HPLC trace of a sample used for biological study of this compound showed a single peak, which corresponded to the target compound.

l-Glutamic acid di-*tert* butyl ester hydrochloride (0.5 g, 1.69 mmol) and triethylamine (0.28 cm^3, 3.82 mmol) were added to methanol (8 cm^3), resulting in the formation a white precipitate. Benzaldehyde (0.18 cm^3, 1.78 mmol) was then added and the mixture stirred under nitrogen for 2.5 hours. Sodium borohydride (0.23 g, 6.07 mmol) was subsequently added portionwise and the mixture was allowed to stir under nitrogen for a further 3 hours. Volatiles were then removed *in vacuo* and the residue partitioned between dichloromethane and aqueous hydrochloric acid (1 mol dm^{-3}) and the organic layer extracted, washed with brine, dried with magnesium sulphate and the solvent removed *in vacuo*. The resulting white solid was triturated in hexane to afford the title compound (0.29g, 0.75 mmol (based on molecular weight of the monohydrochloride salt), 45%) as a white powder. mp 140-142°C; ν_{max}/cm^{-1}(ATR); 2982 (sp^3C-H st), 2631 (N^+-H st), 1725 (ester C=O st), 1149 (C-O st); δ_H (600 MHz, $CDCl_3$) 10.81 (s, 1H, ***H5***), 9.84 (s, 1H, ***H5***), 7.63 (d, 2H, ***H8***), 7.37 (m, 3H, ***H9*** ,***H10***), 4.24 (dd, 2H, ***H6***), 3.62 (s, 1H, ***H4***), 2.47 (m, 4H, ***H11, H12***), 1.51 (s, 9H, ***H15***), 1.35 (s, 9H, ***H1***); δ_C(151 MHz, $CDCl_3$) 171.3 (***C13***) , 166.7 (***C3***) , 131.0 (***C8***) , 130.0 (***C7***) , 129.7, 129.3 (***C9, C10***) , 84.9 (***C14***) , 81.3 (***C2***) , 57.5 (***C4***) , 49.7 (***C6***) , 31.3 , 25.2 (***C11***, ***C12***), 28.2 (***C15***), 28.1 (***C1***); (ES-MS^+) 350.2 (100 %, $[M+H]^+$); HR-MS Found 350.2330 , $C_{20}H_{32}NO_4$ $[M+H]^+$requires 350.2331.

8.5.17. Di-tert-butyl (2S)-2-[(1R)-(benzyl)(tert-butoxycarbonylmethyl)amino]glutarate, $BnGl_3$

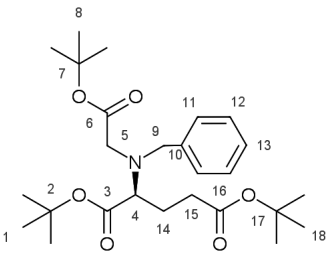

Bn-Glu-tBu (0.40g, 1.04 mmol) was added to acetonitrile (3.5 cm^3, Aldrich anhydrous) and potassium carbonate (0.57 g, 4.13 mmol), potassium iodide (30 mg, 0.18 mmol) salts were added along with t-butyl bromoacetate (0.23 cm^3, 1.57 mmol) and the mixture was heated at 60°C under nitrogen. TLC (ethyl acetate:hexanes 20:80 v/v) indicated that consumption of starting material was achieved within 6 hours, but heating was maintained for a further 16 hours prior to cooling to room temperature and removal of solids by filtration. The filtrate was concentrated *in vacuo* and subjected to column chromatography (method ii, diethyl ether:hexanes 0:100→40:60 compound eluted in ca. 15:85 v/v diethyl ether:hexanes) to afford the title compound (0.24 g, 0.52 mmol, 50%) as a colourless oil. ν_{max}/cm^{-1}(ATR); 2974 (sp^3 C-H st), 1719 (ester C=O st), 1137 (ester C-O st); δ_H (700 MHz, $CDCl_3$) ; 7.40-7.22 (m, 5H, ***H11***, ***H12, H13***) , 3.95 (d, J = 13.5 Hz, 1H, ***H5***), 3.74 (d, J = 13.5 Hz, 1H, ***H5***), 3.43 (d, J = 17.0 Hz, 1H, ***H9***), 3.30 (m, J = 17.0 Hz, 2H, ***H9***, ***H4***), 2.48 (ddd, J = 16.5, 9.5, 6.0 Hz, 1H, ***H15***), 2.26 (ddd, J = 16.5, 9.5, 6.0 Hz, 1H, ***H15***), 1.91 (m, 2H, ***H14***), 1.50 (s, 9H, ***H8***), 1.43 (s, 9H, ***H18***), 1.40 (s, 9H, ***H1***); δ_C(176 MHz, $CDCl_3$); 172.9 (***C16***) , 171.9 (***C6***), 170.9 (***C3***) , 129.3 ,

128.4 , 127.4 (***C10, C11, C12, C13***) , 81.5 (***C17***) , 80.9 (***C7***) , 80.2 (***C2***) , 62.4 (***C4***) , 56.7 (***C5***) , 52.7 (***C9***) , 32.0 (***C15***) , 28.5 (***C18***) , 28.3 (***C8***) , 28.2 (***C1***), 25.2 (***C14***) . (ES-MS$^+$) 464.3 (100 %, $[M+H]^+$); HR-MS Found 464.3009, $C_{26}H_{42}NO_6$ $[M+H]^+$requires 464.3012.

8.5.18. Di-tert-butyl (2S)-2-[(tert-butoxycarbonylmethyl)amino]glutarate, 32

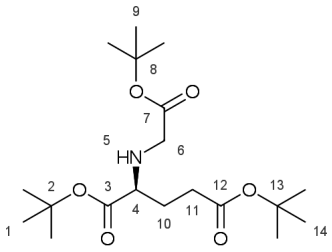

Via the protected intermediate $BnGl_3$: Ethanol (25 cm^3) was used to dissolve **$BnGl_3$** (0.08 g, 0.03 mmol) and the colourless solution was evacuated and back-filled with nitrogen three times prior to the addition of 5% palladium on charcoal (7 mg, 3 μmol wrt Pd). Once the catalyst was added, the reaction mixture was evacuated and back-filled with hydrogen gas from a balloon three times prior to stirring at room temperature. Reaction progress was monitored by the use of ^{1}H NMR which indicated that debenzylation was achieved within 4 hours. The reaction mixture was subsequently allowed to stand for a few minutes under a flow of nitrogen prior to catalyst removal via filtration over Celite®. Concentration of the filtrate *in vacuo,* followed by re-dissolution of the residue in chloroform and a second solvent removal *in vacuo* led to isolation of the title molecule (51 mg, 0.14 mmol, 79%) as a colourless oil.

Direct synthesis from commercially available starting material: l-Glutamic acid di-*tert* butyl ester hydrochloride (1.5 g, 5.8 mmol) was stirred at room temperature in chloroform under argon in the presence of activated zinc dust (3.0g, 46 mmol) for one hour.* The zinc dust was then filtered off, and the solvent removed from the filtrate *in vacuo* to afford the free base. The resulting oil was dissolved in acetonitrile (28 cm^3, dried over molecular sieves). When the solution was nearly homogeneous, anhydrous triethylamine (1.21 cm^3, 8.68 mmol) was added at once, followed by the dropwise addition of t-butyl bromoacetate (0.89 cm^3, 6.1 mmol). Finally, a catalytic amount of potassium iodide (ca. 0.1 g) was added and the resulting mixture stirred at room temperature under argon for 24 hours. After the solvent was removed *in vacuo*, the oily residue was partitioned between water and dichloromethane (2x) and the combined organic extracts were subsequently washed in brine prior to being dried with magnesium sulphate and the solvent being removed *in vacuo*. The resulting oil was dissolved in the minimum volume of dichloromethane and subjected to column chromatogra-

*Zinc dust was activated by suspension and ultrasonic agitation in 1 mol dm^{-3} hydrochloric acid for ten minutes under an argon atmosphere. The grey solid was then collected by filtration under a flow of nitrogen, washed in quick succession with water, ethanol and then diethyl ether (ca. 100 cm^3 each) and dried under high vacuum prior to use.

phy (method i, silica, ethyl acetate:hexanes 30:70→60:40) to afford the pure compound (0.44 g, 1.2 mmol, 21%) as a colourless oil. ν_{max}/cm^{-1}(ATR) 2970 (N-H st), 2930 (sp^3 C-H), 1731 (ester C=O st), 1149 (ester C-O st); δ_H (700 MHz, $CDCl_3$) 3.29 (d, J = 17.0 Hz, 1H, ***H6***), 3.22 (d, J = 17.0 Hz, 1H, ***H6***), 3.14 (dd, 1H, ***H4***), 2.34 (t, ***H11***), 1.92 (m, 2H, ***H5***, ***H10***), 1.82 (m, 1H, ***H10***), 1.46 (s, 9H, ***H1***), 1.44 (s, 9H, ***H14***), 1.43 (s, 9H, ***H9***); δ_C(176 MHz, $CDCl_3$) 173.8 (***C3***) , 172.8 (***C12***) , 171.3 (***C7***) , 81.7 (***C2***) , 81.5 (***C13***) , 80.5 (***C8***) , 60.8 (***C4***) , 50.2 (***C6***) , 32.2 (***C11***) 28.6 (***C10***) , 28.4 (***C1, C9, C14***); (ES-MS$^+$) 374.2 (100 %, $[M+H]^+$); HR-MS Found 374.2538, $C_{19}H_{36}NO_6$ $[M+H]^+$requires 374.2543.

8.5.19. Di-tert-butyl (S)-2-{[(2-pyridyl)methyl](tert-butoxycarbonylmethyl)amino}glutarate, $PyGl_3$-tBu

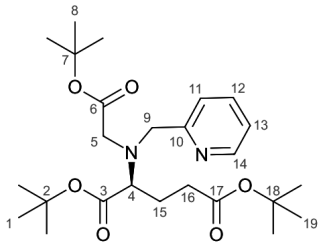

Aminoester **32** (0.16 g, 0.43 mmol) was dissolved in 1,2-dichloroethane (3 cm^3), and pyridine-2-carboxaldehyde (37μL, 0.39 mmol) added, prior to the addition of sodium triacetoxyborohydride (0.18 g, 0.85 mmol) at once. The reaction mixture was then stirred at room temperature under nitrogen for five hours, prior to the addition of a further equivalent of sodium triacetoxyborohydride (0.18 g, 0.85 mmol). After this addition, the reaction mixture was allowed to stir for a further 24 hours, after which the reaction was quenched by the addition of a saturated solution of sodium carbonate (5 cm^3). Dichloromethane (5 cm^3) was then added and the organic layer collected. The organic layer was then washed with saturated sodium carbonate (2x) and then brine (2x), prior to being dried over magnesium sulphate. The solvent was removed *in vacuo*, to give a yellow oil (0.13 g), that was purified via column chromatography (method i, silica, gradient used was diethyl ether:hexanes 0:100→100:0) to give the title compound (0.02 g, 0.04 mmol, 1%), as a colourless oil. δ_H (700 MHz, $CDCl_3$) 8.45 (d, 1H, ***H14***), 7.66 (d, 1H, ***H11***), 7.63 (dd, 1H, ***H12***), 7.10 (dd, 1H, ***H13***), 4.00 (d, J = 15.5 Hz, 1H, ***H9***), 3.89 (d, J = 15.5 Hz, 1H, ***H9***), 3.44 (d, J = 17.0, 1.5 Hz, 1H, ***H5***), 3.38 (d, J = 17.0, 1.5 Hz, 1H, ***H5***), 3.28 (ddd, 1H, ***H4***), 2.44 (m, 1H, ***H16***), 2.32 (m, 1H, ***H16***), 1.96 (m, 1H, ***H15***), 1.84 (m, 1H, ***H15***), 1.45 (s, 9H, ***H19***), 1.37 (s, 18H, ***H1, H8***); δ_C(176 MHz, $CDCl_3$) 172.6 (***C17***), 171.7 (***C3***), 170.8 (***C6***), 159.7 (***C10***), 148.7 (***C14***), 136.6 (***C12***), 122.8 (***C11***), 121.9 (***C13***), 81.3 (***C18***), 80.6 (***C2***), 80.1 (***C7***), 63.7 (***C4***), 58.4 (***C9***), 53.6 (***C5***), 32.0 (***C16***), 28.2 (***C19***), 28.0 (***C1, C8***), 25.3 (***C15***); (ES-MS$^+$) 465.1 (100 %, $[M+H]^+$); HR-MS Found 465.2972, $C_{25}H_{21}N_2O_6$ $[M+H]^+$requires 465.2965.

8.5.20. Di-tert-butyl (2S)-2-{(1R)-(tert-butoxycarbonylmethyl)[(2-pyridyl)carbonyl]amino} glutarate, PyCO-Gl$_3$-tBu*

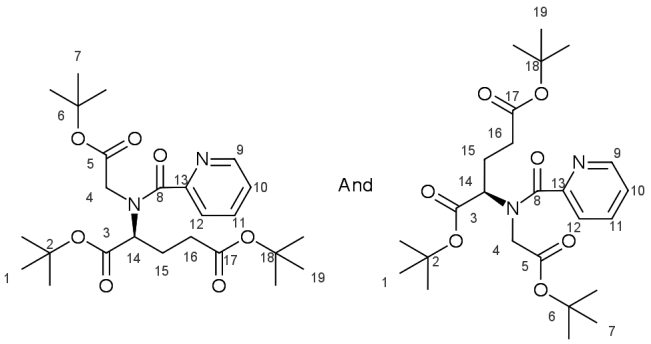

Picolinoyl chloride hydrochloride (0.12 g, 0.67 mmol) was added to anhydrous dichloromethane, and 4-dimethylaminopyridine (7 mg, 0.06 mmol) added prior to cooling the mixture to -78°C. Anhydrous triethylamine (0.21 cm^3, 2.9 mmol) was then added, followed by aminoester **32** (0.22 g, 0.59 mmol). The reaction mixture was allowed to stir at -78°C for two hours under argon prior to being raised to room temperature. After 4 hours another equivalent of picolinoyl chloride hydrochloride (0.12 g, 0.67 mmol) was added along with more triethylamine (0.21 cm^3, 2.9 mmol). The reaction was then worked up via partitioning between saturated sodium carbonate (25 cm^3) and dichloromethane when a steady state was confirmed via ES-LCMS (after 42 hours). The organic layer was then washed with brine, dried over magnesium sulphate and the solvent removed *in vacuo*. The residue was purified via preparative reverse-phase column chromatography (water:acetonitrile , 0.1% v/v formic acid as additive 0:100→100:0 compound eluted in ca. 20:80 v/v water:acetonitrile) to give the title compound (0.03 g, 0.06 mmol, 10%), as a colourless oil. δ_H (700 MHz, $CDCl_3$, Two rotomers in a 1:1.2 ratio†) 8.52 (d, 1H, ***H9***), 8.49 (d, 1H, ***H9***), 7.86 (d, 1H, ***H12***), 7.74 (m, 1H, ***H11***), 7.29 (t, 1H, ***H10***), 5.21 (dd, 1H, ***H14***), 4.93 (dd, 1H, ***H14***), 4.64 (d, J = 18.5 Hz, 1H, ***H4***), 4.36 (d, J = 17.0 Hz, 1H, ***H4***), 4.17 (d, J = 18.5 Hz, 1H, ***H4***), 3.77 (d, J = 17.0 Hz, 1H, ***H4***), 2.95-1.60 (m, 4H, ***H15*** and ***H16***), 1.47 (s, 9H, ***H19***),1.46 (s, 9H, ***H19***), 1.43 (s, 9H, ***H1***), 1.42 (s, 9H, ***H1***), 1.37 (s, 9H, ***H7***), 1.29 (s, 9H, ***H7***); δ_C(176 MHz, $CDCl_3$) 172.4 (***C17***), 172.3 (***C17***), 170.1 (***C3***), 170.0 (***C3***), 169.5 (***C8***), 168.9 (***C8***), 168.8 (***C5***), 167.9 (***C5***), 153.9 (***C13***), 153.5 (***C13***), 148.2 (***C9***), 147.5 (***C9***), 137.0 (***C11***), 136.9 (***C11***), 125.3 (***C12***), 124.9 (***C10***), 124.8 (***C10***), 124.50, 82.3(***C10***), 82.1-80.4 (***C2***, ***C6***, ***C18***), 61.1 (***C14***), 58.3 (***C14***), 49.7 (***C4***), 46.6 (***C4***), 32.3 (***C16***), 31.8 (***C16***), 28.2-27.9 (***C1***, ***C7***, ***C19***), 25.3 (***C15***), 24.9 (***C15***); (ES-MS$^+$) 479.3 (100 %, $[M+H]^+$); HR-MS Found 479.2751, $C_{25}H_{39}N_2O_7$ $[M+H]^+$requires 479.2757.

*This reaction was not found to be reproducible.

†Different chemical shifts that refer to the same proton environment in the characterisation data correspond to signals from an individual rotomer.

8.5.21. 2-{2-[2-(3-Oxo-2H-isoindol-2-oyl)ethylamino]ethyl}-2H-isoindole-1,3-dione,[149] 33

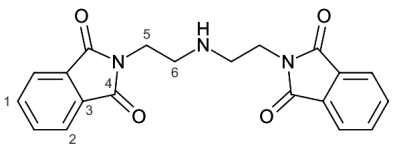

Bis(2-chloroethyl)amine hydrochloride (4.0 g, 22.4 mmol) and potassium phthalimide (15 g, 81.0 mmol) were dissolved in dimethylformamide (50 cm^3) and the mixture was heated at 100°C under nitrogen for 16 hours. This mixture was then poured into a slurry of basic ice-water (50 g ice, 50 cm^3 water and 5 g potassium carbonate) and stirred for 2 hours to precipitate the title compound as a white solid, which was collected by filtration and dried under high vacuum (4.8 g, 13.2 mmol, 59%) . δ_H (400 MHz, $CDCl_3$) 7.66 (m, 8H, ***H1***, ***H2***), 3.77 (t, J = 6.0 Hz, 4H, ***H5***), 2.95 (t, J = 6.0 Hz, 4H, ***H6***); δ_C (101 MHz, $CDCl_3$) 168.4 (***C4***), 133.7 (***C3***), 132.1 , 123.13 (***C1, C2***), 47.2 , 37.53 (***C5, C6***).

8.5.22. tert-Butyl {bis[2-(3-oxo-2H-isoindol-2-oyl)ethyl]amino}acetate,[149] 33-tBu

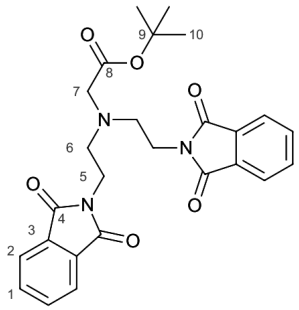

Imide **33** (1.85 g, 5.1 mmol) was dissolved in acetonitrile (27 cm^3, dried over molecular sieves) and potassium carbonate (2.11 g, 15.3 mmol) and potassium iodide (ca. 0.25 g) were then suspended in the solution. t-Butyl bromoacetate (0.82 cm^3, 5.6 mmol) was then added to the reaction mixture at once, and the mixture was heated at 60°C under nitrogen for 14 hours. Once cooled to room temperature, solids were removed via filtration, and the solvent removed from the filtrate *in vacuo*. Hexane was then added to the oily residue, and the title compound precipitated as a white solid (1.43 g, 3.0 mmol, 59%), that was collected via filtration after agitation in an ultrasonic bath. δ_H (400 MHz, $CDCl_3$) 7.68 (m, 8H, ***H1***, ***H2***), 3.72 (t, J = 6.5 Hz, 4H, ***H5***), 3.45 (s, 2H, ***H7***), 3.03 (t, J = 6.5 Hz, 4H, ***H6***), 1.41 (s, 9H, ***H10***); δ_C (101 MHz, $CDCl_3$) 170.6 (***C8***), 168.4 (***C4***), 133.8 (***C3***), 132.3, 123.2 (***C1***, ***C2***), 81.2 (***C9***), 51.8, 36.2 (***C5***, ***C6***), 28.3 (***C10***).

8.5.23. 2-Amino-1-[(benzyl)(2-aminoethyl)amino]ethane[301], 35

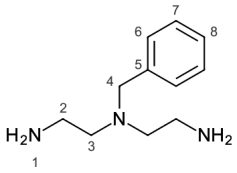

Synthesis of 2-(2-{(Benzyl)[2-(3-oxo-2H-isoindol-2-oyl)ethyl]amino}ethyl)-2H-isoindole-1,3-dione, 35-Phth. Imide **33** (1.5 g, 4.1 mmol), was dissolved in acetonitrile (17 cm^3, dried over molecular sieves), and potassium carbonate (1.14 g, 8.3 mmol) added prior to the addition of benzyl bromide (0.52 cm^3, 4.4 mmol) at once to the suspension. The mixture was then heated at 60°C under argon for 15 hours, after which time the reaction mixture was filtered hot and the solvent removed from the filtrate *in vacuo*. The residue was then partitioned between water and dichloromethane, and the dichloromethane layer extracted and washed with brine. After drying the organic extract with magnesium sulphate and removal of the solvent *in vacuo*, the residue was heated at 60°C under high vacuum to remove the residual benzyl bromide, to afford the title product (1.36 g, 3.0 mmol, 73%) as a yellow oil. δ_H (400 MHz, $CDCl_3$) 7.70 (m, 8H), 6.98 (m, 5H), 3.77 (t, 4H), 2.81 (t, 4H), 1.59 (s, 2H).

Synthesis of 2-Amino-1-[(benzyl)(2-aminoethyl)amino]ethane from 35. Imide **25-Phth** (1.37 g, 3.0 mmol), was dissolved in a methanolic solution of hydrazine monohydrate (50 cm^3, 0.5 mol dm^{-3} in methanol) and the solution was stirred under argon at room temperature for 20 hours, during which time a flocculent white precipitate formed. The precipitate was then filtered using a sinter funnel (2x) and the solvent was removed *in vacuo*. The residue was then dissolved in chloroform and washed twice with aqueous ammonia (50 cm^3, 5 wt. % ammonia). The organic layer was then dried over magnesium sulphate and the solvent removed *in vacuo* to afford the title compound (0.46 g, 2.4 mmol, 79%) as a pale yellow oil that was kept in an argon-flushed round bottom flask in a freezer to prevent reactions with the air. δ_H (400 MHz, $CDCl_3$) 7.29 (m, 5H, ***H6***, ***H7***, ***H8***), 3.58 (s, 2H, ***H4***), 2.75 (t, J = 6.5 Hz, 4H, ***H2***), 2.52 (t, J = 6.5 Hz, 4H, ***H3***), 1.37 (s, 4H, ***H1***); δ_C (101 MHz, $CDCl_3$) 139.6 (***C5***), 128.8 , 128.3, 127.0 (***C6***, ***C7***, ***C8***), 59.2 (***C4***), 57.40 (***C3***), 39.84 (***C2***); (ES-MS^+) 194.2 (100 %, $[M+H]^+$, M= $C_{11}H_{19}N_3$).

8.5.24. Di-tert-butyl bromomalonate[307], 36*

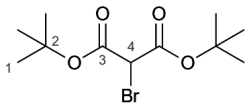

Di-t-butyl malonate (5 cm^3, 22.3 mmol) was dissolved in tetrohydrofuran (anhydrous, 45 cm^3) and the reaction mixture was cooled under argon using an acetone/dry ice bath. Using a pressure-equalising dropping funnel, n-butyllithium (1.6 mol dm^{-3} in hexanes, 18 cm^3, 29 mmol) was added dropwise to the solution which was kept at low temperature for 45 minutes. Using a syringe, bromine (1.5 cm^3, 29 mmol) was added at once and the reaction mixture was allowed to reach room temperature. After being allowed to stir for 2 hours at room temperature, the solvent was removed *in vacuo* and the residue partitioned (2x) between saturated carbonate and chloroform. The combined organic extracts were dried over magnesium sulphate and the solvent removed *in vacuo*. The residue was purified via column chromatography (method i, silica, diethyl ether:hexanes 0:100→10:90) to give the title compound (4.9 g, 17 mmol, 75%) as a pungent, lachrymatory, pale yellow oil. δ_H (400 MHz, $CDCl_3$) 4.68 (s, 1H, ***H4***), 1.51 (s, 18H, ***H1***); δ_C (101 MHz, $CDCl_3$) 163.7 (***C3***), 84.0 (***C2***), 45.87 (***C4***), 27.8 (***C1***); GC-MS (EI^+) 225.0 (^{81}Br-M-OtBu$^{\bullet+}$, M= $C_{11}H_{19}BrO_4$).

8.5.25. Di-tert-butyl bromomethylmalonate[338], Me-36

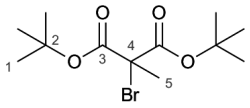

Methylation of di-t-butyl malonate. Di-t-butyl malonate (3 cm^3, 13.3 mmol) was dissolved in anhydrous tetrahydrofuran (20 cm^3) and was added dropwise to a suspension of sodium hydride (60 wt. %, 0.54 g, 13.5 mmol) also in anhydrous tetrahydrofuran (20 cm^3). Once the gas evolution subsided, the reaction mixture was allowed to stir at room temperature under argon for 5 minutes prior to the dropwise addition of methyl iodide (0.83 cm^3, 13.3 mmol) via syringe. The reaction mixture was then stirred for a further 20 hours at room temperature. The reaction was then quenched with a saturated solution of ammonium chloride and the crude product extracted using dichloromethane. The organic extract was then dried over magnesium sulphate and the solvent was removed *in vacuo*. The residue was then purified by column chromatography (method i, silica, diethyl ether:hexanes 0:100→10:90) to give the title compound (1.0 g, 4.3 mmol, 32%)†. δ_H (400 MHz, $CDCl_3$) 3.22 (q, J = 7.0 Hz, 1H), 1.46 (s, 18H), 1.32 (d, J = 7.0 Hz, 3H); δ_C (101 MHz, $CDCl_3$) 169.8, 81.3, 48.3, 28.0,

*A small amount of an impurity that could not be removed by column chromatography was detected, but in further steps the reagent functioned as expected if an excess was used. This is accounted for in the equivalents of reactions using **36**.

†Conventional TLC staining methods, were ineffective for visualising the compound. Instead, the co-elution of elemental iodine was used to gauge elution progress.

13.5; GC-MS (EI$^+$) 215.1 (M-$CH_4^{\bullet+}$, M= $C_{12}H_{22}O_4$).

Bromination of di-tert-butyl methylmalonate. This procedure was performed analogously to that for **36** (***Section 8.5.24***) except the following quantities were used: Di-tert-butyl methylmalonate (1.0 g, 4.3 mmol), n-butyllithium (1.6 mol dm^{-3} in hexanes, 2.9 cm^3, 4.6 mmol), bromine (0.27 cm^3, 5.3 mmol). The target compound (1.1 g, 3.6 mmol, 83%) was isolated as a colourless oil. δ_H (400 MHz, $CDCl_3$) 1.99 (s, 3H, ***H5***), 1.48 (s, 18H, ***H1***); δ_C (101 MHz, $CDCl_3$) 166.6 (***C3***), 83.5 (***C2***), 59.8 (***C4***), 27.8 (***C1***), 26.7 (***C5***); GC-MS (EI$^+$) 307.2 (^{79}Br-M-OtBu$^{\bullet+}$, M= $C_{12}H_{21}BrO_4$).

8.5.26. 2,2,2-Trifluoro-1-{2-[2-(2,2,2-trifluoroacetylamino)ethylamino]ethylamino}-1-ethanone[309], trifluoroacetate salt, 37

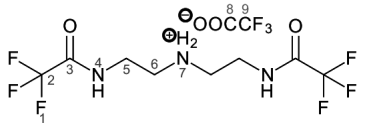

Diethylene triamine (1 cm^3, 9.3 mmol) was dissolved in acetonitrile (15 cm^3, spiked with 0.2 cm^3 water) and ethyl trifluoroacetate (3.8 cm^3, 31.9 mmol) was added to the solution which was refluxed for 18 hours. The title compound (3.66 g, 8.9 mmol, 96%), was isolated as a buff solid after removal of the volatiles *in vacuo*. δ_H (700 MHz, DMSO-d^6) 9.62 (t, J = 6.0 Hz, 2H, ***H4***), 8.84 (s, 2H, ***H7***), 3.50 (q, J = 6.0 Hz, 4H, ***H5***), 3.14 (t, J = 6.0 Hz, 4H, ***H6***); δ_C (176 MHz, DMSO-d^6) 158.6 (d, J = 31.4 Hz, ***C9***), 156.9 (d, J = 36.6 Hz, ***C3***), 116.6 (m, ***C2, C8***), 45.4 (***C6***), 35.8 (***C5***); δ_F (376 MHz, DMSO-d^6) -73.7 (***F9***), -74.5 (***F2***); (ES-MS$^+$) 296.9 (100 %, [M+H-CF_3COOH]$^+$, M= $C_{12}H_{15}F_9N_3O_4$).

8.5.27. {Bis[2-(2,2,2-trifluoroacetylamino)ethyl]amino}acetonitrile, 37-CN

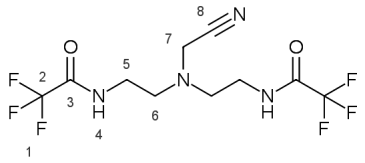

Trifluoroacetamide **37** (1.25 g, 3.0 mmol) was dissolved in acetonitrile (10 cm^3, dried over molecular sieves) and Hunig's base (1.6 cm^3, 9.2 mmol) was added. A catalytic amount (ca. 0.2 g) of potassium iodide was added prior to the addition of chloroacetonitrile (0.21cm^3, 3.3 mmol) at once. The resulting mixture was then heated at 60^{o}C for 18 hours under nitrogen. At this point, reaction progress was monitored by ES-LCMS, and more chloroacetonitrile (1.05 cm^3, 1.7 mmol) added in an attempt to convert residual starting material. Since no progress was observed after a further 4.5 hours of heating, the reaction mixture was cooled in a freezer, filtered and volatile material was removed *in*

vacuo from the filtrate. Water was added to precipitate the title compound (0.21 g, 0.63 mmol, 19%) as a white solid. mp 107-110°C; δ_H (700 MHz, DMSO-d^6) 9.24 (t, J = 6.0 Hz, 2H, ***H4***), 3.78 (s, 2H, ***H7***), 3.24 (dt, 4H, ***H5***), 2.58 (t, 4H, ***H6***); δ_C(176 MHz, DMSO-d^6) 156.8 (q, J = 36.0 Hz, ***C3***), 116.4 (m, ***C2***, ***C8***), 52.3 (***C6***), 41.9 (***C7***), 37.4 (***C5***); δ_F (376 MHz, DMSO-d^6) -74.5 (***F1***); (ES-MS$^+$) 335.9 (100 %, $[M+H]^+$); HR-MS Found 335.0934 , $C_{10}H_{13}N_4O_2F_6$ $[M+H]^+$ requires 335.0943.

8.5.28. tert-Butyl [bis(2-hydroxyethyl)amino]acetate[339], 39

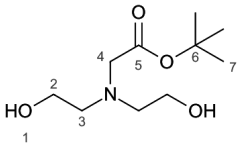

Diethanolamine (3.12 g, 29.7 mmol) was dissolved in anhydrous dichloromethane (10 cm^3), followed by t-butyl bromoacetate (1.1 cm^3, 7.5 mmol) and potassium iodide (0.25g, 1.5 mmol). The reaction mixture was stirred at room temperature under nitrogen for 20 hours prior to the addition of water. The reaction mixture was then partitioned (3x) between water and chloroform, and the combined organic extracts washed with brine. The title compound (1.5 g, 6.84 mmol, 91%) was afforded as a colourless oil after drying the organic layers over magnesium sulphate and solvent removal *in vacuo*. δ_H (700 MHz, $CDCl_3$) 3.58 (t, 4H, ***H2***), 3.32 (s, 2H, ***H4***), 3.23 (s, 2H, ***H1***), 2.82 (t, 4H, ***H3***), 1.46 (s, 9H, ***H7***);δ_C(176 MHz, $CDCl_3$) 172.4 (***C5***), 81.9 (***C6***), 59.8 (***C2***), 57.8 (***C3***), 56.7 (***C4***), 28.1 (***C7***); (ES-MS$^+$) 220.1 (100 %, $[M+H]^+$, M= $C_{10}H_{21}NO_4$).

8.5.29. Benzyl 2,5-dihydro-1H-pyrrole-1-carboxylate, 41

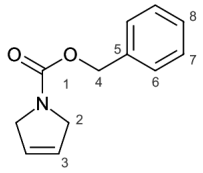

Benzyl chloroformate (0.96 cm^3, 6.74 mmol) and 3-pyrroline (0.5 cm^3, 6.58 mmol) were dissolved in dichloromethane (22 cm^3) prior to the dropwise addition of triethylamine (1.4cm^3, 10.0 mmol). Once the addition was complete, the cloudy reaction mixture was stirred at room temperature under argon for 18 hours, at which point TLC analysis (silica, diethyl ether:hexanes 60:40 v/v) indicated completion. The reaction mixture was then partitioned between aqueous sodium carbonate and dichloromethane (2x), and the combined organic extracts washed with brine prior to drying over magnesium sulphate and solvent removal *in vacuo*. Purification of the residue via column chromatography (method ii, diethyl ether:hexanes 0:100→100:0, compound eluted in ca. 50:50 v/v diethyl ether:hexanes) afforded the title compound (0.72 g, 3.55 mmol, 54%) as a colourless oil. δ_H (400

MHz, $CDCl_3$) 7.23 (m, 5H, ***H6***, ***H7***, ***H8***), 5.67 (m, 2H, ***H3***), 5.05 (s, 2H, ***H4***), 4.09 (m, 4H, ***H2***); δ_C (101 MHz, $CDCl_3$) 154.6 (***C1***), 137.0 , 128.5, 128.0, 127.9, 125.8, 125.7 (***C3***, ***C5***, ***C6***, ***C7***, ***C8***), 66.8 (***C4***), 53.4 (***C2***); GC-MS (EI^+) 203.9 ($M^{\bullet+}$, M= $C_{12}H_{13}NO_2$).

8.5.30. tert-Butyl [bis(2-chloroethyl)amino]acetate, 43

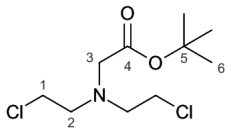

Diol **39** (0.49 g, 2.23 mmol) was dissolved in anhydrous dichloromethane (5 cm^3) and thionyl chloride (0.65 cm^3, 8.96 mmol) was added dropwise to the solution, which was refluxed under nitrogen for 1 hour. After cooling to room temperature, the excess thionyl chloride was quenched by the addition of a solution of saturated sodium carbonate. The title compound (0.48 g, 1.88 mmol, 84%) was afforded after extraction from this mixture using dichloromethane (2x). δ_H (700 MHz, $CDCl_3$) 3.53 (t, J = 7.0 Hz, 4H, ***H1***), 3.41 (s, 2H, ***H3***), 3.08 (t, J = 7.0 Hz, 4H, ***H2***), 1.46 (s, 9H, ***H6***); δ_C(176 MHz, $CDCl_3$) 170.5 (***C4***), 81.5 (***C5***), 56.5 (***C2***), 56.2 (***C3***), 42.3 (***C1***), 28.2 (***C6***); (ES-MS^+) 256.1 (100 %, $[M+H]^+$); HR-MS Found 256.0876, $C_{10}H_{20}NO_2Cl_2$ $[M+H]^+$requires 256.0871.

8.5.31. tert-Butyl [bis(2-iodoethyl)amino]acetate, 44

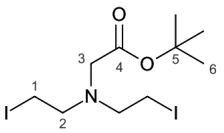

Dichloride **43** (0.79 g, 3.08 mmol), was dissolved in acetone (50 cm^3) and sodium iodide (4.6, 30.9 mmol) was added and the mixture refluxed for 16 hours, at which point TLC analysis (silica, dichloromethane) indicated completion. The solvent was then removed *in vacuo* and the residue partitioned between water and dichloromethane. The extracted organic layer was dried over magnesium sulphate and the solvent removed *in vacuo*. Diethyl ether was then added to this residue which was agitated in an ultrasonic bath. The solid material was filtered off and the diethyl ether removed *in vacuo* to afford the title compound (0.81 g, 1.84 mmol, 60%). δ_H (700 MHz, $CDCl_3$) 3.35 (s, 4H, ***H3***), 3.14 (t, J = 8.0, 2H, ***H1***), 3.06 (t, J = 8.0 2H, ***H2***), 1.45 (s, 4H, ***H6***);δ_C(176 MHz, $CDCl_3$) 170.3 (***C4***), 81.5 (***C5***), 57.0 (***C2***), 55.3 (***C3***), 28.2 (***C6***), 4.4 (***C1***); (ES-MS^+) 439.9 (100 %, $[M+H]^+$); HR-MS Found 439.9579, $C_{10}H_{20}NO_2I_2$ $[M+H]^+$requires 439.9584.

8.5.32. Diethyl {[(2,4-dimethoxyphenyl)methyl]amino}malonate[340], 45

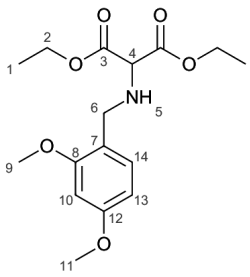

Diethyl aminomalonate hydrochloride (1 g, 4.7 mmol) was dissolved in 1,2-dichloroethane (17 cm^3) and triethylamine (0.98 cm^3, 7.0 mmol) was added, followed by the addition of 2,4-dimethoxy benzaldehyde (0.77 g, 4.6 mmol) and sodium triacetoxyborohydride (2.0 g, 9.4 mmol). The mixture was allowed to stir at room temperature under nitrogen for 24 hours. Following this, the reaction mixture was basified by the addition of saturated sodium carbonate and then partitioned between saturated sodium carbonate and dichloromethane. The organic extract was dried over magnesium sulphate and the solvent removed *in vacuo*. The residue was purified by column chromatography (method i, silica, acetonitrile:dichloromethane 0:100→50:50 compound eluted in ca. 30:70 v/v acetonitrile:dichloromethane) to afford the title compound (1.05 g, 3.2 mmol, 68%) as a yellow oil. δ_H (700 MHz, $CDCl_3$) 7.13 (d, 2H, ***H14***), 6.42 (m, 2H, ***H10***, ***H13***), 4.17 (dq, J = 7.2, 0.8 Hz, 4H, ***H2***), 4.04 (d, J = 0.8 Hz, 1H, ***H4***), 3.80 (s, 3H, ***H9***), 3.79 (s, 3H, ***H11***), 3.76 (s, 2H, ***H6***), 2.38 (s, 1H, ***H5***) 1.25 (td, J = 7.2, 0.8 Hz, 6H, ***H1***); δ_C(176 MHz, $CDCl_3$) 168.8 (***C3***), 160.5 (***C12***), 158.9 (***C8***), 130.8 (***C14***), 119.6 (***C7***), 103.9 (***C13***), 98.6 (***C10***), 64.5 (***C4***), 61.8 (***C2***), 55.5 (***C11***), 55.2 (***C9***), 47.0 (***C6***), 14.2 (***C1***); (ES-MS^+) 326.1 (100 %, $[M+H]^+$, M= $C_{16}H_{23}NO_6$).

8.5.33. Diethyl benzylaminomethylmalonate, 46

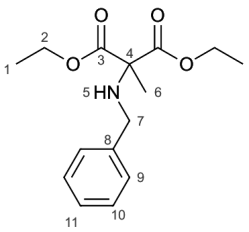

Benzylamine (0.86 cm^3, 7.8 mmol) was dissolved in acetonitrile (19 cm^3, dried over molecular sieves) and potassium carbonate (1.19 g, 8.6 mmol) was suspended in the solution. Diethyl bromomethylmalonate (1.5 cm^3, 7.8 mmol) was then dissolved in the mixture, which was heated at 40°C under argon for 21 hours, followed by heating at 60°C for a further 9 hours, at which point TLC analysis (silica, in dichloromethane) showed the depletion of starting material. Once cooled, the reaction mixture was filtered and the solvent removed *in vacuo* and the residue partitioned between aqueous sodium

bicarbonate and dichloromethane. The organic layer was extracted, dried over magnesium sulphate and purified by column chromatography (method i, silica, diethyl ether:hexanes 0:100→80:20 v/v) to afford the title compound (0.51 g, 1.8 mmol, 23%) as a pale yellow to colourless oil. δ_H (700 MHz, $CDCl_3$) 7.30 (m, 2H, ***H9***), 7.26 (m, 2H, ***H10***), 7.20 (m, 1H, ***H11***), 4.16 (q, J = 7.1 Hz, 4H, ***H2***), 3.66 (s, 2H, ***H7***), 1.57 (s, 3H, ***H6***), 1.21 (t, J = 7.1 Hz, 6H, ***H1***); δ_C(176 MHz, $CDCl_3$) 170.6 (***C3***), 139.7 (***C8***), 128.4 (***C10***), 128.3 (***C9***), 127.1 (***C11***), 66.8 (***C4***), 61.6 (***C2***), 48.1 (***C7***), 19.6 (***C6***), 14.0 (***C1***); (ES-MS^+) 280.1 (100 %, $[M+H]^+$); HR-MS Found 280.1563, $C_{15}H_{22}NO_4$ $[M+H]^+$requires 280.1549.

8.5.34. Di-tert-butyl benzylaminomalonate[315], 47

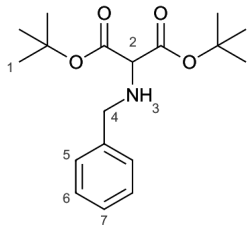

Bromomalonate **36** (1.0 g, 3.4 mmol), and potassium carbonate (0.51 g, 3.7 mmol) were added to acetonitrile (8 cm^3, dried over molecular sieves) and benzylamine (0.37 cm^3, 3.4 mmol) was added dropwise to the mixture, which was then allowed to stir under argon at room temperature for 2 hours, at which point TLC analysis (diethyl ether:hexanes 20:80 v/v) showed the consumption of starting material. The reaction mixture was then filtered, the solvent removed from the filtrate *in vacuo* and the residue purified via column chromatography (method i, silica, diethyl ether:hexanes 0:100→30:70 v/v) to afford the title compound (0.41 g, 1.3 mmol, 38%) as a yellow oil.* δ_H (400 MHz, $CDCl_3$) 7.35 (m, 5H, ***H5*** , ***H6***, ***H7***), 3.91 (m, 3H, ***H2***, ***H4***), 3.06 (s, 1H, ***H4***), 1.46 (s, 18H, ***H1***).

*The rapid formation of a solid crust on samples of this compound was construed as evidence of its reaction with air. Thus, it is advised that the compound is used as soon as it is made.

8.5.35. Di-tert-butyl (2-tert-butyldimethylsiloxyethylamino)malonate, 48

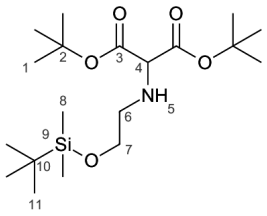

Preparation of TBDMS-protected ethanolamine. tert-Butyldimethylsilyl chloride (5.3 g, 35.2 mmol) and imidazole (4.5 g, 66.1 mmol) were dissolved in dichloromethane (20 cm^3, anhydrous) and ethanolamine (2 cm^3, 33.1 mmol) was added dropwise to the solution at room temperature under an argon atmosphere. Once the addition was complete, the reaction mixture was stirred at room temperature for 90 minutes, after which time a solution of saturated sodium carbonate was slowly added (until basic pH) to the stirring reaction mixture, which was then transferred to a separating funnel. The aqueous layer was washed with dichloromethane (2x) and the combined organic extracts were dried over magnesium sulphate and the solvent removed *in vacuo*. The residue was then redissolved in diethyl ether, filtered through a sinter funnel and the solvent removed *in vacuo* again to afford the title compound (3.71 g, 21.2 mmol, 64%) as a yellow oil. δ_H (400 MHz, $CDCl_3$) 3.62 (t, J = 5.5 Hz, 4H), 2.77 (t, J = 5.5 Hz, 4H), 0.89 (s, 9H), 0.06 (s, 6H);δ_C(101 MHz, $CDCl_3$) 65.1, 44.2, 25.9, 18.3, -5.3.

Di-tert-butyl (2-tert-butyldimethylsiloxyethylamino)malonate. **36**, (0.86 g, 2.9 mmol), potassium carbonate (0.34 g, 2.5 mmol) were added to acetonitrile (6 cm^3, dried over molecular sieves) prior to the addition of the TBDMS-protected ethanolamine prepared above (0.48 g, 2.5 mmol) to the solution at once. The reaction mixture was then allowed to stir at room temperature under argon for 19 hours, at which point TLC analysis (silica, diethyl ether/hexanes 20:80 v/v) showed consumption of the protected ethanolamine. The reaction mixture was then filtered and the solvent removed *in vacuo* prior to purification of the residue via column chromatography (method i, silica, diethyl ether:hexanes 0:100→30:70 v/v) to afford the title compound (0.63 g, 1.6 mmol, 64%). δ_H (700 MHz, $CDCl_3$) 3.92 (s, 1H, *H**4***), 3.73 (t, 2H, *H**7***), 2.71 (t, 2H, *H**6***), 2.34 (s, 1H, *H**5***), 1.47 (s, 18H, *H**1***), 0.90 (s, 9H, *H**11***), 0.06 (s, 1H, *H**8***); δ_C(176 MHz, $CDCl_3$) 167.6 (*C**3***), 82.1 (*C**2***), 66.5 (*C**7***), 62.5 (*C**4***), 49.2 (*C**6***), 27.9 (*C**1***), 25.9 (*C**10***), 18.26 (*C**11***), -5.36 (*C**8***); δ_{Si}(139 MHz, $CDCl_3$) 19.9 (*Si**9***); (ES-MS^+) 390.2 (100 %, $[M+H]^+$); HR-MS Found 390.2666, $C_{19}H_{40}NO_5Si$ $[M+H]^+$requires 390.2676.

8.6. Determination of ligand stock solution concentrations via quantitative ^{1}H NMR

8.6.1. Preparation of t-butanol standard solution

Deuterium oxide (ca. 7 cm^3), was added to a volumetric flask (10 cm^3), which was then placed on a five-digit balance which was then tared. t-Butanol (0.100 cm^3, Aldrich anhydrous) was then added to the volumetric flask, and the change in weight recorded. The solution was then made up to the mark using the requisite amount of deuterium oxide. From the mass of t-butanol added, the molar concentration of t-butanol in deuterium oxide could be calculated.

8.6.2. Determination of ligand solution concentration

A mass of the ligand to be studied (corresponding to a solution concentration of 0.5 or 0.25 mol dm^{-3} , based on the ligand structural formula), was dissolved in dipotassium hydrogen phosphate (0.2 mol dm^{-3} for non phenolate ligands, and 0.4 mol dm^{-3} for phenolate ligands), and aqueous sodium hydroxide (6 mol dm^{-3} , added in 5μL increments) was added if the ligand precipitation occurred. An aliquot of this solution (50 μL) was then diluted tenfold in dipotassium hydrogen phosphate (450μL, 0.2 mol dm^{-3}), and an equal volume of the t-butanol stock solution prepared in ***Section 8.6.1*** was added to the diluted ligand solution, which was mixed thoroughly and transferred to an NMR tube prior to ^{1}H NMR spectrum acquisition on a Bruker Avance 400 NMR spectrometer using a bespoke quantitative water suppression experiment. Integral ratios could then be measured using standard offline NMR processing software e.g. MestReNova after manual phase and baseline corrections, from which the *in situ* ligand concentration was calculated using the equations in ***Section 2.2***. This value was one-tenth of the concentration of the original stock. Using the measured concentration, the original stock could then be manipulated as necessary.

8.7. Analysis of biological properties

All techniques were performed aseptically unless indicated otherwise.

8.7.1. Preparation of overnight cultures of *E. coli* JM101 from freezer stocks

Revival of bacteria from low temperature storage (-78^{o}C) was performed by using a sterile pipette tip to streak an aliquot of frozen culture to an LB agar plate at room temperature. The plate was then incubated at 37^{o}C overnight to afford single colonies of *E. coli* JM101 and were stored in a commercial refrigerator for up to a week. Generation of a culture of approximately 10^9CFU/cm^3 was performed by picking up a single colony of *E. coli* via a sterile pipette tip that was then ejected into

10 cm^3 sterile Oxoid (stock no. CM0129) Tryptone Soya Broth (TSB). The inoculated media was incubated at 37°C overnight with shaking to generate a turbid suspension of cells.

8.7.2. Assessment of relationship between colony forming units and optical density at 600nm (OD_{600})

An overnight culture of *E. coli* JM101 was prepared in a manner identical to that described in section ***8.7.1***. Once grown, serial twofold dilution on this culture was performed in TSB (Oxoid CM0129B) in a BD 48-well treated tissue culture plate until the $\frac{1}{1024}$ dilution. The optical densities at 600 nm (OD_{600}) of each dilution ($\frac{1}{2}$x, $\frac{1}{4}$x, $\frac{1}{8}$x, $\frac{1}{16}$x, $\frac{1}{32}$x, $\frac{1}{64}$x, $\frac{1}{128}$x, $\frac{1}{256}$x, $\frac{1}{512}$x and $\frac{1}{1024}$x) were then recorded and a subsequent serial tenfold dilution of each of these dilutions was performed until the 10^{-8} dilution was reached, using aqueous saline. Aliquots of each dilution in saline (10μL) were then spotted onto LB agar plates in the manner described by Miles and Misra[341], and the plates incubated at 37°C overnight. Visible colonies were then counted and adjusted to reflect the number of colony forming units in 1 cm^3 of the parent dilution (CFU cm^{-3}) . Only counts from inocula presenting between five and fifty unambiguously single colonies were used. The experiment was performed in duplicate, and average values of OD_{600} and CFU cm^{-3} were used to derive a linear relation between the two values.

8.7.3. Growth inhibition studies on *E. Coli* JM101

An overnight culture was prepared according to ***Section 8.7.1***. This culture was then subjected to a 1 in 900 dilution, from which tissue culture plates could be populated. VWR 96-well treated tissue culture plates were used for all studies. For negative controls, 180μL sterile TSB and 20μL diluting solvent (typically 0.2 M K_2HPO_4, specific concentrations are given in the main text) were used. For positive controls, 180μL diluted culture and 20μL diluting solvent were used. Positive and negative controls were separated by at least one well on all plates studied. Solutions of ligand in the diluting solvent (adjusted to pH 7 using 5M NaOH$\pm$0.5 unless otherwise indicated) were subject to filter sterilisation using 0.22μm syringe filters (when sufficient material was available) prior to serial dilution to concentrations ten times those to be used *in situ*. Therefore, 20 μL solutions of the 10x ligand solutions were added to the plate, followed by the addition of 180μL of diluted culture giving a cell density of the order of 10^6CFU/cm^3. All growth curves were performed in triplicate.

Optical density readings at 600 and 620 nm at 37°C were performed on a BioTek synergy H4 kinetic plate reader set to read once an hour for 16 hours. Prior to each reading, the plate was shaken for ten seconds.

8.7.4. Assessment of inhibitory concentrations against *E. Coli* JM101 for ICP-MS studies

An overnight culture was prepared according to ***Section 8.7.1*** and subjected to a tenfold dilution resulting in a cell density of 10^8 CFU/ cm^3, verified by use of a CASY model TT cell counter. Ligand stock solutions were then prepared in an appropriate diluting solvent (typically 0.2M $K_2HPO_4$and 5M NaOH to aid dissolution, specific concentrations are given in the main text) to 100x the intended concentration *in situ*.

Autoclaved, oven-dried 100cm^3conical flasks equipped with sponge bungs were then charged with 19.6 cm^3sterile TSB, 200μL of 100x ligand solution, or 200μL of the diluting solvent for the positive control. Aliquots (200μL) of the diluted overnight culture were then added to each flask to give cultures of density 10^6 CFU/ cm^3. These cultures were then incubated for 16 hours at 37°C with shaking. Once elapsed, the OD_{600} and CFU/ cm^3 (via cell counter) values for the positive control and for each ligand concentration were recorded. Percentage inhibition was calculated by division of these OD_{600} and CFU/ cm^3 values for each ligand concentration by those recorded for the positive control.

8.7.5. Preparation of ligand-treated cultures of *E. coli* JM101 for ICP-MS analysis

An overnight culture was prepared according to ***Section 8.7.1***, subjected to a tenfold dilution resulting in a cell density of 10^8 CFU/ cm^3, and 0.5 cm^3 of the diluted sulture was added to an acid-washed 250 cm^3 conical flask containing 49 cm^3 sterile TSB and 0.5 cm^3 of a 100x ligand stock solution (***Section 8.7.4***). These cultures were then incubated for 16 hours at 37°C with shaking. After this incubation period, 45 cm^3 of this large scale culture was transferred to a 50 cm^3 Falcon tube and centrifuged at 10°C for 40 minutes at 4000 rpm. In the meantime, the cell count of the large-scale culture was measured using a CASY model TT cell counter using the residual culture in the conical flask, to assess the actual extent of growth inhibition. Once centrifugation was complete, the supernatant was discarded and the cells resuspended in a washing buffer (10 cm^3) consisting of 0.5 mol dm^{-3} sorbitol and 10mM HEPES, pH= 7.8 prior to re-centrifugation for 10 minutes at 10°C at 4000 rpm. Once again, the supernatant was discarded, and the cells were resuspended in a further 10 cm^3 of the washing buffer. An additional cycle of centrifugation for 10 minutes was then performed. After this cycle was complete, the cells were resuspended in a 5 cm^3 of the washing buffer and centrifuged at for 15 minutes at 10°C and 4500 rpm. The supernatant was then decanted off, and the cells were resuspended in 5 cm^3 of high-purity 65% nitric acid and left to digest for at least 48 hours prior to analysis.

8.7.6. ICP-MS analysis of cell digests

A diluent composed of aqueous nitric acid (400 cm^3, 2 % v/v), an ICP-MS standard solution (500 cm^3,100 ppb Ag in 2 % nitric acid) and 65% high-purity nitric acid (50 cm^3) was used to prepare a $\frac{1}{10}$x, $\frac{1}{20}$x, and $\frac{1}{100}$x, dilution of the cell digest. Using the same diluent, 0, 0.1, 0.2, 0.5, 1, 2, 5, 10, 20, 50, 100, 200, 500 and 1000 ppb standard solutions were prepared from a multi-element stock solution containing calcium, magnesium, cobalt, copper, iron, manganese, nickel and zinc, all at 1000 ppm, to generate the calibration curve. All ICP-MS analyses were performed by Dr. Deenah Osman.

8.7.7. Assessment of *E. Coli* JM101 growth inhibition via a disc-diffusion based method

An overnight culture of *E. Coli* JM101 was prepared in a manner identical to that described in ***Section 8.7.1*** and subjected to a tenfold dilution in TSB to give a cell density of 10^8 CFU/ cm^3. An aliquot (100 μL) of this culture was subsequently used to inoculate warmed (55°C) agar overlays (4 cm^3 each, 0.6% w/v agar in water) and each inoculated overlay was rapidly poured onto pre-warmed plates loaded with LB agar (20 cm^3) to give a combined agar height of 6mm. Once the inoculated plates were cooled to room temperature, four sterile paper discs ($\varnothing$=1 cm)* were placed on each quadrant. Solutions (20μL) of the ligand under study in DMSO/water (3:1 v/v) at the desired concentrations were loaded onto each disc using a Gilson pipette. The plates were then allowed to stand for five minutes to allow the solution to permeate the agar before being incubated overnight at 37°C on a single incubator shelf.

Following incubation, the plates were placed against a blank background and photographed with a ruler in shot to serve as an internal scale. Care was taken to position the camera as close to perpendicular to the background as possible. The resulting images were then processed using the NIH ImageJ suite[342] to enhance the contrast between the zones of inhibited and normal bacterial growth from which the zone of inhibition could be measured.

8.8. Estimation of partition coefficients

8.8.1. General procedure for the preparation of Fe^{3+} complexes of free ligands

The ligand to be complexed (typically 0.02 mmol) was added at once to a stock solution of Iron (III) chloride (typically 12.5 mM, 1 cm^3, 0.125 mmol) in a conical-bottomed Schlenk tube. If necessary, water was added in 1 cm^3 portions to facilitate dissolution of the ligand and the yellow solution was stirred under nitrogen for at least 1 hour. If precipitation occurred during this time then aqueous sodium hydroxide (10 wt. %) was carefully added until a homogeneous solution was again obtained and the mixture heated at 50°C for at least 1 more hour.

*Prepared from Whatman No. 1 filter paper using an ordinary circle cutter. Once cut, the discs may be placed in a glass Petri dish, autoclaved and dried in the usual way.

Aqueous sodium hydroxide (10 wt. %) was then added via Gilson pipette in 10μL aliquots until the pH of the reaction mixture was around 4 and a persistent rust-coloured precipitate was observed. The reaction mixture was then filtered through a 0.22μm syringe filter to afford the final complex in solution.

Fe-AmGly$_2$. Yellow-orange in solution. λ_{max}(PBS) /nm 250, 380; λ_{max}(DMSO) /nm 405; (ES-MS$^+$) 459.9 (100 %, [M+H]$^+$); (ES-MS$^-$) 458.1 (100 %, [M-H]$^-$); HR-MS Found 458.0571, $C_{14}H_{19}N_4O_{10}{}^{54}Fe$ [M+H]$^+$ requires 458.0576.

Fe-EDTA. Pale yellow in solution. (ES-MS$^+$) 345.9 (100 %, [M+H]$^+$, M= $C_{10}H_{12}FeN_2O_8$); (ES-MS$^-$) 344.2 (100 %, [M-H]$^-$).

Fe-HBED. Wine-red in solution. λ_{max}(PBS) /nm 277, 315, 490; (ES-MS$^-$) 440.1 (100 %, [M-H]$^-$); HR-MS Found 438.0727, $C_{20}H_{20}N_2O_6{}^{54}Fe$ [M-H]$^-$ requires 438.0717.

Fe-AmBn$_2$. Pale yellow in solution. λ_{max}(PBS) /nm 283; (ES-MS$^+$) 524.9 (100 %, [M+H]$^+$); HR-MS Found 522.1411, $C_{24}H_{28}N_4O_6{}^{54}Fe$ [M+H]$^+$ requires 522.1405.

Fe-AmGly$_1$. Yellow-orange in solution. λ_{max}(PBS) /nm 283, 374; λ_{max}(DMSO) /nm 398; (ES-MS$^-$) 401.0 (100 %, [M-H]$^-$); HR-MS Found 401.0377, $C_{12}H_{17}N_3O_9{}^{54}Fe$ [M-H]$^-$ requires 401.0361.

Fe-BrHBED. Wine-red in solution. λ_{max}(PBS) /nm 242, 283, 475;λ_{max}(DMSO) /nm 286, 468; (ES+MS$^+$) 599.5 (100 %, [M+H]$^+$); (ES-MS$^-$) 597.7 (100 %, [M-H]$^-$); HR-MS Found 597.8857, $C_{20}H_{18}N_2O_6Br_2{}^{54}Fe$ [M-H]$^-$ requires 597.8752.

Fe-EHPG. Wine-red in solution. λ_{max}(PBS) /nm 282, 484;λ_{max}(DMSO) /nm 288, 467; (ES-MS$^-$) 412.1 (100 %, [M-H]$^-$); HR-MS Found 410.0422, $C_{18}H_{16}N_2O_6{}^{54}Fe$ [M-H]$^-$ requires 410.0404.

Fe-MeEHPG. Wine-red in solution. (ES-MS$^-$) 440.1 (100 %, [M-H]$^-$, M= $C_{20}H_{21}FeN_2O_6$).

Fe-DTPA. Pale yellow in solution. λ_{max}(PBS) /nm 260; λ_{max}(DMSO) /nm 280; (ES-MS$^-$) 445.2 (100 %, [M-H]$^-$, M= $C_{14}H_{20}FeN_3O_{10}$).

Fe-EGTA. Pale yellow in solution. λ_{max}(PBS) /nm 273; (ES-MS$^-$) 432.0 (100 %, [M-H]$^-$, M= $C_{14}H_{21}FeN_2O_{10}$).

Fe-NOTA. Pale yellow in solution. λ_{max}(DMSO) /nm 260.

8.8.2. General procedure for estimating the partition coefficients of Fe^{3+} complexes

Preliminary work. Solutions prepared in the manner described in ***Section 8.8.1*** were subject to a $\frac{1}{10}$x dilution into a modified PBS system (K_2HPO_4 0.075 mol dm^{-3}, KH_2PO_4 0.025 mol dm^{-3}, KCl 0.15 mol dm^{-3} , adjusted to pH 7.4) to provide a buffered stock that was subject to additional serial dilution. Typically, the serial dilutions made from this stock were ($\frac{1}{10}$x, $\frac{1}{20}$x, $\frac{1}{40}$x, and $\frac{1}{50}$x), all of which had their UV-Vis spectra recorded in glass cuvettes. Serial dilution was then repeated from the $\frac{1}{10}$x stock using DMSO using the same dilution factors and the UV-Vis spectra of these solutions were recorded also. From the spectra recorded in DMSO, a wavelength exceeding 350 nm that exhibited sufficient absorption ($0.1 \leq A \leq 1$) was selected for the next part of the experiment.

Experimental procedure. A $\frac{1}{20}$x dilution in the modified PBS system was prepared of the metal complex stock prepared in ***Section 8.8.1*** and the pH of the diluted solution adjusted to pH$\approx$7.4 . An aliquot of known volume ($\geq$750μL) was then added to a 2 cm^3 sample vial, to which an equal volume of dichloroethane was added. The vial was sealed and mixed in a vertical turntable overnight. After the mixing period phases were separated by centrifugation at 2500 rpm for 1 minute. A sample of each phase (40μL) was then added to plastic Eppendorf tubes charged with DMSO (960μL) and the resulting mixture was vortexed to a homogeneous solution. Portions (200μL) of the DMSO solutions from each phase was then loaded onto a 96-well plate (VWR 734-2327). This part of the experiment was performed in duplicate, and the samples from the replicate were loaded onto the same plate.

Prior to reading the absorbance values at the wavelength determined above, a linear absorbance response was confirmed by loading 200μL of the $\frac{1}{10}$x, $\frac{1}{20}$x, $\frac{1}{40}$x, and $\frac{1}{50}$x solutions prepared previously in DMSO and measuring their absorbance in plate along with that of a solvent blank. Two samples of each dilution were placed on different rows to check for the effect of aberrations on the plate, which was then read.

Analysis of the data. Absorbance values for the solvent blanks were subtracted from the calibration and analyte wells. The absorption of the wells containing the tested dichloroethane and buffer phases was compared to adjacent empty wells after solvent subtraction, and the absorbance of the analyte wells was set to zero if the absorbance values were similar. Once this additional correction was performed, the absorbance of the dichloroethane layer was divided by the absorbance of the buffer layer for each replicate to calculate the distribution coefficient for each replicate. These individual values were averaged to give the reported distribution coefficient.

8.8.3. Procedure for free ligand partition coefficients

The ligand to be studied (ca. 10-20 mg), was dissolved in a modified PBS system (1 cm^3, K_2HPO_4 0.075 mol dm^{-3}, KH_2PO_4 0.025 mol dm^{-3}, KCl 0.15 mol dm^{-3}, D_2O used instead of water) in an

Eppendorf tube and the pD adjusted to $\approx$7. This solution was then placed into a glass sample vial and the volume increased to 2cm^3 using more PBS. $CDCl_3$ (2 cm^3) was then added to the sample vial which was then agitated vigorously by hand. The vial lid was then removed to allow for pressure equilibration and replaced. Following this initial equilibration, the vial was placed in a vertical turntable and allowed to mix for at least 2 hours.

For measurement, the phases were separated via centrifugation at 1500 rpm for at least two minutes prior to sampling of each phase (the aqueous phase being sampled first) by drawing up a known volume (usually 800-1000 μL) in silicone-free plastic syringes and spiking the samples of either phase with t-butanol (1 vol. %) as an internal standard (***Section 2.2***). The samples were then transferred into NMR tubes and normal ^{1}H spectra acquired. If phase partitioning was observed, the spectra could be re-run under quantitative conditions and the integral ratios calculated to derive the chlroform-buffer partition coefficient, P_{CDCl_3}.

8.9. Fura-2 partitioning experiments

It is the opinion of this author that the procedure for this experiment is best presented as a protocol, due to the iterative nature of the experiment. ***Section A****,* covers the methodology.

A. Fura-2 partitioning protocol

A.1. Preparation

A.1.1. Ligand stocks:

- Make up 0.11M stock of the ligand in 18.2 MΩ water. Change pH to dissolve as necessary.
- Quantify solution stock concentration using the procedure in ***Section (8.6).***
- Dilute back to 0.1M using integral ratio.
- Serial dilute to 100μM in pH 7.0 HEPES at 0.1M KCl (referred to as the "**buffer system**" from here).
- The resulting ligand solution is solution **A**.

A.1.2. Metal ion stocks:

- Make up 10ml of a 10mM stock of $CaCl_2$or $ZnCl_2$ in a 15 ml falcon tube in 18.2 MΩ water.
- Verify by ICP-MS and if necessary introduce a dilution correction.
- Dilute 10mM stock to make 5 cm^3 1mM stock in the **buffer system**.
- From this stock make sub-stocks of the following concentrations in the buffer system (Solutions **B-1** to **B-11**):

Row	**Volume 1 mM stock** /μL	**Buffer system volume** /μL
1	0	1000
2	80	920
3	160	840
4	240	760
5	320	680
6	400	600
7	480	520
8	560	440
9	640	360
10	720	280
11	800	200

A.2. Selection of metal ion stock (Metal ion fluorescence titration)

A.2.1. Fura-2 concentration adjustment

- Prepare 20μM stock solution from 1 mM **Fura-2** stock stored in DMSO, using the **buffer system**.
- The stock is kept in the freezer in DMSO usually there are 50 μL in each Eppendorf..
- Verify concentration by UV-Vis, using ϵ_{363}=**28000 M^{-1}cm^{-1}**.
- Keep stock cold and in dark until needed. This is solution **C**.

A.3. Titration in plate

- Add 95 μL **buffer system** to each well in a 96-well plate to be used in this stage of the experiment.
- Add 5 μL of each M^{2+} stock made (solutions **B-1** to **B-11**) to each of these wells.
- Add 100 μL of the **Fura-2** solution (solution **C**) to each of these wells.
- Aspirate with a pipette.
- Incubate 10 min at 25^{o}C.
- Record emission spectrum (λ_{ex}=340 nm) for each well.
- Plot emission intensity at λ=510 nm and see which solutions comprise the linear part of the titration curve (fluorescence intensity vs [M^{2+}]). Determine where the linear part ends/saturation is achieved.
- Choose a solution that falls on the linear part of the titration curve for all subsequent experiments.
- Repeat measurement for this stock and plot its fluorescence value on the same curve as the one to check linearity.
- If it's in linear region then proceed, if not choose a more dilute value and try again. This metal ion stock is solution **D**.

A.4. Check for ligand autofluorescence

- Add 175 μL of **buffer system** to new wells on the plate, one for each ligand.
- Add 5 μL of the selected Ca^{2+} or Zn^{2+} stock (solution **D**) to these wells.

- To new wells on the same plate, add 20 μL of a ligand stock (solution **A**).
- Aspirate with a pipette.
- Incubate 10 mins at 25^{o}C.
- Record fluorescence at λ_{em}=510 nm (λ_{ex}=340 nm).
- If values significant then subtract from fluorescence intensity in subsequent steps.

A.5. Metal ion partitioning experiments

A.5.1. Fura-2 First

- Add 75 μL **buffer system**.
- Add 100μL **Fura-2** stock (solution **C**) to new wells in the plate for each ligand to be studied.
- Add 5 μL metal ion stock (solution **D**) to these wells.
- Add 20 μL ligand stock (solution **A**) to wells.
- Aspirate with a pipette.
- Incubate 10 min at 25^{o}C.
- Record fluorescence at λ_{em}=510 nm (λ_{ex}=340 nm).

A.5.2. Ligand First

- Add 75 μL **buffer system** to new wells on plate for each ligand.
- Add 20 μL ligand stock (solution **A**) to wells.
- Add 5 μL metal ion stock (solution **D**) to these wells.
- Add 100 μL **Fura-2** stock (solution **C**) to new wells in the plate for each ligand to be studied.
- Aspirate with a pipette.
- Incubate 10 min at 25^{o}C.
- Record fluorescence at λ_{em}=510 nm (λ_{ex}=340 nm).
- Check values of fluorescence from either order of addition are within experimental error of one another (only possible with technical repeats) to ensure equilibrium has been reached. If not, incubate the plate for a further ten minutes and read again. Repeat as necessary, noting how long it takes to reach equilibrium.

A.6. Analysis of the data

- Plot out linear part of titration curve obtained in A.3. Fit a line to express fluorescence intensity as a function of $[M^{2+}]$.
- Use the line to determine M^{2+} depletion from **Fura-2** using fluorescence intensity values obtained when in competition with each ligand.

B. Some precursors to AAZTA ligands

These intermediates were synthesised over the course of this work, either as a way to differentiate the *endo*- and exocyclic amine groups in the ligand. Some attempts were made to prepare a lipophilic variant of **AAZTA**, but they are not discussed here owing to their similarity to previously published work.[343]

B.1. Tert-butyl [6-methyl-6-nitro-4-(tert-butoxycarbonylmethyl)-1,4-diazepin-1-yl]acetate, NO_2-AAZ-tBu

This compound was synthesised to compliment the routes devised by Waldron. In the Waldron synthesis of precursors to orthogonally functionalised **AAZTA** derivatives, the dimethoxybenzyl protecting group was used to generate a versatile intermediate (***Scheme 57***) in four steps.

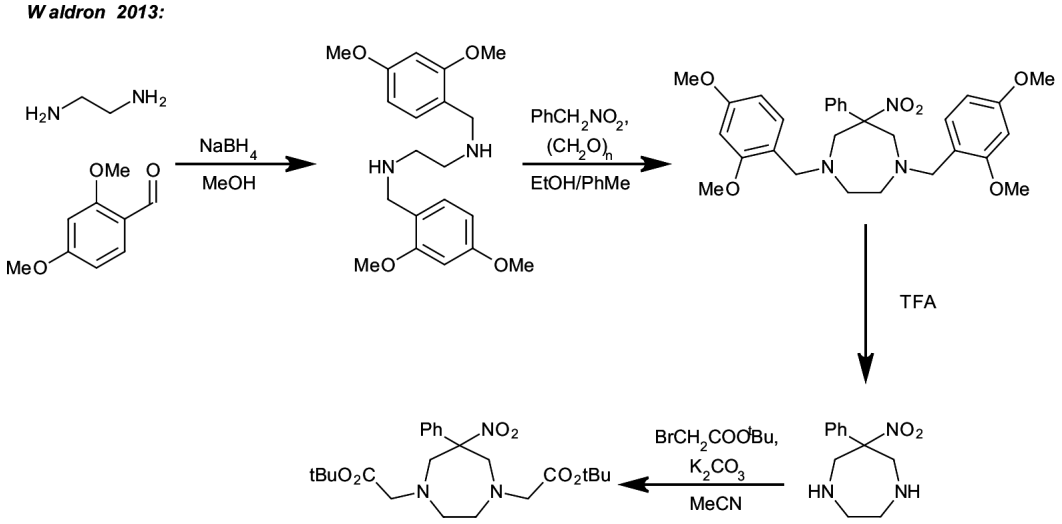

Scheme 57: Waldron route to orthogonally functionalisable **AAZTA** precursors.

In contrast, the title compound was synthesised in a total of three steps, representing what could be a more efficient synthesis of a similar intermediate if only exocyclic amine functionalisation was desired (***Scheme 58***).

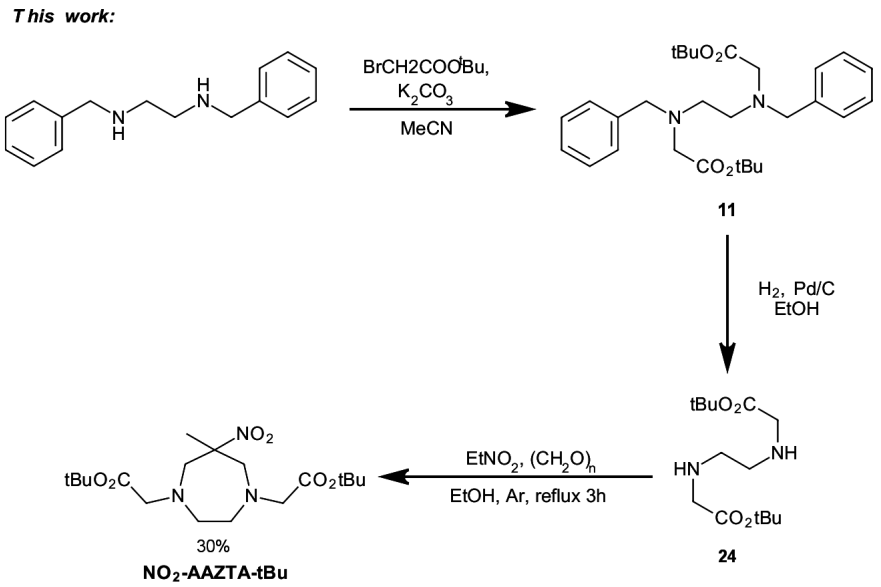

Scheme 58: A three-step route to **NO_2-AAZTA-tBu**.

Further development of a route using this intermediate was discontinued because attempts to reduce the nitro group of **NO_2-AAZ-tBu** using hydrogen gas were unsuccessful. An experimental procedure for **NO_2-AAZ-tBu** follows:

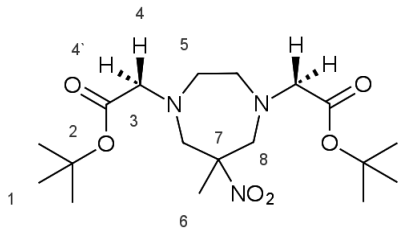

Compound **12** (52 mg, 0.18 mmol) was dissolved in ethanol (ca. 5 cm^3) and paraformaldehyde (16 mg, 0.54 mmol) was added at once. Shortly after, nitroethane (14.2μL, 0.20 mmol) was added into the reaction mixture via a Gilson pipette and the mixture refluxed under argon for three hours, and which point ^{1}H NMR spectroscopy indicated completion of the reaction. Once cooled, the reaction mixture was partitioned between saturated sodium carbonate and dichloromethane and the organic layer extracted (3x). The organic layers were dried using magnesium sulphate and the volume reduced *in vacuo* for purification by column chromatography (silica, microscale method, compound eluted in 20:79:1 ethyl acetate:hexanes:triethylamine). Removal of the solvent afforded the title compound (23.2 mg, 0.06 mmol, 30%) as a colourless oil. ν_{max}/cm^{-1}(ATR) 2976 (sp^3C-H st), 1729 (ester C=O st), 1534 (NO_2st), 1148 (ester C-O st); δ_H (700 MHz, $CDCl_3$) 3.65 (d, J = 14.9 Hz, 2H, ***H8***$_{eq}$), 3.48 (d, J = 17.3 Hz, 2H, ***H4***), 3.33 (d, J = 17.3 Hz, 2H, ***H4'***), 3.12 (d, J = 14.9 Hz, 2H, ***H8***$_{eq}$), 2.94 – 2.83 (m, 4H, ***H5***), 1.46 (s, 21H, ***H1***, ***H6***); δ_C(176 MHz, $CDCl_3$) 171 (***C3***) , 92 (***C7***) , 81 (***C2***) , 62 (***C8***) , 61 (***C4***) , 56 (***C5***) , 28 (***C1***) , 24 (***C6***); (ES-MS^+) 388.0 (100 %, $[M+H]^+$); HR-MS Found 388.2429, $C_{18}H_{34}N_3O_6$ $[M+H]^+$requires 388.2448.

B.2. o-({4-[(o-Hydroxyphenyl)methyl]-6-methyl-6-nitro-1,4-diazepin-1-yl} methyl)phenol, NO_2-AAZ-HB

This was intended as a precursor to an **AAZTA** derivative bearing two phenolic donors attached to the endocyclic nitrogens so as to give a ligand that could form strong complexes with Fe^{3+}. Using the precursor **4-H-21**, which could be prepared in large quantities **NO_2-AAZ-HB** could easily be prepared (***Scheme 59***), but reduction of the nitro group could not be achieved using palladium-catalysed hydrogenation using both hydrogen gas and transfer hydrogenation procedures, or nickel-based reagents such as nickel boride, or Raney® nickel.

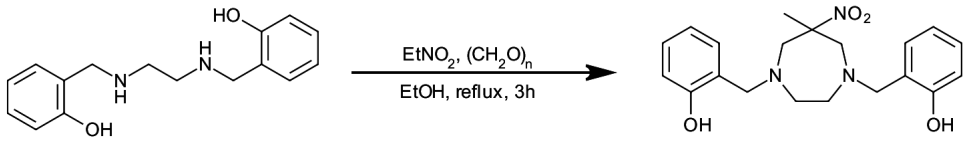

4-H-21 — 23% — **NO_2-AAZ-HB**

Scheme 59: Synthesis of **NO_2-AAZ-HB**.

An experimental procedure for **NO_2-AAZ-HB** is overleaf.

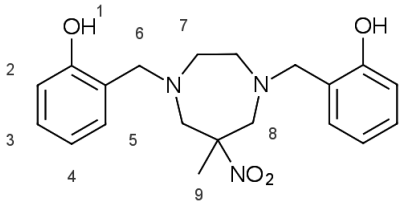

Aminophenol **4-H-21** (0.26 g, 0.95 mmol) was partially dissolved in ethanol (4 cm^3) and stirred at room temperature while paraformaldehyde (85 mg, 2.83 mmol based on repeat unit M=30 g mol^{-1}) and nitroethane (71μL, 0.99 mmol) were added sequentially. The solution was then refluxed for three hours and monitored by TLC (90:10 v/v dichloromethane:methanol) which indicated the consumption of starting material within two hours. After cooling to room temperature, the solvent was removed *in vacuo* and purified by column chromatography (method ii, dichloromethane:hexane, compound eluted in 50:50 v/v dichloromethane:hexane) to give a white solid that was crystallised via slow evaporation from chloroform to give beautiful white crystals (0.08 g, 0.22 mmol, 23%). Slow evaporation of this material from a solution of dimethyl sulphoxide gave crystals that were suitable for X-ray crystallography. ν_{max}/cm^{-1}(ATR) 2968, 2850 (sp^3C-H st), 1535 (NO_2st), 1248 (phenol C-O st); δ_H (400 MHz, $CDCl_3$) 9.36 (s, 2H, ***H1***), 7.24- 6.68 (m, 8H, ***H2, H3, H4, H5***), 3.99 (d, J = 13.4 Hz, 2H, ***H8***), 3.74 (d, J = 13.4 Hz, 2H, ***H6***), 3.60 (d, J = 14.5 Hz, 2H, ***H6***), 3.07 (d, J = 14.5 Hz, 2H, ***H8***), 2.79 (m, 4H, ***H7***), 1.53 (d , 6H*, ***H9***);† (ES-MS^+) 372.0 (100 %, $[M+H]^+$); HR-MS Found 372.1927 , $C_{20}H_{26}N_3O_4$ $[M+H]^+$requires 372.1923; X-ray crystallography: $C_{20}H_{25}N_3O_4$, M_r=371.43, monoclinic ($P2_1/n$); *a* = 15.4949(13) Å, *b* = 6.1756(6) Å, *c* = 20.1254(18) ; crystal size = 0.37 × 0.11 × 0.07 mm^3; T= 120K;

*The origin of this splitting pattern is currently unknown.

†The rapid precipitation of this compound from a variety of deuterated solvents has rendered the acquisition of satisfactory ^{13}C NMR data difficult.

C. A listing of single crystal X-ray structures

These structures are displayed by order of appearance in the experimental, or their similarities to discussed compounds. All structures with the exception of those in ***Tables 50***, ***54***, ***55*** and ***64*** (which were crystallised and solved by Dr. Javier Pitarch-Jarque), were solved by Dr. Dmitry Yufit. Only hydrogen atoms involved in intromolecular hydrogen bonding have been shown in the interests of clarity. In some cases, to emphasise the interesting long range order, figures rendered using the Mercury software package by Dr. Javier Pitarch-Jarque have been used.

C.1. Structures of $AmGly_2$

C.1.1. Dipotassium salt

Table 48: Crystal data and structure refinement for the dipotassium salt of **$AmGly_2$**.

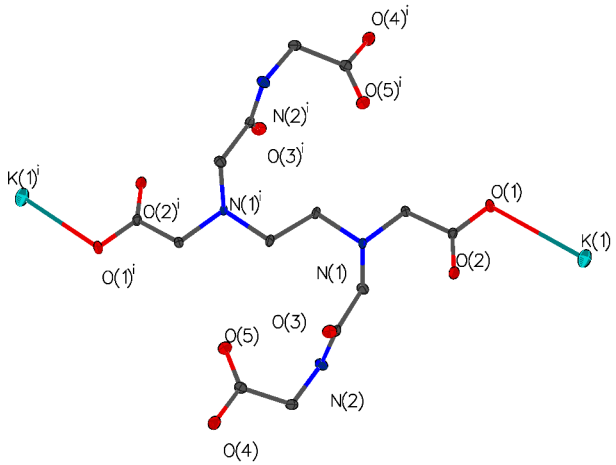

Identification code	13srv218
Empirical formula	$[C_{14}H_{20}N_4O_{10}]^{2-}$ x $2K^+$
Formula weight	482.54
Temperature /K	120
Crystal system	monoclinic
Space group	$P2_1/c$
a /Å	6.6561(4)
b /Å	14.2304(8)
c /Å	10.5791(6)
α /°	90.00
β /°	94.267(2)
γ /°	90.00
Volume/ $Å^3$	999.26(10)
Z	2
ρ_{calc} mg/mm^3	1.604
m $/mm^{-1}$	0.536
F(000)	500.0
Crystal size $/mm^3$	0.274 × 0.161 × 0.132
2Θ range for data collection	5.72 to 57.98°
Index ranges	$-9 \leq h \leq 9$, $-15 \leq k \leq 19$, $-14 \leq l \leq 13$
Reflections collected	10537
Independent reflections	2646[R(int) = 0.0266]
Data/restraints/parameters	2646/0/168
Goodness-of-fit on F^2	1.100
Final R indexes [$I >= 2\sigma(I)$]	R_1 = 0.0467, wR2 = 0.1486
Final R indexes [all data]	R_1 = 0.0529, wR_2 = 0.1552

C.1.2. Zwitterionic form

Table 49: Crystal data and structure refinement for the **AmGly$_2$** zwitterion.

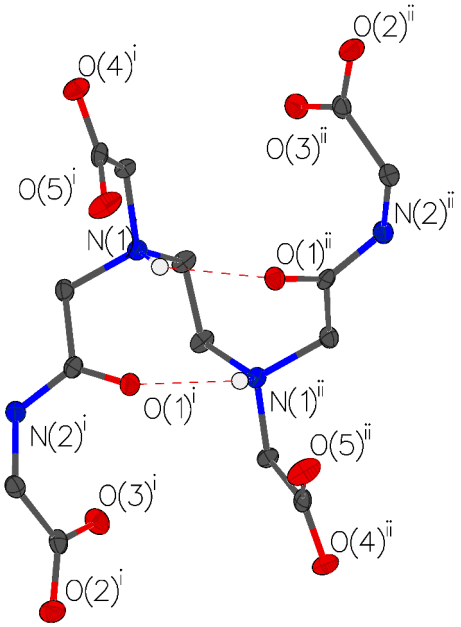

Identification code	13srv271
Empirical formula	$C_{14}H_{22}N_4O_{10}$
Formula weight	406.36
Temperature /K	120
Crystal system	orthorhombic
Space group	$P2_12_12$
a /Å	17.3349(11)
b /Å	9.3065(5)
c /Å	5.3951(4)
α /°	90.00
β /°	90.00
γ /°	90.00
Volume/ Å^3	870.38(10)
Z	2
ρ_{calc} mg/mm^3	1.551
m /mm^{-1}	0.133
F(000)	428.0
Crystal size /mm^3	0.3599 × 0.1611 × 0.0820
2Θ range for data collection	6.42 to 55.98°
Index ranges	-22 ≤ h ≤ 22, -12 ≤ k ≤ 11, -6 ≤ l ≤ 7
Reflections collected	4500
Independent reflections	2095[R(int) = 0.0442]
Data/restraints/parameters	2095/0/171
Goodness-of-fit on F^2	1.014
Final R indexes [$I >= 2\sigma(I)$]	R_1 = 0.0449, wR_2 = 0.0721
Final R indexes [all data]	R_1 = 0.0620, wR_2 = 0.0793

C.1.3. Mg^{2+} complex

Table 50: Crystal data and structure refinement for the **Mg-AmGly$_2$** complex.

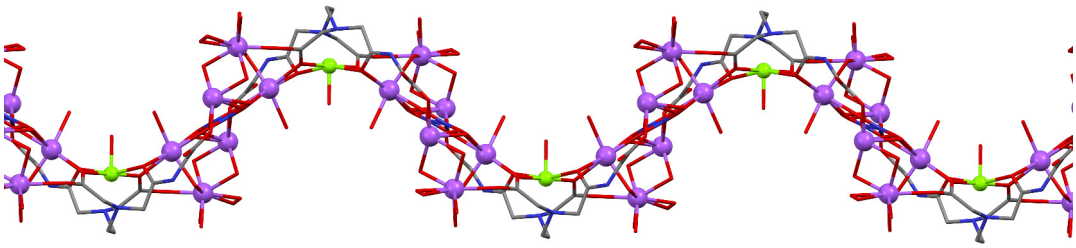

Identification code	Gly Mg
Empirical formula	$C_{14}H_{32}MgN_5Na_3O_{21}$
Formula weight	699.72
Temperature /K	293(2)
Crystal system	monoclinic
Space group	C2/c
a /Å	12.1907(6)
b /Å	9.6223(6)
c /Å	23.9144(9)
α /°	90
β /°	90.473(4)
γ /°	90
Volume/ Å^3	2805.1(2)
Z	4
ρ_{calc} mg/mm^3	1.657
m /mm^{-1}	0.21
F(000)	1456
Crystal size /mm^3	? × ? × ?
2Θ range for data collection	6.684 to 49.998
Index ranges	$-14 \leq h \leq 13$, $-11 \leq k \leq 10$, $-27 \leq l \leq 28$
Reflections collected	6515
Independent reflections	2433 [R_{int} = 0.0392, R_{sigma} = 0.0454]
Data/restraints/parameters	2433/0/224
Goodness-of-fit on F^2	1.056
Final R indexes [$I >= 2\sigma(I)$]	R_1 = 0.0548, wR_2 = 0.1494
Final R indexes [all data]	R_1 = 0.0666, wR_2 = 0.1610

C.2. Structure of $AmNH_2$

Table 51: Crystal data and structure refinement for the **$AmNH_2$** zwitterion.

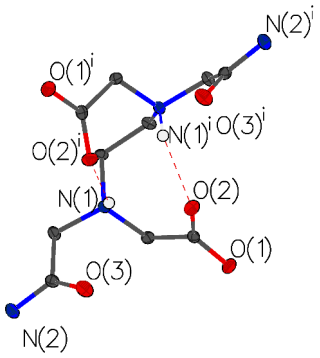

Identification code	14SRV154
Empirical formula	$C_{10}H_{18}N_4O_6$
Formula weight	290.28
Temperature /K	120.0
Crystal system	orthorhombic
Space group	Fdd2
a /Å	32.9984(14)
b /Å	14.0107(6)
c /Å	5.3942(2)
α /°	90.00
β /°	90.00
γ /°	90.00
Volume/ Å^3	2493.92(19)
Z	8
ρ_{calc} mg/mm^3	1.546
m /mm^{-1}	0.128
F(000)	1232.0
Crystal size /mm^3	0.37 × 0.094 × 0.06
2Θ range for data collection	4.94 to 60
Index ranges	$-46 \leq h \leq 46$, $-19 \leq k \leq 19$, $-7 \leq l \leq 7$
Reflections collected	12180
Independent reflections	1001 [R_{int} = 0.0499, R_{sigma} = 0.0205]
Data/restraints/parameters	1001/1/127
Goodness-of-fit on F^2	1.047
Final R indexes [$I >= 2\sigma(I)$]	R_1 = 0.0279, wR_2 = 0.0674
Final R indexes [all data]	R_1 = 0.0304, wR_2 = 0.0690

C.3. Structure of 6a

Table 52: Crystal data and structure refinement for **6a**.

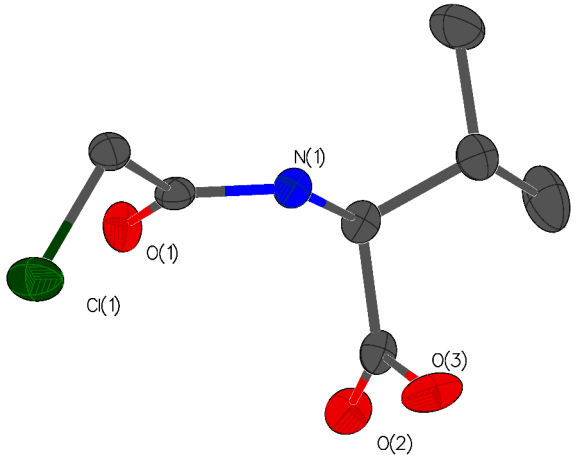

Identification code	14srv003
Empirical formula	$C_7H_{12}NO_3Cl$
Formula weight	193.63
Temperature /K	120
Crystal system	orthorhombic
Space group	$P2_12_12$
a /Å	12.2940(4)
b /Å	14.2498(5)
c /Å	5.5498(2)
α /°	90.00
β /°	90.00
γ /°	90.00
Volume/ Å^3	972.25(6)
Z	4
ρ_{calc} mg/mm^3	1.323
m /mm^{-1}	3.276
F(000)	408.0
Crystal size /mm^3	0.452 × 0.096 × 0.03
2Θ range for data collection	9.5 to 147.78°
Index ranges	$-15 \leq h \leq 14$, $-17 \leq k \leq 17$, $-6 \leq l \leq 6$
Reflections collected	7507
Independent reflections	1895 [R_{int} = 0.0315, R_{sigma} = 0.0240]
Data/restraints/parameters	1895/0/157
Goodness-of-fit on F^2	1.080
Final R indexes [$I >= 2\sigma(I)$]	R_1 = 0.0234, wR_2 = 0.0584
Final R indexes [all data]	R_1 = 0.0249, wR_2 = 0.0600

C.4. Structure of methyl (2-bromoacetylamino)acetate

Table 53: Crystal data and structure refinement for Methyl (2-bromoacetylamino)acetate.

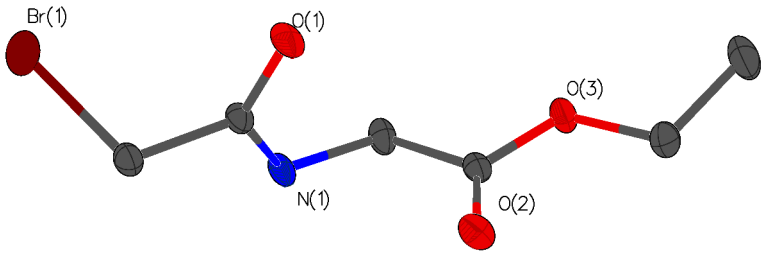

Identification code	14srv159
Empirical formula	$C_6H_{10}NO_3Br$
Formula weight	224.06
Temperature /K	100.0
Crystal system	monoclinic
Space group	$P2_1/c$
a /Å	11.269(2)
b /Å	9.5839(19)
c /Å	7.9133(15)
α /°	90.00
β /°	94.7056(19)
γ /°	90.00
Volume/ Å^3	851.7(3)
Z	4
ρ_{calc} mg/mm^3	1.747
m /mm^{-1}	4.390
F(000)	448.0
Crystal size /mm^3	0.1 × 0.1 × 0.002
2Θ range for data collection	6.48 to 58
Index ranges	$-15 \leq h \leq 15$, $-13 \leq k \leq 13$, $-7 \leq l \leq 10$
Reflections collected	8560
Independent reflections	2286 [R_{int} = 0.0397, R_{sigma} = 0.0365]
Data/restraints/parameters	2286/0/101
Goodness-of-fit on F^2	1.124
Final R indexes [$I >= 2\sigma(I)$]	R_1 = 0.0367, wR_2 = 0.1011
Final R indexes [all data]	R_1 = 0.0404, wR_2 = 0.1028

C.5. Structures of $AmGly_1$

C.5.1. Free ligand

Table 54: Crystal data and structure refinement for the **$AmGly_1$** Zwitterion

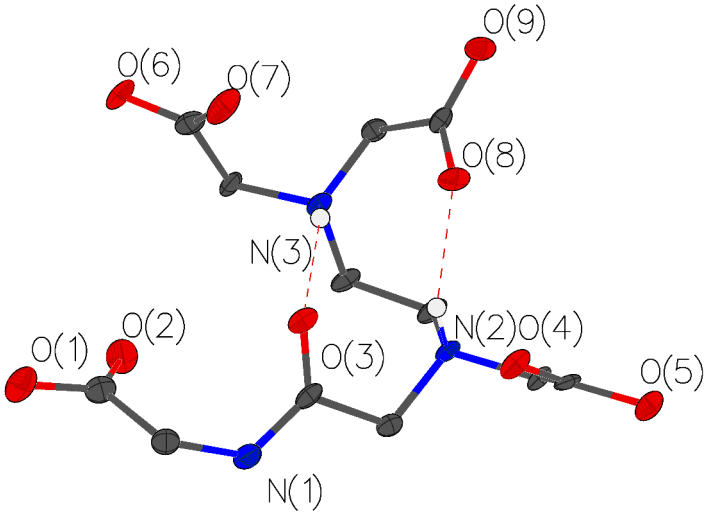

Identification code	jp441
Empirical formula	$C_{12}H_{19}N_3O_9$
Formula weight	349.3
Temperature /K	293(2)
Crystal system	monoclinic
Space group	$P2_1/c$
a /Å	5.4251(3)
b /Å	9.5386(4)
c /Å	28.5858(18)
α /°	90
β /°	91.682(5)
γ /°	90
Volume/ $Å^3$	1478.62(13)
Z	4
ρ_{calc} mg/mm^3	1.569
m /mm^{-1}	0.136
F(000)	736
Crystal size /mm^3	? × ? × ?
2Θ range for data collection	7.126 to 49.982
Index ranges	$-6 \leq h \leq 6$, $-11 \leq k \leq 11$, $-29 \leq l \leq 33$
Reflections collected	7345
Independent reflections	2603 [R_{int} = 0.0630, R_{sigma} = 0.0855]
Data/restraints/parameters	2603/0/219
Goodness-of-fit on F^2	1.011
Final R indexes [$I >= 2\sigma(I)$]	R_1 = 0.0559, wR_2 = 0.1059
Final R indexes [all data]	R_1 = 0.0877, wR_2 = 0.1185

C.5.2. Ca^{2+} complex

Table 55: Crystal data and structure refinement for **Ca-AmGly$_1$**.

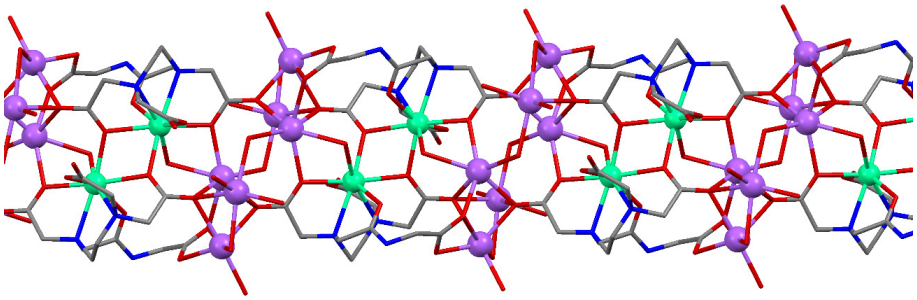

Identification code	ED3A Ca
Empirical formula	$C_{12}H_{20.5}CaClN_3Na_3O_{16.5}$
Formula weight	615.31
Temperature /K	293(2)
Crystal system	monoclinic
Space group	P2/n
a /Å	13.8850(9)
b /Å	8.8663(5)
c /Å	21.6439(16)
α /°	90
β /°	105.003(7)
γ /°	90
Volume/ Å^3	2573.7(3)
Z	4
ρ_{calc} mg/mm^3	1.588
m /mm^{-1}	0.476
F(000)	1262
Crystal size /mm^3	? × ? × ?
2Θ range for data collection	7.188 to 49.998
Index ranges	$-12 \leq h \leq 16$, $-6 \leq k \leq 10$, $-25 \leq l \leq 14$
Reflections collected	9692
Independent reflections	4530 [R_{int} = 0.0354, R_{sigma} = 0.0610]
Data/restraints/parameters	4530/0/357
Goodness-of-fit on F^2	1.057
Final R indexes [$I >= 2\sigma(I)$]	R_1 = 0.0575, wR_2 = 0.1442
Final R indexes [all data]	R_1 = 0.0750, wR_2 = 0.1558

C.6. Structure of 11

Table 56: Crystal data and structure refinement for **11**.

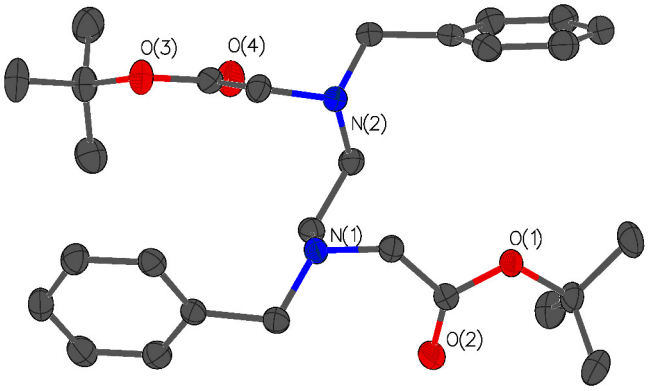

Identification code	14srv004
Empirical formula	$C_{28}H_40N_2O_4$
Formula weight	468.62
Temperature /K	120
Crystal system	tetragonal
Space group	P-4
a /Å	22.2406(6)
b /Å	22.2406(6)
c /Å	5.4929(2)
α /°	90.00
β /°	90.00
γ /°	90.00
Volume/ Å^3	2717.03(14)
Z	4
ρ_{calc} mg/mm^3	1.146
m /mm^{-1}	0.076
F(000)	1016.0
Crystal size /mm^3	0.48 × 0.24 × 0.2
2Θ range for data collection	3.66 to 55°
Index ranges	$-28 \leq h \leq 28$, $-28 \leq k \leq 28$, $-7 \leq l \leq 7$
Reflections collected	30203
Independent reflections	3446 [R_{int} = 0.0501, R_{sigma} = 0.0283]
Data/restraints/parameters	3446/0/467
Goodness-of-fit on F^2	1.066
Final R indexes [$I >= 2\sigma(I)$]	R_1 = 0.0355, wR_2 = 0.0781
Final R indexes [all data]	0.21/-0.17

C.7. Structure of 4-H-21-OMe

Table 57: Crystal data and structure refinement for **4-H-21-OMe**.

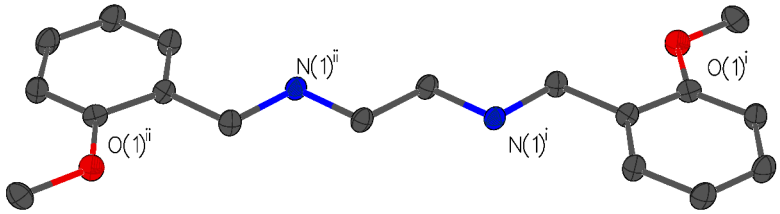

Identification code	14srv048
Empirical formula	$C_{18}H_{24}N_2O_2$
Formula weight	300.39
Temperature /K	120.0(2)
Crystal system	monoclinic
Space group	$P2_1/n$
a /Å	7.2450(3)
b /Å	5.5692(3)
c /Å	20.0255(9)
α /°	90.0
β /°	95.571(3)
γ /°	90.0
Volume/ Å^3	804.19(6)
Z	2
ρ_{calc} mg/mm^3	1.241
m /mm^{-1}	0.081
F(000)	324.0
Crystal size /mm^3	0.49 × 0.25 × 0.14
2Θ range for data collection	4.0872 to 65.3608°
Index ranges	$-10 \leq h \leq 10$, $-8 \leq k \leq 8$, $-29 \leq l \leq 30$
Reflections collected	11326
Independent reflections	2344[R(int) = 0.0384]
Data/restraints/parameters	2344/0/148
Goodness-of-fit on F^2	1.060
Final R indexes [$I >= 2\sigma(I)$]	R_1 = 0.0494, wR_2 = 0.1177
Final R indexes [all data]	R_1 = 0.0649, wR_2 = 0.1278

C.8. Structure of 4-R-21-tBu compounds

C.8.1. Structure of 4-F-21-tBu

Table 58: Crystal data and structure refinement for **4-F-21-tBu**.

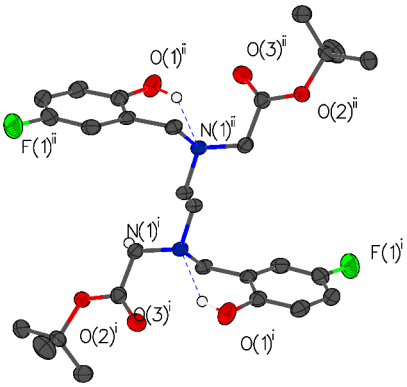

Identification code	15srv011
Empirical formula	$C_{28}H_{38}F_2N_2O_6$
Formula weight	536.60
Temperature /K	120.0
Crystal system	monoclinic
Space group	$P2_1/c$
a /Å	13.1139(10)
b /Å	10.2607(7)
c /Å	10.8035(6)
α /°	90.00
β /°	92.594(6)
γ /°	90.00
Volume/ Å^3	1452.22(17)
Z	2
ρ_{calc} mg/mm^3	1.227
m /mm^{-1}	0.094
F(000)	572.0
Crystal size /mm^3	0.36 × 0.24 × 0.12
2Θ range for data collection	5.48 to 57.98
Index ranges	$-17 \leq h \leq 17$, $-13 \leq k \leq 13$, $-14 \leq l \leq 14$
Reflections collected	22165
Independent reflections	3863 [R_{int} = 0.0766, R_{sigma} = 0.0583]
Data/restraints/parameters	3863/0/248
Goodness-of-fit on F^2	1.025
Final R indexes [$I >= 2\sigma(I)$]	R_1 = 0.0538, wR_2 = 0.0960
Final R indexes [all data]	R_1 = 0.0914, wR_2 = 0.1109

C.8.2. Structure of 4-Cl-21-tBu

Table 59: Crystal data and structure refinement for **4-Cl-21-tBu**.

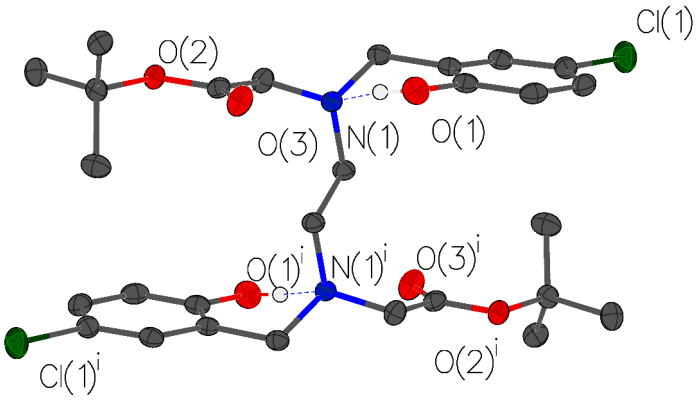

Identification code	15srv079
Empirical formula	$C_{28}H_{38}Cl_2N_2O_6$
Formula weight	569.50
Temperature /K	120.0
Crystal system	monoclinic
Space group	$P2_1/c$
a /Å	15.0443(5)
b /Å	8.8106(3)
c /Å	11.2961(4)
α /°	90.00
β /°	106.053(4)
γ /°	90.00
Volume/ Å^3	1438.92(9)
Z	2
ρ_{calc} mg/mm^3	1.314
m /mm^{-1}	0.269
F(000)	604.0
Crystal size /mm^3	0.38 × 0.23 × 0.08
2Θ range for data collection	5.42 to 58
Index ranges	$-20 \leq h \leq 20$, $-11 \leq k \leq 12$, $-15 \leq l \leq 15$
Reflections collected	19026
Independent reflections	3817 [R_{int} = 0.0509, R_{sigma} = 0.0401]
Data/restraints/parameters	3817/0/248
Goodness-of-fit on F^2	1.029
Final R indexes [$I >= 2\sigma(I)$]	R1 = 0.0435, wR2 = 0.1016
Final R indexes [all data]	R_1 = 0.0625, wR_2 = 0.1133

C.8.3. Structure of 4-Br-21-tBu

Table 60: Crystal data and structure refinement for **4-Br-21-tBu**.

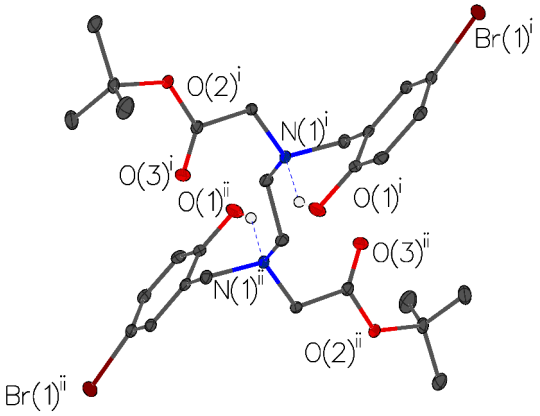

Identification code	14srv283
Empirical formula	$C_{28}H_{38}Br_2N_2O_6$
Formula weight	658.42
Temperature /K	120.0
Crystal system	triclinic
Space group	P-1
a /Å	6.03170(10)
b /Å	9.8716(2)
c /Å	12.9407(2)
α /°	105.2066(17)
β /°	98.9882(19)
γ /°	97.3798(18)
Volume/ Å^3	722.72(2)
Z	1
ρ_{calc} mg/mm^3	1.513
m /mm^{-1}	2.848
F(000)	338.0
Crystal size /mm^3	0.28 × 0.14 × 0.08
2Θ range for data collection	4.34 to 60
Index ranges	$-8 \leq h \leq 8$, $-13 \leq k \leq 13$, $-18 \leq l \leq 18$
Reflections collected	11986
Independent reflections	4207 [R_{int} = 0.0304, R_{sigma} = 0.0397]
Data/restraints/parameters	4207/0/248
Goodness-of-fit on F^2	1.018
Final R indexes [$I >= 2\sigma(I)$]	R_1 = 0.0295, wR_2 = 0.0613
Final R indexes [all data]	R_1 = 0.0407, wR_2 = 0.0645

C.8.4. Structure of 4-MeO-21-tBu

Table 61: Crystal data and structure refinement for **4-MeO-21-tBu**.

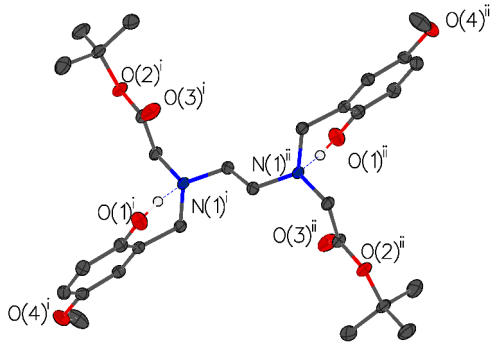

Identification code	15srv043
Empirical formula	$C_{30}H_{44}N_2O_8$
Formula weight	560.67
Temperature /K	120.0
Crystal system	triclinic
Space group	P-1
a /Å	6.4286(2)
b /Å	10.1382(4)
c /Å	12.8531(4)
α /°	104.525(3)
β /°	92.917(3)
γ /°	107.035(3)
Volume/ Å^3	768.31(5)
Z	1
ρ_{calc} mg/mm^3	1.212
m /mm^{-1}	0.087
F(000)	302.0
Crystal size /mm^3	0.49 × 0.24 × 0.14
2Θ range for data collection	4.38 to 60
Index ranges	$-9 \leq h \leq 8$, $-14 \leq k \leq 14$, $-18 \leq l \leq 18$
Reflections collected	12161
Independent reflections	4474 [R_{int} = 0.0302, R_{sigma} = 0.0392]
Data/restraints/parameters	4474/0/269
Goodness-of-fit on F^2	1.029
Final R indexes [$I >= 2\sigma(I)$]	R_1 = 0.0442, wR_2 = 0.1003
Final R indexes [all data]	R_1 = 0.0622, wR_2 = 0.1102

C.8.5. Structure of NOON-tBu

Table 62: Crystal data and structure refinement for **NOON-tBu**.

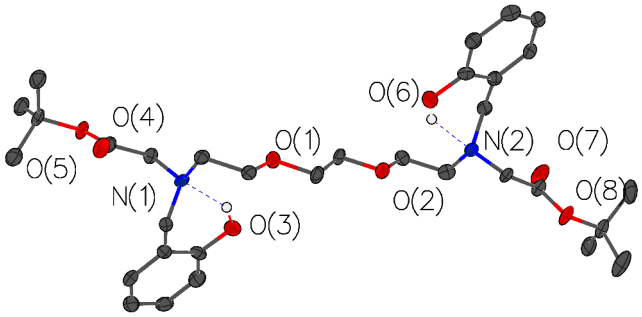

Identification code	14srv166
Empirical formula	$C_{32}H_{48}N_2O_8$
Formula weight	588.72
Temperature /K	120.0
Crystal system	orthorhombic
Space group	$Pca2_1$
a /Å	10.5409(5)
b /Å	10.0117(5)
c /Å	29.6434(14)
α /°	90.00
β /°	90.00
γ /°	90.00
Volume/ Å^3	3128.3(3)
Z	4
ρ_{calc} mg/mm^3	1.250
m /mm^{-1}	0.089
F(000)	1272.0
Crystal size /mm^3	0.28 × 0.16 × 0.05
2Θ range for data collection	2.74 to 55
Index ranges	$-13 \leq h \leq 13$, $-12 \leq k \leq 13$, $-38 \leq l \leq 38$
Reflections collected	30025
Independent reflections	7159 [R_{int} = 0.1269, R_{sigma} = 0.0958]
Data/restraints/parameters	7159/1/387
Goodness-of-fit on F^2	0.904
Final R indexes [$I >= 2\sigma(I)$]	R_1 = 0.0669, wR_2 = 0.1487
Final R indexes [all data]	R_1 = 0.1138, wR_2 = 0.1678

C.9. Structures of NOON

C.9.1. Free ligand

Table 63: Crystal data and structure refinement for **NOON**.

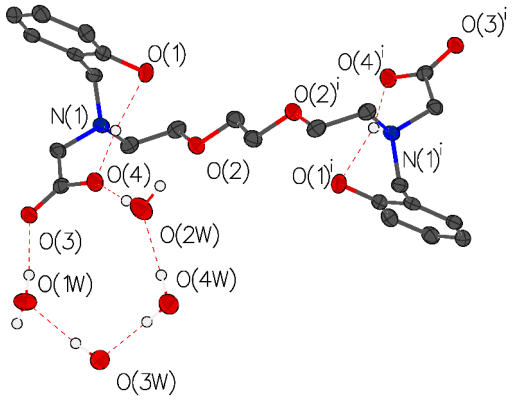

Identification code	14srv278
Empirical formula	$C_{24}H_{32}N_2O_8$ x 5.33 H_2O
Formula weight	572.60
Temperature /K	120.0
Crystal system	trigonal
Space group	P-3
a /Å	18.8263(5)
b /Å	18.8263(5)
c /Å	7.2192(2)
α /°	90.00
β /°	90.00
γ /°	120.00
Volume/ Å^3	2215.90(10)
Z	3
ρ_{calc} mg/mm^3	1.287
m /mm^{-1}	0.891
F(000)	922.0
Crystal size /mm^3	0.28 × 0.03 × 0.03
2Θ range for data collection	5.42 to 144.9
Index ranges	$-20 \leq h \leq 23$, $-23 \leq k \leq 22$, $-8 \leq l \leq 8$
Reflections collected	25927
Independent reflections	2917 [R_{int} = 0.0990, R_{sigma} = 0.0480]
Data/restraints/parameters	2917/9/254
Goodness-of-fit on F^2	1.066
Final R indexes [$I >= 2\sigma(I)$]	R_1 = 0.0534, wR_2 = 0.1098
Final R indexes [all data]	R_1 = 0.0849, wR_2 = 0.1221

C.9.2. Ca^{2+} complex

Table 64: Crystal data and structure refinement for **Ca-NOON**.

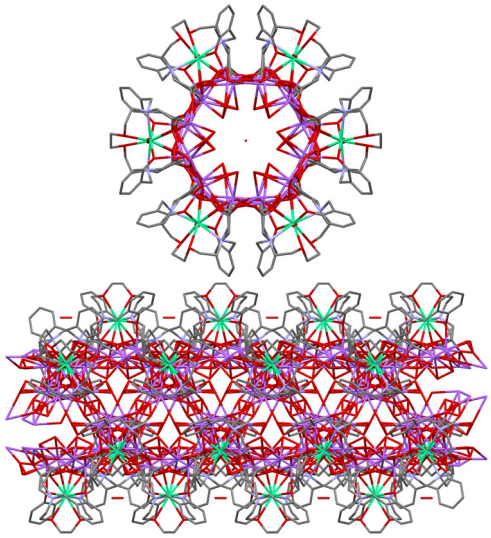

Identification code	jp439
Empirical formula	$C_{144}H_{186}Ca_6N_{12}Na_{12}O_{71}$
Formula weight	3737.47
Temperature /K	N/A
Crystal system	trigonal
Space group	P-3c1
a /Å	23.7597(17)
b /Å	23.7597(17)
c /Å	9.3476(7)
α /°	90
β /°	90
γ /°	120
Volume/ Å^3	4570.0(6)
Z	1
ρ_{calc} mg/mm^3	1.3579
m /mm^{-1}	0.294
F(000)	1956.9
Crystal size /mm^3	N/A × N/A × N/A
2Θ range for data collection	6.82 to 49.98
Index ranges	-14 ≤ h ≤ 33, -32 ≤ k ≤ 11, -6 ≤ l ≤ 13
Reflections collected	11059
Independent reflections	2674 [R_{int} = 0.0543, R_{sigma} = 0.0848]
Data/restraints/parameters	2674/33/262
Goodness-of-fit on F^2	1.091
Final R indexes [$I >= 2\sigma(I)$]	R_1 = 0.0850, wR_2 = 0.2107
Final R indexes [all data]	R_1 = 0.1130, wR_2 = 0.2309

C.10. Structure of 26

Table 65: Crystal data and structure refinement for 26.

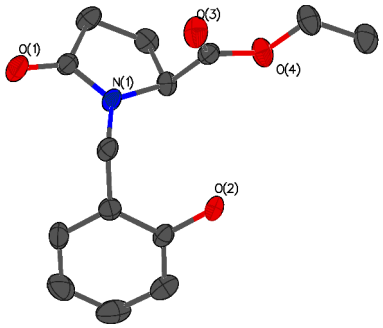

Identification code	14srv127
Empirical formula	$C_{14}H_{17}NO_4$
Formula weight	263.29
Temperature /K	120.0
Crystal system	triclinic
Space group	P1
a /Å	6.8353(3)
b /Å	7.5669(3)
c /Å	7.7552(3)
α /°	96.5965(19)
β /°	112.7236(19)
γ /°	106.441(2)
Volume/ Å^3	343.27(2)
Z	1
ρ_{calc} mg/mm^3	1.274
m /mm^{-1}	0.775
F(000)	140.0
Crystal size /mm^3	0.28 × 0.21 × 0.14
2Θ range for data collection	12.6 to 139.9°
Index ranges	$-7 \leq h \leq 8$, $-9 \leq k \leq 9$, $-9 \leq l \leq 9$
Reflections collected	2382
Independent reflections	1722 [R_{int} = 0.0554, R_{sigma} = 0.0965]
Data/restraints/parameters	1722/3/174
Goodness-of-fit on F^2	1.086
Final R indexes [$I >= 2\sigma(I)$]	R_1 = 0.0767, wR_2 = 0.2019
Final R indexes [all data]	R_1 = 0.0797, wR_2 = 0.2218

C.11. Structure of HB-28

Table 66: Crystal data and structure refinement for **HB-28**.

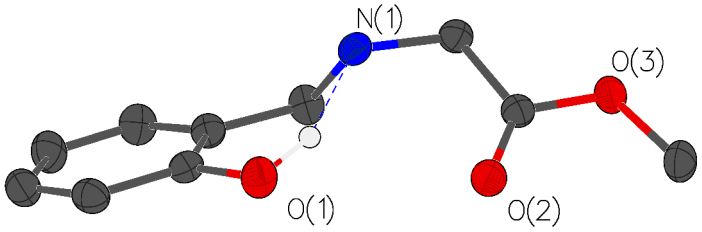

Identification code	14srv139
Empirical formula	$C_{10}H_{13}NO_3$
Formula weight	195.21
Temperature /K	120.0
Crystal system	orthorhombic
Space group	Pbca
a /Å	9.2513(8)
b /Å	9.0842(8)
c /Å	22.8517(19)
α /°	90.00
β /°	90.00
γ /°	90.00
Volume/ Å^3	1920.5(3)
Z	8
ρ_{calc} mg/mm^3	1.350
m /mm^{-1}	0.100
F(000)	832.0
Crystal size /mm^3	0.42 × 0.18 × 0.16
2Θ range for data collection	3.56 to 60°
Index ranges	-13 ≤ h ≤ 12, -12 ≤ k ≤ 12, -32 ≤ l ≤ 32
Reflections collected	18663
Independent reflections	2799 [R_{int} = 0.0546, R_{sigma} = 0.0331]
Data/restraints/parameters	2799/0/179
Goodness-of-fit on F^2	0.987
Final R indexes [$I >= 2\sigma(I)$]	R_1 = 0.0404, wR_2 = 0.1049
Final R indexes [all data]	R_1 = 0.0590, wR_2 = 0.1146

C.12. Structure of NO_2-AAZ-HB

Table 67: Crystal data and structure refinement for **NO_2-AAZ-HB**.

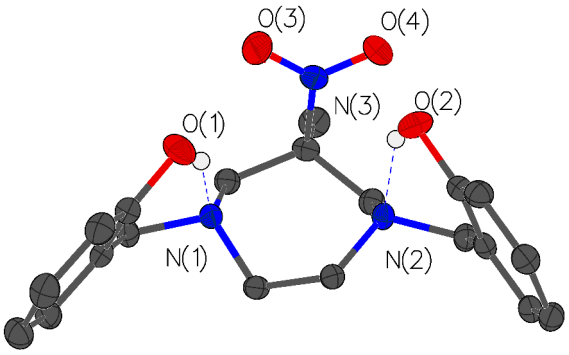

Identification code	14srv144
Empirical formula	$C_{20}H_{25}N_3O_4$
Formula weight	371.43
Temperature /K	120.0
Crystal system	monoclinic
Space group	$P2_1/n$
a /Å	15.4949(13)
b /Å	6.1756(6)
c /Å	20.1254(18)
α /°	90.00
β /°	107.437(3)
γ /°	90.00
Volume/ Å^3	1837.3(3)
Z	4
ρ_{calc} mg/mm^3	1.343
m /mm^{-1}	0.095
F(000)	792.0
Crystal size /mm^3	0.37 × 0.11 × 0.07
2Θ range for data collection	5.52 to 56°
Index ranges	$-20 \leq h \leq 20$, $-8 \leq k \leq 8$, $-25 \leq l \leq 26$
Reflections collected	40351
Independent reflections	4432 [R_{int} = 0.1513, R_{sigma} = 0.0868]
Data/restraints/parameters	4432/0/344
Goodness-of-fit on F^2	1.024
Final R indexes [$I >= 2\sigma(I)$]	R_1 = 0.0549, wR_2 = 0.1189
Final R indexes [all data]	R_1 = 0.1010, wR_2 = 0.1385

D. Calculation of molecular weights from CHN data via JASPER

The following is a representative procedure for the calculation of molecular weights via CHN analysis, which were reported in (***Table*** 7) for samples of certain compounds.

1. Obtain a CHN analysis of the sample under study. For this example, **$AmGly_1$** is used:

chn20150311	14580	03/11/2015	943-JAGWRM-RSm ed3a	32.2	5.4	9.15

2. Draw the structure of the free acid in a program such as ChemDraw to obtain the expected CHN analysis values.

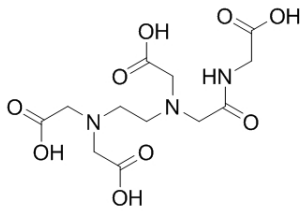

$AmGly_1$

Elemental Analysis (expected): C, 41.26; H, 5.48; N, 12.03; O, 41.22
Found: C: 32.2 H: 5.4 N: 9.15

3. Input the required data into the JASPER interface. In this example, hydrochloric acid and water have been postulated as the main impurities. This is because no organic impurities were detectable by ^{1}H and ^{13}C NMR techniques, and the sample will have been exposed to hydrochloric acid and water as part of the purification procedure.

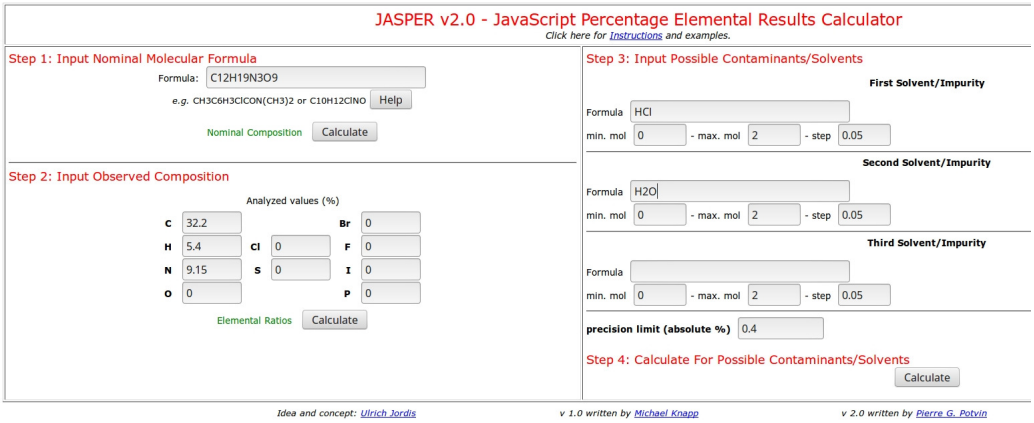

4. This gives a “corrected” molecular formula:

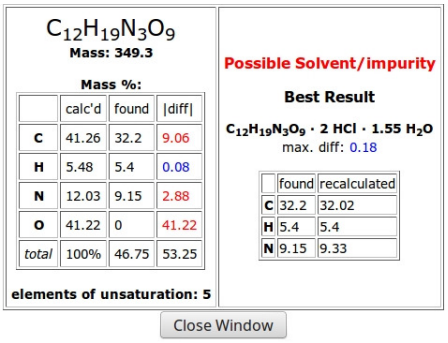

$C_{12}H_{19}N_3O_9$

Mass: 349.3

Mass %:

	calc'd	found	|diff|
C	41.26	32.2	9.06
H	5.48	5.4	0.08
N	12.03	9.15	2.88
O	41.22	0	41.22
total	100%	46.75	53.25

elements of unsaturation: 5

Possible Solvent/impurity

Best Result

$C_{12}H_{19}N_3O_9 \cdot 2\ HCl \cdot 1.55\ H_2O$
max. diff: 0.18

	found	recalculated
C	32.2	32.02
H	5.4	5.4
N	9.15	9.33

Close Window

5. These values can then be used to calculate a molecular weight from CHN analysis.

References

[1] J. R. Hart, *J. Chem. Educ.*, 1984, **61**, 1060.

[2] J. R. Hart, *J. Chem. Educ.*, 1985, **62**, 75.

[3] O. J. Grundler, A. T. M. van der Steen and J. Wilmot, in *Overview of the European Risk Assessment on EDTA*, ACS Symposium Series, 2005, ch. 21, pp. 336–347.

[4] WHO, *WHO model list of essential medicines: 18th list, April 2013*, World Health Organization, 2013.

[5] F. Munz, *US Patent US2130505 A*, 1938.

[6] G. Schwarzenbach, *The Analyst*, 1955, **80**, 713.

[7] S. Chaberek, F. Bersworth and A. E. Martell, *Arch. Biochem. Biophys.*, 1955, **55**, 321–337.

[8] M. B. Zucker and J. Borrelli, *Blood*, 1954, **9**, 602–8.

[9] G. Banfi, G. L. Salvagno and G. Lippi, *Clin. Chem. Lab. Med.*, 2007, **45**, 565–76.

[10] W. G. Mitchell, *Exp. Biol. Med.*, 1953, **83**, 346–348.

[11] A. Wallace, C. P. North, R. T. Mueller and N. Hemaidan, *Proceedings of The American Society For Horticultural Science*, 1953, **62**, 116–118.

[12] R. B. Johnson, *J. Bacteriol.*, 1954, **68**, 604.

[13] B. Nowack and J. M. VanBriesen, in *Chelating Agents in the Environment*, ACS Symposium Series, 2005, ch. 2, pp. 1–18.

[14] C. Oviedo and J. Rodríguez, *Química Nova*, 2003, **26**, 901–905.

[15] K. Pirkanniemi, *Ph.D. thesis*, University of Kuopio, 2007.

[16] I. S. S. Pinto, I. F. F. Neto and H. M. V. M. Soares, *Env. Sci. Pollut. Res.*, 2014, **21**, 11893–11906.

[17] D. Schowanek, T. C. Feijtel, C. M. Perkins, F. A. Hartman, T. W. Federle and R. J. Larson, *Chemosphere*, 1997, **34**, 2375–2391.

[18] `https://commons.wikimedia.org/wiki/File%3AGram_negative_cell_wall.svg`.

[19] C. R. H. Raetz and C. Whitfield, *Annu. Rev. Biochem.*, 2002, **71**, 635–700.

[20] M. Schindler and M. J. Osborn, *Biochem.*, 1979, **18**, 4425–4430.

[21] L. A. Clifton, M. W. A. Skoda, A. P. Le Brun, F. Ciesielski, I. Kuzmenko, S. A. Holt and J. H. Lakey, *Langmuir*, 2015, **31**, 404–412.

[22] H. Labischinski, G. Barnickel, H. Bradaczek, D. Naumann, E. T. Rietschel and P. Giesbrecht, *J. Bacteriol.*, 1985, **162**, 9–20.

[23] M. Vaara, *Microbiol. Rev.*, 1992, **56**, 395–411.

[24] A. Laatiris, M. El Achouri, M. R. Infante and Y. Bensouda, *Microbiol. Res.*, 2008, **163**, 645–50.

[25] H. Nikaido, *Science*, 1994, **264**, 382–8.

[26] A. Inoue and K. Horikoshi, *Nature*, 1989, **338**, 264–266.

[27] J. A. Caetano, M. A. Lima, M. D. C. Miranda, J. C. Serufo and P. R. L. Ponte, *Rev. Esc. Enferm. USP*, 2011, **45**, 153–160.

[28] M. Vaara, *Microbiol. Rev.*, 1992, **56**, 395–411.

[29] L. Leive, *Biochem. Biophys. Res. Commun.*, 1965, **21**, 290 – 296.

[30] J. Voss, *J. Gen. Microbiol.*, 1967, **48**, 391–400.

[31] H. Haque and A. Russell, *Antimicrob. Agents Chemother.*, 1974, **6**, 200–206.

[32] H. Haque and A. D. Russell, *Antimicrob. Agents Chemother.*, 1974, **5**, 447–452.

[33] B. A. Key, G. W. Gray and S. G. Wilkinson, *Biochem J*, 1970, **117**, 721–732.

[34] A. B. Spicer and D. F. Spooner, *J. Gen. Microbiol.*, 1974, **80**, 37–50.

[35] D. P. Brunner, R. A. Caputo and R. W. Treick, *Biochem. Biophys. Res. Commun.*, 1977, **74**, 919 – 925.

[36] R. E. Hancock and P. G. Wong, *Antimicrob. Agents Chemother.*, 1984, **26**, 48–52.

[37] J. S. Chapman and N. H. Georgopapadakou, *Antimicrob. Agents Chemother.*, 1988, **32**, 438–442.

[38] R. P. Darveau and R. E. Hancock, *J. Bacteriol.*, 1983, **155**, 831–8.

[39] N. A. Amro, L. P. Kotra, K. Wadu-Mesthrige, A. Bulychev, S. Mobashery and G.-y. Liu, *Langmuir*, 2000, **16**, 2789–2796.

[40] M. Vaara and T. Vaara, *Antimicrob. Agents Chemother.*, 1983, **24**, 114–122.

[41] M. Vaara, J. Fox, G. Loidl, O. Siikanen, J. Apajalahti, F. Hansen, N. Frimodt-Møller, J. Nagai, M. Takano and T. Vaara, *Antimicrob. Agents Chemother.*, 2008, **52**, 3229–36.

[42] K. J. Waldron, J. C. Rutherford, D. Ford and N. J. Robinson, *Nature*, 2009, **460**, 823–30.

[43] P. C. Wilkins and R. G. Wilkins, *Inorganic chemistry in biology*, Oxford University Press Oxford, 1997, vol. 199.

[44] C. Housecroft and A. Sharpe, *Inorganic Chemistry*, Pearson, 3rd edn., 2005.

[45] N. Nelson, *The EMBO Journal*, 1999, **18**, 4361–4371.

[46] K. W. Becker and E. P. Skaar, *FEMS Microbiol. Rev.*, 2014, **38**, 1235–1249.

[47] S. Silver, P. Johnseine and K. King, *J. Bacteriol.*, 1970, **104**, 1299–306.

[48] G. Porcheron, A. Garénaux, J. Proulx, M. Sabri and C. M. Dozois, *Frontiers in Cellular and Infection Microbiology*, 2013, **3**, 90.

[49] E. R. Frawley and F. C. Fang, *Mol. Microbiol.*, 2014, **93**, 609–16.

[50] B. Troxell and H. M. Hassan, *Frontiers in Cellular and Infection Microbiology*, 2013, **3**, 59.

[51] T. Bergan, J. Klaveness, A. J. Aasen and n, *Chemotherapy*, 2001, **47**, 10–14.

[52] T. Zhou, Y. Ma, X. Kong and R. C. Hider, *Dalton Trans.*, 2012, **41**, 6371–89.

[53] Y.-Y. Xie, M.-S. Liu, P.-P. Hu, X.-L. Kong, D.-H. Qiu, J.-L. Xu, R. C. Hider and T. Zhou, *Med. Chem. Res.*, 2012, **22**, 2351–2359.

[54] B. Xu, X.-L. Kong, T. Zhou, D.-H. Qiu, Y.-L. Chen, M.-S. Liu, R.-H. Yang and R. C. Hider, *Bioorg. Med. Chem. Lett.*, 2011, **21**, 6376–80.

[55] M.-X. Zhang, C.-F. Zhu, Y.-J. Zhou, X.-L. Kong, R. C. Hider and T. Zhou, *Chem. Biol. Drug. Des.*, 2014, **84**, 659–668.

[56] S. M. Damo, T. E. Kehl-Fie, N. Sugitani, M. E. Holt, S. Rathi, W. J. Murphy, Y. Zhang, C. Betz, L. Hench, G. Fritz, E. P. Skaar and W. J. Chazin, *Proc. Natl. Acad. Sci. U. S. A.*, 2013, **110**, 3841–3846.

[57] T. G. Nakashige, B. Zhang, C. Krebs and E. M. Nolan, *Nat. Chem. Biol.*, 2015, **11**, 765–771.

[58] D. M. Gagnon, M. B. Brophy, S. E. J. Bowman, T. A. Stich, C. L. Drennan, R. D. Britt and E. M. Nolan, *J. Am. Chem. Soc.*, 2015, **137**, 3004–3016.

[59] A. K. Katz, J. P. Glusker, S. A. Beebe and C. W. Bock, *J. Am. Chem. Soc.*, 1996, **118**, 5752–5763.

[60] J. P. Glusker, A. K. Katz and C. W. Bock, *Metal coordination of several divalent cations: Mg^{2+}, Ca^{2+}, Be^{2+}, and Zn^{2+}*, Conference abstract (The XVII Congress and General Assembly of the International Union of Crystallography), 1996.

[61] J. Huheey, E. Keiter and R. Keiter, *Inorganic Chemistry: Principles of Structure and Reactivity*, Pearson Education, 2000.

[62] A. Martell, R. Hancock and R. Motekaitis, *Coord. Chem. Rev.*, 1994, **133**, 39–65.

[63] R. D. Hancock, *J. Chem. Educ.*, 1992, **69**, 615.

[64] E. Chinea, S. Dominguez, A. Mederos, F. Brito, J. M. Arrieta, A. Sanchez and G. Germain, *Inorg. Chem.*, 1995, **34**, 1579–1587.

[65] R. D. Hancock and A. E. Martell, *Chem. Rev.*, 1989, **89**, 1875–1914.

[66] A. D. McNaught, *Compendium of chemical terminology*, Blackwell Science Oxford, 1997.

[67] C. Rücker and K. Kümmerer, *Green Chemistry*, 2012, **14**, 875.

[68] OECD, *Test No. 301: Ready Biodegradability*, 1992.

[69] OECD, *Test No. 306: Biodegradability in Seawater*, 1992.

[70] OECD, *Test No. 302A: Inherent Biodegradability: Modified SCAS Test*, 1981.

[71] OECD, *Test No. 304A: Inherent Biodegradability in Soil*, 1981.

[72] R. S. Boethling, E. Sommer and D. DiFiore, *Chem. Rev.*, 2007, **107**, 2207–2227.

[73] J. M. Tiedje, *Appl. Microbiol.*, 1975, **30**, 327–329.

[74] R. A. Thomas, K. Lawlor, M. Bailey and L. E. Macaskie, *Appl. Environ. Microbiol.*, 1998, **64**, 1319–1322.

[75] M. Witschel, S. Nagel and T. Egli, *J. Bacteriol.*, 1997, **179**, 6937–6943.

[76] A. D. Satroutdinov, E. G. Dedyukhina, T. I. Chistyakova, M. Witschel, I. G. Minkevich, V. K. Eroshin and T. Egli, *Env. Sci. Tech.*, 2000, **34**, 1715–1720.

[77] A. D. Satroutdinov, T. I. Chistyakova, E. G. Dedyukhina and I. G. Minkevich, in *Microbial Degradation of EDTA: New EDTA-Degrading Bacterial strains*, ACS Symposium Series, 2005, ch. 9, pp. 171–182.

[78] T. Klüner, D. C. Hempel and B. Nörtemann, *Applied Microbiology and Biotechnology*, 1998, **49**, 194–201.

[79] Y. Liu, T. M. Louie, J. Payne, J. Bohuslavek, H. Bolton and L. Xun, *Appl. Environ. Microbiol.*, 2001, **67**, 696–701.

[80] L. Chen, T. Liu and C. Ma, *J. Phys. Chem. A*, 2010, **114**, 443–454.

[81] Y. Suzuki and N. Koyama, *Biodegradation*, 2008, **20**, 39–44.

[82] J. J. Lauff, D. B. Steele, L. A. Coogan and J. M. Breitfeller, *Appl. Environ. Microbiol.*, 1990, **56**, 3346–53.

[83] M. Witschel and T. Egli, *Biodegradation*, 1997, **8**, 419–28.

[84] C. G. van Ginkel, R. Geerts and P. D. Nguyen, in *Biodegradation of L-Glutamatediacetate by Mixed Cultures and an Isolate*, ACS Symposium Series, 2005, ch. 11, pp. 183–194.

[85] V. Sýkora, P. Pitter, I. Bittnerova and T. Lederer, *Water Res.*, 2001, **35**, 2010 – 2016.

[86] P. Pitter and V. Sýkora, *Chemosphere*, 2001, **44**, 823 – 826.

[87] D. F. Browning, T. J. Wells, F. L. S. França, F. C. Morris, Y. R. Sevastsyanovich, J. A. Bryant, M. D. Johnson, P. A. Lund, A. F. Cunningham, J. L. Hobman, R. C. May, M. A. Webber and I. R. Henderson, *Mol. Microbiol.*, 2013, **87**, 939–950.

[88] G. Stevenson, B. Neal, D. Liu, M. Hobbs, N. H. Packer, M. Batley, J. W. Redmond, L. Lindquist and P. Reeves, *J. Bacteriol.*, 1994, **176**, 4144–4156.

[89] C. Sekse, J. Bohlin, E. Skjerve and G. E. Vegarud, *Microbial Informatics and Experimentation*, 2012, **2**, 5.

[90] H. Du, T.-M. Lo, J. Sitompul and M. W. Chang, *Biochem. Biophys. Res. Commun.*, 2012, **424**, 657–62.

[91] F. Liu, A. Soh Yan Ni, Y. Lim, H. Mohanram, S. Bhattacharjya and B. Xing, *Bioconjug Chem*, 2012, **23**, 1639–1647.

[92] A. J. H. Marshall and L. J. V. Piddock, *J. Antimicrobial. Chemother.*, 1994, **34**, 465–483.

[93] *Cold Spring Harbor Protocols*, 2010, **2010**, a660.

[94] A. Leydier, Y. Lin, G. Arrachart, R. Turgis, D. Lecercle, A. Favre-Reguillon, F. Taran, M. Lemaire and S. Pellet-Rostaing, *Tetrahedron*, 2012, **68**, 1163–1170.

[95] J. Coates, P. G. Sammes and R. M. West, *J. Chem. Soc., Perkin Trans. 2*, 1996, 1283–1287.

[96] D. Burdinski, J. Lub, J. A. Pikkemaat, D. Moreno Jalón, S. Martial and C. Del Pozo Ochoa, *Dalton Trans.*, 2008, 4138.

[97] J. Lohse and O. Wernberg, *Acta Chem. Scand.*, 1995, **49**, 768–770.

[98] C. H. Cullen, G. J. Ray and C. M. Szabo, *Magn. Reson. Chem.*, 2013.

[99] S. A. Richards and J. C. Hollerton, *Essential practical NMR for organic chemistry*, John Wiley & Sons, 2010.

[100] T. Rundlöf, M. Mathiasson, S. Bekiroglu, B. Hakkarainen, T. Bowden and T. Arvidsson, *J. Pharm. Biomed. Anal.*, 2010, **52**, 645–651.

[101] C. Peng, M. N. Chan and C. K. Chan, *Env. Sci. Tech.*, 2001, **35**, 4495–4501.

[102] G. F. Pauli, B. U. Jaki and D. C. Lankin, *J. Nat. Prod.*, 2005, **68**, 133–149.

[103] J. A. Aguilar and S. J. Kenwright, *The Analyst*, 2016, **141**, 236–42.

[104] *JASPER v2.0 - JavaScript Percentage Elemental Results Calculator*, `http://www.chem.yorku.ca/profs/potvin/Jasper/jasper2.htm`.

[105] D. C. Harris, *Quantitative Chemical Analysis*, Freeman, 3rd edn., 1991.

[106] B. D. Corbin, E. H. Seeley, A. Raab, J. Feldmann, M. R. Miller, V. J. Torres, K. L. Anderson, B. M. Dattilo, P. M. Dunman, R. Gerads, R. M. Caprioli, W. Nacken, W. J. Chazin and E. P. Skaar, *Science*, 2008, **319**, 962–965.

[107] A. W. J. Logan, S. J. Sprague, R. W. Foster, L. B. Marx, V. Garzya, M. S. Hallside, A. L. Thompson and J. W. Burton, *Org. Lett.*, 2014, **16**, 4078–4081.

[108] M. D. Rolfe, C. J. Rice, S. Lucchini, C. Pin, A. Thompson, A. D. S. Cameron, M. Alston, M. F. Stringer, R. P. Betts, J. Baranyi, M. W. Peck and J. C. D. Hinton, *J. Bacteriol.*, 2011, **194**, 686–701.

[109] J. R. Swathy, M. U. Sankar, A. Chaudhary, S. Aigal and T. Anshup, Pradeep, *Sci. Rep.*, 2014, **4**, 7161.

[110] A. I. Graham, S. Hunt, S. L. Stokes, N. Bramall, J. Bunch, A. G. Cox, C. W. McLeod and R. K. Poole, *J. Biol. Chem.*, 2009, **284**, 18377–18389.

[111] H. Irving and D. H. Mellor, *J. Chem. Soc. (Resumed)*, 1955, 3457.

[112] A. E. Martell, R. J. Motekaitis *et al.*, *Determination and use of stability constants*, VCH publishers, 1992.

[113] I. Johnson and M. Spence, *The molecular probes handbook*, Life Technologies Corporation, 2010.

[114] Z. Xiao and A. G. Wedd, *Nat. Prod. Rep.*, 2010, **27**, 768–789.

[115] OECD, *Test No. 107: Partition Coefficient (n-octanol/water): Shake Flask Method*, `DOI:10.1787/20745753`.

[116] A. Leo, C. Hansch and D. Elkins, *Chem. Rev.*, 1971, **71**, 525–616.

[117] P. D. Leeson and B. Springthorpe, *Nat. Rev. Drug Discov.*, 2007, **6**, 881–90.

[118] R. Mannhold, G. I. Poda, C. Ostermann and I. V. Tetko, *J. Pharm. Sci.*, 2009, **98**, 861–93.

[119] Z. Szakács, S. Béni and B. Noszál, *Talanta*, 2008, **74**, 666 – 674.

[120] C. W. Sheu, D. Salomon, J. L. Simmons, T. Sreevalsan and E. Freese, *Antimicrob. Agents Chemother.*, 1975, **7**, 349–363.

[121] F. Li, Y. Mulyana, M. Feterl, J. M. Warner, J. G. Collins and F. R. Keene, *Dalton Trans.*, 2011, **40**, 5032–8.

[122] A. K. Gorle, M. Feterl, J. M. Warner, L. Wallace, F. R. Keene and J. G. Collins, *Dalton Trans.*, 2014, **43**, 16713–25.

[123] C. W. Sheu and E. Freese, *J. Bacteriol.*, 1973, **115**, 869–875.

[124] G. Steyaert, G. Lisa, P. Gaillard, G. Boss, F. Reymond, H. H. Girault, P.-A. Carrupt and B. Testa, *J. Chem. Soc. Faraday. Trans.*, 1997, **93**, 401–406.

[125] P. Atkins and J. De Paula, *Physical Chemistry*, Oxford University Press, 8th edn., 2006.

[126] B. O. Keller, J. Sui, A. B. Young and R. M. Whittal, *Anal. Chim. Acta*, 2008, **627**, 71–81.

[127] A. F. Danil de Namor and D. Alfredo Pacheco Tanaka, *J. Chem. Soc. Faraday. Trans.*, 1998, **94**, 3105–3110.

[128] H. Santacruz, R. E. Navarro, L. Machi, R. Sugich-Miranda and M. Inoue, *Polyhedron*, 2011, **30**, 690–696.

[129] D. A. Jaeger, M. F. Peacock and D. S. Bohle, *Langmuir*, 2003, **19**, 4859–4862.

[130] J. F. Carvalho, S. H. Kim and C. A. Chang, *Inorg. Chem.*, 1992, **31**, 4065–4068.

[131] J. J. Michels, J. Huskens and D. N. Reinhoudt, *J. Am. Chem. Soc.*, 2002, **124**, 2056–2064.

[132] A. Scozzafava, L. Menabuoni, F. Mincione and C. T. Supuran, *J. Med. Chem.*, 2002, **45**, 1466–1476.

[133] K.-Y. Choi, J. J. Oh and Y.-I. Lee, *Microchem. J.*, 1997, **55**, 357–366.

[134] T. Takeshita, T.-A. Shimohara and S. Maeda, *J. Am. Oil Chem. Soc.*, 1982, **59**, 104–107.

[135] C. H. W. Hirs, S. Moore and W. H. Stein, *J. Am. Chem. Soc.*, 1954, **76**, 6063–6065.

[136] C. H. W. Hirs, S. Moore and W. H. Stein, *J. Biol. Chem.*, 1952, **195**, 669–683.

[137] B. J. Johnson, *J. Chem. Educ.*, 2014, **91**, 1212–1215.

[138] S. Moore and W. H. Stein, *J. Biol. Chem.*, 1951, **192**, 663–681.

[139] J. Clayden, N. Greeves, S. Warren and P. Wothers, *Organic Chemistry*, Oxford University Press, 2001.

[140] A. El-Faham and F. Albericio, *Chem. Rev.*, 2011, **111**, 6557–6602.

[141] N. Nakajima and Y. Ikada, *Bioconjug. Chem.*, 1995, **6**, 123–130.

[142] J. A. Rowley, G. Madlambayan and D. J. Mooney, *Biomaterials*, 1999, **20**, 45–53.

[143] D. Maffeo and J. A. G. Williams, *Inorg. Chim. Act.*, 2003, **355**, 127–136.

[144] O. Reany, T. Gunnlaugsson and D. Parker, *J. Chem. Soc. Perkin. Trans. 2*, 2000, 1819–1831.

[145] T. W. Greene and P. G. M. Wuts, in *Protective Groups in Organic Synthesis*, John Wiley & Sons, Inc., 3rd edn., 2002.

[146] M. K. Anwer, D. Sherman, J. G. Roney and A. F. Spatola, *J. Org. Chem.*, 1989, **54**, 1284–1289.

[147] R. A. W. Johnstone, A. H. Wilby and I. D. Entwistle, *Chem. Rev.*, 1985, **85**, 129–170.

[148] S. D. Bull, S. G. Davies, G. Fenton, A. W. Mulvaney, R. S. Prasad and A. D. Smith, *J. Chem. Soc., Perkin Trans. 1*, 2000, 3765–3774.

[149] J. S. Davies and L. Al-Jamri, *J. Pept. Sci.*, 2002, **8**, 663–670.

[150] M. Weigl and B. Wünsch, *Tetrahedron*, 2002, **58**, 1173–1183.

[151] H. Miyake, M. Watanabe, M. Takemura, T. Hasegawa, Y. Kojima, M. B. Inoue, M. Inoue and Q. Fernando, *J. Chem. Soc. Dalton. Trans.*, 2002, 1119–1125.

[152] M. Tropiano, O. A. Blackburn, J. A. Tilney, L. R. Hill, M. P. Placidi, R. J. Aarons, D. Sykes, M. W. Jones, A. M. Kenwright, J. S. Snaith, T. J. Sorensen and S. Faulkner, *Chem. Eur. J.*, 2013, **19**, 16566–16571.

[153] Z. Baranyai, L. Tei, G. B. Giovenzana, F. K. Kálmán and M. Botta, *Inorg. Chem.*, 2012, **51**, 2597–2607.

[154] L. Tei, Z. Baranyai, M. Botta, L. Piscopo, S. Aime and G. B. Giovenzana, *Org. Biomol. Chem.*, 2008, **6**, 2361–2368.

[155] G. C. R. Ellis-Davies, *Tetrahedron Lett.*, 1998, **39**, 953–956.

[156] G. C. R. Ellis-Davies and J. H. Kaplan, *Proc. Nat. Acad. Sci.*, 1994, **91**, 187–191.

[157] E. W. Price, J. F. Cawthray, G. A. Bailey, C. L. Ferreira, E. Boros, M. J. Adam and C. Orvig, *J. Am. Chem. Soc.*, 2012, **134**, 8670–8683.

[158] C. M. Micklitsch, Q. Yu and J. P. Schneider, *Tetrahedron Lett.*, 2006, **47**, 6277–6280.

[159] T. Storr, B. R. Cameron, R. A. Gossage, H. Yee, R. T. Skerlj, M. C. Darkes, S. P. Fricker, G. J. Bridger, N. A. Davies, M. T. Wilson, K. P. Maresca and J. Zubieta, *Eur. J. Inorg. Chem.*, 2005, **2005**, 2685–2697.

[160] D. G. van der Poll, H. M. Kieler-Ferguson, W. C. Floyd, S. J. Guillaudeu, K. Jerger, F. C. Szoka and J. M. Fréchet, *Bioconjug. Chem.*, 2010, **21**, 764–773.

[161] J.-d. Twibanire and T. B. Grindley, *Polymers*, 2014, **6**, 179–213.

[162] E. Kume and R. Miyamoto, *Kidorui = Rare earths*, 2009, 210–211.

[163] L. A. Clapp, C. J. Siddons, J. R. Whitehead, D. G. VanDerveer, R. D. Rogers, S. T. Griffin, S. B. Jones and R. D. Hancock, *Inorg. Chem.*, 2005, **44**, 8495–502.

[164] A. E. Martell and R. M. Smith, *Critical stability constants*, Springer, 1974, vol. 3.

[165] R. B. Conolly, *Toxicol. Sci.*, 2003, **77**, 151–157.

[166] M. Kohn, *J. Mol. Endocrinol.*, 2002, **29**, 113–123.

[167] X.-W. Zhu, S.-S. Liu, L.-T. Qin, F. Chen and H.-L. Liu, *Ecotoxicol. Environ. Saf.*, 2013, **89**, 130–136.

[168] M. Beecroft and G. J. Sharples, *Unpublished Results*, 2015.

[169] C. Piergentili and N. J. Robinson, *Unpublished Results*, 2012.

[170] D. C. Dominguez, *Mol. Microbiol.*, 2004, **54**, 291–297.

[171] T. H. Hohle and M. R. O'Brian, *Mol. Microbiol.*, 2014, n/a–n/a.

[172] T. H. Hohle and M. R. O'Brian, *Mol. Microbiol.*, 2009, **72**, 399–409.

[173] T. E. Kehl-Fie and E. P. Skaar, *Curr. Opin. Chem. Biol.*, 2010, **14**, 218–224.

[174] S. Puri, T. H. Hohle and M. R. O'Brian, *Proc. Nat. Acad. Sci.*, 2010, **107**, 10691–10695.

[175] P. Letkeman and A. E. Martell, *Inorg. Chem.*, 1979, **18**, 1284–1289.

[176] R. J. Motekaitis and A. E. Martell, *J. Am. Chem. Soc.*, 1970, **92**, 4223–4230.

[177] A. Fisher and D. Naughton, *Trans. Met. Chem.*, 2004, **29**, 315–319.

[178] H. Irving and R. J. P. Williams, *J. Chem. Soc. (Resumed)*, 1953, 3192.

[179] A. Fisher and D. Naughton, *J. Struct. Chem.*, 2007, **48**, 711–714.

[180] R. A. Bulman, N. Jobanputra, R. Kuroda, A. McKinnon and P. J. Sadler, *Inorg. Chem.*, 1987, **26**, 2483–2486.

[181] S. Ulvenlund, A. S. Georgopoulou, D. M. P. Mingos, I. Baxter, S. E. Lawrence, A. J. P. White and D. J. Williams, *J. Chem. Soc. Dalton. Trans.*, 1998, 1869–1878.

[182] M. B. Inoue, P. Oram, M. Inoue and Q. Fernando, *Inorg. Chim. Act.*, 1996, **246**, 401 – 412.

[183] B. Xu, X.-L. Kong, T. Zhou, D.-H. Qiu, Y.-L. Chen, M.-S. Liu, R.-H. Yang and R. C. Hider, *Bioorg. Med. Chem. Lett.*, 2011, **21**, 6376–80.

[184] R. C. Hedstrom, R. K. Schockley and R. G. Eagon, *J. Bacteriol.*, 1981, **148**, 995–997.

[185] K. Matsushita, O. Adachi, E. Shinagawa and M. Ameyama, *J. Biochem.*, 1978, **83**, 171–181.

[186] *Cold Spring Harbor Protocols*, 2006, pdb.rec8247.

[187] R. Delgado, S. Quintino, M. Teixeira and A. Zhang, *J. Chem. Soc. Dalton. Trans.*, 1997, 55–64.

[188] E. J. New, A. Congreve and D. Parker, *Chem. Sci.*, 2010, **1**, 111.

[189] R. L. Bertrand, *J. Theor. Biol.*, 2014, **359**, 72–79.

[190] K. J. Waldron and N. J. Robinson, *Nat. Rev. Microbiol.*, 2009, **7**, 25–35.

[191] C. D. Georgiou, H. Fang and R. B. Gennis, *J. Bacteriol.*, 1987, **169**, 2107–12.

[192] R. Crichton and J. R. Boelaert, *Inorganic biochemistry of iron metabolism: from molecular mechanisms to clinical consequences*, John Wiley & Sons, 2nd edn., 2001.

[193] H. D. Madhani and E. P. Skaar, *PLoS Pathogens*, 2010, **6**, e1000949.

[194] S. C. Andrews, A. K. Robinson and F. Rodríguez-Quiñones, *FEMS Microbiol. Rev.*, 2003, **27**, 215–237.

[195] W. R. Harris, C. J. Carrano, S. R. Cooper, S. R. Sofen, A. E. Avdeef, J. V. McArdle and K. N. Raymond, *J. Am. Chem. Soc.*, 1979, **101**, 6097–6104.

[196] A. Evers, R. D. Hancock, A. E. Martell and R. J. Motekaitis, *Inorg. Chem.*, 1989, **28**, 2189–2195.

[197] C. J. Carrano, S. R. Cooper and K. N. Raymond, *J. Am. Chem. Soc.*, 1979, **101**, 599–604.

[198] J. B. Neilands, T. J. Erickson and W. H. Rastetter, *J. Biol. Chem.*, 1981, **256**, 3831–2.

[199] Y.-J. Zhou, M.-S. Liu, A. R. Osamah, X.-L. Kong, S. Alsam, S. Battah, Y.-Y. Xie, R. C. Hider and T. Zhou, *Eur. J. Med. Chem.*, 2015, **94**, 8–21.

[200] M.-X. Zhang, C.-F. Zhu, Y.-J. Zhou, X.-L. Kong, R. C. Hider and T. Zhou, *Chem. Biol. Drug. Des.*, 2014, **84**, 659–668.

[201] P. N. Turowski, S. J. Rodgers, R. C. Scarrow and K. N. Raymond, *Inorg. Chem.*, 1988, **27**, 474–481.

[202] R. Ma, R. J. Motekaitis and A. E. Martell, *Inorg. Chim. Acta*, 1994, **224**, 151–155.

[203] F. Yunta, S. García-Marco, J. J. Lucena, M. Gómez-Gallego, R. Alcázar and M. A. Sierra, *Inorg. Chem.*, 2003, **42**, 5412–5421.

[204] M. A. Sierra, M. Gómez-Gallego, R. Alcázar, J. J. Lucena, F. Yunta and S. García-Marco, *Dalton Trans.*, 2004, 3741–3747.

[205] F. L. Eplattenier, I. Murase and A. E. Martell, *J. Am. Chem. Soc.*, 1967, **89**, 837–843.

[206] C. J. Bannochie and A. E. Martell, *J. Am. Chem. Soc.*, 1989, **111**, 4735–4742.

[207] A. E. Frost, H. H. Freedman, S. J. Westerback and A. E. Martell, *J. Am. Chem. Soc.*, 1958, **80**, 530–536.

[208] B. Peter and S. Carsten, *WO Patent App. PCT/EP1997/002568*, 1997.

[209] S. Goswami, S. Maity, A. K. Das and A. C. Maity, *Tetrahedron Lett.*, 2013, **54**, 6631–6634.

[210] D. Reinhard, L. Schöttner, V. Brosius, F. Rominger and M. Mastalerz, *Eur. J. Org. Chem.*, 2015, **2015**, 3274–3285.

[211] N. U. Hofsløkken, L. Skattebøl, F. Johansson, S. K. Bertilsson, P. G. Andersson, J. Møller, A. Senning, X.-K. Yao, H.-G. Wang, J. P. Tuchagues and M. Ögren, *Acta Chem. Scand.*, 1999, **53**, 258–262.

[212] J. G. Wilson, *Aust. J. Chem.*, 1987, **40**, 1695.

[213] N. A, S. F, M.-N. A and O. R, *World Patent No. WO2009037235 A1*, 2009.

[214] E. Wong, S. Liu, S. Rettig and C. Orvig, *Inorg. Chem.*, 1995, **34**, 3057–3064.

[215] S. Velusamy and T. Punniyamurthy, *Eur. J. Org. Chem.*, 2003, **2003**, 3913–3915.

[216] D. H. T. Phan, B. Kim and V. M. Dong, *J. Am. Chem. Soc.*, 2009, **131**, 15608–15609.

[217] J. A. Sclafani, M. T. Maranto, T. M. Sisk and S. A. Van Arman, *J. Org. Chem.*, 1996, **61**, 3221–3222.

[218] A. Mehta, R. Jaouhari, T. J. Benson and K. T. Douglas, *Tetrahedron Lett.*, 1992, **33**, 5441–5444.

[219] M. M. Hansen and J. R. Riggs, *Tetrahedron Lett.*, 1998, **39**, 2705–2706.

[220] http://research.chem.psu.edu/brpgroup/pKa_compilation.pdf.

[221] S. Kazumi and H. Daikichi, *Japanese patent JPH0710819 (A)*, 1995.

[222] E. M. Gale, S. Mukherjee, C. Liu, G. S. Loving and P. Caravan, *Inorg. Chem.*, 2014, **53**, 10748–10761.

[223] B. Nörtemann, in *Biogeochemistry of Chelating Agents*, 2005, vol. 910, pp. 150–170.

[224] M. J. Matar, L. Ostrosky-Zeichner, V. L. Paetznick, J. R. Rodriguez, E. Chen and J. H. Rex, *Antimicrob. Agents Chemother.*, 2003, **47**, 1647–1651.

[225] J. Hinton and K. D. Ingram, *J. Food Safety*, 2011, **31**, 357–364.

[226] H. Dickert, K. Machka and I. Braveny, *Infection*, 1981, **9**, 18–24.

[227] B. Bonev, J. Hooper and J. Parisot, *J. Antimicrob. Chemother.*, 2008, **61**, 1295–1301.

[228] G. Da Violante, N. Zerrouk, I. Richard, G. Provot, J. C. Chaumeil and P. Arnaud, *Biol. Pharm. Bull.*, 2002, **25**, 1600–1603.

[229] http://www.microbelibrary.org/component/resource/laboratory-test/3189-kirby-bauer-disk-diffusion-susceptibility-test-protocol, An ASM resource.

[230] P. Levene and H. S. Simms, *J. Biol. Chem.*, 1923, **55**, 801–813.

[231] T. E. Needham, *Ph.D. thesis*, University of Rhode Island, 1970.

[232] L. Lattuada, A. Barge, G. Cravotto, G. B. Giovenzana and L. Tei, *Chem. Soc. Rev.*, 2011, **40**, 3019–3049.

[233] P. Caravan, J. J. Ellison, T. J. McMurry and R. B. Lauffer, *Chem. Rev.*, 1999, **99**, 2293–2352.

[234] G. J. Stasiuk and N. J. Long, *Chem. Commun.*, 2013, **49**, 2732.

[235] S. Aime, L. Anelli, M. Botta, M. Brocchetta, S. Canton, F. Fedeli, E. Gianolio and E. Terreno, *J. Biol. Inorg. Chem.*, 2002, **7**, 58–67.

[236] A. de Sá, C. S. Bonnet, C. F. G. C. Geraldes, E. Tóth, P. M. T. Ferreira and J. P. André, *Dalton Trans.*, 2013, **42**, 4522–4532.

[237] L. Pettit, *Chemistry International – Newsmagazine for IUPAC*, 2006, **28**, 14.

[238] C. J. Anderson, F. Dehdashti, P. D. Cutler, S. W. Schwarz, R. Laforest, L. A. Bass, J. S. Lewis and D. W. McCarthy, *J. Nucl. Med.*, 2001, **42**, 213–221.

[239] S. Aime, L. Calabi, C. Cavallotti, E. Gianolio, G. B. Giovenzana, P. Losi, A. Maiocchi, G. Palmisano and M. Sisti, *Inorg. Chem.*, 2004, **43**, 7588–7590.

[240] A. J. Wilkinson, *Ph.D. thesis*, University of Durham, 2004.

[241] G. Anderegg, F. Arnaud-Neu, R. Delgado, J. Felcman and K. Popov, *Pure Appl. Chem.*, 2005, **77**, 1445.

[242] E. T. Clarke and A. E. Martell, *Inorg. Chim. Acta*, 1991, **181**, 273 – 280.

[243] E. T. Clarke and A. E. Martell, *Inorg. Chim. Acta*, 1991, **190**, 37–46.

[244] A. Bianchi, L. Calabi, C. Giorgi, P. Losi, P. Mariani, D. Palano, P. Paoli, P. Rossi and B. Valtancoli, *J. Chem. Soc, Dalton. Trans.*, 2001, 917–922.

[245] M. J. Van der Merwe, J. C. A. Boeyens and R. D. Hancock, *Inorg. Chem.*, 1985, **24**, 1208–1213.

[246] A. Bevilacqua, R. I. Gelb, W. B. Hebard and L. J. Zompa, *Inorg. Chem.*, 1987, **26**, 2699–2706.

[247] S. Cortes, E. Brucher, C. F. G. C. Geraldes and A. D. Sherry, *Inorg. Chem.*, 1990, **29**, 5–9.

[248] H. Hama and S. Takamoto, *Nippon Kagaku Kaishi*, 1975, 1182–1185.

[249] S. Chaves, R. Delgado and J. Da Silva, *Talanta*, 1992, **39**, 249–254.

[250] R. Delgado and J. F. da Silva, *Talanta*, 1982, **29**, 815–822.

[251] X. Zhu and S. Z. Lever, *Electrophoresis*, 2002, **23**, 1348–1356.

[252] P. Caravan, C. Comuzzi, W. Crooks, T. J. McMurry, G. R. Choppin and S. R. Woulfe, *Inorg. Chem.*, 2001, **40**, 2170–2176.

[253] G. Anderegg, P. Nägeli, F. Müller and G. Schwarzenbach, *Helv. Chim. Acta.*, 1959, **42**, 827–836.

[254] G. Anderegg, *Helv. Chim. Acta*, 1964, **47**, 1801–1814.

[255] D. L. Wright, J. H. Holloway and C. N. Reilley, *Anal. Chem.*, 1965, **37**, 884–892.

[256] G. L. Smith and D. J. Miller, *Biochim. Biophys. Acta*, 1985, **839**, 287–299.

[257] K. H. Schroeder, *Acta. Chem. Scand.*, 1963, **17**, 1509–1514.

[258] J. H. Holloway and C. N. Reilley, *Anal. Chem.*, 1960, **32**, 249–256.

[259] K. Doi and M. Tanaka, *Anal. Chim. Acta*, 1974, **71**, 464–467.

[260] L. A. Clifton, S. A. Holt, A. V. Hughes, E. L. Daulton, W. Arunmanee, F. Heinrich, S. Khalid, D. Jefferies, T. R. Charlton, J. R. P. Webster, C. J. Kinane and J. H. Lakey, *Angew. Chem. Int. Ed. Engl.*, 2015, **54**, 11952–5.

[261] M. Regueiro-Figueroa, L. M. P. Lima, V. Blanco, D. Esteban-Gómez, A. de Blas, T. Rodríguez-Blas, R. Delgado and C. Platas-Iglesias, *Inorg. Chem.*, 2014, **53**, 12859–12869.

[262] A. Takács, R. Napolitano, M. Purgel, A. C. Bényei, L. Zékány, E. Brücher, I. Tóth, Z. Baranyai and S. Aime, *Inorg. Chem.*, 2014, **53**, 2858–2872.

[263] Z. Baranyai, F. Uggeri, G. Giovenzana, A. Bényei, E. Brücher and S. Aime, *Chem. Eur. J.*, 2009, **15**, 1696–1705.

[264] F. K. Kálmán and G. Tircsó, *Inorg. Chem.*, 2012, **51**, 10065–10067.

[265] G. Tircsó, A. Bényei, R. Király, R. Lázár, I and; Pál and E. Brücher, *Eur. J. Inorg. Chem.*, 2007, **2007**, 701–713.

[266] J. R. Morey, C. A. McDevitt and T. E. Kehl-Fie, *BioMetals*, 2015, **28**, 509–519.

[267] J. T. Gerig, P. Singh, L. A. Levy and R. E. London, *J. Inorg. Biochem.*, 1987, **31**, 113–121.

[268] R. J. Motekaitis, A. E. Martell and M. J. Welch, *Inorg. Chem.*, 1990, **29**, 1463–1467.

[269] E. Garcia-España, *Personal communication*, 2015.

[270] L. Alderighi, P. Gans, A. Ienco, D. Peters, A. Sabatini and A. Vacca, *Coord. Chem. Rev.*, 1999, **184**, 311–318.

[271] T. Hill and P. Lewicki, *Statistics: Methods and Applications*, StatSoft, 2007.

[272] M. Orama, H. Hyvönen, H. Saarinen and R. Aksela, *J. Chem. Soc. Dalton. Trans.*, 2002, 4644–4648.

[273] I. Gorelov and V. Babich, *Zh. Neorg. Khim.*, 1971, **16**, 902.

[274] K. Majlesi, K. Zare and F. Teimouri, *J. Chem. Eng. Data*, 2004, **49**, 439–443.

[275] A. Craggs, G. J. Moody and J. D. R. Thomas, *Analyst*, 1979, **104**, 961–972.

[276] T. Bohigian and A. E. Martell, *Prog. Rep. US. Atom. En. Comm. Con.*, 1960, At30–1–1823.

[277] R. J. Motekaitis and A. E. Martell, *J. Coord. Chem.*, 1994, **31**, 67–78.

[278] AkzoNobel, *Dissolvine ®GL technical brochure*, 2014.

[279] G. D. Fasman, H. A. Sober *et al.*, *Handbook of biochemistry and molecular biology*, CRC press Cleveland, 1977, vol. 4.

[280] W. R. Harris, R. J. Motekaitis and A. E. Martell, *Inorg. Chem.*, 1975, **14**, 974–978.

[281] *United States Environmental Protection Agency, Estimation Programs Interface Suite™ for Microsoft® Windows, v 4.11*, 2012.

[282] I. Lázár, R. Király and Z. Takács, *J. Coord. Chem.*, 2000, **51**, 293–304.

[283] M. Mashihara, T. Ando and I. Murase, *Bull. Chem. Soc. Jpn.*, 1973, **46**, 844–847.

[284] J. Henig, E. Toth, J. Engelmann, S. Gottschalk and H. A. Mayer, *Inorg. Chem.*, 2010, **49**, 6124–6138.

[285] https://orgprepdaily.wordpress.com/2006/09/19/evans-asymmetric-glyoxylate-ene-reaction/

[286] B. Sreenivasulu and J. J. Vittal, *Angew. Chem. Int. Ed. Engl.*, 2004, **116**, 5893–5896.

[287] L. J. Prins, M. M. Blázquez, A. Kolarović and G. Licini, *Tetrahedron Lett.*, 2006, **47**, 2735–2738.

[288] R. Pal and D. Parker, *Org. Biomol. Chem.*, 2008, **6**, 1020.

[289] T. Gunnlaugsson, D. F. Brougham, A.-M. Fanning, M. Nieuwenhuyzen, J. E. O'Brien and R. Viguier, *Org. Lett.*, 2004, **6**, 4805–4808.

[290] Y.-H. Chiu, and J. W. Canary, *Inorg. Chem.*, 2003, **42**, 5107–5116.

[291] M. Lanznaster, A. Neves, A. J. Bortoluzzi, A. M. C. Assumpcao, I. Vencato, S. P. Machado and S. M. Drechsel, *Inorg. Chem.*, 2006, **45**, 1005–11.

[292] P. Caravan, S. J. Rettig and C. Orvig, *Inorg. Chem.*, 1997, **36**, 1306–1315.

[293] K. Ananda and V. Suresh Babu, *J. Pept. Res.*, 2001, **57**, 223–226.

[294] A. F. Abdel-Magid and S. J. Mehrman, *Org. Process Res. Dev.*, 2006, **10**, 971–1031.

[295] B. Müller and H. Vahrenkamp, *Eur. J. Inorg. Chem.*, 1999, **1999**, 137–144.

[296] Z. Wang, D. Pei, Y. Zhang, C. Wang and J. Sun, *Molecules*, 2012, **17**, 5151–63.

[297] W. A. White and H. Weingarten, *J. Org. Chem.*, 1967, **32**, 213–214.

[298] M. Valencic, T. van der Does and E. de Vroom, *Tetrahedron Lett.*, 1998, **39**, 1625–1628.

[299] S. Das, D. Addis, S. Zhou, K. Junge and M. Beller, *J. Am. Chem. Soc.*, 2010, **132**, 1770–1771.

[300] Y. Li, A. Silamkoti, G. Kolavi, L. Mou, S. Gulati, G. M. Air and W. J. Brouillette, *Bioorg. Med. Chem.*, 2012, **20**, 4582–4589.

[301] E. K. Lermontova, M. Huan, A. V. Churakov, J. A. K. Howard, M. V. Zabalov, S. S. Karlov and G. S. Zaitseva, *Dalton Trans.*, 2009, 4695.

[302] C. Galaup, J.-M. Couchet, S. Bedel, P. Tisnès and C. Picard, *J. Org. Chem.*, 2005, **70**, 2274–2284.

[303] G. Bechara, N. Leygue, C. Galaup, B. Mestre-Voegtlé and C. Picard, *Tetrahedron*, 2010, **66**, 8594–8604.

[304] G. Bechara, N. Leygue, C. Galaup, B. Mestre and C. Picard, *Tetrahedron Lett.*, 2009, **50**, 6522–6525.

[305] D. Burdinski, J. A. Pikkemaat, J. Lub, P. de Peinder, L. Nieto Garrido and T. Weyhermuller, *Inorg. Chem.*, 2009, **48**, 6692–6712.

[306] B. M. Trost and L. S. Melvin, *J. Am. Chem. Soc.*, 1976, **98**, 1204–1212.

[307] B. M. Trost and W. J. Frazee, *J. Am. Chem. Soc.*, 1977, **99**, 6124–6126.

[308] R. N. Salvatore, C. H. Yoon and K. W. Jung, *Tetrahedron*, 2001, **57**, 7785–7811.

[309] M. C. O'Sullivan and D. M. Dalrymple, *Tetrahedron Lett.*, 1995, **36**, 3451–3452.

[310] G. Tojo and M. I. Fernandez, *Oxidation of Alcohols to Aldehydes and Ketones*, Springer, 2006.

[311] Y. Fricke, N. Kopp and B. Wünsch, *Synthesis*, 2010, **2010**, 791–796.

[312] K. C. Nicolaou, V. A. Adsool and C. R. H. Hale, *Org. Lett.*, 2010, **12**, 1552–1555.

[313] B. T. Golding, M. J. Kebbell and I. M. Lockhart, *J. Chem. Soc, Perkin Trans. 2*, 1987, 705.

[314] A. Polavarapu, J. A. Stillabower, S. G. W. Stubblefield, W. M. Taylor and M.-H. Baik, *J. Org. Chem.*, 2012, **77**, 5914–21.

[315] I. Ugarriza, U. Uria, L. Carrillo, J. L. Vicario and E. Reyes, *Chem. Eur. J.*, 2014, **20**, 11650–11654.

[316] H. A. Keane, W. Hess and J. W. Burton, *Chem. Commun.*, 2012, **48**, 6496–8.

[317] W. Hess and J. W. Burton, *Adv. Synth. Catal.*, 2011, **353**, 2966–2970.

[318] W. Hess and J. W. Burton, *Chem. Eur. J.*, 2010, **16**, 12303–12306.

[319] M. Kadirvel, M. Fairclough, C. Cawthorne, E. J. Rowling, M. Babur, A. McMahon, P. Birkket, A. Smigova, S. Freeman, K. J. Williams and G. Brown, *Bioorg. Med. Chem.*, 2014, **22**, 341–349.

[320] J. E. Saavedra, *J. Org. Chem.*, 1985, **50**, 2271–2273.

[321] P. R. Greene and C. D. Bain, *Spectroscopy Europe*, 2004, **16**, 8–15.

[322] M. Ali, M. Woods, P. Caravan, A. Opina, M. Spiller, J. Fettinger and A. Sherry, *Chem. Eur. J.*, 2008, **14**, 7250–7258.

[323] M. Woods and A. D. Sherry, *Inorg. Chem.*, 2003, **42**, 4401–4408.

[324] M. Pniok, V. Kubíček, J. Havlíčková, J. Kotek, A. Sabatie-Gogová, J. Plutnar, S. Huclier-Markai and P. Hermann, *Chem. Eur. J.*, 2014, **20**, 7944–7955.

[325] C. J. Broan, J. P. L. Cox, A. S. Craig, R. Kataky, D. Parker, A. Harrison, A. M. Randall and G. Ferguson, *J. Chem. Soc. Perkin. Trans. 2*, 1991, 87.

[326] H. Morimoto, T. Tsubogo, N. D. Litvinas and J. F. Hartwig, *Angew. Chem. Int. Ed. Engl.*, 2011, **50**, 3793–3798.

[327] W. C. Still, M. Kahn and A. Mitra, *J. Org. Chem.*, 1978, **43**, 2923–2925.

[328] M. S. Dunn and T. Brophy, *J. Biol. Chem.*, 1932, **99**, 221–229.

[329] E. S. Claudio, M. A. ter Horst, C. E. Forde, C. L. Stern, M. K. Zart and H. A. Godwin, *Inorg. Chem.*, 2000, **39**, 1391–1397.

[330] J. Li and Y. Sha, *Molecules*, 2008, **13**, 1111–1119.

[331] A. I. Almansour, N. Arumugam, R. Suresh Kumar, J. Carlos Menéndez, H. A. Ghabbour, H.-K. Fun and R. Ranjith Kumar, *Tetrahedron Lett.*, 2015, **56**, 6900–6903.

[332] H. K. Chenault, J. Dahmer and G. M. Whitesides, *J. Am. Chem. Soc.*, 1989, **111**, 6354–6364.

[333] N. Cakić, T. Z. Verbić, R. M. Jelić, C. Platas-Iglesias and G. Angelovski, *Dalton Trans.*, 2016, **45**, 6555–6565.

[334] R. S. Dickins and A. Badari, *Dalton Trans.*, 2007, 3661–3668.

[335] T. A. Immel, M. Grätzke, E. Batroff, U. Groth and T. Huhn, *J. Inorg. Biochem.*, 2012, **106**, 68–75.

[336] S. Ménage, J.-B. Galey, J. Dumats, G. Hussler, M. Seité, I. G. Luneau, G. Chottard and M. Fontecave, *J. Am. Chem. Soc.*, 1998, **120**, 13370–13382.

[337] B. P. Waldron, D. Parker, C. Burchardt, D. S. Yufit, M. Zimny and F. Roesch, *Chem. Commun.*, 2013, **49**, 579–581.

[338] J. Wilent and K. S. Petersen, *J. Org. Chem.*, 2014, **79**, 2303–7.

[339] R. B. Greenwald, H. Zhao, K. Yang, P. Reddy and A. Martinez, *J. Med. Chem.*, 2004, **47**, 726–34.

[340] G. Simig, G. Doleschall, G. Hornyák, J. Fetter, K. Lempert, J. Nyitrai, P. Huszthy, T. Gizur and M. Kajtár-Peredy, *Tetrahedron*, 1985, **41**, 479–484.

[341] A. A. Miles, S. S. Misra and J. O. Irwin, *J. Hygiene*, 1938, **38**, 732–49.

[342] C. A. Schneider, W. S. Rasband and K. W. Eliceiri, *Nat. Methods*, 2012, **9**, 671–675.

[343] E. Gianolio, G. B. Giovenzana, D. Longo, I. Longo, I. Menegotto and S. Aime, *Chem. Eur. J.*, 2007, **13**, 5785–5797.